

Arthritis & Rheumatology

An Official Journal of the American College of Rheumatology
www.arthritisrheum.org and wileyonlinelibrary.com

Editor

S. Louis Bridges, Jr., MD, PhD, *New York*

Deputy Editors

Karen H. Costenbader, MD, MPH, *Boston*

Mariana J. Kaplan, MD, *Bethesda*

Kenneth G. Saag, MD, MSc, *Birmingham*

Daniel H. Solomon, MD, MPH, *Boston*

Co-Editors

David T. Felson, MD, MPH, *Boston*

Richard F. Loeser Jr., MD, *Chapel Hill*

Journal Publications Committee

Chair - Betty Tsao, PhD, *Charleston*

Member - ARP Liaison

Cynthia Crowson, PhD, *Stewartville*

Members

Elana Bernstein, MD, MSc, *New York*

Krati Chauhan, MD, PhD, *Burlington*

Daniel B. Horton, MD, MSCE, *New Brunswick*

Suraj Rajasimhan, PharmD, *Columbia*

Faria Latif Sami, MD, *Birmingham*

Himanshu Vashistha, PhD, MBA, *Great Neck*

Editorial Staff

Susan Case, *Vice President, Strategic Marketing,*

Communications and Publishing, Maryland

Maggie Parry, *Director, Quality and Production, Georgia*

Brian T. Robinson, *Director, Digital Content, Pennsylvania*

Chris Reynolds, *Product Manager, Georgia*

Christy Austin, *Publishing Coordinator, Washington*

Laura Bolte, *Managing Editor, North Carolina*

Associate Editors

Rohit Aggarwal, MD, *Pittsburgh*

Ivona Aksentijevich, MD, PhD, *Bethesda*

Marta Alarcón-Riquelme, MD, PhD, *Stockholm, Sweden*

Neil Basu, MD, PhD, *Scotland*

Ashira D. Blazer, MD, MSCI, *Baltimore*

Nunzio Bottini, MD, PhD, *Los Angeles*

Alberto Carli, MD, *New York*

John Carrino, MD, MPH, *New York*

Andrew Cope, MD, PhD, *London, UK*

Jeffrey Curtis, MD, MS, MPH, *Birmingham*

Nicola Dalbeth, MBChB, MD, FRCP, *Auckland, NZ*

Maria Danila, MD, MS, *Birmingham*

Christopher Denton, PhD, FRCP, *London, UK*

Doruk Erkan, MD, *New York*

Richard A. Furie, MD, *Great Neck*

Hassan Ghomrawi, PhD, MPH, *Birmingham*

J. Michelle Kahlenberg, MD, PhD, *Ann Arbor*

Wan-Uk Kim, MD, PhD, *Seoul, Korea*

Jason S. Knight, MD, PhD, *Ann Arbor*

Carl D. Langefeld, PhD, *Winston-Salem*

Yvonne C. Lee, MD, MMSc, *Chicago*

Katherine Liao, MD, MPH, *Boston*

Tony R. Merriman, PhD, *Birmingham*

Rachel E. Miller, PhD, *Chicago*

Yukinori Okada, MD, PhD, *Osaka, Japan*

Karen B. Onel, MD, *New York*

Dana Orange, MD, MS, *New York*

Janet E. Pope, MD, MPH, FRCP, *London, Ontario, Canada*

Lisa G. Rider, MD, *Bethesda*

Christopher T. Ritchlin, MD, MPH, *Rochester*

William H. Robinson, MD, PhD, *Palo Alto*

Amr Sawalha, MD, *Pittsburg*

Carla R. Scanzello, MD, PhD, *Philadelphia*

Georg Schett, MD, *Erlangen, Germany*

Gabriela Schmajuk, MD, *Palo Alto*

Raphaële Seror, MD, PhD, *Becetre, France*

Leena Sharma, MD, *Chicago*

Jasvinder Singh, MD, MPH, *Houston*

Robert F. Spiera, MD, *New York*

Yoshiya Tanaka, MD, PhD, *Kitakyushu, Japan*

Fei Wang, PhD, *New York*

Baohong Zhao, PhD, *New York*

Advisory Editors

Ayaz Aghayev, MD, *Boston*

Joshua F. Baker, MD, MSCE, *Philadelphia*

Bonnie Bermas, MD, *Dallas*

Jamie Collins, PhD, *Boston*

Kristen Demoruelle, MD, PhD, *Denver*

Christopher Denton, PhD, FRCP, *London*

Anisha Dua, MD, MPH, *Chicago*

John FitzGerald, MD, *Los Angeles*

Lauren Henderson, MD, MMSc, *Boston*

Monique Hinchcliff, MD, MS, *New Haven*

Hui-Chen Hsu, PhD, *Birmingham*

Mohit Kapoor, PhD, *Toronto*

Seoyoung Kim, MD, ScD, MSCE, *Boston*

Vasileios Kyttaris, MD, *Boston*

Carl D. Langefeld, PhD, *Winston-Salem*

Christian Lood, PhD, *Seattle*

Dennis McGonagle, FRCPI, PhD, *Leeds*

Julie Paik, MD, MHS, *Baltimore*

Julie Zikherman, MD, *San Francisco*

AMERICAN COLLEGE OF RHEUMATOLOGY

Carol Langford, MD, MHS, *Cleveland, President*

William Harvey, MD, MSc, *Boston, President-Elect*

Anne Bass, MD, *New York, Treasurer*

Angus Worthing, MD, *Washington, DC, Secretary*

Steven Echard, IOM, CAE, *Atlanta, Executive Vice-President*

© 2025 American College of Rheumatology. All rights reserved, including rights for text and data mining and training of artificial technologies or similar technologies. No part of this publication may be reproduced, stored or transmitted in any form or by any means without the prior permission in writing from the copyright holder. Authorization to copy items for internal and personal use is granted by the copyright holder for libraries and other users registered with their local Reproduction Rights Organization (RRO), e.g. Copyright Clearance Center (CCC), 222 Rosewood Drive, Danvers, MA 01923, USA (www.copyright.com), provided the appropriate fee is paid directly to the RRO. This consent does not extend to other kinds of copying or use such as copying for general distribution, for advertising or promotional purposes, for creating new collective works, for resale, or for artificial intelligence tools or technologies. Special requests should be addressed to: permissions@wiley.com.

Access Policy: Subject to restrictions on certain backfiles, access to the online version of this issue is available to all registered Wiley Online Library users 12 months after publication. Subscribers and eligible users at subscribing institutions have immediate access in accordance with the relevant subscription type. Please go to onlineibrary.wiley.com for details.

The views and recommendations expressed in articles, letters, and other communications published in Arthritis & Rheumatology are those of the authors and do not necessarily reflect the opinions of the editors, publisher, or American College of Rheumatology. The publisher and the American College of Rheumatology do not investigate the information contained in the classified advertisements in this journal and assume no responsibility concerning them. Further, the publisher and the American College of Rheumatology do not guarantee, warrant, or endorse any product or service advertised in this journal.

Cover design: Todd Machen

© This journal is printed on acid-free paper.

Arthritis & Rheumatology

An Official Journal of the American College of Rheumatology
www.arthritisrheum.org and wileyonlinelibrary.com

VOLUME 77 • July 2025 • NO. 7

In This Issue.....	A4
Journal Club.....	A5
Clinical Connections	A6

Special Articles

Notes from the Field: The National Academies' 2024 Diagnostic Criteria for Long COVID: Concerns That Could Affect the Rheumatology Community <i>Leonard H. Calabrese, Michael Putman, Jeffrey A. Sparks, Zachary Wallace, Alfred H. J. Kim, Kevin L. Winthrop, and Cassandra Calabrese</i>	785
Editorial: Air Pollution's Hidden Toll: Risks for Rheumatoid Arthritis and Rheumatoid Arthritis-Associated Lung Disease <i>Sofia Ajeganova and Jeremy Sokolove</i>	789
Review: Immune Aging in Rheumatoid Arthritis <i>Cornelia M. Weyand and Jörg J. Goronzy</i>	792
Editorial: Systemic Sclerosis: A Multisystem Disease; Time to Think Beyond Scleroderma <i>Yannick Allanore and Shervin Assassi</i>	805

Rheumatoid Arthritis

Associations of Fire Smoke and Other Pollutants With Incident Rheumatoid Arthritis and Rheumatoid Arthritis-Associated Interstitial Lung Disease <i>Vanessa L. Kronzer, Yangyuna Yang, Punyasha Roul, James L. Crooks, Cynthia S. Crowson, John M. Davis III, Jeffrey A. Sparks, Jeffrey R. Pierce, Katelyn O'Dell, Brian C. Sauer, Grant W. Cannon, Joshua F. Baker, Ted R. Mikuls, and Bryant R. England</i>	808
Genome-Wide Aggregated Trans Effects Analysis Identifies Genes Encoding Immune Checkpoints as Core Genes for Rheumatoid Arthritis <i>Athina Spiliopoulou, Andrii Iakovliev, Darren Plant, Megan Sutcliffe, Seema Sharma, Cankut Cubuk, Myles Lewis, Costantino Pitzalis, Anne Barton, and Paul M. McKeigue</i>	817
Cytotoxic Response of CD4 ⁺ T Cells Orchestrated by SLAMF4 in Rheumatoid Arthritis <i>Mégane Lacaud, Houda-Ghoulane Bouzidi, Mylène Petit, Magali Breckler, Delphine Lemeiter, Johanna Sigaux, Elodie Rivière, Luca Semerano, Marie-Christophe Boissier, Natacha Bessis, and Jérôme Biton</i>	827

Psoriatic Arthritis

Metabolic Stress Expands Polyfunctional, Proinflammatory Th ₁₇ Cells in Patients With Psoriatic Arthritis for Whom There is Interleukin-23-Independent Interleukin-17 Production <i>Carmel B. Stober, Louise Ellis, Jane C. Goodall, Marc Veldhoen, and J. S. Hill Gaston</i>	842
An Immunosenescent CD8 ⁺ T Cell Subset in Patients with Axial Spondyloarthritis and Psoriatic Arthritis Links Spontaneous Motility to Telomere Shortening and Dysfunction <i>Giorgia Paldino, Valentina Tedeschi, Valentina Proganò, Erica Salvati, Valerio Licursi, Eleonora Vertecchi, Alexandru L. Bivolaru, Emanuele Molteni, Rossana Scrivo, Mattia Congia, Alberto Cauli, Rosalba Caccavale, Marino Paroli, Martina Kunkl, Loretta Tuosto, Rosa Sorrentino, and Maria Teresa Fiorillo</i>	854

Systemic Lupus Erythematosus

Induction of Type I Interferon-Dependent Activation and Migration of Inflammatory Dendritic Cells to Local Lymph Nodes by UV Light Exposure <i>Xizhang Sun, Jaime L. Chao, Michael Gerner, and Keith B. Elkon</i>	867
--	-----

Sjögren's Syndrome

Brief Report: Distinct Pathophysiologic Pathways Support Stratification of Sjögren's Disease Based on Symptoms, Clinical, and Routine Biological Data <i>Yann Nguyen, Maxime Beydon, Jacques-Eric Gottenberg, Jacques Morel, Aleth Perdriger, Emmanuelle Dernis, Divi Cornec, Valérie Devauchelle-Pensec, Damien Sène, Philippe Dieudé, Marion Couderc, Anne-Laure Fauchais, Claire Larroche, Olivier Vittecoq, Carine Salliot, Eric Hachulla, Véronique Le Guern, Xavier Mariette, Raphaële Seror, and Gaëtane Nocturne</i>	876
---	-----

Vasculitis

Proteomic Profiling of the Large-Vessel Vasculitis Spectrum Identifying Shared Signatures of Innate Immune Activation and Stromal Remodeling

Robert T. Maughan, Erin Macdonald-Dunlop, Lubna Haroon-Rashid, Louise Sorensen, Natalie Chaddock, Shauna Masters, Andrew Porter, Marta Peverelli, Charis Pericleous, Andrew Hutchings, James Robinson, Taryn Youngstein, Raashid A. Luqmani, Justin C. Mason, Ann W. Morgan, and James E. Peters. 884

Systemic Sclerosis

Absence of Functional Autoantibodies Targeting Angiotensin II Receptor Type 1 and Endothelin-1 Type A Receptor in Circulation and Purified IgG From Patients With Systemic Sclerosis

Wieke M. van Oostveen, Eva M. Hoekstra, E. W. Nivine Levarht, Ilana B. Kotliar, Thomas P. Sakmar, René E. M. Toes, Jeska K. de Vries-Bouwstra, Laura H. Heitman, and Cynthia M. Fehres. 901

Critical Role for Transglutaminase 2 in Scleroderma Skin Fibrosis and in the Development of Dermal Sclerosis in a Mouse Model of Scleroderma

Angela Y. Y. Tam, Korska Khan, Shiwen Xu, Marianne Bergin, Linghong Huang, Erik Arroyo Colon, Danyi Cheng, Elisabetta A. M. Verderio, Voon Ong, Christopher P. Denton, John Atkinson, Tim S. Johnson, and David J. Abraham 914

Serum Type I Interferon Score for Prediction of Clinically Meaningful Disease Progression in Limited Cutaneous Systemic Sclerosis

Stefano Di Donato, Rebecca Ross, Ranjitha Karanth, Vishal Kakkar, Enrico De Lorenzis, Lesley-Anne Bissell, Kristina Clark, Philip Yee, Christopher P. Denton, and Francesco Del Galdo 929

Clinical Image

Clinical Images: Transient Perivascular Inflammation of the Carotid Artery Syndrome

Neeharika Namineni, Sowmya Mahalingam, and Abhijeet Danve 942

Clinical Images: A Treatable Cause of Bilateral Leg Edema and Pleural Effusion: Yellow Nail Syndrome with IgG4-Related Disease

Seiya Oba and Yusuke Matsuo. 944

Letter

Targeting Long Noncoding RNA H19 in Subchondral Bone Osteocytes and Cartilage Degradation in Osteoarthritis: Comment on the Article by Wang et al

An-Fang Huang and Wang-Dong Xu 946

Reply

Wayne Y. W. Lee and Rongliang Wong. 947

Limitations in the Real-World Emulation of the HORIZON-Pivotal Fracture Trial: Comment on the Article by D'Andrea et al

Peng Shih-Kuei, Poi Kuo, and James Cheng-Chung Wei 948

Reply

Elvira D'Andrea and Shirley Wang. 948

Avoiding Placebo as Control Treatment in Rheumatology Trials: Can We Do Better? Comment on the Article by Kivitz et al

Maarten Boers 949

2023 American College of Rheumatology/American College of Chest Physicians Guideline for the Screening and Monitoring of Interstitial Lung Disease in People with Systemic Autoimmune Rheumatic Diseases: Comment on the Article by Johnson et al

Julian Segan, Michael Putman, and Richard Conway. 950

Reply

Sindhu R. Johnson, Marcy B. Bolster, Sonye K. Danoff, Michael George, Gordon Guyatt, Reza D. Mirza, Dinesh Khanna, Aberdeen Allen Jr, Amy Turner, and Elana J. Bernstein 951

Erratum

Correction to: Discovery of a Novel Missense Variant in NLRP3 Causing Atypical Cryopyrin-Associated Periodic Syndromes With Hearing Loss as the Primary Presentation, Responsive to Anti-Interleukin-1 Therapy 953

Cover image: The feature on the cover (from Tam et al, pages 914–928) shows the histologic section of mouse skin stained with Masson's trichrome. The image captures the skin of a genetically engineered mutant mouse globally deficient in transglutaminase 2 (TG2). This mouse was used to study the role of TG2 in an experimentally induced in vivo model of scleroderma skin fibrosis.

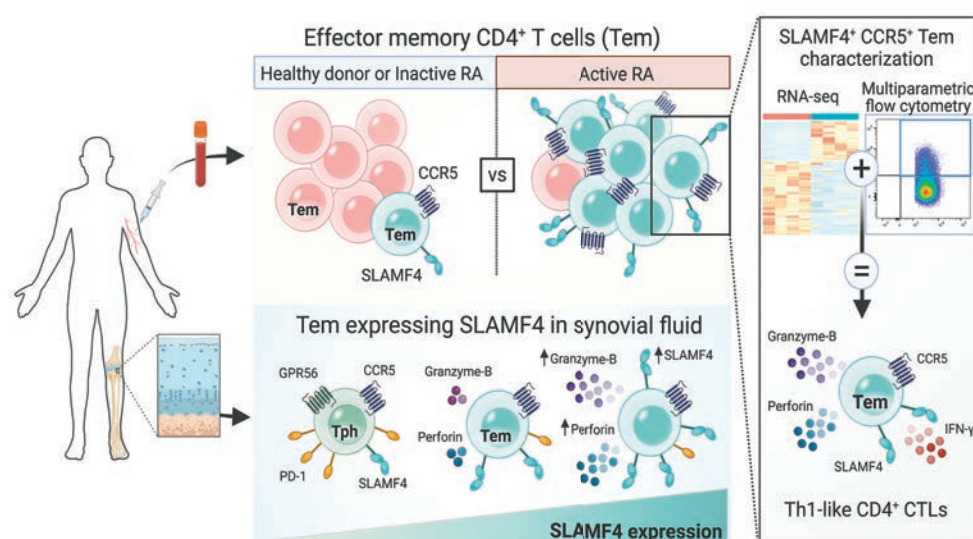
Clinical Connections

Cytotoxic Response of CD4⁺ T Cells Orchestrated by SLAMF4 in RA

Lacaud et al, *Arthritis Rheumatol.* 2025;77:827-841.

CORRESPONDENCE

Jérôme Biton, PhD: jerome.biton@univ-paris13.fr



KEY POINTS

- SLAMF4⁺ Tem are expanded in peripheral blood of patients with ACPA⁺ RA with active disease, and display both Th1 and cytotoxic CD4⁺ T cell features.
- SAP sustains the Th1 and cytotoxic functions of SLAMF4⁺ Tem.
- CCR5 expression appears to connect SLAMF4⁺ SAP⁺ Tem to RA pathophysiology.
- SLAMF4^{high} SAP⁺ CCR5⁺ Tem represent the main subset of cytotoxic CD4⁺ T cells in synovial fluid, suggesting that their inhibition may be of therapeutic interest.

SUMMARY

CD4⁺ T cells play a central role in the pathogenesis of rheumatoid arthritis (RA), but the specific mechanisms sustaining their chronic and deleterious responses remain insufficiently understood. By investigating the involvement of signaling lymphocytic activation molecule family (SLAMF) receptors in this process, Lacaud et al identified effector memory CD4⁺ T cells (Tem) expressing SLAMF4 as a cytotoxic and inflammatory subset expanded in RA.

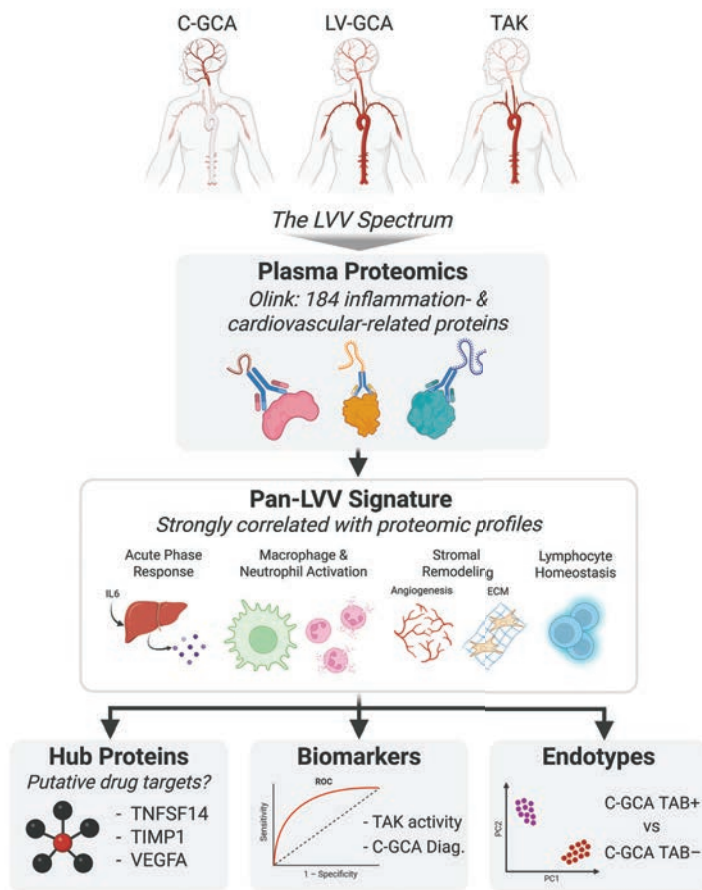
In the peripheral blood of patients with anti-citrullinated protein autoantibodies (ACPA)⁺ RA, SLAMF4⁺ Tem were overrepresented in individuals with active disease. This enrichment was specifically restricted to SLAMF4⁺ Tem coexpressing the inflammatory tissue-homing receptor CCR5 and the adaptor molecule SLAM-associated protein (SAP), the latter mediating downstream signaling upon SLAMF4 activation. Gene Set Enrichment Analysis of RNA-sequencing data, combined with multiparametric flow cytometry, revealed that SLAMF4⁺ SAP⁺ CCR5⁺ Tem exhibited both a Th1 (IFN-γ⁺, Tbet⁺) and a cytotoxic phenotype (granzyme-B⁺, perforin⁺, CX3CR1⁺). In synovial fluid of patients with RA, Tem highly expressing SLAMF4 represented the main cytotoxic subset of CD4⁺ T cells. In contrast, those with intermediate/low SLAMF4 expression corresponded to a minor subpopulation of peripheral helper T cells (Tph) characterized by high PD-1 and GPR56 expression. These findings highlight the potential contribution of SLAMF4^{high} SAP⁺ CCR5⁺ Tem to RA pathogenesis.

Proteomic Profiling of the Large-Vessel Vasculitis Spectrum

Maughan et al, *Arthritis Rheumatol.* 2025;77:884-900.

CORRESPONDENCE

James E. Peters, PhD, MRCP: j.peters@imperial.ac.uk



KEY POINTS

- Comparison of C-GCA, LV-GCA, and TAK proteomic profiles revealed a high degree of similarity suggesting shared pathobiology.
- Proteins altered in both diseases indicated a prominent acute phase response, macrophage and neutrophil activation, stromal remodeling, and lymphocyte signaling.
- Network-based analysis highlighted importance of immune–stromal crosstalk in LVV.
- LVV plasma protein profiles correlated with LVV artery phenotype suggesting that the plasma proteome could provide a noninvasive readout of arterial disease states.

SUMMARY

Large-vessel vasculitis (LVV) encompasses a group of diseases characterized by granulomatous inflammation of large- and medium-sized arteries. The two primary forms of LVV are giant cell arteritis (GCA) and Takayasu arteritis (TAK). Despite histopathologic similarities between GCA and TAK, there are differences in genetic risk factors, demographics (particularly age of onset), and arterial tropism. GCA is classified into cranial GCA (C-GCA), involving the extracranial branches of the carotid artery, and large-vessel GCA (LV-GCA), involving the aorta and its first-order branches, although both may co-exist.

Maughan et al performed plasma proteomic profiling in TAK, C-GCA, LV-GCA, and controls. Biopsy-proven C-GCA was proteomically distinct to biopsy-negative C-GCA, indicating that the latter is a molecularly distinct entity and questioning the reliability of diagnosis made purely on clinical grounds. There was strong correlation between the proteomic profiles of TAK, LV-GCA, and biopsy-proven C-GCA, suggesting sharing of the molecular effector pathways across these forms of vasculitis. A 'pan-LVV' protein signature common to TAK, LV-GCA, and C-GCA included proteins involved in innate immunity, lymphocyte signaling, and stromal remodeling. Bioinformatic network analysis highlighted immune–stromal crosstalk in LVV and proteins (e.g., TNFSF14) that could be targeted therapeutically to address both inflammation and the arterial proliferative response. The researchers developed multi-protein biomarkers for TAK disease activity and C-GCA diagnosis that outperformed current laboratory markers.

In this Issue

Highlights from this issue of *A&R* | By Lara C. Pullen, PhD

Distinct Pathophysiologic Pathways Support Stratification of Sjögren Disease

Studies have suggested that activation of B cells could contribute to systemic complications in Sjögren disease (SjD). In this issue, Nguyen et al (p. 876) report that three SjD clusters display distinct expressions of interferon (IFN) signature and markers of T and B cell activation, confirming that distinct pathophysiologic mechanisms determine these three clusters.

The researchers studied patients in the Assessment of Systemic Signs and Evolution in Sjögren's Syndrome (ASSESS) cohort. In a previous study, they stratified them into three groups based on symptoms, clinical presentation, and routine biologic data: low systemic activity with high symptoms (LSAHS), high systemic activity (HSA), and B cell active with low symptoms (BALS). This BALS cluster

was found to have the highest risk for disease progression. When the authors analyzed the cytokine profiles of the patients, they found that distinct cytokine patterns supported the stratification of the patients. For example, the LSAHS cluster had lower levels of cytokines involved in T and B lymphocyte activation, and a lower IFN signature.

The BALS and HSA clusters could be differentiated by the IFN signature, with the BALS cluster having the higher IFN signature. Interestingly, when focusing on the BALS cluster, the authors found that the IFN signature might be a prognostic marker to help identify patients at risk of new immunosuppressant for systemic manifestations or at risk of incident lymphoma. Thus, this study suggests that a high IFN signature could be used as a prognostic biomarker in SjD.

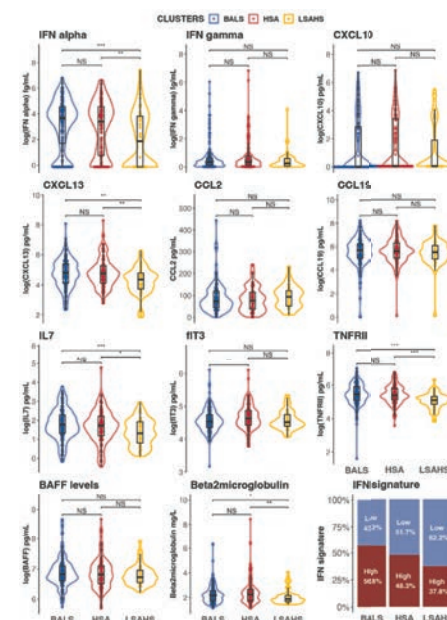


Figure 1. Comparison of cytokine levels and IFN signatures according to the three defined clusters: BALS, HSA, and LSAHS.

UV Light Exposure Linked to Migration of Inflammatory Dendritic Cells

Dendritic cells (DCs) play a central role not only in the immune response initiated in the skin after skin damage but also as key antigen-presenting cells in systemic lupus erythematosus. Several studies have demonstrated that microbial stimulation of type I interferon (IFN-I) in the skin and other organs can generate inflammatory DCs, and multiple investigators have reported that repetitive lower-dose ultraviolet light radiation (UVR) can cause an increase in the IFN-I response in a lupus-prone mouse strain compared with wild-type mice. In this issue, Sun et al (p. 867) describe a previously unknown relationship between skin UVR and the migration

of the inflammatory conventional DC subset (inf cDC2) population to draining lymph nodes (dLN). The new findings build upon previous work from the group, showing that cyclic GMP-AMP synthase is required for the initial six-hour IFN-I stimulation after UVR in the skin; however, after this, other sensors become activated.

In the current study, the investigators used a short-term model to evaluate the acute response of adaptive immune cells. They found that IFN-I activated inf cDC2 in the dLN of C57BL/6 mice after UVR. B6 mice had higher numbers of CD64+ myeloid cells and inf cDC2 in the dLN after UVR; IFN receptor knockout mice did not.

The researchers further investigated the hypothesis that IFN-I is integral to the pathophysiology of photosensitivity by studying transgenic mice lacking Trex1, a DNase III homolog. This highly abundant endoplasmic reticulum-tethered 3'-5' DNA exonuclease degrades excess or damaged DNA in the cytosol. In patients with lupus with Trex1 mutations, UVR causes enhanced photosensitivity in response to phototesting. The researchers found that *Trex1*-mutant mice exhibited an exaggerated IFN-I response in the skin and a higher proportion of inf cDC2 in the dLN compared with wild-type mice. The results suggest that the described pathway may be relevant to lupus.

CD8+ T Cell Subset Links Spontaneous Motility to Telomere Attrition

Studies have linked the chronic inflammation associated with rheumatic or other disorders to alterations of the telomere/telomerase system. In axial spondyloarthritis

p. 854

(axSpA), researchers have documented premature senescence of CD8+ and CD4+ T cells in patients younger than 35 who present with inappropriate telomere shortening, thymic output shrinkage, and altered telomerase activity.

Despite the growing body of evidence linking chronic inflammation with telomere shortening, the molecular mechanisms underlying the association remain unelucidated. One possible explanation for the association is the importance of the lamin

isoforms that bind to the linker of the nucleoskeleton-cytoskeleton complex. Researchers have found that the loss of these isoforms softens the cell nucleus, enhances constricted cell migration, and contributes to migration-induced DNA damage. In this issue, Paldino et al (p. 854) report that patients with SpA have an enriched, terminally differentiated CD8+ T cell subset with a senescent and cytotoxic/proinflammatory profile, as well as an intrinsic invasive potential. Although these cells spontaneously migrate regardless of specific cytokine gradients, they can also migrate efficiently in response to a chemotactic gradient.

Spontaneously migrating CD8+ T cells from all cohorts (radiographic axSpA,

psoriatic arthritis, and rheumatoid arthritis) exhibited a more pronounced DNA damage response activation and a higher number of telomeric damage foci per cell. Moreover, all patients (except healthy donors) had an increase in the subset of terminally differentiated effector memory T cells and a decrease in the central memory subset among the migrated CD8+ T cells. The researchers also found a significantly higher expression of the fractalkine receptor, CX3CR1, in spontaneously migrating versus nonmigrating CD8+ T cells. They conclude that this cell population may represent a key player in disease pathogenesis, as it couples intrinsic motion with a cytotoxic and proinflammatory profile.

Journal Club

A monthly feature designed to facilitate discussion on research methods in rheumatology.

Serum Type I IFN Score for Prediction of Clinically Meaningful Disease Progression in Limited Cutaneous SSc

Di Donato et al, *Arthritis Rheumatol.* 2025;77:929-941.

Patients with limited cutaneous systemic sclerosis (lcSSc), the most common subset of systemic sclerosis (SSc), can experience life-threatening complications, including lung fibrosis, pulmonary hypertension, and severe gastrointestinal tract disease. Outcomes are heterogeneous, and predictive markers are needed to identify those at greatest risk of major complications. Although autoantibody profiles are predictive of risk, these may be less applicable to lcSSc, in which high-risk patterns are much less frequent. The simple composite serum chemokine IFN score has been used in other autoimmune rheumatic diseases; we applied this to lcSSc and showed that it predicts increased risk for disease progression.

A novel aspect of our approach is that we used a new time-to-clinical-progression score, which was developed for an event-driven clinical trial of mycophenolate mofetil in SSc (MINIMISE). The MINIMISE instrument measures clinically important disease progression analogous to clinical worsening, and therefore, any intervention or predictor that differentiates MINIMISE outcome is self-evidently meaningful. The same chemokine serum IFN signature was well validated in previous studies in other autoimmune rheumatic diseases, and a threshold or high IFN score was previously derived for diffuse cutaneous SSc. Our findings show feasibility to identify patients with lcSSc at high risk of clinical

worsening who may benefit most from treatment approaches targeting the IFN pathway.

Questions

1. What is the likely effect of background treatment within an observational cohort on IFN signature, and how might this confound the results of this study?
2. How does the chemokine IFN score used in this study compare with other scores and with signatures based on peripheral blood gene expression rather than protein assay?
3. Does the IFN score categorization complement autoantibody-based subgroups in lcSSc?
4. How does the MINIMISE endpoint compare with and complement other initiatives to develop composite measures in SSc such as Sclero-ID, CRISS, and CRISTAL?
5. Is the IFN signature more predictive of outcomes in patients with features of overlap or mixed connective tissue disease where the IFN signature has previously been reported in other studies?

CD8+ T Cell Subset Links Spontaneous Motility to Telomere Attrition

Studies have linked the chronic inflammation associated with rheumatic or other disorders to alterations of the telomere/telomerase system. In axial spondyloarthritis

p. 854

(axSpA), researchers have documented premature senescence of CD8+ and CD4+ T cells in patients younger than 35 who present with inappropriate telomere shortening, thymic output shrinkage, and altered telomerase activity.

Despite the growing body of evidence linking chronic inflammation with telomere shortening, the molecular mechanisms underlying the association remain unelucidated. One possible explanation for the association is the importance of the lamin

isoforms that bind to the linker of the nucleoskeleton-cytoskeleton complex. Researchers have found that the loss of these isoforms softens the cell nucleus, enhances constricted cell migration, and contributes to migration-induced DNA damage. In this issue, Paldino et al (p. 854) report that patients with SpA have an enriched, terminally differentiated CD8+ T cell subset with a senescent and cytotoxic/proinflammatory profile, as well as an intrinsic invasive potential. Although these cells spontaneously migrate regardless of specific cytokine gradients, they can also migrate efficiently in response to a chemotactic gradient.

Spontaneously migrating CD8+ T cells from all cohorts (radiographic axSpA,

psoriatic arthritis, and rheumatoid arthritis) exhibited a more pronounced DNA damage response activation and a higher number of telomeric damage foci per cell. Moreover, all patients (except healthy donors) had an increase in the subset of terminally differentiated effector memory T cells and a decrease in the central memory subset among the migrated CD8+ T cells. The researchers also found a significantly higher expression of the fractalkine receptor, CX3CR1, in spontaneously migrating versus nonmigrating CD8+ T cells. They conclude that this cell population may represent a key player in disease pathogenesis, as it couples intrinsic motion with a cytotoxic and proinflammatory profile.

Journal Club

A monthly feature designed to facilitate discussion on research methods in rheumatology.

Serum Type I IFN Score for Prediction of Clinically Meaningful Disease Progression in Limited Cutaneous SSc

Di Donato et al, *Arthritis Rheumatol.* 2025;77:929-941.

Patients with limited cutaneous systemic sclerosis (lcSSc), the most common subset of systemic sclerosis (SSc), can experience life-threatening complications, including lung fibrosis, pulmonary hypertension, and severe gastrointestinal tract disease. Outcomes are heterogeneous, and predictive markers are needed to identify those at greatest risk of major complications. Although autoantibody profiles are predictive of risk, these may be less applicable to lcSSc, in which high-risk patterns are much less frequent. The simple composite serum chemokine IFN score has been used in other autoimmune rheumatic diseases; we applied this to lcSSc and showed that it predicts increased risk for disease progression.

A novel aspect of our approach is that we used a new time-to-clinical-progression score, which was developed for an event-driven clinical trial of mycophenolate mofetil in SSc (MINIMISE). The MINIMISE instrument measures clinically important disease progression analogous to clinical worsening, and therefore, any intervention or predictor that differentiates MINIMISE outcome is self-evidently meaningful. The same chemokine serum IFN signature was well validated in previous studies in other autoimmune rheumatic diseases, and a threshold or high IFN score was previously derived for diffuse cutaneous SSc. Our findings show feasibility to identify patients with lcSSc at high risk of clinical

worsening who may benefit most from treatment approaches targeting the IFN pathway.

Questions

1. What is the likely effect of background treatment within an observational cohort on IFN signature, and how might this confound the results of this study?
2. How does the chemokine IFN score used in this study compare with other scores and with signatures based on peripheral blood gene expression rather than protein assay?
3. Does the IFN score categorization complement autoantibody-based subgroups in lcSSc?
4. How does the MINIMISE endpoint compare with and complement other initiatives to develop composite measures in SSc such as Sclero-ID, CRISS, and CRISTAL?
5. Is the IFN signature more predictive of outcomes in patients with features of overlap or mixed connective tissue disease where the IFN signature has previously been reported in other studies?

NOTES FROM THE FIELD

The National Academies' 2024 Diagnostic Criteria for Long COVID: Concerns That Could Affect the Rheumatology Community

Leonard H. Calabrese,¹ Michael Putman,² Jeffrey A. Sparks,³ Zachary Wallace,⁴ Alfred H. J. Kim,⁵ Kevin L. Winthrop,⁶ and Cassandra Calabrese¹

Introduction

Shortly after the COVID-19 pandemic began, it became clear that some people with COVID-19 had prolonged or, in some cases, incomplete recovery. Patient-led groups took an early and important role in advocating for affected people, coining the term “long COVID.”¹ The term postacute sequelae of COVID-19 (PASC) is often used interchangeably with long COVID, with the latter enduring as the more commonly used diagnostic label in both scientific and lay literature. Over time long COVID and PASC have come to encompass a myriad of over 200 symptoms, the majority of which did not have clear pathologic correlates.² Similar postinfectious sequelae, including clinical syndromes resembling myalgic encephalomyelitis/chronic fatigue syndrome (ME/CFS) and fibromyalgia, have been previously described following numerous other infectious diseases but not to the scale of that seen with COVID-19.^{3,4}

As with any condition, affected patients share features. There is a female predominance reported in long COVID, and many fulfill diagnostic and/or classification criteria for ME/CFS and/or fibromyalgia. Symptoms of dysautonomia are also common.⁵ Observational studies have also identified a range of pathologically confirmed post-COVID complications affecting multiple organs, including the endocrine, cardiovascular, and neurologic systems. Incident autoimmune diseases after COVID-19 have been reported, with large observational studies describing a modest but statistically significant association.^{1,5} However, these studies may be biased by unmeasured confounding (eg, health care use, etc).

Establishing a widely accepted definition of long COVID to facilitate clinical care and research is an urgent priority. A definition would guide clinical diagnosis and facilitate research to define underlying pathophysiology and identify effective management

strategies. Collectively, these advances may improve the suffering that people with these conditions often describe. Early in the pandemic, several organizations proposed different case definitions (Table 1) for long COVID. These definitions varied with regard to the need for microbiologic documentation, the duration of symptoms required, and the necessity to rule out alternative diagnoses. The limitations of these definitions have been recently reviewed.⁶

The National Academies' definition of long COVID

Given the urgent clinical and research need for a rigorous definition for long COVID, the US Department of Health and Human Services asked the National Academy of Science Engineering and Medicine (the “National Academies”) to develop a definition. The expectation was that this definition would promote consistency in diagnosis, raise public awareness, help patients access care and benefits, and facilitate research. To define long COVID, the committee established by the National Academies engaged more than 1,300 participants, including key opinion leaders working in the field, systematically reviewed the relevant literature, and applied rigorous methods as well as the input of many key opinion leaders working in the field. The proposed definition was published in 2024⁷ and summarized in Table 1.

The signatories to this research letter have been actively engaged in various aspects of the response to the COVID-19 pandemic from a rheumatology perspective. We understand and appreciate the challenges that the National Academies faced in formulating a definition and the substantial effort contributed by those involved. By explicit design, the committee developed a case definition that sought to be accurate and precise, accessible

¹Leonard H. Calabrese, DO, Cassandra Calabrese, DO: Cleveland Clinic Lerner College of Medicine, Cleveland, Ohio; ²Michael Putman, MD, MSCI: Medical College of Wisconsin, Milwaukee; ³Jeffrey A. Sparks, MD, MSc, Brigham and Women's Hospital, Harvard University, Boston, Massachusetts; ⁴Zachary Wallace, MD, MSc: Massachusetts General Hospital, Harvard Medical School, Boston; ⁵Alfred H. J. Kim, MD, PhD: Washington University School of Medicine, St. Louis, Missouri; ⁶Kevin L. Winthrop, MD, MPH, Oregon Health and Science University, Portland.

Author disclosures are available at <https://onlinelibrary.wiley.com/doi/10.1002/art.43114>.

Address correspondence via email to Leonard H. Calabrese, DO, at calabrl@ccf.org.

Submitted for publication September 17, 2024; accepted in revised form January 7, 2025.

Table 1. Selected definitions of long COVID*

	US Centers for Disease Control and Prevention	World Health Organization	RECOVER	National Academies
High-level summary	“Signs, symptoms, and conditions that continue or develop after initial COVID-19 infection”	“The continuation or development of new symptoms 3 months after the initial SARS-CoV-2 infection, with these symptoms lasting for at least 2 months with no other explanation”	“A definition of postacute sequelae of COVID-19 (PASC) using self-reported symptoms”	“Continuous, relapsing and remitting, or progressive disease state that affects one or more organ systems”
Positive SARS-CoV-2 laboratory test required	No	No	Yes	No
Minimum time since COVID-19 onset	90 days	90 days	Assessed at 180 days, but may have had shorter symptom duration	90 days
Symptoms included	“People with long COVID can have a wide range of symptoms that can last weeks, months, or even years after infection”	“While common symptoms of long COVID can include fatigue, shortness of breath and cognitive dysfunction over 200 different symptoms have been reported that can have an impact on everyday functioning”	Smell and/or taste, postexertional malaise, chronic cough, brain fog, thirst, palpitations, chest pain, fatigue, sexual desire or capacity, dizziness, gastrointestinal, abnormal movements, and hair loss	Shortness of breath, cough, persistent fatigue, postexertional malaise, difficulty concentrating, memory changes, recurring headache, lightheadedness, fast heart rate, sleep disturbance, problems with taste or smell, bloating, constipation, and diarrhea
Systemic autoimmune rheumatic diseases included	None	None	None	Connective tissue diseases and autoimmune disorders, such as lupus, rheumatoid arthritis, and Sjögren disease
Other diseases included	None	None	None	Yes

* RECOVER, Researching COVID to Enhance Recovery.

and understandable, and, above all, acceptable to those who are suffering, especially those experiencing work disability and in need of support. Importantly, the authors also emphasized that a case definition that was highly sensitive would be limited by a high rate of false positives and that expert history-taking and clinical judgment would be required to assess a given patient's likelihood of whether they qualified to be diagnosed as having long COVID. We appreciate the merits of this stated attempt but must emphasize that clinical judgment is not static and will be influenced by critical appraisal of ongoing research and our current levels of understanding of the intersection of long COVID and its relationship to rheumatic and immunologic diseases, and thus, the implementation of this case definition will no doubt likely change over time. For the present, however, we have concerns regarding the clinical use of the National Academies' definition and how this definition may currently impact the field of rheumatic disease.

First concern: low specificity

The newly proposed case definition is, by the National Academies' stated design, highly sensitive while lacking specificity. As

stated by the committee, they attempted to be inclusive while avoiding wrongly including patients whose conditions are not related to prior SARS-CoV-2 infections. We worry that a balance was not struck. No specific symptoms are required to qualify, and nearly any symptom would be sufficient for diagnosis. Further, the condition being attributed to COVID-19 can occur at any time point (ie, days, months, or even years) after an infection, and neither diagnostic certainty of COVID-19 infection nor having had symptoms of COVID-19 are required. We are concerned that such broad inclusion criteria do not advance a clinician's ability to differentiate postinfectious syndromes from the background non-specific, intermittent somatic symptoms (ie pain, fatigue, sleep disturbances, and abdominal pain) of unclear etiology, which are frequently encountered in rheumatology practices and the general population.⁸

Second concern: inclusion of incident rheumatic disease

The National Academies' long COVID definition states that “patients can present with diagnosable conditions such as

fibromyalgia, connective tissue diseases,...and autoimmune disorders such as lupus, rheumatoid arthritis, and Sjögren disease.” We will not further discuss fibromyalgia, which appears to bear a complex relationship to long COVID and has been previously reviewed in the literature.⁹ Instead, we will focus on the decision to include autoimmune rheumatic disorders as features that support a diagnosis of long COVID.

In just a few years, we have advanced our understanding of the immunologic consequences of COVID-19 infection and hypothesized regarding their potential associations with long COVID risk.¹ These immunologic consequences include the presence of ongoing low-level inflammation, upregulation of an interferon response, aberrant neutrophil activity, and mounting autoreactivity.^{1,5,10,11} Recognizing these associations, we strongly believe that it is premature to conclude that any of these immune perturbations are causally related to any symptoms or end-organ complications attributed to long COVID, and the presence of these immunologic features are insufficient to establish a diagnosis of long COVID. It can be argued that among the strongest evidence for the induction of autoimmunity from COVID-19 is the development of an array of autoantibodies following infection, including some autoantibodies used in clinical practice (eg, antinuclear antibodies), but this observation is not unique to SARS-CoV-2 and has been described in the context of other infections.^{4,10} Further, the autoantibody response observed in some is often transient, and there are conflicting data about whether these autoantibodies correlate with long COVID symptoms or end-organ pathology.^{10,12}

We do not support the National Academies’ decision to label a new diagnosis of rheumatic disease in the post-COVID-19 period as long COVID. To support the inclusion of rheumatic and other autoimmune diseases in their definition, the National Academies relied on electronic medical record (EMR) database studies, which have important and often overlooked limitations when used in observational research. In addition to confounding and time-related biases common to observational studies, EMR-based studies may be affected by misclassification when exposure, covariates, and outcomes are defined by billing codes (eg, under- or overcoding). They may also come to biased conclusions when important potential confounders such as health care use are not considered. Many autoimmune diseases lack validated diagnostic coding algorithms; for others, proposed, or even validated, approaches to identifying cases often have high false positive rates.

Inconsistency of literature linking COVID-19 with incident rheumatic diseases

A comprehensive review of the growing number of epidemiologic studies examining the relationship of COVID-19 and autoimmune diseases is beyond the scope of this research letter, but at the minimum, these reports have been inconsistent. For example, among four of the largest epidemiologic studies

exploring the association of COVID-19 and lupus, one found a significantly increased risk,¹³ whereas another found no significantly increased risk¹⁴; the other two studies^{15,16} found COVID-19 to be potentially protective against the risk of lupus. Do we believe that COVID-19 confers protection against lupus? Certainly not. The conflicting results from these studies suggest that it is premature to include rheumatic diseases as a criterion for the diagnosis of long COVID. Although previous literature suggest that other types of infections may trigger rheumatic diseases (eg, hepatitis B-associated polyarteritis nodosa and hepatitis C-associated cryoglobulinemic vasculitis), the attribution of an infection to incident rheumatic disease in an individual patient is often circumspect at best and would not appreciably change the management approach in the vast majority.

Conclusions

We strongly endorse recommendations from the National Academies that further work is needed; more detailed epidemiologic investigations of long COVID risk using orthogonal methodologies, clinical trials of immune targeting therapies for long COVID, and basic and translational studies such as the recent use of animal models using passive transfer of IgG from people with long COVID to study autoimmunity.¹ It is quite possible that long COVID is a heterogeneous group of disorders with many clinical endotypes involving numerous pathogenic mechanisms and disease trajectories such that a single disease definition may not suffice. Although we have raised important concerns, we admit that we do not have the answers to these important questions. From a clinical perspective of the rheumatology practitioner and the individual patient, the current case definition clearly provides much leeway in diagnosing long COVID based on our history and clinical judgment when needed for patient care. Thus, there is a need to disseminate this declarative and procedural knowledge throughout the profession. From an educational perspective, there is no other field moving as rapidly as that of COVID-19 and its postinfectious sequelae, and thus, this topic must have an ongoing place in our educational agenda. Finally, as rheumatologists, we care for people living with many diseases that share features with long COVID, and our research into these disorders may inform our understanding of long COVID. As a profession, we are therefore well-positioned to engage in the ongoing discussions regarding the potential associations among SARS-CoV-2 infection, long COVID, and rheumatic disease.

AUTHOR CONTRIBUTIONS

All authors were involved in drafting the article or revising it critically for important intellectual content, and all authors approved the final version to be published.

REFERENCES

1. Al-Aly Z, Davis H, McCorkell L, et al. Long COVID science, research and policy. *Nat Med* 2024;30(8):2148–2164.
2. Al-Aly Z, Topol E. Solving the puzzle of long Covid. *Science* 2024; 383(6685):830–832.
3. Thaweethai T, Jolley SE, Karlson EW, et al; RECOVER Consortium. Development of a definition of postacute sequelae of SARS-CoV-2 infection. *JAMA* 2023;329(22):1934–1946.
4. Choutka J, Jansari V, Hornig M, et al. Unexplained post-acute infection syndromes. *Nat Med* 2022;28(5):911–923.
5. Davis HE, McCorkell L, Vogel JM, et al. Long COVID: major findings, mechanisms and recommendations. *Nat Rev Microbiol* 2023;21(3): 133–146.
6. Haslam A, Olivier T, Prasad V. The definition of long COVID used in interventional studies. *Eur J Clin Invest* 2023;53(8):e13989.
7. National Academies of Sciences, Engineering, and Medicine. A Long COVID Definition: A Chronic, Systemic Disease State with Profound Consequences. The National Academies Press; 2024:186.
8. Barsky AJ, Silbersweig DA. The amplification of symptoms in the medically ill. *J Gen Intern Med* 2023;38(1):195–202.
9. Clauw DJ, Calabrese L. Rheumatology and long COVID: lessons from the study of fibromyalgia. *Ann Rheum Dis* 2024;83(2):136–138.
10. Altmann DM, Whettlock EM, Liu S, et al. The immunology of long COVID. *Nat Rev Immunol* 2023;23(10):618–634.
11. Woodruff MC, Ramonell RP, Lee FE, et al. Broadly-targeted autoreactivity is common in severe SARS-CoV-2 Infection. *medRxiv Preprint* posted online October 23, 2020. doi:[10.1101/2020.10.21.20216192](https://doi.org/10.1101/2020.10.21.20216192)
12. Klein J, Wood J, Jaycox JR, et al. Distinguishing features of long COVID identified through immune profiling. *Nature* 2023;623(7985): 139–148.
13. Chang R, Yen-Ting Chen T, Wang SI, et al. Risk of autoimmune diseases in patients with COVID-19: a retrospective cohort study. *EClinicalMedicine* 2023;56:101783.
14. Tesch F, Ehm F, Vivirito A, et al. Incident autoimmune diseases in association with SARS-CoV-2 infection: a matched cohort study. *Clin Rheumatol* 2023;42(10):2905–2914.
15. Hileman CO, Malakooti SK, Patil N, et al. New-onset autoimmune disease after COVID-19. *Front Immunol* 2024;15:1337406.
16. Lim SH, Ju HJ, Han JH, et al. Autoimmune and autoinflammatory connective tissue disorders following COVID-19. *JAMA Netw Open* 2023; 6(10):e2336120.

EDITORIAL

Air Pollution's Hidden Toll: Risks for Rheumatoid Arthritis and Rheumatoid Arthritis–Associated Lung Disease

Sofia Ajeganova¹  and Jeremy Sokolove² 

Air pollution presents an important factor for the global burden of disease. Poor air quality has become a growing issue due to urbanization and climate changes. Ambient (outdoor) air pollution in both cities and rural areas was estimated to cause 4.2 million premature deaths worldwide per year in 2019, attributed to cardiovascular and respiratory disease and cancers. Because the incidence of autoimmune inflammatory diseases rapidly rose after industrialization and the widely accepted hypothesis that the overt clinical presentation of such diseases results from the interaction between genetic predisposition and environmental factors, the role of ambient inhaled air pollutants on the risk of immune-mediated diseases has received more attention. Indeed, it has been found that chronic exposure to levels of air pollutants above the threshold for human protection is associated with a 10% higher risk of developing various immune-mediated diseases.¹ Understanding the factors behind such an increased risk and etiopathogenesis is crucial to find new targets of therapy and appropriate prevention strategies.

Rheumatoid arthritis (RA) is a complex polygenic inflammatory disease that develops through immune activation in genetically susceptible individuals following environmental challenges.² Epidemiologic, clinical, and molecular studies suggest a potential role of the lung as the important site for initiation of RA-related autoimmunity.³ Smoking is a major predisposing factor, and there is a dose-dependent interaction between smoking and RA-risk genes in the risk of developing seropositive RA.⁴ Local immunity toward citrullinated proteins and accompanying inflammation might be present in the lungs early during RA disease development.⁵ Thus, it is plausible to suggest that environmental factors that trigger RA development could also contribute to increased RA-related interstitial lung disease (RA-ILD). Many patients with RA are nonsmokers. Besides cigarette smoke, other airborne particles, such as inhaled air pollutants and occupational inhalable agents (silica, textile dust, quartz dust, herbicides), may trigger pulmonary oxidative stress, inducing autoimmune responses

and systemic inflammation. Early epidemiologic studies have implicated associations between RA and long-term exposure to various ambient air pollutants, especially exposure to fine particulate matter <2.5 μm in diameter ($\text{PM}_{2.5}$).^{6–8} Of different air pollutants measures, exposure to $\text{PM}_{2.5}$ has been most closely linked to anti-citrullinated protein antibody (ACPA) titers.⁹ ACPA-negative, or seronegative RA, constituting about one-third of all patients with RA, may have genetic and environmental pathogenesis different to seropositive RA, but it has been insufficiently studied. Evidence for the impact of air pollutants on the risk of RA is inconsistent, probably due to differences in exposure assessment, composition of air pollutants, control for covariates, and different age of the studied populations, and little is known about association between air pollutants and development of RA-ILD.¹⁰

$\text{PM}_{2.5}$ air pollution originates from natural sources (such as forest fire smokes) and anthropogenic sources (such as fossil fuel, vehicle emissions, cigarette smoking, and industrial sources). Although public health gains have been achieved through reductions in nonsmoke $\text{PM}_{2.5}$, wildfires have burned increasing acreages since the 1980s. The cumulative impact of increased burns and fires, a growing source of air pollution including $\text{PM}_{2.5}$, raises concerns and questions about the long-term health impact. Are small-in-size $\text{PM}_{2.5}$ particles more pathogenic and toxic than larger PM_{10} particles or sulfur dioxide (SO_2), carbon monoxide (CO), nitrogen oxides (NOx), and ozone (O_3)? Does fire smoke-related $\text{PM}_{2.5}$ have similar toxicity as total $\text{PM}_{2.5}$? Is acute or chronic exposure to air pollutants necessary to affect risk of the disease? Does duration of exposure to air pollutants determine the risk of seropositive and/or seronegative RA?

The complex interactions between environmental and individual exposures make it challenging to attribute outcome to a single environmental exposure, especially when there is a lag between the exposure and overt clinical disease. To estimate the effect of environmental exposures, population-level environmental exposures, together with individual risk factors, are necessary to

¹Sofia Ajeganova, MD, PhD: Karolinska Institute, Stockholm, Sweden;
²Jeremy Sokolove, MD: Stanford University, Stanford, California.

Author disclosures are available at <https://onlinelibrary.wiley.com/doi/10.1002/art.43115>.

Address correspondence via email to Sofia Ajeganova, MD, PhD, at sofia.ajeganova@ki.se.

Submitted for publication November 12, 2024; accepted in revised form December 18, 2024.

include in the study. In this issue of *Arthritis & Rheumatology*, Kronzer et al¹¹ report the analysis of exposure to fire smoke–related PM_{2.5} and other air pollutants on the risk of incident RA and RA-ILD after RA diagnosis. Researchers effectively used a case–control study design based on a huge administrative and electronic dataset of the Department of Veterans Affairs (VA) with over 70,000 veterans. A validated algorithm to define RA and a stringent set of criteria to define RA-ILD were applied. Of all, 9,701 patients with incident RA with at least five years of preceding observation (mean age 65 years, 86% male, 56% current smokers, 63% seropositive), of them 531 patients with RA-ILD, were identified in 2014 to 2018 and included for the analysis, along with 68,851 controls matched on age, sex, and VA enrollment year. Pollution level data were extracted from the nationwide ground pollutant monitoring data and averaged over all available time points at all monitors within 50 km of the zip code area. Primary exposure was mean daily smoke PM_{2.5}, which consisted of fire-related PM_{2.5}, nonfire PM_{2.5}, and overall total PM_{2.5} over the United States at a 15 × 15-km resolution, integrated with at least five years preceding VA address data. Averaged secondary pollutants PM₁₀, SO₂, CO, NO_x, and O₃ were measured based on available monitoring data within 50 km of the zip code area. Additional data included duration of fire smoke pollutant exposure before index date, ethnicity, body mass index, and smoking status at the index date.

This huge case–control study using national VA data and nationwide pollutant monitoring suggests association between higher exposure to fire smoke–related PM_{2.5} of one to five years before RA diagnosis and development of RA, and exposure to fossil fuel–related NO_x is the most associated with overall RA risk or seronegative RA. Analysis restricted to never-smokers showed no meaningful differences in point estimates. There was no evidence of interactions between fire smoke PM_{2.5} and smoking status, age, sex, and race and ethnicity on risk of RA in this study. The further novelty is the finding of association between higher exposure to fire smoke–related PM₂ and risk of RA-ILD. Matched case–control design, which was used in this analysis, can be as credible as randomized studies to study rare outcomes.¹²

The main analysis indicated that more recent exposure to fire smoke–related PM_{2.5} within one to three years and three to five years before RA diagnosis was associated with RA risk consistently in the quartiles of the exposure (adjusted odds ratio [aOR] 1.12, 95% confidence interval [CI] 1.03–1.23, and aOR 1.13, 95% CI 1.02–1.26, per 1 µg/m³). Given the design, it is still likely that the results reflect temporal associations between ambient PM_{2.5} and RA, even though for the averaged long-term exposure of longer than five years, the association was not found here. Thus, the current study raises questions about the window for which the effect of air pollution is most evident, and this merits further investigation. Most biologic associations would present at a concentration–response function and stronger effects for long-term exposures. However, stronger associations at lower rather than higher PM_{2.5} exposures have been previously reported.¹³

Effects could also be nonlinear at different exposure times and across different concentrations of air pollutants. Further, composition of PM_{2.5} can vary across regions and seasons, and the different chemical species and mixtures that comprise PM_{2.5} can have different impacts on health. Moreover, PM_{2.5} at low and high concentrations might represent particles with different toxicity in patients with a high genetic risk or without such a risk. One aspect in which future studies should focus is the identification of specific PM_{2.5} components that may be driving the association with RA.

The novel finding of approximately two-fold higher risk of RA-ILD (aOR 1.98, 95% CI 1.08–3.62, per 1 µg/m³) related to PM_{2.5} is notable, especially considering that prevalence of RA-ILD was likely underreported in administrative dataset (no systematic screening). The pathogenic effects of air pollutants, especially prolonged exposure to high levels of PM_{2.5} on lungs and respiratory diseases, including ILD, idiopathic pulmonary fibrosis, and exacerbation of RA-ILD, have been previously reported. The current study by Kronzer et al¹¹ shows that exposure to fire smoke PM_{2.5} may be associated with RA-ILD development. Interestingly, to note here, the higher mean age, the more male patients and smokers there were among the studied patients than in commonly reported cohorts with RA (ie, population with known risk factors for RA-ILD). Possible mechanisms by which RA-ILD occurs and progresses merit further investigations.

When considering the evidence presented in the article together, the association between prolonged exposure to air pollutants and risk of RA overall (for exposure to fire smoke PM_{2.5}, PM₁₀, or fossil fuel–related NO_x), or seronegative RA (for exposure to O₃ or PM₁₀), was small, and estimates for several secondary air pollutants (SO₂, CO) were inconsistent across the concentrations and exposure terms and were even seemingly “protective.” The effect sizes may have been attenuated because of the high degree of overlap in the mixture of air pollutants usually correlated in space because they have common sources.

The study demonstrates the utility of geocoding of exposure to air pollutants based on postal codes. However, ambient measures may not accurately reflect personal exposures varying depending on age, season, occupation, socioeconomic status, and habits. Null associations with some air pollutants may be related to possible misclassification of absolute pollutant exposures because of sparse monitoring in rural areas. However, because ambient air pollution policies are proposed at the group level rather than at the individual level, the results of environmental research may still be used to inform community-level prevention and intervention efforts, even if they do not address the individual exposure–outcome response. Exposure to the mixture of multiple air pollutants could also obscure estimated effects. The authors acknowledge the potential for residual confounding and the possibility of unmeasured prior exposures in individual service careers because many military veterans have been exposed to open burn pits, which are known to contain a variety of pollutants, and have often been exposed to other negative environmental phenomena

including gasoline exhaust, dust, ambient air pollution, and fumes from equipment.

This study adds to the existing literature and highlights the health risk posed by air pollutants for RA and RA-ILD. There is still much to be learned about this complex (gene) environmental exposure–effect relationship in the pathogenesis of autoimmune diseases, the temporal biologic effect of exposure to air pollutants, and the long-term effects of exposure to multiple air pollutants. Programs for controlling and reduction of air pollutants, along with screening adapted for at-risk population can potentially result in positive effects on health outcomes.

AUTHOR CONTRIBUTIONS

Drs Ajeganova and Sokolove drafted the article, revised it critically for important intellectual content, and approved the final version to be published.

REFERENCES

1. Adami G, Pontalti M, Cattani G, et al. Association between long-term exposure to air pollution and immune-mediated diseases: a population-based cohort study. *RMD Open* 2022;8(1):e002055.
2. Klareskog L, Ronnelid J, Saevarsdottir S, et al. The importance of differences; on environment and its interactions with genes and immunity in the causation of rheumatoid arthritis. *J Intern Med* 2020; 287(5):514–533.
3. Joshua V, Chatzidionisyou K, Catrina AI. Role of the lung in individuals at risk of rheumatoid arthritis. *Best Pract Res Clin Rheumatol* 2017; 31(1):31–41.
4. Kallberg H, Ding B, Padyukov L, et al. Smoking is a major preventable risk factor for rheumatoid arthritis: estimations of risks after various exposures to cigarette smoke. *Ann Rheum Dis* 2011;70(3):508–511.
5. Catrina AI, Ytterberg AJ, Reynisdottir G, et al. Lungs, joints and immunity against citrullinated proteins in rheumatoid arthritis. *Nat Rev Rheumatol* 2014;10(11):645–653.
6. Chang KH, Hsu CC, Muo CH, et al. Air pollution exposure increases the risk of rheumatoid arthritis: a longitudinal and nationwide study. *Environ Int* 2016;94:495–499.
7. Ho WC, Chou LW, Wang RY, et al. Association between exposure to ambient air pollution and the risk of rheumatoid arthritis in Taiwan: a population-based retrospective cohort study. *Int J Environ Res Public Health* 2022;19(12):7006.
8. Zhang J, Fang XY, Wu J, et al. Association of combined exposure to ambient air pollutants, genetic risk, and incident rheumatoid arthritis: a prospective cohort study in the UK Biobank. *Environ Health Perspect* 2023;131(3):37008.
9. Alex AM, Kunkel G, Sayles H, et al. Exposure to ambient air pollution and autoantibody status in rheumatoid arthritis. *Clin Rheumatol* 2020;39(3):761–768.
10. Zhao N, Al-Aly Z, Zheng B, et al. Fine particulate matter components and interstitial lung disease in rheumatoid arthritis. *Eur Respir J* 2022;60(1):2102149.
11. Kronzer VL, Yang Y, Roul P, et al. Associations of fire smoke and other pollutants with incident rheumatoid arthritis and rheumatoid arthritis-associated interstitial lung disease. *Arthritis Rheumatol* 2025;77(7): 808–816.
12. Vandembroucke JP. When are observational studies as credible as randomised trials? *Lancet* 2004;363(9422):1728–1731.
13. Stafoggia M, Oftedal B, Chen J, et al. Long-term exposure to low ambient air pollution concentrations and mortality among 28 million people: results from seven large European cohorts within the ELAPSE project. *Lancet Planet Health* 2022;6(1):e9–e18.

REVIEW

Immune Aging in Rheumatoid Arthritis

Cornelia M. Weyand  and Jörg J. Goronzy

Rheumatoid arthritis (RA) is a life-long autoimmune disease caused by the confluence of genetic and environmental variables that lead to loss of self-tolerance and persistent joint inflammation. RA occurs at the highest incidence in individuals >65 years old, implicating the aging process in disease susceptibility. Transformative approaches in molecular immunology and in functional genomics have paved the way for pathway paradigms underlying the replacement of immune homeostasis with autodestructive immunity in affected patients, including the process of immune aging. Patients with RA have a signature of premature immune aging, best understood for CD4⁺ T cells, which function as pathogenic effectors in this HLA class II-associated disease. Premature immune aging is present in healthy HLA-DRB1*04⁺ individuals, placing accelerated immune aging before joint inflammation. Aging-related molecular abnormalities directly implicated in turning RA CD4⁺ T cells into proinflammatory effector cells are linked to malfunction of subcellular organelles, such as mitochondria, lysosomes, lipid droplets, and the endoplasmic reticulum. Resulting changes in T cell behavior include cellular hypermobility, tissue invasiveness, unopposed mammalian target of rapamycin complex (mTORC)1 activation, excessive release of tumor necrosis factor, lysosomal failure, clonal expansion, and immunogenic cell death. Aged and metabolically reprogrammed T cells in patients with RA are accompanied by age-associated B cells, which specialize in autoantibody production. Clonal hematopoiesis drives myeloid cell aging by producing aged monocytes and hypermetabolic macrophages, which sustain the process of inflammaging. Here, we synthesize insights into the relationship of RA risk and immune aging and discuss mechanisms through which immune aging can cause autoimmunity.

Introduction

Over the last century, we have been gifted an additional 30 years of life, and for those born today, 100-year lives will be common, creating the challenge to build longevity-ready communities and align health span to life span. Researchers in the biologic and social sciences have mobilized to realize the potential of living long and living well, and much progress has been made in understanding the biology of aging. Biologic aging is the major cause of chronic disease and disability and refers to the gradual decline across numerous biologic systems that occurs with advancing chronological age. Among these systems, the immune system has taken center stage given its pivotal role in protecting the host against infection and malignancies and securing tissue homeostasis and repair. Diseases caused by failing immune defense and poor tissue regeneration are, by far, the leading causes of morbidity and mortality in developed countries.

In the traditional view, autoimmunity is an aberration of protective immunity, initiated and sustained by the erroneous recognition of self-antigen, and is therefore thought to be most prevalent in those with a strong and highly efficient immune system. With advances in the collection of society-spanning data, it is now clear that the vast majority of individuals diagnosed with autoimmune disease are in the second half of life,¹ when the immune system is compromised because of the process of immune aging.^{2–4} In a recent population-based cohort study of 22 million individuals in the United Kingdom, the incidence and prevalence of 19 of the most common autoimmune diseases were evaluated, including rheumatoid arthritis (RA).¹ Only a few autoimmune diseases were commonly diagnosed before the age of five years (Addison disease, celiac disease, type 1 diabetes, psoriasis, vitiligo), but for most autoimmune diseases, incidence increased with age, particularly for autoimmune thyroid disease, pernicious anemia, and RA. Figure 1 shows the age-dependent incidence of RA compared to polymyalgia rheumatica (PMR) and

Supported by the NIH (grants R01-AR-042527, R01-AI-108906, R01-HL-142068, U01-AI-179609, and R01-HL-117913 to Dr Weyand and grants R01-AI-108891, R01-AG-045779, U19-AI-057266, and R01-AI-129191 to Dr Goronzy).

Cornelia M. Weyand, MD, PhD, Jörg J. Goronzy, MD, PhD: Mayo Clinic Alix School of Medicine, Mayo Clinic College of Medicine and Science, Rochester, Minnesota, and Stanford University School of Medicine, Stanford, California.

Author disclosures and graphical abstract are available at <https://onlinelibrary.wiley.com/doi/10.1002/art.43105>.

Address correspondence via email to Cornelia M. Weyand, MD, PhD, at cweyand@stanford.edu.

Submitted for publication August 7, 2024; accepted in revised form December 18, 2024.

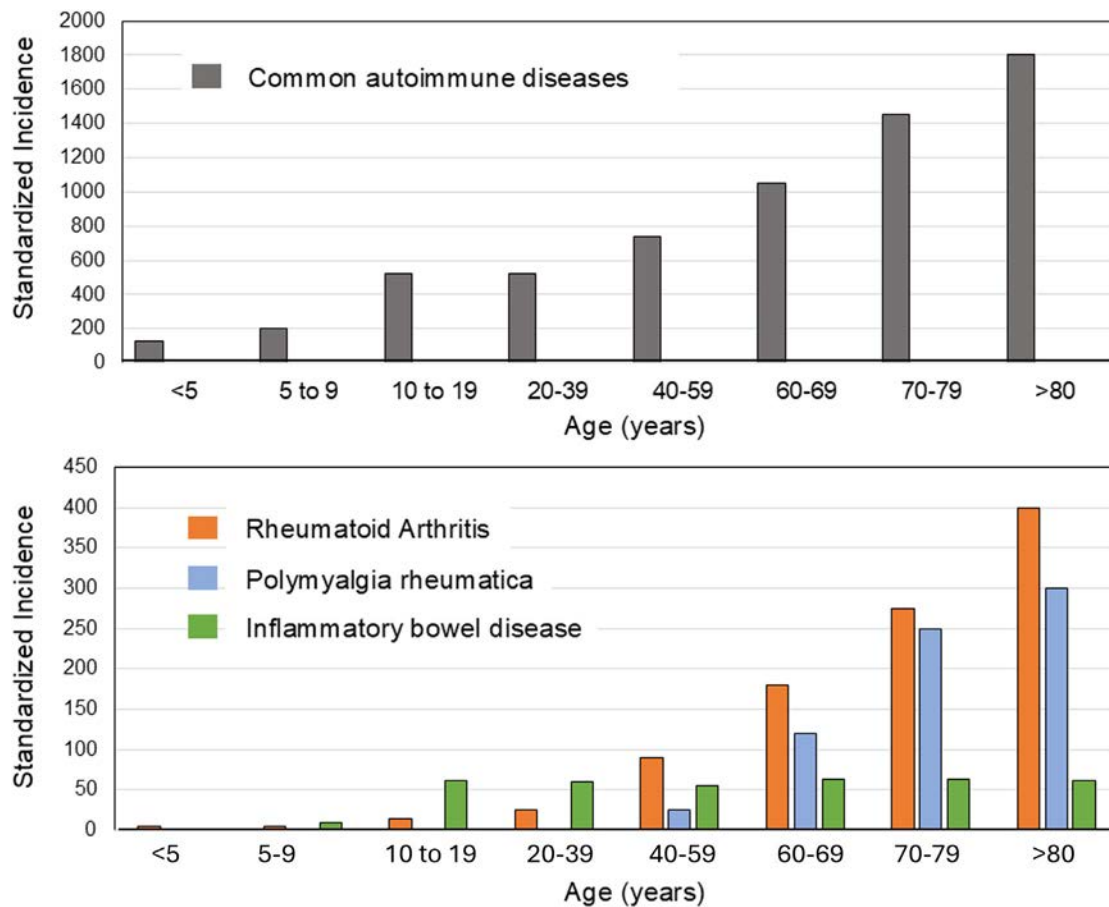


Figure 1. Aging as a risk factor for rheumatoid arthritis. Data are modified from the study by Conrad et al.¹ Age- and sex-standardized incidence rates were calculated for eight age categories. “Common autoimmune diseases” refers to the primary incidence of the 19 autoimmune disorders investigated in this study (top). Incidence rates for rheumatoid arthritis are compared to age-dependent incidence rates for polymyalgia rheumatica and inflammatory bowel disease (bottom).

inflammatory bowel disease. PMR is a classic age-associated disease, with essentially no cases among individuals <50 years of age. The median age of RA diagnosis among the 22 million individuals was at 65 years, with steeply rising incidence rates among those in the seventh and eighth decades of life. Thus, RA occurs in a host with an aged immune system. These epidemiologic data stand in stark contrast to the concept that the immune systems of patients with RA are particularly proficient, able to correctly assign innate and adaptive immune cells toward the recognition of foreign and self-antigens. To the opposite, these epidemiologic data provide strong support that immune aging is a risk factor for autoimmunity.^{5,6}

In this review, we will highlight the substantial advances made in conceptualizing the immunopathology of RA in the context of aging-related immune failure and the prematurity of immune aging in patients whose biologic aging precedes chronological aging. Indeed, RA emerges as an ideal model system to investigate the relationship between immune aging and loss of self-tolerance and to delineate the implications for the fundamental understanding of how the immune system

deviates from protection to injury across the spectrum of health and disease.

Cellular senescence

A central feature of the aging process is the induction of cellular senescence, a stable and terminal state of growth arrest, in which cells can no longer proliferate but persist and regulate neighboring cells through the secretion of an array of growth factors and cytokines. Senescent T cells are typically resistant to apoptotic cell death by up-regulating cell survival pathways, such as the Bcl-2 family of antiapoptotic proteins.⁷⁻⁹ Over the last decade, aging research has morphed into senescence research, and the term “senescence” is broadly used to describe aged cells. Accordingly, the process of immune aging is sometimes designated as immunosenescence. We will outline in this article why the term “immunosenescence” is inaccurate and arguably confusing. Most importantly, immune cells remain highly sensitive to apoptosis, even after extensive proliferative stress. Apoptosis is, by far, the most important mechanism to secure immune cell

contraction after antigen-driven proliferation and under homeostatic conditions.^{10–12} Thus, lymphocytes and macrophages (Mφs) are subject to aging-induced changes but do not undergo irreversible cell cycle block and therefore are not truly senescent.

Originally identified as a mechanism limiting the number of population doublings in cultured fibroblasts, cellular senescence has been linked to telomere attrition and to DNA damage-signaled cell cycle arrest. It is now recognized as a central process contributing to tissue regeneration and as a cellular defense against hyperproliferation, thus critically impacting embryogenesis, wound healing, and protection against cancer.¹³ Senescent cells are characteristically arrested in the G1 phase of the cell cycle. Up-regulation of the cyclin-dependent kinase (CDK) inhibitors p21 and p16 leads to inhibition of CDK4 and CDK6, repression of E2F transcription factors, and ultimately repression of their target genes. Acquisition of the senescent state is associated with morphologic changes (increased size and volume, irregular nuclear shape) and senescence-associated heterochromatin foci. Most importantly, senescent cells acquire a hypersecretory state known as the senescence-associated secretory phenotype (SASP), releasing an array of proinflammatory cytokines, growth factors, angiogenesis factors, and proteases that can disrupt microenvironments and compromise tissue structure and function. Indeed, senescent cells may become a nidus for sterile tissue inflammation, identifying them as “cells of interest” in chronic destructive tissue inflammation.^{14,15}

Expectedly, DNA damage-induced signaling has a major impact on the structure and function of cellular organelles. Elevated activity of the senescence-associated β -galactosidase is a classic marker of senescence and marks the heightened stimulation of the lysosomal pathway. A shift in mitochondrial function (mito-senescence) leads to up-regulation of the Bcl-2 family proteins (BAX, BAK), rendering senescent T cells resistant to apoptosis. Indeed, genetic loss of mitochondrial transcription factor A (TFAM), the main transcription factor of the mitochondrial genome, produces transgenic mice with a multitude of age-associated morbidities.¹⁶ The hypersecretory state of senescent cells must impose pressure on the endoplasmic reticulum controlling the folding and packing of secreted proteins, but precise studies are needed to understand the impact of endoplasmic reticulum (ER) senescence.

Senescent cells have recently drawn attention as potential therapeutic targets. In transgenic mice, purging of p16-expressing senescent cells can increase the mean life span and health span. These data have spurred the development of senolytic agents, selected to eliminate senescent cells in vivo. Clinical trials are underway to evaluate whether senolytic drugs can slow the aging process and associated morbidities, such as atherosclerosis, neurodegenerative disease, osteoporosis, chronic kidney disease, etc.¹⁷ Recently published results from a clinical trial testing senolytics in aging-associated osteopenia have been disappointing.¹⁸ Another class of SASP-targeting drugs are the senomorphics, designed to

modify SASP factors in vivo. In contrast to senolytics, senomorphics do not kill senescent cells, but rather they target pathways directly relevant for the induction, production, and secretion of SASP factors, for example, the transcription factors STAT3, NF- κ B, CCAAT/enhancer binding protein, and the p38 MAPK, phosphatidylinositol 3-kinase/Akt, mammalian target of rapamycin (mTORC) 1, and JAK/STAT signaling pathways. Therapeutics neutralizing SASP factors are also recognized as classic senomorphics. Rheumatologists are well familiar with senomorphics, having used anticytokine antibodies (anti-tumor necrosis factor [anti-TNF], anti-interleukin-6 [anti-IL-6], etc) for decades.

Therapeutic targeting of senescent cells and SASP factors raises the important question of whether they are exclusively detrimental.¹⁹ Given the critical role of cellular senescence in tissue remodeling and repair, persistent elimination may be to the disadvantage of the host. Although progress has been made in measuring SASP product abundance at defined time points, we have insufficient data to discriminate between beneficial and detrimental effects of cytokines and growth factors, challenging the use of SASP factors as biomarkers of aging and aging-related inflammation and the therapeutic goal of depleting senescent cells.

“Senescence” and “SASP” have become widely used terms to identify aged and stressed cells and their secretome. These terms may be valuable to identify stromal cells that have accumulated a high burden of DNA damage and have entered terminal growth arrest, but they are imprecise terms to describe the state of T cells and B cells in older individuals and in patients with chronic inflammatory disease.²⁰ The function of T cells and B cells in the immune system is inseparable from massive clonal expansion and a complex program of cellular differentiation. Recent data have demonstrated that T cells are essentially immortal, capable of repairing proliferation-imposed damage and undergoing self-renewal like stem cells.²¹ The secretome of highly differentiated T cells is rich in cytokines, which are needed to mount a successful immune response, but does not signal senescence. Apoptotic cell death curtails the size of the T cell compartment after antigen-induced expansion, eliminating T cells in irreversible proliferative arrest.^{10,22,23} Therefore, we will not apply the term “immunosenescence” in this review and instead will use the more precise term “immune aging.”

T cell aging in RA

Aged CD4⁺ T cells were first isolated from the rheumatoid joint²⁴ in 1996 and were subsequently confirmed in a number of studies.^{24–26} End-differentiated CD4⁺CD28[−] T cells were highly enriched in synovial tissue and were distinctly autoreactive in humans and mice.^{24,27} In patients with multiple sclerosis, CD4⁺CD28[−] T cells are highly responsive to disease-inducing autoantigens.²⁸ Molecular phenotyping focused attention on the telomeres of these unusual CD4⁺ T cells, showing premature

telomeric erosion in RA T cells with a 25-year left shift.^{29,30} The telomeric defect was present among naive CD4⁺ T cells of patients with RA, compatible with the defect being acquired before antigen-induced clonal expansion. In healthy individuals, premature telomeric shortening occurred in those who had inherited the RA-associated HLA-DRB1*04 haplotype, eliminating RA and RA synovitis as the driving factor.³⁰

The length of telomeric sequences is a well-recognized hallmark of cellular aging and has allowed definition of cell types affected by age-inappropriate aging. In patients with RA and in healthy HLA-DR4⁺ individuals, not only CD4⁺ T cells but also neutrophils have premature telomeric shortening.³⁰ Sharing of accelerated telomeric erosion in myeloid and lymphoid cell populations points toward the hematopoietic stem cell (HSC) as the target of the yet unidentified inducer of premature aging.^{31,32} Multiple mechanisms function as drivers of stem cell exhaustion during aging, including excessive apoptosis, premature differentiation, cytostatic DNA damage, growing mutational burden, and DNA damage-driven disruptions in intercellular communication compromising stem cell niches.^{33,34} HSC aging is characterized by the expansion of numbers, the decline in pluripotency, and the skewing toward the myeloid lineage.³⁵ Defective proliferative capacity and accelerated telomere shortening in circulating HSCs of patients with RA has been reported.³¹ It has been proposed that the reduced HSC pool is a major driver of premature T cell aging in RA.³⁶ In that model, reduced HSC proliferation leads to reduced T cell precursors. To maintain peripheral T cell numbers, adult individuals increase proliferation of postthymic T cells (homeostatic proliferation) and thus impose proliferative pressure. Increased proliferative pressure inevitably induces premature T cell aging. Premature senescence in HSCs of patients with RA has also profound clinical implications, predicting excess toxicity for treatment approaches that rely on depletion of HSCs or their progeny.³⁷

Most information available about the mechanisms and the relevance of T cell aging in RA stems from the study of helper and effector CD4⁺ T cells. It is highly likely that T cell aging affects the functional competence of other T cell populations, such as Treg cells. A clearly age-related mechanism of Treg cell failure has been described for another autoimmune disease.^{38,39} In large vessel vasculitis and in older healthy individuals, CD8⁺ Treg cells lose the ability to secrete immunoinhibitory exosomes into the extracellular space, leaving CD4⁺ T cells unsuppressed. Understanding the relevance of this mechanism in RA requires further examination.

DNA damage in RA T cells. Cellular aging is tightly integrated with DNA damage. Maintaining tissue homeostasis and responding to environmental cues imposes replication stress on all tissues but specifically on the adaptive immune system, which needs to undergo massive expansion to protect the host against pathogens and tumors. Cellular replication is inevitably linked to

DNA breaks and the accumulation of mutations. For highly proliferative cells to maintain genome integrity, they need a superbly functioning DNA repair machinery and access to energy sustaining the repair activity. Quiescent T cells can survive by using fast, low-fidelity nonhomologous end-joining, but proliferating T cells rely on the more accurate homologous recombination (HR) to maintain genome integrity.⁴⁰ Irreparable DNA damage of the nuclear genome or of telomeric sequences is a classical inducer of senescence, but like other lymphoid cells, stressed T cells are driven into apoptosis. Equipped with a sophisticated machinery to sense cellular stress and DNA damage, lymphoid and myeloid cells prefer apoptosis as the mechanism culling out poorly functional cells.⁴¹ T cells remain sensitive to DNA damage-induced apoptosis but steadily accumulate DNA lesions as they undergo cycles of clonal expansion and contraction.

RA T cells are deficient in the DNA repair enzyme ATM,⁴² with DNA damage load high in untreated patients with newly diagnosed RA (Figure 2). Transcriptome analysis has yielded evidence for transcriptional repression of the genes encoding for DNA repair molecules (*ATM*, *NBS1*, *RAD50*, *MRE11*, *TP53*), impairing both the sensing and the repair of DNA double-strand breaks. Genome instability predisposes RA T cells to premature death, exposing patients with RA to attrition of naive CD4⁺ T cells. Analysis of T cell receptor diversity within the naive CD4⁺ T cell pool has confirmed repertoire contraction, likely caused by excessive cell death.⁴² During adult life, replenishment of the T cell pool is mostly dependent on replication of postthymic T cells, a process termed “homeostatic proliferation.”^{2,36} Excessive T cell loss must therefore lead to compensatory T cell expansion, altogether ideal conditions to induce immune aging. Studies exploring how RA T cells rich in DNA breaks adapt to their inability of timely DNA repair have shown that the cells seek protection from genotoxic stress by up-regulating the DNA-protein kinase catalytic subunit (DNA-PKcs), deviating them toward the use of error-prone non-homologous end-joining as a DNA repair pathway and the continuous accumulation of mutations.⁴³ Notably, in patient-derived T cells, up-regulated DNA-PKcs activates the JNK stress pathway, rendering the cells susceptible to cell death but also to functional reprogramming.

Insufficient DNA repair in RA T cells extends to the telomeric ends (Figure 2). Like stem cells, healthy T cells can elongate their telomeres by up-regulating telomerase. RA T cells are characterized by shallow telomerase up-regulation, restriction of clonal size, and homeostatic control of the T cell compartment.⁴⁴ Notably, not only does the breakdown of the DNA repair machinery have relevance for the nuclear DNA and the telomeric DNA, but it also affects mitochondrial DNA and leads to mitochondrial failure.^{45,46} Recent data have also implicated DNA polymerase β , a key enzyme in base excision repair, in unresolved DNA damage in RA T cells⁴⁷ (Figure 2).

A critical question is whether the aging phenotype of RA T cells alters the functionality of the cells and whether T cell aging

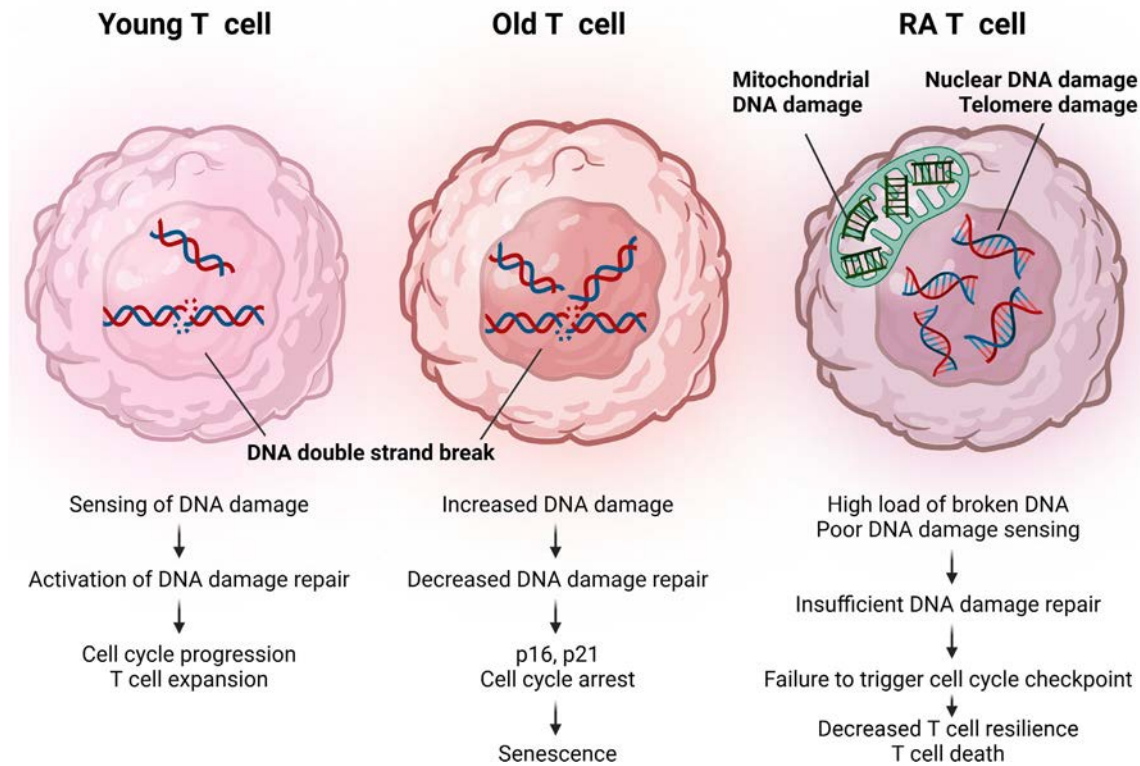


Figure 2. Functional consequences of DNA damage in young and old T cells. As highly proliferative cells, T cells are prone to accumulate DNA breaks. In young T cells (left), the DNA repair machinery senses and repairs the broken DNA. In old T cells (middle), a decline in DNA repair triggers the senescence program, slows cell cycle progression, and curbs clonal expansion. CD4⁺ T cells from patients with RA have a high load of damaged nuclear and mitochondrial DNA due to defective DNA repair (right). The cell enters a stress response program but fails to activate the cell cycle checkpoint. Cells passing through the cell cycle are at high risk to die, often dying an immunogenic cell death that stimulates tissue inflammation. RA, rheumatoid arthritis.

has direct relevance for the disease process (Figure 3). This question has been addressed experimentally. The reliance of CD4⁺ T cells on HR to keep the DNA breakage load low and avoid triggering of the universal stress response makes these cells highly dependent on the MRE11A-RAD50-NBS1 complex, a multiprotein complex critically important in DNA damage recognition and orchestration of repair. The nuclease MRE11A contributes to DNA end processing and resection. RA CD4⁺ T cells typically have low expression of MRE11A, and cellular localization studies have linked MRE11A deficiency to telomeric breakage and unraveling of juxtacentromeric heterochromatin.⁴⁸ Most importantly, MRE11A-deficient CD4⁺ T cells start to express the senescence marker CD57, become tissue invasive, cause synovitis in a chimeric human-synovium mouse model, and facilitate the accumulation of p16⁺ senescent T cells in the synovial tissue (Figure 3).

How can RA T cells continue to clonally expand and drive chronic persistent synovitis if they accumulate high levels of unrepaired DNA double-strand breaks? Cell cycle checkpoints are thought to prevent T cells with damaged DNA from entering S phase and replicating their DNA and efficiently arrest T cells at the G1-S transition. Obviously, RA T cells fail to arrest and

proceed through the cell cycle, remaining dependent on persistent CDK activity. Induction of the CDK inhibitor p21 depends on appropriate DNA damage sensing, yet this mechanism is nonoperational in RA T cells (Figure 2). Thus, RA T cells are not truly senescent. The term “cell cycle inertia” has been coined to describe cells that ignore cell cycle checkpoints and progress through the cell cycle despite high mutational load.⁴⁹

In essence, RA CD4⁺ T cells have only limited features of senescence: they accrue DNA double-strand breaks, which compromise their functionality and activate an adaptation program that incites pathogenic behavior (Figures 2 and 3). RA CD4⁺ T cells lack one characteristic sign of cellular senescence: the entry into permanent T cell cycle arrest. Like tumor cells, they progress through the cell cycle despite irreparable DNA damage, strongly predisposing them to undergo inflammatory cell death.

Aging-associated T cell transcription factors. T cells are long lived, undergo cycles of massive expansion and contraction, and differentiate into a diverse set of memory and effector cells. T cell function in older individuals is impaired, exemplified by the progressively rising risk of developing malignancies and

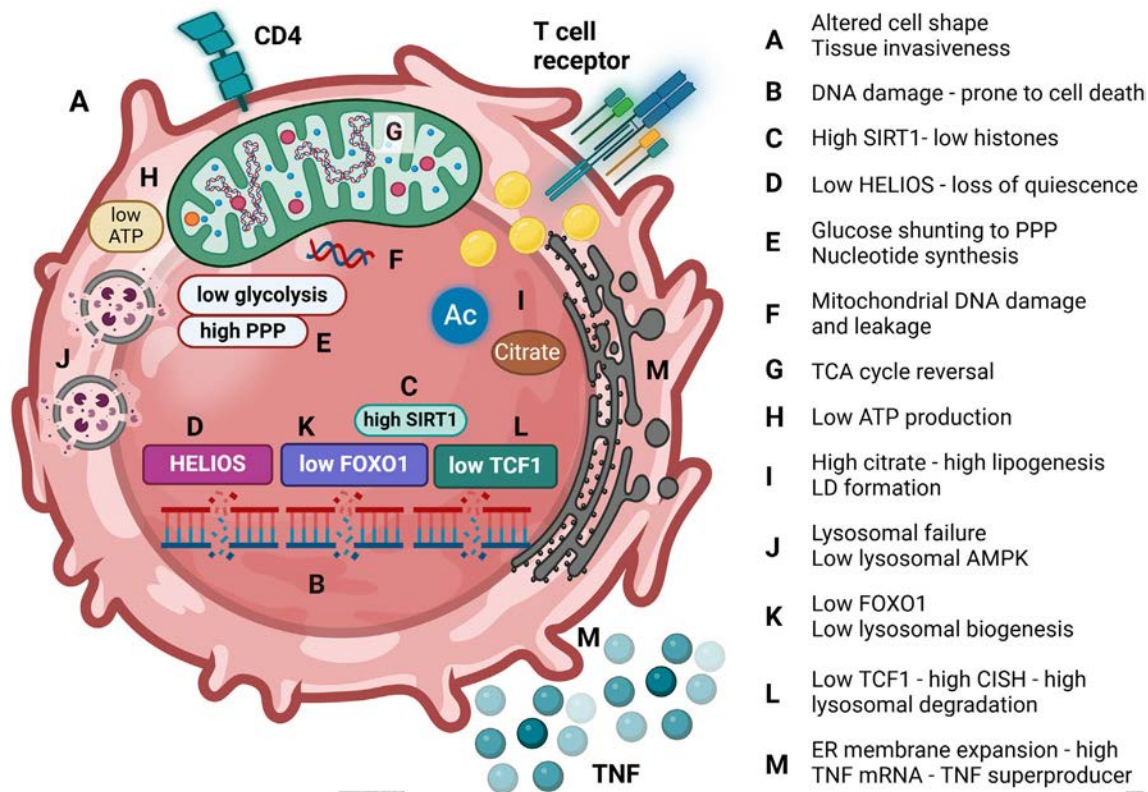


Figure 3. Molecular and functional features of CD4⁺ T cell aging in RA. CD4⁺ T cells from patients with RA share molecular and functional modules with T cells from older adults. Known molecules, transcription factors, and pathways are mapped in the cell. Functional consequences of the aging-associated features are often related to changes in organelle function, affecting the fitness of mitochondria, lysosomes, and the ER. Pathogenic consequences of aging-imposed functional abnormalities are indicated and range from tissue invasiveness to excessive TNF production, dysfunctional cell death, and inappropriate handling of cellular waste. AMPK, AMP-activated protein kinase; CoA, coenzyme A; ER, endoplasmic reticulum; LD, lipid droplet; mRNA, messenger RNA; PPP, pentose phosphate pathway; RA, rheumatoid arthritis; SIRT1, Sirtuin 1; TCA, tricarboxylic acid cycle; TNF, tumor necrosis factor.

infections in older adults. Mechanistic studies comparing T cell fitness in young and older adults have provided valuable insights into how the aging process affects T cell competency, T cell survival, and T cell replenishment (Figure 3). Unbiased screening of T cells isolated from older adults have identified transcription factors and scaffolding molecules that are either up-regulated or down-regulated in aged T cells. The following three transcription factors control downstream pathways that have immediate impact on the ability of T cells to maintain a competent T cell pool or interfere with effector functions that render the older host susceptible to inflammation.

HELIOS⁵⁰: CD4⁺ T cells from older donors have reduced expression of the transcription factor HELIOS. HELIOS controls the transition from quiescence to differentiation. HELIOS^{low} T cells from older individuals escape from quiescence and force T cells into differentiation. This creates ideal conditions for T cell exhaustion.

FOXO1^{51,52}: Loss of the transcription factor FOXO1 in T cells from older adults causes down-regulation of lysosomal biogenesis. Such T cells eliminate undigested waste through exosomal

expulsion, seeding the tissue environment with proinflammatory DAMPs.

TCF1 and CISH⁵³: Aged T cells have reduced expression of TCF1, a transcription factor critically involved in maintaining T cell youth and stemness. Loss of TCF1 in aged T cells leads to the increased expression of CISH. One major functional outcome relates to lysosomal dysfunction. Specifically, CISH^{high} T cells degrade their lysosomes at a higher rate, further compromising lysosomal function and waste management in older T cells. Studies are needed to connect the rewiring of the transcription factor network with the functional deviation of T cells in the RA synovium.

Organelle dysfunction in RA T cells. The major driver for T cell aging is the replicative pressure inherent to the T cell life cycle. Antigenic stimulation elicits a massive clonal expansion to generate the effector cells needed for mounting a successful immune response. Even under resting conditions, T cells need to be constantly replenished. After the age of 20 years, most newly built T cells derive from proliferative activity of postthymic

T cells. Proliferative turnover imposes high bioenergetic and biosynthetic pressure. So it is not unexpected that one of the hallmarks of aging is the deterioration of mitochondrial function.^{54,55} The main transcription factor controlling mitochondrial function is TFAM, and genetic deletion of TFAM selectively in CD4⁺ T cells leads to a pronounced aging phenotype not only in immune cells but also in many other organ systems.⁵⁶ These studies have supported the concept that mitochondrial aging is a pinnacle event in immune cell aging and gives rise to high inflammatory burden in the host.

A characteristic signature for RA T cells is low mitochondrial performance^{57–60} (Figure 3). This is true for T cells in the circulation as well as for T cells in the synovial tissue. Quantification of mitochondrial-derived ATP shows about half as much ATP production in the patient's T cells compared to controls. Underlying mechanisms have been elucidated.^{45,59} First, damage of mitochondrial DNA leads to failure of the electron transport chain, which is ultimately responsible for ATP production.⁴⁵ Second, the tricarboxylic acid (TCA) cycle underperforms,⁶¹ impairing the catabolism of carbohydrates, fats, and proteins. Specifically, instead of oxidizing acetyl-coenzyme A (acetyl-CoA), the TCA cycle in RA T cells reverts and overproduces citrate.⁶² Excess citrate is pumped into the cytosol, where cytosolic acetyl-CoA is increased and drives protein acetylation. One of the target proteins is the cytoskeletal protein tubulin, which is highly acetylated in RA T cells. Consequently, these T cells become polarized and tissue invasive.⁶²

Excess citrate in RA T cells promotes lipogenesis and leads to intracellular accumulation of lipid droplets.⁶³ These lipid droplets are storage organelles that primarily protect the cell from lipid toxicity. In RA T cells, they also serve as a reservoir for membrane lipids, allowing the cell to form podosomal extensions and fostering T cell mobility and tissue invasion.

Reversal of the mitochondrial TCA in RA T cells promotes citrate accumulation but also low concentrations of succinate and malate.⁶⁴ Low availability of malate reduces mitochondrial aspartate production and interrupts the malate–aspartate shuttle. Consequences include insufficient aspartate in the cytosol and insufficient regeneration of cytosolic NAD. Indeed, availability of cytosolic NAD communicates the metabolic status of the cell to the ER. Consequently, RA T cells expand their ER membranes, entering a state of ER stress.⁶⁴ The expansion of ER membranes offers a platform for the recruitment of ribosomes, particularly those that carry messenger RNA (mRNA) encoding for membrane proteins. One of these proteins is the cytokine TNF. RA T cells accumulate TNF mRNA on the ER membranes and turn into TNF superproducers (Figure 3).

Mitochondrial failure in RA T cells not only has implications for ER functioning, but it also directly affects glycolytic competency. Glycolysis produces pyruvate, which needs to be imported into the mitochondria for oxidative breakdown. The inability of the mitochondria in RA T cells to handle pyruvate results in a shutdown of the glycolytic pathway.^{65–67}

Transcriptional repression of the key glycolytic enzyme PFKFB3 causes a slowdown in glycolysis and shunting of glucose into the pentose phosphate pathway.^{65,67} The low demand for glucose renders the RA T cell relatively resistant to glucose-low environments, exemplified in the inflamed synovial tissue.⁶⁸ Only T cells that can survive without a glucose supply are able to persist in this glucose-depleted microenvironment. These data raise the question about which nutrient resources T cells can access to survive in the rheumatoid joint. Available data⁶⁸ show high levels of the amino acids glutamine and glutamate in inflamed synovium and dependence of synovial Mφs on these amino acid for survival and function. T cells have transporters for these amino acids and can shift from glucose consumption to amino acid use.

Not unexpectedly, low mitochondrial performance in RA T cells has implication for all the other organelles (Figure 3). Particularly affected appears to be the endolysosomal system.⁶⁹ Aged CD4 T cells have several defects impairing lysosomal function and, with that, the handling of cellular waste. Systematic analysis of the transcription factor network in aged CD4 T cells has pinpointed transcription factors that are immediately involved in regulating lysosomal biogenesis. Down-regulation of FOXO1 and up-regulation of CISH lead to a decline in the formation of new lysosomal enzymes and increased degradation of available lysosomes.^{51,53} Aged CD4⁺ T cells fail to digest cellular waste appropriately and turn into littering effector cells. The deposition of insufficiently degraded cellular waste provides a strong inflammatory nidus.

Molecular studies in RA CD4⁺ T cells have yielded insights into another aspect of lysosomal function, harboring the two major metabolic sensors of the cell: AMP-activated protein kinase (AMPK) and mechanistic target of rapamycin complex 1 (mTORC1).⁷⁰ To assess the cell's ability to undergo proliferation, mTORC1 senses the amino acid content of the lysosomal lumen and undergoes activation if a sufficient amino acid supply is present. Cells with low ATP production activate AMPK, which in turn inactivates mTORC1. In RA T cells, recruitment of AMPK to the lysosomal surface no longer functions, and mTORC1 is unopposed.⁷⁰ Essentially, RA T cells lack a protective feedback loop that prevents proliferation of starving cells and instead proliferate despite limiting energy resources.

In essence, RA T cells in the tissue and in the circulation are under high metabolic stress, imposed by mitochondrial malfunction. With barely enough energy resources to survive, RA T cells adapt a survival strategy that directly promotes pathogenic effector functions. Breakdown of the endolysosomal system and leakage of mitochondrial DNA into the cytoplasm cause deposition of highly inflammatory cellular waste into the cell's surroundings. Low mitochondrial performance signals to the ER, biasing co-translational translocation, which enhances production of the key proinflammatory cytokine TNF. Most importantly, inappropriate lipogenesis and

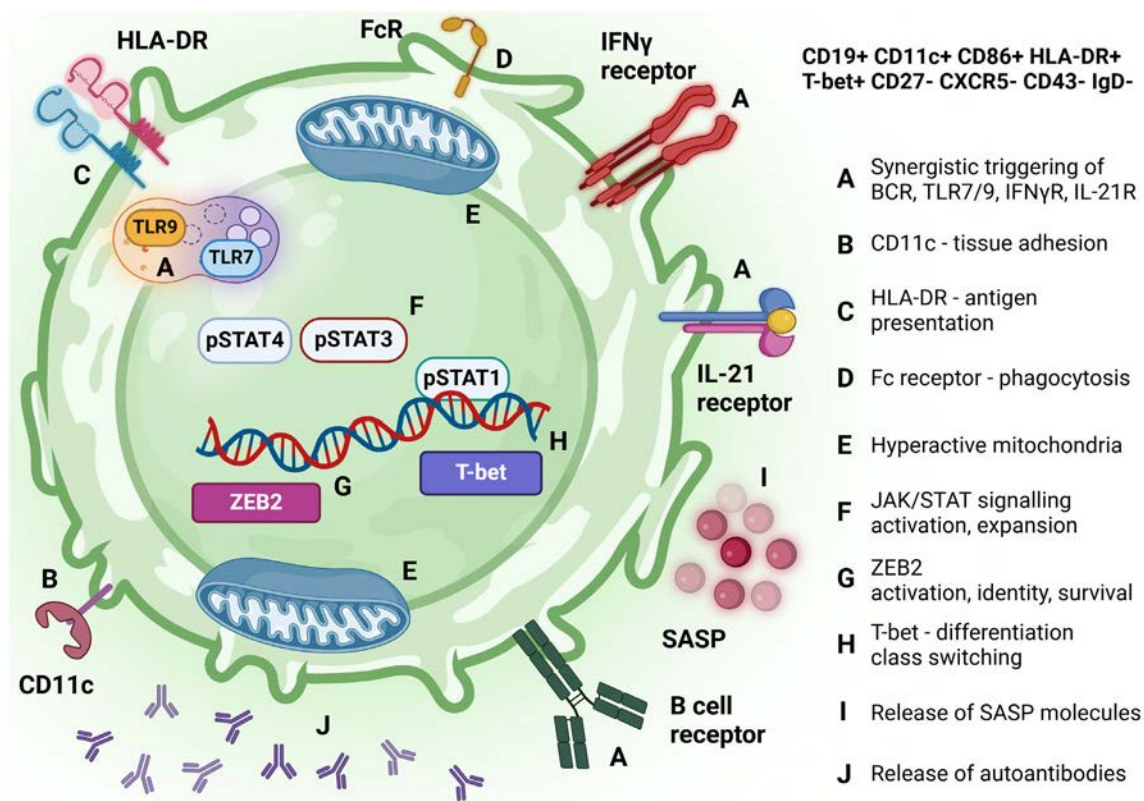


Figure 4. Molecular and functional features of ABCs. ABCs are a transcriptionally and functionally unique B cell population. They express CD19, CD11c, CD86, HLA-DR, and the transcription factor T-bet. They are negative for CD21, CD27, CXCR5, CD43, and IgD. They expand in response to infection and chronic stimulation and typically accumulate with age. They are activated through the coordinated action of antigen, TLR ligands, and cytokines. ABCs are a specialized subset of memory B cells that contribute to autoimmune disease by producing autoantibodies. Distinguishing features are listed and mapped in the cell. ABC, age-associated B cell; BCR, B cell receptor; FcR, Fc receptor; IFN γ R, interferon- γ receptor; IL-21R, interleukin-21 receptor; SASP, senescence-associated secretory phenotype; TLR, Toll-like receptor.

suppressed glycolysis stimulate formation of lipid droplets, polarization of the cells, and building of membrane extensions, all promoting tissue invasion (Figure 3). The ability to survive in the absence of glucose enables RA T cells to enter the glucose-depleted synovial tissue space and persist in a harsh nutritional environment.

In summary, RA CD4⁺ T cells are prematurely aged, display a distinct phenotype, and are proinflammatory effector cells that directly contribute to tissue inflammation. Their pinnacle abnormality lies in defective DNA repair capacity, which causes instability of the mitochondrial genome. A lack of mitochondrial fitness forces the cell into an adaptation program that affects the function of endosomes, lysosomes, and the ER. Key metabolic consequences are low production of ATP and of TCA cycle intermediates. Functional consequences of the metabolic reprogramming range from excess TNF generation to lipid droplet formation, hypermotility, and tissue invasiveness. Accumulation of damaged DNA, mitochondrial failure, and high proinflammatory potential are all features of cellular aging and dovetail with the original observation that RA T cells have premature telomeric erosion.

Age-associated B cells in RA

Obviously, B cells are not unaffected by progressive age, and over the last decade, a specialized B cell subset that is age-associated has been defined and has been directly implicated in autoimmunity⁷¹ (Figure 4). Originally, these B cells came to attention because of their phenotype (CD11c⁺) and reactivity to Toll-like receptor (TLR) ligands.⁷² They are now recognized as autoreactive memory B cells, containing immediate precursors to autoantibody-secreting cells.⁷³ In humans, age-associated B cells (ABCs) display obvious similarities to atypical DN2 memory B cells (CD21^{low} CD27⁻), and both populations are firmly established as the source of pathogenic autoantibodies and as disease drivers in systemic lupus erythematosus.

ABCs have a distinct phenotype that has enabled biomarker studies, correlating disease activity with the frequency and distribution of these aged B cells. Early on, they were identified as CD19⁺ CD43⁻ CD93⁻ CD21/35⁻ CD23⁻ CD11c⁺ CD11b⁺.⁷⁴ Recent studies have linked ABC identity to a gene expression module including *CD19*, *CD86*, *FCRLA*, *FCRL3*, *FCRL5*, *FCGR2B*, *MS4A1*, and *ITGAX*, combined with the lack of *CD27*,

CR2, *CXCR5*, *FCER2*, and *IGHD*.⁷⁵ A distinctive feature of ABCs is the expression of the transcription factor T-bet.

As expected for aging-related cells, ABCs emerge in an inflammatory cytokine environment, responding to combined signaling through the B cell receptor and endosomal TLRs. They are responsive to signaling by interferon- γ (IFN γ) and IL-21, identifying them as ideal partners for end-differentiated T cells that release IFN γ and IL-21 as their effector cytokines. ABC-generating conditions are reminiscent to those necessary for the extrafollicular plasma blast response. They are typically encountered in the setting of chronic bacterial and viral infection, highlighting that this B cell subset is the product of persistent immune stimulation, a scenario typical for the older adult.

In line with the overarching theme that aged T cells and B cells acquire innate-like functions, ABCs express a unique subset of transcription factors and are endowed with a unique profile of effector functions, providing the aged host with the ability to skip the restriction of antigen recognition and acquire antigen-nonspecific reactivity, often directed against self (Figure 4). Recent studies have defined critical transcription factors beyond T-bet that are essential in the activation, differentiation, survival, and acquisition of effector functions in ABCs and have identified zinc finger E-box binding homeobox 2 (ZEB2), a member of the Zfh1 family of two-handed zinc finger/homeodomain proteins.⁷⁵ *ZEB2* mutations are associated with Hirschsprung disease and Mowat–Wilson syndrome, but this transcriptional repressor appears to have a critical role in the process of B cell aging. In mechanistic studies, ZEB2-dependent ABC differentiation required signaling through the JAK/STAT pathway, specifically involving STAT1, STAT3, and STAT4. These data are in keeping with the concept that an environment rich in T cell–derived cytokines (IFN γ , IL-21) enables ABCs to thrive.

Critical for their contribution to the pathogenesis of autoimmune disease is the functional specification of ABCs, including their ability to collaborate with other inflammatory cells and prosper in a host that has a low threshold for inflammatory activity. ABCs are highly dynamic and are chronically reactivated, an important characteristic for their role in chronically persistent autoimmune disease.⁷³ The ABC population contains precursors of plasmablasts, differentiates into autoantibody-secreting B cells, and then differentiates back into ABCs, without entering a stable, long-term memory compartment.⁷³ However, their role as pathogenic contributors to autoimmunity exceeds far beyond their involvement as a class-switched B cell subset. ABCs express CD11c and chemokine receptors such as CXCR3, which deviate them away from lymphoid tissues toward inflammatory tissue sites. They express elevated levels of HLA–DR and costimulatory molecules, optimizing their ability to serve as a partner of proinflammatory T cells. Their cytokine secretion profile is dominated by IL-12p70 and IL-23, while lacking IL-10.⁷⁶ Equipped with Fc receptors, ABCs exhibit high phagocytic capacity, a function dependent on the DNA-binding molecule ZEB2.⁷⁵ They share

with T-bet-expressing T cells the expression of cytotoxic molecules, such as perforin, granzyme A, and natural killer cell receptor group 7 (Figure 4).

Studies of murine ABCs have emphasized a characteristic metabolic profile.⁷⁷ Up-regulation of both extramitochondrial glycolysis and mitochondrial oxygen consumption identifies ABCs as a hypermetabolic population.⁷⁷ This hypermetabolic state correlates with the release of SASP markers and the secretion of autoreactive specificities. Whether ABCs enhance and amplify the inflammatory tissue environment by releasing metabolic intermediates or reactive oxygen species is not known. Their ability to adapt their bioenergetic performance to their functional portfolio separates old B cells from old T cells, which have obvious signs of irreparable mitochondrial stress (Figure 3).

Emerging data support that ABCs are critical effectors cells in RA, have potential as actionable biomarkers, and represent promising therapeutic targets. Like presenescent T cells, ABCs are present during the early phase of RA. Studies in early patients with RA naive to disease-modifying antirheumatic drugs have shown that ABCs are the predominant population of B cells in the synovial fluid.⁷⁶ Low frequencies of ABCs in the peripheral blood are in line with the ability of these age-induced B cells to home to inflamed tissue sites. Their role in the tissue infiltrates appears to extend beyond antibody secretion. ABCs induce high inflammatory activity in synovial fibroblasts,⁷⁸ adding to their inflammation-inducing and sustaining functions in the older host.

In summary, ABCs are a standard part of the immune system in the older adult, where factors other than just specificity control their expansion and survival. Their hallmark is the production of autoantibodies, and ABC-derived autoantibodies have pathogenic function. They are expanded in RA and contribute to the immune aging phenotype of patients with RA (Figure 4).

M ϕ aging in RA

Lymphocyte aging is shaped by the extreme proliferative pressure that T cells and B cells are under and the need for such cells to persist in humans for almost 100 years. Different rules apply to myeloid cells, which are critically important in innate immunity but also as antigen-presenting cells in adaptive immune responses. Neutrophils live for days to possibly weeks. Their aging phenotype is mostly a reflection of HSC aging. Similarly, monocyte and M ϕ aging is inseparable from HSC aging. Released from the bone marrow, circulating monocytes can survive hours to days before they are recruited into tissues, where they locally differentiate into M ϕ s.^{79,80} Such bone marrow–derived M ϕ s intermingle with tissue-resident M ϕ s (TRMs). TRMs colonize their homing organs early during embryonic development from the yolk sac, adapt to organ-specific conditions, and assume a vital function in tissue homeostasis. They reside in

distinct tissue niches, and their functions are tailored toward the particular needs of the organ they live in. Best known TRMs are the brain microglia, lung alveolar M ϕ s, liver Kupffer cells, cardiac M ϕ s, intestinal M ϕ s, and skin Langerhans cells. “True” TRMs are functionally distinct from the monocyte-derived M ϕ s that are born in the bone marrow and infiltrate into tissue sites in response to tissue injury, infection, foreign bodies, and metabolic deviations. In young mice, TRMs are often self-maintained, retain proliferative capacity, and build new TRMs in the tissue sites. Whether and how TRMs are maintained over lifetime is unknown, but emerging data suggest that TRMs are eventually replenished by bone marrow-derived monocytes. Little is known about the composition of tissue M ϕ populations in adult humans, particularly under conditions of chronic long-lasting inflammation, which almost certainly destroys the self-renewal capacity of tissue-residing cell populations. Current data support the concept that tissue M ϕ s in adult humans are hybrid populations, partially TRMs, and partially bone marrow derived.⁸¹ Thus, HSC aging is the dominant determinant of myeloid cell aging in RA.

Under steady-state conditions, most adult HSCs are quiescent and protected from the detrimental effects of proliferative stress. When needed, HSCs initiate demand-adapted hematopoiesis, exit quiescence, and differentiate. Upon aging, HSCs are exposed to persistent and chronic low-grade inflammatory stimuli, a process that has been named inflammaging. The aged HSC pool has reduced homing and repopulating capacity, is biased to differentiate into myeloid cells, accumulates DNA damage, and displays reduced clonal diversity and an epigenetic drift.^{35,82} Because of the enormous proliferative demand on HSCs, the cells have a cumulative increase in somatic mutational load. It has been estimated that HSC acquire mutations at a rate of 14 to 17 mutations per cell per year,⁸³ a fraction of which is nondetrimental and nonlethal and instead increases stem cell fitness, resulting in selective expansion of mutated HSCs. Mutant clonal outgrowth causes the onset of clonal hematopoiesis of indeterminate potential (CHIP). CHIP is diagnosed when an expanded somatic blood cell clone carrying leukemia driver mutations (eg, in *DNMT3A*, *TET2*, *ASXL1*, *TP53*, *JAK2*, *SF3B1*) is present at a variant allele

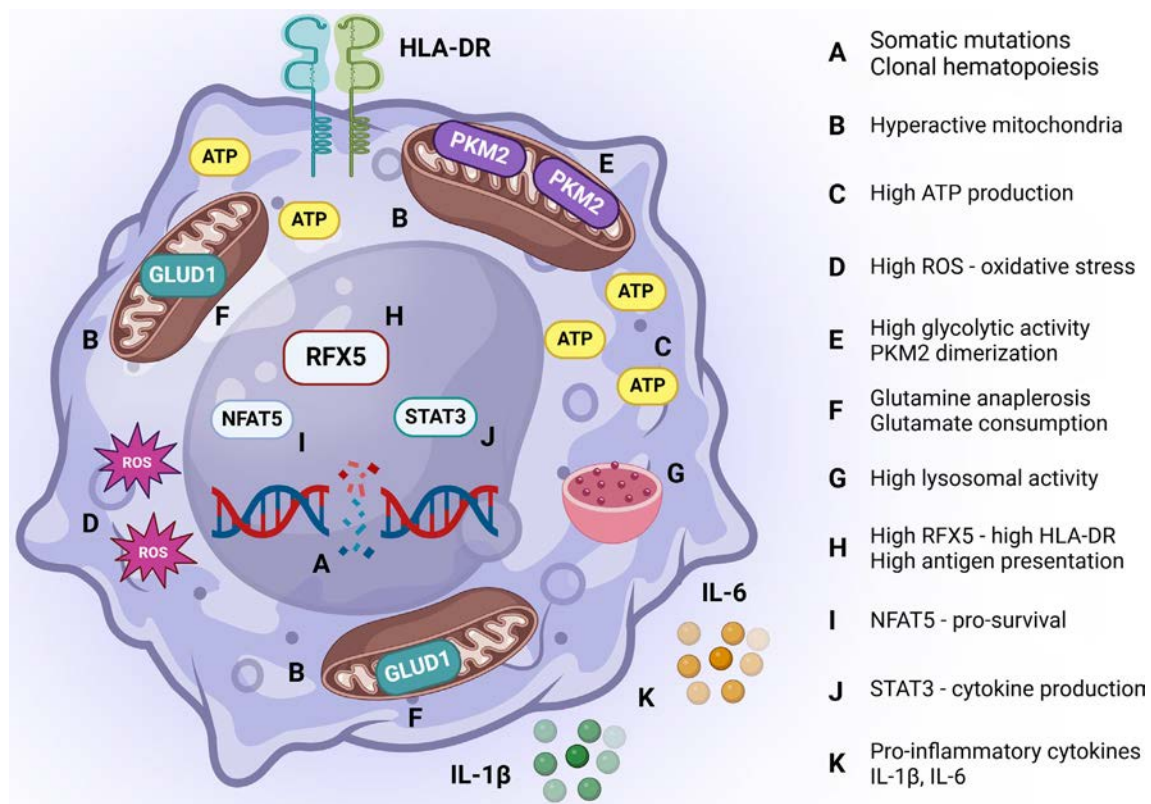


Figure 5. Distinguishing features of hyperstimulated macrophages in rheumatoid arthritis. Myeloid cell aging is closely related to the accumulation of somatic mutations in hematopoietic stem cells, followed by selective expansion of mutated clones (clonal hematopoiesis). Offspring of mutated clones have proinflammatory features. A typical finding of macrophages in rheumatoid arthritis is their hypermetabolic phenotype. Two mitochondrial enzymes have been described to support pathogenic macrophage functions: glutamate dehydrogenase supports metabolic fitness through glutamine anaplerosis and, in parallel, increases antigen-presenting capacity by up-regulating HLA-DR; PKM2 directly regulates the production of proinflammatory cytokines. GLUD1, glutamate dehydrogenase 1; IL, interleukin; PKM2, pyruvate kinase M2; RFX5, regulatory factor X5; ROS, reactive oxygen species.

frequency of >2%. CHIP carriers are at increased risk of developing myeloid hematologic malignancies; their all-cause mortality is markedly increased, mainly because of high risk for cardiovascular disease and stroke.⁸⁴ CHIP incidence is closely correlated with age and is present in <1% of individuals <40 years old and in 10% to 20% of individuals >70 years old.⁸⁵ Indeed, sensitive methods may allow detection of somatic mutations in blood cells in 95% of 50- to 60-year-olds.⁸⁵ Here, low-grade smoldering inflammation functions as a major selective pressure to induce CHIP, but then in turn, CHIP carriers are prone to higher inflammatory responses, noticeable as higher IL-6, TNF, IL-1, and IL-18 serum levels.⁸⁶ Specifically, myeloid cells carrying *DNMT3A*, *TET2*, and *JAK2* mutations have been identified as highly inflammatory effector cells.^{87,88} In a Finnish cohort of patients with RA, 17% of tested patients had CHIP, most commonly caused by *DNMT3A* mutations,⁸⁹ and a recent Mendelian randomization study has suggested a causal relationship between RA and CHIP.⁹⁰

The high prevalence of mutated HSCs in patients with RA is consistent with more pronounced aging of the bone marrow stem cell, as first described by the accelerated telomeric loss of neutrophils in patients with RA.³⁰ These data support the concept that acceleration of the aging process in RA affects innate and adaptive immune cells (Figure 5).

Although the loss of immune tolerance that manifests with the production of autoantibodies precedes joint inflammation by decades⁹¹ and thus occurs outside the joint, rheumatoid synovitis is highly dependent on local stromal cells and M ϕ s, thus subject to myeloid cell aging. In established disease, M ϕ s in the joint are highly diverse, falling into several clearly distinguishable populations.⁶⁸ Metabolic analysis has identified them as hypermetabolic cells that adapt to the glucose-depleted tissue microenvironment by switching to glutaminolysis.⁶⁸ Interestingly, the metabolic switch and adaptation to the low glucose concentrations in synovial tissue is mechanistically linked to functional adaptations. Synovial M ϕ s up-regulate the mitochondrial enzyme glutamate dehydrogenase 1, which optimizes glutamine consumption, and the antigen-presenting machinery in a coordinated manner. The hypermetabolic phenotype of synovial M ϕ s is maintained in monocyte-derived M ϕ s⁹² shared between patients with RA and patients with coronary artery disease (CAD). A hallmark of CAD M ϕ s is high mitochondrial stress that directly contributes to their inflammatory output⁹³ and is mechanistically linked to the posttranslational modification of the glycolytic enzyme pyruvate kinase M2. Survival of synovial M ϕ s in patients with RA is associated with high expression of the transcription factor NFAT5, which in turn is up-regulated by hypoxia and TLR-4 ligand stimulation.⁹⁴ These data exemplify that myeloid cell aging, metabolic adaptations, and chronic tissue inflammation are closely interlinked (Figure 5).

Conclusions

The risk of being diagnosed with RA is highest in individuals >60 years of age, when the immune system has a strong imprint of aging. Patients being diagnosed earlier in life have a signature of premature immune aging. Aged innate and adaptive immune cells contribute to the loss of self-tolerance. Deriving from HSCs that have accumulated somatic mutations, older myeloid cells with a robust bias toward proinflammatory functions infiltrate into peripheral tissues, where they intermingle with tissue-resident M ϕ s to drive tissue inflammation. Because of defects in the repair of mitochondrial DNA, aged T cells are under high metabolic stress, which affects the functionality of their subcellular organelles and turns them into proinflammatory effector cells. Expanded by chronic stimulation in a proinflammatory environment, ABCs acquire innate-like functions and pivot toward autoantibody production. Resetting the tolerance loss in RA will require rejuvenation of the immune system.

ACKNOWLEDGMENTS

The authors would like to give sincere thanks to the members of the Weyand and Goronzy research teams and the patients who have contributed to this work. We are thankful for the support of the Encrantz Family Discovery Program and the Mary and Mark Davis Program in Rheumatoid Arthritis.

AUTHOR CONTRIBUTIONS

All authors contributed to at least one of the following manuscript preparation roles: conceptualization AND/OR methodology, software, investigation, formal analysis, data curation, visualization, and validation AND drafting or reviewing/editing the final draft. As corresponding author, Dr Weyand confirms that all authors have provided the final approval of the version to be published and takes responsibility for the affirmations regarding article submission (eg, not under consideration by another journal), the integrity of the data presented, and the statements regarding compliance with institutional review board/Declaration of Helsinki requirements.

REFERENCES

1. Conrad N, Misra S, Verbakel JY, et al. Incidence, prevalence, and co-occurrence of autoimmune disorders over time and by age, sex, and socioeconomic status: a population-based cohort study of 22 million individuals in the UK. *Lancet* 2023;401(10391):1878–1890.
2. Goronzy JJ, Weyand CM. Mechanisms underlying T cell ageing. *Nat Rev Immunol* 2019;19(9):573–583.
3. Alhaj Hussien K, Louis V, Canque B. A new model of human lymphopoiesis across development and aging. *Trends Immunol* 2024;45(7):495–510.
4. de Mol J, Kuiper J, Tsiantoulas D, et al. The dynamics of B cell aging in health and disease. *Front Immunol* 2021;12:733566.
5. Zheng Y, Liu Q, Goronzy JJ, et al. Immune aging - a mechanism in autoimmune disease. *Semin Immunol* 2023;69:101814.
6. Liu Q, Zheng Y, Goronzy JJ, et al. T cell aging as a risk factor for autoimmunity. *J Autoimmun* 2023;137:102947.

7. Di Micco R, Krizhanovsky V, Baker D, et al. Cellular senescence in ageing: from mechanisms to therapeutic opportunities. *Nat Rev Mol Cell Biol* 2021;22(2):75–95.
8. Suryadevara V, Hudgins AD, Rajesh A, et al. SenNet recommendations for detecting senescent cells in different tissues. *Nat Rev Mol Cell Biol* 2024;25(12):1001–1023.
9. Kumari R, Jat P. Mechanisms of cellular senescence: cell cycle arrest and senescence associated secretory phenotype. *Front Cell Dev Biol* 2021;9:645593.
10. McKinstry KK, Strutt TM, Swain SL. Regulation of CD4+ T-cell contraction during pathogen challenge. *Immunol Rev* 2010;236(1):110–124.
11. Snow AL, Pandiyan P, Zheng L, et al. The power and the promise of restimulation-induced cell death in human immune diseases. *Immunol Rev* 2010;236(1):68–82.
12. Zhan Y, Carrington EM, Zhang Y, et al. life and death of activated T cells: how are they different from naïve T cells? *Front Immunol* 2017;8:1809.
13. Gorgoulis V, Adams PD, Alimonti A, et al. Cellular senescence: defining a path forward. *Cell* 2019;179(4):813–827.
14. Wang B, Han J, Elisseeff JH, et al. The senescence-associated secretory phenotype and its physiological and pathological implications. *Nat Rev Mol Cell Biol* 2024;25(12):958–978.
15. Schafer MJ, Zhang X, Kumar A, et al. The senescence-associated secretome as an indicator of age and medical risk. *JCI Insight* 2020;5(12):e133668.
16. Desdín-Micó G, Soto-Herederó G, Aranda JF, et al. T cells with dysfunctional mitochondria induce multimorbidity and premature senescence. *Science* 2020;368(6497):1371–1376.
17. Chaib S, Tchonia T, Kirkland JL. Cellular senescence and senolytics: the path to the clinic. *Nat Med* 2022;28(8):1556–1568.
18. Farr JN, Atkinson EJ, Achenbach SJ, et al. Effects of intermittent senolytic therapy on bone metabolism in postmenopausal women: a phase 2 randomized controlled trial. *Nat Med* 2024;30(9):2605–2612.
19. Kita A, Yamamoto S, Saito Y, et al. Cellular senescence and wound healing in aged and diabetic skin. *Front Physiol* 2024;15:1344116.
20. Gems D, Kern CC. Is “cellular senescence” a misnomer? *Geroscience* 2022;44(5):2461–2469.
21. Künzli M, Masopust D. CD4⁺ T cell memory. *Nat Immunol* 2023;24(6):903–914.
22. van den Berg SPH, Derksen LY, Drylewicz J, et al. Quantification of T-cell dynamics during latent cytomegalovirus infection in humans. *PLoS Pathog* 2021;17(12):e1010152.
23. Lee KP, Epstein B, Lake CM, et al. Molecular and temporal control of restimulation-induced cell death (RICD) in T lymphocytes. *Front Cell Death* 2023;2:2.
24. Schmidt D, Goronzy JJ, Weyand CM. CD4⁺ CD7[−] CD28[−] T cells are expanded in rheumatoid arthritis and are characterized by autoreactivity. *J Clin Invest* 1996;97(9):2027–2037.
25. Pawlik A, Ostaneck L, Brzosko I, et al. The expansion of CD4⁺CD28[−] T cells in patients with rheumatoid arthritis. *Arthritis Res Ther* 2003;5(4):R210–R213.
26. Fasth AE, Snir O, Johansson AA, et al. Skewed distribution of proinflammatory CD4⁺CD28null T cells in rheumatoid arthritis. *Arthritis Res Ther* 2007;9(5):R87.
27. Jiang J, Liu C, Liu M, et al. OX40 signaling is involved in the autoactivation of CD4⁺CD28[−] T cells and contributes to the pathogenesis of autoimmune arthritis. *Arthritis Res Ther* 2017;19(1):67.
28. Broux B, Pannemans K, Zhang X, et al. CX(3)CR1 drives cytotoxic CD4⁺CD28[−] T cells into the brain of multiple sclerosis patients. *J Autoimmun* 2012;38(1):10–19.
29. Koetz K, Bryl E, Spickschen K, et al. T cell homeostasis in patients with rheumatoid arthritis. *Proc Natl Acad Sci USA* 2000;97(16):9203–9208.
30. Schönland SO, Lopez C, Widmann T, et al. Premature telomeric loss in rheumatoid arthritis is genetically determined and involves both myeloid and lymphoid cell lineages. *Proc Natl Acad Sci USA* 2003;100(23):13471–13476.
31. Colmegna I, Diaz-Borjon A, Fujii H, et al. Defective proliferative capacity and accelerated telomeric loss of hematopoietic progenitor cells in rheumatoid arthritis. *Arthritis Rheum* 2008;58(4):990–1000.
32. Goronzy JJ, Fujii H, Weyand CM. Telomeres, immune aging and autoimmunity. *Exp Gerontol* 2006;41(3):246–251.
33. Mejia-Ramirez E, Florian MC. Understanding intrinsic hematopoietic stem cell aging. *Haematologica* 2020;105(1):22–37.
34. Flach J, Milyavsky M. Replication stress in hematopoietic stem cells in mouse and man. *Mutat Res* 2018;808:74–82.
35. Beerman I. Accumulation of DNA damage in the aged hematopoietic stem cell compartment. *Semin Hematol* 2017;54(1):12–18.
36. Goronzy JJ, Weyand CM. Successful and maladaptive T cell aging. *Immunity* 2017;46(3):364–378.
37. Colmegna I, Weyand CM. Haematopoietic stem and progenitor cells in rheumatoid arthritis. *Rheumatology (Oxford)* 2011;50(2):252–260.
38. Wen Z, Shimojima Y, Shirai T, et al. NADPH oxidase deficiency underlies dysfunction of aged CD8⁺ Tregs. *J Clin Invest* 2016;126(5):1953–1967.
39. Jin K, Wen Z, Wu B, et al. NOTCH-induced rerouting of endosomal trafficking disables regulatory T cells in vasculitis. *J Clin Invest* 2021;131(1):e136042.
40. Prochazkova J, Loizou JI. Programmed DNA breaks in lymphoid cells: repair mechanisms and consequences in human disease. *Immunology* 2016;147(1):11–20.
41. Hünig T, Schimpl A. Systemic autoimmune disease as a consequence of defective lymphocyte death. *Curr Opin Immunol* 1997;9(6):826–830.
42. Shao L, Fujii H, Colmegna I, et al. Deficiency of the DNA repair enzyme ATM in rheumatoid arthritis. *J Exp Med* 2009;206(6):1435–1449.
43. Shao L, Goronzy JJ, Weyand CM. DNA-dependent protein kinase catalytic subunit mediates T-cell loss in rheumatoid arthritis. *EMBO Mol Med* 2010;2(10):415–427.
44. Fujii H, Shao L, Colmegna I, et al. Telomerase insufficiency in rheumatoid arthritis. *Proc Natl Acad Sci USA* 2009;106(11):4360–4365.
45. Li Y, Shen Y, Jin K, et al. The DNA repair nuclease MRE11A functions as a mitochondrial protector and prevents T cell pyroptosis and tissue inflammation. *Cell Metab* 2019;30(3):477–492.e6.
46. Li Y, Goronzy JJ, Weyand CM. DNA damage, metabolism and aging in pro-inflammatory T cells: rheumatoid arthritis as a model system. *Exp Gerontol* 2018;105:118–127.
47. Gu L, Sun Y, Wu T, et al. A novel mechanism for macrophage pyroptosis in rheumatoid arthritis induced by Pol β deficiency. *Cell Death Dis* 2022;13(7):583.
48. Li Y, Shen Y, Hohensinner P, et al. Deficient activity of the nuclease MRE11A induces T cell aging and promotes arthritogenic effector functions in patients with rheumatoid arthritis. *Immunity* 2016;45(4):903–916.
49. Nathans JF, Cornwell JA, Afifi MM, et al. Cell cycle inertia underlies a bifurcation in cell fates after DNA damage. *Sci Adv* 2021;7(3):eabe3882.
50. Zhang H, Jadhav RR, Cao W, et al. Aging-associated HELIOS deficiency in naïve CD4⁺ T cells alters chromatin remodeling and promotes effector cell responses. *Nat Immunol* 2023;24(1):96–109.
51. Jin J, Li X, Hu B, et al. FOXO1 deficiency impairs proteostasis in aged T cells. *Sci Adv* 2020;6(17):eaba1808.

52. Jin J, Kim C, Xia Q, et al. Activation of mTORC1 at late endosomes misdirects T cell fate decision in older individuals. *Sci Immunol* 2021; 6(60):eabg0791.
53. Jin J, Mu Y, Zhang H, et al. CISH impairs lysosomal function in activated T cells resulting in mitochondrial DNA release and inflamming. *Nat Aging* 2023;3(5):600–616.
54. Suomalainen A, Nunnari J. Mitochondria at the crossroads of health and disease. *Cell* 2024;187(11):2601–2627.
55. López-Otín C, Blasco MA, Partridge L, et al. Hallmarks of aging: an expanding universe. *Cell* 2023;186(2):243–278.
56. Carrasco E, Gómez de Las Heras MM, Gabandé-Rodríguez E, et al. The role of T cells in age-related diseases. *Nat Rev Immunol* 2022; 22(2):97–111.
57. Qiu J, Wu B, Goodman SB, et al. Metabolic control of autoimmunity and tissue inflammation in rheumatoid arthritis. *Front Immunol* 2021; 12:652771.
58. Weyand CM, Wu B, Huang T, et al. Mitochondria as disease-relevant organelles in rheumatoid arthritis. *Clin Exp Immunol* 2023;211(3): 208–223.
59. Wu B, Goronzy JJ, Weyand CM. Metabolic fitness of T cells in autoimmune disease. *Immunometabolism* 2020;2(2):e200017.
60. Weyand CM, Goronzy JJ. Immunometabolism in the development of rheumatoid arthritis. *Immunol Rev* 2020;294(1):177–187.
61. Weyand CM, Zeisbrich M, Goronzy JJ. Metabolic signatures of T-cells and macrophages in rheumatoid arthritis. *Curr Opin Immunol* 2017; 46:112–120.
62. Wu B, Qiu J, Zhao TV, et al. Succinyl-CoA ligase deficiency in pro-inflammatory and tissue-invasive T cells. *Cell Metab* 2020;32(6): 967–980.e5.
63. Shen Y, Wen Z, Li Y, et al. Metabolic control of the scaffold protein TKS5 in tissue-invasive, proinflammatory T cells. *Nat Immunol* 2017; 18(9):1025–1034.
64. Wu B, Zhao TV, Jin K, et al. Mitochondrial aspartate regulates TNF biogenesis and autoimmune tissue inflammation. *Nat Immunol* 2021; 22(12):1551–1562.
65. Yang Z, Shen Y, Oishi H, et al. Restoring oxidant signaling suppresses proarthritogenic T cell effector functions in rheumatoid arthritis. *Sci Transl Med* 2016;8(331):331ra38.
66. Weyand CM, Yang Z, Goronzy JJ. T-cell aging in rheumatoid arthritis. *Curr Opin Rheumatol* 2014;26(1):93–100.
67. Yang Z, Fujii H, Mohan SV, et al. Phosphofructokinase deficiency impairs ATP generation, autophagy, and redox balance in rheumatoid arthritis T cells. *J Exp Med* 2013;210(10):2119–2134.
68. Hu Z, Zhao TV, Huang T, et al. The transcription factor RFX5 coordinates antigen-presenting function and resistance to nutrient stress in synovial macrophages. *Nat Metab* 2022;4(6):759–774.
69. Jin J, Zhang H, Weyand CM, et al. Lysosomes in T cell immunity and aging. *Front Aging* 2021;2:809539.
70. Wen Z, Jin K, Shen Y, et al. N-myristoyltransferase deficiency impairs activation of kinase AMPK and promotes synovial tissue inflammation. *Nat Immunol* 2019;20(3):313–325.
71. Cancro MP. Age-associated B cells. *Annu Rev Immunol* 2020;38: 315–340.
72. Rubtsov AV, Rubtsova K, Fischer A, et al. Toll-like receptor 7 (TLR7)-driven accumulation of a novel CD11c⁺ B-cell population is important for the development of autoimmunity. *Blood* 2011;118(5):1305–1315.
73. Nickerson KM, Smita S, Hoehn KB, et al. Age-associated B cells are heterogeneous and dynamic drivers of autoimmunity in mice. *J Exp Med* 2023;220(5):e20221346.
74. Hao Y, O'Neill P, Naradikian MS, et al. A B-cell subset uniquely responsive to innate stimuli accumulates in aged mice. *Blood* 2011; 118(5):1294–1304.
75. Dai D, Gu S, Han X, et al. The transcription factor ZEB2 drives the formation of age-associated B cells. *Science* 2024;383(6681):413–421.
76. Vidal-Pedrola G, Naamane N, Cameron JA, et al. Characterization of age-associated B cells in early drug-naïve rheumatoid arthritis patients. *Immunology* 2023;168(4):640–653.
77. Frasca D, Romero M, Garcia D, et al. Hyper-metabolic B cells in the spleens of old mice make antibodies with autoimmune specificities. *Immun Ageing* 2021;18(1):9.
78. Qin Y, Cai ML, Jin HZ, et al. Age-associated B cells contribute to the pathogenesis of rheumatoid arthritis by inducing activation of fibroblast-like synoviocytes via TNF- α -mediated ERK1/2 and JAK-STAT1 pathways. *Ann Rheum Dis* 2022;81(11):1504–1514.
79. Lazarov T, Juarez-Carreño S, Cox N, et al. Physiology and diseases of tissue-resident macrophages. *Nature* 2023;618(7966):698–707.
80. Gordon S, Plüddemann A. The mononuclear phagocytic system. Generation of diversity. *Front Immunol* 2019;10:1893.
81. Wculek SK, Forisch S, Miguel V, et al. Metabolic homeostasis of tissue macrophages across the lifespan. *Trends Endocrinol Metab* 2024; 35(9):793–808.
82. Kovtonyuk LV, Fritsch K, Feng X, et al. Inflamm-aging of hematopoiesis, hematopoietic stem cells, and the bone marrow microenvironment. *Front Immunol* 2016;7:502.
83. Caiado F, Kovtonyuk LV, Gonullu NG, et al. Aging drives Tet2^{+/−} clonal hematopoiesis via IL-1 signaling. *Blood* 2023;141(8):886–903.
84. Genovese G, Kähler AK, Handsaker RE, et al. Clonal hematopoiesis and blood-cancer risk inferred from blood DNA sequence. *N Engl J Med* 2014;371(26):2477–2487.
85. Young AL, Challen GA, Birmann BM, et al. Clonal haematopoiesis harbouring AML-associated mutations is ubiquitous in healthy adults. *Nat Commun* 2016;7(1):12484.
86. Bick AG, Weinstock JS, Nandakumar SK, et al; NHLBI Trans-Omics for Precision Medicine Consortium. Inherited causes of clonal haematopoiesis in 97,691 whole genomes. *Nature* 2020;586(7831): 763–768.
87. Sano S, Oshima K, Wang Y, et al. Tet2-mediated clonal hematopoiesis accelerates heart failure through a mechanism involving the IL-1 β /NLRP3 inflammasome. *J Am Coll Cardiol* 2018;71(8): 875–886.
88. Cull AH, Snetsinger B, Buckstein R, et al. Tet2 restrains inflammatory gene expression in macrophages. *Exp Hematol* 2017;55: 56–70.e13.
89. Savola P, Lundgren S, Keränen MAI, et al. Clonal hematopoiesis in patients with rheumatoid arthritis. *Blood Cancer J* 2018;8(8):69.
90. Zhang J, Zhou C, Guan S. Association between rheumatoid arthritis and clonal hematopoiesis: a Mendelian randomization study. *Twin Res Hum Genet* 2024;27(3):1–5.
91. Deane KD, Holers VM. Rheumatoid arthritis pathogenesis, prediction, and prevention: an emerging paradigm shift. *Arthritis Rheumatol* 2021;73(2):181–193.
92. Zeisbrich M, Yanes RE, Zhang H, et al. Hypermetabolic macrophages in rheumatoid arthritis and coronary artery disease due to glycogen synthase kinase 3 β inactivation. *Ann Rheum Dis* 2018;77(7): 1053–1062.
93. Shirai T, Nazarewicz RR, Wallis BB, et al. The glycolytic enzyme PKM2 bridges metabolic and inflammatory dysfunction in coronary artery disease. *J Exp Med* 2016;213(3):337–354.
94. Choi S, You S, Kim D, et al. Transcription factor NFAT5 promotes macrophage survival in rheumatoid arthritis. *J Clin Invest* 2017; 127(3):954–969.

EDITORIAL

Systemic Sclerosis: A Multisystem Disease; Time to Think Beyond Scleroderma

Yannick Allanore¹  and Shervin Assassi² 

The heterogeneity in the natural history of systemic sclerosis (SSc) is a major challenge both for clinical management and for trial design. It is dictated by the complex interplay between vascular injury and dysregulation of the immune response, culminating in the fibrosis of various target organs. Stratification of the patients is critical to adapt the management according to the patient profile and disease concerns. So far, skin fibrosis (diffuse vs limited) has been the main criterion used to risk-stratify patients with SSc. The key differences in the two clinical cutaneous subsets are the type and speed of progression of organ damage. Measurement of skin involvement can, therefore, be used as a surrogate for disease activity, severity, and death in patients with diffuse cutaneous SSc (dcSSc) as opposed to limited cutaneous SSc (lcSSc), for which it has no prognostic value.¹ Indeed, the lack of relevance of the skin score as a surrogate in lcSSc has excluded this subset from many clinical trials, depriving these patients of the potential benefits of novel treatment options. This gap appears unfortunate because lcSSc represents about two-thirds of the whole SSc population of patients.² It is also established that patients with lcSSc have an altered quality of life and can develop severe organ manifestations.^{3,4} The best example is probably the risk of lung manifestations, with pulmonary arterial hypertension (PAH) being predominant in lcSSc, whereas interstitial lung disease (ILD), although less common in this disease subset, can also be progressive.⁴ In addition to the divergent organ manifestations, the other key difference between lcSSc and dcSSc is the timing of such complications. Indeed, lcSSc is seen as a slower progressive disease in which silent remodeling may act during years before leading to clinical manifestations. This has implications for clinical research and clinical trials in lcSSc, for which composite index and time to events are the two key components to take into consideration for performing clinical trials.

In the study by Di Donato et al,⁵ [Correction added on 12 February 2025, after first online publication: second paragraph, “Di Stefano” has been corrected to “Di Donato”.] a composite

endpoint in lcSSc has been explored, and this provides some very promising results. Indeed, the authors aimed at measuring the performance of a biomarker in lcSSc and therefore measured the probability of organ damages in a population with lcSSc. They have been inspired by a not yet published trial that used a similar methodology to investigate the effects of mycophenolate mofetil in lcSSc (NCT04927390). The authors enrolled 149 patients with lcSSc, having a median (interquartile range) baseline disease duration from first non-Raynaud phenomenon symptom of 8 (10) years.

Within an average follow-up time of 94.5 months (95% confidence interval 78.4–113.3), 47 of 149 patients (32.5%) developed the endpoint. The most common event was newly diagnosed PAH ($n = 13$; 27.3%), followed by SSc-related death ($n = 9$; 19%), progression of ILD ($n = 6$; 13%), SSc-related cardiac events ($n = 6$; 13%), worsening of the modified Rodnan Skin Score (mRSS) ($n = 5$; 11%), gastrointestinal complications ($n = 4$; 8.5%), severe digital vasculopathy requiring hospitalization ($n = 3$; 6.4%), and scleroderma renal crisis ($n = 1$; 2.1%). A limitation of this study is that a significant number of patients already had disease manifestations at the baseline visit. For example, PAH was already present in nine patients at the baseline visit. Prior studies have indicated that patients with SSc with PAH have higher serum interferon (IFN)-inducible chemokine levels than those without this manifestation.⁶ Moreover, IFN therapy has been associated with the occurrence of PAH in patients receiving this therapeutic modality for the treatment of other diseases.⁷ Although the presence of PAH at the baseline visit was not significantly associated with IFN score positivity in the study, future studies examining patients with early disease can provide additional information on discerning whether the increased serum IFN-inducible chemokine levels are the cause or a consequence of PAH.

As pointed out by the authors, the relatively long baseline disease duration of eight years raises the possibility that some of the results are influenced by survival bias. For example, there was no association between disease duration and IFN positivity status.

¹Yannick Allanore, MD, PhD: Cochin Hospital, Paris Cité Université, INSERM U1016, Paris, France; ²Shervin Assassi, MS, MD: UTHealth Houston, Houston, Texas.

Author disclosures are available at <https://onlinelibrary.wiley.com/doi/10.1002/art.43121>.

Address correspondence via email to Yannick Allanore, MD, PhD, at yannick.allanore@me.com.

Submitted for publication January 1, 2025; accepted in revised form January 8, 2025.

A possible explanation for this lack of association is that there is a preferential depletion of the IFN-positive patient population (because of its higher mortality rate), which would counteract a potential trend in increasing IFN positivity frequency with the accumulating disease damage over time. Therefore, future studies examining patients with early disease can provide additional insights into the relationship between IFN signature and SSc disease manifestations.

The weight of the respective components in a composite index is critical to estimate. In this study,⁵ the impact of having a skin score worsening is quite small, contributing to only 5 of 47 events (11%); of these events, 2 out of 5 patients also had cardiac events. This is illustrated by a mean value mRSS of 1.59 (2.05) in the group without an event versus 3.17 (3.36) in the group characterized by at least one event (mRSS values ranges from 0 to 51). This highlights that skin fibrosis cannot be a robust endpoint to assess disease progression in lcSSc at advanced stages. It underscores that we may think beyond skin fibrosis (ie, the literal meaning of the word, scleroderma) when we aim at measuring disease progression in lcSSc.

The study adds to the body of evidence underscoring the role of IFN pathway activation in SSc disease pathogenesis and progression. Several genes in this pathway, such as *IRF5*, *IRF7*, *IRF8*, and *STAT4*, have been robustly linked to SSc susceptibility.⁸ Moreover, an activated IFN signature is the most prominent feature of SSc peripheral blood cell gene expression profile.⁸ Consistent with the results of this study, IFN signature was not more common in patients with dcSSc than in those with lcSSc in the previous observational studies, underscoring its potential utility as biomarker for disease severity in both clinical subsets of disease.⁹ In this study,⁵ the strongest association at the baseline visit was anti-Ro52 positivity. This finding is consistent with the previously reported association of the IFN gene expression signature with anti-SSA positivity in patients with SSc.¹⁰ Anti-Ro52 is a common autoantibody in SSc and can co-occur with other SSc-related autoantibodies. In a previous international study, 6.5% of patients with SSc had monospecific anti-Ro52 antibodies, whereas 20.6% of study population had anti-Ro52 antibodies overlapping with other SSc-related antibodies.¹¹ Anti-Ro52 antibodies have been consistently associated with ILD, underscoring its link to an important internal organ manifestation occurring both in dcSSc and lcSSc subsets.

In Scleroderma Lung Study II, baseline serum IFN cytokine score predicted better response to immunosuppression, whereas it showed a trend for worse ILD course when patients were taken off immunosuppression, underscoring its value as a potential predictive biomarker for response to immunosuppression.¹² Moreover, active immunosuppression significantly reduced the IFN-inducible chemokine levels. In the study, only 8.7% of participants were treated with mycophenolate mofetil. Future longitudinal studies are needed to characterize the dynamic changes of this biomarker over time and to determine

whether the direction of the predictive significance of IFN cytokine score depends on the treatment status with immunosuppressive agents.

Altogether, the Di Donato et al study⁵ pioneers the field of outcome measures for lcSSc and the relevance of the use of composite index. The items to be used and their definition still need to be further validated, but this is the subject of ongoing research.¹³ Moreover, the current study demonstrates that type I IFN activation is common in SSc-relevant disease manifestations beyond skin involvement. The data require independent validation in longitudinal studies but suggest that IFN score may aid in the measurement of disease activity and in enriching for clinically meaningful events over time in clinical trials of patients with lcSSc.¹⁴ Moreover, Di Donato et al provide further support for type I IFN as a therapeutic target in SSc.⁵ This offers great opportunities to capitalize on the prior progress in treating interferonopathies and the availability of several medications to counteract IFN activation.¹⁵ Altogether, these data position SSc on the list of candidate diseases to be treated by anti-IFN therapies, with the potential of improving the disease beyond skin involvement and reaching the ultimate goal of disease modification by improving several disease manifestations.

AUTHOR CONTRIBUTIONS









Drs Allanore and Assassi drafted the article, revised it critically for important intellectual content, and approved the final version to be published.

REFERENCES

1. Khanna D, Furst DE, Clements PJ, et al. Standardization of the modified Rodnan skin score for use in clinical trials of systemic sclerosis. *J Scleroderma Relat Disord* 2017;2(1):11–18.
2. Allanore Y. Limited cutaneous systemic sclerosis: the unfairly neglected subset. *J Scleroderma Relat Disord* 2016;1:241–246.
3. Frantz C, Avouac J, Distler O, et al. Impaired quality of life in systemic sclerosis and patient perception of the disease: a large international survey. *Semin Arthritis Rheum* 2016;46(1):115–123.
4. Frantz C, Huscher D, Avouac J, et al; EUSTAR co-authors. Outcomes of limited cutaneous systemic sclerosis patients: results on more than 12,000 patients from the EUSTAR database. *Autoimmun Rev* 2020;19(2):102452.
5. Di Donato S, Ross R, Karanth R, et al. Serum Type I interferon score predicts clinically meaningful disease progression in limited cutaneous systemic sclerosis. *Arthritis Rheumatol* 2025;77(7):929–941.
6. George PM, Oliver E, Dorfmueller P, et al. Evidence for the involvement of type I interferon in pulmonary arterial hypertension. *Circ Res* 2014;114(4):677–688.
7. Savale L, Sattler C, Günther S, et al. Pulmonary arterial hypertension in patients treated with interferon. *Eur Respir J* 2014;44(6):1627–1634.
8. Kakkar V, Assassi S, Allanore Y, et al. Type 1 interferon activation in systemic sclerosis: a biomarker, a target or the culprit. *Curr Opin Rheumatol* 2022;34(6):357–364.
9. Liu X, Mayes MD, Tan FK, et al. Correlation of interferon-inducible chemokine plasma levels with disease severity in systemic sclerosis. *Arthritis Rheum* 2013;65(1):226–235.

10. Assassi S, Mayes MD, Arnett FC, et al. Systemic sclerosis and lupus: points in an interferon-mediated continuum. *Arthritis Rheum* 2010; 62(2):589–598.
11. Wodkowski M, Hudson M, Proudman S, et al; Canadian Scleroderma Research Group (CSRG); Australian Scleroderma Cohort Study (ASCS); Genetics versus Environment in Scleroderma Outcome Study (GENISOS). Monospecific anti-Ro52/TRIM21 antibodies in a tri-nation cohort of 1574 systemic sclerosis subjects: evidence of an association with interstitial lung disease and worse survival. *Clin Exp Rheumatol* 2015;33(4 Suppl 91):S131–S135.
12. Assassi S, Li N, Volkmann ER, et al. Predictive significance of serum interferon-inducible protein score for response to treatment in systemic sclerosis-related interstitial lung disease. *Arthritis Rheumatol* 2021;73(6):1005–1013.
13. Lescoat A, Murphy SL, Roofeh D, et al. Considerations for a combined index for limited cutaneous systemic sclerosis to support drug development and improve outcomes. *J Scleroderma Relat Disord* 2021;6(1):66–76.
14. Gerges E, Cauvet A, Schwarz M, et al. Association of serum interferon alpha-2a levels with disease severity and prognosis in systemic sclerosis. *Rheumatology (Oxford)* Published online October 10, 2024. doi:<https://doi.org/10.1093/rheumatology/keae546>
15. Khanna D, Denton CP, Assassi S, et al. A randomised, parallel-group, double-blind, placebo-controlled phase 3 study to Determine the effectiveness of the type I interferon receptor antibody, Anifrolumab, In SYstemic sclerosis: DAISY study design and rationale. *Clin Exp Rheumatol* 2024;42(8):1635–1644.

Associations of Fire Smoke and Other Pollutants With Incident Rheumatoid Arthritis and Rheumatoid Arthritis–Associated Interstitial Lung Disease

Vanessa L. Kronzer,¹  Yangyuna Yang,² Punyasha Roul,² James L. Crooks,³ Cynthia S. Crowson,¹ 
John M. Davis III,¹  Jeffrey A. Sparks,⁴  Jeffrey R. Pierce,⁵ Katelyn O'Dell,⁶ Brian C. Sauer,⁷ 
Grant W. Cannon,⁷  Joshua F. Baker,⁸ Ted R. Mikuls,²  and Bryant R. England² 

Objective. The aim of this study was to determine whether pollutants such as fire smoke–related particulate matter <2.5 μm (PM_{2.5}) are associated with incident rheumatoid arthritis (RA) and RA-associated interstitial lung disease (RA-ILD).

Methods. This patient–control study used Veterans Affairs (VA) data from October 1, 2009, to December 31, 2018. We identified patients with incident RA and RA-ILD using validated algorithms, matching each patient to ≤ 10 controls on age, sex, and VA enrollment year. We obtained pollutants including fire smoke PM_{2.5}, carbon monoxide, nitrogen oxides (NO_x), ozone, overall PM_{2.5}, PM₁₀, and sulfur dioxide (SO₂) at least one year before the index date. We fit conditional logistic regression models to estimate adjusted odds ratios (aORs) with 95% confidence intervals (CIs) for incident RA and RA-ILD, adjusted for confounders.

Results. We identified 9,701 patients with incident RA (mean age 65 years, 86% male), including 531 patients with RA-ILD (mean age 69 years, 91% male), and 68,852 matched controls. Fire smoke PM_{2.5} was not associated with RA (aOR 1.07, 95% CI 0.92–1.23) but was associated with RA-ILD (aOR 1.98, 95% CI 1.08–3.62, per 1 $\mu\text{g}/\text{m}^3$). Increased levels of NO_x were associated with RA (aOR 1.16, 95% CI 1.06–1.27, highest vs lowest quartile). The highest quartiles of ozone (aOR 1.19, 95% CI 1.06–1.34) and PM₁₀ (aOR 1.25, 95% CI 1.10–1.43) were associated with seronegative RA. Carbon monoxide, overall PM_{2.5}, and SO₂ were not, or negatively, associated with RA and RA-ILD.

Conclusion. Increased fire smoke PM_{2.5} was associated with RA-ILD, whereas NO_x, ozone, and PM₁₀ were associated with RA risk. Thus, air pollution may increase the risk of RA and RA-ILD.

INTRODUCTION

Wildfires are reaching record and alarming levels in the United States.^{1,2} Such changes could have large impacts on

human health because increased levels of particulate matter <2.5 μm (PM_{2.5}), the main pollutant in fire smoke, are associated with the onset of diabetes,³ multiple sclerosis,⁴ and Parkinson disease⁵ and all-cause death.⁶ Importantly, several respiratory

The funders had no role in the decision to publish or preparation of this manuscript. The content is solely the responsibility of the authors and does not necessarily represent the official views, positions, or policies of their universities, affiliated academic health care centers, the NIH, the Department of Veterans Affairs (VA), or the US government.

Supported by the Rheumatology Research Foundation Scientist Development Award and National Institute of Arthritis and Musculoskeletal and Skin Diseases, NIH (grant P30-AR-072577 and Value and Evidence in Rheumatology using bioinformatics and advanced analytics Pilot & Feasibility Award to Dr Kronzer); National Aeronautics and Space Administration Health and Air Quality Applied Sciences Team (grant 80NSSC21K0429R to Dr Pierce); and VA Clinical Science Research and Development (grant IK2-CX-002203 to Dr England). Dr Sparks's work was supported by the National Institute of Arthritis and Musculoskeletal and Skin Diseases, NIH (grants R01-AR-080659, R01-AR-077607, P30-AR-070253, and P30-AR-072577); R. Bruce and Joan M. Mickey Research Scholar Fund; and Gordon and Llura Gund Foundation Llura Gund Award. Dr Mikuls's work was supported by the VA Merit Award (grant BX004600), NIH (grant U54-GM-115458), and US Department of Defense (grant PR200793).

¹Vanessa L. Kronzer, MD, MSCI, Cynthia S. Crowson, PhD, John M. Davis III, MD, MS: Mayo Clinic, Rochester, Minnesota; ²Yangyuna Yang, PhD, Punyasha

Roul, MS, Ted R. Mikuls, MD, MSPH, Bryant R. England, MD, PhD: VA Nebraska-Western Iowa Health Care System and University of Nebraska Medical Center, Omaha; ³James L. Crooks, PhD: National Jewish Health, Denver, Colorado; ⁴Jeffrey A. Sparks, MD, MMSc: Brigham and Women's Hospital and Harvard Medical School, Boston, Massachusetts; ⁵Jeffrey R. Pierce, PhD: Colorado State University, Fort Collins; ⁶Katelyn O'Dell, PhD: George Washington University, Washington, District of Columbia; ⁷Brian C. Sauer, PhD, Grant W. Cannon, MD: Salt Lake City VA and University of Utah; ⁸Joshua F. Baker, MD, MSCE: Corporal Michael J. Crescenz VA and University of Pennsylvania, Philadelphia.

Additional supplementary information cited in this article can be found online in the Supporting Information section (<http://onlinelibrary.wiley.com/doi/10.1002/art.43113>).

Author disclosures and graphical abstract are available at <https://onlinelibrary.wiley.com/doi/10.1002/art.43113>.

Address correspondence via email to Vanessa L. Kronzer, MD, MSCI, at kronzer.vanessa@mayo.edu.

Submitted for publication April 9, 2024; accepted in revised form December 18, 2024.

irritants have been found to be associated with increased risk of rheumatoid arthritis (RA), including cigarette smoking,⁷ occupational inhalant exposures,^{8,9} and respiratory tract diseases,^{10,11} especially in the 5 to 10 years before RA onset.¹² Thus, fire smoke may also be a risk factor for RA. Indeed, PM_{2.5} appears to be associated with anti-citrullinated protein antibody (ACPA) production, a hallmark of RA.^{13–15} Some studies of overall PM_{2.5} have shown positive associations with RA^{16–18} and others none.^{19–21} However, none studied fire smoke exposure specifically.

Another important and unresolved question is whether other pollutants like carbon monoxide (CO), nitrogen oxides (NO_x), ozone, PM₁₀, and sulfur dioxide (SO₂) increase the risk of RA. For example, one study showed that NO₂ and SO₂ increase the risk of RA,²² but others have shown no association of NO_x^{19,20,23} or SO₂.^{19,23} Although some studies have suggested CO,^{9,23,24} ozone,^{20,23,24} and PM₁₀ might increase RA risk, these reports studied exposures less than three years before RA onset and/or did not adjust for key confounders like smoking.¹⁷ Finally, although some studies suggest pollutants might increase the risk of interstitial lung abnormalities²⁵ and idiopathic pulmonary fibrosis,²⁶ none have studied the association between pollutants and RA-associated interstitial lung disease (RA-ILD).

To address these gaps, we leveraged national Veterans Affairs (VA) data, the largest integrated health care system in the United States,²⁷ and nationwide pollutant monitoring data from the Environmental Protection Agency (EPA).²⁸ We aimed to determine the associations between fire smoke and other pollutant exposures with the risk of RA and RA-ILD and to identify the timing of any such associations. We hypothesized that increasing levels of fire smoke and other pollutant exposures would be associated with increased risk of both RA and RA-ILD, especially five or more years before RA onset.

PATIENTS AND METHODS

Study population and design. This patient–control study used national VA data, which contain detailed administrative and electronic health data on US veterans enrolled in VA health care.²⁷ The index date for this study was the time of RA diagnosis (or matched date), as indicated by the date fulfilling all components of the RA algorithm. This study received institutional review board approval (00012917; 1619487).

Incident RA and RA-ILD. The primary outcomes for this study were incident RA and RA-ILD. We identified patients with incident RA using a validated algorithm requiring at least two RA codes (International Classification of Diseases, Ninth Revision [ICD-9] 714.0, 714.1, 714.2, and 714.81; and ICD-10 M05.x, M06.x, excluding M06.1, and M06.4), a rheumatologist diagnosis of RA, and either a prescription of a disease-modifying antirheumatic drug (DMARD) or positive rheumatoid factor (RF) or ACPA.²⁹ To ensure incident diagnoses, we also required a one-

year period after VA enrollment with no RA diagnostic codes or DMARD fills. This algorithm has >90% positive predictive value (PPV) for RA by the American College of Rheumatology criteria³⁰ and 85% PPV for classifying incident versus prevalent RA.³¹ Patients with RA were categorized as being seropositive or seronegative based on RF and/or ACPA.

Among these patients with RA, we defined RA-ILD as the presence of two RA-ILD codes at least 30 days apart (ICD-9 515.x, 516.3, 516.8, and 516.9; and ICD-10 J84.1, J84.89, and J84.9) along with either a pulmonologist diagnosis of ILD or procedure codes for a chest computed tomography scan plus either pulmonary function tests or lung biopsy. RA-ILD assessment included data after RA diagnosis. This algorithm has a PPV for RA-ILD of 81%.³²

To ensure all participants could have at least five years of preceding pollutant exposure data, we a priori restricted the analysis to patients with incident RA and RA-ILD with at least five years of preceding address data available. Because address data began October 1, 2009, we included patients with incident RA from October 1, 2014, to the time of extraction of data on patients with RA on December 31, 2018. We also required them to have available PM_{2.5} data because they were the primary exposure of interest for this study. Availability of the other pollutant exposures was not required.

Controls. We matched patients with incident RA to up to ≤10 controls without RA based on year of birth, sex, and VA enrollment year. We did not match on smoking status to avoid introducing selection bias.³³ We required that controls have none of the billing codes for RA mentioned in the Incident RA and RA-ILD section. Like patients, we required they have at least five years preceding address data and available PM_{2.5} data for pollutant exposure assessment.

Fire smoke PM_{2.5}, other pollutants, and covariates.

Our primary exposure was 24-hour average fire smoke PM_{2.5} exposure (in micrograms per meter cubed). This fire smoke exposure was a fused product of ground pollutant monitoring from the EPA Air Quality System²⁸ and satellite-based smoke plume imagery from the National Oceanic and Atmospheric Administration Hazard Mapping System.³⁴ By overlaying these two data sources, this fused product produces daily grids of smoke-related PM_{2.5}, nonsmoke PM_{2.5}, and overall total PM_{2.5} over the contiguous United States at a 15 × 15 km resolution, starting in 2006.³⁴ We interpolated these grids with address data from the National Change of Address Database maintained by the US Postal Service, which are updated quarterly.

We obtained secondary pollutants of interest including 1-hour maximum (max) CO, 1-hour max NO_x, 8-hour max ozone, 24-hour average PM₁₀, and 1-hour max SO₂ interpolated from the EPA ground pollutant monitoring above²⁸ using a previously validated method.^{34,35} Specifically, we assigned daily

concentrations of each pollutant to Zip Code Tabulation Areas (ZCTAs) using the median of the measurements at all monitors within the ZCTAs and within 50 km of the ZCTA centroid.²⁸ We chose 50 km to minimize missing data. For all pollutants, we categorized mean exposure into quartiles for ease of interpretation, along with deciles in a post hoc sensitivity analysis. Due to the narrow range of exposures including PM_{2.5}, we also reported results for continuous values.

To minimize the potential for reverse causation, in which people may alter air exposures between RA symptom onset and clinical diagnosis, we included pollutant exposure measurements occurring at least one year before index date. To identify the timing of any potential associations, we also divided this pollutant exposure into time windows (over one to three, over three to five, and over five years before the index date). We took the mean of all the daily pollutant reads that were available within each time window. We obtained the following covariates from the VA corporate data warehouse: age at index date, self-reported sex (male vs female), VA enrollment year, duration of fire smoke pollutant exposure data

before index date (continuous), race and ethnicity (Asian, Black, Hispanic White, White non-Hispanic, or unknown), body mass index nearest preceding index date (<20, 20–24.9, 25–29.9, 30–34.9, 35–39.9, or ≥40 kg/m²), and smoking status at index date (current, former, or never).

Statistical analysis. We performed conditional logistic regression models for each pollutant exposure to obtain adjusted odds ratios (aORs) with 95% confidence intervals (CIs) for RA (with subgroup analysis by RA serostatus) and RA-ILD, adjusting for the above covariates. We also performed stratified analyses by exposure time windows (more than one to three, more than three to five, and more than five years before index date). For sensitivity analyses, we stratified by geographic region (Midwest, Northeast, South, and West) and smoking status (never vs ever) using unconditional logistic regression because patients with RA and controls were no longer matched. Second, we performed multiplicative interactions between fire smoke PM_{2.5} and age (>65 vs ≤65 years), sex, race and ethnicity, and smoking status

Table 1. Characteristics of patients with incident RA and matched controls*

Characteristic	Patients with RA (n = 9,701), n (%)	Patients with RA-ILD (n = 531), n (%)	Controls (n = 68,851), n (%)
Age at index, mean (±SD), y ^a	65 (±11)	69 (±9)	63 (±11)
Male ^a	8,292 (86)	484 (91)	57,043 (83)
VA enrollment period ^a			
1997–2001	5,548 (57)	329 (62)	37,347 (54)
2002–2006	2,785 (29)	147 (28)	21,160 (31)
2007–2011	1,306 (14)	52 (10)	10,072 (15)
2012–2016	62 (0.6)	3 (0.6)	272 (0.4)
Time of PM _{2.5} data before index, mean (±SD), y	7.0 (±1.4)	6.8 (±1.4)	6.9 (±1.4)
Race and ethnicity			
Asian/other	321 (3.3)	14 (3)	1930 (2.8)
Black	1,825 (19)	99 (19)	13,821 (20)
Hispanic White	335 (3.5)	25 (5)	1,865 (2.7)
White non-Hispanic	6,735 (69)	374 (70)	41,008 (60)
Unknown/missing	485 (5)	19 (4)	10,227 (15)
BMI at index, kg/m ²			
<20	126 (1.3)	3 (0.6)	1,061 (1.5)
20 to <25	1,506 (16)	87 (16)	10,526 (15)
25 to <30	3,523 (36)	211 (40)	24,418 (36)
30 to <35	2,902 (30)	157 (30)	17,706 (26)
35 to <40	1,158 (12)	54 (10)	7,103 (10)
≥40	485 (5)	19 (4)	3,220 (4.7)
Missing	1 (<1)	–	4,817 (7)
Smoking status at index			
Never	1,317 (14)	49 (9)	13,516 (20)
Former	2,858 (30)	143 (27)	16,169 (24)
Current	5,439 (56)	332 (63)	31,664 (46)
Unknown/missing	87 (0.9)	7 (1.3)	7,502 (11)
Geographic region			
Midwest	1,975 (20)	104 (20)	13,747 (20)
Northeast	1,503 (16)	82 (15)	6,956 (10)
South	4,183 (43)	240 (45)	33,825 (49)
West	2,029 (21)	104 (20)	14,211 (21)
Unknown	10 (0.1)	1 (0.2)	104 (0.2)

* BMI, body mass index; ILD, interstitial lung disease; PM_{2.5}, particulate matter <2.5 μm; RA, rheumatoid arthritis; VA, Veterans Affairs.

^a The indicated factors were matched.

(ever vs never) for risk of RA. Third, we performed a post hoc analysis categorizing PM_{2.5} exposure data into deciles.

Throughout this study, any individuals missing exposure or covariate data were excluded from that model (ie, complete patient analysis). To examine the effects of missing covariates on our results, we performed a sensitivity analysis with multiple imputation for missing covariates using fully conditional specification with 10 imputed datasets. We used a significance threshold of two-sided alpha of 0.05. We outlined all analyses in a prespecified protocol and performed analyses using Stata version 18 (StataCorp LLC).

RESULTS

Patient characteristics. We identified 30,146 patients with incident RA (Supplementary Figure 1). Of these, 9,701 patients with incident RA met study eligibility criteria (mean age 65 years, 86% male) and were matched to 68,851 controls. Within these, 531 also met criteria as patients with RA-ILD

(mean age 69 years, 91% male; Table 1). Median time between RA and RA-ILD was 0.0 years (interquartile range −2.1 to 1.4). Of patients with RA with serological data, 63% were seropositive, whereas 80% of patients with RA-ILD were seropositive.

Pollutants and incident RA. The mean duration of PM_{2.5} exposure data available for this study was 7.0 years in patients with RA and 6.9 years in controls (Table 1), with a range of 4.3 to 9.0 years. Mean pollutant levels did not show large absolute differences between patients with RA and controls (Supplementary Table 1). Fire smoke PM_{2.5} was not associated with RA overall (aOR 1.07, 95% CI 0.92–1.23, per 1 µg/m³; Table 2). Post hoc analyses showed that the second and tenth deciles of exposure were associated with higher RA risk (Supplementary Table 2). Increased NOx levels were associated with an increased risk of RA (aOR 1.16, 95% CI 1.06–1.27 for highest vs lowest quartile; Table 2). In addition, the highest quartiles of ozone (aOR 1.19, 95% CI 1.06–1.34) and PM₁₀ (aOR 1.25, 95% CI 1.10–1.43) exposure were associated with patients with RA who were

Table 2. Association between preceding fire smoke and other pollutant exposures and incident RA*

Pollutant	Overall RA (n = 9,701), continuous exposure, adjusted OR (95% CI) ^{a,b}	Overall RA (n = 9,701), quartiled exposure, adjusted OR (95% CI) ^a	Seropositive RA (n = 5,588), quartiled exposure, adjusted OR (95% CI) ^a	Seronegative RA (n = 3,347), quartiled exposure, adjusted OR (95% CI) ^a
Fire smoke PM _{2.5} , µg/m ³	1.07 (0.92–1.23)	1.00 (ref)	1.00 (ref)	1.00 (ref)
Quartile 2	–	0.95 (0.89–1.02)	0.99 (0.90–1.08)	0.90 (0.80–1.00)
Quartile 3	–	0.91 (0.85–0.97)	0.98 (0.90–1.07)	0.82 (0.73–0.92)
Quartile 4	–	1.01 (0.95–1.08)	1.08 (0.99–1.18)	0.93 (0.83–1.04)
CO, ppm	0.78 (0.67–0.91)	1.00 (ref)	1.00 (ref)	1.00 (ref)
Quartile 2	–	0.92 (0.85–0.99)	0.91 (0.81–1.01)	0.88 (0.77–1.02)
Quartile 3	–	0.84 (0.77–0.91)	0.90 (0.80–0.99)	0.77 (0.66–0.89)
Quartile 4	–	0.81 (0.74–0.88)	0.78 (0.70–0.88)	0.85 (0.73–0.98)
NOx, ppb	1.02 (1.00–1.03)	1.00 (ref)	1.00 (ref)	1.00 (ref)
Quartile 2	–	1.18 (1.08–1.29)	1.17 (1.04–1.31)	1.17 (1.01–1.36)
Quartile 3	–	1.08 (0.99–1.18)	1.14 (1.01–1.28)	0.98 (0.84–1.14)
Quartile 4	–	1.16 (1.06–1.27)	1.16 (1.03–1.31)	1.15 (0.99–1.34)
O ₃ , ppm	0.97 (0.91–1.03)	1.00 (ref)	1.00 (ref)	1.00 (ref)
Quartile 2	–	0.99 (0.93–1.06)	0.97 (0.89–1.06)	1.05 (0.94–1.18)
Quartile 3	–	0.89 (0.83–0.95)	0.85 (0.78–0.93)	0.92 (0.82–1.04)
Quartile 4	–	0.97 (0.91–1.04)	0.90 (0.83–0.99)	1.19 (1.06–1.34)
PM _{2.5} , µg/m ³	0.94 (0.93–0.96)	1.00 (ref)	1.00 (ref)	1.00 (ref)
Quartile 2	–	0.90 (0.85–0.96)	0.94 (0.86–1.02)	0.83 (0.75–0.92)
Quartile 3	–	0.81 (0.76–0.86)	0.81 (0.75–0.89)	0.77 (0.69–0.86)
Quartile 4	–	0.72 (0.68–0.77)	0.76 (0.70–0.83)	0.65 (0.58–0.73)
PM ₁₀ , µg/m ³	1.03 (0.98–1.08)	1.00 (ref)	1.00 (ref)	1.00 (ref)
Quartile 2	–	0.83 (0.77–0.89)	0.78 (0.71–0.87)	0.99 (0.87–1.14)
Quartile 3	–	0.88 (0.81–0.95)	0.83 (0.75–0.91)	1.05 (0.92–1.19)
Quartile 4	–	1.02 (0.94–1.10)	0.96 (0.87–1.06)	1.25 (1.10–1.43)
SO ₂ , ppb	0.98 (0.97–0.98)	1.00 (ref)	1.00 (ref)	1.00 (ref)
Quartile 2	–	0.96 (0.89–1.04)	0.99 (0.90–1.10)	0.95 (0.83–1.08)
Quartile 3	–	1.01 (0.94–1.10)	1.02 (0.92–1.13)	1.01 (0.89–1.16)
Quartile 4	–	0.78 (0.72–0.85)	0.80 (0.71–0.89)	0.77 (0.67–0.88)

* Bold values indicate $P < 0.05$. CI, confidence interval; CO, carbon monoxide; NOx, nitrogen oxides; O₃, ozone; OR, odds ratio; PM_{2.5}, particulate matter <2.5 µm; ppb, parts per billion; ppm, parts per million; RA, rheumatoid arthritis; ref, reference; SO₂, sulfur dioxide.

^a The ref group was individuals with the lowest quartile of pollutant exposure. The patients were matched with controls on age, sex, and enrollment while adjusting for duration of pollutant exposure data, race and ethnicity, body mass index, and smoking status.

^b Values are per 1 unit exposure for all except O₃ (0.01 units) and NOx and PM₁₀ (10 units).

seronegative, but not seropositive, when compared to the lowest quartile. In contrast, CO (aOR 0.78, 95% CI 0.67–0.91, per 1 part per million), overall PM_{2.5} (aOR 0.94, 95% CI 0.93–0.96, per 10 µg/m³), and SO₂ (aOR 0.98, 95% CI 0.97–0.98, per 1 part per billion) were negatively associated with RA risk.

Pollutants and RA-ILD. Higher fire smoke PM_{2.5} was significantly associated with RA-ILD (aOR 1.98, 95% CI 1.08–3.62, per 1 µg/m³; Table 3). Post hoc analyses showed that fire smoke PM_{2.5} concentrations of 0.28 µg/m³ and higher seemed to drive this elevated risk (Supplementary Table 2). Except for the highest quartile of CO being negatively associated, no other pollutants were associated with RA-ILD.

Pollutant timing and RA. When stratifying by pollutant timing, we found fire smoke PM_{2.5} exposure to be most associated with RA in the one to three years (aOR 1.12, 95% CI 1.03–1.23, per 1 µg/m³) and three to five years (aOR 1.13, 95% CI 1.02–1.26, per 1 µg/m³) before RA index date (Figure 1; Table 4). Higher smoke PM_{2.5} exposure more than five years before RA diagnosis was

negatively associated with RA risk. In contrast, NOx showed the strongest point estimates in the three to five years and more than five years before RA onset. Finally, PM₁₀ exposure was most strongly associated with RA in the three to five years before RA onset (aOR 1.08, 95% CI 1.03–1.14 for highest vs lowest quartile).

Sensitivity analyses. Sensitivity analyses stratifying by geographic region showed NOx had the highest OR for RA in the West (OR 1.50, 95% CI 1.21–1.85 for highest vs lowest quartile; Supplementary Table 3). Restricting analyses to never-smokers showed no meaningful differences in point estimates (Supplementary Table 3). We also found no evidence of interactions between fire smoke PM_{2.5} and age, sex, race and ethnicity, and smoking status on risk of RA (*P* > 0.3 for each, data not shown). Regarding missing covariate data, 576 patients with RA (6%) and 13,716 controls (20%) were missing at least one covariate. However, results for each of the seven pollutants did not differ after performing multiple imputation for missing covariates (data not shown). Of note, 7,282 of study participants (9%) were

Table 3. Association between preceding fire smoke and other pollutant exposures and RA-ILD*

Pollutant	Patients with RA-ILD (n = 531), mean concentration (±SD)	Controls (n = 3,605), mean concentration (±SD)	Continuous exposure in patients with RA-ILD, adjusted OR (95% CI) ^{a,b}	Quartiled exposure in patients with RA-ILD, adjusted OR (95% CI) ^a
Fire smoke PM _{2.5} , µg/m ³	0.27 (±0.15)	0.26 (±0.14)	1.98 (1.08–3.62)	1.00 (ref)
Quartile 2	–	–	–	1.16 (0.87–1.55)
Quartile 3	–	–	–	1.06 (0.79–1.43)
Quartile 4	–	–	–	1.45 (1.09–1.93)
CO, ppm	0.57 (±0.22)	0.59 (±0.22)	0.54 (0.27–1.09)	1.00 (ref)
Quartile 2	–	–	–	1.05 (0.72–1.52)
Quartile 3	–	–	–	0.94 (0.63–1.39)
Quartile 4	–	–	–	0.59 (0.39–0.89)
NOx, ppb	43.2 (±22.6)	43.2 (±24.7)	0.99 (0.93–1.05)	1.00 (ref)
Quartile 2	–	–	–	1.20 (0.92–1.77)
Quartile 3	–	–	–	0.97 (0.64–1.47)
Quartile 4	–	–	–	1.03 (0.70–1.52)
O ₃ , ppm	0.04 (±0.00)	0.04 (±0.00)	0.90 (0.67–1.19)	1.00 (ref)
Quartile 2	–	–	–	0.95 (0.71–1.27)
Quartile 3	–	–	–	0.89 (0.66–1.22)
Quartile 4	–	–	–	0.89 (0.65–1.21)
PM _{2.5} , µg/m ³	8.96 (±1.62)	8.99 (±1.58)	0.99 (0.93–1.06)	1.00 (ref)
Quartile 2	–	–	–	1.12 (0.85–1.47)
Quartile 3	–	–	–	0.97 (0.72–1.30)
Quartile 4	–	–	–	0.94 (0.70–1.25)
PM ₁₀ , µg/m ³	18.7 (±5.0)	18.8 (±5.3)	1.04 (0.92–1.32)	1.00 (ref)
Quartile 2	–	–	–	0.78 (0.56–1.10)
Quartile 3	–	–	–	0.94 (0.67–1.32)
Quartile 4	–	–	–	1.07 (0.77–1.51)
SO ₂ , ppb	3.48 (±3.52)	3.93 (±4.39)	0.97 (0.93–1.00)	1.00 (ref)
Quartile 2	–	–	–	1.11 (0.77–1.60)
Quartile 3	–	–	–	1.29 (0.90–1.84)
Quartile 4	–	–	–	0.86 (0.58–1.26)

* Bold values indicate *P* < 0.05. CI, confidence interval; CO, carbon monoxide; ILD, interstitial lung disease; NOx, nitrogen oxides; O₃, ozone; OR, odds ratio; PM_{2.5}, particulate matter <2.5 µm; ppb, parts per billion; ppm, parts per million; RA, rheumatoid arthritis; ref, reference; SO₂, sulfur dioxide.

^a The ref group was individuals with the lowest quartile of pollutant exposure. The patients were matched with controls on age, sex, and enrollment while adjusting for duration of pollutant exposure data, race and ethnicity, body mass index, and smoking status.

^b Values are per 1 unit exposure for all except O₃ (0.01 units) and NOx and PM₁₀ (10 units).

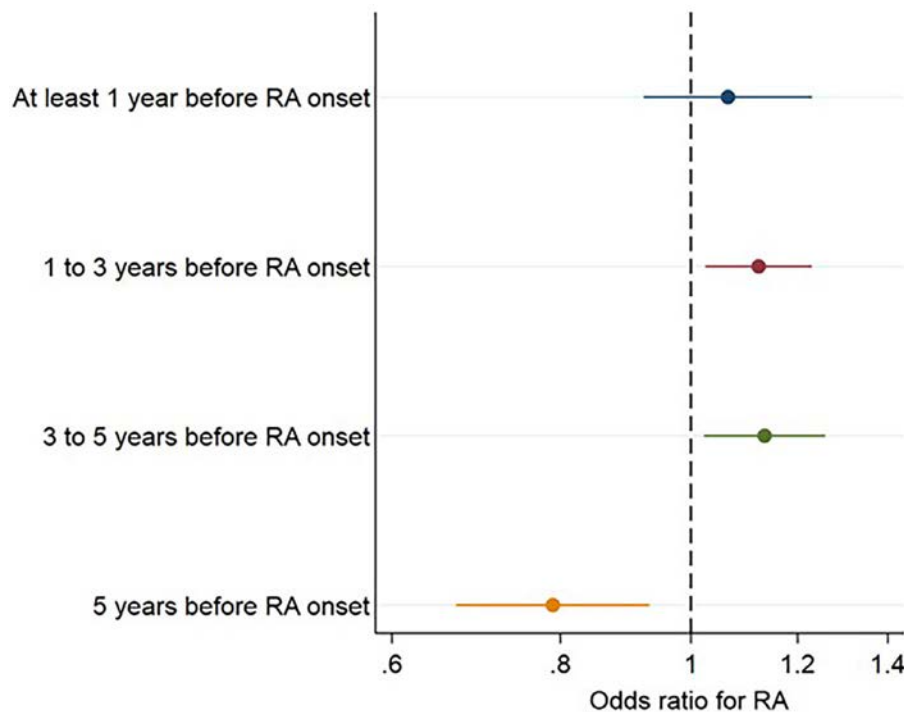


Figure 1. Forest plot depicting associations of fire smoke $PM_{2.5}$ with risk of RA by exposure time period. Models are per $1\text{-}\mu\text{g}/\text{m}^3$ increase in $PM_{2.5}$ and adjusted for age, sex, enrollment, duration of pollutant exposure data, race and ethnicity, body mass index, and smoking status. $PM_{2.5}$, particulate matter $<2.5\text{ }\mu\text{m}$; RA, rheumatoid arthritis.

missing all fire smoke $PM_{2.5}$ exposure data, and 25,984 (33%) were missing at least one of the other five pollutant exposures in this study. Participants missing all fire smoke $PM_{2.5}$ exposure data were more likely to be controls and live in the West (Supplementary Table 4).

DISCUSSION

This large patient-control study using national VA data and nationwide pollutant monitoring found that high fire smoke $PM_{2.5}$ exposure was associated with RA-ILD, along with incident RA one to five years later. NO_x, a pollutant generated largely from fossil fuel combustion,³⁶ was also associated with incident RA, and ozone and PM_{10} were associated with incident seronegative RA. Several other pollutants including CO, overall $PM_{2.5}$, and SO₂ were not, or negatively, associated with incident RA and RA-ILD. Overall, these findings add to the growing body of literature on inhalant exposures and RA risk and suggest that reducing fire smoke and fossil fuel emissions may have benefits for RA and RA-ILD prevention. They also highlight the need for more robust infrastructure for studying the impact of pollutants on health in the United States.

The first key finding from this study was that high fire smoke $PM_{2.5}$ exposure was associated with incident RA-ILD. No prior studies have examined fire smoke $PM_{2.5}$ and RA or RA-ILD risk,

though others have found an association between overall $PM_{2.5}$ and RA.^{16–18} Our study did not show a significant association between fire smoke $PM_{2.5}$ and overall RA except in stratified analyses in the one to five years before RA onset. The association between $PM_{2.5}$ and RA both with and without ILD has strong biologic rationale because both $PM_{2.5}$ ^{13–15} and wood-fire smoke³⁷ have previously been associated with ACPA development to a higher degree than cigarette smoke. Furthermore, elemental carbon from $PM_{2.5}$ is associated with increased risk of interstitial lung abnormalities.²⁵ Importantly, the observed association between fire smoke $PM_{2.5}$ and RA-ILD occurred even despite the study period not including recent record-breaking wildfire years.^{38,39} Therefore, future studies are needed to determine whether higher levels of fire smoke $PM_{2.5}$ exposure have an even stronger effect.

The second key finding from this study was that high levels of other pollutants such as NO_x were associated with incident RA overall, whereas ozone and PM_{10} were associated with incident seronegative RA. Prior literature on the association between NO_x and RA has mostly shown a positive association.^{18,21,22,24} Studies showing no association with RA had lower NO_x levels than ours and these other studies,^{19,20,23} perhaps explaining this discrepancy. Indeed, even the third quartile of NO_x exposure was not associated with RA in our study. The three prior studies of ozone and RA all showed a positive association as well.^{20,23,24} Only one study has shown an association between PM_{10} and RA,¹⁷ whereas most show no association.^{16,18,19,22–24}

Table 4. Association between the timing of preceding pollutant exposures and incident RA*

Pollutant/years before RA	Continuous exposure for patients with RA, adjusted OR (95% CI) ^{a,b}			Quartiled exposure for patients with RA, adjusted OR (95% CI) ^a		
	More than one to three years	More than three to five years	More than five years	More than one to three years	More than three to five years	More than five years
Fire smoke	1.12 (1.03–1.23)	1.13 (1.02–1.26)	0.79 (0.67–0.93)	1.00 (ref)	1.00 (ref)	1.00 (ref)
PM _{2.5} , µg/m ³						
Quartile 2	–	–	–	1.26 (1.18–1.35)	1.19 (1.12–1.28)	1.06 (0.98–1.15)
Quartile 3	–	–	–	1.21 (1.13–1.30)	1.11 (1.03–1.19)	1.06 (0.97–1.16)
Quartile 4	–	–	–	1.18 (1.10–1.27)	1.12 (1.04–1.20)	0.92 (0.84–1.00)
CO, ppm	0.72 (0.60–0.86)	0.73 (0.62–0.86)	0.80 (0.69–0.93)	1.00 (ref)	1.00 (ref)	1.00 (ref)
Quartile 2	–	–	–	0.99 (0.90–1.08)	0.96 (0.88–1.05)	1.00 (0.91–1.10)
Quartile 3	–	–	–	0.86 (0.78–0.94)	0.85 (0.78–0.94)	0.80 (0.72–0.88)
Quartile 4	–	–	–	0.81 (0.74–0.89)	0.83 (0.76–0.91)	0.82 (0.74–0.90)
NOx, ppb	1.01 (0.99–1.02)	1.02 (1.00–1.04)	1.02 (1.01–1.04)	1.00 (ref)	1.00 (ref)	1.00 (ref)
Quartile 2	–	–	–	1.13 (1.03–1.24)	1.17 (1.06–1.28)	1.31 (1.18–1.46)
Quartile 3	–	–	–	1.11 (1.01–1.21)	1.03 (0.93–1.14)	1.08 (0.97–1.20)
Quartile 4	–	–	–	1.16 (1.06–1.28)	1.17 (1.06–1.29)	1.27 (1.14–1.41)
O ₃ , ppm	1.02 (0.96–1.08)	0.99 (0.94–1.05)	0.94 (0.89–1.00)	1.00 (ref)	1.00 (ref)	1.00 (ref)
Quartile 2	–	–	–	1.04 (0.97–1.12)	1.01 (0.95–1.09)	0.96 (0.89–1.03)
Quartile 3	–	–	–	0.98 (0.92–1.05)	0.96 (0.90–1.03)	0.93 (0.85–1.00)
Quartile 4	–	–	–	1.01 (0.94–1.09)	1.00 (0.93–1.08)	0.92 (0.85–1.00)
PM _{2.5} , µg/m ³	0.94 (0.92–0.95)	0.96 (0.94–0.97)	0.95 (0.94–0.97)	1.00 (ref)	1.00 (ref)	1.00 (ref)
Quartile 2	–	–	–	0.87 (0.81–0.92)	0.94 (0.89–1.00)	0.94 (0.88–1.00)
Quartile 3	–	–	–	0.75 (0.70–0.80)	0.81 (0.76–0.87)	0.84 (0.79–0.90)
Quartile 4	–	–	–	0.72 (0.67–0.77)	0.81 (0.76–0.86)	0.72 (0.67–0.78)
PM ₁₀ , µg/m ³	1.04 (0.98–1.09)	1.08 (1.03–1.14)	1.00 (0.94–1.06)	1.00 (ref)	1.00 (ref)	1.00 (ref)
Quartile 2	–	–	–	0.84 (0.78–0.92)	0.84 (0.77–0.91)	0.88 (0.81–0.95)
Quartile 3	–	–	–	0.98 (0.90–1.06)	0.97 (0.90–1.05)	0.78 (0.71–0.85)
Quartile 4	–	–	–	1.03 (0.95–1.12)	1.11 (1.03–1.21)	0.98 (0.90–1.07)
SO ₂ , ppb	0.97 (0.96–0.98)	0.98 (0.97–0.98)	0.99 (0.98–0.99)	1.00 (ref)	1.00 (ref)	1.00 (ref)
Quartile 2	–	–	–	0.94 (0.87–1.02)	0.96 (0.88–1.05)	1.02 (0.93–1.11)
Quartile 3	–	–	–	1.01 (0.93–1.10)	1.11 (1.02–1.20)	1.00 (0.92–1.10)
Quartile 4	–	–	–	0.80 (0.73–0.87)	0.83 (0.76–0.90)	0.81 (0.73–0.89)

* Bolded values are statistically significant. CI, confidence interval; CO, carbon monoxide; NOx, nitrogen oxides; O₃, ozone; OR, odds ratio; PM_{2.5}, particulate matter <2.5 µm; ppb, parts per billion; ppm, parts per million; RA, rheumatoid arthritis; ref, reference; SO₂, sulfur dioxide.

^a The ref group was individuals with the lowest quartile of pollutant exposure. The patients were matched with controls on age, sex, and enrollment while adjusting for duration of pollutant exposure data, race and ethnicity, body mass index, and smoking status.

^b Values are per 1 unit exposure for all except O₃ (0.01 units) and NOx and PM₁₀ (10 units).

Importantly, the associations we observed for ozone and PM₁₀ were only present for seronegative RA. However, this association of ozone and PM₁₀ with seronegative RA risk is consistent with prior links between respiratory tract diseases and seronegative RA onset.¹² The association of so many respiratory irritants with RA onset suggests that respiratory irritation itself, not specific irritants, leads to RA onset. Thus, many diverse forms of pollution may be harmful.

Although the above associations between fire smoke and RA-ILD and NOx and RA were modest in size, small effects can translate into large health effects on a population level. For example, taking into account the incidence of RA-ILD in the United States⁴⁰ and the effect sizes observed in this study, halving fire smoke PM_{2.5} exposure would correspond to 876 fewer patients with RA-ILD in the United States each year. Similarly, halving NOx exposure would be associated with 1,385 fewer patients with RA in the United States each year.⁴¹ Thus, small pollutant reductions can have massive health implications.

Regarding the timing of pollutant exposures, we observed that fire smoke PM_{2.5} was most strongly associated with RA in the one to five years before the date of RA diagnosis, whereas NOx exposure more than three years and PM₁₀ exposure three to five years before RA diagnosis demonstrated the highest risk. The longer time window for NOx was also previously observed in a population-based study in Sweden.²² The association with more recent fire smoke exposures contrasted with our hypothesis that associations would be strong more than five years before diagnosis. This may be a result of reverse causation or detection bias. Alternatively, fire smoke may be an environmental trigger that has a more immediate effect on increasing risk. For example, previous studies with short follow-up also showed PM_{2.5} to be associated with RA^{16,17} and RA flare.⁴² Future mechanistic studies could help distinguish whether fire smoke triggers initial RA-related autoimmunity itself or drives later downstream inflammatory processes such as epitope spreading.

The other pollutants studied including CO, overall PM_{2.5}, the third quartile of fire smoke PM_{2.5}, and SO₂ were not associated, or even inversely associated, with RA and RA-ILD. One reason for the negative PM_{2.5} results could be the elevated point estimates starting in the second decile. Another reason could be that prior studies showing an association between overall PM_{2.5} and RA^{16–18} had higher levels than ours and others showing no association.^{20,21} Although ours and some prior studies have not observed an association between SO₂ and RA,^{19,23} this study and the others did not include exposure data >10 years before RA onset, when it was previously found to be associated.²² However, given the lack of reported protective associations in prior literature and known inflammatory nature of these compounds,^{43–45} these “protective” associations are likely spurious. We speculate they may have resulted from selection bias due to the nonrandom missingness of pollutant data, especially for the nonfire smoke pollutants, which had higher missingness and wider grids. These inverse associations for other pollutants raise the question of whether the observed positive associations for fire smoke PM_{2.5} and NO_x are underestimated due to a similar underlying bias. Regardless, these inconsistencies highlight the need for more robust monitoring systems in the United States for a more accurate assessment of the connection between pollutants and human health.

Strengths of this study include using the largest available integrated health data system in the United States, robust data linkages, and longer duration of pollutant exposure history compared to previous studies. There are also limitations. Perhaps most importantly, selection bias, for example due to increased missing data in controls and individuals from rural areas, may have biased results, creating potentially spurious protective associations we observed for some pollutants. Results may not generalize well to other populations because the VA population has an overrepresentation of male sex and smoking history, which likely impact inhalant exposures and RA onset.^{8,9,22} The use of administrative algorithms for RA and RA-ILD likely resulted in misclassification of outcomes, though this would also be anticipated to bias results toward the null. Misclassification of pollutant exposures may have biased results, especially due to sparse monitoring in rural areas, using monitors up to 50 km away for nonfire smoke pollutants and relying on quarterly postal address data that do not account for travel. The greater frequency of missing covariate data in controls may have resulted in selection bias, though imputed results showed minimal differences. We were not able to adjust for potential confounders such as socioeconomic status,²² season,⁴⁶ occupational exposures⁹ including burn pits,⁸ or genetics.⁹ We chose not to adjust for certain respiratory diseases such as asthma or chronic obstructive pulmonary disease because such diseases may mediate the association between pollutants and RA.¹¹ Results may have been due to chance due to multiple testing. Sensitivity analyses by geographic region and smoking status could be biased due to the unmatched, unconditional model design. Finally, this study did not capture recent high fire smoke years

(2020–2023) or pollutant exposure data >10 years before RA diagnosis, in which certain pollutants have been most strongly associated with RA.²²

In summary, greater fire smoke PM_{2.5} exposure was associated with RA-ILD and RA in the subsequent one to five years. Fossil fuel–related NO_x was also associated with incident RA, though several other pollutants were not, or negatively, associated with RA. Given the potential sources of bias with current monitoring systems, these findings spark a call to action to develop more comprehensive monitoring systems in the United States. Confirmation of these findings would suggest that addressing wildfire smoke and fossil fuel emissions may have large-scale population-level health benefits by reducing the risk of RA and RA-ILD.

ACKNOWLEDGMENTS

We thank Alexander Maas for the inspiration and Emily Fischer and Bonne Ford for their important contributions to the fire smoke algorithm necessary to conduct this project.

AUTHOR CONTRIBUTIONS











All authors contributed to at least one of the following manuscript preparation roles: conceptualization AND/OR methodology, software, investigation, formal analysis, data curation, visualization, and validation AND drafting or reviewing/editing the final draft. As corresponding author, Dr Kronzer confirms that all authors have provided the final approval of the version to be published, and takes responsibility for the affirmations regarding article submission (eg, not under consideration by another journal), the integrity of the data presented, and the statements regarding compliance with institutional review board/Declaration of Helsinki requirements.

REFERENCES

1. Climate change indicators: wildfires. US Environmental Protection Agency. Updated January 14, 2025. Accessed November 1, 2023. <https://www.epa.gov/climate-indicators/climate-change-indicators-wildfires>
2. Westerling AL. Increasing western US forest wildfire activity: sensitivity to changes in the timing of spring. *Philos Trans R Soc Lond B Biol Sci* 2016;371:20150178. Erratum in: *Philos Trans R Soc Lond B Biol Sci* 2016;371:20160373.
3. Sørensen M, Poulsen AH, Hvidtfeldt UA, et al. Exposure to source-specific air pollution and risk for type 2 diabetes: a nationwide study covering Denmark. *Int J Epidemiol* 2022;51:1219–1229.
4. Bergamaschi R, Monti MC, Trivelli L, et al. PM_{2.5} exposure as a risk factor for multiple sclerosis. An ecological study with a Bayesian mapping approach. *Environ Sci Pollut Res Int* 2021;28:2804–2809.
5. Jo S, Kim YJ, Park KW, et al. Association of NO₂ and other air pollution exposures with the risk of Parkinson disease. *JAMA Neurol* 2021;78:800–808.
6. Faustini A, Rapp R, Forastiere F. Nitrogen dioxide and mortality: review and meta-analysis of long-term studies. *Eur Respir J* 2014;44:744–753.
7. Di Giuseppe D, Discacciati A, Orsini N, et al. Cigarette smoking and risk of rheumatoid arthritis: a dose-response meta-analysis. *Arthritis Res Ther* 2014;16:R61.

8. Ebel AV, Lutt G, Poole JA, et al. Association of agricultural, occupational, and military inhalants with autoantibodies and disease features in US veterans with rheumatoid arthritis. *Arthritis Rheumatol* 2021;73:392–400.
9. Tang B, Liu Q, Ilar A, et al. Occupational inhalable agents constitute major risk factors for rheumatoid arthritis, particularly in the context of genetic predisposition and smoking. *Ann Rheum Dis* 2023;82:316–323.
10. Kronzer VL, Huang W, Zaccardelli A, et al. Association of sinusitis and upper respiratory tract diseases with incident rheumatoid arthritis: a case-control study. *J Rheumatol* 2022;49:358–364.
11. Kronzer VL, Westerlind H, Alfredsson L, et al. Respiratory diseases as risk factors for seropositive and seronegative rheumatoid arthritis and in relation to smoking. *Arthritis Rheumatol* 2021;73:61–68.
12. Kronzer VL, Huang W, Crowson CS, et al. Timing of sinusitis and other respiratory tract diseases and risk of rheumatoid arthritis. *Semin Arthritis Rheum* 2022;52:151937.
13. Zhao N, Smargiassi A, Hatzopoulou M, et al. Long-term exposure to a mixture of industrial SO₂, NO₂, and PM_{2.5} and anti-citrullinated protein antibody positivity. *Environ Health* 2020;19:86.
14. Alex AM, Kunkel G, Sayles H, et al. Exposure to ambient air pollution and autoantibody status in rheumatoid arthritis. *Clin Rheumatol* 2020;39:761–768.
15. Bernatsky S, Smargiassi A, Joseph L, et al. Industrial air emissions, and proximity to major industrial emitters, are associated with anti-citrullinated protein antibodies. *Environ Res* 2017;157:60–63.
16. Park JS, Choi S, Kim K, et al. Association of particulate matter with autoimmune rheumatic diseases among adults in South Korea. *Rheumatology (Oxford)* 2021;60:5117–5126.
17. Adami G, Pontalti M, Cattani G, et al. Association between long-term exposure to air pollution and immune-mediated diseases: a population-based cohort study. *RMD Open* 2022;8:e002055.
18. Zhang J, Fang XY, Wu J, et al. Association of combined exposure to ambient air pollutants, genetic risk, and incident rheumatoid arthritis: a prospective cohort study in the UK Biobank. *Environ Health Perspect* 2023;131:37008.
19. Hart JE, Källberg H, Laden F, et al. Ambient air pollution exposures and risk of rheumatoid arthritis. *Arthritis Care Res (Hoboken)* 2013; 65:1190–1196.
20. De Roos AJ, Koehoorn M, Tamburic L, et al. Proximity to traffic, ambient air pollution, and community noise in relation to incident rheumatoid arthritis. *Environ Health Perspect* 2014;122:1075–1080.
21. Chang KH, Hsu CC, Muo CH, et al. Air pollution exposure increases the risk of rheumatoid arthritis: a longitudinal and nationwide study. *Environ Int* 2016;94:495–499.
22. Hart JE, Källberg H, Laden F, et al. Ambient air pollution exposures and risk of rheumatoid arthritis: results from the Swedish EIRA case-control study. *Ann Rheum Dis* 2013;72:888–894.
23. Shin J, Lee J, Lee J, et al. Association between exposure to ambient air pollution and rheumatoid arthritis in adults. *Int J Environ Res Public Health* 2019;16:1227.
24. Jung CR, Hsieh HY, Hwang BF. Air pollution as a potential determinant of rheumatoid arthritis: a population-based cohort study in Taiwan. *Epidemiology* 2017;28(Suppl 1):S54–S59.
25. Rice MB, Li W, Schwartz J, et al. Ambient air pollution exposure and risk and progression of interstitial lung abnormalities: the Framingham Heart Study. *Thorax* 2019;74:1063–1069.
26. Conti S, Harari S, Caminati A, et al. The association between air pollution and the incidence of idiopathic pulmonary fibrosis in Northern Italy. *Eur Respir J* 2018;51:1700397.
27. VA Informatics and Computing Infrastructure (VINCI). US Department of Veterans Affairs. Accessed November 3, 2023. <https://www.research.va.gov/programs/vinci/default.cfm>
28. RSIG-related downloadable data files. US Environmental Protection Agency. Updated January 2, 2025. Accessed November 3, 2023. <https://www.epa.gov/hesc/rsig-related-downloadable-data-files>
29. England BR, Roul P, Yang Y, et al. Risk of COVID-19 in rheumatoid arthritis: a national Veterans Affairs matched cohort study in at-risk individuals. *Arthritis Rheumatol* 2021;73:2179–2188.
30. Aletaha D, Neogi T, Hawker G, et al. 2010 Rheumatoid arthritis classification criteria: an American College of Rheumatology/European League Against Rheumatism collaborative initiative. *Arthritis and Rheumatism* 2010;62:2569–2581.
31. Chung CP, Rohan P, Krishnaswami S, et al. A systematic review of validated methods for identifying patients with rheumatoid arthritis using administrative or claims data. *Vaccine* 2013;31(Suppl 10): K41–K61.
32. England BR, Roul P, Mahajan TD, et al. Performance of administrative algorithms to identify interstitial lung disease in rheumatoid arthritis. *Arthritis Care Res (Hoboken)* 2020;72:1392–1403.
33. Pearce N. Analysis of matched case-control studies. *BMJ* 2016;352: i969.
34. O'Dell K, Ford B, Fischer EV, et al. Contribution of wildland-fire smoke to US PM_{2.5} and its influence on recent trends. *Environ Sci Technol* 2019;53:1797–1804.
35. Lipner EM, O'Dell K, Brey SJ, et al. The associations between clinical respiratory outcomes and ambient wildfire smoke exposure among pediatric asthma patients at National Jewish Health, 2012–2015. *Geohealth* 2019;3:146–159.
36. Song W, Liu XY, Hu CC, et al. Important contributions of non-fossil fuel nitrogen oxides emissions. *Nat Commun* 2021;12:243.
37. Sigari N, Moghimi N, Shahraki FS, et al. Anti-cyclic citrullinated peptide (CCP) antibody in patients with wood-smoke-induced chronic obstructive pulmonary disease (COPD) without rheumatoid arthritis. *Rheumatol Int* 2015;35:85–91.
38. Particulate matter (PM_{2.5}) trends. US Environmental Protection Agency. Updated August 16, 2024. Accessed November 8, 2023. <https://www.epa.gov/air-trends/particulate-matter-pm25-trends>
39. Final rule to strengthen the national air quality health standard for particulate matter fact sheet. US Environmental Protection Agency. 2024. Accessed March 19, 2024. <https://www.epa.gov/system/files/documents/2024-02/pm-naaqs-overview.pdf>
40. Raimundo K, Solomon JJ, Olson AL, et al. Rheumatoid arthritis-interstitial lung disease in the United States: prevalence, incidence, and healthcare costs and mortality. *J Rheumatol* 2019;46:360–369.
41. Myasoedova E, Davis J, Matteson EL, et al. Is the epidemiology of rheumatoid arthritis changing? Results from a population-based incidence study, 1985–2014. *Ann Rheum Dis* 2020;79:440–444.
42. Adami G, Viapiana O, Rossini M, et al. Association between environmental air pollution and rheumatoid arthritis flares. *Rheumatology (Oxford)* 2021;60:4591–4597.
43. Li R, Kou X, Tian J, et al. Effect of sulfur dioxide on inflammatory and immune regulation in asthmatic rats. *Chemosphere* 2014;112: 296–304.
44. She X, Gao X, Wang K, et al. Effects of noise and low-concentration carbon monoxide exposure on rat immunity. *J Occup Health* 2021; 63:e12235.
45. Tsai MH, Chi MC, Hsu JF, et al. Urban particulate matter enhances ROS/IL-6/COX-II production by inhibiting microRNA-137 in synovial fibroblast of rheumatoid arthritis. *Cells* 2020;9:1378.
46. Wu Q, Xu Z, Dan YL, et al. Association between traffic-related air pollution and hospital readmissions for rheumatoid arthritis in Hefei, China: a time-series study. *Environ Pollut* 2020;268:115628.

Genome-Wide Aggregated *Trans* Effects Analysis Identifies Genes Encoding Immune Checkpoints as Core Genes for Rheumatoid Arthritis

Athina Spiliopoulou,¹  Andrii Iakovliev,¹  Darren Plant,²  Megan Sutcliffe,³  Seema Sharma,² 
Cankut Cubuk,⁴  Myles Lewis,⁴  Costantino Pitzalis,⁴  Anne Barton,²  and Paul M. McKeigue¹ 

Objective. The sparse effector “omnigenic” hypothesis postulates that the polygenic effects of common single nucleotide polymorphisms (SNPs) on a typical complex trait are mediated by *trans* effects that coalesce on expression of a relatively sparse set of core genes. The objective of this study was to identify core genes for rheumatoid arthritis by testing for association of rheumatoid arthritis with genome-wide aggregated *trans* effects (GATE) scores for expression of each gene as transcript in whole blood or as circulating protein levels.

Methods. GATE scores were calculated for 5,400 cases and 453,705 non-cases of primary rheumatoid arthritis in UK Biobank participants of European ancestry.

Results. Testing for association with GATE scores identified 16 putative core genes for rheumatoid arthritis outside the HLA region, of which six—*TP53BP1*, *PDCD1*, *TNFRSF14*, *LAIR1*, *LILRA4*, and *IDO1*—were supported by Mendelian randomization analysis based on the marginal likelihood of the causal effect parameter. Five of these 16 genes were validated by a reported association of rheumatoid arthritis with SNPs within 200 kb of the transcription site, eight by association of the measured protein level with rheumatoid arthritis in UK Biobank, 10 by experimental perturbation in mouse models of inflammatory arthritis, and two—*CTLA4* and *PDCD1*—by evidence that drugs targeting the gene cause or ameliorate inflammatory arthritis in humans. Fourteen of these 16 genes are in pathways affecting immunity or inflammation, and six—*CD5*, *CTLA4*, *TIGIT*, *LAIR1*, *TNFRSF14*, and *PDCD1*—encode receptors that have been characterized as immune checkpoints exploited by cancer cells to escape the immune response.

Conclusion. These results highlight the key role of immune checkpoints in rheumatoid arthritis and identify possible therapeutic targets.

INTRODUCTION

Rheumatoid arthritis is an immune-mediated inflammatory disease with a prevalence of about 1% in most populations. The genetic information for discrimination, equal to the logarithm to base two of the recurrence risk ratio in first-degree relatives,¹ is

about 2.3 bits,² of which the HLA region accounts for about 0.8 bits.³ Although the catalog of genome-wide association studies (GWAS) lists 337 genomic regions outside the HLA region that contain single nucleotide polymorphisms (SNPs) associated with rheumatoid arthritis at the conventional genome-wide threshold of $P < 5 \times 10^{-8}$, the genes in these regions are mostly broadly

The views expressed are those of the authors and not necessarily those of the National Health Service, the National Institute for Health Research, or the Department of Health.

Supported by the UK Medical Research Council (MR/V012509/1) and by the National Institute for Health Research Barts Biomedical Research Centre (NIHR 203330). The development of the GENOSCORES platform was supported by a Springboard Award (SBF006/1109) from the Academy of Medical Sciences, supported in turn by the Wellcome Trust, the UK Government Department of Business, Energy and Industrial Strategy, the British Heart Foundation, and Diabetes UK. The transcriptomic study was supported by the NIHR Manchester Biomedical Research Centre (203308) and Versus Arthritis (VA 21754). Dr Iakovliev's work was supported by the Medical Research Council Cross Disciplinary Fellowship (XDF) Programme (MC_FE_00035).

¹Athina Spiliopoulou, PhD, Andrii Iakovliev, PhD, Paul M. McKeigue, FFPH, PhD: University of Edinburgh, Edinburgh, Scotland; ²Darren Plant, PhD, Seema Sharma, MD, Anne Barton, MD, PhD: University of Manchester and

the National Institute for Health and Care Research Manchester Biomedical Research Centre, Manchester University NHS Foundation Trust, Oxford Road, Manchester, United Kingdom; ³Megan Sutcliffe, PhD: University of Manchester, Manchester, United Kingdom; ⁴Cankut Cubuk, PhD, Myles Lewis, MD, PhD, Costantino Pitzalis, MD, PhD: Queen Mary University of London and Barts Health NHS Trust and NIHR Barts Biomedical Research Centre, London, United Kingdom.

UK Biobank data are available to approved researchers in the Research Analysis Platform. The application form for requesting access can be found at <https://www.ukbiobank.ac.uk/>. Summary statistics from the Keio transcriptomics study are publicly available. Summary statistics from the Manchester transcriptomics study is available from <http://doi.org/10.5281/zenodo.14673156>. The GENOSCORES platform used to compute locus-specific genotypic scores is accessible via an online application programming interface (web API), at <https://genoscores.cphs.mvm.ed.ac.uk/>. Access requests to the GENOSCORES platform and the corresponding R package should be directed to the corresponding author.

expressed and are not in pathways specifically relevant to immune-mediated disease.⁴ Although the treatment of rheumatoid arthritis has been revolutionized by drugs that target specific proteins mediating inflammation, the contribution of GWAS to discovery of drug targets for rheumatoid arthritis has been limited.⁵

Conventional GWAS analyses focus on identifying the nearby genes (usually within 200 kb) that mediate the effects of common variants on disease through *cis* effects. However, for a typical gene, most of the SNP heritability of levels of the transcript or encoded protein is attributable to *trans* effects of variants that are distant from the transcription site.⁶ On this basis, the “omnigenic” sparse effector model was proposed as a fundamental rethink of the genetic architecture of complex traits.⁷ This postulates that most of the polygenic effects on a typical complex trait are mediated through weak *trans* effects of common variants that coalesce on expression of a relatively sparse set of “core” effector genes in relevant tissues. The availability of summary statistics from large GWAS studies of transcripts in whole blood or proteins in plasma has made it possible to test this hypothesis by constructing genotypic predictors of gene expression based on aggregated *trans* effects and testing these genotypic scores for association with the disease or trait under study. We have reported an application of this genome-wide aggregated *trans* effects (GATE) analysis pipeline to type 1 diabetes, which identified a set of putative core genes regulating the differentiation and activity of CD4+ Treg cells.⁸ The objective of this study was to investigate whether GATE analysis can identify core genes for rheumatoid arthritis.

MATERIALS AND METHODS

Ethical approval. Ethical approval for the UK Biobank was previously obtained from the North West Centre for Research Ethics Committee (11/NW/0382). Informed consent was obtained for all study participants. The work described herein was approved by the UK Biobank under application 23652. Ethical approval for the transcriptomics study was granted by the North West 6 Central Manchester South Research Ethics Committee (COREC 04/Q1403/37). All patients provided written consent.

Case definition. The case definition of rheumatoid arthritis in the UK Biobank cohort was based on any of three criteria: (1) hospital discharge or death certificate with an International Classification of Diseases diagnostic code for rheumatoid arthritis; (2) any primary care diagnosis of rheumatoid arthritis; or (3) self-reported diagnosis of rheumatoid arthritis supported by

prescription of a disease-modifying antirheumatic drug at baseline or during follow-up. Of 487,152 individuals with nonmissing phenotype and genotype data, 5,958 had ever been diagnosed with rheumatoid arthritis. When those with a diagnosis of Sjögren's disease antedating the diagnosis of rheumatoid arthritis were excluded, 5,731 cases of primary rheumatoid arthritis remained. The full dataset was pruned to ensure that no pairs of individuals with kinship coefficient >0.05 remained. As summary statistics for *cis* and *trans* effects of SNP genotypes on gene expression were available only from studies of individuals of European ancestry, the dataset for *trans* effects analysis was restricted to those participants who reported their ethnic origin as white. After applying these exclusions, there were 451,447 individuals, of whom 5,292 were classified as cases. Of these, 2,015 were classified as incident cases, on the basis that the first mention of a diagnosis of rheumatoid arthritis was later than the date on which they were assessed.

GATE analysis. Methods for GATE analysis have been described previously.⁸ The data sources and analytical steps are illustrated in Figure 1. The list of SNPs that were typed or imputed in UK Biobank was uploaded to the GENOSCORES server. A database query extracts the univariate coefficients of regression of expression of each target gene on each of these SNPs, filtered by setting a threshold of $P < 10^{-5}$. For each target gene and each clump of associated SNPs containing at least one SNP associated with expression of the gene at $P < 10^{-6}$, the vector of coefficients is multiplied by the inverse correlation matrix among SNP genotypes computed from the 1000 Genomes reference panel to obtain a vector of multivariable weights that are corrected for linkage disequilibrium (LD). A pseudoinverse solution is implemented to handle ill-conditioned matrices in clumps with highly correlated SNPs. For each gene and each clump of associated SNPs, a locus-specific score is computed by multiplying the vector of adjusted weights by the matrix of SNP genotypes in the target dataset. The locus-specific scores for each gene are summed over *trans*-quantitative trait loci (QTLs) to obtain genome-wide aggregated *trans* scores.

Trans-expression QTL (*trans*-eQTL) scores were computed from eQTLGen phase 1, in which only 10,317 trait-associated SNPs were tested for *trans* associations.⁹ For these scores, the threshold for defining clumps of associated SNPs was relaxed to $P < 10^{-5}$ because for these trait-associated SNPs, the prior probability of an effect on gene expression is higher than it is for random SNPs. *Trans*-protein QTL (*trans*-pQTL) scores were computed from three studies of circulating proteins:

Additional supplementary information cited in this article can be found online in the Supporting Information section (<http://onlinelibrary.wiley.com/doi/10.1002/art.43125>).

Author disclosures are available at <https://onlinelibrary.wiley.com/doi/10.1002/art.43125>.

Address correspondence via email to Paul M. McKeigue, FFPH, PhD, at paul.mckeigue@ed.ac.uk.

Submitted for publication September 17, 2024; accepted in revised form January 7, 2025.

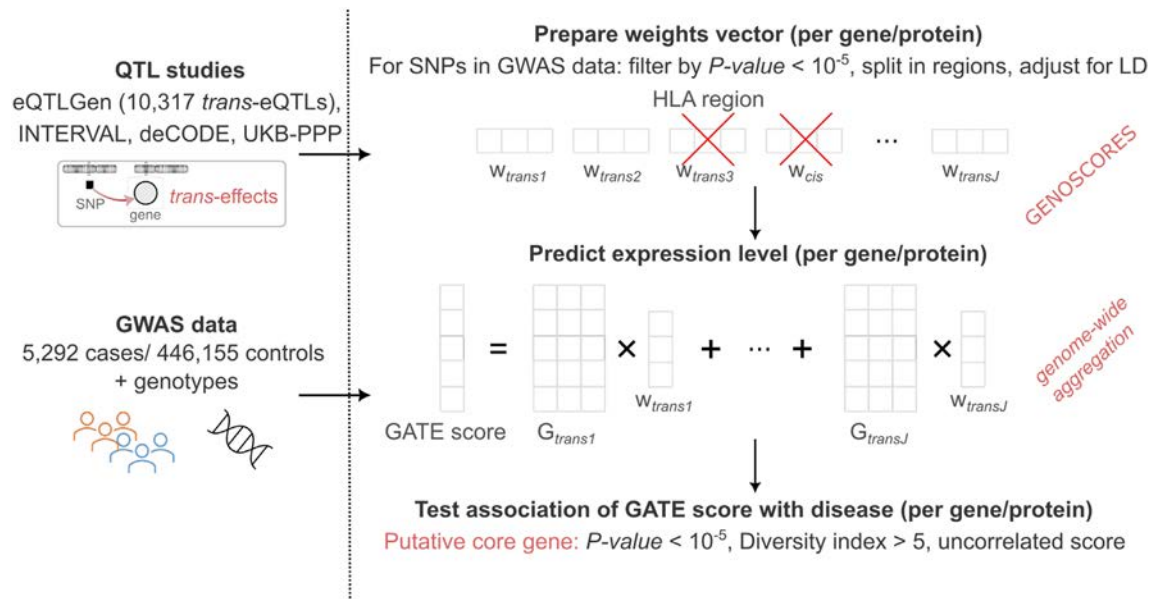


Figure 1. Graphic illustration of the data sources and analytical steps for identification of core genes for rheumatoid arthritis. eQTL, expression QTL; GATE, genome-wide aggregated *trans* effects; GWAS, genome-wide association study; LD, linkage disequilibrium; QTL, quantitative trait locus; SNP, single nucleotide polymorphism; UKB-PPP, UK Biobank Pharma Proteomics Project.

- 1,478 proteins on the SomaLogic panel measured in plasma on 3,301 blood donors in the INTERVAL study.¹⁰
- 4,719 proteins on the SomaLogic version 4 panel measured in plasma on 35,559 Icelanders in the deCODE study¹¹; 2,207 aptamers on this platform that appeared to cross-react with *CFH*, encoding complement factor H, were excluded. The criteria for identifying these aptamers were a *trans*-pQTL at the *CFH* locus, no *cis*-pQTL, and association of the *trans* score with age-related macular degeneration.
- 2,923 proteins on the Olink Explore panel measured in plasma on 54,306 participants in UK Biobank.¹²

As the HLA region is a hotspot for *trans*-QTLs for genes involved in immunity and inflammation¹³ and associations of these *trans*-QTLs with autoimmune disease are heavily confounded by the direct effects of HLA antigens, the HLA region (from 25 to 34 Mb on chromosome 6) was excluded from the computation of genome-wide *trans* scores. *Cis*-eQTLs and *cis*-pQTLs were excluded from the aggregated *trans* scores and tested for association with the disease separately.

Statistical analysis. When testing for association with genotypic scores for Olink proteins calculated from the UK Biobank proteomics study, the 54,306 participants who were included in the proteomics study were excluded from tests of association of the genotypic scores with the outcome. A logistic regression model was fitted with rheumatoid arthritis as response variable with sex and the first 20 genotypic principal components as covariates. The fitted values from this null model were used to

compute tests for association with the *cis* score and aggregated *trans* score predicting the levels of a transcript or circulating protein. These tests were computed as efficient score tests based on the gradient and second derivative of the log-likelihood at the null. Log odds ratios in the tables have been standardized by multiplying them by the SD of the score so that the coefficient is the log odds ratio associated with an increase of the score by one SD.

As an index of the effective number of unlinked *trans*-QTLs contributing to each genome-wide *trans* score, we calculated the diversity index or Hill number.¹⁴ For each gene, the diversity index was computed from the variances $\sigma_1, \dots, \sigma_K$ of the K locus-specific *trans* scores as $2^{-\sum_{i=1}^K \log_2 p_i}$, where $p_i = \sigma_i^2 / \sum_j \sigma_j^2$. This index can take values from 1, if one of the QTLs has much larger variance than the others, to K , if the variances of the locus-specific *trans* scores are equal.

For each putative core gene identified through aggregating the effects of at least 10 *trans*-QTLs, an instrumental variable (“Mendelian randomization”) analysis was undertaken. This was based on constructing a scalar genetic instrument from each *trans*-QTL and marginalizing over the distribution of direct (pleiotropic) effects of the instrument on the outcome to compute the likelihood of the causal effect parameter as described elsewhere.¹⁵ *Cis*-QTLs were excluded from these analyses because *cis*-acting SNPs frequently alter the splicing of the gene product so that effects on the measured level of transcript or circulating protein do not correspond to effects on function. A null result in these Mendelian randomization analyses does not exclude a causal effect because even with 10 or more instruments (*trans*-QTLs), there may not be enough information in the data to learn the posterior distribution of direct effects.

Table 1. Putative core genes identified through aggregated *trans*-eQTL scores*

Gene	Chrom	Transcription site	<i>Trans</i> score			<i>Cis</i> score		Reported GWAS hit within 200 kb
		Start position (Mb)	Effective number of <i>trans</i> -eQTLs	Log odds ratio	<i>P</i>	Log odds ratio	<i>P</i>	
<i>IL10RA</i>	11	117.99	5.8	0.064	3×10^{-6}	-0.015	0.3	
<i>CD5</i>	11	61.10	8.9	0.066	2×10^{-6}	0.033	0.02	<i>CD6, CD5, VPS37C</i>
<i>CTLA4</i>	2	203.85	9.6	0.112	6×10^{-16}	-0.037	0.007	<i>CD28, CTLA4, ICOS</i>
<i>STAP1</i>	4	67.56	6.4	-0.070	4×10^{-7}	-0.014	0.3	
<i>FBLN7</i>	2	112.14	7.5	0.068	3×10^{-6}	-0.008	0.6	
<i>SLAMF1</i>	1	160.61	5.7	0.070	4×10^{-7}	0.009	0.5	<i>SLAMF6</i>

* Log odds ratios are scaled as the difference in log odds associated with a score difference of one SD. Threshold for inclusion in this table is *trans* score association at $P < 10^{-5}$ and effective number of *trans*-eQTLs >5. Chrom, chromosome; eQTL, expression quantitative trait locus; GWAS, genome-wide association study; Mb, megabase.

Filtering and validation criteria. As before,⁸ the GATE scores were filtered to retain only those scores for which the effective number of *trans*-QTLs was greater than five. This retained 413 aggregated *trans*-eQTL scores for 413 unique genes and 3,256 aggregated *trans*-pQTL scores for 2,586 unique genes. For the initial list of putative core genes, we set a threshold of $P < 10^{-5}$ for association of disease with GATE scores.

We defined six criteria for validation as a core gene:

1. Any SNP association with rheumatoid arthritis, reported in the GWAS catalog, at the conventional threshold of $P <$



Figure 2. Correlations between aggregated *trans*-eQTL scores for putative core genes. Rows and columns of the correlation matrix are ordered by hierarchical clustering on the absolute value of correlation. Diagonal elements of the correlation matrix are equal to one; they are set to zero for easier visualisation of the off-diagonal values. eQTL, expression quantitative trait locus. Color figure can be viewed in the online issue, which is available at <http://onlinelibrary.wiley.com/doi/10.1002/art.43125/abstract>.

5×10^{-8} within 200 kb of the transcription site of the target gene. As *cis*-SNPs were excluded from the GATE score, this is orthogonal validation. The 200-kb cutoff is based on the distribution of distances from protein QTL variants to transcription start site.¹⁶ Although this criterion would not be appropriate for identifying the gene that mediates the *cis* effect of a disease-associated SNP, if the gene has already been identified through *trans* effects as a putative core gene for the disease and there is a SNP association near its transcription site, then this gene is the most likely mediator of the *cis* effect.

2. Instrumental variable analysis ("Mendelian randomization"), based on marginalizing over the distribution of pleiotropic effects of *trans*-QTLs, supports a causal effect of the transcript or protein at $P < 0.01$. This criterion is evaluated only if the target gene has at least 10 *trans*-QTLs because, otherwise, there is not enough information to infer the distribution of pleiotropic effects.
3. Association of disease with the measured level of the encoded protein in the UK Biobank proteomics study, in the same direction as the association with the aggregated *trans* score, with magnitude (standardized log odds ratio) of the protein association at least twice that of the *trans* score association. Evidence of causality is strengthened if levels of the protein are associated with incident rheumatoid arthritis, excluding those already diagnosed at baseline.
4. Drugs targeting the gene product, its ligand, or its receptor cause inflammatory arthritis or have shown efficacy against rheumatoid arthritis in a phase 2 trial.
5. Perturbation of the gene by knockout, transduction, or overexpression, or perturbation of the gene product by an inhibitor or an agonist, alters the severity of disease in an experimental model of inflammatory arthritis.
6. Rare variants in the gene cause a monogenic form of the disease. From searching PubMed, 11 genes were identified as reported monogenic causes of inflammatory arthritis: *LACC1*, *LRBA*, *NFIL3*, *UNC13D*, *NOD2*, *NLRP3*, *MEFV*, *TNFAIP3*, *PRF1*, *STX11*, *ACP5*.^{17–21}

Table 2. Putative core genes identified through aggregated *trans*-pQTL scores*

pQTL study	N	Gene	Chrom	Transcription site	Trans score			Cis score		Reported GWAS hit within 200 kb
				Start position (Mb)	Effective number of trans-pQTLs	Log odds ratio	P value	Log odds ratio	P value	
DeC	5,292	PNLIPRP2	10	116.62	6.2	0.061	9×10^{-6}	-0.007	0.6	
UKB	4,650	TP53BP1	15	43.40	8.3	0.072	8×10^{-7}			
UKB	4,650	CXCL10	4	76.02	7.6	0.091	1×10^{-9}	0.019	0.2	
UKB	4,650	CXCL9	4	76.00	7.8	0.086	3×10^{-9}	-0.007	0.6	
UKB	4,650	IDO1	8	39.90	8.2	0.065	9×10^{-6}	-0.025	0.1	
UKB	4,650	PDCD1	2	241.85	21.3	0.096	1×10^{-10}	-0.005	0.7	GAL3ST2
UKB	4,650	TNFRSF14	1	2.56	9.8	0.067	4×10^{-6}	-0.024	0.1	TNFRSF14, MMEL1
UKB	4,650	LAIR1	19	54.35	6.1	0.069	4×10^{-6}	-0.006	0.7	
DeC	5,292	TIGIT	3	114.28	6.1	0.082	2×10^{-9}	0.004	0.8	
DeC	5,292	LILRA4	19	54.33	9.1	0.063	5×10^{-6}	-0.009	0.5	

* Log odds ratios are scaled as the difference in log odds associated with a score difference of one SD. Threshold for inclusion in this table is *trans* score association at $P < 10^{-5}$ and effective number of *trans*-pQTLs > 5 . Chrom, chromosome; DeC, deCODE; GWAS, genome-wide association study; Mb, megabase; pQTL, protein quantitative trait locus; UKB, UK Biobank.

RESULTS

Trans-eQTL scores. Table 1 shows the six putative core genes identified through association with aggregated *trans*-eQTL scores. For three of these genes—*CD5*, *CTLA4*, and *SLAMF1*—associations of rheumatoid arthritis with SNPs within 200 kb of the transcription site are listed in the GWAS catalog. For these SNP associations, gene names recorded in the GWAS catalog in the fields “Reported Gene” or “Mapped Gene” are shown in the last column of Table 1. As previously reported for type 1 diabetes,⁸ the *cis*-eQTL association of *CTLA4* is in the opposite direction to the association with the aggregated *trans* score; this may be explained by *cis*-acting SNPs that alter the splicing of this gene.

Figure 2 shows that the aggregated *trans*-eQTL scores for the six putative core genes are only weakly correlated, indicating that they do not share most of their *trans*-eQTLs. Supplementary Table S1 shows that multiple regions containing SNPs previously identified as associated with rheumatoid arthritis are *trans*-eQTLs for one or more of these putative core genes. Notably, seven regions outside the HLA region that contain SNPs associated with rheumatoid arthritis are *trans*-eQTLs for *CTLA4*.

To test whether genetic effects on the proportions of immune cell types could explain the associations of rheumatoid arthritis with *trans* scores for predicted gene expression, we used summary statistics from the Sardinia study of immune cell phenotypes in peripheral blood²² to calculate genome-wide scores for each immune cell phenotype. We tested these scores for association with rheumatoid arthritis. Supplementary Table S2 shows that rheumatoid arthritis was associated inversely with the proportion of CD4+ T cells that were Treg cells and positively associated with the absolute count of CD4+ T cells. Although *CTLA4* is expressed on CD4+ T cells, the association of rheumatoid arthritis with the polygenic score for CD4+ T cell count was much weaker than the association with the GATE score for *CTLA4*.

Trans-pQTL scores. Table 2 shows the 10 putative core genes identified through association with aggregated *trans*-pQTL scores. The strongest GATE score association with rheumatoid arthritis is for *PDCD1*, which encodes the immune checkpoint receptor programmed cell death protein 1 (PD-1). Supplementary Table S3 shows that the *trans*-pQTLs contributing to this GATE score include 12 regions containing genes previously associated with rheumatoid arthritis through GWAS studies: *SDF4*, *AP4B1*, *PTPN22*, *CTLA4*, *BACH2*, *TRAF1*, *IL2RA*, *TSPAN14*, *PTPN11*, *ILF3*, *FUT2* and *AIRE*. This coalescence of *trans* effects of disease-associated SNPs on expression of a disease-relevant target gene is consistent with the sparse effector hypothesis.

Supplementary Figure S1 shows that the aggregated *trans*-pQTL scores for seven of these putative core genes are correlated, indicating that they share *trans*-pQTLs. The highest correlation (0.6) is between the scores for *CXCL10* and *CXCL9*. Supplementary Table S3 shows that these two genes share nine *trans*-pQTL regions containing genes—*PTPN22*, *GCKR*, *IL18R1*, *STAT4*, *CCR1*, *IFNG-AS1*, *PTPN11*, *PTPN2*, and *TYK2*—previously identified as associated with rheumatoid arthritis. This sharing of *trans*-QTLs means that we cannot distinguish, without other evidence, which of these two target genes is most likely to be causal.

To investigate whether these results were replicated in independent datasets, we searched the “expression quantitative trait score” (eQTS) summary statistics released by the eQTLGen Consortium.⁹ Their study used summary statistics from two published GWAS of rheumatoid arthritis to construct polygenic risk scores that were tested for association with gene expression in an individual-level dataset. Supplementary Table S4 shows that for three of the genes in Tables 1 or 2—*PDCD1*, *TIGIT*, and *CTLA4*—expression levels were associated with polygenic scores for rheumatoid arthritis.

Table 3. Tests of association of rheumatoid arthritis (at baseline or follow-up) with plasma levels of proteins measured in the UK Biobank cohort and encoded by putative core genes or by genes within 200 kb of a reported GWAS hit*

		Measured level of protein				Trans score				
Gene	GWAS hit	Noncases	Cases	Log odds ratio	P value	Effective number of trans-pQTLs	r ²	Ratio r ² / h ² _{trans}	Log odds ratio	P value
Genes in Tables 1 or 2 with protein levels measured in UK Biobank										
PDCD1	GAL3ST2	50,779	698	0.60	2 × 10 ⁻⁶⁵	21.3	0.034	0.17	0.10	1 × 10 ⁻¹⁰
LAIR1		50,426	684	0.47	4 × 10 ⁻⁴⁵	6.1	0.006	0.04	0.07	4 × 10 ⁻⁶
CXCL10		50,674	688	0.45	1 × 10 ⁻³¹	7.6	0.015	0.16	0.09	1 × 10 ⁻⁹
TNFRSF14	TNFRSF14, MMEL1	50,507	686	0.43	3 × 10 ⁻²⁹	9.8	0.010	0.07	0.07	4 × 10 ⁻⁶
CXCL9		50,674	688	0.37	7 × 10 ⁻²¹	7.8	0.015	0.12	0.09	3 × 10 ⁻⁹
SLAMF1	SLAMF6	49,524	677	0.24	1 × 10 ⁻¹⁰	10.3	0.013	0.15	0.05	3 × 10 ⁻⁴
TIGIT		43,025	589	0.22	1 × 10 ⁻⁸	4.0	0.004	0.24	0.01	0.6
CD5	CD6, CD5, VPS37C	50,790	698	0.17	6 × 10 ⁻⁶	11.3	0.022	0.13	0.04	0.005
IL10RA		49,524	677	0.12	0.001	3.9	0.001	1.55	0.03	0.05
TP53BP1		42,549	583	0.13	0.001	8.3	0.022	0.25	0.07	8 × 10 ⁻⁷
CTLA4		43,828	598	-0.12	0.003					
PNLIPRP2		50,426	684	-0.05	0.2	5.4	0.004	0.04	0.04	0.007
LILRA4		42,371	589	0.04	0.3	7.0	0.003		0.01	0.7
IDO1		42,660	584	-0.02	0.6	7.8	0.020	0.15	0.05	2 × 10 ⁻⁴
Genes within 200 kb of a GWAS hit and trans score association with rheumatoid arthritis at P < 0.001										
LGALS9	KSR1, NOS2	50,431	685	0.64	9 × 10 ⁻⁶⁴	8.6	0.015	0.10	0.06	3 × 10 ⁻⁵
IL2RA	IL2RA	50,102	681	0.51	3 × 10 ⁻⁴²	11.6	0.016	0.09	0.06	9 × 10 ⁻⁵
TNFRSF9	TNFRSF9, PARK7	50,067	683	0.46	4 × 10 ⁻³⁸	9.0	0.017	0.09	0.06	1 × 10 ⁻⁴
CD274	+	50,067	683	0.46	5 × 10 ⁻³⁶	8.3	0.017	0.16	0.05	5 × 10 ⁻⁴
CD27	TNFRSF1A, LTBR	50,608	687	0.44	8 × 10 ⁻³⁵	24.2	0.021	0.11	0.06	1 × 10 ⁻⁴
CD48	ITLN1	50,590	688	0.21	7 × 10 ⁻⁸	15.6	0.035	0.17	0.06	1 × 10 ⁻⁴
SLAMF7	ITLN1	50,386	684	0.06	0.1	20.5	0.035	0.22	0.05	9 × 10 ⁻⁴
GP1BB	SEPT5-GP1BB, TBX1	42371	589	-0.02	0.6	9.8	0.041	0.25	0.05	3 × 10 ⁻⁴

* Associations are adjusted for age, sex, and continental ancestry. Log odds ratios are scaled as difference in log odds associated with a covariate difference of one SD. *Trans* scores are based on proteins measured in UK Biobank only. For *TIGIT*, *PNLIPRP2*, and *LILRA4*, these associations differ from those in Table 2, which are based on *trans*-pQTLs for proteins measured in the DeCODE study. Similarly, for *CD5*, *IL10RA*, and *SLAMF1*, these differ from those in Table 1, which are based on *trans*-eQTLs for transcripts measured in the eQTLGen study. The plus sign denotes GWAS hits that have not been attributed to a gene. GWAS, genome-wide association study; pQTL, protein quantitative trait locus.

Nearby GWAS hits. For five of the 16 putative core genes—*CD5*, *CTLA4*, *SLAMF1*, *PDCD1*, and *TNFRSF14*—that were identified through association of GATE scores with rheumatoid arthritis, associations of rheumatoid arthritis with SNPs within 200 kb of the transcription site are listed in the GWAS catalog. The attribution of the GWAS hit to the target gene is supported by a *cis*-QTL association for *CTLA4*. For *CD5*, *CTLA4*, and *TNFRSF14*, the target gene is included in the GWAS catalog as one of the attributed genes. The association with SNPs in the *SLAMF1* region had been attributed to *SLAMF6*, and the association with SNPs in the *PDCD1* region had been attributed to *GAL3ST2*, 40 kb upstream of *PDCD1*.

Mendelian randomization. Supplementary Table S5 shows that of the 10 putative core genes identified through aggregated *trans* effects on protein levels, six were supported at $P < 0.01$ by a Mendelian randomization analysis based on

computing the marginal likelihood of the causal effect parameter.¹⁵ Scatter plots of the coefficients for the effects of the *trans*-pQTLs are shown for *LAIR1*, *TP53BP1*, *TNFRSF14*, and *PDCD1* in Supplementary Figures S2–S5. The coefficients for the effects of the pQTLs on rheumatoid arthritis are plotted against the coefficients for the effects of the pQTLs on circulating levels of the protein. The slope of the straight line shown in each plot is the maximum likelihood estimate of the causal effect parameter based on marginalizing over the posterior distribution of the direct (pleiotropic) effects. If there were no direct effects of the *trans*-pQTLs on rheumatoid arthritis and no uncertainty in the estimates of coefficients of regression of disease and protein levels on the *trans*-pQTLs, the points in this plot would lie on a straight line through the origin, and the slope of this line would be the causal effect parameter. We emphasize that Mendelian randomization analysis has limitations and that the results should be interpreted as only one line of evidence to be combined with evidence from other sources.

Associations with measured levels of proteins and transcripts. Of the 54,306 individuals in the UK Biobank proteomics study, 688 had a diagnosis of primary rheumatoid arthritis at baseline or during follow-up. Table 3 shows that of the 14 putative core genes for which the protein encoded by the gene was measured in the UK Biobank proteomics study, nine met the criterion of association in the same direction as the *trans* score effect with a standardized log odds ratio at least twice as high for the measured protein as for the GATE score that predicts the protein level. Because these associations of protein levels with rheumatoid arthritis include cases already diagnosed, they may be altered by the effects of the disease or by drug treatment.

The lower part of Table 3 shows eight additional candidates for core gene status identified as genes within 200 kb of a GWAS hit that have a GATE score associated with rheumatoid arthritis at the less stringent threshold of $P < 0.001$ (on the basis that a nearby GWAS hit increases the prior probability of a causal effect). For five of these eight genes—*LGALS9*, *IL2RA*, *TNFRSF9*, *CD274*, and *CD27*—levels of the encoded protein were strongly associated with rheumatoid arthritis. Supplementary Table S6 shows that for 10 of the 14 proteins associated with rheumatoid arthritis at baseline or follow-up at a standardized log odds ratio >0.2 , these associations persisted after restriction to incident cases diagnosed during follow-up.

Table 3 shows that the squared correlations (r^2) between the GATE scores and the measured protein levels are typically only about 2% and that the proportion of variance explained by the GATE score is typically 10% to 20% of the total SNP heritability attributable to *trans* effects (h^2_{trans}) estimated previously in the UK Biobank proteomics dataset.¹² If the association of the protein with disease is causal, the effect size associated with the measured protein level should be about seven times the effect size associated with the GATE score (the ratio of effect sizes scales with the correlation of the score with the measured value). For the top five genes in Table 3, the ratio of measured protein effect size to GATE score effect size is between four and seven, broadly consistent with this prediction.

To compare whole blood transcript levels in cases of rheumatoid arthritis and healthy controls, we examined two microarray studies: a published study of 66 cases of rheumatoid arthritis not yet treated with a conventional synthetic disease-modifying antirheumatic drug (csDMARD) and 35 healthy controls in Keio, Japan²³ and an unpublished study of 55 csDMARD-treated cases of rheumatoid arthritis and 10 healthy controls in Manchester, England. Supplementary Table S7 shows that expression levels of *CD5* and *LILRA4* were inversely associated with rheumatoid arthritis in both studies. These associations with transcript levels were opposite in direction to the associations with the soluble proteins in UK Biobank, consistent with the possibility that the soluble proteins act as decoys to down-regulate the cellular receptor. We

emphasize that to characterize case-control differences in whole blood transcript levels will require larger studies using methods that distinguish splice variants and control for cell-type proportions.

Summary of validation. Supplementary Table S8 tabulates the genes in Tables 1, 2, or 3 for which experimental perturbation has demonstrated an effect in a mouse model of inflammatory arthritis. For two of these genes, there is at least preliminary clinical evidence of efficacy of drugs targeting the encoded protein against rheumatoid arthritis. Table 4 summarizes the results of applying five criteria for validation of each putative core gene, excluding the sixth criterion of monogenic disease, which was not met by any of these genes. The strongest evidence is for *PDCD1*, which meets all five criteria: nearby GWAS hit, protein association, Mendelian randomization support, validation from perturbation in an experimental model, and effects of a targeted agonist against rheumatoid arthritis in a phase 2 trial.

DISCUSSION

From aggregated *trans* effects, this study identified 16 genes outside the HLA region as putative core genes for rheumatoid arthritis. Six of these—*CD5*, *CTLA4*, *TIGIT*, *LILRA4*, *PDCD1*, and *TNFRSF14*—encode proteins that have been identified as immune checkpoints, defined broadly as receptors on immune cells that are exploited by cancer cells to escape the immune response.^{24–27} Inflammatory arthritis and other autoimmune reactions are common adverse effects of inhibitors of these immune checkpoints used in cancer therapy. *LILRA4* encodes leukocyte immunoglobulin-like receptor subfamily A member 4, a cell surface protein expressed on plasmacytoid dendritic cells; it has been proposed that *LILRA4* is an “innate checkpoint,” analogous to the checkpoints identified in the adaptive immune system.²⁸

For 10 of these genes, experimental perturbation in a mouse model has been shown to influence inflammatory arthritis.^{29–38} For two putative core genes—*CTLA4* and *PDCD1*—there is at least preliminary evidence of efficacy against rheumatoid arthritis in clinical trials of drugs that target the protein.^{39,40}

Of the six immune checkpoint genes identified through GATE analysis as putative core genes for rheumatoid arthritis, GATE scores for four—*CD5*, *CTLA4*, *PDCD1*, and *TIGIT*—are associated with type 1 diabetes also⁸ (result for *PDCD1* to be reported elsewhere). The other two—*LILRA4* and *TNFRSF14*—appear to be more specifically associated with rheumatoid arthritis. *TNFRSF14* was originally identified as a receptor for glycoprotein D of herpes simplex virus; it is now considered to be an immune checkpoint that inhibits immune response by binding to B- and T-lymphocyte attenuator, encoded by *BTLA*, and to CD160, an Ig-like glycoprotein expressed on $\gamma\delta$ T cells. A

TNFRSF14-Ig fusion protein aggravated autoimmune arthritis in the collagen-induced arthritis mouse model.³⁴

Of the 16 putative core genes identified through GATE analysis, 11 are expressed specifically by immune cells, mostly T cells. The genes not expressed specifically by immune cells are *IDO1*, *FBLN7*, *STAP1*, *TP53BP1*, and *PNLIPRP2*. *IDO1* modulates immune checkpoint-mediated immunosuppression by mechanisms that are not yet clear.⁴¹ *STAP1* has been reported to up-regulate activation of T cells via the T cell receptor.⁴² For *FBLN7* and *TP53BP1*, there is some experimental support for a role in inflammatory arthritis. *FBLN7* encodes the extracellular matrix protein fibulin-7, which binds to human monocytes via integrins $\alpha_5\beta_1$ and $\alpha_2\beta_1$; in a mouse model of systemic inflammation, it inhibits chemokine-mediated migration of macrophages.⁴³ *TP53BP1* encodes the p53-binding protein 1 that is required for accumulation of p53 to facilitate repair of DNA double-strand breaks. Knockout of the gene encoding p53 in mice increases disease severity in the collagen-induced arthritis model.³² *PNLIPRP2*, which is only just above the *P*-value threshold of 10^{-5} and has no support from association of measured protein levels with disease, may be a chance finding.

Six additional candidates for core gene status are identified by the combination of a GATE score association with rheumatoid arthritis at $P < 0.001$, a reported GWAS hit within 200 kb of the transcription site, and association of measured protein levels with rheumatoid arthritis. For five of these genes—*LGALS9*, *IL2RA*, *TNFRSF9*, *CD274*, and *CD27*—there is experimental validation from perturbation in a mouse model of inflammatory arthritis.^{38,44–47} For three of these five genes, the GWAS hit had been attributed to another nearby gene or not attributed at all. The association with *CD274* that encodes the ligand for the PD-1 receptor is further support for a key role of PD-1 signaling

in rheumatoid arthritis. *LGALS9* encodes galectin-9, one of four ligands for the immune checkpoint receptor TIM-3, also known as hepatitis A virus cellular receptor 2; blockade of TIM-3 ameliorates arthritis in a mouse model.⁴⁸

The *trans*-pQTL scores calculated in this study are for the predicted level of the circulating protein. In cases where this protein is the soluble form of a cellular receptor, the associations of disease with levels of the soluble form are not necessarily in the same direction as the associations with expression of the receptor. Thus, for PD-1, the measured level of the soluble protein and the GATE score for the protein level are positively associated with rheumatoid arthritis. This effect is in the opposite direction to what would be predicted from clinical experience with antagonists and agonists of the PD-1 receptor. A possible explanation for this is that the soluble protein acts as a decoy for the ligand for the cellular receptor.^{49,50}

Strengths of this study are that the cases and non-cases are from a single cohort, that diagnoses based on primary care records or self-report are validated by drug prescriptions, and that the design effectively rules out reverse causation because the background prevalence of rheumatoid arthritis in the population samples from which genetic scores were constructed was only about 1%. The main limitation of this study is that for genetic prediction from *trans* effects on gene expression in whole blood, it relies on eQTL-Gen phase 1, in which only 10,316 trait-associated SNPs were tested for *trans* associations. Another limitation is that the eQTLGen summary statistics were not directly adjusted for cell-type proportions in each blood sample, although they were adjusted for principal components as a proxy for cell-type proportions. We addressed this by examining the associations of rheumatoid arthritis with polygenic scores for immune cell phenotypes; CD4+ T cells were the only cell type for which a polygenic score was positively associated with rheumatoid arthritis. As the GATE score associations with rheumatoid arthritis do not match the expression profile

Table 4. Summary of validation status of putative core genes for rheumatoid arthritis identified through GATE analysis*

Gene	GWAS hit	Protein association	Mendelian randomization	Experimental validation in mouse model	Drug effect in humans
<i>IL10RA</i>				+	
<i>CD5</i>	+	+		+	
<i>CTLA4</i>	+			+	+
<i>STAP1</i>					
<i>FBLN7</i>					
<i>SLAMF1</i>	+	+			
<i>PNLIPRP2</i>					
<i>TP53BP1</i>			+	+	
<i>CXCL10</i>		+		+	
<i>CXCL9</i>		+		+	
<i>IDO1</i>			+		
<i>PDCD1</i>	+	+	+	+	+
<i>TNFRSF14</i>	+	+	+	+	
<i>LAIR1</i>		+	+	+	
<i>TIGIT</i>		+		+	
<i>LILRA4</i>			+		

* GATE, genome-wide aggregated *trans* effects; GWAS, genome-wide association study.

of this cell type, it is unlikely that confounding by cell-type proportions can explain these associations. These limitations will be overcome when more comprehensive summary statistics are available from the whole blood transcriptomics study that is now planned for a subset of the UK Biobank cohort. For *trans*-pQTLs in whole blood, comprehensive summary statistics on SNP associations are available for 2,923 proteins on the Olink platform measured on 54,000 participants in UK Biobank, but even with this large sample size, the GATE scores typically explain only about 10% of the estimated SNP heritability attributable to *trans* effects. We are nevertheless able to detect associations of these GATE scores with disease because the underlying associations, estimated from the associations of measured protein levels with disease, are typically strong.

Where variants with pleiotropic effects on gene expression have large effects on disease risk, GATE analysis alone cannot reliably distinguish causal genes from genes that are regulated by these pleiotropic variants. For this reason, we excluded *trans*-QTLs in the HLA region from the computation of GATE scores, as in our earlier study of type 1 diabetes. Where variants have large direct effects on disease risk, the eQTS method⁹ is expected to be less powerful than GATE analysis because such variants dilute the association of the target gene with the polygenic risk score. This may explain why only three of the 16 putative core genes were replicated in the eQTS summary statistics, even though the eQTS analysis was not limited to the 10,316 SNPs used in eQTLGen phase 1.

The coalescence of disease-associated SNP effects on expression of a small number of target genes, demonstrated in this study, provides broad support for the sparse effector hypothesis, at least for immune-mediated inflammatory disease. As disease-relevant genes are enriched with redundant enhancer domains and depleted of *cis*-eQTLs of large effect,^{51,52} they are often not detected by a conventional SNP-by-SNP GWAS analysis. Whatever theoretical questions remain to be resolved, it is clear that GATE analysis identifies disease-relevant genes that include at least some promising therapeutic targets, in contrast with conventional SNP-by-SNP analysis of a GWAS, which identifies mostly SNPs of tiny effect near genes that often have no obvious relevance to disease-specific pathways. Because GATE scores typically account for only a small proportion of the variance of gene expression, they are unlikely to be useful for stratifying disease with respect to prognosis and prediction of drug response. The proteins and transcripts encoded by the genes that are identified by GATE analysis as core genes have much stronger associations with disease; establishing whether they are useful as clinical predictors will require validation studies in cohorts.

AUTHOR CONTRIBUTIONS

All authors contributed to at least one of the following manuscript preparation roles: conceptualization AND/OR methodology, software, investigation, formal analysis, data curation, visualization, and validation AND drafting or reviewing/editing the final draft. As corresponding author, Dr McKeigue confirms that all authors have provided the final approval of



the version to be published and takes responsibility for the affirmations regarding article submission (eg, not under consideration by another journal), the integrity of the data presented, and the statements regarding compliance with institutional review board/Declaration of Helsinki requirements.

REFERENCES

- McKeigue P. Quantifying performance of a diagnostic test as the expected information for discrimination: relation to the C-statistic. *Stat Methods Med Res* 2019;28(6):1841–1851.
- Kuo C-F, Grainge MJ, Valdes AM, et al. Familial aggregation of rheumatoid arthritis and co-aggregation of autoimmune diseases in affected families: a nationwide population-based study. *Rheumatology (Oxford)* 2017;56(6):928–933.
- Schaid DJ, Lin WY. One- and two-locus models for mapping rheumatoid arthritis-susceptibility genes on chromosome 6. *BMC Proc* 2007; 1(Suppl 1):S103.
- Ishigaki K, Sakaue S, Terao C, et al; BioBank Japan Project. Multi-ancestry genome-wide association analyses identify novel genetic mechanisms in rheumatoid arthritis. *Nat Genet* 2022;54(11):1640–1651.
- Fang H, Chen L, Knight JC. From genome-wide association studies to rational drug target prioritisation in inflammatory arthritis. *Lancet Rheumatol* 2020;2(1):e50–e62.
- Liu X, Li YI, Pritchard JK. Trans effects on gene expression can drive omnigenic inheritance. *Cell* 2019;177(4):1022–1034.e6.
- Boyle EA, Li YI, Pritchard JK. An expanded view of complex traits: from polygenic to omnigenic. *Cell* 2017;169(7):1177–1186.
- Iakovliev A, McGurnaghan SJ, Hayward C, et al. Genome-wide aggregated trans-effects on risk of type 1 diabetes: a test of the “omnigenic” sparse effector hypothesis of complex trait genetics. *Am J Hum Genet* 2023;110(6):913–926.
- Võsa U, Claringbould A, Westra HJ, et al; BIOS Consortium; i2QTL Consortium. Large-scale cis- and trans-eQTL analyses identify thousands of genetic loci and polygenic scores that regulate blood gene expression. *Nat Genet* 2021;53(9):1300–1310.
- Sun BB, Maranville JC, Peters JE, et al. Genomic atlas of the human plasma proteome. *Nature* 2018;558(7708):73–79.
- Feringstad E, Sulem P, Atlason BA, et al. Large-scale integration of the plasma proteome with genetics and disease. *Nat Genet* 2021; 53(12):1712–1721.
- Sun BB, Chiou J, Traylor M, et al; Alnylam Human Genetics; AstraZeneca Genomics Initiative; Biogen Biobank Team; Bristol Myers Squibb; Genentech Human Genetics; GlaxoSmithKline Genomic Sciences; Pfizer Integrative Biology; Population Analytics of Janssen Data Sciences; Regeneron Genetics Center. Plasma proteomic associations with genetics and health in the UK Biobank. *Nature* 2023; 622(7982):329–338.
- Fehrmann RSN, Jansen RC, Veldink JH, et al. Trans-eQTLs reveal that independent genetic variants associated with a complex phenotype converge on intermediate genes, with a major role for the HLA. *PLoS Genet* 2011;7(8):e1002197.
- Hill MO. Diversity and evenness: a unifying notation and its consequences. *Ecology* 1973;54(2):427–432.
- McKeigue PM, Spiliopoulou A, Iakovliev A, et al. Inference of causal and pleiotropic effects with multiple weak genetic instruments: application to effect of adiponectin on type 2 diabetes. *medRxiv Preprint* posted online December 17, 2023. doi:<https://doi.org/10.1101/2023.12.15.23300008>
- Fauman EB, Hyde C. An optimal variant to gene distance window derived from an empirical definition of cis and trans protein QTLs. *BMC Bioinformatics* 2022;23(1):169.

17. Miceli-Richard C, Lesage S, Rybojad M, et al. CARD15 mutations in Blau syndrome. *Nat Genet* 2001;29(1):19–20.
18. Diogo D, Kurreeman F, Stahl EA, et al; Consortium of Rheumatology Researchers of North America; Rheumatoid Arthritis Consortium International. Rare, low-frequency, and common variants in the protein-coding sequence of biological candidate genes from GWASs contribute to risk of rheumatoid arthritis. *Am J Hum Genet* 2013;92(1):15–27.
19. Zhou Q, Wang H, Schwartz DM, et al. Loss-of-function mutations in TNFAIP3 leading to A20 haploinsufficiency cause an early-onset auto-inflammatory disease. *Nat Genet* 2016;48(1):67–73.
20. McGonagle D, Wadat A, Savic S. Mechanistic immunological based classification of rheumatoid arthritis. *Autoimmun Rev* 2018;17(11):1115–1123.
21. La Bella S, Rinaldi M, Di Ludovico A, et al. Genetic background and molecular mechanisms of juvenile idiopathic arthritis. *Int J Mol Sci* 2023;24(3):1846.
22. Orrù V, Steri M, Sole G, et al. Genetic variants regulating immune cell levels in health and disease. *Cell* 2013;155(1):242–256.
23. Tasaki S, Suzuki K, Kassai Y, et al. Multi-omics monitoring of drug response in rheumatoid arthritis in pursuit of molecular remission. *Nat Commun* 2018;9(1):2755.
24. Ren S, Tian Q, Amar N, et al. The immune checkpoint, HVEM may contribute to immune escape in non-small cell lung cancer lacking PD-L1 expression. *Lung Cancer* 2018;125:115–120.
25. Ruth JH, Gurra-Rubio M, Athukorala KS, et al. CD6 is a target for cancer immunotherapy. *JCI Insight* 2021;6:e145662.
26. Helou DG, Shafiei-Jahani P, Hurrell BP, et al. LAIR-1 acts as an immune checkpoint on activated ILC2s and regulates the induction of airway hyperreactivity. *J Allergy Clin Immunol* 2022;149(1):223–236.e6.
27. Alotaibi FM, Min WP, Koropatnick J. CD5 blockade, a novel immune checkpoint inhibitor, enhances T cell anti-tumour immunity and delays tumour growth in mice harbouring poorly immunogenic 4T1 breast tumour homografts. *Front Immunol* 2024;15:1256766.
28. Tiberio L, Laffranchi M, Zucchi G, et al. Inhibitory receptors of plasmacytoid dendritic cells as possible targets for checkpoint blockade in cancer. *Front Immunol* 2024;15:1360291.
29. Henningsson L, Eneljung T, Jirholt P, et al. Disease-dependent local IL-10 production ameliorates collagen induced arthritis in mice. *PLoS One* 2012;7(11):e49731.
30. Miura Y, Isogai S, Maeda S, et al. CTLA-4-Ig internalizes CD80 in fibroblast-like synoviocytes from chronic inflammatory arthritis mouse model. *Sci Rep* 2022;12(1):16363.
31. Plater-Zyberk C, Taylor PC, Blaylock MG, et al. Anti-CD5 therapy decreases severity of established disease in collagen type II-induced arthritis in DBA/1 mice. *Clin Exp Immunol* 1994;98(3):442–447.
32. Simelyte E, Rosengren S, Boyle DL, et al. Regulation of arthritis by p53: critical role of adaptive immunity. *Arthritis Rheum* 2005;52(6):1876–1884.
33. Zhao W, Dong Y, Wu C, et al. TIGIT overexpression diminishes the function of CD4 T cells and ameliorates the severity of rheumatoid arthritis in mouse models. *Exp Cell Res* 2016;340(1):132–138.
34. Pierer M, Schulz A, Rossol M, et al. Herpesvirus entry mediator-Ig treatment during immunization aggravates rheumatoid arthritis in the collagen-induced arthritis model. *J Immunol* 2009;182:3139–3145.
35. Kim S, Easterling ER, Price LC, et al. The role of leukocyte associated immunoglobulin-like receptor-1 (LAIR-1) in suppressing collagen-induced arthritis. *J Immunol* 2017;199:2692–2700.
36. Kwak HB, Ha H, Kim HN, et al. Reciprocal cross-talk between RANKL and interferon-gamma-inducible protein 10 is responsible for bone-erosive experimental arthritis. *Arthritis Rheum* 2008;58(5):1332–1342.
37. Boff D, Crijns H, Janssens R, et al. The chemokine fragment CXCL9(74–103) diminishes neutrophil recruitment and joint inflammation in antigen-induced arthritis. *J Leukoc Biol* 2018;104(2):413–422.
38. Wood MK, Daoud A, Talor MV, et al. Programmed death ligand 1-expressing macrophages and their protective role in the joint during arthritis. *Arthritis Rheumatol* 2024;76(4):553–565.
39. Maxwell L, Singh JA. Abatacept for rheumatoid arthritis. *Cochrane Database Syst Rev* 2009;2009(4):CD007277.
40. Tuttle J, Drescher E, Simón-Campos JA, et al. A phase 2 trial of pere-solimab for adults with rheumatoid arthritis. *N Engl J Med* 2023;388(20):1853–1862.
41. Zhai L, Ladomersky E, Lenzen A, et al. IDO1 in cancer: a Gemini of immune checkpoints. *Cell Mol Immunol* 2018;15(5):447–457.
42. Kagohashi K, Sasaki Y, Ozawa K, et al. Role of signal-transducing adaptor protein-1 for T cell activation and pathogenesis of autoimmune demyelination and airway inflammation. *J Immunol* 2024;212:951–961.
43. Sarangi PP, Chakraborty P, Dash SP, et al. Cell adhesion protein fibulin-7 and its C-terminal fragment negatively regulate monocyte and macrophage migration and functions in vitro and in vivo. *FASEB J* 2018;32(9):4889–4898.
44. Seki M, Oomizu S, Sakata KM, et al. Galectin-9 suppresses the generation of Th17, promotes the induction of regulatory T cells, and regulates experimental autoimmune arthritis. *Clin Immunol* 2008;127(1):78–88.
45. Sakaguchi S, Sakaguchi N, Asano M, et al. Immunologic self-tolerance maintained by activated T cells expressing IL-2 receptor alpha-chains (CD25). Breakdown of a single mechanism of self-tolerance causes various autoimmune diseases. *J Immunol* 1995;155:1151–1164.
46. Seo SK, Choi JH, Kim YH, et al. 4-1BB-mediated immunotherapy of rheumatoid arthritis. *Nat Med* 2004;10(10):1088–1094.
47. Ofiazoglu E, Boursalian TE, Zeng W, et al. Blocking of CD27-CD70 pathway by anti-CD70 antibody ameliorates joint disease in murine collagen-induced arthritis. *J Immunol* 2009;183:3770–3777.
48. Nozaki Y, Akiba H, Akazawa H, et al. Inhibition of the TIM-1 and -3 signaling pathway ameliorates disease in a murine model of rheumatoid arthritis. *Clin Exp Immunol* 2024;218(1):55–64.
49. Gu D, Ao X, Yang Y, et al. Soluble immune checkpoints in cancer: production, function and biological significance. *J Immunother Cancer* 2018;6(1):132.
50. Khan M, Zhao Z, Arooj S, et al. Soluble PD-1: predictive, prognostic, and therapeutic value for cancer immunotherapy. *Front Immunol* 2020;11:587460.
51. Wang X, Goldstein DB. Enhancer domains predict gene pathogenicity and inform gene discovery in complex disease. *Am J Hum Genet* 2020;106(2):215–233.
52. Mostafavi H, Spence JP, Naqvi S, et al. Systematic differences in discovery of genetic effects on gene expression and complex traits. *Nat Genet* 2023;55(11):1866–1875.

Cytotoxic Response of CD4⁺ T Cells Orchestrated by SLAMF4 in Rheumatoid Arthritis

Mégane Lacaud,¹ Houda-Ghozlane Bouzidi,¹ Mylène Petit,² Magali Breckler,¹ Delphine Lemeiter,¹ Johanna Sigaux,² Elodie Rivière,² Luca Semerano,² Marie-Christophe Boissier,² Natacha Bessis,¹  and Jérôme Biton¹ 

Objective. This study aimed to assess whether signaling lymphocytic activation molecule family receptors (SLAMFs) are involved in the shaping of the pathologic response of CD4⁺ T cells in rheumatoid arthritis (RA).

Methods. Peripheral blood (PB) and synovial fluid (SF) mononuclear cells from patients with RA were freshly isolated. In RA, we used a multimodal approach to determine the involvement of numerous subpopulations of CD4⁺ T cells expressing SLAMFs. Experimentally, multiple flow cytometry panels, RNA sequencing, and stimulations were used. Analyses involved high-dimensional unsupervised clustering of flow cytometry data and pathway enrichment analyses of transcriptomic data.

Results. In PB of patients with RA with active disease, SLAMF4⁺ effector memory CD4⁺ T cells (Tem) represented the only overrepresented subpopulation of CD4⁺ T cells expressing SLAMFs. This positive correlation between RA activity and SLAMF4⁺ Tem was restricted to those coexpressing the intracellular molecule SLAM-associated protein (SAP) and the tissue-homing receptor CCR5. Gene Set Enrichment Analysis of RNA sequencing data reveals that SLAMF4⁺ CCR5⁺ Tem display a cytotoxicity-related gene signature. Moreover, based on the differential expression of cytotoxicity markers (GPR56, CX3CR1, granzyme-B, perforin, and granulysin), unsupervised clustering of flow cytometry data identified distinct subpopulations of PB cytotoxic Tem. Among them, only SLAMF4^{high} SAP⁺ CCR5⁺ Tem (Cytotox-F4^{high} Tem) were correlated with RA activity. Remarkably, Cytotox-F4^{high} Tem emerged as the only cytotoxic population of CD4⁺ T cells (CD4⁺ CTLs) present in SF of patients with active disease.

Conclusion. This study emphasizes that Cytotox-F4^{high} Tem represent a significant CD4⁺ CTL subpopulation involved in RA, suggesting that their inhibition represent a promising therapeutic interest.

INTRODUCTION

Rheumatoid arthritis (RA) affects 0.5% to 1% of the adult population,¹ making it one of the most common autoimmune disorders worldwide. RA leads to joint destruction, disability, and reduced life expectancy.² The infiltration of different immune cell populations into the joint represents a major component of RA pathophysiology. This includes the recruitment and activation of natural killer (NK) cells, monocytes/macrophages, B cell-producing autoantibodies such as anti-citrullinated protein

antibodies (ACPA), and autoreactive CD4⁺ and CD8⁺ T cells, among others. Regarding CD4⁺ T cells, significant studies recently reinforced their major role in RA pathophysiology.^{3–8} For instance, high-dimensional analysis identified an additional CD4⁺ T cell subpopulation expanded in the synovium of patients with RA, named peripheral helper T (Tph) cells (PD-1^{high} CXCR5⁺). In RA, Tph cells have been shown to drive B cell activation and autoantibody production.⁶ Unlike follicular helper T (Tfh) cells, which interact with B cells within lymphoid organs, Tph cells provide help to B cells within inflamed tissues.⁵ In RA, other recent works

Supported by the French Society of Rheumatology, the Arthritis-Courtin Foundation, Chloé Recherche Foundation, the Université Sorbonne Paris Nord and Sandoz, Inc. France.

¹Mégane Lacaud, PhD, Houda-Ghozlane Bouzidi, MS, Magali Breckler, PhD, Delphine Lemeiter, MS, Natacha Bessis, PhD, Jérôme Biton, PhD: Inserm UMR-1125 and Université Sorbonne Paris Nord, Bobigny, France; ²Mylène Petit, MS, Johanna Sigaux, MD, PhD, Elodie Rivière, MD, PhD, Luca Semerano, MD, PhD, Marie-Christophe Boissier, MD, PhD: Inserm UMR-1125, Université Sorbonne Paris Nord and Avicenne Hospital, Assistance Publique Hôpitaux de Paris, Bobigny, France.

Drs Lacaud and Bouzidi are co-first authors and contributed equally to this work.

Additional supplementary information cited in this article can be found online in the Supporting Information section (<http://onlinelibrary.wiley.com/doi/10.1002/art.43124>).

Author disclosures are available at <https://onlinelibrary.wiley.com/doi/10.1002/art.43124>.

Address correspondence via email to Jérôme Biton, PhD, at jerome.biton@univ-paris13.fr.

Submitted for publication May 17, 2024; accepted in revised form January 7, 2025.

strengthened the place of Tph cells and of cytotoxic CD4⁺ T cells (CD4⁺ CTLs). These studies notably identified additional subpopulations of Tph cells and of CD4⁺ CTLs, such as CXCL13^{high} GPR56⁺ Tph cells,⁷ HLA-DR⁺ CD27[−] CD4⁺ CTLs,⁶ and cytotoxic age-associated helper T (ThA) cells.⁸

Despite an increasingly detailed characterization of the immunopathogenesis of RA, approximately 30% of patients do not respond adequately to targeted therapies,⁹ and only a minority achieve sustained remission. This underlines the need to identify new therapeutic targets. Regarding proinflammatory CD4⁺ Foxp3[−] T cells (Tconv), a major remaining objective is to identify additional parameters that support their pathologic functions, and then to focus on those that are therapeutically targetable. Among the receptors capable of modulating Tconv responses, the signaling lymphocytic activation molecule family (SLAMF) represents a group of receptors whose role in RA remains insufficiently explored. In fact, six SLAMFs have the potential to regulate the response of CD4⁺ T cells. These SLAMFs (SLAMF1, -F3, -F4, -F5, -F6, and -F7) possess immunoreceptor tyrosine-based inhibitory motifs (ITSMs) in their intracytoplasmic part.¹⁰ Once SLAMFs are engaged, their ITSMs are phosphorylated and serve as recruitment sites for the intracellular adapter molecule SLAM-associated protein (SAP).¹⁰ Then, SAP recruits the tyrosine-protein kinase Fyn and/or Lck, enabling the activation of signaling pathways essential for cell activation.¹¹

The connection between autoimmune diseases and SLAMFs is notably highlighted by several single nucleotide polymorphisms associated with systemic lupus erythematosus (SLE),^{12,13} multiple sclerosis,¹⁴ and RA.¹⁵ The involvement of SLAMF receptors has been well studied in SLE,¹⁶ in which SLAMF1 plays a crucial role in the interaction between CD4⁺ T and B cells.¹⁷ Additionally, CD4⁺ T cells exhibit overexpression of SLAMF1 and SLAMF7, and the frequency of terminally differentiated effector memory CD4⁺ T cells (Tem) expressing SLAMF1 is associated with SLE activity.¹⁶ Collectively, significant data in SLE illustrate the major role of SLAMFs in shaping Tconv responses in an autoimmune context. In RA, Tph cells are known to induce plasma cell differentiation through SLAMF5 interactions, and CD4⁺ CD28[−] T cells exhibit high expression of various NK receptors, including SLAMF4 and SLAMF7.¹⁸ However, research linking SLAMF expression to Tconv responses in RA is more limited. Given the critical role of Tconv in RA pathogenesis, further exploration of SLAMF-mediated modulation of Tconv responses in this disease is warranted. Therefore, our aim was to better characterized SLAMF involvement in shaping the proinflammatory responses of CD4⁺ T cells in RA.

PATIENTS AND METHODS

Patients. Individuals meeting the American College of Rheumatology/EULAR revised criteria for RA were selected.¹⁹ Individuals meeting the Assessment of SpondyloArthritis

International Society classification criteria for axial spondyloarthritis (SpA) were selected.²⁰ Patients with RA and SpA were recruited and peripheral blood (PB) samples were obtained as part of their medical management in the rheumatology department of Avicenne Hospital (Bobigny, France). RA activity was defined using Disease Activity Score-28 using the erythrocyte sedimentation rate (DAS28-ESR) or C-reactive protein level (DAS28-CRP) as follows: remission: DAS28-CRP or DAS28-ESR ≤ 2.6 ; low activity: DAS28-CRP or DAS28-ESR > 2.6 and ≤ 3.2 ; moderate activity: DAS28-CRP or DAS28-ESR > 3.2 and ≤ 5.1 ; and high activity: DAS28-CRP or DAS28-ESR > 5.1 . In some experiments, RA activity was defined as follows: RA remission-low: DAS28-CRP ≤ 3.2 ; RA moderate-high: DAS28-CRP > 3.2 . SpA activity was defined using the Bath Ankylosing Spondylitis Disease Activity Index.

Rheumatoid factor, ACPA seropositivity, and other clinical parameters were obtained by review of electronic medical records. Excepted those from Supplementary Figure 1B and E, all patients with RA included in this study were seropositive for ACPA. Patients with ACPA⁺ RA included in this study were naïve from biologic disease-modifying antirheumatic drugs (bDMARDs) or treated by tumor necrosis factor (TNF) inhibitors (etanercept, infliximab, and adalimumab), abatacept, or tocilizumab (see Supplementary Table 1 for more details). In some experiments, patients with ACPA[−] RA and patients with SpA were used as controls (see online Supplementary Table 1 for more details). PB from healthy donors (HDs) was obtained from donors recruited from the “Etablissement Français du Sang” of Avicenne Hospital. In the figures involving HDs, the latter were age-matched with RA patients.

Synovial fluid (SF) samples were obtained as excess material from patients with ACPA⁺ RA undergoing therapeutic arthrocentesis as directed by the treating rheumatologist. Of note, the majority of patients who underwent arthrocentesis had an active disease. The study was approved by the local ethics committee (NI-2016-11-01), and written informed consent was obtained from all patients before study entry.

Processing of blood and SF samples, flow cytometry (cell phenotyping).

Peripheral blood mononuclear cells (PBMCs) and SF mononuclear cells were freshly isolated by density-gradient sedimentation using Ficoll-Paque (Eurobio Scientific). Freshly isolated mononuclear cells were stained using antibodies listed in online Supplementary Table 2. Briefly, for surface cell staining, antibody dilutions were made using the BD Horizon Brilliant Stain Buffer (BD Biosciences) according to the manufacturer's recommendations. The anti-Foxp3 staining set (Thermo Fisher Scientific) was used for intracellular staining of Foxp3, SAP, cytokines (interferon [IFN]- γ , TNF- α), and cytotoxic molecules (granzyme-B, perforin, and granzyme), according to the manufacturer's recommendations. Flow cytometry acquisition was performed on a BD FACSymphony A3 Cell

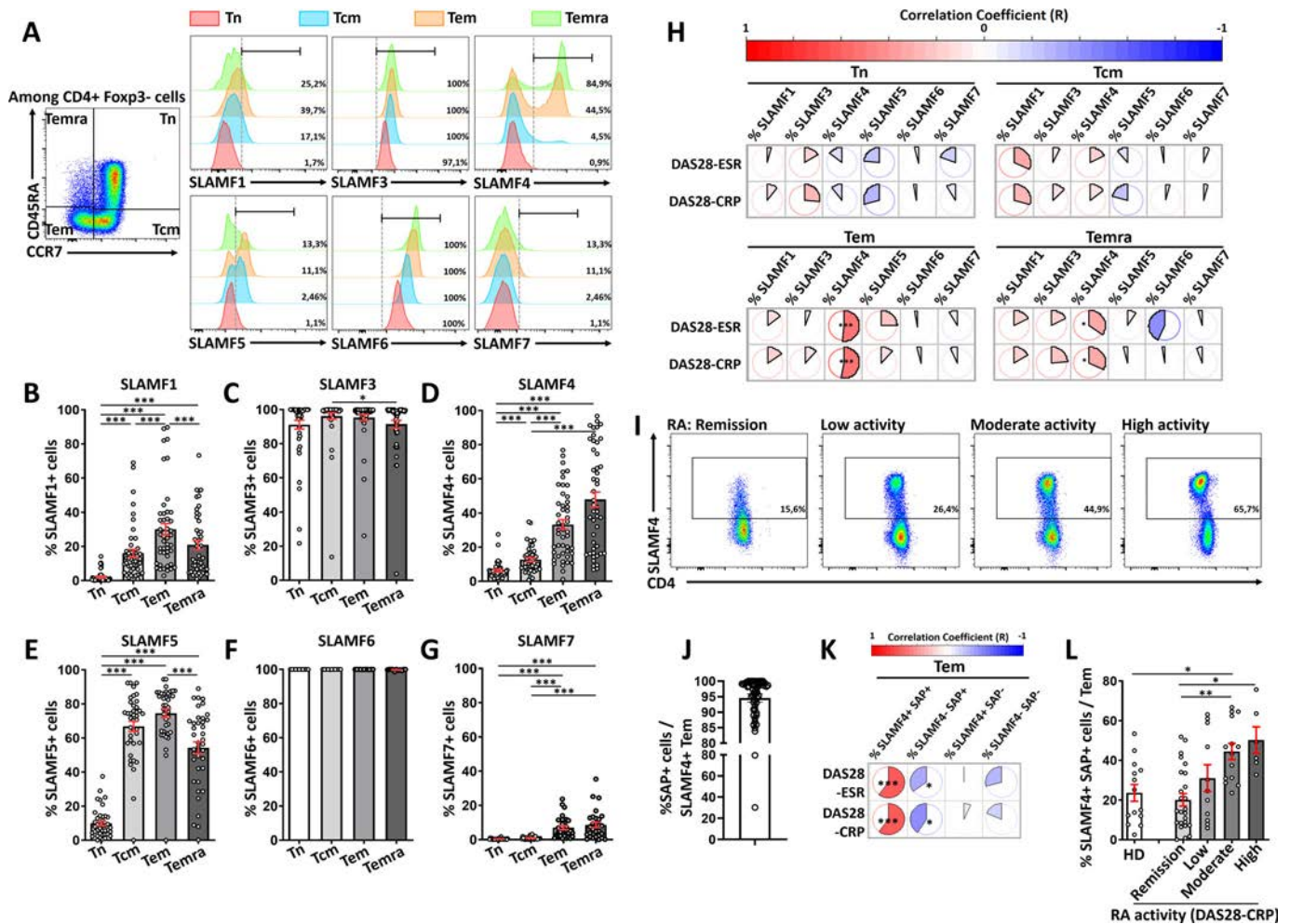


Figure 1. SLAMF4⁺ SAP⁺ Tem are associated with RA activity. (A–L) Flow cytometry experiments were performed using PB mononuclear cells (PBMCs) from patients with ACPA⁺ RA in (A–L) and HD in (L). (A) Representative monoparametric histograms of the expression of SLAMFs; and (B) percentage of SLAMF1⁺, (C) -F3⁺, (D) -F4⁺, (E) -F5⁺, (F) -F6⁺, and (G) -F7⁺ cells among Tn, Tcm, Tem, and Temra in patients with RA (n = 46). (H) Correlations between DAS28-ESR or DAS28-CRP vs percentage of SLAMF⁺ cells among Tn, Tcm, Tem, and Temra in patients with RA (n = 46). Red and blue colors indicate positive and negative correlations, respectively. The filled fraction of the circle in each of the pie charts corresponds to the absolute value of the associated Spearman correlation coefficient. (I) Representative dot plots of SLAMF4 expression among Tem according to DAS28-CRP. (J) Percentage of SAP⁺ cells among SLAMF4⁺ Tem. (K) Correlations between DAS28-ESR or DAS28-CRP vs percentage of SLAMF4⁺ SAP⁺ among Tem in patients with RA (n = 56). (L) Percentage of SLAMF4⁺ SAP⁺ cells among Tem in HD (n = 14) and patients with RA (n = 56) according to disease activity (DAS28-CRP). (B–G, J, and L) Data are expressed as mean ± SEM. (B–G) A Friedman test was used. (L) A Kruskal-Wallis test was applied. (H and K) A Spearman test was applied. **P* < 0.05, ***P* < 0.01, ****P* < 0.001. DAS28-CRP, Disease Activity Score-28 using the C-reactive protein level; DAS28-ESR, Disease Activity Score-28 using the erythrocyte sedimentation rate; HD, healthy donor; PB, peripheral blood; RA, rheumatoid arthritis; SAP, SLAM-associated protein; SLAMF, signaling lymphocytic activation molecule family; Tcm, central memory CD4⁺ T cells; Tem, effector memory CD4⁺ T cells; Temra, effector memory CD4⁺ T cells re-expressing CD45RA; Tn, naïve CD4⁺ T cells.

Analyzer (BD Biosciences) using FACSDiva software. Results were analyzed using FlowJo software v10.9.0 (TreeStar, Inc). Detailed methods are described in the Supplementary Methods.

Cytokine expression. To study IFN- γ , TNF- α , and CXCL13 expression, PBMCs were cultured for two hours (IFN- γ , TNF- α) or four hours (CXCL13) (before staining) in flat-bottom 96-well plates at a density of 10^6 cells per 200 μ L in the presence

of RPMI 1640 with 10% fetal bovine serum (FBS), 100 U/mL penicillin, 100 mg/mL streptomycin, 1 M HEPES. PBMCs were cultured with or without (unstimulated cells) 25 ng/mL of phorbol 12-myristate 13-acetate (PMA) and 0.5 μ g/mL of ionomycin (Sigma-Aldrich) in the presence of brefeldin A (1/1,000) and monensin (0.7/1,000) (stimulated and unstimulated cells) (BD Biosciences). In some experiments, for CXCL13 expression, instead of PMA/ionomycin, a 24-hour coated anti-CD3 antibody stimulation was used (1 μ g/mL) (BD Biosciences, clone OKT3).

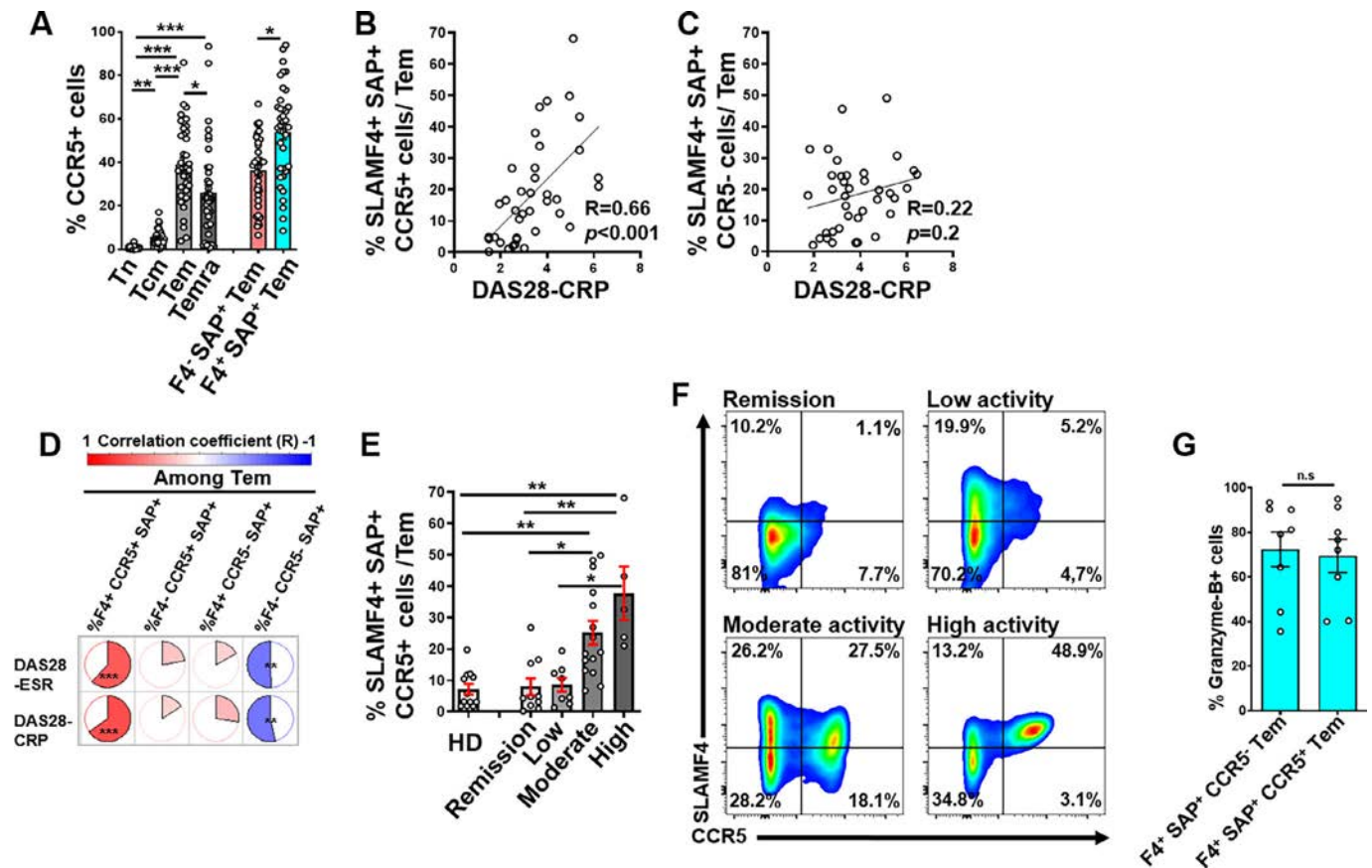


Figure 2. CCR5 expression by SLAMF4⁺ SAP⁺ Tem is necessary to establish a link with RA activity. (A–G) Flow cytometry experiments were performed using PBMCs from patients with RA ($n = 38$) in (A)–(F) or ($n = 8$) in (G) and from HD ($n = 12$) in (E). (A) Percentage CCR5⁺ cells among Tn, Tcm, Tem, Temra, and F4^{+/−} SAP⁺ Tem. (B) Correlation between the DAS28-CRP and percentage of F4⁺ SAP⁺ CCR5⁺ cells among Tem (patients with RA). (C) Correlation between the DAS28-CRP and percentage SLAMF4⁺ SAP⁺ CCR5[−] cells among Tem (patients with RA). (D) Correlations between RA activity (DAS28-ESR and DAS28-CRP) vs percentage F4^{+/−} SAP⁺ CCR5^{+/−} cells among Tem. Graphical representation is the same as in Figure 1H. (E) Percentage F4⁺ SAP⁺ CCR5⁺ cells among Tem in HD and patients with RA according to disease activity defined using DAS28-CRP. (F) Representative dot plots of SLAMF4 and CCR5 expression among SAP⁺ Tem according to RA activity (DAS28-CRP). (G) Percentage granzyme-B⁺ cells among F4⁺ SAP⁺ CCR5^{+/−} Tem in patients with RA ($n = 8$). (A, E and G) Data are expressed as mean \pm SEM. (A) A Friedman test was applied, because of space constraints only selected statistically significant differences are labeled. (B–D) A Spearman test, (E) a Kruskal-Wallis test, and (G) a Wilcoxon signed-rank test were used. * $P < 0.05$, ** $P < 0.01$, *** $P < 0.001$. DAS28-CRP, Disease Activity Score-28 using the C-reactive protein level; DAS28-ESR, Disease Activity Score-28 using the erythrocyte sedimentation rate; F4, SLAMF4; HD, healthy donor; n.s., not significant; PBMC, peripheral blood mononuclear cell; RA, rheumatoid arthritis; SAP, SLAM-associated protein; SLAMF, signaling lymphocytic activation molecule family; Tcm, central memory CD4⁺ T cells; Tem, effector memory CD4⁺ T cells; Temra, effector memory CD4⁺ T cells re-expressing CD45RA; Tn, naïve CD4⁺ T cells. Color figure can be viewed in the online issue, which is available at <http://onlinelibrary.wiley.com/doi/10.1002/art.43124/abstract>.

For the last four hours of cultures, brefeldin A (1/1,000) and monensin (0.7/1,000) were added (BD Biosciences). Unstimulated cells were used as control and stained with the same antibody mix than stimulated cells. Then, cell surface and intracellular staining were performed as described above and in Supplementary Methods.

Cells sorting. Cells sorting was performed on a BD FACSAria II sorter. Cell purity was routinely >95%. For subsequent RNA analyses, sorted cells were immediately lysed in RLT lysis buffer (Qiagen) with 1% β -mercaptoethanol (Sigma). Details are provided in Supplementary Methods.

In vitro stimulation (granzyme-B secretion). Sorted F4⁺ and F4[−] Tem were cultured in U-bottom 96-well plates at a density of 3×10^5 cells per 200 μ L in the presence of RPMI 1640 with 10% FCS, 100 U/mL penicillin, 100 mg/mL streptomycin, 1 M HEPES, with (stimulated cells) or without (unstimulated cells) 2 μ g/mL of soluble anti-CD3 (clone HIT3) (eBioscience). After 24 hours of culture, granzyme-B levels in culture supernatants were measured using commercially available enzyme-linked immunosorbent assay kits (DuoSet Granzyme-B; R&D Systems) according to the manufacturer's instructions.

Flow cytometry unsupervised analyses. The plugins Downsampler (V3), PaCMAP (V1.0.0), and FlowSOM (3.0.18 PP),

from FlowJo software v10.9.0 (TreeStar, Inc), were used to perform unsupervised analyses. Detailed descriptions are in the Supplementary Methods.

RNA sequencing and data analyses. RNA extractions were realized with a Norgen kit. RNA concentrations were obtained using fluorometric Qubit RNA assay (Life Technologies). The quality of the RNA (RNA integrity number) was determined on the Agilent 2100 Bioanalyzer (Agilent Technologies) using a pico chip kit. To construct the libraries, 1 ng of high quality total RNA sample (RNA integrity number >6.5) was processed using NEB-Next low input RNA library prep kit (New England BioLabs) according to manufacturer's instructions. Polymerase chain reaction enrichment with a single barcode was then realized to obtain the final library. Libraries were then quantified with Qubit HS DNA assay (Life Technologies) and library profiles assessed using the DNA High Sensitivity LabChip kit on an Agilent 2100 Bioanalyzer (Agilent Technologies). Libraries were sequenced on a NextSeq 500 instrument (Illumina). Fastq files were then aligned using STAR algorithm (version 2.7.6a), on the Ensembl release 101 reference. Reads were then counted using RSEM (v1.3.1), and the statistical analyses on the read counts were performed with R software (version 3.6.3) and the DESeq2 package (DESeq2_1.26.0). We used the standard DESeq2 normalization method. The Wald test with the contrast function and the Benjamini-Hochberg false discovery rate (FDR) control procedure were used to identify the differentially expressed genes. R scripts and parameters used to perform analyses are available on the platform: https://github.com/GENOM-IC-Cochin/RNA-Seq_analysis. Details are provided in Supplementary Methods.

To investigate enriched functions and pathways of the 100 most significantly up-regulated genes (Fold change >2 and FDR <8 × 10⁻⁶) in SLAMF4⁺ CCR5⁺ Tem, we used the Cytoscape (v3.9.1) plugin ClueGo/CluePedia (v2.5.9).^{21,22} Details are provided in Supplementary Methods.

Statistical analysis. Data distribution was determined using a Shapiro-Wilk normality test. For analyses with two comparisons, quantitative unpaired data were assessed using an unpaired *t*-test if normally distributed, or a Mann-Whitney U test if not. For more than two comparisons, a one-way analysis of variance (ANOVA) with Tukey's post hoc comparisons was used for normally distributed unpaired data, and a Kruskal-Wallis test with Dunn's post hoc comparisons was used otherwise. For paired data involving two comparisons, a paired *t*-test was used if the data were normally distributed, or a Wilcoxon signed-rank test if not. For more than two comparisons, a one-way repeated measures ANOVA with Tukey's post hoc comparisons was used for normally distributed paired data, and a Friedman test with Dunn's post hoc comparisons was used otherwise. Categorical data were compared using a chi-square test. Correlations between quantitative parameters were assessed using the Spearman test.

Statistical analyses were performed with GraphPad Prism software version 8.0.2. Data are presented as the mean ± SEM in all Figures and as mean ± SD in Supplementary Table 1. A value of *P* < 0.05 was considered as significant. The statistical tests applied for each comparison are specified in the corresponding figure and table legends.

Principal component analysis correlation circles (Supplementary Figure 2) and multiple correlation representations were performed using R software (<http://www.r-project.org/>). In RNA sequencing analysis, a Wald test with the contrast function and the Benjamini-Hochberg FDR control procedure were used to identify the differentially expressed genes. FDR < 0.05 with a fold change >2 was considered as significant.

RESULTS

Tem coexpressing SLAMF4 and SAP are overrepresented in patients with ACPA⁺ RA with active disease. In patients with ACPA⁺ RA (Supplementary Table 1), we focused on the six SLAMFs (SLAMF1, -F3, -F4, -F5, -F6, and -F7) potentially able to impact the response of Tconv. Their expression was assessed among four PB Tconv subpopulations, namely naïve CD4⁺ T cells (Tn; CD45RA⁺ CCR7⁺), central memory CD4⁺ T cells (Tcm; CD45RA⁻ CCR7⁺), Tem (CD45RA⁻ CCR7⁻), and effector memory CD4⁺ T cells re-expressing CD45RA (Temra; CD45RA⁺ CCR7⁻) (Supplementary Figure 3A and B). First, SLAMF3 and SLAMF6 were almost expressed by all Tconv, regardless of their activation status (Figure 1A, C, and F). The frequency of SLAMF1 and SLAMF5 expressing cells was maximal among Tem (Figure 1A, B, and E), whereas that of SLAMF4 and SLAMF7 still increased until the Temra stage (Figure 1A, D, and G).

Next, we investigated the relationship between RA activity (measured with DAS28-ESR and DAS28-CRP scores) and SLAMF expression by the four Tconv subpopulations studied. Remarkably, only the frequency of SLAMF4⁺ cells among Tem showed a strong and significant positive correlation with disease activity (percentage SLAMF4⁺ cells among Tem vs DAS28-ESR and DAS28-CRP, *R* = 0.51 and *R* = 0.58, respectively) (Figure 1H and I). By contrast, although these correlations were also significant among Temra, they were much weaker (Figure 1H). Based on these results, we then focused on SLAMF4⁺ Tem. Although most F4⁺ Tem expressed SAP (Figure 1J), approximately 5% of them were SAP⁻. Because SLAMFs cannot activate Tem in the absence of SAP, we examined whether SLAMF4⁺ SAP^{+/−} Tem were differentially associated with RA activity.¹¹ In fact, among SLAMF4⁺ Tem, only those expressing SAP were associated with RA activity (Figure 1K). As a result, the frequency of SLAMF4⁺ SAP⁺ (F4⁺ SAP⁺) cells among Tem was higher in patients with highly active RA, compared to those in remission and to HDs (Figure 1L). The use of bDMARDs did not significantly impact this finding (Supplementary Figure 4).

Finally, we evaluated whether our results were applicable to another chronic inflammatory rheumatic disease with different pathologic mechanisms from RA, namely SpA. Our results showed that F4⁺ SAP⁺ Tem were not associated with disease activity in patients with SpA (Supplementary Figure 1C and F). Moreover, given that some evidence suggests that ACPA⁻ and ACPA⁺ RA might represent two distinct pathologic entities,²³ we also checked our findings in ACPA⁻ RA. Importantly, we did not find any correlations in patients with ACPA⁻ RA (Supplementary Figure 1B and E). Consequently, the rest of this study focused on patients with ACPA⁺ RA.

F4⁺ SAP⁺ Tem display both Th1 cell and CD4⁺ CTL characteristics. To evaluate the proinflammatory properties of F4⁺ Tem, we determined their capacity to produce TNF- α and IFN- γ . First, TNF- α expression was similarly high in F4⁺ SAP⁺ and F4⁻ SAP⁺ Tem (Figure 3A–C). However, the expression of IFN- γ (Figure 3D–F) and the frequency of cells coexpressing TNF- α and IFN- γ were dramatically higher in F4⁺ SAP⁺ Tem than in F4⁻ SAP⁺ Tem (Figure 3G and H). In the absence of SAP, F4⁺ Tem had a lower expression of IFN- γ (Supplementary Figure 5A–C). Moreover, in addition to its strong expression by NK and CD8⁺ T cells, some studies reported that CD4⁺ CTLs also overexpressed SLAMF4.^{18,24,25} Figure 3I and J showed that granzyme-B expression was mostly limited to F4⁺ Tem and F4⁺ Temra. Of note, SAP expression by F4⁺ Tem was necessary to sustain that of granzyme-B (Supplementary Figure 5D and E). Next, we checked the ability of sorted F4⁺ Tem to secrete granzyme-B in response to anti-CD3 antibody stimulation. Figure 3K showed a much higher granzyme-B concentration in the supernatant of anti-CD3 activated F4⁺ Tem compared to that of F4⁻ Tem. This result supported that F4⁺ SAP⁺ Tem possessed the capacity to secrete granzyme-B contained in their lytic granules. Altogether, the present data indicated that F4⁺ SAP⁺ Tem possessed both proinflammatory and cytotoxic properties.

CCR5 links cytotoxic F4⁺ SAP⁺ Tem to RA pathophysiology. CCR5 is a chemokine receptor well known to be involved in immune cell migration toward inflammatory tissues.²⁶ Moreover, it has been shown that most T cells express CCR5 in the joints of RA patients.^{26–28} Consequently, we assessed whether PB F4⁺ SAP⁺ Tem expressed CCR5, and if so, to what extent this impacted their link with RA activity (Supplementary Table 1). As expected, CCR5 was hardly expressed by Tn and Tcm, whereas it was expressed by approximately 40% of Tem (Figure 2A). The frequency of CCR5 expressing cells was higher in F4⁺ SAP⁺ Tem than in F4⁻ SAP⁺ Tem (Figure 2A). Remarkably, F4⁺ SAP⁺ CCR5⁺ Tem were positively correlated with disease activity, whereas this was not the case for their CCR5⁻ counterparts (Figure 2B–D). Therefore, the frequency of F4⁺ SAP⁺ CCR5⁺ cells among Tem was higher in patients with highly active RA than in those in remission and in HD (Figure 2E and F). Next, we sought

to evaluate the impact of CCR5 on granzyme-B and cytokine expression by F4⁺ SAP⁺ Tem. We were unable to do this for cytokines, because the available methods (PMA-ionomycin or anti-CD3 stimulation) to study their expression dramatically decrease that of CCR5. Regarding granzyme-B, no stimulation step was required to study its expression. Importantly, PB F4⁺ SAP⁺ CCR5⁺ Tem had a similar expression of granzyme-B than their CCR5⁻ counterparts (Figure 2G).

The presence of PB CD4⁺ CTLs consistent with F4⁺ SAP⁺ CCR5⁺ Tem has been observed in patients with autoimmune diseases, but also in older individuals, such as supercentenarians.^{29,30} As expected, both F4⁺ SAP⁺ CCR5⁺ and CCR5⁻ Tem proportion increased with the age of RA patients (Supplementary Figure 2A–D). However, principal component analysis correlation circles clearly indicated that PB F4⁺ SAP⁺ CCR5⁺ Tem were mainly linked to RA activity, whereas their CCR5⁻ counterparts were rather associated with patient's age (Supplementary Figure 2E–H). Finally, only F4⁺ SAP⁺ Tem expressing CCR5 are associated with disease activity in PB, regardless of patient's age.

F4⁺ SAP⁺ CCR5⁺ Tem correspond to a Th1 like CD4⁺ CTL subpopulation. To further characterize PB F4⁺ CCR5⁺ Tem, we compared their transcriptome to that of their F4⁻ counterparts. Cells were sorted according to SLAMF4 and CCR5 expression (Supplementary Figure 6) but not on that of SAP, to avoid cell fixation and permeabilization. Of note, the expression of *SH2D1A* encoding SAP was not significantly different in F4⁺ CCR5⁺ versus F4⁻ CCR5⁺ Tem (Supplementary Figure 7A). Unsupervised analyses of enriched functions and pathways of the 100 most up-regulated genes in F4⁺ CCR5⁺ Tem revealed an overrepresentation of genes related to mononuclear cell migration (*CCL4*, *CCL5*, *XCL2*, *CX3CR1*) and with leukocyte-mediated cytotoxicity (*PRF1*, *GZMB*, *KLRD1*) (Figure 4A–C). Additionally, supervised analysis confirmed that F4⁺ CCR5⁺ Tem overexpressed genes associated with a cytotoxic signature (Figure 4D–F; Supplementary Figure 7B).^{31,32} This signature included genes encoding cytotoxic molecules (*GZMA*, *GZMB*, *GZMH*, *GNLY*, *PRF1*, *FASLG*, and *KLRD1*) and molecules involved in immune cell degranulation or in their killing activity (*KLRK1* and *NKG7*). An increased expression of genes related to the cytotoxic functions of T lymphocytes was also observed (*CRTAM*, *EOMES*, *ZNF683*, and *ZEB2*).^{32–35} *ADGRG1* encoding GPR56, an adhesion G-protein coupled receptor that has been suggested to be a marker of cytotoxic T cells,³⁶ was also overexpressed by F4⁺ CCR5⁺ Tem (Figure 4D–F). Regarding genes known to be down-regulated in CD4⁺ CTLs, a decreased expression of *ZEB1*, *CD27*, and *CD28* was observed among F4⁺ CCR5⁺ Tem (Figure 4E; Supplementary Figure 7C).

RNA sequencing data also showed that the expression of most chemokine receptors and homing molecules was down-regulated in F4⁺ CCR5⁺ Tem (Supplementary Figure 7E), except for *CX3CR1* and *S1PR5* (Figure 4E and F), whose expression is

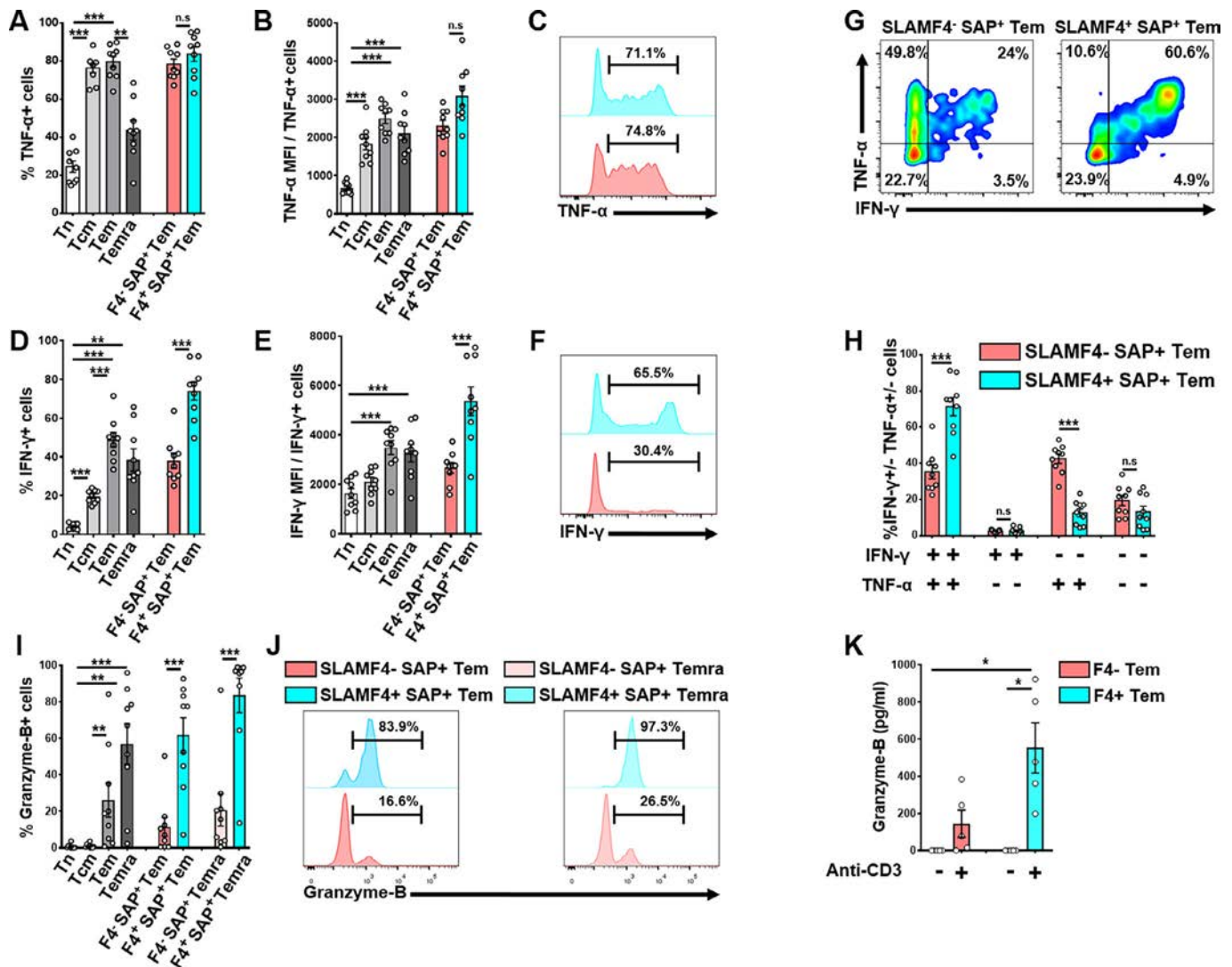
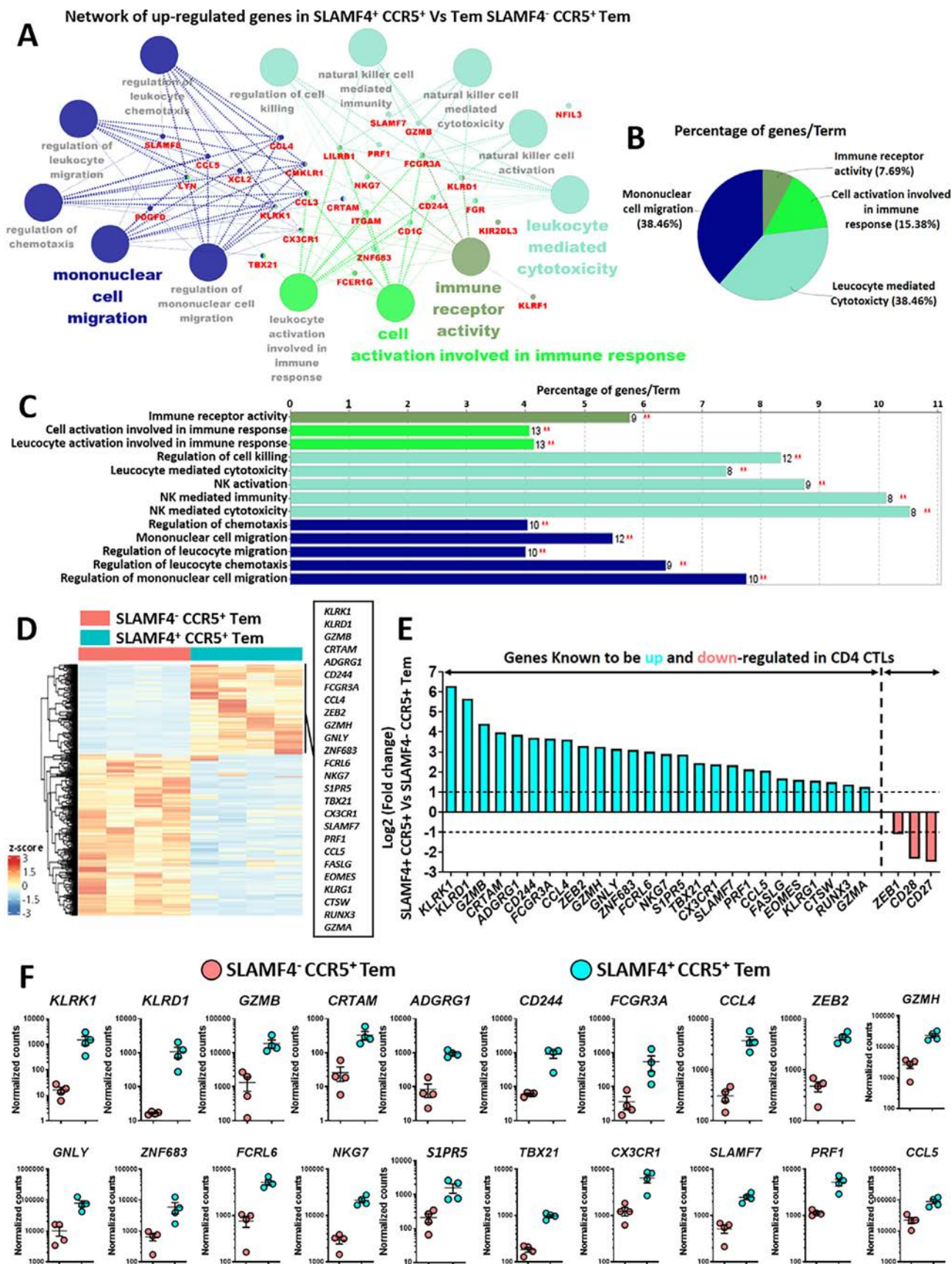


Figure 3. SLAMF4⁺ SAP⁺ Tem highly express IFN-γ and granzyme-B. (A–K) Flow cytometry experiments were performed using PBMCs from patients with RA (n = 9 in A–J; n = 5 in K). (A–J) PBMCs were stimulated 2 hours with PMA-ionomycin. (A) Percentage of TNF-α⁺ cells, (B) TNF-α MFI/TNF⁺ cells, (D) percentage of IFN-γ⁺ cells, (E) IFN-γ MFI/IFN-γ⁺ cells, among Tn, Tcm, Tem, Temra, and SLAMF4⁺ SAP⁺ Tem. (C and F) Representative monoparametric histograms of (C) TNF-α and (F) IFN-γ expression by F4⁺ SAP⁺ Tem (red curve) and F4⁺ SAP⁺ Tem (blue curve). (G) Representative dot plots of TNF-α and IFN-γ coexpression by F4⁺ SAP⁺ Tem. (H) Frequency of TNF-α⁺ IFN-γ⁺ cells among F4⁺ SAP⁺ Tem. (I) % granzyme-B⁺ cells among Tn, Tcm, Tem, Temra, F4⁺ SAP⁺ Tem and F4⁺ SAP⁺ Temra. (J) Representative monoparametric histograms of granzyme-B expression by F4⁺ SAP⁺ Tem and F4⁺ SAP⁺ Temra. (K) Granzyme-B concentration (ELISA) in sorted F4⁺ and F4⁺ Tem stimulated with or without anti-CD3 antibody. (A, B, D, E, H, I, and K) Data are expressed as mean ± SEM. (A, B, D, E, and H) A one-way repeated measures ANOVA was used. (I and K) A Friedman test was used. **P* < 0.05, ***P* < 0.01, ****P* < 0.001. ANOVA, analysis of variance; ELISA, enzyme-linked immunosorbent assay; F4, SLAMF4; IFN, interferon; MFI, mean fluorescence intensity; n.s., not significant; PBMC, peripheral blood mononuclear cell; PMA, phorbol myristate acetate; RA, rheumatoid arthritis; SAP, SLAM-associated protein; SLAMF, signaling lymphocytic activation molecule family; Tcm, central memory CD4⁺ T cells; Tem, effector memory CD4⁺ T cells; Temra, effector memory CD4⁺ T cells re-expressing CD45RA; Tn, naïve CD4⁺ T cells; TNF, tumor necrosis factor. Color figure can be viewed in the online issue, which is available at <http://onlinelibrary.wiley.com/doi/10.1002/art.43124/abstract>.

known to be up-regulated in CD4⁺ CTLs.³⁷ Regarding the expression of genes allowing the identification of the main subtypes of Th cells (Supplementary Figure 7D), only *TBX21* encoding the Th1 marker Tbet was up-regulated (Figure 4F). Finally, a flow cytometry panel dedicated to the study of CD4⁺ CTLs confirmed a higher expression of Th1 (Tbet) and cytotoxicity markers (granzyme-B, perforin, granzyme, GPR56, and CX3CR1) in F4⁺ SAP⁺ CCR5⁺ Tem (Supplementary Figure 7F–H). Altogether, flow cytometry

and RNA sequencing data identified F4⁺ SAP⁺ CCR5⁺ Tem as a subpopulation of Th1-like CD4⁺ CTLs.

F4⁺ SAP⁺ CCR5⁺ Tem represent a less frequent population of Th1 like CD4⁺ CTLs than those previously described as being involved in RA. Next, we determined the extent to which F4⁺ SAP⁺ CCR5⁺ Tem represented an original subset of CD4⁺ CTLs. Consequently, we first evaluated the



(Figure legend continues on next page.)

overlap between F4⁺ SAP⁺ CCR5⁺ Tem and the CD4⁺ CTL subset originally described as expanded in RA, namely CD4⁺ CD28[−] T cells. Supplementary Figure 8A–C showed that F4⁺ SAP⁺ CCR5⁺ Tem were half as frequent as CD4⁺ CD28[−] T cells. Moreover, dimensionality reduction analysis of flow cytometry data identified that F4⁺ SAP⁺ CCR5⁺ Tem and CD4⁺ CD28[−] T cells only partially overlapped, with an overlap index of less than 50% (Supplementary Figure 8D–G). More precisely, regarding CD4⁺ CD28[−] T cells, we identified three cell subsets that did not match with F4⁺ SAP⁺ CCR5⁺ Tem (Supplementary Figure 8H–L). The first one corresponded to a subset of CD4⁺ CD28[−] Tem lacking CCR5 expression (green population) (Supplementary Figure 8H–J). CCR5[−] cells represented approximately 40% of CD4⁺ CD28[−] Tem (Supplementary Figures 8J and 9A). This analysis also highlighted the presence of CD4⁺ CD28[−] T cells corresponding to Temra (light blue population) (Supplementary Figure 8H, I, and K), and of a subset of CD4⁺ CD28[−] Tem that did not express SLAMF4 (orange population) (Supplementary Figure 8H, I, and L). Indeed, in some patients, up to half of CD4⁺ CD28[−] T cells were Temra (Supplementary Figure 9B), whereas F4[−] CD4⁺ CD28⁺ Tem had a lower expression of granzyme-B compared to their SLAMF4⁺ counterparts (Supplementary Figure 9D and E). Finally, regarding F4⁺ SAP⁺ CCR5⁺ Tem, we identified a minor population of cells expressing CD28 (pink population) (Supplementary Figure 8H and M) that retained a significant expression of granzyme-B (Supplementary Figure 9G and H).

Additionally, we determined whether F4⁺ SAP⁺ CCR5⁺ Tem corresponded to a more recently described population of CD4⁺ CTLs, namely HLA-DR⁺ CD27[−] Tem.⁶ Our data showed that most F4⁺ SAP⁺ CCR5⁺ Tem corresponded to HLA-DR[−] CD27[−] Tem and not to HLA-DR⁺ CD27[−] Tem (Supplementary Figure 10A and B). Moreover, whatever the expression of HLA-DR and CD27 by Tem, only those expressing SLAMF4 expressed granzyme-B (Supplementary Figure 10C–H).

In RA and other autoimmune diseases, an additional subset of CD4⁺ CTLs has been recently described. This subset of cytotoxic CXCR3^{mid} CD25[−] CXCR5[−] CCR6[−] CCR4[−] Tem were designated as ThA cells.⁸ Indeed, a majority of F4⁺ Tem, but also of F4⁺ SAP⁺ CCR5⁺ Tem, corresponded to CXCR3^{mid} CD25[−] CXCR5[−] CCR6[−]

CCR4[−] cells (Supplementary Figure 11D–G), confirming RNA sequencing data (Supplementary Figure 7). Conversely, less than 65% of ThA cells expressed SLAMF4 (Supplementary Figure 11H), whereas less than half of ThA cells expressed CCR5 (Supplementary Figure 11I). As a result, F4⁺ SAP⁺ CCR5⁺ Tem accounted for only 35% of total ThA cells (Supplementary Figure 11J and K). Consequently, F4⁺ SAP⁺ CCR5⁺ Tem represented a much less frequent subpopulation than ThA cells. Importantly, granzyme-B expression by ThA cells was restricted to those expressing SLAMF4 (Supplementary Figure 11L and M). Besides their cytotoxic properties, ThA cells also exhibit a B cell helper function notably through the production of CXCL13. Importantly, CXCL13 gene was not expressed by F4⁺ CCR5⁺ Tem (Supplementary Figure 7E). At the protein level, CXCL13 expression by F4⁺ SAP⁺ Tem was very low and not significantly different from that of F4[−] SAP⁺ Tem (Supplementary Figure 11Q and R). Indeed, the higher expression of CXCL13 was observed for Tcm (Supplementary Figure 11O and P).³⁸ Altogether, multiple flow cytometry and RNA sequencing experiments identified F4⁺ SAP⁺ CCR5⁺ Tem as a subpopulation distinct from HLA-DR⁺ CD27[−] Tem and much less frequent than ThA cells and CD4⁺ CD28[−] T cells.

Cytotox-F4^{high} Tem are the only subset of CD4⁺ CTLs found in SF. In SF, we assessed the presence of F4⁺ SAP⁺ CCR5⁺ Tem. First, SF was highly enriched in Tem compared to PB, whereas Tn and Temra were virtually absent (Supplementary Figure 12A and B). In PB, SLAMF4 was expressed by both Tem and Temra, whereas its expression in SF was mostly restricted to Tem (Supplementary Figure 12C). In SF, Tem frequency being higher than in PB, and SLAMF4 expression being restricted to Tem, F4⁺ SAP⁺ Tem were overrepresented in this compartment (Supplementary Figure 12D). Moreover, most of them expressed CCR5 (Supplementary Figure 12E). Therefore, only the subpopulation of F4⁺ SAP⁺ Tem expressing CCR5 was enriched in SF (Supplementary Figure 12F).

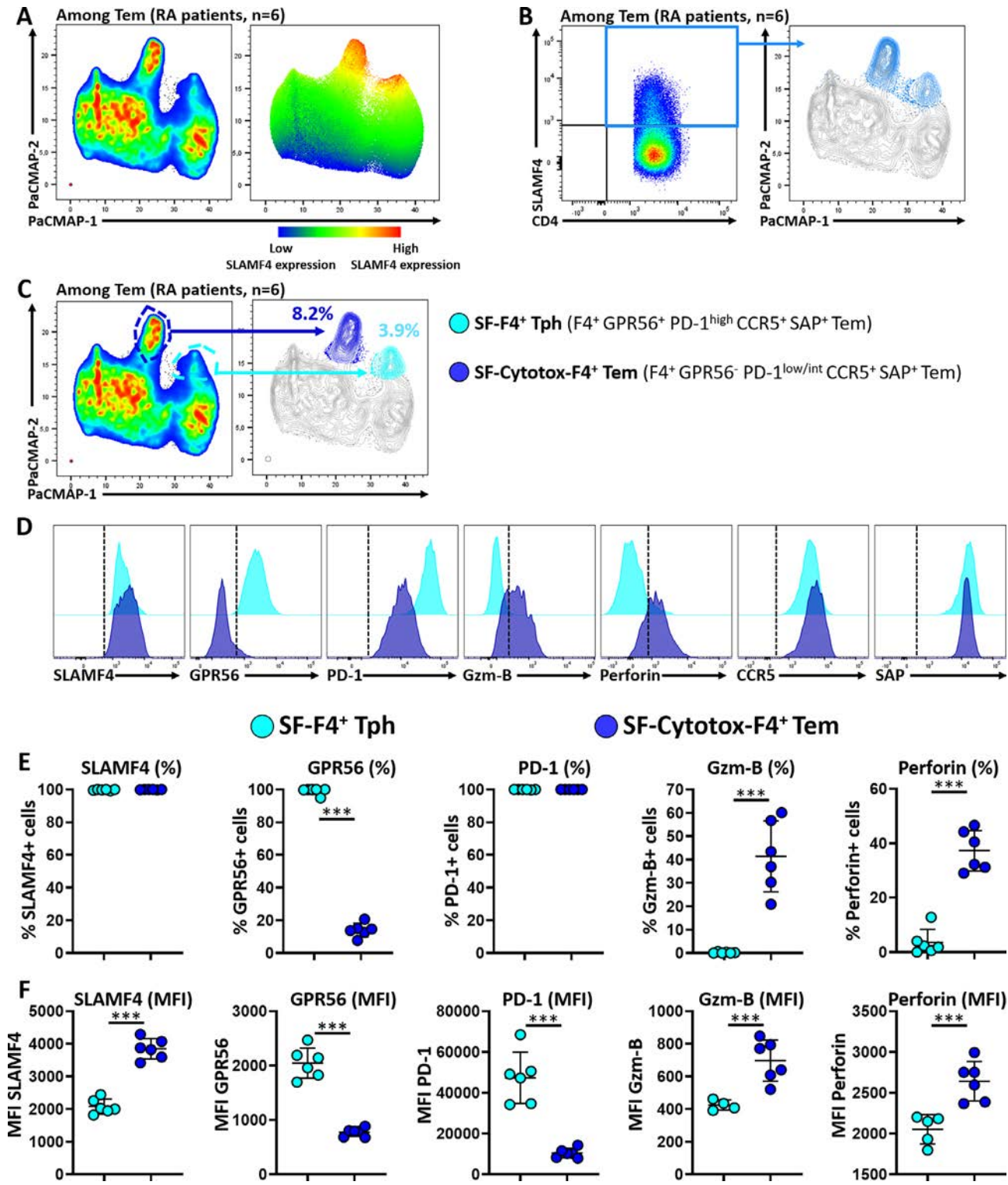
We then evaluated whether F4⁺ SAP⁺ CCR5⁺ Tem represented the main population of CD4⁺ CTLs in SF of RA patients. First, granzyme-B and perforin expression was mostly restricted to Tem (Supplementary Figure 13A–C), and among them, to F4⁺

(Figure legend continued from previous page.)

Figure 4. Cytotoxic and Th1-related transcripts are enriched in SLAMF4⁺ CCR5⁺ Tem. (A–F) RNA sequencing experiments were performed on sorted PB F4⁺ CCR5⁺ and F4[−] CCR5⁺ Tem from patients with RA (n = 4). (A) Enriched functions and pathways of the 100 most significantly up-regulated genes in F4⁺ CCR5⁺ vs F4[−] CCR5⁺ Tem. The network of pathways was created using the ClueGo and CluePedia plugins in Cytoscape. (B) Pie chart showing the most significant terms. (C) Histogram showing the up-regulated terms in F4⁺ CCR5⁺ vs F4[−] CCR5⁺ Tem. (D) Heatmap showing the 274 up-regulated (red) and 530 down-regulated (blue) DEGs in SLAMF4⁺ CCR5⁺ Tem vs their SLAMF4[−] counterparts. The list of genes in the box to the left of the heatmap highlighted the presence of genes known to be overexpressed in CD4⁺ CTLs. (E) Histogram showing the log2(Fold change) of the genes (blue histograms) shown in the box in (D) and of genes known to be down-regulated (pink histograms) in CD4⁺ CTLs. (F) Histograms showing the expression profile of genes associated with a CD4⁺ CTL signature in F4⁺ CCR5⁺ Tem vs F4[−] CCR5⁺ Tem. (A–F) A Benjamini-Hochberg FDR <0.05 and a log2(Fold change) >1 were used as cutoff to determine DEGs. CD4⁺ CTL, cytotoxic population of CD4⁺ T cell; DEG, differentially expressed gene; F4, SLAMF4; FDR, false discovery rate; NK, natural killer; PB, peripheral blood; RA, rheumatoid arthritis; SLAMF, signaling lymphocytic activation molecule family; Tem, effector memory CD4⁺ T cells. Color figure can be viewed in the online issue, which is available at <http://onlinelibrary.wiley.com/doi/10.1002/art.43124/abstract>.

SAP⁺ CCR5⁺ Tem (Supplementary Figure 13D–F). However, F4⁺ SAP⁺ CCR5⁺ Tem exhibited reduced expression of cytotoxic molecules in SF compared to PB (Supplementary Figure 7H). Thus, we investigated whether some of them corresponded to a

noncytotoxic subpopulation in SF. Initially, we focused on Tph cells due to their high enrichment in SF, which represents approximately 30% of total CD4⁺ T cells.⁵ In addition, GPR56, a marker of peripheral CD4⁺ CTLs that is highly expressed by F4⁺ SAP⁺ CCR5⁺ Tem



(Figure legend continues on next page.)

in PB (Supplementary Figure 7F), is restrictively expressed by CXCL13^{high} Tph cells in SF.⁷ We thus hypothesized that noncytotoxic SF F4⁺ SAP⁺ CCR5⁺ Tem might correspond to GPR56⁺ Tph cells. In Figures 5A–C, we identified two subsets of Tem expressing SLAMF4 within this compartment. The first subset of F4⁺ SAP⁺ CCR5⁺ Tem exhibited a cytotoxic phenotype (designated as SF-Cytotox-F4⁺ Tem, dark blue population). The second, less frequent, corresponded to cells exhibiting a Tph cell phenotype (designated as SF-F4^{int} Tph, light blue population) (Figure 5A–C). SF-F4^{int} Tph cells expressed SLAMF4 at a lower level than SF-Cytotox-F4⁺ Tem, did not express cytotoxic molecules, and possessed a full phenotype of Tph cells (GPR56⁺ PD-1^{high} ICOS⁺ CXCR5⁺ cells) (Figure 5D–F; Supplementary Figure 14A–F). Importantly, the more frequent subpopulation, namely SF-Cytotox-F4⁺ Tem, was mainly characterized by higher expression of SLAMF4 and cytotoxic molecules (granzyme-B and perforin) (Figure 5D–F). SF-Cytotox-F4⁺ Tem did not express GPR56 and also displayed a lower level of PD-1 expression than SF-F4^{int} Tph cells (Figure 5D–F). In addition, among SF-Cytotox-F4⁺ Tem, those with the highest expression of SLAMF4 had the strongest expression of granzyme-B and perforin (Supplementary Figure 13G–L). In SF, these data highlighted that a strong expression of SLAMF4 was essential for Tem to display a cytotoxic phenotype. Consistently, further analyses of PB data revealed that only PB-SLAMF4^{high} SAP⁺ CCR5⁺ Tem (Cytotox-F4^{high} Tem), most of which expressed SAP and CCR5, demonstrated the dual characteristic of being both highly cytotoxic and associated with RA activity (dark blue population) (Figure 6; Supplementary Figure 15). Overall, the present study identified that Cytotox-F4^{high} Tem represent a CD4⁺ CTL population linked to RA activity in PB and the only one able to maintain a robust expression of granzyme-B and perforin in SF.

DISCUSSION

By providing an in-depth characterization of CD4⁺ CTLs within the context of RA, this work underscored the pivotal role of SLAMF4 in shaping the cytotoxic response of CD4⁺ T cells in

this disease. We also showed that SAP is an indispensable partner to support the cytotoxic properties of F4⁺ Tem. It is worth noting that CD4⁺ CTLs, originally described as CD4⁺ CD28[−] T cells, have long been suggested to be involved in RA pathophysiology.^{39–41} Moreover, recent studies have refocused attention on CD4⁺ CTLs in this disease.^{3,7,8} However, SLAMF4 expression and its involvement in the cytotoxic properties of CD4⁺ T cells were not investigated. For instance, HLA-DR⁺ CD27[−] Tem has been proposed to represent cytotoxic cells particularly expanded in RA.⁶ Our work showed that most F4⁺ SAP⁺ CCR5⁺ Tem did not correspond to HLA-DR⁺ CD27[−] Tem. Indeed, we observed that the cytotoxic properties of HLA-DR^{+/−} CD27[−] Tem were mainly restricted to those expressing SLAMF4. Consequently, HLA-DR did not appear to drive the cytotoxic activity of CD4⁺ T cells in RA. A more recent study showed that GPR56 expression by PB CD4⁺ T cells is associated with a cytotoxic profile, whereas in SF it identified a subpopulation of CXCL13^{high} Tph cells.⁷ In line with these data, we observed that most cytotoxic Cytotox-F4^{high} Tem expressed GPR56 in PB (PB-Cytotox-F4⁺ Tem) but not in SF. Additionally, we identified a discrete population of noncytotoxic SF Tem (SF-F4⁺ Tph) that expressed SLAMF4 at an intermediate level and exhibited a Tph cell phenotype (PD-1^{high} GPR56⁺ ICOS⁺ CXCR5⁺). In patients with RA, as shown by us and others,^{7,8} some CD4⁺ T cells expressing cytotoxic markers display a phenotype or characteristics of Tph cells in PB (ThA cells) and SF (SF-F4⁺ Tph, GPR56⁺ CXCL13^{high} Tph). Consequently, the existence of a lineage relationship between CD4⁺ CTLs and some Tph cell subpopulations expressing cytotoxicity markers deserves further investigation.

To our knowledge, at the protein level, only one study has reported expression of SLAMF4 by CD4⁺ CTLs (CD4⁺ CD28[−] T cells) in PB of patients with RA.¹⁸ However, the link between RA activity and SLAMF4 expression by PB CD4⁺ CTLs, as well as the presence of F4⁺ CD4⁺ CTLs in SF, had never been reported. Here, we found that the frequency of SLAMF4⁺ Tem, coexpressing SAP and CCR5, was positively correlated with RA activity. Moreover, we showed that CD4⁺ T cells displaying a

(Figure legend continued from previous page.)

Figure 5. Cytotox-F4⁺ Tem (F4⁺ GPR56[−] PD-1^{low/inter} CCR5⁺ SAP⁺ Tem) represent the main CD4⁺ CTL subpopulation in SF of RA. (A–F) Flow cytometry experiments were performed using SFMCs (n = 6) (same patients with RA as Supplementary Figure 13). (A) Dimensionality reduction, based on the expression of SLAMF4, GPR56, PD-1, granzyme-B, perforin, SAP, and CCR5, was done among Tem using the PaCMAP method applied on concatenated files from six patients with RA. (A, right panel) Distribution and the level of SLAMF4 expression (red color indicated a high expression). (B) Gate corresponding to SLAMF4⁺ Tem (blue gate) was projected to the PaCMAP used in (A). (C) PaCMAP projection showing the two subpopulations of SLAMF4⁺ Tem. (D) Monoparametric histograms showing the expression of SLAMF4, GPR56, PD-1, granzyme-B, perforin, CCR5, and SAP among SF-F4⁺ Tph and SF-Cytotox-F4⁺ Tem. (E) Histograms showing percentages of SLAMF4⁺, GPR56⁺, PD-1⁺, granzyme-B⁺, and perforin⁺ cells among SF-F4⁺ Tph and SF-Cytotox-F4⁺ Tem. (F) Histograms showing the MFI of markers mentioned in (E) among SF-F4⁺ Tph and SF-Cytotox-F4⁺ Tem. (E and F) Data are expressed as mean ± SEM and a Wilcoxon signed-rank test or a paired *t*-test was used according to data distribution (***) *P* < 0.001). CD4⁺ CTL, cytotoxic population of CD4⁺ T cell; Gzm-B, granzyme-B; MFI, mean fluorescence intensity; PaCMAP, Pairwise Controlled Manifold Approximation; RA, rheumatoid arthritis; SAP, SLAM-associated protein; SF-F4, synovial fluid–SLAMF4; SFMC, synovial fluid mononuclear cells; SLAMF, signaling lymphocytic activation molecule family; Tem, effector memory CD4⁺ T cells; Tph, peripheral helper T cells. Color figure can be viewed in the online issue, which is available at <http://onlinelibrary.wiley.com/doi/10.1002/art.43124/abstract>.

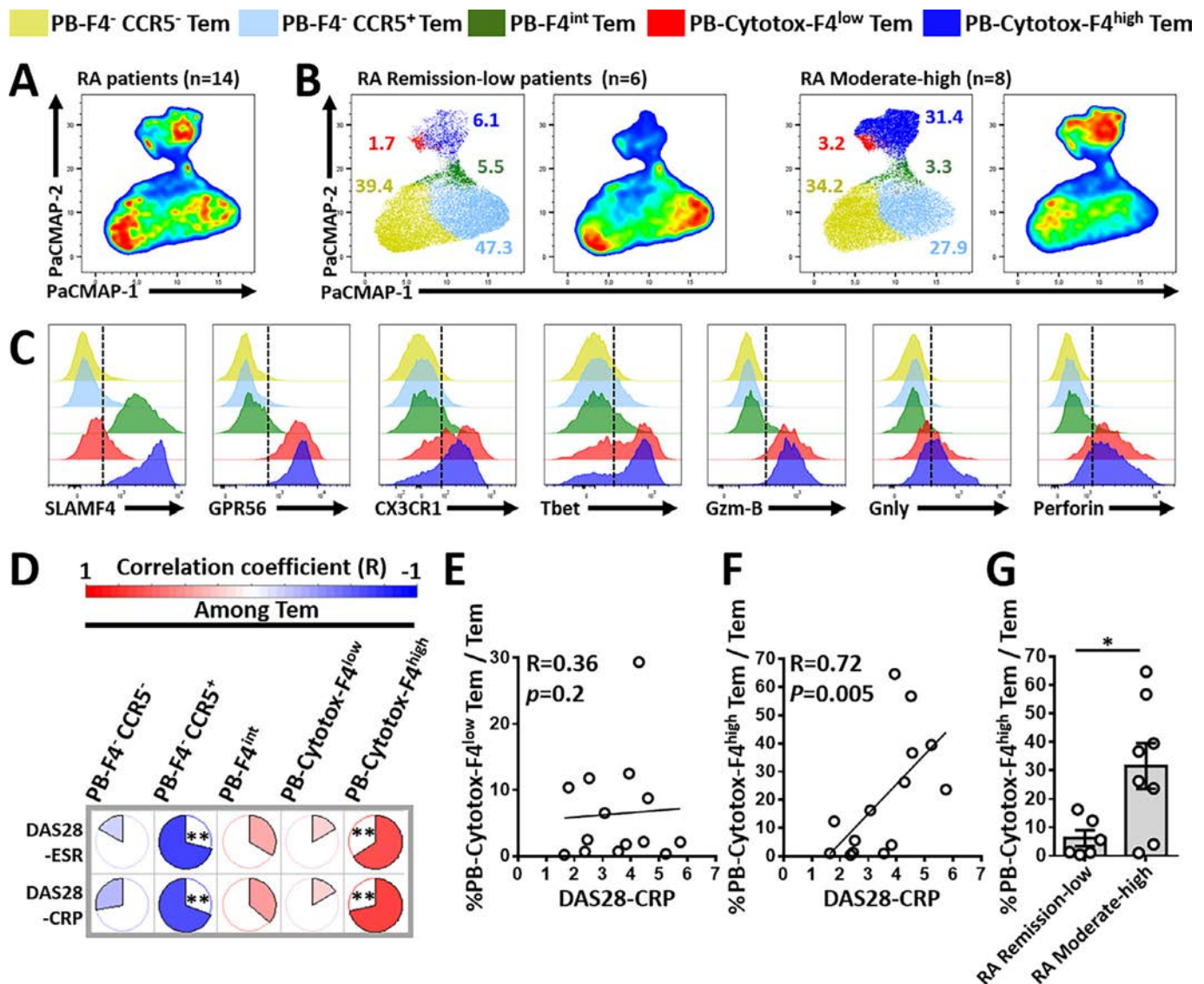


Figure 6. Only CD4⁺ CTLs highly expressing SLAMF4 (Cytotox-F4^{high} Tem) are linked to RA activity in PB (same patients as Supplementary Figure 15F–H) (n = 14). (A) PaCMAP projection was done among Tem (concatenated files from 14 patients with RA). Cell subsets were determined by the expression of SLAMF4, GPR56, CX3CR1, Tbet, CCR5, granzyme-B, granulysin, perforin, and SAP using the FlowSOM algorithm. (B) PaCMAP projections showing cell subset frequency according to RA activity (RA remission-low: DAS28-CRP ≤3.2; RA moderate-high: DAS28-CRP >3.2). (C) Monoparametric histograms showing the expression of molecules mentioned in (A) among the Tem subsets identified in (B). (D) Graphical representation of Spearman correlations between RA activity (DAS28-ESR and DAS28-CRP) vs percentage PB-F4⁺ CCR5⁺ Tem (gold population in B), percentage PB-F4⁺ CCR5⁺ Tem (light blue population in B), percentage PB-F4^{int} Tem (green population in B), percentage PB-Cytotox-F4^{low} Tem (red population in B), and percentage PB-Cytotox-F4^{high} Tem (dark blue population in B). (E and F) Spearman correlation between the DAS28-CRP vs percentage PB-Cytotox-F4^{low} Tem among Tem and vs percentage PB-Cytotox-F4^{high} Tem among Tem, respectively. (G) Percentage PB-Cytotox-F4^{high} Tem among Tem in patients with RA remission-low and RA moderate-high. (D–F) A Spearman test was applied. (G) Data are expressed as mean ± SEM, and a Mann-Whitney U test was used. (*P < 0.05, **P < 0.01). CD4⁺ CTL, cytotoxic population of CD4⁺ T cell; DAS28-CRP, Disease Activity Score-28 using the C-reactive protein level; DAS28-ESR, Disease Activity Score-28 using the erythrocyte sedimentation rate; F4, SLAMF4; Gzm-B, granzyme-B; PaCMAP, Pairwise Controlled Manifold Approximation; PB, peripheral blood; RA, rheumatoid arthritis; SAP, SLAM-associated protein; SLAMF, signaling lymphocytic activation molecule family; Tem, effector memory CD4⁺ T cells. Color figure can be viewed in the online issue, which is available at <http://onlinelibrary.wiley.com/doi/10.1002/art.43124/abstract>.

cytotoxic phenotype in SF were restricted to SF-Cytotox-F4⁺ Tem. In RA, we also observed that a significant part of PB F4⁺ CD4⁺ CD28⁻ T cells are Temra and not Tem. Given that F4⁺ Temra are absent in SF and weakly associated with RA activity

in PB, it seems important to distinguish these two types of F4⁺ CD4⁺ CTLs in this disease. As shown by our data, this is not possible by simply defining CD4⁺ CTLs as cells not expressing CD28. Independently of RA, CD4⁺ CTLs have long been considered to

be Temra derived from Tem following persistent or repeated antigen exposure, notably in the context of viral infections.^{31,37,42} In RA, we observed a low proportion of Cytotox-F4⁺ Temra compared to their Tem counterparts. This might suggest that the latter do not switch adequately to this terminal stage of differentiation, which leads to cell exhaustion or senescence. This hypothesis might sustain an exacerbated and chronic CD4⁺ T cell cytotoxic response in RA.

CCR5 is a chemokine receptor notably known to be involved in immune cell migration toward the inflammatory joint in response to its ligands (CCL3, CCL4, and RANTES).²⁶ Our data showed that most Tem expressed CCR5 in SF, whereas peripheral F4⁺ SAP⁺ Tem lacking CCR5 expression were not associated with RA activity. One could assume that the expression of CCR5 allows F4⁺ SAP⁺ Tem to migrate to the inflammatory joint, thereby establishing a link between them and joint inflammation in RA. Regarding other chemokine receptors, most were weakly or not expressed by F4⁺ SAP⁺ CCR5⁺ Tem. This included CXCR3, CXCR5, CCR6, and CCR4, whose expression levels were used to identify ThA cells (CXCR3^{int} CD25⁻ CXCR5⁻ CCR6⁻ CCR4⁻ Tem). However, F4⁺ SAP⁺ CCR5⁺ Tem represent a much less frequent subpopulation than ThA cells. Independently of RA, these four chemokine receptors have been used to distinguish between Tfh (CXCR5⁺), Th1 cells (CXCR3⁺ CCR4⁻ CCR6⁺), Th2 cells (CXCR3⁻ CCR4⁺ CCR6⁻), and Th17 cells (CXCR3⁻ CCR4⁺ CCR6⁺),⁴³ whereas the nonexpression of CD25 allowed to exclude most Treg cells. Consequently, the phenotype used to identify ThA cells allows the exclusion of noncytotoxic Th subsets (Th1, Th2, Th17, Treg, and Tfh), rather than a specific identification of CD4⁺ CTLs. In agreement, F4⁻ ThA cells had a much lower granzyme-B expression compared to their F4⁺ counterparts. Despite some overlap, ThA cells also differ from F4⁺ SAP⁺ CCR5⁺ Tem in their ability to produce CXCL13. Anyway, unlike Cytotox-F4^{high} Tem, the therapeutic inhibition of CD4⁺ CTL subpopulations defined by the lack of expression of CD27, CD28, or of chemokine receptors remains a complex challenge.

Our study has some limitations. First, because our results were obtained in patients with ACPA⁺ RA, additional studies will be needed to determine whether Cytotox-F4^{high} Tem exhibit autoreactive properties in the context of citrulline immunity. We also recognize the need for additional works to investigate the association between Cytotox-F4^{high} Tem and the response to the different available targeted treatments. Beyond the scope of the present work, it would also be interesting to compare the association of the different CD4⁺ CTL subsets described as being involved in RA, including Cytotox-F4^{high} Tem, with RA activity. Additionally, we checked the ability of F4⁺ Tem to secrete granzyme-B. However, we did not evaluate their cytotoxic activity, mainly because traditional cytotoxicity assays employ nonphysiologic conditions by using cancer cell lines as targets (such as K562 or P815 cells).^{8,18} Moreover, the functional involvement of cytotoxic CD4⁺ CTLs in the synovium, including that of Cytotox-F4^{high} Tem,

remains incompletely known and warrants further investigation. For instance, concerning Treg and CD4⁺ CTLs, both can exhibit cytotoxic responses *in vitro* against each other.⁴⁴ This raises the possibility that in the joint, CD4⁺ CTLs may alter the regulatory responses triggered by Treg cells. Another hypothesis is that perforin produced by CD4⁺ CTLs may promote the hypercitrullination of neutrophil extracellular traps, through a calcium and peptidylarginine deiminases dependent mechanism.⁴⁵ In this case, the cytotoxic properties of CD4⁺ CTLs may promote the production of autoantibodies such as ACPA. Besides their cytotoxic properties, Cytotox-F4^{high} Tem could also participate, through their Th1 profile (IFN- γ and TNF- α), in the activation of a large panel of immune and non-immune cells involved in the pathophysiology of RA. For instance, TNF- α produced by CX3CR1-expressing CD4⁺ CTLs following their interaction with fractalkine-expressing fibroblast-like synoviocytes (FLS) amplifies FLS expansion.⁴⁶ This might suggest an important role of CD4⁺ CTLs in the pannus formation.

Significant recent studies reinforced the involvement of CD4⁺ CTLs in the pathophysiology of RA.⁷⁻⁹ Here, we identified SLAMF4, together with SAP and CCR5, as important contributors in the orchestration of the cytotoxic response of CD4⁺ T cells in RA. From a therapeutic perspective, targeting F4⁺ SAP⁺ CCR5⁺ Tem without affecting other SLAMF4⁺ immune cells, such as CD8⁺ T cells and NK cells, is challenging. It could be partially achieved using bispecific antibodies (bsAbs) designed to target two molecules expressed specifically on F4⁺ SAP⁺ CCR5⁺ Tem. Such bsAbs, known as cis-binding bsAbs, preferentially bind to cells coexpressing both targets.^{47,48} Altogether, it might be expected that an anti-CD4/SLAMF4 cis-binding bsAbs with depleting properties would be able to target F4⁺ CD4⁺ T cells, while sparing other SLAMF4⁺ cells.

Nonetheless, further studies aiming to characterize more precisely the role of Cytotox-F4^{high} Tem in the pathophysiology of RA will contribute to determine their relevance as a potential therapeutic target in RA.

ACKNOWLEDGMENTS

We thank the patients who donated samples. We thank Dr Nathalie Saldenberg Kermanac, Dr Caroline Beal, Dr Salima Challal, and all the medical staff of the Rheumatology department of the Avicenne Hospital (Bobigny, France). We thank Elisabetta Dondi and Laure Aubard from the fluorescence platform (Université Sorbonne Paris Nord, Bobigny) and Léa Paolini (INSERM UMR-1125, Université Sorbonne Paris Nord, Bobigny) for cells sorting. We thank Frank Letourneur, Lucie Adoux and Benjamin Saintpierre from the GenomIC platform (Cochin Institute, Paris) for RNA sequencing experiments and bioinformatics analysis. We thank Samuel Bitoun for providing us with some samples of SF (Rheumatology Department, Université Paris-Saclay, INSERM U1184, Hôpital Bicêtre, APHP, FHU CARE).

AUTHOR CONTRIBUTIONS

All authors contributed to at least one of the following manuscript preparation roles: conceptualization AND/OR methodology, software,

investigation, formal analysis, data curation, visualization, and validation AND drafting or reviewing/editing the final draft. As corresponding author, Dr Biton confirms that all authors have provided the final approval of the version to be published, and takes responsibility for the affirmations regarding article submission (eg, not under consideration by another journal), the integrity of the data presented, and the statements regarding compliance with institutional review board/Declaration of Helsinki requirements.

ROLE OF THE STUDY SPONSOR


Sandoz, Inc had no role in the study design or in the collection, analysis, or interpretation of the data, the writing of the manuscript, or the decision to submit the manuscript for publication. Publication of this article was not contingent upon approval by Sandoz, Inc.

REFERENCES

- Cross M, Smith E, Hoy D, et al. The global burden of rheumatoid arthritis: estimates from the global burden of disease 2010 study. *Ann Rheum Dis* 2014;73(7):1316–1322.
- Listing J, Kekow J, Manger B, et al. Mortality in rheumatoid arthritis: the impact of disease activity, treatment with glucocorticoids, TNF α inhibitors and rituximab. *Ann Rheum Dis* 2015;74(2):415–421.
- Fonseka CY, Rao DA, Raychaudhuri S. Leveraging blood and tissue CD4 $^{+}$ T cell heterogeneity at the single cell level to identify mechanisms of disease in rheumatoid arthritis. *Curr Opin Immunol* 2017;49:27–36.
- Zhang F, Wei K, Slowikowski K, et al; Accelerating Medicines Partnership Rheumatoid Arthritis and Systemic Lupus Erythematosus (AMP RA/SLE) Consortium. Defining inflammatory cell states in rheumatoid arthritis joint synovial tissues by integrating single-cell transcriptomics and mass cytometry. *Nat Immunol* 2019;20(7):928–942.
- Rao DA, Gurish MF, Marshall JL, et al. Pathologically expanded peripheral T helper cell subset drives B cells in rheumatoid arthritis. *Nature* 2017;542(7639):110114.
- Fonseka CY, Rao DA, Teslovich NC, et al. Mixed-effects association of single cells identifies an expanded effector CD4 $^{+}$ T cell subset in rheumatoid arthritis. *Sci Transl Med* 2018;10(463):eaag0305.
- Argyriou A, Wadsworth MH II, Lendvai A, et al. Single cell sequencing identifies clonally expanded synovial CD4 $^{+}$ T_{PH} cells expressing GPR56 in rheumatoid arthritis. *Nat Commun* 2022;13(1):4046.
- Goto M, Takahashi H, Yoshida R, et al. Age-associated CD4 $^{+}$ T cells with B cell-promoting functions are regulated by ZEB2 in autoimmunity. *Sci Immunol* 2024;0:eadk1643.
- Smolen JS, Aletaha D, Barton A, et al. Rheumatoid arthritis. *Nat Rev Dis Primers* 2018;4(1):18001.
- Wu N, Veillette A. SLAM family receptors in normal immunity and immune pathologies. *Curr Opin Immunol* 2016;38:45–51.
- Gartshteyn Y, Askanase AD, Mor A. SLAM associated protein signaling in T cells: tilting the balance toward autoimmunity. *Front Immunol* 2021;12:654839.
- You Y, Wang Z, Deng GH, et al. Detection and functional evaluation of -262A/T and -188A/G polymorphisms of SLAM gene in patients with systemic lupus erythematosus. *J Rheumatol* 2010;37(11):2268–2272.
- Kumar KR, Li L, Yan M, et al. Regulation of B cell tolerance by the lupus susceptibility gene Ly108. *Science* 2006;312(5780):1665–1669.
- Beecham AH, Patsopoulos NA, Xifara DK, et al; International IBD Genetics Consortium (IBDGC). Analysis of immune-related loci identifies 48 new susceptibility variants for multiple sclerosis. *Nat Genet* 2013;45(11):1353–1360.
- Suzuki A, Yamada R, Kochi Y, et al. Functional SNPs in CD244 increase the risk of rheumatoid arthritis in a Japanese population. *Nat Genet* 2008;40(10):1224–1229.
- Humbel M, Bellanger F, Horisberger A, et al. SLAMF receptor expression identifies an immune signature that characterizes systemic lupus erythematosus. *Front Immunol* 2022;13:843059.
- Karampetsou MP, Comte D, Suárez-Fueyo A, et al. Signaling lymphocytic activation molecule family member 1 engagement inhibits T cell-B cell interaction and diminishes interleukin-6 production and plasmablast differentiation in systemic lupus erythematosus. *Arthritis Rheumatol* 2019;71(1):99–108.
- Fasth AER, Björkström NK, Anthoni M, et al. Activating NK-cell receptors co-stimulate CD4(+)CD28(-) T cells in patients with rheumatoid arthritis. *Eur J Immunol* 2010;40(2):378–387.
- Aletaha D, Neogi T, Silman AJ, et al. 2010 Rheumatoid arthritis classification criteria: an American College of Rheumatology/European League Against Rheumatism collaborative initiative. *Ann Rheum Dis* 2010;69(9): 1580–1588. <https://doi.org/10.1136/ard.2010.138461>
- Rudwaleit M, van der Heijde D, Landewé R, et al. The Assessment of SpondyloArthritis international Society classification criteria for peripheral spondyloarthritis and for spondyloarthritis in general. *Ann Rheum Dis* 2011;70(1): 25–31. <https://doi.org/10.1136/ard.2010.133645>
- Bindea G, Mlecnik B, Tosolini M, et al. Spatiotemporal dynamics of intratumoral immune cells reveal the immune landscape in human cancer. *Immunity* 2013;39(4):782–795.
- Mlecnik B, Bindea G, Angell HK, et al. Integrative analyses of colorectal cancer show immunoscore is a stronger predictor of patient survival than microsatellite instability. *Immunity* 2016;44(3): 698–711.
- Li K, Wang M, Zhao L, Liu Y, et al. ACPA-negative rheumatoid arthritis: from immune mechanisms to clinical translation. *EBioMedicine* 2022;83:104233.
- Sun L, Gang X, Li Z, et al. Advances in understanding the roles of CD244 (SLAMF4) in immune regulation and associated diseases. *Front Immunol* 2021;12:648182.
- Mucida D, Husain MM, Muroi S, et al. Transcriptional reprogramming of mature CD4 $^{+}$ helper T cells generates distinct MHC class II-restricted cytotoxic T lymphocytes. *Nat Immunol* 2013;14(3): 281–289.
- Patel DD, Zachariah JP, Whichard LP. CXCR3 and CCR5 ligands in rheumatoid arthritis synovium. *Clin Immunol* 2001;98(1):39–45.
- Loetscher P, Ugucioni M, Bordoli L, et al. CCR5 is characteristic of Th1 lymphocytes. *Nature* 1998;391(6665):344–345.
- Qin S, Rottman JB, Myers P, et al. The chemokine receptors CXCR3 and CCR5 mark subsets of T cells associated with certain inflammatory reactions. *J Clin Invest* 1998;101(4):746–754.
- Vallejo AN, Nestel AR, Schirmer M, et al. Aging-related deficiency of CD28 expression in CD4 $^{+}$ T cells is associated with the loss of gene-specific nuclear factor binding activity. *J Biol Chem* 1998; 273(14):8119–8129.
- Hashimoto K, Kouno T, Ikawa T, et al. Single-cell transcriptomics reveals expansion of cytotoxic CD4 T cells in supercentenarians. *Proc Natl Acad Sci USA* 2019;116(48):24242–24251.
- Patil VS, Madrigal A, Schmiedel BJ, et al. Precursors of human CD4 $^{+}$ cytotoxic T lymphocytes identified by single-cell transcriptome analysis. *Sci Immunol* 2018;3(19):eaan8664.
- Cenerenti M, Saillard M, Romero P, et al. The era of cytotoxic CD4 T cells. *Front Immunol* 2022;13:867189.
- Takeuchi A, Badr MS, Miyauchi K, et al. CRTAM determines the CD4 $^{+}$ cytotoxic T lymphocyte lineage. *J Exp Med* 2016;213(1):123–138.
- Pearce EL, Mullen AC, Martins GA, et al. Control of effector CD8 $^{+}$ T cell function by the transcription factor Eomesodermin. *Science* 2003;302(5647):1041–1043.

35. Oja AE, Vieira Braga FA, Remmerswaal EBM, et al. The transcription factor Hobit identifies human cytotoxic CD4⁺ T cells. *Front Immunol* 2017;8:325.
36. Peng YM, van de Garde MDB, Cheng KF, et al. Specific expression of GPR56 by human cytotoxic lymphocytes. *J Leukoc Biol* 2011;90(4):735–740.
37. Weiskopf D, Bangs DJ, Sidney J, et al. Dengue virus infection elicits highly polarized CX3CR1⁺ cytotoxic CD4⁺ T cells associated with protective immunity. *Proc Natl Acad Sci USA* 2015;112(31):E4256–E4263.
38. Wong MT, Chen J, Narayanan S, et al. Mapping the diversity of follicular helper t cells in human blood and tonsils using high-dimensional mass cytometry analysis. *Cell Rep* 2015;11(11):1822–1833.
39. Warrington KJ, Takemura S, Goronzy JJ, et al. CD4⁺,CD28⁻ T cells in rheumatoid arthritis patients combine features of the innate and adaptive immune systems. *Arthritis Rheum* 2001;44(1):13–20.
40. Martens PB, Goronzy JJ, Schaid D, et al. Expansion of unusual CD4⁺ T cells in severe rheumatoid arthritis. *Arthritis Rheum* 1997;40(6):1106–1114.
41. Scarsi M, Ziglioli T, Airò P. Decreased circulating CD28-negative T cells in patients with rheumatoid arthritis treated with abatacept are correlated with clinical response. *J Rheumatol* 2010;37(5):911–916.
42. Tian Y, Babor M, Lane J, et al. Unique phenotypes and clonal expansions of human CD4 effector memory T cells re-expressing CD45RA. *Nat Commun* 2017;8(1):1473.
43. Mahnke YD, Brodie TM, Sallusto F, et al. The who's who of T-cell differentiation: human memory T-cell subsets. *Eur J Immunol* 2013;43(11):2797–2809.
44. Czystowska M, Strauss L, Bergmann C, et al. Reciprocal granzyme/perforin-mediated death of human regulatory and responder T cells is regulated by interleukin-2 (IL-2). *J Mol Med (Berl)* 2010;88(6):577–588.
45. Romero V, Fert-Bober J, Nigrovic PA, et al. Immune-mediated pore-forming pathways induce cellular hypercitrullination and generate citrullinated autoantigens in rheumatoid arthritis. *Sci Transl Med* 2013;5(209):209ra150.
46. Sawai H, Park YW, He X, et al. Fractalkine mediates T cell-dependent proliferation of synovial fibroblasts in rheumatoid arthritis. *Arthritis Rheum* 2007;56(10):3215–3225.
47. Shi N, Zhou Y, Liu Y, et al. PD-1/LAG-3 bispecific antibody potentiates T cell activation and increases antitumor efficacy. *Front Immunol* 2022;13:1047610.
48. Klein C, Brinkmann U, Reichert JM, et al. The present and future of bispecific antibodies for cancer therapy. *Nat Rev Drug Discov* 2024;23(4):301–319.

Metabolic Stress Expands Polyfunctional, Proinflammatory Th₁₇ Cells in Patients With Psoriatic Arthritis for Whom There is Interleukin-23–Independent Interleukin-17 Production

Carmel B. Stober,¹  Louise Ellis,² Jane C. Goodall,² Marc Veldhoen,^{3,4,5} and J. S. Hill Gaston²

Objective. Genetic associations and blockade of the interleukin (IL)-23/IL-17 axis with monoclonal antibodies support a role for this pathway in patients with psoriatic arthritis (PsA). This study examines the requirement of IL-23 for IL-17 production and the role of the metabolic microenvironment in the expansion of Th₁₇-derived cells in patients with PsA.

Methods. Th₁₇ cell frequencies in synovial fluid or peripheral blood from patients with PsA were evaluated by flow cytometry using chemokine receptor 6, CD161, and T-bet as phenotypic markers, and the cytokines interferon γ , granulocyte–macrophage colony-stimulating factor (GM-CSF), and IL-17 were assessed by flow cytometry and enzyme-linked immunosorbent assay. The impact of IL-23 and metabolic stress on T cell differentiation was investigated.

Results. Polyfunctional positive IL-17 (IL-17^{pos}) CD4 ($P < 0.0001$) and CD8 ($P < 0.0001$), and GM-CSF^{pos} Th₁₇-derived cells ($P < 0.0001$) were increased in the inflamed joints of patients with PsA, with a proportional decrease in the peripheral blood of patients. We demonstrate IL-23-independent IL-17 release by CD4 T cells in patients with PsA, in which the absence of IL-23 during Th₁₇ differentiation reduced IL-17 by mean \pm SEM 31% \pm 5.8%. Exogenous IL-23 increased IL-17, negatively regulated GM-CSF, and cooperated with transforming growth factor β to augment IL-17. Polyfunctional Th₁₇ and Th₁₇-derived cells, but not Th₁ cells, were expanded by metabolic stress in patients with PsA.

Conclusion. We confirmed the abundance of polyfunctional type 17 CD4 and CD8 cells in the inflamed joints of patients with PsA. We demonstrate IL-23-independent expansion of Th₁₇ cells, for which IL-23 negatively regulates GM-CSF. This may account for therapeutic differences in IL-17 and IL-23 inhibition in patients with PsA or other spondyloarthritides. Polyfunctional IL-17^{pos} Th₁₇ and Th₁₇-derived but not Th₁ cells were expanded by metabolic stress, and metabolic stress may itself represent a unique therapeutic target.

INTRODUCTION

Psoriasis (Ps) is a common chronic inflammatory skin condition affecting 1% to 3% of the world population,¹ and up to 30% of patients with Ps have psoriatic arthritis (PsA).² Genetic studies have highlighted the importance of the interleukin (IL)-23 pathway, with a unique PsA risk variant identified at the IL-23 receptor

(IL-23R) locus.^{3,4} The clinical importance of the IL-23/Th₁₇ pathway in patients with PsA has also been validated by the efficacy of antibodies targeting IL-23 or IL-17. We showed elevated frequencies of Th₁₇ cells in the synovial fluid (SF) of patients with PsA,^{5,6} with more recent evidence revealing that these T cells are associated with polyfunctional cytokine expression.^{7–9} However, the benefit of therapies targeting the IL-23/Th₁₇ pathway

Supported by the Cambridge Arthritis Research Endeavour (registered charity). Dr Stober's work was supported by the National Institute for Health Research (NIHR) as a clinical lecturer at the University of Cambridge (NIHR2046). Dr Goodall's work was supported by a senior fellowship from Versus Arthritis (19639). Dr Veldhoen's work was supported by the European Union European Research Council program (280307-Epithelial_Immunol) and the European Union Horizon 2020 European Research Area project (667824-EXCELLtoINNOV).

¹Carmel B. Stober, PhD, MBChB, MRCP: University of Cambridge and Addenbrooke's Hospital, Cambridge University Hospitals NHS Foundation Trust, Cambridge, United Kingdom; ²Louise Ellis, BSc, Jane C. Goodall, PhD, J. S. Hill Gaston, MA, PhD, BMBCh, FRCP, FMedSci: University of Cambridge, Cambridge University Hospitals NHS Foundation Trust, Cambridge,

United Kingdom; ³Marc Veldhoen, PhD: GIMM - Gulbenkian Institute for Molecular Medicine, Avenida Prof. Egas Moniz, Lisbon, Portugal; ⁴Marc Veldhoen, PhD: Faculdade de Medicina da Universidade de Lisboa, Avenida Prof. Egas Moniz, Lisbon, Portugal; ⁵Marc Veldhoen, PhD: The Babraham Institute, Cambridge, United Kingdom.

Additional supplementary information cited in this article can be found online in the Supporting Information section (<http://acrjournals.onlinelibrary.wiley.com/doi/10.1002/art.43095>).

Address correspondence via email to Carmel B. Stober, PhD, MBChB, MRCP, at cbs24@medschl.cam.ac.uk.

Submitted for publication May 6, 2024; accepted in revised form May 10, 2024.

are more impressive for patients with Ps than for patients with PsA, and IL-23 inhibition has been ineffective in patients with axial disease.¹⁰ This implies differences in tissue-specific effector cells and the possibility that cytokines in addition to IL-17 contribute to pathogenicity in patients with PsA.

Granulocyte-macrophage colony-stimulating factor (GM-CSF) is a hematopoietic growth factor that promotes the maturation and activation of monocytes, dendritic cells, and neutrophils and enhances the release of pro-inflammatory cytokines. In experimental autoimmune encephalomyelitis (EAE), an autoimmune mouse model of multiple sclerosis (MS), GM-CSF produced by Th₁₇ was essential for disease,^{11–13} whereas IL-17A and IL-17F were not required.¹⁴ In these models, pathogenic Th₁₇-derived or ex-Th₁₇ cells possessed features of Th₁₇ but no longer produced IL-17; they coexpressed the Th₁-associated transcription factor T-bet in addition to retinoic acid receptor-related orphan nuclear receptor (ROR) γ t, but also secreted GM-CSF, and were expanded by IL-23.^{15–17} GM-CSF-producing T cells have been observed at sites of inflammation in human diseases including cerebrospinal fluid from patients with MS,^{18,19} SF from patients with rheumatoid arthritis (RA) and juvenile idiopathic arthritis,²⁰ and peripheral blood (PB) from patients with spondyloarthritis.⁷

The role of IL-23 in Th₁₇ cell differentiation has remained controversial because naive T cells lack IL-23R,^{21,22} although transforming growth factor (TGF) β , IL-1, and IL-6 induce the expression of the Th₁₇ cell-specific transcription factor ROR γ t, leading to the expression of *Il23r* and *Il17a*.²³ Naive T cells differentiated with TGF β and IL-6 are nonpathogenic,²⁴ but exposure to IL-23 conferred pathogenicity.²⁵ It was therefore hypothesized that IL-6 is absolutely required for Th₁₇ cell differentiation,²⁶ whereas IL-23 was necessary for expansion and stabilization of the Th₁₇ cell phenotype^{22,27} and the induction of pathogenic Th₁₇ and Th₁₇-derived subsets that produce GM-CSF.^{17,22} A relationship between metabolic stress, IL-23R expression, and Th₁₇ cell development was demonstrated in murine studies, in which exposure of T cells to increased salt concentrations expanded pathogenic Th₁₇ cells, up-regulated pro-inflammatory

GM-CSF, and accelerated autoimmunity.^{28,29} Moreover, a high-salt diet in mice and a pilot human study reduced several intestinal bacteria, promoted hypertension, and increased the frequency of Th₁₇ cells.³⁰

We confirm increased frequencies of polyfunctional type 17 and positive GM-CSF (GM-CSF^{pos}) Th₁₇-derived cells in inflamed joints, with a relative reduction of these subsets in the PB of patients with PsA. We demonstrate IL-23-independent IL-17 release by Th₁₇ cells, and in contrast to murine studies, IL-23 negatively regulates GM-CSF. We identify metabolic stress as a putative target for intervention in patients with PsA, in which inhibiting glycolysis reduces IL-17, whereas ionic and endoplasmic reticular (ER) stress expand polyfunctional Th₁₇ and Th₁₇-derived cells but not Th₁ cells in patients with PsA.

PATIENTS AND METHODS

Patient samples. PB (n = 60) and SF (n = 10) samples were obtained from patients with PsA attending the rheumatology service at Addenbrooke's Hospital who fulfilled Criteria of the Classification of Psoriatic Arthritis criteria.³¹ Table 1 summarizes the demographics of patients with PsA recruited to the study, including erythrocyte sedimentation rate and C-reactive protein values, number of tender or swollen joints, and the proportion of patients receiving biologic, synthetic, or no disease-modifying antirheumatic drugs. Blood was taken from healthy donor (HD) volunteers (n = 24). The study was approved by the Addenbrooke's Hospital and Repatriation General Hospital local ethics committees.

Cell isolation. SF mononuclear cells (SFMCs) and peripheral blood mononuclear cells (PBMCs) were purified by density centrifugation.⁵ Naive CD4 T cells were isolated using the naive CD4 T cell isolation kit II human (Miltenyi Biotec; Supplementary Figure 1).

Table 1. Demographic and clinical characteristics of patients with PsA*

Characteristic	All PsA (n = 60), median (IQR)	SF (n = 10), median (IQR)	PsA vs SF, P value	HD (n = 24), median (IQR)	PsA vs HD, P value
Male, n (%)	37 (62)	8 (80)	0.21	17 (71)	0.41
Age, y	48 (40–58)	53 (43–68)	0.33	40 (32–48)	0.05
ESR, mm/h	8 (5–19)	13 (7–39)	0.17	–	–
CRP, ng/mL	4 (4–14)	20 (4–41)	0.09	–	–
68 TJC	2 (1–5)	1 (1–2)	0.42	–	–
66 SJC	1 (0–3)	1 (1–2)	0.98	–	–
Treatment, n (%)					
Biologic \pm synthetic DMARD	13 (22)	0	–	–	–
Synthetic DMARD	25 (42)	6 (60)	–	–	–
No DMARD	22 (37)	4 (40)	–	–	–

* 60 patients with psoriatic arthritis (PsA) were recruited to this study, including 10 patients who provided synovial fluid (SF). Bold P values are considered statistically significant. CRP, C-reactive protein; DMARD, disease-modifying antirheumatic drug; ESR, erythrocyte sedimentation rate; HD, healthy donor; IQR, interquartile range; SJC, swollen joint count; TJC, tender joint count.

Cell stimulation. PBMCs and SFMCs were treated with phorbol 12-myristate 13-acetate (PMA), ionomycin, and BD GolgiStop (BD Biosciences).⁵ Alternatively, cells were incubated with Dynabeads human T-activator CD3/28 beads (ratio of bead to cell of 1:1) \pm IL-23 or IL-12 at 10 ng/mL or IL-2 at 100 U/mL and supernatants were harvested at 72 hours for the quantification of GM-CSF, IL-17, or interferon (IFN) γ by enzyme-linked immunosorbent assay (ELISA; Ready-SET-Go!, eBioscience). Naive T cells were cultured in X-vivo medium (Lonza) with Th₁₇ differentiation: IL-1 β , IL-6, anti-IFN γ , \pm IL-23 \pm TGF β ; Th₁ differentiation: IL-12 \pm IL-23 (BD Pharmingen); and Dynabeads human T-activator CD3/28 beads. T cell differentiation was also performed in 2 to 10 nM thapsigargin, an additional 50 mM NaCl, or 2 mM 2-deoxy-D-glucose (2-DG). Supernatants were harvested for ELISA, and cells were restimulated with PMA, ionomycin, and BD GolgiStop before harvesting and staining for flow cytometric analysis.

Flow cytometry. Cells were stained with Zombie-NIR, blocked with 1% mouse serum, and stained extracellularly for CD3, CD4, chemokine receptor (CCR) 6, and CD161, and fixed, permeabilized, and stained intracellularly with antibodies to IL-17, IFN γ , and GM-CSF (BD Cytofix/Cytoperm) or appropriate isotype controls. For intracellular T-bet staining, the Transcription Factor Staining buffer set (eBioscience) was used. A Fortessa Flow Cytometry System (BD Biosciences) and FlowJo software (TreeStar) were used for analysis, with assistance provided by the National Institute for Health Research Cambridge Biomedical Research Centre phenotyping hub.

Statistical analysis. Statistical analysis was performed using Prism 6 software. Two groups were compared using Student's *t*-test and three or more groups were compared with one-way analysis of variance and Tukey's multiple comparison test. When the effects of treatment were explored, paired *t*-tests were used, and *P* < 0.05 was considered significant.

RESULTS

Polyfunctional GM-CSF^{pos} and IL-17^{pos} T cells are abundant in the inflamed joints of patients with PsA and are decreased in PB from patients with PsA compared with PB from HDs. The frequency of SF and PB CD4 and CD3+CD4^{neg} (mostly CD8) T cells producing GM-CSF, IFN γ , or IL-17 were evaluated in patients with PsA (Figure 1A–C). IFN γ , GM-CSF, and IL-17 were higher in inflamed joints relative to PB from patients, although they were only significant for CD4 T cells (Figure 1G, *P* < 0.0001). GM-CSF has defined pathogenicity of Th₁₇ cells;^{11–13,15–17} therefore, GM-CSF coexpression was investigated (Figure 1D and E).

GM-CSF^{pos} polyfunctional T cells were abundant in inflamed joints, where mean \pm SEM 74% \pm 4.2% CD4 (Figure 1I) and mean

\pm SEM 79% \pm 4.2% CD8 (Figure 1K) T cells coexpressed GM-CSF with another cytokine. This was reflected by reduced CD4 (Figure 1H, *P* < 0.001) and CD8 (Figure 1J, *P* < 0.01) T cells from the SF of patients with PsA expressing only GM-CSF when compared with PB from patients with PsA (*n* = 60), also confirmed using matched patient SF and PB CD4 (Supplementary Figure 2E, *n* = 4) and CD8 (Supplementary Figure 2D, *n* = 4) T cells. GM-CSF^{pos} polyfunctional T cells were increased in PB from HDs compared with PB from patients with PsA, and observed for CD4 (Figure 1H and I) and CD8 (Figure 1J and K) T cells. Because only 0.7% to 4.8% of GM-CSF^{pos} cells were IL-17^{pos} (Figure 1I and K), the expression of IL-17 with other cytokines was evaluated.

Polyfunctional IL-17^{pos} T cells were increased in SF from patients with PsA relative to PB from patients with PsA, and observed for CD4 (Figure 1M; mean \pm SEM 57% \pm 4.6% SF from patients with PsA vs mean \pm SEM 33% \pm 2.1% PB from patients with PsA; *P* < 0.0001) and CD8 (Figure 1O; mean \pm SEM 65% \pm 7.1% SF from patients with PsA vs mean \pm SEM 36% \pm 3.3% PB from patients with PsA; *P* < 0.0001) T cells. Polyfunctional IL-17^{pos}GM-CSF^{pos}IFN γ ^{pos} CD4 (Figure 1L, *P* < 0.0001) and CD8 (Figure 1N, *P* < 0.0001) were abundant in SF compared with PB, also confirmed using matched patient SF and PB CD4 (Supplementary Figure 2G, *n* = 4) and CD8 (Supplementary Figure 2F, *n* = 4) T cells. Polyfunctional IL-17^{pos} cells were less abundant in patients with PsA compared with PB from HDs; the highest proportions of IL-17^{pos}GM-CSF^{pos}IFN γ ^{pos} CD4 (Figure 1L) and CD8 (Figure 1N) T cells were observed in SF from patients with PsA, which is greater than from PB from HDs, which in turn is greater than from PB from patients with PsA. We therefore confirm accumulation of polyfunctional GM-CSF^{pos} and IL-17^{pos} CD4 and CD8 T cells in inflamed joints, with a relative reduction in patients with PsA compared with PB from HDs.

GM-CSF^{pos} and IL-17^{pos} polyfunctional CD4 T cells express Th₁₇-associated phenotypic markers and T-bet.

The expression of Th₁₇-associated phenotypic markers was evaluated in inflamed joints and PB from patients with PsA. CD161, a cell-surface C-type lectin-like receptor closely associated with Th₁₇ and the transcription factor ROR γ t, was most abundant in IL-17^{pos} PB subsets (Figure 2C). The Th₁₇-associated CCR6 was also highly expressed by IL-17^{pos} Th₁₇ cells (Figure 2D), with no significant difference in either CD161 (Figure 2C) or CCR6 (Figure 2D) if IL-17^{pos} PB cells coexpressed other cytokines. IFN γ ^{pos} PB cells not producing GM-CSF or IL-17 (likely classic Th₁) displayed the lowest surface levels of CD161 (Figure 2A) and CCR6 (Figure 2B). GM-CSF expression correlated with intermediate levels of CD161, significantly higher than for classic Th₁ (Figure 2A, *P* < 0.01) but lower than IL-17^{pos} PB cells (Figure 2C, *P* < 0.0001). Intermediate expression levels of CCR6 were also observed in cells expressing GM-CSF without IL-17 (Figure 2B).

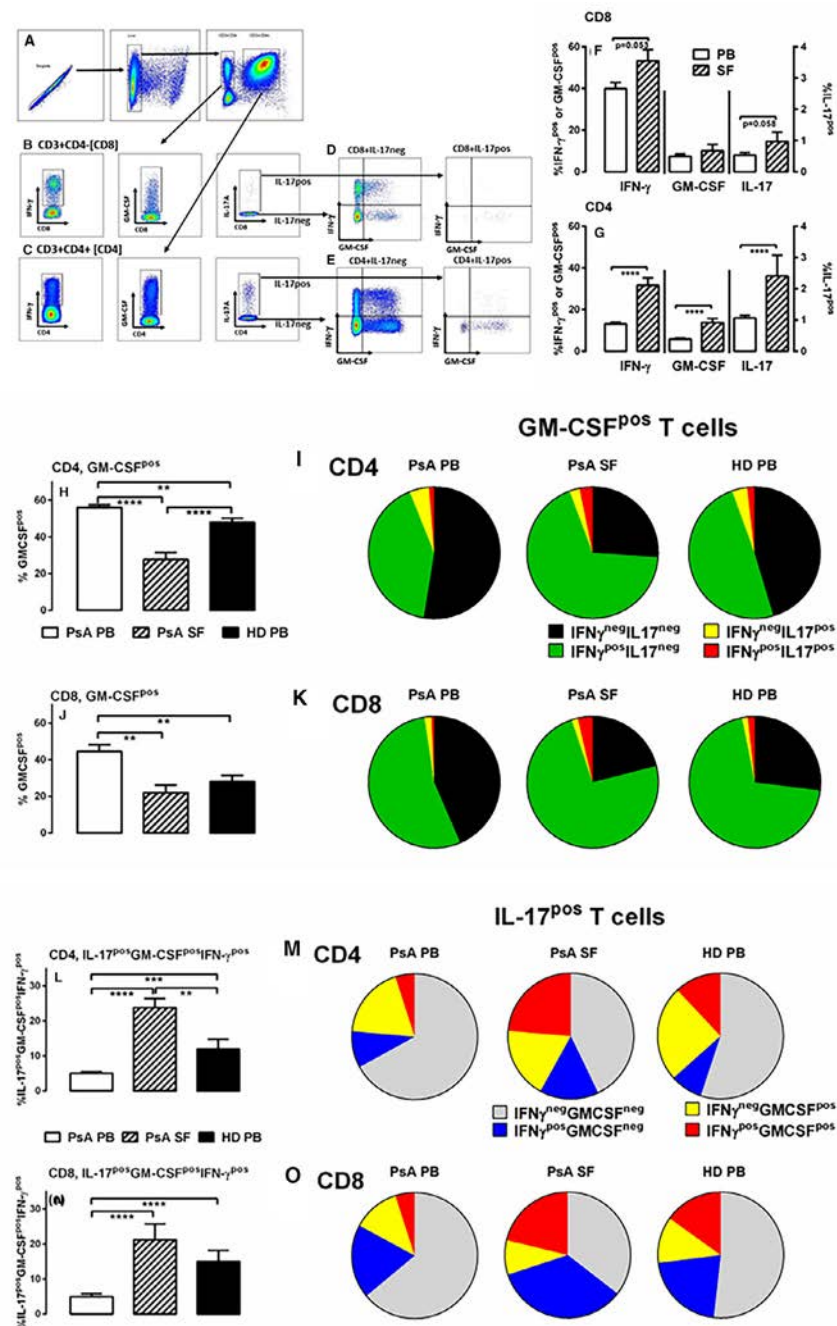


Figure 1. Polyfunctional GM-CSF^{pos} and IL-17^{pos} T cells are abundant in inflamed joints of patients with PsA and are decreased in PB of patients with PsA compared with PB from HDs. PB from patients with PsA (n = 60), SF from patients with PsA (n = 10), or PB from HDs (n = 24) were analyzed. PBMCs or SFMCs were stimulated with PMA and ionomycin, before analysis by flow cytometry. (A) PBMCs (or SFMCs) were gated on FSC/SSC to identify lymphocytes, dead cells were excluded, and further gated as (B) CD3+CD4^{neg} (CD8) or (C) CD3+CD4⁺ (CD4) T cells, expressing either IFN γ , GM-CSF, or IL-17. The frequency of (F) CD8 or (G) CD4 T cells that were IFN γ ^{pos}, GM-CSF^{pos}, or IL-17^{pos} were compared in PB and SF from patients with PsA. Polyfunctional cytokine expression was then evaluated where (D, upper) CD8 or (E, lower) CD4 T cells were gated as (D and E, left) IL-17 negative or (D and E, right) IL-17 positive, and then gated on IFN γ and GM-CSF expression. (H) CD4 and (J) CD8 were compared in GM-CSF^{pos} (IFN γ ^{neg}IL-17^{neg}) subsets, and (L) CD4 and (N) CD8 IL-17^{pos}GM-CSF^{pos}IFN γ ^{pos} subsets were compared in PB and SF from patients with PsA and PB from HDs. The coexpression of GM-CSF with other cytokines in (I) CD4 and (K) CD8 T cells; and the coexpression of IL-17 with other cytokines in (M) CD4 and (O) CD8 T cells; in PB and SF from patients with PsA and PB from HDs are demonstrated in pie charts. Data are represented as mean \pm SEM and are analyzed by one-way ANOVA with Tukey's multiple comparison test. * P < 0.05; ** P < 0.01; *** P < 0.001; **** P < 0.0001. ANOVA, analysis of variance; FSC, forward scatter; GM-CSF, granulocyte-macrophage colony-stimulating factor; HD, healthy donor; IFN, interferon; IL, interleukin; neg, negative; PB, peripheral blood; PBMC, PB mononuclear cells; PMA, phorbol 12-myristate 13-acetate; pos, positive; PsA, psoriatic arthritis; SF, synovial fluid; SFMC, SF mononuclear cells; SSC, side scatter.

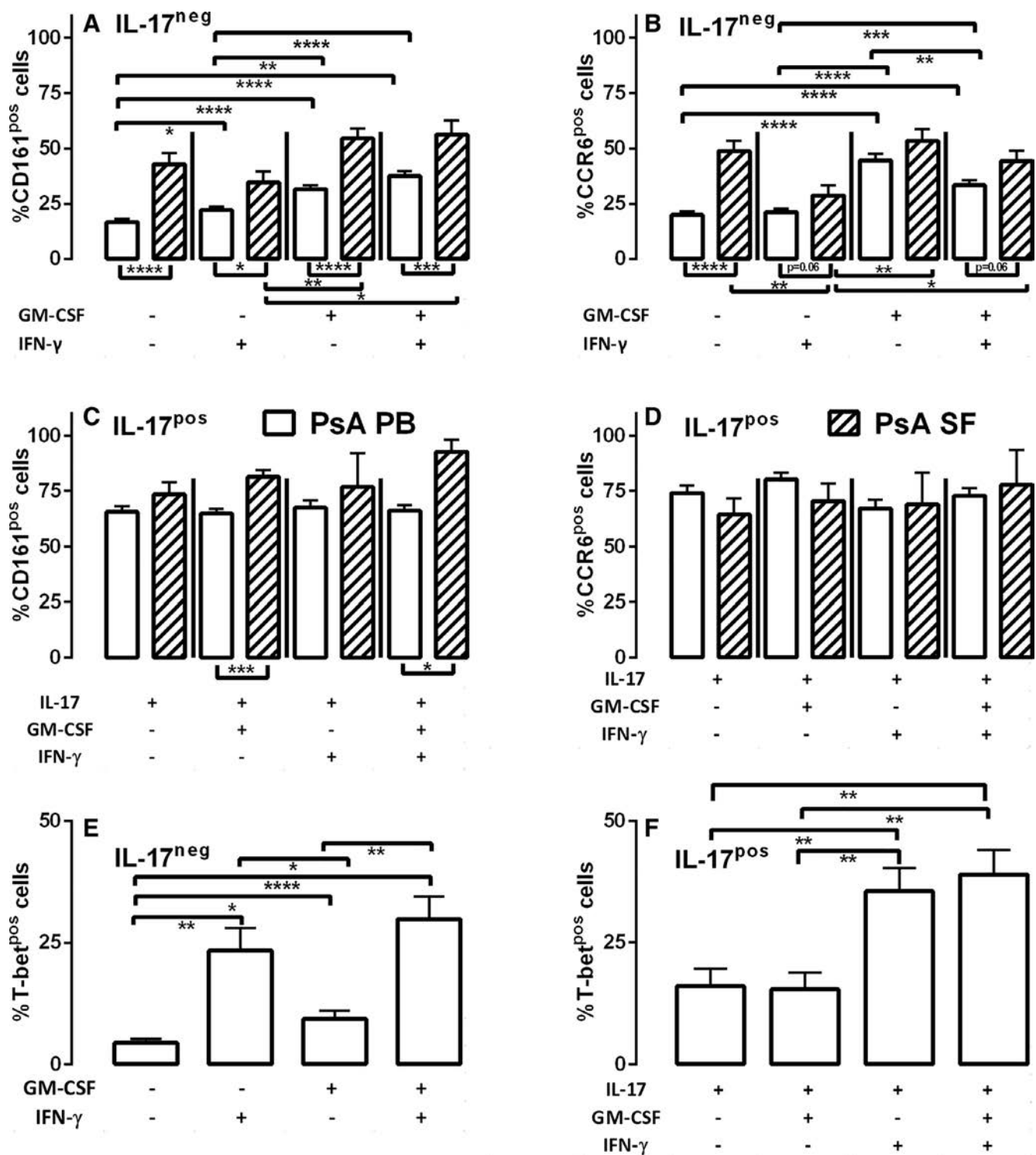


Figure 2. GM-CSF^{pos} and IL-17^{pos} polyfunctional CD4 T cells express Th₁₇-associated phenotypic markers and T-bet. Cells of PB from patients with PsA (n = 38, open bars) and SF from patients with PsA (n = 9, hatched bars) were incubated with PMA and ionomycin before staining and analysis by flow cytometry. Cells were gated as CD3+CD4+ T cells and evaluated as (A and C) CD161^{pos} or (B and D) CCR6^{pos} cells according to cytokine expression profiles (as in Figure 1E). Alternatively, PB from patients with PsA (n = 10) was stimulated with PMA and ionomycin, gated as CD3+CD4+ T cells, and examined based upon cytokine and T-bet expression. (E and F) T-bet expression in (E) IL-17^{neg} or (F) IL-17^{pos} CD4 T cells coexpressing GM-CSF \pm IFN γ . Data are represented as mean \pm SEM, and analyzed by one-way ANOVA with Tukey's multiple comparison test. **P* < 0.05; ***P* < 0.01; ****P* < 0.001; *****P* < 0.0001. ANOVA, analysis of variance; CCR, chemokine receptor; GM-CSF, granulocyte-macrophage colony-stimulating factor; HD, healthy donor; IFN, interferon; IL, interleukin; neg, negative; PB, peripheral blood; PMA, phorbol 12-myristate 13-acetate; pos, positive; PsA, psoriatic arthritis; SF, synovial fluid.

In inflamed joints, mean \pm SEM 43% \pm 5.1% and 49% \pm 4.7% of cytokine-negative cells expressed CD161 (Figure 2A) and CCR6 (Figure 2B), respectively, which is higher than equivalent PB T cells. GM-CSF^{pos} SF T cells demonstrated increased CD161 expression relative to GM-CSF^{pos} PB subsets, and significantly higher than SF Th₁ cells (Figure 2A). GM-CSF expression by IL-17^{pos} SF T cells also coincided with higher CD161 levels compared with PB counterparts (Figure 2C). CCR6 expression was lower in Th₁ SF cells when compared with cytokine-negative and GM-CSF^{pos} SF T cells (Figure 2B).

The pathogenicity of Th₁₇-derived cells, and the switch of Th₁₇ to Th₁ coincides with expression of the Th₁-associated transcription factor, T-bet.^{15–17} We demonstrate T-bet expression correlates with IFN γ , and was higher in GM-CSF^{pos} cells coexpressing IFN γ (Figure 2E, $P < 0.001$). Similarly, IFN γ coexpression in IL-17^{pos} cells was associated with increased T-bet expression

(Figure 2F, $P < 0.01$). GM-CSF^{pos}IFN γ ^{pos} cells that no longer produce IL-17 but express Th₁₇-associated markers therefore likely represent Th₁₇-derived subsets, for which T-bet acquisition in these and IL-17^{pos}GM-CSF^{pos}IFN γ ^{pos} polyfunctional T cells may represent a transition from a Th₁₇ to Th₁ phenotype.

Exogenous IL-23 increases IL-17 but inhibits GM-CSF release by Teff cells in patients with PsA. In mice, IL-23 expands pathogenic GM-CSF^{pos} Th₁₇ cells,^{11–13} therefore, the effect of exogenous IL-23 on cytokine release was compared in patients with PsA and in HDs. Stimulated Teff cells from patients with PsA released higher GM-CSF (Figure 3A, $P < 0.05$), lower IFN γ (Figure 3G, $P < 0.05$) and similar levels of IL-17 (Figure 3D) compared with HDs. In contrast to murine studies, exogenous IL-23 decreased GM-CSF release by both patients with PsA (Figure 3A; mean \pm SD 31% \pm 3.0% reduction; $P < 0.0001$) and

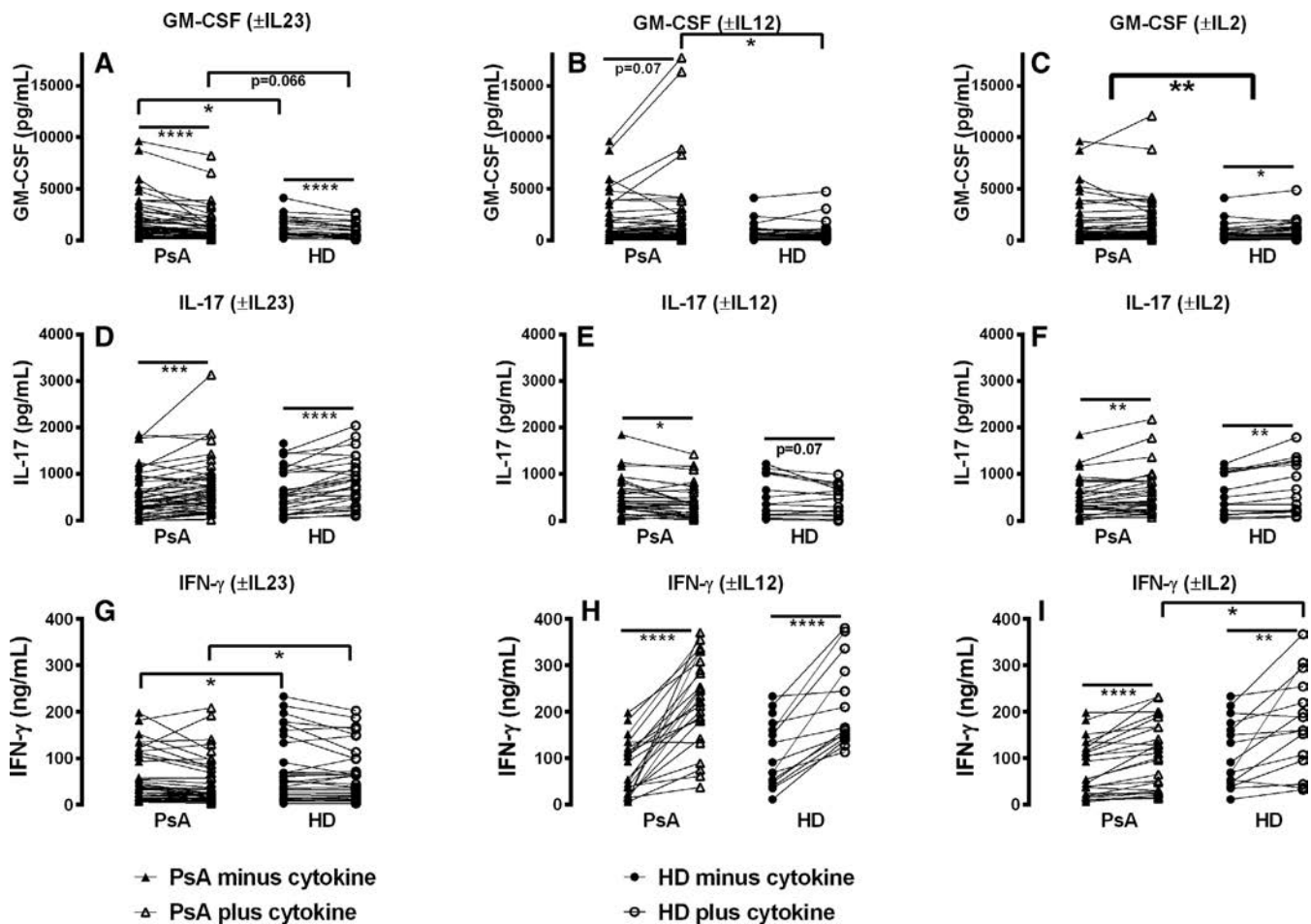


Figure 3. Exogenous IL-23 increases IL-17 but inhibits GM-CSF release by Teff cells in patients with PsA. PBMCs from patients with PsA ($n = 50$) and HDs ($n = 26$) were stimulated with anti-CD3/28 in the absence or presence of exogenous IL-23, IL-12, or IL-2, and supernatants tested for (A–C) GM-CSF, (D–F) IL-17, or (G–I) IFN γ by ELISA. Matched pairs of PBMC from patients with PsA (\blacktriangle) or HDs (\bullet) without exogenous cytokine were compared with PBMCs from patients with PsA (\triangle) or HDs (\circ) with exogenous IL-23, IL-12, or IL-2. Samples from patients with PsA were also compared with PBMCs from HDs within treatment groups. Data are represented as paired samples, with data analyzed by paired or unpaired Student's t -test. * $P < 0.05$; ** $P < 0.01$; *** $P < 0.001$; **** $P < 0.0001$. ELISA, enzyme-linked immunosorbent assay; GM-CSF, granulocyte-macrophage colony-stimulating factor; HD, healthy donor; IFN, interferon; IL, interleukin; PB, peripheral blood; PBMC, PB mononuclear cell; PsA, psoriatic arthritis.

HDs (Figure 3A; mean \pm SEM 33% \pm 4.4% reduction; $P < 0.001$) T cells. IL-23 increased IL-17 in patients with PsA (Figure 3D; mean \pm SEM 57% \pm 13.5% increase; $P < 0.001$) and in HDs (Figure 3D; mean \pm SEM 70% \pm 15.7% increase; $P < 0.0001$), and there was no net effect of IL-23 on IFN γ (Figure 3G).

Exogenous IL-12 augmented IFN γ production (Figure 3H; mean \pm SEM 636% \pm 150.2% increase; $P < 0.0001$) and slightly increased GM-CSF in patients with PsA (Figure 3B; mean \pm SEM 26% \pm 9.0% increase; $P = 0.07$). IL-17 release was inhibited by IL-12, although only significant for patients with PsA (Figure 3E, $P < 0.01$).

Polymorphisms in *IL2RA* have been associated with increased frequencies of GM-CSF-producing T cells.¹⁸ We found no net effect of exogenous IL-2 on GM-CSF release in patients with PsA, although there was a slight increase in HDs (Figure 3C, $P < 0.05$). IL-2 enhanced IL-17 release in patients with PsA and in HDs (Figure 3F; mean \pm SEM 39% \pm 11.9% increase; $P < 0.001$) and also IFN γ in both patients with PsA (Figure 3I; mean \pm SEM 59% \pm 12.6% increase; $P < 0.0001$) and HDs (Figure 3I; mean \pm SEM 85% \pm 26.5% increase; $P < 0.01$).

IL-17 release by Th₁₇ cells from patients with PsA is only partially IL-23 dependent, whereas IL-23 cooperates with TGF β . We sought to explore the effects of IL-23 and TGF β on IL-17, GM-CSF, and IFN γ production by naive T cells differentiated under Th₁₇-polarizing or Th₁-polarizing conditions, in patients with PsA. Naive CD4 T cells were differentiated with Th₁₇-polarizing cytokines (IL-1 β , IL-6, anti-IFN γ) with or without IL-23 \pm TGF β (Supplementary Figure 3); or the Th₁-polarizing cytokine IL-12 \pm IL-23 (Supplementary Figure 4).

IL-23-independent IL-17 production was confirmed, in that the absence of IL-23 during Th₁₇ differentiation reduced IL-17 production by mean \pm SEM 31% \pm 5.8% (Figure 4A; $P < 0.001$), and IL-17^{pos} T cell frequency by mean \pm SEM 31% \pm 8.2% (Figure 4B, Supplementary Figure 3A, $P < 0.01$). TGF β removal during Th₁₇ differentiation markedly reduced IL-17 release by mean \pm SEM 70% \pm 7.3% (Figure 4A, $P < 0.0001$) and the frequency of IL-17^{pos} cells by mean \pm SEM 74% \pm 4.4% (Figure 4B and Supplementary Figure 3A; $P < 0.0001$). IL-23 and TGF β cooperated to augment IL-17 release in that removing both cytokines reduced IL-17 production by mean \pm SEM 84% \pm 6.3% (Figure 4A, $P < 0.0001$) and IL-17^{pos} cells by mean \pm SEM 87% \pm 2.0% (Figure 4B and Supplementary Figure 3A, $P < 0.0001$).

In contrast to IL-17, the absence of IL-23 during Th₁₇ differentiation increased GM-CSF by mean \pm SEM 79 \pm 19% (Figure 4C; $P < 0.01$), and the frequency of GM-CSF^{pos} T cells by mean \pm SEM 99% \pm 17% (Figure 4D and Supplementary Figure 3B; $P < 0.0001$). There was no net effect of IL-23 on IFN γ (Figure 4E and F). Removing TGF β increased both GM-CSF and IFN γ release by mean \pm SEM 61% \pm 20%

(Figure 4C; $P < 0.01$) and mean \pm SEM 122% \pm 34% (Figure 4E; $P < 0.01$) respectively. IL-23 cooperated with TGF β as removal of both cytokines increased GM-CSF release by mean \pm SEM 185% \pm 52% (Figure 4C; $P < 0.01$) and GM-CSF^{pos} cells by mean \pm SEM 128% \pm 37% (Figure 4D and Supplementary Figure 3B; $P < 0.01$).

Given the marked reduction in IL-17^{pos} cells on removing TGF β , cytokine coexpression was only examined in the presence or absence of IL-23. There was an overall decrease in the frequency of IL-17^{pos} Th₁₇ (Figure 4B), but an increase in GM-CSF^{pos} Th₁₇ cells (Figure 4D) on removing IL-23. This corresponded to a proportional increase in polyfunctional IL-17^{pos} T cells coexpressing especially GM-CSF (Figure 4G; mean \pm SEM 32% \pm 3.2% without IL-23 vs mean \pm SEM 41% \pm 2.6% with IL-23; $P < 0.01$).

Th₁-polarized cells did not produce IL-17, and the levels of IFN γ and GM-CSF were significantly higher (Supplementary Figure 4) than for Th₁₇-polarized CD4 T cells (Supplementary Figure 3). IFN γ release by Th₁-polarized cells was 10-fold that for Th₁₇ polarization (mean \pm SEM 344 \pm 52.4 ng/mL for Th₁ vs mean \pm SEM 33 \pm 12.1 ng/mL for Th₁₇; $P < 0.0001$), and three-fold higher for GM-CSF (5,016 \pm 778 pg/mL for Th₁ vs 1,627 \pm 260 pg/mL for Th₁₇; $P < 0.001$). Similarly, the percentage of cells producing IFN γ (mean \pm SEM 71% \pm 1.6% for Th₁ vs mean \pm SEM 20% \pm 3.0% for Th₁₇; $P < 0.0001$) or GM-CSF (mean \pm SEM 51% \pm 5.1% for Th₁ vs mean \pm SEM 22% \pm 2.7% for Th₁₇; $P < 0.0001$) was higher with Th₁-polarizing conditions. The presence of IL-23 during Th₁ differentiation reduced GM-CSF release (Figure 4C, $P < 0.001$) and the frequency of GM-CSF^{pos} cells (Figure 4D, Supplementary Figure 4A vs B, middle panel; mean \pm SEM 51% \pm 5.1% minus IL-23 vs mean \pm SEM 18% \pm 3.1% plus IL-23; $P < 0.001$) but did not affect IFN γ (Figure 4E and F). We therefore confirm that IL-17 production by adaptive immune cells is only partially IL-23-dependent in patients with PsA, and IL-23 cooperates with TGF β to augment IL-17 release. Conversely, the presence of IL-23 reduces GM-CSF release by Th₁₇-derived and classic Th₁ cells, in addition to polyfunctional IL-17^{pos} T cells.

Polyfunctional Th₁₇ and Th₁₇-derived cells are amplified by metabolic stress. The effect of metabolic stress using Th₁₇ or Th₁-polarizing conditions was evaluated in patients with PsA. Metabolic stress was induced by (1) limiting glycolysis with 2-DG, (2) exposure to high-salt medium (ionic stress), or (3) stimulation of ER stress with thapsigargin,³² and supernatants harvested for quantification by ELISA. Harvested CD4 T cells were restimulated with PMA and ionomycin, and cytokine release was evaluated by flow cytometry.

Ionic stress with high salt and ER stress with thapsigargin increased IL-17 (Figure 5A and B, Supplementary Figure 5A), GM-CSF (Figure 5C and D, Supplementary Figure 5B), and IFN γ (Figure 5E and F, Supplementary Figure 5C) under Th₁₇ polarizing

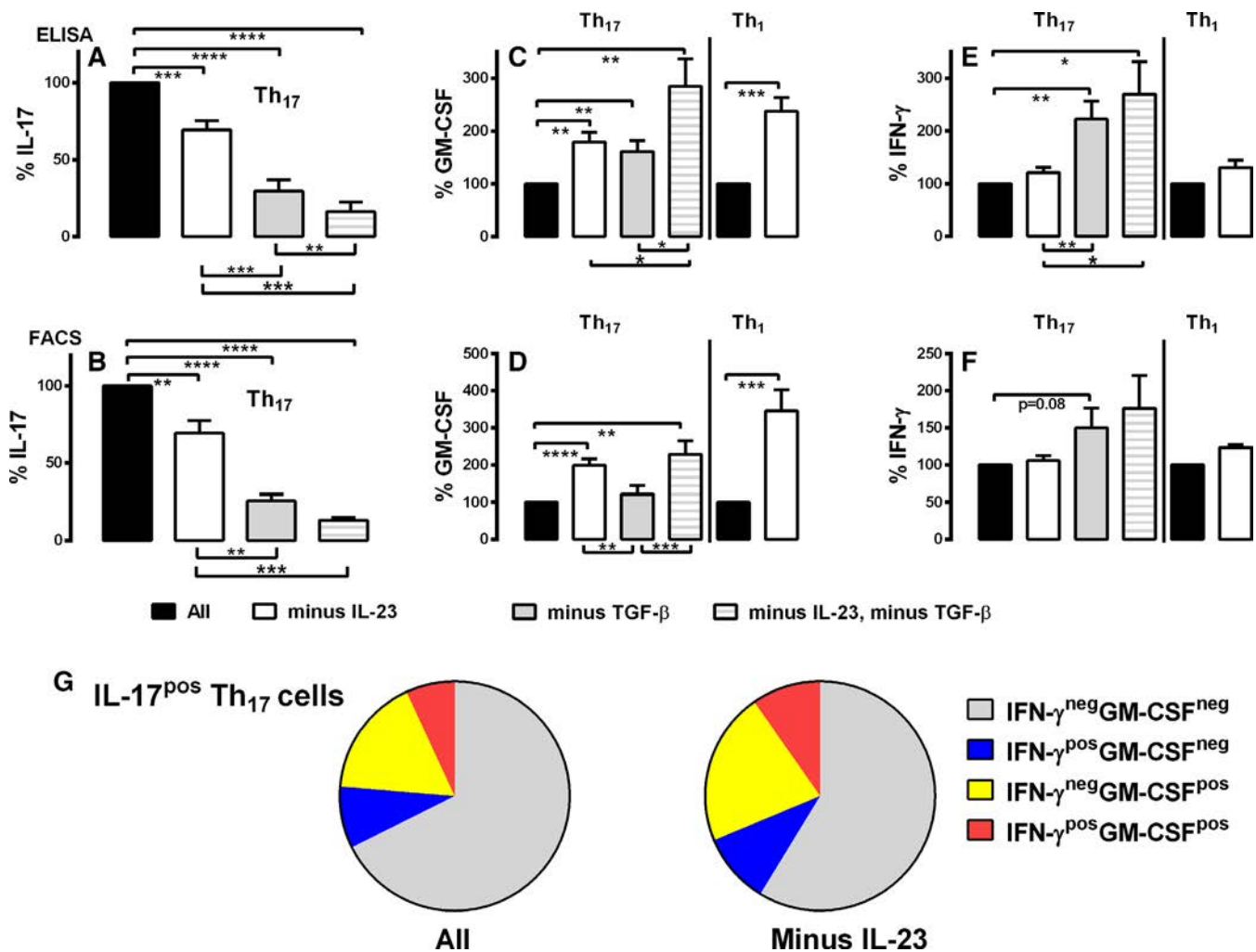


Figure 4. IL-17 release by Th₁₇ cells from patients with PsA is only partially IL-23 dependent, whereas IL-23 cooperates with TGFβ. Naive CD4 T cells of patients with PsA were differentiated in (A–G) Th₁₇-polarizing (n = 14) or (C–F) Th₁-polarizing (n = 12) conditions with removal of cytokines as detailed and stimulated with anti-CD3/28 Dynabeads for five to seven days, and supernatants were tested for (A) IL-17, (C) GM-CSF, or (E) IFNγ by ELISA. Cells were harvested and restimulated with PMA and ionomycin before staining and analysis by flow cytometry. Cells were gated as live, CD3⁺CD4⁺ T cells, and evaluated as (B) IL-17^{pos}, (D) GM-CSF^{pos}, or (F) IFNγ^{pos} T cells. Data comparing cytokine removal is normalized relative to Th₁₇-polarizing conditions with IL-23 and TGFβ; or Th₁ polarizing conditions with IL-23. (G) Pie charts demonstrating IL-17^{pos} T cells with the coexpression of GM-CSF ± IFNγ differentiated under Th₁₇ polarizing conditions in the presence or absence of IL-23. Data are represented as mean ± SEM, with data analyzed by one-way ANOVA with Tukey's multiple comparison test. **P* < 0.05; ***P* < 0.01; ****P* < 0.001; *****P* < 0.0001. ANOVA, analysis of variance; ELISA, enzyme-linked immunosorbent assay; FACS, fluorescence-activated cell sorting; GM-CSF, granulocyte-macrophage colony-stimulating factor; IFN, interferon; IL, interleukin; PMA, phorbol 12-myristate 13-acetate; pos, positive; PsA, psoriatic arthritis; TGF, transforming growth factor. Color figure can be viewed in the online issue, which is available at <http://onlinelibrary.wiley.com/doi/10.1002/art.43095/abstract>.

conditions. 2-DG slightly increased GM-CSF (Figure 5C and D) but inhibited IL-17 (Figure 5A and B) and IFNγ (Figure 5E and F). 2-DG correspondingly decreased GM-CSF^{pos} polyfunctional cells expressing IFNγ ± IL-17 and IL-17^{pos} polyfunctional T cells. Thapsigargin was most effective at expanding polyfunctional subsets in which GM-CSF^{pos} polyfunctional Th₁₇-derived cells increased from mean ± SEM 36% ± 3.4% to 63% ± 3.4% (Figure 5G; *P* < 0.0001), and IL-17^{pos} polyfunctional Th₁₇ from mean ± SEM 32% ± 3.2% to 65% ± 3.1% (Figure 5H; *P* < 0.0001). Thapsigargin preferentially expanded IFNγ expression in GM-CSF^{pos} (Figure 5G) and IL-17^{pos} (Figure 5H)

polyfunctional Th₁₇, whereas high salt augmented IL-17^{pos} cells coexpressing GM-CSF (Figure 5H; mean ± SD 24% ± 3.2% to 45% ± 4.7%; *P* < 0.001).

As observed for Th₁₇-polarized cells, IFNγ frequency within Th₁-differentiated cells was reduced with 2-DG (Supplementary Figure 6; mean ± SEM 34% ± 2% decrease for Th₁ vs mean ± SEM 60% ± 5% for Th₁₇) whereas there was no significant effect on GM-CSF (Supplementary Figure 6A, C, and D). There was a modest increase in IFNγ (mean ± SEM 18% ± 5% increase for Th₁ vs mean ± SEM 254% ± 30% for Th₁₇) and GM-CSF (mean ± SEM 33% ± 21% increase for Th₁ vs mean ± SEM 215% ±

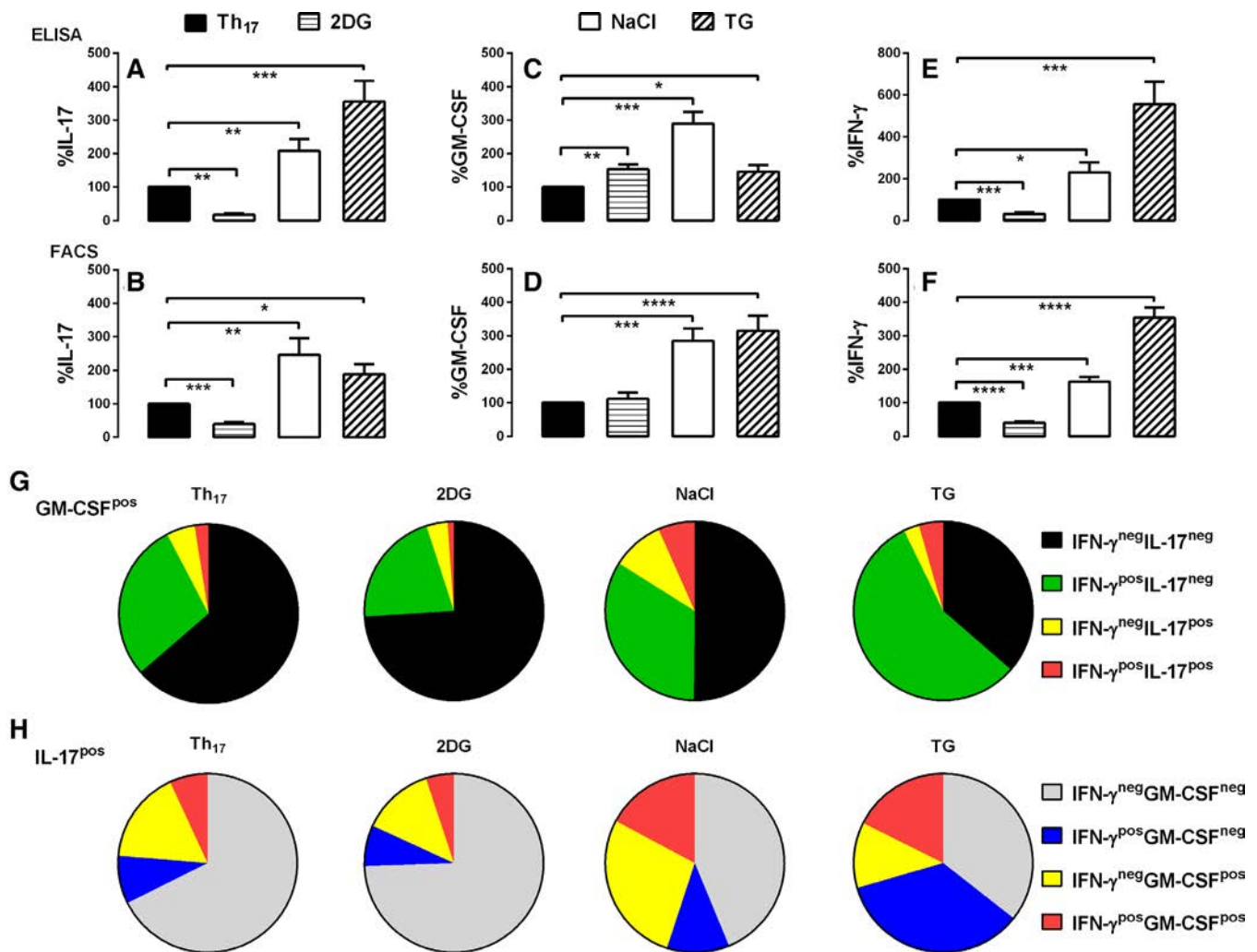


Figure 5. Polyfunctional Th₁₇ and Th₁₇-derived cells are amplified by metabolic stress. Naive CD4 T cells from patients with PsA were differentiated in Th₁₇-polarizing conditions in the absence (Th₁₇) or presence of the metabolic mediators 2-DG, NaCl, or TG and stimulated with anti-CD3/28 Dynabeads for five to seven days, and supernatants were tested for (A) IL-17, (C) GM-CSF, or (E) IFN γ by ELISA (normalized to 100% for Th₁₇ cells without metabolic mediators). Cells were then restimulated with PMA and ionomycin, before staining and analysis by flow cytometry. (B, D, and F) Percent change in proportion of single cytokine^{pos} cells (normalized to 100% for Th₁₇ cells without metabolic mediators) and analysis by FACS for (B) IL-17, (D) GM-CSF, or (F) IFN γ . (G) GM-CSF^{pos} cells coexpressing IFN γ \pm IL-17 were displayed in pie charts as Th₁₇ without metabolic mediators, or in the presence of 2-DG, NaCl, or TG. (H) IL-17^{pos} cells coexpressing IFN γ \pm GM-CSF were displayed in pie charts as Th₁₇ without metabolic mediators, or in the presence of 2-DG, NaCl, or TG. Data are represented as mean \pm SEM, with data analyzed by paired *t*-test using Tukey's multiple comparison test. **P* < 0.05; ***P* < 0.01; ****P* < 0.001; *****P* < 0.0001. 2-DG, 2-deoxy-D-glucose; ELISA, enzyme-linked immunosorbent assay; FACS, fluorescence-activated cell sorting; GM-CSF, granulocyte-macrophage colony-stimulating factor; IFN, interferon; IL, interleukin; pos, positive; PsA, psoriatic arthritis; TG, thapsigargin; TGF, transforming growth factor. Color figure can be viewed in the online issue, which is available at <http://onlinelibrary.wiley.com/doi/10.1002/art.43095/abstract>.

44% for Th₁₇) with thapsigargin. High salt did not expand Th₁₇-differentiated cells (Supplementary Figure 6), whereas a decrease in cell viability was observed in some donors (Supplementary Figure 6A and B), although no overall net decrease in cytokine release was observed for pooled donors (Supplementary Figure 6C and D).

We therefore demonstrate that metabolic stress expands putatively pathogenic polyfunctional Th₁₇ and Th₁₇-derived cells but minimally affects Th₁ subsets. We also reveal important differences in the regulation of IL-17 and GM-CSF, including differential effects on limiting glycolysis as well as reciprocal regulation by IL-

23. The cytokine milieu and metabolic microenvironment experienced during the expansion of naive CD4 T cells will likely influence the T cell phenotypes obtained, in which there is considerable Th₁₇ plasticity, and such factors may be important in maintaining these subsets at sites of disease.

DISCUSSION

We demonstrate increased proportions of GM-CSF^{pos} Th₁₇-derived and IL-17^{pos} polyfunctional T cells in the inflamed joints of patients with PsA, which are reduced in frequency in the PB

of patients with PsA when compared with PB from HDs. Polyfunctional T cells may traffic to inflamed joints and are retained or expanded within the joint. IL-17^{pos} T cells are by definition Th₁₇, in which the coexpression of pro-inflammatory GM-CSF implies a pathogenic phenotype.^{11–15} These polyfunctional Th₁₇ cells coexist with GM-CSF^{pos} cells no longer producing IL-17 but demonstrating features of Th₁₇ (CCR6^{pos}, CD161^{pos}), described as Th₁₇-derived, ex-Th₁₇, or nonclassic Th₁ cells. The pathogenicity of Th₁₇-derived cells or the switch of Th₁₇ to Th₁ correlates with expression of T-bet.^{15–17} In contrast, nonpathogenic Th₁₇ cells that play a role in barrier function in the intestine coproduce anti-inflammatory mediators such as IL-10, have an ex-Th₁₇ regulatory phenotype, and are not influenced by IL-23.³³ Th₁₇ cells therefore exhibit considerable plasticity and may transform to a Th₁₇-derived phenotype at sites of disease.³⁴ Th₁₇-derived cells have a more differentiated phenotype, enhanced survival capability, increased proliferative capacity, and are polyfunctional in terms of cytokine production relative to classic Th₁ and Th₁₇ cells, suggesting they are more likely to contribute to disease pathogenesis.³⁴

We confirm IL-23-dependent, but also IL-23-independent IL-17 production by adaptive immune cells, in which the absence of IL-23 during Th₁₇ differentiation reduced IL-17 by mean \pm SEM 31% \pm 5.8%. In a Th₁₇ fate reporter mouse model, chronic inflammation caused a switch to alternative cytokines by Th₁₇ cells that no longer produced IL-17 (Th₁₇-derived cells), for which this conversion was IL-23 dependent.¹⁷ IL-23 also drove pathogenic T cell responses and reduced regulatory T cell activity in intestinal inflammation, whereas IL-23R activation induced T-bet signaling and the generation of pathogenic polyfunctional T cells expressing IL-17A with IFN γ .^{35,36} In contrast to murine studies in which IL-23 augments GM-CSF,^{11,12} we show that GM-CSF is negatively regulated by IL-23 in human Th₁₇ and Th₁ cells. Removing IL-23 during Th₁₇ differentiation increased the frequency of polyfunctional IL-17^{pos} T cells coexpressing GM-CSF. There are therefore key differences in murine and human Th₁₇ cells and IL-23-responsiveness, and it is plausible that augmentation of GM-CSF when blocking IL-23 could be a factor determining differences observed between IL-17 and IL-23 inhibition in human disease.¹⁰ We also confirmed dependence on TGF β for IL-17 release by human naive CD4 T cells differentiated under Th₁₇-polarizing conditions.³⁷ TGF β cooperated with IL-23 in our study to enhance IL-17 production. TGF β therefore appears to be an essential cytokine for human Th₁₇ differentiation, although previous studies have shown that other pro-inflammatory mediators including IL-1 β , IL-6, and IL-23 are required to confer pathogenicity.^{22–27,38} The plasticity of Th₁₇ cells and the associated cytokine milieu means that targeting of IL-17 alone will only transiently inhibit Th₁₇ or Th₁₇-derived cells in chronic inflammatory settings.

We show that both ionic pressure with high salt and ER stress with thapsigargin expand polyfunctional Th₁₇-derived and IL-17^{pos} Th₁₇ cells in vitro, in accordance with previous murine data.³² Limiting glycolysis with 2-DG can increase IL-17,³²

whereas we showed that 2-DG inhibited IL-17 and IFN γ , but increased GM-CSF. Shi et al³⁹ also demonstrated that blocking glycolysis with 2-DG inhibited Th₁₇ development, in which the dichotomy of 2-DG is likely influenced by glucose availability and in particular the expression of the glycolytic intermediate metabolite, phosphoenolpyruvate.⁴⁰ There is further in vivo evidence to support metabolic stress as a mediator of Th₁₇ expansion, in which a high-salt diet fed to mice increased the severity of EAE, whereas serum glucocorticoid kinase (SGK) 1 deficient mice exhibited less severe EAE.^{28,29} SGK1 governed sodium transport, salt homeostasis, IL-23R expression, and stabilization of the Th₁₇ phenotype, thus linking metabolic and inflammatory pathways. Furthermore, mice fed a high-salt diet had an altered microbiome in which *Lactobacillus murinus* was depleted, and *L. murinus* treatment prevented salt-induced exacerbation of murine EAE by modulating Th₁₇ cells.³⁰ A human study of moderate salt challenge also showed reduced survival of *Lactobacilli* spp, with a concomitant increase in Th₁₇ and blood pressure.³⁰ In a murine model of collagen-induced arthritis, clinical and histologic arthritis were more severe in mice fed a high-salt diet, the expression of intestinal and synovial IL-17 was higher, and higher salt levels were demonstrated in mice with RA when compared with the SF from mice with osteoarthritis.⁴¹

The impact of ionic stress on Th₁₇ expansion is influenced by the cytokine microenvironment. Matthias et al⁴² showed that high salt exposure induced several anti-inflammatory mediators in Th₁₇ cells, including the regulatory transcription factor FOXP3, TGF β , IL-10, and CTLA-4. However, the presence of pro-inflammatory cytokines prevented the upregulation of anti-inflammatory mediators in human Th₁₇ cells, and in murine EAE, high salt was only pathogenic when Th₁₇ cells were primed in the presence of pro-inflammatory mediators (IL-6, IL-1 β , IL-23) and absence of TGF β .⁴² Brucklacher-Waldert et al³² confirmed a requirement for pro-inflammatory mediators to augment IL-17 release with thapsigargin and high salt, but in contrast with Matthias et al,⁴² TGF β increased IL-17 release elicited by high salt. Overall, these data highlight the complex interaction of cytokine and metabolic microenvironments in influencing the pro- versus anti-inflammatory Th₁₇ subsets that ensue.

Matthias et al^{42–44} reported that high salt augmented IL-17 but with a concomitant reduction in IFN γ and shift from Th₁ to Th₂ responses. In our study, we showed the effect of salt on IFN γ was context-dependent in that high salt augmented IFN γ and GM-CSF release in Th₁₇-polarizing but not Th₁-polarizing conditions. TGF β is an inducer of SGK1,²⁹ and NaCl can increase the production of TGF β by NaCl-induced NFAT5,^{42,45} demonstrating an autocrine effect of TGF β on Th₁₇ cells, and positive relationship with NaCl. A putative candidate is the relationship between SGK1 and IL-23 downstream signaling, in which SGK1 stabilizes IL-23R expression and the Th₁₇ phenotype by deactivation of FOXO1, a direct repressor of IL-23R expression.²⁹ Collectively, these

studies provide a direct molecular link between Th₁₇ immunity and ionic stress that may be crucial to the development and expansion of pathogenic Th₁₇ subsets.

The ER is an organelle that facilitates protein folding, trafficking, and degradation to maintain protein homeostasis, and ER stress agents such as thapsigargin disturb ER proteostasis, thus activating the unfolded protein response. There are several physiologic mediators of ER stress including hypoxia, in which XBP1 is a downstream transcription factor activated by ER stress, which directly regulates *Rorc* and thus Th₁₇ cell differentiation. XBP1 also forms a transcriptional complex with hypoxia-inducible factor (HIF) 1 α , a metabolic sensor of hypoxia and a key transcriptional regulator of Th₁₇ cell polarization operating via direct transcriptional activation of *Rorc*.^{39,46,47} The potent augmentation of GM-CSF^{pos} Th₁₇-derived and IL-17^{pos} polyfunctional Th₁₇ cells by thapsigargin identifies the ER stress response as a putative molecular target. Subudhi et al⁴⁸ showed metabolic coordination between skin epithelium and type 17 immunity in plaque psoriasis, in which blocking HIF1 α in psoriatic lesions ex vivo impaired glycolysis and phenocopied IL-17 inhibition.⁴⁸ They showed that epithelial pathology was fueled by glycolysis to enhance lactate production, whereas pharmacological inhibition of lactate-producing enzymes or lactate transporters attenuated skin pathology and IL-17A expression in vivo, linking metabolic stress and type 17 immunity for patients with psoriatic disease.⁴⁸ Lactate accumulation occurs in metabolically active inflamed joints, and uptake of lactate by the SLC5A12 transporter into CD4 T cells augments IL-17 production.⁴⁹

A limitation of our study was the number of phenotypic markers and intracellular cytokines used to characterize the defined T cell subsets in contrast to more recent studies in patients with PsA. Steel et al⁹ described an abundance of polyfunctional IL-17A^{pos}CD8^{pos} SF T (Tc₁₇) cells, possessing features of Th₁₇ cells (expressing *RORC/IL23R/CCR6/CD161*) and Tc1 (granzyme A/B). These Tc₁₇ cells demonstrated a tissue-resident memory (T_{RM}) cell signature and had increased levels of CXCR6 hypothesized to retain the subset within the joint by binding to the ligand CXCL16; the latter also increased in the synovial joints of patients with PsA. Penvaka et al⁵⁰ described clonally expanded CD8^{pos} T cells in SF from patients with PsA, with abundant expression of CXCR3, in which CXCR3 plays a role in chemotaxis during inflammation. Polyfunctional T cells within our study likely include T_{RM} cells, in which approximately 50% of GM-CSF^{pos} CD4 and CD8 SF cells coexpressed CD69, compared with 20% of corresponding PB cells (data not shown because they have not extensively been characterized).

In summary, we hypothesize that the abundance polyfunctional GM-CSF^{pos} and IL-17^{pos} type 17 cells in the SF of patients with PsA represents the appearance or accumulation in the joint of Th₁₇-derived subsets (or nonclassic Th₁) that express Th₁₇ cell-associated markers. IL-23 augments the frequency of IL-17^{pos} cells, but there is probable IL-23-independent Th₁₇

differentiation and IL-17 release by adaptive immune cells. In contrast to murine studies, IL-23 negatively regulates GM-CSF in human T cells. TGF β is required for Th₁₇ differentiation and cooperates with IL-23 to augment IL-17 production. IL-17^{pos} Th₁₇ and GM-CSF^{pos} Th₁₇-derived polyfunctional T cell subsets, but not classic Th₁ cells, are expanded by metabolic stress, for which there is accumulating evidence linking metabolic stress with type 17 immunity. Our data therefore support GM-CSF inhibition and/or modulation of metabolic stress as novel therapeutic targets for patients with PsA.

ACKNOWLEDGMENTS

Many thanks to Dominique Raut-Roy, who was the research nurse supporting this study. Assistance with flow cytometry was provided by the National Institute for Health Research Cambridge Biomedical Research Centre phenotyping hub.

AUTHOR CONTRIBUTIONS



All authors contributed to at least one of the following manuscript preparation roles: conceptualization AND/OR methodology, software, investigation, formal analysis, data curation, visualization, and validation AND drafting or reviewing/editing the final draft. As corresponding author, Dr Stober confirms that all authors have provided the final approval of the version to be published, and takes responsibility for the affirmations regarding article submission (eg, not under consideration by another journal), the integrity of the data presented, and the statements regarding compliance with institutional review board/Declaration of Helsinki requirements.

REFERENCES

1. Michalek IM, Loring B, John SM. A systematic review of worldwide epidemiology of psoriasis. *J Eur Acad Dermatol Venereol* 2017;31(2):205–212.
2. Eder L, Haddad A, Rosen CF, et al. The incidence and risk factors for psoriatic arthritis in patients with psoriasis: a prospective cohort study. *Arthritis Rheumatol* 2016;68(4):915–923.
3. Bowes J, Budu-Aggrey A, Huffmeier U, et al. Dense genotyping of immune-related susceptibility loci reveals new insights into the genetics of psoriatic arthritis. *Nat Commun* 2015;6:6046.
4. Stuart PE, Nair RP, Tsoi LC, et al. Genome-wide association analysis of psoriatic arthritis and cutaneous psoriasis reveals differences in their genetic architecture. *Am J Hum Genet* 2015;97(6):816–836.
5. Benham H, Norris P, Goodall J, et al. Th17 and Th22 cells in psoriatic arthritis and psoriasis. *Arthritis Res Ther* 2013;15(5):R136.
6. Menon B, Gullick NJ, Walter GJ, et al. Interleukin-17+CD8+ T cells are enriched in the joints of patients with psoriatic arthritis and correlate with disease activity and joint damage progression. *Arthritis Rheumatol* 2014;66(5):1272–1281.
7. Al-Mossawi MH, Chen L, Fang H, et al. Unique transcriptome signatures and GM-CSF expression in lymphocytes from patients with spondyloarthritis. *Nat Commun* 2017;8(1):1510.
8. Steel KJA, Srenathan U, Ridley M, et al. Polyfunctional, proinflammatory, tissue-resident memory phenotype and function of synovial interleukin-17A+CD8+ T cells in psoriatic arthritis. *Arthritis Rheumatol* 2020;72(3):435–447.

9. Wade SM, Canavan M, McGarry T, et al. Association of synovial tissue polyfunctional T-cells with DAPSA in psoriatic arthritis. *Ann Rheum Dis* 2019;78(3):350–354.
10. Baeten D, Ostergaard M, Wei JC, et al. Risankizumab, an IL-23 inhibitor, for ankylosing spondylitis: results of a randomised, double-blind, placebo-controlled, proof-of-concept, dose-finding phase 2 study. *Ann Rheum Dis* 2018;77(9):1295–1302.
11. Codarri L, Gyöveszi G, Tosevski V, et al. ROR γ t drives production of the cytokine GM-CSF in helper T cells, which is essential for the effector phase of autoimmune neuroinflammation. *Nat Immunol* 2011;12(6):560–567.
12. El-Behi M, Ciric B, Dai H, et al. The encephalitogenicity of T(H)17 cells is dependent on IL-1- and IL-23-induced production of the cytokine GM-CSF. *Nat Immunol* 2011;12(6):568–575.
13. Sonderegger I, Iezzi G, Maier R, et al. GM-CSF mediates autoimmunity by enhancing IL-6-dependent Th17 cell development and survival. *J Exp Med* 2008;205(10):2281–2294.
14. Haak S, Croxford AL, Kreyenborg K, et al. IL-17A and IL-17F do not contribute vitally to autoimmune neuro-inflammation in mice. *J Clin Invest* 2009;119(1):61–69.
15. Brucklacher-Waldert V, Ferreira C, Innocentin S, et al. Tbet or continued ROR γ t expression is not required for Th17-associated immunopathology. *J Immunol* 2016;196(12):4893–4904.
16. Duhon R, Glatigny S, Arbelaez CA, et al. Cutting edge: the pathogenicity of IFN- γ -producing Th17 cells is independent of T-bet. *J Immunol* 2013;190(9):4478–4482.
17. Hirota K, Duarte JH, Veldhoen M, et al. Fate mapping of IL-17-producing T cells in inflammatory responses. *Nat Immunol* 2011;12(3):255–263.
18. Hartmann FJ, Khademi M, Aram J, et al. Multiple sclerosis-associated IL2RA polymorphism controls GM-CSF production in human TH cells. *Nat Commun* 2014;5:5056.
19. Noster R, Riedel R, Mashreghi MF, et al. IL-17 and GM-CSF expression are antagonistically regulated by human T helper cells. *Sci Transl Med* 2014;6(241):241ra80.
20. Piper C, Pesenacker AM, Bending D, et al. T cell expression of granulocyte-macrophage colony-stimulating factor in juvenile arthritis is contingent upon Th17 plasticity. *Arthritis Rheumatol* 2014;66(7):1955–1960.
21. Bettelli E, Carrier Y, Gao W, et al. Reciprocal developmental pathways for the generation of pathogenic effector TH17 and regulatory T cells. *Nature* 2006;441(7090):235–238.
22. Langrish CL, Chen Y, Blumenschein WM, et al. IL-23 drives a pathogenic T cell population that induces autoimmune inflammation. *J Exp Med* 2005;201(2):233–240.
23. Ivanov I, McKenzie BS, Zhou L, et al. The orphan nuclear receptor ROR γ directs the differentiation program of proinflammatory IL-17+ T helper cells. *Cell* 2006;126(6):1121–1133.
24. McGeachy MJ, Bak-Jensen KS, Chen Y, et al. TGF- β and IL-6 drive the production of IL-17 and IL-10 by T cells and restrain T(H)-17 cell-mediated pathology. *Nat Immunol* 2007;8(12):1390–1397.
25. Lee Y, Awasthi A, Yosef N, et al. Induction and molecular signature of pathogenic TH17 cells. *Nat Immunol* 2012;13(10):991–999.
26. Korn T, Bettelli E, Gao W, et al. IL-21 initiates an alternative pathway to induce proinflammatory T(H)17 cells. *Nature* 2007;448(7152):484–487.
27. Veldhoen M, Hocking RJ, Flavell RA, et al. Signals mediated by transforming growth factor- β initiate autoimmune encephalomyelitis, but chronic inflammation is needed to sustain disease. *Nat Immunol* 2006;7(11):1151–1156.
28. Kleiweietfeld M, Manzel A, Titze J, et al. Sodium chloride drives autoimmune disease by the induction of pathogenic TH17 cells. *Nature* 2013;496(7446):518–522.
29. Wu C, Yosef N, Thalhamer T, et al. Induction of pathogenic TH17 cells by inducible salt-sensing kinase SGK1. *Nature* 2013;496(7446):513–517.
30. Wilck N, Matus MG, Kearney SM, et al. Salt-responsive gut commensal modulates T(H)17 axis and disease. *Nature* 2017;551(7682):585–589.
31. Taylor W, Gladman D, Helliwell P, et al. Classification criteria for psoriatic arthritis: development of new criteria from a large international study. *Arthritis Rheum* 2006;54(8):2665–2673.
32. Brucklacher-Waldert V, Ferreira C, Stebbins M, et al. Cellular stress in the context of an inflammatory environment supports TGF- β -independent T helper-17 differentiation. *Cell Rep* 2017;19(11):2357–2370.
33. Stockinger B, Omenetti S. The dichotomous nature of T helper 17 cells. *Nat Rev Immunol* 2017;17(9):535–544.
34. Basdeo SA, Cluxton D, Sulaimani J, et al. Ex-TH₁₇ (nonclassical Th₁) cells are functionally distinct from classical Th₁ and Th17 cells and are not constrained by regulatory T cells. *J Immunol* 2017;198(6):2249–2259.
35. Ahern PP, Izcue A, Maloy KJ, et al. The interleukin-23 axis in intestinal inflammation. *Immunol Rev* 2008;226:147–159.
36. Krausgruber T, Schiering C, Adelman K, et al. T-bet is a key modulator of IL-23-driven pathogenic CD4(+) T cell responses in the intestine. *Nat Commun* 2016;7:11627.
37. Manel N, Unutmaz D, Littman DR. The differentiation of human T(H)-17 cells requires transforming growth factor- β and induction of the nuclear receptor ROR γ mat. *Nat Immunol* 2008;9(6):641–649.
38. Veldhoen M, Stockinger B. TGF β 1, a “jack of all trades”: the link with pro-inflammatory IL-17-producing T cells. *Trends Immunol* 2006;27(8):358–361.
39. Shi LZ, Wang R, Huang G, et al. HIF1 α -dependent glycolytic pathway orchestrates a metabolic checkpoint for the differentiation of TH17 and Treg cells. *J Exp Med* 2011;208(7):1367–1376.
40. Huang TY, Hirota M, Sasaki D, et al. Phosphoenolpyruvate regulates the Th₁₇ transcriptional program and inhibits autoimmunity. *Cell Rep* 2023;42(3):112205.
41. Jung SM, Kim Y, Kim J, et al. Sodium chloride aggravates arthritis via Th₁₇ polarization. *Yonsei Med J* 2019;60(1):88–97.
42. Matthias J, Heink S, Picard F, et al. Salt generates antiinflammatory Th₁₇ cells but amplifies pathogenicity in proinflammatory cytokine microenvironments. *J Clin Invest* 2020;130(9):4587–4600.
43. Matthias J, Maul J, Noster R, et al. Sodium chloride is an ionic checkpoint for human T_H2 cells and shapes the atopic skin microenvironment. *Sci Transl Med* 2019;11(480):eaau0683.
44. Matthias J, Zielinski CE. Shaping the diversity of Th2 cell responses in epithelial tissues and its potential for allergy treatment. *Eur J Immunol* 2019;49(9):1321–1333.
45. Gutcher I, Donkor MK, Ma Q, et al. Autocrine transforming growth factor- β promotes in vivo Th₁₇ cell differentiation. *Immunity* 2011;34(3):396–408.
46. Dang EV, Barbi J, Yang HY, et al. Control of T(H)₁₇/T(reg) balance by hypoxia-inducible factor 1. *Cell* 2011;146(5):772–784.
47. Wang H, Flach H, Onizawa M, et al. Negative regulation of Hif1 α expression and TH₁₇ differentiation by the hypoxia-regulated micro-RNA miR-210. *Nat Immunol* 2014;15(4):393–401.
48. Subudhi I, Konieczny P, Prystupa A, et al. Metabolic coordination between skin epithelium and type 17 immunity sustains chronic skin inflammation. *Immunity* 2024;57(7):1665–1680.e7.
49. Pucino V, Certo M, Bulusu V, et al. Lactate buildup at the site of chronic inflammation promotes disease by inducing CD4(+) T cell metabolic rewiring. *Cell Metab* 2019;30(6):1055–1074.e8.
50. Penkava F, Velasco-Herrera MDC, Young MD, et al. Single-cell sequencing reveals clonal expansions of pro-inflammatory synovial CD8 T cells expressing tissue-homing receptors in psoriatic arthritis. *Nat Commun* 2020;11(1):4767.

An Immunosenescent CD8+ T Cell Subset in Patients with Axial Spondyloarthritis and Psoriatic Arthritis Links Spontaneous Motility to Telomere Shortening and Dysfunction

Giorgia Paldino,¹ Valentina Tedeschi,¹ Valentina Proganò,¹ Erica Salvati,² Valerio Licursi,² Eleonora Vertecchi,² Alexandru L. Bivolaru,¹ Emanuele Molteni,¹ Rossana Scrivo,¹  Mattia Congia,³ Alberto Cauli,³ Rosalba Caccavale,⁴ Marino Paroli,⁴ Martina Kunkl,⁵ Loretta Tuosto,¹ Rosa Sorrentino,¹ and Maria Teresa Fiorillo¹ 

Objective. A pathogenetic role of CD8+ T lymphocytes in radiographic axial spondyloarthritis (r-axSpA) and other spondyloarthritis (SpA) is sustained by genome-wide association studies and by the expansion of public T cell clones in the target tissues. This study investigates the migration of CD8+ T cells along with their phenotype and functions in patients with r-axSpA and psoriatic arthritis (PsA).

Methods. Peripheral blood CD8+ and CD4+ T cells were isolated from patients with r-axSpA (n = 128), PsA (n = 60), and rheumatoid arthritis (RA) (n = 74) and healthy donors (HDs) (n = 79). Transwell migration assay was performed in the presence of different chemokines. CD8+ T cell immunoprofiling and effector functions were assessed by multiparametric flow cytometry. Transcriptome signature was evaluated by RNA sequencing analysis, whereas telomere length and dysfunction were measured by reverse transcriptase–polymerase chain reaction and immunofluorescence–fluorescence in situ hybridization, respectively.

Results. A significantly higher number of CD8+ T cells migrating in the absence of chemokine stimuli was found in patients with SpA compared with HDs and patients with RA. This subset, producing cytotoxic (granzyme B, perforin, granulysin) and proinflammatory molecules (tumor necrosis factor), was significantly enriched in terminally differentiated (CCR7–CD45RA+) and senescent (CD28–CD57+) cells having a gene expression profile characterized by cytolytic signature and natural killer markers. Remarkably, these spontaneously migrating CD8+ T cells showed DNA damage response activation, telomere shortening, and dysfunction.

Conclusion. These data describe a terminally differentiated CD8+ T cell subset with a senescent and cytotoxic/proinflammatory profile and an intrinsic invasive potential enriched in patients with SpA that represents a possible player in disease pathogenesis.

INTRODUCTION

Experimental animal models and clinical data strongly point at T lymphocytes as key players in the pathogenesis of radiographic

axial spondyloarthritis (r-axSpA), historically termed ankylosing spondylitis.¹ R-axSpA is the prototype of a group of chronic inflammatory rheumatic diseases, named spondyloarthritis (SpA), that share pathogenic mechanisms and clinical features.^{2,3} These disorders also

Supported by the Ceschina Foundation and Sapienza University of Rome through “Progetti di Ateneo” and partially by Consiglio Nazionale delle Ricerche (project DBA.AD005.225-NUTRAGE-FOE2021).

¹Giorgia Paldino, PhD, Valentina Tedeschi, PhD, Valentina Proganò, MSc, Alexandru L. Bivolaru, MSc, Emanuele Molteni, MD, Rossana Scrivo, MD, PhD, Loretta Tuosto, PhD, Rosa Sorrentino, PhD, Maria Teresa Fiorillo, PhD: Sapienza University of Rome, Rome, Italy; ²Erica Salvati, PhD, Valerio Licursi, PhD, Eleonora Vertecchi, PhD: Institute of Molecular Biology and Pathology, National Research Council, Rome, Italy; ³Mattia Congia, MD, Alberto Cauli, MD, PhD: Azienda Ospedaliero-Universitaria di Cagliari, Cagliari, Italy; ⁴Rosalba Caccavale, MD, Marino Paroli, MD: Sapienza University of Rome Polo Pontino, Latina, Italy; ⁵Martina Kunkl, PhD: Sapienza University of Rome

and Scientific Institute for Research, Hospitalization and Healthcare Santa Lucia Foundation, Rome, Italy.

Drs Paldino and Tedeschi are co-first authors and contributed equally to this work.

All data relevant to the study are included in the article or uploaded as supplementary information. RNA sequencing data are available through the National Center for Biotechnology Information's Gene Expression Omnibus repository, under accession number GSE266295 (<https://www.ncbi.nlm.nih.gov/geo/query/acc.cgi?acc=GSE266295>).

Additional supplementary information cited in this article can be found online in the Supporting Information section (<http://onlinelibrary.wiley.com/doi/10.1002/art.43109>).

comprise psoriatic arthritis (PsA), arthritis associated with inflammatory bowel disease (IBD), reactive arthritis, and undifferentiated peripheral SpA.^{1,2}

R-axSpA primarily involves sacroiliac joints and spine; however, inflammation at the peripheral joints and extra-musculoskeletal manifestations (acute anterior uveitis, psoriasis, and IBD) may also occur.⁴ The strong association with the human leucocyte antigen (HLA)-B*27 and the endoplasmic reticulum associated aminopeptidases 1 and 2 genes supports a guilty involvement of (auto)antigen presentation to CD8+ T cells.^{5–7} Additionally, other genes related to CD8+ T cell development and functions (*TBX21*, *EOMES*, *RUNX3*, and *ZMIZ1*) were associated with r-axSpA susceptibility by genome-wide association studies.^{6,8} Recently, r-axSpA-associated CD8+ T cell clonotypes with public T cell receptors (TRBV9+) and cross-reactive to self and microbial HLA-B*27-restricted antigens were found expanded in the synovial and ocular fluids of patients with SpA.^{9,10} Importantly, selective antibody-targeted depletion of these expanded TRBV9+ CD8+ T cells has been proven successful in r-axSpA treatment.¹¹

However, mechanisms and anatomic sites where these CD8+ T cell clonotypes are activated are currently unknown.¹² It has been hypothesized that damage to dermal or mucosal barriers (as observed in psoriasis or IBD, respectively), along with the exposure of the immune system to microorganisms, may have a pathogenetic relevance.¹³ Accordingly, a gut-joint axis of inflammation in SpA has been recently proposed; however, the CD8+ T cell migration profile and the chemokines involved are little-known.^{14,15}

In addition, the physiological exposure during a lifetime to latent pathogens leads to persistent stimulation of CD8+ T cells that induces a premature immunosenescence.^{16,17} Nevertheless, the contribution of this event as a possible cause or effect in rheumatic immune-mediated inflammatory diseases remains unresolved.

In this study, we describe a subset of circulating CD8+ T cells enriched in patients with SpA compared with HDs and patients with rheumatoid arthritis (RA) with an intrinsic migratory capability independent of chemotactic stimuli. These cells exhibit an immunosenescent phenotype with telomere shortening, DNA damage response (DDR) activation, and telomere attrition, along with cytolytic and proinflammatory properties.

MATERIALS AND METHODS

Study participants. A total of 128 patients with r-axSpA, 60 patients with PsA, 74 patients with RA, and 79 age-matched healthy donors (HDs) were enrolled in this study (Table 1). Patients

with r-axSpA, PsA, and RA were classified according to standard criteria.^{18–20} Patients and controls were recruited at the Rheumatology Units of Sapienza University of Rome (Policlinico Umberto I, Roma, and ICOT Hospital, Latina) and the University of Cagliari (Azienda Ospedaliero-Universitaria, Cagliari). HLA-B*27 expression was checked both by serological analysis using ME1 monoclonal antibody (mAb) and by genomic analysis using Micro SSP Allele-specific HLA class I DNA typing tray B*27 (ONE LAMBDA, Thermo Fisher) according to the manufacturer's instructions. The study received approval by the Ethics Committees of Sapienza University of Rome (0018614/2019 and 6893/2022) and the University of Cagliari (PG/2018/16312). All participants provided written informed consent before enrollment.

Peripheral blood mononuclear cells separation and T cells isolation.

Peripheral blood mononuclear cells were isolated on density gradient Lympholyte solution (Cederlane Laboratories) from blood samples in sodium citrate within 24 hours from blood draw. CD8+ and CD4+ T lymphocytes were positively isolated by the respective isolation kits (Miltenyi Biotec). Each subset was resuspended at 10^6 cells/mL density in Roswell Park Memorial Institute Medium (RPMI) (Euroclone) supplemented with 5% fetal bovine serum (Biochrom), glutamine 2 mM (Euroclone), amphotericin B 2.5 µg/mL (Euroclone), and penicillin/streptomycin 100 U/mL/100 µg/mL (Euroclone). All experiments were performed after overnight culture.

Transwell migration assay. CD8+ or CD4+ T cells were resuspended at 1.5×10^5 cells in chemotaxis buffer (CB) (0.5% bovine serum albumin [BSA], 25 mM 4-(2-hydroxyethyl)-1-piperazine ethanesulfonic acid in RPMI) at room temperature (RT) and subjected to migration using 96-well transwell plates (Transwell, Corning) in the presence of the chemokine (CXCL9, CXCL10, and CXCL12 at 100 nM; CXCL11 and CCL20 at 300 nM) or in CB alone as control. Afterward, the plate was left at 37°C with 5% CO₂ for 90 minutes. A further condition (Input) was used to normalize the number of migrated cells as follows: $(1.5 \times 10^5 \times \text{number of migrated cells})/\text{number of Input cells}$. Then, migrated cells, non-migrated cells, and the Input were fixed in 1% weight/volume (w/v) paraformaldehyde/phosphate buffered saline (PBS) 1× and counted by FACSCalibur (Becton Dickinson) before the analysis by FlowJo software V.10.9.0 (Tree Star Inc).

CD8+ T cell immunophenotype. The immunoprofile of migrated and non-migrated CD8+ T cells was assessed after 20 seconds of incubation at 4°C with fluorochrome-conjugated antibodies (Supplementary Table 1). Cells were then washed in PBS 1× and fixed in 2% w/v paraformaldehyde/PBS 1× for

Author disclosures are available at <https://onlinelibrary.wiley.com/doi/10.1002/art.43109>.

Address correspondence via email to Maria Teresa Fiorillo, PhD, at mariateresa.fiorillo@uniroma1.it.

Submitted for publication May 15, 2024; accepted in revised form December 18, 2024.

Table 1. Characteristics of patients with radiographic r-axSpA, PsA, and RA, and HD enrolled in this study*

Patient characteristics	r-axSpA (n = 128)	PsA (n = 60)	RA (n = 74)	HD (n = 79)	r-axSpA vs HD, P value	PsA vs HD, P value	RA vs HD, P value
Age, mean \pm SD, y	50 \pm 14.1	55 \pm 14.0	56 \pm 13.6	51 \pm 15.0	ns	ns	ns
Disease duration, mean \pm SD, y	14.1 \pm 12.1	10.3 \pm 8.9	10.5 \pm 7.7	na	—	—	—
Sex ratio (% of men)	72	53	24	49	0.0011	ns	0.0014
HLA-B*27 (% positivity)	80	18	12	8	< 0.0001	ns	ns
BASDAI, mean \pm SD	3 \pm 2.4	na	na	na	—	—	—
ASDAS-CRP, mean \pm SD	2.1 \pm 1.1	nd	na	na	—	—	—
DAS28-CRP, mean \pm SD	na	na	3 \pm 1.3	na	—	—	—
DAPSA, mean \pm SD	na	11 \pm 9.9	na	na	—	—	—
CRP, mean \pm SD, mg/l	5 \pm 11.3	4 \pm 7.9	2 \pm 4.3	nd	—	—	—
ESR, mean \pm SD, mm/h	18 \pm 17.7	15 \pm 14.1	21 \pm 18.5	nd	—	—	—
bDMARDs, %	77	77	80	nd	—	—	—
NSAIDs, %	9	0	0	nd	—	—	—
csDMARDs, %	9	17	28	nd	—	—	—
None, %	10	7	4	nd	—	—	—
Glucocorticoids, %	2	5	8	nd	—	—	—
Other, %	2	2	3	nd	—	—	—

* P values were determined by Kruskal-Wallis test, except for sex ratio and HLA-B*27 positivity, where chi-square test has been applied; P values < 0.05 were considered significant. ASDAS-CRP, ankylosing spondylitis disease activity score with C-reactive protein, determined in 104 out 128 patients with r-axSpA; BASDAI, Bath Ankylosing Spondylitis Disease Activity Index; bDMARDs, biologic disease-modifying antirheumatic drugs (anti-TNF α , anti-IL17, anti-IL6 receptor agents); CRP, C-reactive protein; csDMARDs, conventional synthetic disease-modifying antirheumatic drugs; DAS28-CRP, disease activity score in 28 joints with C-reactive protein; DAPSA, disease activity in psoriatic arthritis; ESR, erythrocyte sedimentation rate; HD, healthy donor; HLA-B*27, human leucocyte antigen; IL, interleukin; na, not applicable; nd, not determined; none, not in therapy; ns, not significant; other, beta-blockers/angiotensin-converting enzyme; inhibitors/antidiabetics (several patients take more drugs simultaneously); NSAIDs, nonsteroidal anti-inflammatory drugs; PsA, psoriatic arthritis; RA, rheumatoid arthritis; r-axSpA, radiographic axial spondyloarthritis; TNF α , tumor necrosis factor alpha.

subsequent flow cytometry acquisition and analysis, as previously described.

Proinflammatory and cytolytic molecules production.

Migrated and non-migrated cells were treated with brefeldin A (10 μ g/mL) at 37°C for 16 hours. Cells were stained with anti-CD3 (Supplementary Table 1) for 20 seconds on ice, fixed with 4% paraformaldehyde for 20 seconds on ice, and permeabilized with 1% BSA/0.1% saponin/PBS 1 \times for 5 seconds at RT. Finally, cells were stained by anti-granzyme B, anti-perforin, anti-granulysin, and anti-tumor necrosis factor alpha (TNF α) mAbs (Supplementary Table 1). Cells fixed in 2% w/v paraformaldehyde/PBS 1 \times were then acquired with FACSCalibur and analyzed as previously described.

RNA isolation, RNA library construction, and RNA sequencing. RNA from the migrated and non-migrated CD8+ T cells of eight patients with r-axSpA was extracted by QIAGEN RNeasy Plus Micro Kit according to the manufacturer's instructions. Ovation SoLo RNA-seq Library Preparation kit (Tecan Genomics) was used for library preparation following the manufacturer's instructions. After quantification, RNA quality was tested by Agilent 2100 Bioanalyzer RNA assay (Agilent technologies) or Caliper (PerkinElmer). Final libraries were checked with Qubit 2.0 Fluorometer (Invitrogen) and Agilent Bioanalyzer DNA assay or Caliper (PerkinElmer). The libraries were sequenced on paired-end 150 bp mode on NovaSeq 6000 (Illumina). Detailed

information about RNA sequencing is provided in the Supplementary Materials.

Telomere length analysis. Genomic DNA from migrated and non-migrated cells was extracted by QIAGEN QIAamp DNA Micro Kit following the manufacturer's instructions. DNA was quantified by Nanodrop (ThermoScientific) and used for telomere length analysis. The telomeric ends repeat and the single copy gene β -globin were measured by quantitative reverse transcriptase–polymerase chain reaction (RT-PCR). RT-PCR details are reported in the Supplementary Materials.

Fluorescence in situ hybridization and immunofluorescence. Migrated and non-migrated CD8+ T cells were plated on poly-L-lysine coated coverslips. Cells were then fixed (2% formaldehyde), permeabilized (0.1% triton X-100/PBS 1X), and blocked in 5% BSA/PBS 1 \times . Samples were incubated with an anti-phosphohistone H2AX antibody (Supplementary Table 1) and then with anti-mouse IgG Alexa fluor 488 conjugate secondary antibody (Cell Signaling). Samples were then refixed in 2% formaldehyde, dehydrated with ethanol series, air-dried and co-denatured for three seconds at 80°C with a Cy3-labeled peptide nucleic acid probe, telomere sequence specific (TelC-Cy3, Panagene), and incubated for two hours in a humidified chamber at RT in the dark. After hybridization, coverslips were washed with 70% formamide, 10 mM Tris-HCl pH 7.2, BSA 0.1%, and then in Tris buffered saline–Tween 0.08%,

dehydrated with ethanol series, counterstained with 4',6-diamidino-2-phenylindole (DAPI) (0.5 µg/mL, Sigma-Aldrich), and mounted on specimen slides in mounting medium (Gelvatol Moviol, Sigma-Aldrich). Fluorescence signals were acquired by a Nikon Crest Spinning disk at 60× magnification. Z-stacks were acquired at 0.6 µm steps and then processed with a Nikon imaging software. For lamin B1 detection, fixed and permeabilized cells were incubated with anti-lamin B1 antibody (Supplementary Table 1) and then with an anti-rabbit IgG Alexa fluor 555, counterstained with DAPI and mounted as previously described. Fluorescence signals were acquired as previously described. Nuclear circularity and area were calculated by ImageJ software.

Statistical analysis. Differences among the cohorts were evaluated by the Kruskal-Wallis test, with Dunn's correction for multiple comparisons, whereas comparison within the same group was done by Wilcoxon test. The comparison between the number of migrated CD8+ and CD4+ T lymphocytes, circularity index (CI), and nuclear area of non-migrated versus migrated CD8+ T cells were performed by the Mann-Whitney test. Correlation between age and telomere length (T/S ratio) was evaluated by simple linear regression analysis. Statistical significance was accepted for *P* values less than 0.05. Results were analyzed using Prism software V.8.0 (GraphPad). RNA-seq analysis was performed using R v.4.3.1. Differentially expressed genes (DEGs) were assessed by comparing migrated with non-migrated CD8+ T cells using a Wald test and a false discovery rate (FDR) under the 0.05 threshold²¹ by applying an independent data filtering based on the mean of normalized counts for each gene and optimizing the number of genes having an adjusted *P* value (FDR) of less than 0.05. R packages ggplot2 v.3.5.0 and Complex Heatmap v.2.16.0 were used to generate volcano plot and heatmaps, respectively.

RESULTS

CD8+ but not CD4+ T cells in patients with SpA exhibit high migration in the absence of chemokine stimuli. Chronic inflammatory conditions in SpA are sustained by continuous trafficking and recruitment of immune cells at target sites. Although a role for CD8+ T lymphocytes in SpA pathogenesis has not been fully clarified, recent findings have relaunched their involvement.^{8–11} Herein, we asked whether an altered CD8+ T migratory pattern might occur in SpA by testing the chemotactic properties of peripheral CD8+ T lymphocytes from patients with r-axSpA and PsA, who both belong to the SpA cluster, compared with age-matched HD. Moreover, to deepen the chronic inflammation impact on the migratory pattern, in a cohort of patients with RA, a rheumatic SpA-unrelated, chronic inflammatory disease was also analyzed. The migration was assessed by transwell assays toward the proinflammatory chemokines

CXCL9, CXCL10, and CXCL11, which bind the CXC chemokine receptor 3²² (Figure 1A–C), or toward the homeostatic chemokine CXCL12, a ligand of CXCR4²³ (Figure 1D). Additionally, the CCL20-CCR6 axis (Figure 1E) was evaluated given its involvement in T cell recruitment to gut mucosa and skin.²⁴

CD8+ T cells from all cohorts properly migrated upon chemokine induction. Those from patients with SpA and RA exhibited a significantly higher response to CXCL9 compared with HD (Figure 1A), whereas the four cohorts showed a comparable chemotaxis to CXCL10, CXCL11, and CXCL12 (Figure 1B–D). Migration in response to CCL20 was generally low, especially in the cohort with RA compared with HD (Figure 1E). However, the observed differences seem to not be related to an altered expression of the cognate receptors (Supplementary Figure 1A–E).

Intriguingly, CD8+ T cells from patients with SpA disclosed an intrinsic higher motility in the absence of chemotactic stimuli when compared with HD and patients with RA (Figure 1A–E). To exclude a biased effect of the small cohorts analyzed, the sample size was increased up to 128 patients with r-axSpA, 60 with PsA, 74 with RA, and 79 HD (Figure 1F). Our data confirmed a higher spontaneous migration of CD8+ T cells in patients with SpA (both HLA-B*27-positive and -negative carriers) (Supplementary Figure 2) versus HDs (mean ± SD for patients with r-axSpA 3,638 ± 518.6; PsA 4,296 ± 574.5; and HD 1,572 ± 137.9). Although less pronounced, this finding extended to patients with RA (mean ± SD 2,575 ± 249.9), which suggests that a chronic inflammatory state could influence the basal motility of CD8+ T cells. We asked whether drug treatment could affect spontaneous migration. Notably, no significant differences of CD8+ T cell basal motility were found in untreated versus biologic disease-modifying antirheumatic drug (bDMARD)-treated patients within cohorts of SpA (r-axSpA and PsA) and RA (Supplementary Figure 3).

To verify whether the migration detected by transwell assay was affected by the cellular ability to deform while crossing the membrane pores or by a nuclear size decrease, the nuclear shape and dimension were evaluated. Hence, migrated and non-migrated CD8+ T cells from seven patients with r-axSpA, PsA, and RA, and HD were stained with anti-lamin B1 mAb and DAPI and analyzed for both nuclear CI and area. Two representative cell types of high (left panels) and low (right panels) nuclear CI are reported (Figure 1G). The nuclear CI was lower in migrated versus non-migrated CD8+ T cells in all cohorts (Figure 1H), which suggests that migration is indeed affected by nuclear deformability. Contrarily, the nuclear area was larger in migrated versus non-migrated CD8+ T cells from r-axSpA, unchanged in cells from PsA and RA cohorts, and reduced in migrated cells from HD (Figure 1I). These findings suggested that, in HDs, cell migration could be favored by a reduced nuclear size, whereas the higher migratory profile in patient cohorts mainly relied on nuclear deformability.

Given the involvement of CD4+ T cells in SpA,²⁵ we concurrently assessed the basal motility of CD4+ and CD8+ T cells from patients (60 patients with r-axSpA, 41 with PsA, 40 with RA) and

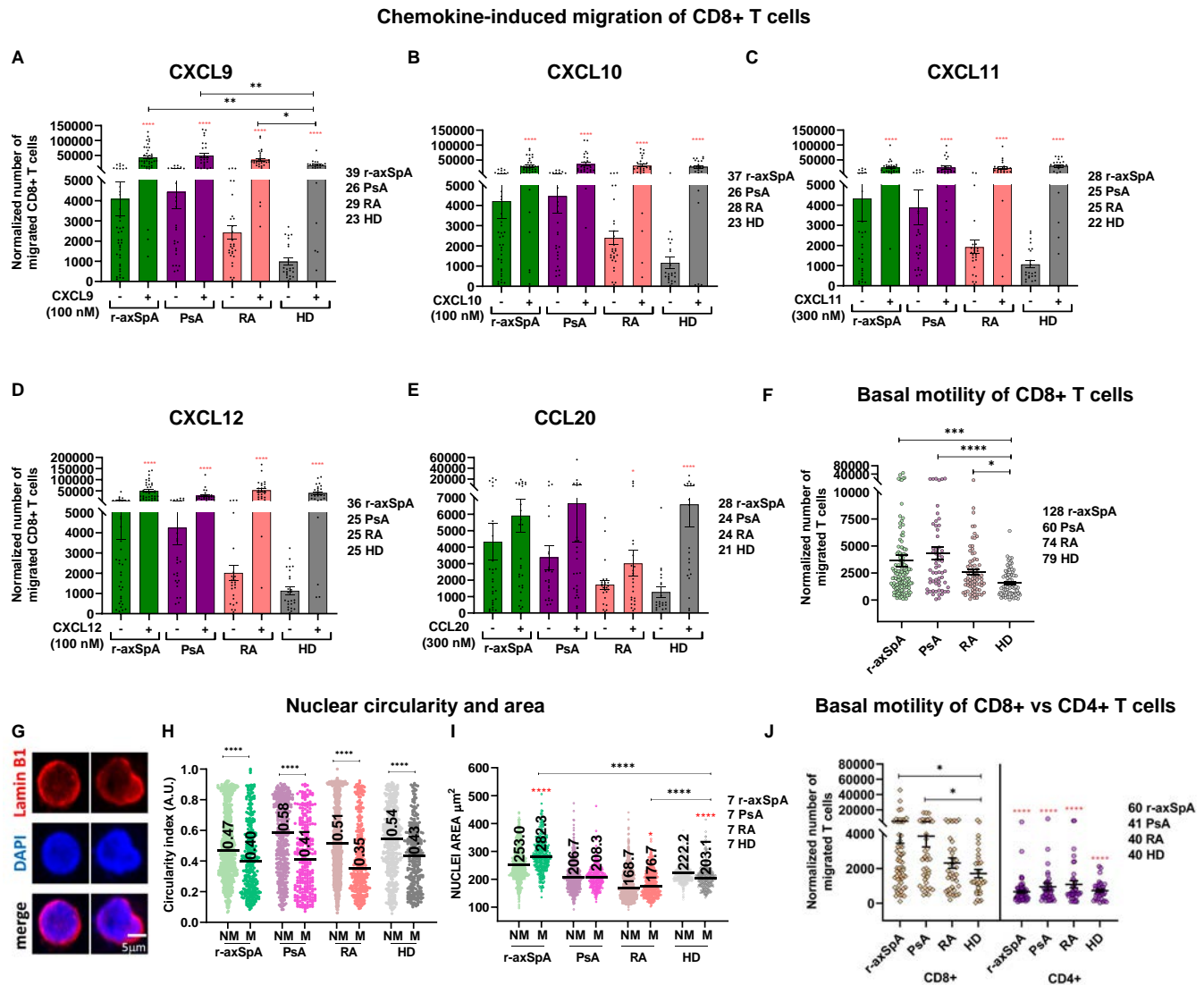


Figure 1. CD8+ but not CD4+ T cells in patients with SpA possess an intrinsic higher motility compared with HD. (A–E) CD8+ T cell migration ability toward the indicated chemokines is shown. (F) The number of cells spontaneously migrating is higher in patients with immune-mediated diseases, especially those with SpA, than in HD. Red asterisks, Wilcoxon test for analysis within the same cohort; * P value < 0.05; **** P value < 0.0001; black asterisks, Kruskal-Wallis test for differences among cohorts; * P value < 0.05; ** P value < 0.01; *** P value < 0.001; **** P value < 0.0001. (G) Upper and middle panels show the nuclear shape of migrated CD8+ T cells stained by anti-lamin B1 mAb and DAPI, respectively; merge is shown in the bottom panel. Left and right panels are representative of cells with high and low CI, respectively. (H) The migrated cells from all cohorts exhibited a lower CI, whereas the nuclear area (I) is larger in migrated versus non-migrated cells of all patients whereas the opposite is found in HD. (J) Comparison of spontaneous migration in CD8+ (on the left) and CD4+ T cells (on the right) of patients and HD. Mann–Whitney test **** P value < 0.0001. The difference in the motility of CD8+ and CD4+ T among the cohorts was analyzed by the Kruskal-Wallis test, * P value < 0.05. Mean \pm SEM in (A–F) and (J) and median in (H) and (I) are reported. A.U., arbitrary units; CI, circularity index; HD, healthy donor; M, migrated CD8+ T cells; mAb, monoclonal antibody; NM, non-migrated; PsA, psoriatic arthritis; RA, rheumatoid arthritis; r-axSpA, radiographic axial spondyloarthritis; SpA, spondyloarthritis.

40 HDs. Within all cohorts, CD8+ T cells displayed a higher intrinsic motility compared with the CD4+ counterpart (Figure 1J). Overall, these observations might suggest that the inflammatory state, caused by both disease and/or aging (mean \pm SD for age: 50 ± 14.1 in r-axSpA; 55 ± 14.0 in PsA; 56 ± 13.6 in RA; and 51 ± 15.0 in HD), has a stronger impact on the basal migratory capabilities of CD8+ than CD4+ T cells.

Transcriptional profiling of spontaneously motile CD8+ T cells. To highlight DEGs correlated to the high intrinsic motility observed in CD8+ T cells of patients with SpA, transcriptomic analysis of migrated versus non-migrated cells was performed (Supplementary Table 2 at accession number GSE266295 and Figure 2). RNA samples were collected from non-migrated and migrated CD8+ T cells from eight patients with

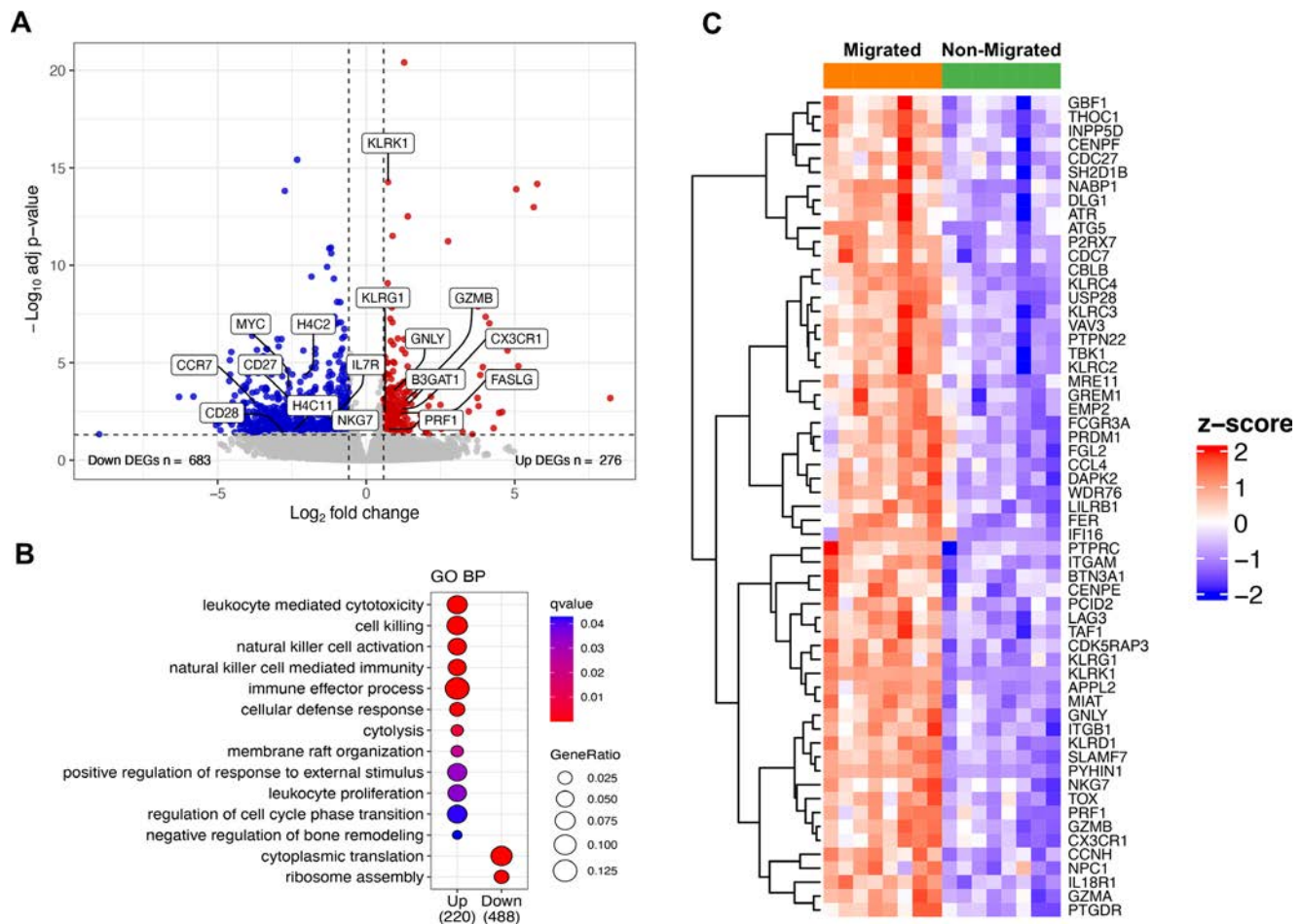


Figure 2. Transcriptome analysis of non-migrated versus migrated CD8+ T cells. (A) Volcano plot showing the distribution of \log_{10} (adjusted P values) values (y-axis) relative to \log_2 (fold changes) values (x-axis) resulting from the comparison of gene expression levels in migrated versus non-migrated CD8+ T cells of eight patients with r-axSpA. Red dots indicate up-regulated DEGs associated with FDR < 0.05 and FC > 1.5 and blue dots indicate DEGs with FDR < 0.05 and FC < -1.5. Selected DEGs are highlighted in the plot. The number of up- and down-regulated genes is reported. (B) Dot plot showing the GO terms enriched in the up-regulated (left) and the down-regulated (right) DEGs. The size of the dots is based on the ratio between the gene number belonging to a GO BP category and the total number of up- or down-regulated genes. The color of the dots shows the q value associated with each term. (C) Heatmap showing row z-score scaled gene expression levels of DEGs belonging to the up-regulated GO BP enriched categories. Genes were hierarchically clustered using Euclidean distances. BP, biological process; DEG, differentially expressed gene; FC, Foldchange; FDR, false discovery rate; GO, gene ontology; r-axSpA, radiographic axial spondyloarthritis.

r-axSpA. Overall, 276 protein coding genes were up-regulated and 683 genes were down-regulated in migrated versus non-migrated CD8+ T cells (FDR < 0.05; foldchange [FC] > 1.5) (Figure 2A). Interestingly, gene ontology (GO) analysis (Figure 2B) highlighted several enriched biologic processes (BPs) in migrated CD8+ T cells pointing out a cytolytic signature and natural killer (NK) features (Figure 2B and C). Indeed, many up-regulated transcripts were related to the activation and cell killing activity shared by NK and CD8+ T cells (*SLAMF7*, *PRDM1*, *PTPRC*, *NKG7*, *SH2D1B*, *IL18R1*, *PTPN22*, *TOX*, *FCGR3A*, *EMP2*, *P2RX7*, *CX3CR1*, *GZMA*, *GZMB*, *GNLY*, *PRF1*, *ITGB1*, *INPP5D*) and others to NK receptors (*KLRD1*, *KLRC4*, *KLRC2*, *KLRC3*, *KLRK1*, *LILRB1*) (Figure 2C). In addition, the down-modulation of GO BPs related to cytoplasmic translation and ribosome assembly (Figure 2B and Supplementary Table 2) and the up-regulation of classical

senescence and exhaustion-related genes (*KLRG1*, *B3GAT1*, *LAG3*) (Figure 2C) suggested that the migrated subset could be less metabolically active and features a terminally differentiated/senescent T cell compartment.

Spontaneously migrating CD8+ T cells possess a terminally differentiated/senescent-like phenotype.

To validate the observations from transcriptomics, naive/memory and senescent profiles of non-migrated versus spontaneously migrated CD8+ T cells were analyzed by flow cytometry (Figure 3 and Supplementary Figure 4). CCR7 and CD45RA expression (Figure 3A) allows for the distinction of four CD8+ T cell subsets: naive (CCR7+CD45RA+), central memory (CCR7+CD45RA-), effector memory (CCR7-CD45RA-), and effector memory cells re-expressing CD45RA (TEMRA) (CCR7

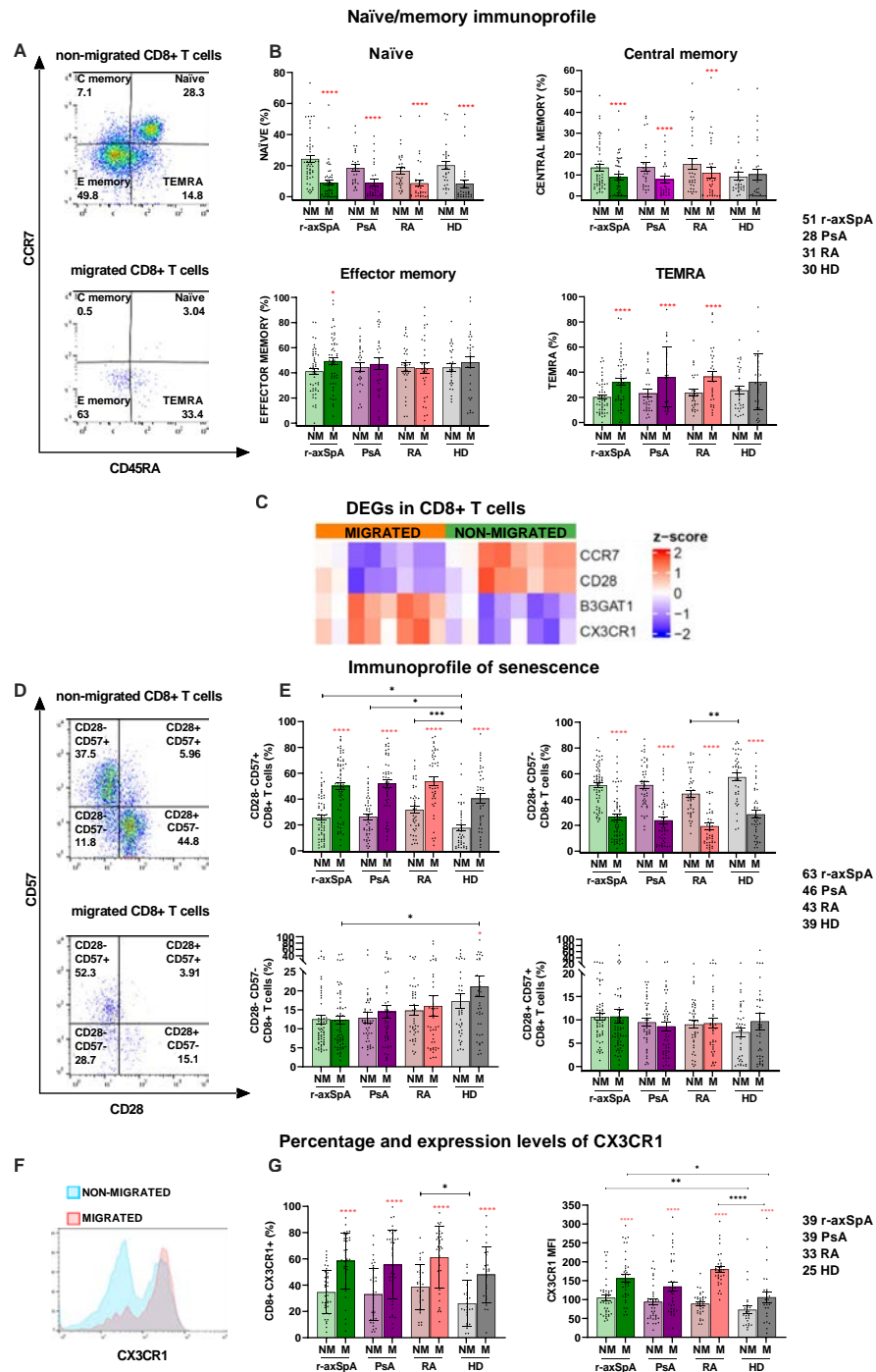


Figure 3. Spontaneously migrating CD8⁺ T cells are enriched in terminally differentiated/senescent cells. (A) Representative flow cytometry plots of naïve/memory composition in non-migrated versus migrated CD8⁺ T cells. (B) After basal migration there was a decrease of CD8⁺ T naïve and central memory cells; the former was in all cohorts and the latter was only in patients, with a parallel enrichment of effector memory cells in the migrated fraction of patients with r-axSpA and TEMRA subset in migrated cells of all patients but not in HD. (C) Heatmap of relevant DEGs (FC > 1.5; FDR < 0.05) in migrated versus non-migrated CD8⁺ T cells (r-axSpA, n = 8). (D) and (E) The analysis of senescence status, which was more pronounced in migrated cells compared with non-migrated ones, as reported in the representative plot (D), has been done by CD28 and CD57 staining. (F) Representative plot showing overlapped CX3CR1 expression in migrated (red line) and non-migrated (blue line) CD8⁺ T cells. (G) The CX3CR1 amount, expressed as percentage and MFI, increased after the migration in the absence of stimuli within all cohorts. Red asterisks; Wilcoxon test pre- and post-migration within the same cohort, *P value < 0.05; ***P value < 0.001; ****P value < 0.0001; black asterisks; Kruskal-Wallis test for the comparison among the four cohorts, *P value < 0.05; **P value < 0.01; ***P value < 0.001. Mean ± SEM is reported in B, E, and G. DEG, differentially expressed gene; FC, Foldchange; FDR, false discovery rate; HD, healthy donor; NM, non-migrated; M, migrated CD8⁺ T cells; MFI, mean level per cell; PsA, psoriatic arthritis; RA, rheumatoid arthritis; r-axSpA, radiographic axial spondyloarthritis.

–CD45RA+). No difference was found among the four cohorts in terms of naive/memory composition either in migrated or non-migrated cells (Figure 3B). Conversely, the frequencies of each subset before and after migration showed the lowering of naive cells in the migrated CD8+ T cell pool from all cohorts (Figure 3B). This was consistent with the CCR7 down-modulation observed in the migrated fraction by RNA-seq analysis (Figure 3C). The same trend was shown by the central memory subset that decreased in migrated CD8+ T cells of all cohorts except HDs (Figure 3B). Additionally, an enrichment of effector memory cells in migrated CD8+ T cells from patients with r-axSpA (Figure 3B) and of TEMRA in the migrated cells from all patients was observed, but not in HDs (Figure 3B).

For the immunosenescent profile, CD28 and CD57 were detected that allowed for the identification of four activation/senescence levels: nonactivated/early-activated CD28+CD57–, activated CD28+CD57+, activated/early-senescent CD28–CD57–, and terminally differentiated-senescent-like CD28–CD57+ T cells (Figure 3D). Consistent with the enrichment of effector memory and TEMRA cells found upon cell migration, an increased percentage of CD28–CD57+ T cells in migrated versus non-migrated cells was observed (Figure 3E). Accordingly, RNA-seq analysis showed CD28 down-modulation and CD57 up-regulation in migrated versus non-migrated CD8+ T cells from patients with r-axSpA who were analyzed (Figure 3C). Interestingly, terminally differentiated-senescent-like CD28–CD57+ T cells were more abundant in non-migrated CD8+ T cells from all patients compared with HDs (Figure 3E). This enrichment was also found before migration in patients with SpA compared with HDs (Supplementary Figure 5). Of note, patients with RA showed a lower occurrence of nonactivated/early-activated CD28+CD57– T subset in non-migrated cells compared with HD (Figure 3E). Additionally, CD28–CD57– cells were found enriched exclusively in migrated cells from HD and more abundant compared with patients with r-axSpA (Figure 3E). No significant differences were observed for CD28+CD57+ cells (Figure 3E). Notably, the comparison of spontaneously migrated versus chemokine-treated cells in patients with SpA showed a higher percentage of TEMRA and senescent cells in the former pool (Supplementary Figure 6). A low percentage of CD8+ T cells expressed PD1, a T cell exhaustion marker, without differences between migrated and non-migrated pools, as anticipated by transcriptomic data (Supplementary Figure 7).

Furthermore, the expression of CX3CR1, a marker of CD8+ T cell differentiation state, highly expressed by long-lived CD8+ T effector memory cells with cytolytic properties,^{26–28} was evaluated after migration (Figure 3F and G). Consistently with RNA-seq data, we found a higher CD8+CX3CR1+ T cell percentage in the migrated pool from all cohorts (Figure 3C, F, and G). Notably, the CD8+CX3CR1+ percentage was higher in non-migrated cells from patients with RA than in HDs (Figure 3G).

These data positively correlated with age of patients, which suggests that physiologic aging with chronic inflammation strongly affect the CD8+ T cell differentiation state. Accordingly, CX3CR1 amount, measured through the mean fluorescence intensity (MFI), was higher in migrated cells from all groups compared with non-migrated cells (Figure 3G). Interestingly, both non-migrated and migrated CD8+ T cells from patients with r-axSpA and migrated cells from patients with RA showed higher CX3CR1 MFI than HD (Figure 3G). Altogether, these data link the higher spontaneous migration with a terminally differentiated/senescent T cell status.

Spontaneously migrating CD8+ T cells exhibit increased cytolytic and proinflammatory functions.

Afterward, we asked whether data from RNA-seq analysis could be confirmed at protein level and translated into functional properties. The production of cytolytic molecules, such as granzyme B, perforin, and granulysin, which have genes that are up-regulated from transcriptomics (Figure 4A–D and Supplementary Figure 8), was then evaluated. Additionally, the TNF α secretion was also assessed (Figure 4D and Supplementary Figure 8); however, its transcript was not among DEGs discriminating non-migrated from migrated cells (Supplementary Table 2) because it represents one major senescence-associated secretory phenotype component and a crucial therapeutic target in SpA. Consistently, granzyme B production was higher in migrated versus non-migrated cells (Figure 4B) in all cohorts, whereas the frequency of perforin-secreting CD8+ T cells increased on migration only in patients with SpA (Figure 4C). Moreover, an increase of granulysin (Figure 4D) and TNF α production (Figure 4E) was observed in migrated versus non-migrated cells both in patients and HDs with no significant differences among the cohorts. Overall, these data indicate that, even without stimulation, the basally migrating CD8+ T cell fraction was capable of producing a higher amount of proteins with cell killing and proinflammatory potential.

Senescent spontaneously migrating CD8+ T cells display shorter and damaged telomeres especially in patients with SpA.

Recent studies highlighted the occurrence of premature T cell senescence in axial SpA and patients with RA, but the underlying mechanisms and the contribution to inflammation at target tissues have not been elucidated as of yet.^{17,29–31} Herein, we evaluated the telomere length in migrated versus non-migrated CD8+ T cells from 24 patients with r-axSpA, 24 with PsA, 24 with RA, and 24 HDs. Figure 5A reports the length of telomeres as a T/S ratio that indicates the number of copies of telomere repeats (T) compared with a single copy control gene (S; β -globin). In line with the senescence state detected by flow cytometry (Figure 3), the migrated CD8+ T cells were characterized by shorter telomeres compared with the

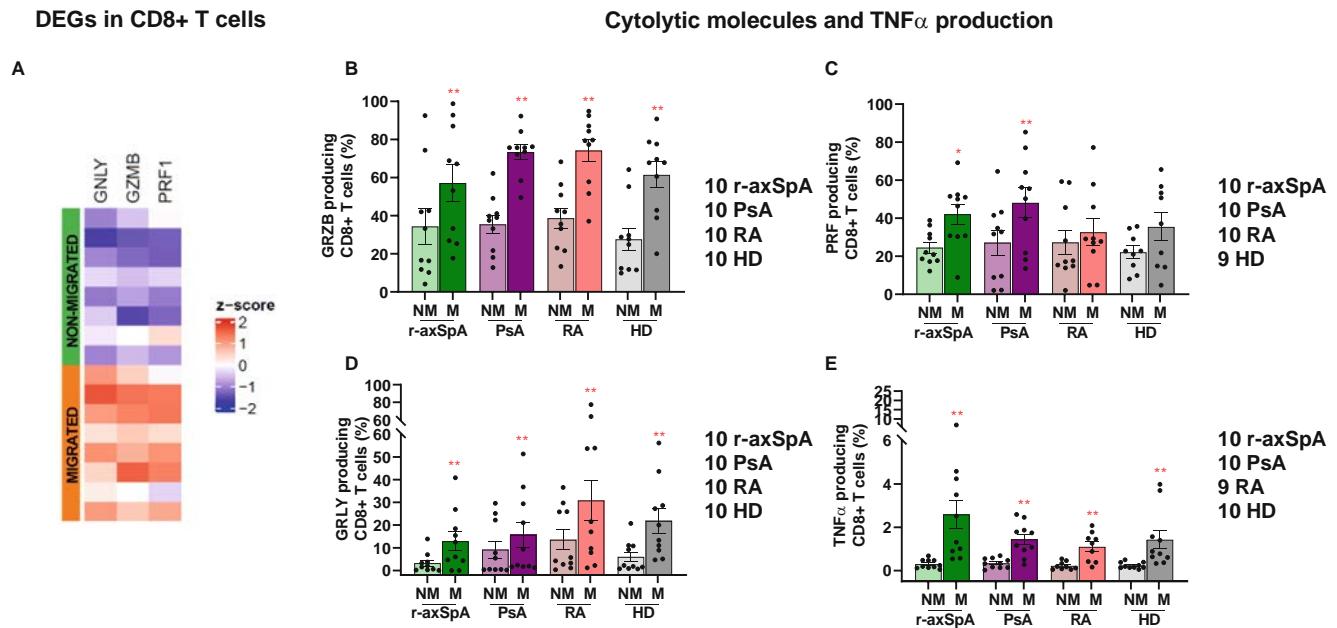


Figure 4. Senescent spontaneously migrating CD8+ T cells exhibit increased cytolytic and proinflammatory functions. (A) Heatmap of up-regulated genes involved in cytolytic functions in migrated versus non-migrated CD8+ T cells (FC > 1.5; FDR < 0.05) of the eight patients with r-axSpA. (B–E). Migrated cells exhibited higher production of granzyme B (B), granulysin (D), and TNF α (E) in all cohorts, whereas a significant increase of perforin production (C) was detected only in migrated cells of patients with SpA; (red asterisks; Wilcoxon test before and after the migration within the same cohort of individuals, **** P value < 0.0001; ** P value < 0.01; * P value < 0.05); (Kruskal-Wallis test for the comparison among the four cohorts, P value ns). Mean \pm SEM is reported. DEG, differentially expressed gene; FC, Foldchange; FDR, false discovery rate; GRLY, granulysin; GRZB, granzyme B; HD, healthy donor; M, migrated CD8+ T cells; NM, non-migrated; ns, not significant; PRF, perforin; PsA, psoriatic arthritis; RA, rheumatoid arthritis; r-axSpA, radiographic axial spondyloarthritis; SpA, spondyloarthritis; TNF α , tumor necrosis factor alpha.

non-migrated counterpart in all groups. The telomere shortening displayed a trend of positive correlation with the age in migrated and non-migrated cells that reached a statistical significance in non-migrated CD8+ T cells from patients with r-axSpA and patients with PsA (Figure 5B).

Data from telomere length measurement (Figure 5A) raised the question of whether shortened telomeres found in spontaneously migrating CD8+ T cells were still able to maintain capping structures that prevent DDR activation and telomere dysfunction (TD). Therefore, the expression of the phosphorylated form of γ -H2AX, a DDR marker, was analyzed in migrated versus non-migrated CD8+ T cells from 14 patients with r-axSpA, 14 with PsA, 14 with RA, and 13 HDs. In parallel, to assess if DDR activation was due to telomere attrition, we analyzed the percentage of cells displaying telomeric signals and γ -H2AX colocalization by immunofluorescence-fluorescence in situ hybridization (IF-FISH) experiments. In all cohorts, a higher percentage of DDR and TD positive cells was detected in migrated cells (Figure 5C–F). Accordingly, the TD number estimation per nucleus revealed an increase of the TD average number in migrated versus non-migrated CD8+ T cells in all cohorts (Figure 5F). More importantly, among the migrated cells, only CD8+ T cells from patients with r-axSpA displayed a significant increase in the TD number compared with HDs (Figure 5F). Overall, these results correlate the spontaneous

migration of CD8+ T cells with an advanced senescent state characterized by telomere shortening, DDR activation, and TD, which was more pronounced in migrated CD8+ T cells from patients with r-axSpA.

DISCUSSION

In this study, we describe a subpopulation of peripheral CD8+ T cells significantly increased in patients of the SpA cluster (r-axSpA and PsA) (Figure 1) that spontaneously migrates regardless of specific chemokine gradients. Notably, this CD8+ T cell subset shows a senescent/terminally differentiated immunoprofile, DDR activation, telomere shortening, and dysfunction and retains cytotoxic and proinflammatory functions (Figures 2–5) and is also detectable with lower frequency in patients with RA and elderly HD participants (mean \pm SD age: 51 \pm 15). Thus, it is conceivable to speculate that these intrinsically “hypermotile” CD8+ T cells could be a byproduct of the inflammaging, which is the basal state of inflammation naturally increasing during aging, and, more importantly, in immune-mediated disorders.

Many studies linked the chronic inflammation associated with rheumatic and other disorders to alterations of the telomere/telomerase system through molecular mechanisms that are still unclear.^{31,32} Yet, nuclear factor kappa B (NF- κ B), a key regulator of inflammation, may induce changes in the telomere

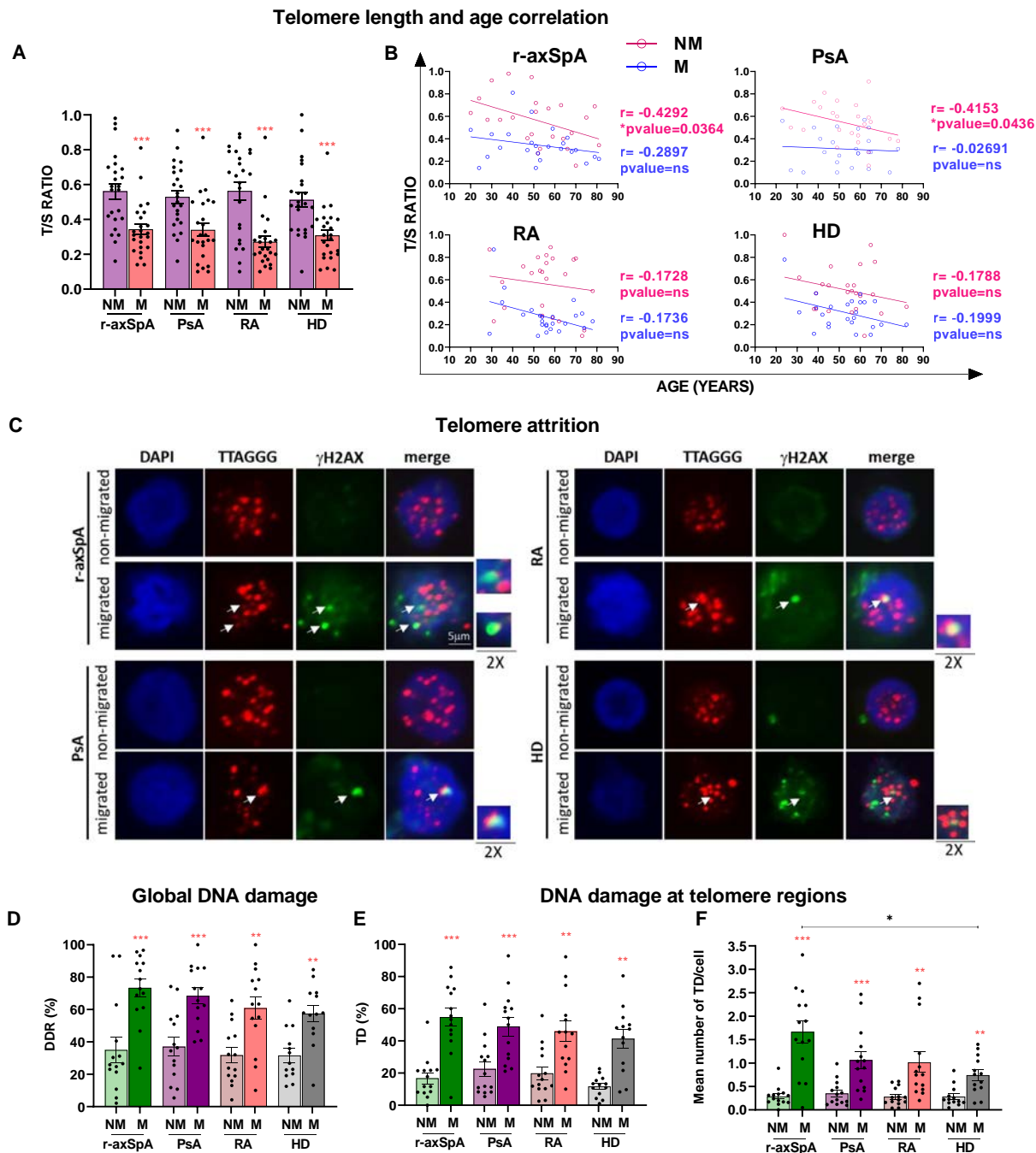


Figure 5. Higher TD in migrated versus non-migrated CD8+ T cells. (A) The analysis of telomere length, expressed as T/S ratio, in non-migrated and migrated CD8+ T cells (r-axSpA, $n = 24$; PsA, $n = 24$; RA, $n = 24$; HD, $n = 24$) showed a shortening in the latter groups in all cohorts. (B) Negative trend of correlation of telomere length with the age both in migrated and non-migrated cells (Spearman r correlation, * P value < 0.05). Cohorts were age-matched (the mean \pm SD age was 52 ± 17.2 in r-axSpA; 53.5 ± 14.6 in PsA; 55.3 ± 13.2 in RA, and 53.4 ± 13.6 in HD). (C) Each panel shows IF-FISH analysis of non-migrated and migrated CD8+ T cells in 1 representative out of 14 patients with r-axSpA, 14 with PsA, 14 with RA, and 13 HD. The merge highlights the DNA damage in the telomeric regions (TD). (D) and (E) panels show the percentage of DNA damage in the whole DNA (% DDR) (D) and in the telomeric regions (% TD) (E), respectively. (F) The telomere dysfunction, expressed in terms of mean number of TD per cell, is reported. Red asterisks, Wilcoxon test before and after the migration within the same cohort of individuals, ** P value < 0.01 ; *** P value < 0.001 ; **** P value < 0.0001 ; black asterisks, Kruskal-Wallis test for the comparison among the four cohorts, * P value < 0.05 . Mean \pm SEM is reported in (A) and (D–F). DDR, DNA damage response; HD, healthy donor; IF-FISH, immunofluorescence-fluorescence in situ hybridization; NM, non-migrated; M, migrated CD8+ T cells; PsA, psoriatic arthritis; RA, rheumatoid arthritis; r-axSpA, radiographic axial spondyloarthritis; TD, telomere dysfunction.

length and telomerase activity through the regulation of several telomere components.³² Moreover, TNF α and p38 MAPK signaling pathways can induce telomere shortening either through direct NF- κ B activation or by promoting the release of activating transcription factor 7 (ATF7) and telomerase from telomeres on ATF7 phosphorylation by p38.³³

A cross-sectional study reported a significantly longer telomere length in PBMCs from patients with r-axSpA, PsA, and RA than in HDs.³⁴ Later on, the same authors described a PBMC telomere length decay more accelerated in patients with PsA than in patients with r-axSpA.³⁵ This finding was attributed to different PBMC telomere physiology dynamics influenced by turnover rate and oxidative stress-induced telomere damage between the two forms of SpA.

In axial SpA, a premature CD8+ and CD4+ T cell senescence was documented in patients younger than 35 years who presented inappropriate telomere shortening, shrinkage of thymic output, and altered telomerase activity; however, the question remains as to whether these alterations precede or follow the clinical disease onset.¹⁷ Our data do not show telomere length differences between patients and controls, neither comparing the spontaneously migrating CD8+ T cells nor the bulky non-migrating cells (Figure 5A). Instead, we find shorter telomeres in migrated compared with non-migrated cells in all groups and a general trend of inverse correlation between telomere length and age that reached statistical significance in the non-migrated but not in the migrated CD8+ T cell pool from patients with SpA. This suggests that other factors besides the age impact the telomere status in the latter (Figure 5A and B).

Interestingly, spontaneously migrating CD8+ T cells from all cohorts exhibited a more pronounced DDR activation and a higher number of telomeric damage foci/cell that outlines a senescence phenotype (Figure 5C–F). In particular, the highest DDR and telomere attrition were found in migrating CD8+ T cells from patients with SpA that also displayed the highest rate of motility (Figures 1 and 5C–F). Notably, the nuclear circularity analysis revealed a certain deformity due to a nonuniform lamin B1 distribution at the nuclear periphery in migrating versus non-migrating CD8+ T cells in all cohorts (Figure 1G and H).

Recently, it has been shown that lamin isoforms bind the linker of nucleoskeleton and cytoskeleton complex and their loss softens the cell nucleus and enhances constricted cell migration that contributes to migration-induced DNA damage.³⁶ Lamin B1 has been implicated in inflammation, cellular senescence, age-associated organ dysfunctions, and human disorders.³⁷ Moreover, growing evidence reports a direct interaction between telomere components and lamins that suggests a possible link between telomere attrition/dysfunction and nuclear architecture.³⁸ Although in migrating CD8+ T cells lamin B1 gene is not modulated, its uneven distribution could alter the stoichiometric assembly of the nuclear lamina inducing alterations of cell mechano-sensitivity and motility.³⁹

Our data revealed a terminally differentiated and senescent profile of CD8+ T cells endowed with intrinsic motion (Figures 2 and 3). Importantly, an increase of TEMRA subset and a decrease of central memory subset was found in the pool of migrated CD8+ T cells from all patients, but not from HD (Figure 3A–C). These immunophenotypic differences suggest that the spontaneously migrated fraction from patients might be enriched in cells chronically stimulated by self and/or microbial antigens from persistent viruses or altered microbiota.^{16,40–42} However, an intestinal origin of these spontaneously migrating CD8+ T cells is not supported by RNA-seq data because α_4 (ITGA4) and β_7 (ITGB7) integrin genes are not up-regulated (data not shown).¹⁷ In patients with r-axSpA, an expansion of circulating cytotoxic CD8+CD28– T cells has been documented and their percentage correlated with the disease status but not with the age.⁴³ A strong enrichment of CD8+CD28–CD57+ T cells, classically defined as terminally differentiated-senescent-like cells, was found in the migrated pool from all cohorts (Figure 3C–E). Remarkably, the percentage of such cells was already higher in the bulky non-migrated cells of patients compared with HDs (Figure 3E), which supports a role for chronic inflammation in accelerating T cell immunosenescence.^{30,44} In addition, the up-regulation of genes implicated in cytotoxic functions and NK-like trait (Figure 2) and the production of cytolytic and proinflammatory proteins (Figure 4) in spontaneously migrated CD8+ T cells delineated a cytotoxic profile. Accordingly, recent single cell cellular indexing of transcriptomes and epitopes by sequencing (CITE-seq) data showed that a hallmark of peripheral effector memory CD8+ T cells in patients with r-axSpA is the overexpression of cytotoxicity-related genes, including GZMH, GZMB, and NKG7.⁴⁵

Our data also evidence a significantly higher expression of the fractalkine receptor, CX3CR1, in spontaneously migrating compared with nonmigrating CD8+ T cells (Figure 3F and G). CX3CR1 graded transcript levels have been proven to reflect the CD8+ T cell differentiation continuum with higher expression levels correlated to stronger cytotoxicity.^{26–28} Recently, a circulating CD8+CCR4+ subpopulation displaying up-regulation of genes promoting osteogenesis has been described in patients with r-axSpA with active disease.⁴⁶ Consistently with our data, those CD8+CCR4+ cells expressing CX3CR1 exhibited an enhanced cytotoxicity. Integrated meta-analyses of gene expression profiles identified CX3CR1 as a marker for rheumatic diseases.⁴⁷ Additionally, a study to develop a predictive disease risk model for r-axSpA acknowledged CX3CR1 as a potential biomarker for early disease diagnosis and progression.⁴⁸

A mechanistic explanation linking CD8+ T cell spontaneous motility with the senescent/cytotoxic phenotype is still lacking. In line with the observed functional phenotype, transcriptomic analysis highlighted in migrated CD8+ T cells, several key genes involved in cell motility, cytoskeleton organization, DNA damage, and telomere stress-induced senescence, but they were not implicated in GO BPs significantly enriched (Figure 2B and

Supplementary Table 2). In patients with RA, Li et al associated premature aging of CD4+ T cells showing a hypermotile, tissue-invasive, and highly arthritogenic in vivo phenotype with a defective expression of the DNA double strand break repair nuclease MRE11A.²⁹ In our study, migrated CD8+ T cells from patients with r-axSpA showed up-regulation of *MRE11* (Figure 2B), which indicates that in our context other mechanisms induce DDR activation. Moreover, our data underlined a low basal motility of CD4+ T cells that might reflect their lower susceptibility to senescence due to a different metabolism.³⁰

The CD8+ T cell subset, which is characterized here, although intrinsically “hypermotile,” is also able to efficiently migrate following a chemotactic gradient (Figure 1A–E). Therefore, we can speculate that these circulating CD8+ T cells could reach the target tissues in patients with SpA attracted by inflammatory chemokine gradients or even by CX3CL1, which has an increased level in inflamed gut and synovial tissues but not in the blood of patients with r-axSpA.⁴⁹ Once in the target tissues, these cells could randomly move in the extracellular matrix supported by their intrinsic motility and create channels that may favor the spreading of other immune cells.⁵⁰ Accordingly, intravital imaging of cytotoxic CD8+ T cells in pancreatic islets of diabetic mice showed that the cell homing kinetics is a stochastic process, which argues against a dominant influence of chemotactic gradients.⁵¹

Overall, these results shed light on a subpopulation of circulating CD8+ T cells that are more frequent in patients in the SpA cluster and that may contribute to chronic inflammation by coupling the intrinsic motion with a cytotoxic/proinflammatory profile. Deeper investigations will be required to understand the mechanistic relationship between TD/senescence and hypermotility, as well as the possible modulatory effects of bDMARDs on the immune and migratory phenotype of this T cell subset.

ACKNOWLEDGMENTS

The authors are grateful to all patients and healthy subjects enrolled in the study and to Dr Federica Lucantoni for excellent technical support. We also want to thank IGA Technology Services of Udine, Italy, for support in the RNA sequencing. Open access publishing facilitated by Università degli Studi di Roma La Sapienza, as part of the Wiley - CRUI-CARE agreement.

AUTHOR CONTRIBUTIONS

All authors contributed to at least one of the following manuscript preparation roles: conceptualization AND/OR methodology, software, investigation, formal analysis, data curation, visualization, and validation AND drafting or reviewing/editing the final draft. As corresponding author, Dr Fiorillo confirms that all authors have provided the final approval of the version to be published, and takes responsibility for the affirmations regarding article submission (eg, not under consideration by another journal), the integrity of the data presented, and the statements regarding compliance with institutional review board/Declaration of Helsinki requirements.

REFERENCES

1. Mauro D, Thomas R, Guggino G, et al. Ankylosing spondylitis: an autoimmune or autoinflammatory disease? *Nat Rev Rheumatol* 2021;17(7):387–404.
2. Navarro-Compán V, Sepriano A, El-Zorkany B, et al. Axial spondyloarthritis. *Ann Rheum Dis* 2021;80(12):1511–1521.
3. Dougados M, Baeten D. Spondyloarthritis. *Lancet* 2011;377(9783):2127–2137.
4. Stolwijk C, van Tubergen A, Castillo-Ortiz JD, et al. Prevalence of extra-articular manifestations in patients with ankylosing spondylitis: a systematic review and meta-analysis. *Ann Rheum Dis* 2015;74(1):65–73.
5. Ranganathan V, Gracey E, Brown MA, et al. Pathogenesis of ankylosing spondylitis - recent advances and future directions. *Nat Rev Rheumatol* 2017;13(6):359–367.
6. Cortes A, Hadler J, Pointon JP, et al; Wellcome Trust Case Control Consortium 2 (WTCCC2). Identification of multiple risk variants for ankylosing spondylitis through high-density genotyping of immune-related loci. *Nat Genet* 2013;45(7):730–738.
7. Costantino F, Breban M, Garchon HJ. Genetics and functional genomics of spondyloarthritis. *Front Immunol* 2018;9:2933.
8. Tang M, Inman RD. Recent advances on the role of cytotoxic T lymphocytes in the pathogenesis of spondyloarthritis. *Semin Immunopathol* 2021;43(2):255–264.
9. Yang X, Garner LI, Zvyagin IV, et al. Autoimmunity-associated T cell receptors recognize HLA-B*27-bound peptides. *Nature* 2022;612(7941):771–777.
10. Deschler K, Rademacher J, Lacher SM, et al. Antigen-specific immune reactions by expanded CD8+ T cell clones from HLA-B*27-positive patients with spondyloarthritis. *J Autoimmun* 2022;133:102901.
11. Britanova OV, Lupyr KR, Staroverov DB, et al. Targeted depletion of TRBV9+ T cells as immunotherapy in a patient with ankylosing spondylitis. *Nat Med* 2023;29(11):2731–2736.
12. Petrelli A, van Wijk F. CD8(+) T cells in human autoimmune arthritis: the unusual suspects. *Nat Rev Rheumatol* 2016;12(7):421–428.
13. Sieper J, Poddubnyy D. Axial spondyloarthritis. *Lancet* 2017;390(10089):73–84.
14. Gracey E, Vereecke L, McGovern D, et al. Revisiting the gut-joint axis: links between gut inflammation and spondyloarthritis. [published correction appears in *Nat Rev Rheumatol* 2020 Sep;16(9):536]. *Nat Rev Rheumatol* 2020;16(8):415–433.
15. Bernardini G, Benigni G, Scivo R, et al. The multifunctional role of the chemokine system in arthritogenic processes. *Curr Rheumatol Rep* 2017;19(3):11.
16. Tedeschi V, Paldino G, Kunkl M, et al. CD8+ T cell senescence: lights and shadows in viral infections, autoimmune disorders and cancer. *Int J Mol Sci* 2022;23(6):3374.
17. Fessler J, Raicht A, Husic R, et al. Premature senescence of T-cell subsets in axial spondyloarthritis. *Ann Rheum Dis* 2016;75(4):748–754.
18. van der Linden S, Valkenburg HA, Cats A. Evaluation of diagnostic criteria for ankylosing spondylitis. A proposal for modification of the New York criteria. *Arthritis Rheum* 1984;27(4):361–368.
19. Taylor W, Gladman D, Helliwell P, et al.; CASPAR Study Group. Classification criteria for psoriatic arthritis: development of new criteria from a large international study. *Arthritis Rheum* 2006;54(8):2665–2673.
20. Aletaha D, Neogi T, Silman AJ, et al. 2010 Rheumatoid arthritis classification criteria: an American College of Rheumatology/European League Against Rheumatism collaborative initiative. *Arthritis Rheum* 2010;62(9):2569–2581.

21. Benjamini Y, Hochberg Y. Controlling the false discovery rate: a practical and powerful approach to multiple testing. *J R Stat Soc Series B Stat Methodol* 1995;57(1):289–300.
22. Dillemans L, De Somer L, Neerincx B, et al. A review of the pleiotropic actions of the IFN-inducible CXC chemokine receptor 3 ligands in the synovial microenvironment. *Cell Mol Life Sci* 2023;80(3):78.
23. Janssens R, Struyf S, Proost P. Pathological roles of the homeostatic chemokine CXCL12. *Cytokine Growth Factor Rev* 2018;44:51–68.
24. Ranasinghe R, Eri R. Pleiotropic immune functions of chemokine receptor 6 in health and disease. *Medicines (Basel)* 2018;5(3):69.
25. Mauro D, Simone D, Bucci L, et al. Novel immune cell phenotypes in spondyloarthritis pathogenesis. *Semin Immunopathol* 2021;43(2):265–277.
26. Böttcher JP, Beyer M, Meissner F, et al. Functional classification of memory CD8(+) T cells by CX3CR1 expression. *Nat Commun* 2015;6(1):8306.
27. Morris SR, Chen B, Mudd JC, et al. Inflammascent CX3CR1+CD57+CD8+ T cells are generated and expanded by IL-15. *JCI Insight* 2020;5(11):e132963.
28. Zwijnenburg AJ, Pokharel J, Varnaité R, et al. Graded expression of the chemokine receptor CX3CR1 marks differentiation states of human and murine T cells and enables cross-species interpretation. *Immunity* 2023;56(8):1955–1974.e10.
29. Li Y, Shen Y, Hohensinner P, et al. Deficient activity of the nuclease MRE11A induces T cell aging and promotes arthritogenic effector functions in patients with rheumatoid arthritis. *Immunity* 2016;45(4):903–916.
30. Mittelbrunn M, Kroemer G. Hallmarks of T cell aging. *Nat Immunol* 2021;22(6):687–698.
31. Heba AC, Toupance S, Arnone D, et al. Telomeres: new players in immune-mediated inflammatory diseases? *J Autoimmun* 2021;123:102699.
32. Lu Y, Ruan Y, Hong P, et al. T-cell senescence: a crucial player in autoimmune diseases. *Clin Immunol* 2023;248:109202.
33. Maekawa T, Liu B, Nakai D, et al. ATF7 mediates TNF- α -induced telomere shortening. *Nucleic Acids Res* 2018;46(9):4487–4504.
34. Tamayo M, Mosquera A, Rego JI, et al. Differing patterns of peripheral blood leukocyte telomere length in rheumatologic diseases. *Mutat Res* 2010;683(1-2):68–73.
35. Tamayo M, Pértiga S, Mosquera A, et al. Individual telomere length decay in patients with spondyloarthritis. *Mutat Res* 2014;765:1–5.
36. Vahabikashi A, Sivagurunathan S, Nicdao FAS, et al. Nuclear lamin isoforms differentially contribute to LINC complex-dependent nucleocytoskeletal coupling and whole-cell mechanics. *Proc Natl Acad Sci USA* 2022;119(17):e2121816119.
37. Kim Y. The impact of altered lamin B1 levels on nuclear lamina structure and function in aging and human diseases. *Curr Opin Cell Biol* 2023;85:102257.
38. Rai R, Sodeinde T, Boston A, Chang S. Telomeres cooperate with the nuclear envelope to maintain genome stability. *BioEssays* 2024;46(2):e2300184.
39. Fracchia A, Asraf T, Salmon-Divon M, et al. Increased lamin B1 levels promote cell migration by altering perinuclear actin organization. *Cells* 2020;9(10):2161.
40. Breban M, Tap J, Leboime A, et al. Faecal microbiota study reveals specific dysbiosis in spondyloarthritis. *Ann Rheum Dis* 2017;76(9):1614–1622.
41. Wang L, Wang Y, Zhang P, et al. Gut microbiota changes in patients with spondyloarthritis: a systematic review. *Semin Arthritis Rheum* 2022;52:151925.
42. Tedeschi V, Paldino G, Alba J, et al. ERAP1 and ERAP2 haplotypes influence suboptimal HLA-B*27:05-restricted anti-viral CD8+ T cell responses cross-reactive to self-epitopes. *Int J Mol Sci* 2023;24(17):13335.
43. Schirmer M, Goldberger C, Würzner R, et al. Circulating cytotoxic CD8(+) CD28(-) T cells in ankylosing spondylitis. *Arthritis Res* 2002;4(1):71–76.
44. Bektas A, Schurman SH, Sen R, et al. Human T cell immunosenescence and inflammation in aging. *J Leukoc Biol* 2017;102(4):977–988.
45. Alber S, Kumar S, Liu J, et al. Single cell transcriptome and surface epitope analysis of ankylosing spondylitis facilitates disease classification by machine learning. *Front Immunol* 2022;13:838636.
46. Martini V, Silvestri Y, Ciurea A, et al. Patients with ankylosing spondylitis present a distinct CD8 T cell subset with osteogenic and cytotoxic potential. *RMD Open* 2024;10(1):e003926.
47. Wang L, Wu LF, Lu X, et al. Integrated analyses of gene expression profiles digs out common markers for rheumatic diseases. *PLoS One* 2015;10(9):e0137522.
48. Gao W, Hou R, Chen Y, et al. A predictive disease risk model for ankylosing spondylitis: based on integrated bioinformatic analysis and identification of potential biomarkers most related to immunity. *Mediators Inflamm* 2023;2023:3220235.
49. Ciccio F, Guggino G, Zeng M, et al. Proinflammatory CX3CR1+/-CD59+ tumor necrosis factor-like molecule 1A+Interleukin-23+ monocytes are expanded in patients with ankylosing spondylitis and modulate innate lymphoid cell 3 immune functions. [published correction appears in *Arthritis Rheumatol* 2021;73:701]. *Arthritis Rheumatol* 2018;70(12):2003–2013.
50. Sadjadi Z, Zhao R, Hoth M, Qu B, Rieger H. Migration of cytotoxic T lymphocytes in 3D collagen matrices. *Biophys J* 2020;119(11):2141–2152.
51. Coppieters K, Amirian N, von Herrath M. Intravital imaging of CTLs killing islet cells in diabetic mice. *J Clin Invest* 2012;122(1):119–131.

Induction of Type I Interferon–Dependent Activation and Migration of Inflammatory Dendritic Cells to Local Lymph Nodes by UV Light Exposure

Xizhang Sun, Jaime L. Chao, Michael Gerner, and Keith B. Elkon 

Objective. Photosensitivity occurs in ~75% of patients with lupus. Although UV light radiation (UVR) stimulates type I interferon (IFN-I) in the skin, how UVR-induced skin inflammation leads to downstream effects is poorly understood. Tissue inflammation causes dendritic cells (DCs) to migrate from organs to draining lymph nodes (dLN), including a recently identified inflammatory conventional DC subset (inf cDC2) that are potent antigen-presenting cells. To explore links between UVR and the early immune response, we examined DC and lymphocyte subset migration to dLN in normal and lupus-prone mouse strains as well as the role of IFN-I.

Methods. Mice received a single dose of UV (500 mJ/cm²) on the dorsal skin. Brachial and inguinal dLN were harvested at one or two days post-UVR. Flow cytometry using the Symphony A3 cytometer and 15-color staining identified myeloid and lymphoid subsets. Statistical significance was determined by Student's *t*-test.

Results. Higher numbers of CD64+ myeloid cells as well as inf cDC2 were detected in the dLN after UVR in B6 mice, but not in IFN receptor knockout (IFNAR KO) mice. In contrast, Trex1 mutant mice had an exaggerated IFN-I response in the skin and a higher proportion of inf cDC2 in the dLN.

Conclusion. These findings reveal a previously unknown relationship between skin UVR and the migration of the inf cDC2 population to dLN. They highlight the role of IFN-I in this process, and the differences between Trex1 mutant and normal mice suggest that this may be of relevance to lupus.

INTRODUCTION

Photosensitivity to sunlight is a very common manifestation of systemic lupus erythematosus (SLE). Not only may UV light radiation (UVR) worsen cutaneous lupus erythematosus (CLE), but it may also initiate systemic disease flares.^{1,2} Although the mechanisms responsible for local and systemic disease exacerbations remain incompletely understood, type I interferon (IFN-I) is thought to be central to the pathogenesis of CLE.³ The IFN-I signature is prominent in the skin of patients with CLE, and we and others have shown that UVR stimulates an IFN-I signature in intact skin or in isolated keratinocytes.^{4–6} Furthermore, IFN-1 receptor blockade significantly improves the Cutaneous LE Disease Area and Severity Index skin score in patients with lupus, indicating the clinical significance of IFN-I in the skin.⁷ Although both IFN-I and neutrophils may

contribute to damage to internal organs after UVR,⁸ it is likely that the adaptive immune system is also recruited into the systemic response.

Sunlight exposure results in multiple biologic effects in the skin that are mediated by UVR (reviewed in Hart et al⁹). At the cellular level, UV induces direct and reactive oxygen species (ROS)–mediated DNA damage, generation of pyrimidine dimers, and photoproducts. These effects lead to inhibition of translation and to cell death (sunburst cells). The immune response to cell damage is also complex and depends on the type, duration, and dose of UVR, as well as host factors. Although acute inflammation is an invariable response to UVR, longer-term effects may vary. One of the best-studied delayed effects of UVR is suppression of antigen-specific contact hypersensitivity reactions, which is largely explained by migration of epidermal Langerhans cells to draining lymph nodes (dLN) with the subsequent generation of

Supported by the NIH (grants R21-AR-077842 to Dr. Elkon and T32-AR-007108 to Dr Chao and R01-AI-134713 to Dr Gerner) and a grant from the Alliance for Lupus Research (to Dr Elkon).

Xizhang Sun, PhD, Jaime L. Chao, PhD, Michael Gerner, PhD, Keith B. Elkon, MD: University of Washington, Seattle.

Additional supplementary information cited in this article can be found online in the Supporting Information section (<https://acrjournals.onlinelibrary.wiley.com/doi/10.1002/art.43108>).

Author disclosures and graphical abstract are available at <https://onlinelibrary.wiley.com/doi/10.1002/art.43108>.

Address correspondence via email to Keith B. Elkon, MD, at KElkon@medicine.washington.edu.

Submitted for publication May 17, 2024; accepted in revised form January 3, 2025.

Treg cells.¹⁰ In addition, UVB generates suppressive cytokines and keratinocyte microvesicles containing platelet-activating factor receptor agonists that also contribute to immunosuppression.¹¹ In contrast to suppressive responses to UVR, the majority of patients with lupus have exaggerated inflammatory responses in the skin,¹² and some experience systemic exacerbations. Because of the prominent role of IFN-I in lupus in general as well as in the skin,^{13–15} we explored the effects of IFN-I on dendritic cell (DC) migration from the skin to dLN. DCs were selected because IFN-I may selectively impact the generation of myeloid cells after UVB exposure^{4,16} and DCs provide the bridge between innate and adaptive immunity.

MATERIALS AND METHODS

Mice, UV, and violet light exposure. The mice used in this study were 12- to 16-week-old females of the following strains: C57BL/6 (B6, wild type), B6.cGAS^{−/−} (kindly provided by Michael Gale, University of Washington), B6.*lfnar*^{−/−} (JAX laboratories), *Trex1* D18N mutant¹⁷ (kindly provided by Fred Perrino, Wake Forest University), and Kikume Green-Red (KikGR)¹⁸ (kindly provided by Kristine Kuhn, University of Colorado, Denver). Mice were anesthetized with isoflurane, and a single dose of UVB (500 mJ/cm²) was delivered to the shaved whole back using FS40T12/UVB bulbs (National Biological Corporation) as described previously.⁵ The narrow-band UVB light energy (290–320 nm, maxima 311 nm) at the dorsal surface was measured with a Photolight IL1400A radiometer with a SEL240/UVB detector (International Light Technologies). In some experiments, the shaved skin was painted with tetramethylrhodamine isothiocyanate (TRITC) right after skin was exposed to UVB light, at 1% in 1:1 mix of acetone:dibutylphthalate 10 μ L per area, total 4 areas per mouse (2 shoulders, 2 near hindlegs) according to published methods.¹⁹ KikGR transgenic mice were exposed to violet light (380–450 nm) as described previously.⁸ A 50-W light-emitting diode lamp with 0.37 numerical aperture fiber (Mightex) at the power of 100 mW and narrow-band 405-nm wavelength was used to expose shaved skin to violet light for 1 hour, followed by UVB-induced sterile injury. In brief, female B6 or KikGR mice (who express the photoconvertible fluorescent coral green fluorescent protein activated by violet light) were either exposed to violet light (405 nm) or not at time 0. One hour after violet light exposure, mice were either exposed to UVR or not. All animal experiments were approved by the Institutional Animal Care and Use Committee of the University of Washington, Seattle.

Detection of IFN-stimulated gene expression

Skin biopsies (6 mm) were performed before irradiation and at different time points after acute UVB injury (6, 24, and 48 hours), and tissue was stored in RNA Later solution (Qiagen). RNA from skin was extracted by RNA Easy kit from Qiagen. Complementary

DNA (cDNA) was synthesized using High Capacity cDNA synthesis kit (Applied Biosciences). IFN-stimulated gene (ISG) transcripts were selected according to previous studies of IFN response to UV and in *Trex*^{−/−} animals^{4,20} and quantified by real-time quantitative polymerase chain reaction and normalized to *18S* (skin) or *Gapdh* (blood) transcript levels using the following primers: *Isg15*, F 5'-AAGCAGCCAGAAGCAGACTC-3' and R 5'-CACCAATCTTCTGGGCAATC-3'; *Isg20*, F 5'-TCACGGA CTACAGAACCCAAG-3' and R 5'-TATCCTCCTTCAGGGCA-TTG-3'; IFN regulatory factor 7 (*Irf7*), F 5'-GTCTCGGCTTGTC-CTTGCT-3' and R 5'-CCAGGTCCATGAGGAAGTGT-3'; *Mx1*, F 5'-CCTCAGGCTAGATGGCAAG-3' and R 5'-CCTCAGGCTA-GATGGCAAG-3'; *Irf1*, F 5'-TGCTGAGATG GACTGTGAGG-3' and R 5'-CTCCACTTTCAGAGCCTTCG-3'; *Irf3*, F 5'-TGGCCT-ACATAAAGCACCTAGATGG-3' and R 5'-CGCAAACCTTTGGC-AAACTTGTCT-3'; *Irf4*, F 5'-AACTGACTGCTCGCAATAATGT-3' and R 5'-GTAACACAGCAATGCCTCTTGT-3'; *Usp18*, F 5'-TTGGGCTCCTGAGGAAACC-3' and R 5'-CGATGTTGTGA-AACCAACCAGA-3'; *Oas1*, F 5'-CAGGAGCTGTACGGCTTCC-3' and R 5'-CCTACCTTGAGTACCTTGAGCAC-3'; *Irf27l2a*, F 5'-CTGTTTGGCTCTGCCATAGGAG-3' and R 5'-CCTAGGATG-GCATTTGTTGATGTGG-3'; *Gapdh*, F 5'-TGGAAGCTGTGG-CGTGAT-3' and R 5'-TGCTTCACCACCTTCTTGAT-3'; and *18s*, F 5'-AACTTTCGATGGTAGTCGCCGT-3' and R 5'-TCCT-TGGATGTGGTAGCCGTTT-3'.

Flow cytometry analysis of cells in the dLN

Lymph nodes (LNs) were obtained from axillary and brachial sites at one and two days after skin exposure to UVB light. In some cases, LNs were obtained from other sites that did not drain UV-exposed skin as controls. LNs were processed as previously described.^{21,22}

Briefly, the tissue was minced finely and digested with 0.8 mg/mL Dispase II (Sigma-Aldrich), 0.2 mg/mL collagenase P (Sigma-Aldrich), and 0.1 mg/mL of deoxyribonuclease I (Worthington) in complete RPMI medium with Ca⁺² and Mg⁺² and 10% fetal bovine serum for 30 minutes at 37°C with shaking. Cells were passed through a 0.7- μ m strainer, resuspended in RPMI, and counted. Cells were treated with Fc Block TruStain FcX (Biolegend) and stained in phosphate-buffered saline + 1% bovine serum albumin. Surface staining was performed using mouse-specific fluorescent antibodies purchased from Biolegend. The following markers were used to define innate immune cell subpopulations: migratory (mig) DCs, CD3[−] B220[−] Ly6G[−] CD26⁺ MHCII[−] high CD11c[−] intermediate (int); cDC1, MHCII⁺ CD26⁺ XCR1⁺ CD172[−]; cDC2, MHCII⁺ CD26⁺ XCR1[−] CD172⁺; resident (res) DCs, CD3[−] CD19[−] Ly6G[−] CD26⁺ MHCII[−] int to +, CD11c[−] high; inflammatory cDC2, CD26⁺ MHCII⁺ XCR1[−] CD172⁺ CD64⁺ MAR1⁺; inflammatory monocytes, CD3[−] CD19[−] Ly6G[−] Ly6C⁺ CD26[−] CD64⁺ Mar1⁺ CD88⁺; Langerhans cells (LCs), CD3[−] CD19[−] Ly6G[−] CD26[−]

MHCII⁺ XCR1[−] Epcam⁺; neutrophils, CD3[−] CD19[−] CD11b⁺ Ly6G⁺. Adaptive immune cells were defined by the following gating schemes: B cells, CD3[−] CD19⁺; CD8⁺ T cells, CD3⁺ CD8⁺ CD4[−]; CD4⁺ conventional T cells (T conv), CD3⁺ CD4⁺ CD8[−] Foxp3[−]; CD4⁺ Treg cells, CD3⁺ CD4⁺ CD8[−] Foxp3⁺. Additional subgating based on CD69, Ki67, and CXCR3 expression was also performed. Stained cells were analyzed on a Symphony A3 flow cytometer (BD) and data analyzed with FlowJo software v10 (Tree Star). The numbers and percent positive populations were determined using fluorescence minus one controls. For statistical analysis, differences between test and control groups were compared by Student's *t*-test using Graph Pad Prism version 10.

RESULTS

Exposure of the skin to UV light causes migration of DCs to dLN. To determine whether UVR to the skin resulted in migration of myeloid cells to local dLN, we exposed three female B6 mice to a single dose of 500 mJ/cm² UV and then examined dLN for the presence of conventional mig DCs, LCs, and Ly6C⁺ CD64⁺ cells (normally classified as monocytes), both at day 1 and day 2 after UVR. Flow cytometry gating for these experiments is depicted in Supplementary Figure 1 (Supplementary Figure 1A at baseline and Supplementary Figure 1B two days post-UVR). As shown in Figure 1A, we observed an increase in mig DCs, res DCs, and Ly6C⁺ CD64⁺ cells, but not LCs, in the dLN two days after UVR. Lack of an increase in LCs two days after UVR is most likely explained by the delayed kinetics of LC migration to dLN, which usually peaks around four days postexposure.²³ To verify that the cells gated as mig DCs in the dLN were indeed skin-derived, we used skin painting with TRITC, a technique used to track migration of cells from the skin.¹⁹ However, skin painting with TRITC itself caused mig DC trafficking to dLN (not shown), so the effect of UV on skin DCs could not be independently assessed by this method. To avoid the confounding effect of TRITC on DC activation, we examined skin DC migration using KikGR mice. All cells in these mice express the protein KikGR, which converts from green to red fluorescence after exposure to violet light, which is of longer wavelength than the UV used in these experiments (see Materials and Methods). After sequential exposure of shaved skin to violet light at time 0 followed by UV light at 60 minutes, we killed the KikGR mice at one day after UV exposure. As shown in a representative experiment (Figure 1B), red-emitting photoconverted migratory DCs were only seen in dLN from mice who were exposed to both violet and UV light, but not mice who received UV light alone. As a control, photoconverted DCs were not observed in the res DCs in the dLN (Figure 1B) and were not found in mice who did not receive UVR (not shown). Presence of nonphotoconverted migratory cells in LNs is consistent with a proportion of these cells migrating into LNs before treatment. Monfrecola et al²⁴ have reported that blue

light (400–475 nm) can alter DC differentiation. Although we cannot entirely exclude an effect of violet light alone on DCs in our experiments, the effects reported on DCs were only observed in monocyte-derived human DCs in vitro exposed to very high doses of blue light (2.5–15 J/cm²), much higher than used in our experiments.

IFN-1 is required for the migration of inflammatory cDC2 to dLN. Bosteels et al²⁵ have previously described an inflammatory conventional DC subset (inf cDC2) that migrates to dLN after virus infection of the lung. This DC subset is characterized by the expression of CD26, CD64, MAR-1, CD172a, and CD11b, as well as by lacking XCR1, CD103, or CD88, thus having phenotypic markers in common with both monocytes (eg, CD64) and cDC2 (eg, CD11c, MHC-II, CD172a, and CD26). The generation of this DC subset was IFN-1 dependent.²⁵ Since we^{4,5} and others have shown that exposing human and mouse skin to UVR generates IFN-I and the observations in Figure 1 indicate that CD64⁺ Ly6C⁺ cells were increased in dLN after UV exposure, we asked whether UV-induced inflammation is capable of generating inf cDC2 and inducing their migration to dLN. To detect inf cDC2, we used CD26 as a marker to resolve conventional DCs from monocyte-derived populations (Supplementary Figure 2).²⁵ B6 mice and B6 mice deficient in IFN α receptor (IFNAR) were exposed to a single dose of UVB, and then dLN as well as control LNs were harvested one and two days postexposure. Although few differences in the numbers of mig DCs or res DCs were observed in dLN between wild-type B6 and IFNAR^{−/−} mice, we observed a significant difference in inf cDC2 in dLN at two days after UV exposure (Figure 2). Inflammatory monocyte (iMO) cells were also reduced in the IFNAR^{−/−} mice compared with wild-type control mice, but the difference did not reach statistical significance (Figure 2). These results indicate that, although the numbers of res DCs and mig DCs in dLN may be increased by multiple mechanisms post-UVR, the increase in inf cDC2 is dependent on IFN-I.

Inf cDC2 do not exclusively depend on cyclic GMP-AMP synthase (cGAS) activation. Bosteels et al²⁵ observed that Toll-like receptor agonists were capable of inducing the induction of inf cDC2. We have previously shown that the early IFN-I production after skin UV exposure in B6 mice is dependent on activation of the cGAS-stimulator of IFN genes (STING) pathway, whereas other IFN-I pathways become active after 24 hours.^{4,5} To determine whether cGAS activation is necessary for inf cDC2 generation and/or migration to dLN, we compared DC migration in the dLN of B6 and cGAS^{−/−} mice. As shown in Figure 3, although the numbers of inf cDC2 were reduced in cGAS knockout at two days after UVR, the differences were not statistically significant. Res DCs and monocytes were also not significantly impacted at this time point (Figure 3), indicating that different sensors⁵ responsible for IFN-1 production play

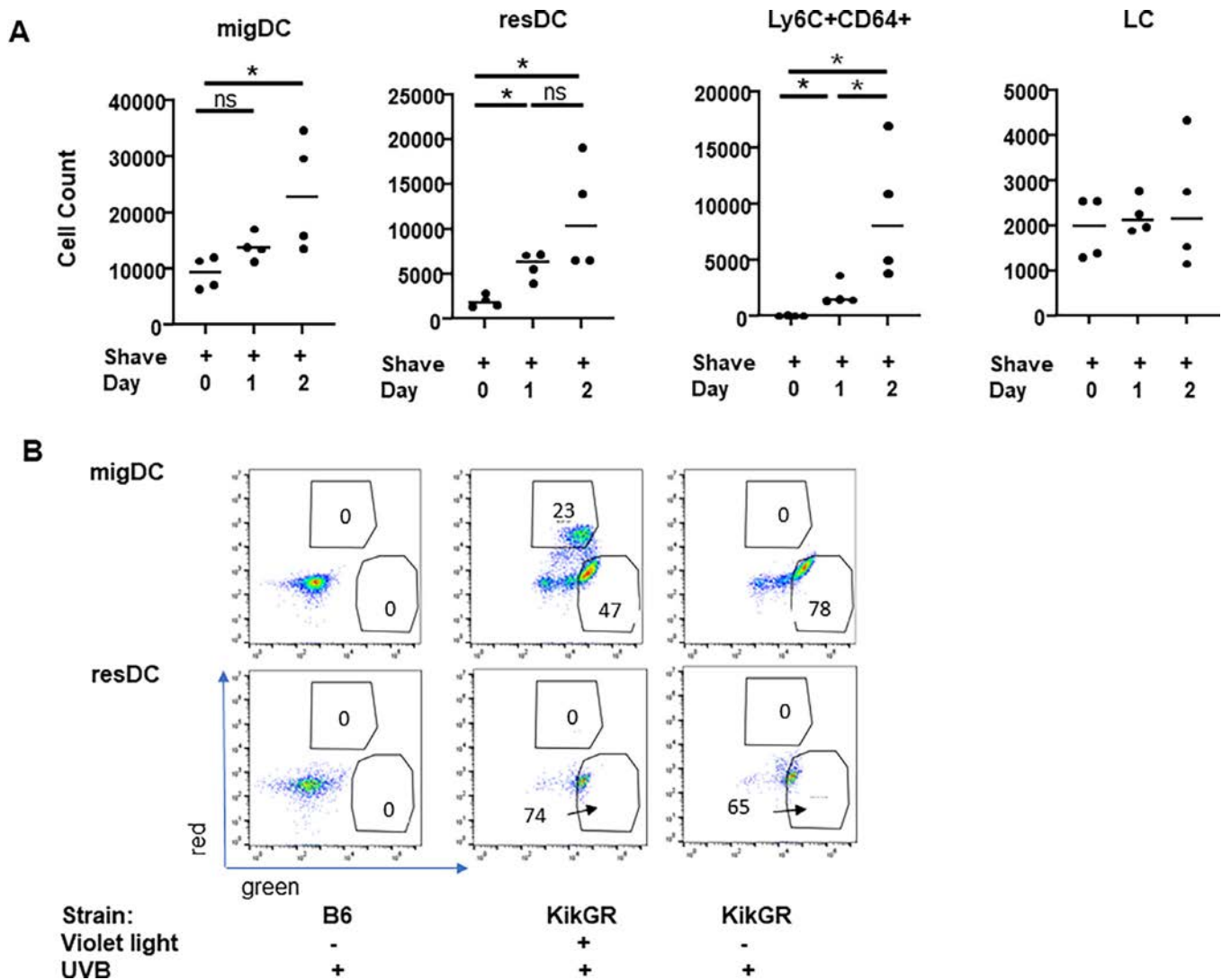


Figure 1. UVR skin exposure results in migration of DCs to the dLN. (A) Female C57BL/6 (B6) mice 8–12 weeks of age were exposed to one dose of UVR (500 mJ/cm²) on the shaved back as described in the Materials and Methods. Cells were collected from the dLN (brachial and inguinal) at time 0 and then at one and two days after UVR. Each dot represents the cell count of mig DCs, res DCs, Ly6C+ CD64+ cells, or LCs as determined by flow cytometry using the phenotypic markers described in the Materials and Methods and the gating schema described in Supplementary Figure 1. (B) Female B6 or KikGR mice (who express the photoconvertible fluorescent coral green fluorescent protein activated by violet light) were either exposed to violet light (405 nm) or not at time 0. One hour after violet light exposure, mice were either exposed to UVR or not as shown in the figure. Cells were collected from the dLN 2 days later and the mig DCs as well as res DCs analyzed for green (not photoconverted) or red (photoconverted) fluorescence by flow cytometry. The result of a representative experiment is shown. **P* < 0.05. DC, dendritic cell; dLN, draining lymph node(s); KikGR, Kikume Green-Red; LC, Langerhans cell; mig, migratory; res, resident; UVR, UV light radiation.

some role in the process of DC and inflammatory monocyte migration at day 2 after UVR.

Trex1 mutant mice have an exaggerated IFN-I response to UV light and increased inf cDC2 in dLN.

Trex1 mutant mice contain a knock-in of the *Trex1* D18N mutation (abbreviated Trex1M), the same mutation that is observed in 1% to 2% of patients with SLE.^{26,27} The Trex1M mouse strain develops a lupus-like disease associated with an IFN-I signature that is dependent on activation of the cGAS-STING pathway.²⁸ To determine how UV exposure in this lupus-prone strain

influences DC migration, we first examined the skin responses of Trex1 mice to UV light. Although ISGs were slightly higher at baseline in Trex1 homozygous mutant mice compared with heterozygous controls, after UV exposure, IFIT3, ISG15, and IRF7 were expressed at severalfold higher levels in Trex1M mice, indicating an exaggerated response (Figure 4A). Because IFN-I was associated with generation of inf cDC2, we next quantified inf cDC2 in the dLN after UV exposure in the skin. Although little difference was observed in the number of mig DCs or res DCs in dLN, a significant increase in inf cDC2 were observed in dLN two days after skin UVR (Figure 4B, Supplementary Figure 3).

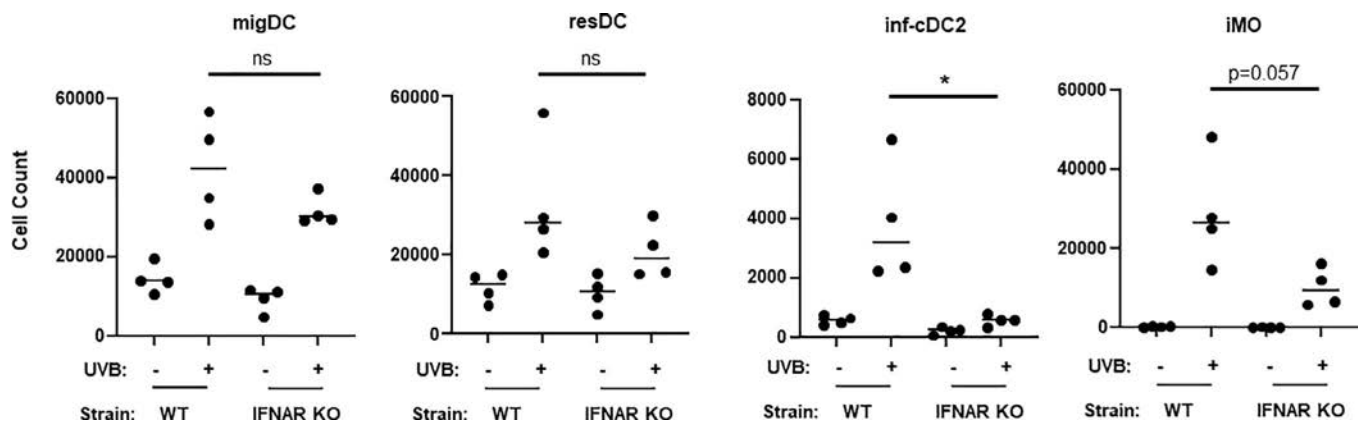


Figure 2. UVR increases the numbers of inf cDC2 in the dLN and is dependent on signaling by IFNAR. Female wild-type B6 or B6 mice lacking the IFN-I receptor (IFNAR KO) were exposed to UVR as in Figure 1 and cells collected from the dLN at two days post-UVR. The cells were analyzed by flow cytometry according to gating shown in Supplementary Figure 2. * $P < 0.05$. DC, dendritic cell; dLN, draining lymph node(s); IFNAR, type 1 interferon receptor; iMO, inflammatory monocyte; inf cDC2, inflammatory conventional cDC2; KO, knockout; mig, migratory; ns, not significant; res, resident; UVR, UV light radiation; WT, wild type.

In contrast, the number of iMO cells was reduced, indicating differential mechanisms driving generation and trafficking of these populations.

UV exposure causes an increase in total B cell and T cell numbers and an increased proportion of activated CD8⁺ T cells in dLN. To determine the acute effects of UVR on Suppadaptive immune cells in dLN, we performed a detailed analysis of B cells and T cell subsets harvested from the dLN and non-draining LN (ndLN). We observed significant increases in the numbers of B cells, T cells, and T cell subsets, including Treg cells, in the dLN, but not in the ndLN (Figure 5A). Because the percentage of cells did not change significantly (CD4 and CD8⁺ T cells are shown in Figure 5B, but similar findings were observed for other T cell subsets), this indicates that the overall cellularity in LNs markedly increases after UVB treatment but that most cell populations are equally affected. When

examining phenotypic markers for T cell activation (CD69), trafficking (CXCR3), and proliferation (Ki67), the numbers of cells exhibiting increases in all of these markers were increased in CD4 and CD8 T cells (not shown and Figure 6A), consistent with the overall increases in these cells (Figure 5A), but only the CD8⁺ T cells showed an increased in the percentage of CD69⁺ cells (Figure 6B), indicating selective activation of this cell type at this early time point after UVR.

DISCUSSION

DCs are central to the immune response initiated in the skin after skin damage and are also regarded as the key antigen-presenting cell (APC) implicated in SLE.^{29–31} After skin injury, including that induced by UVB exposure, dermal DC1 and DC2 migrate to the dLN, where they encounter T cells (reviewed in Kashem et al.²³). The functional effects on T cells

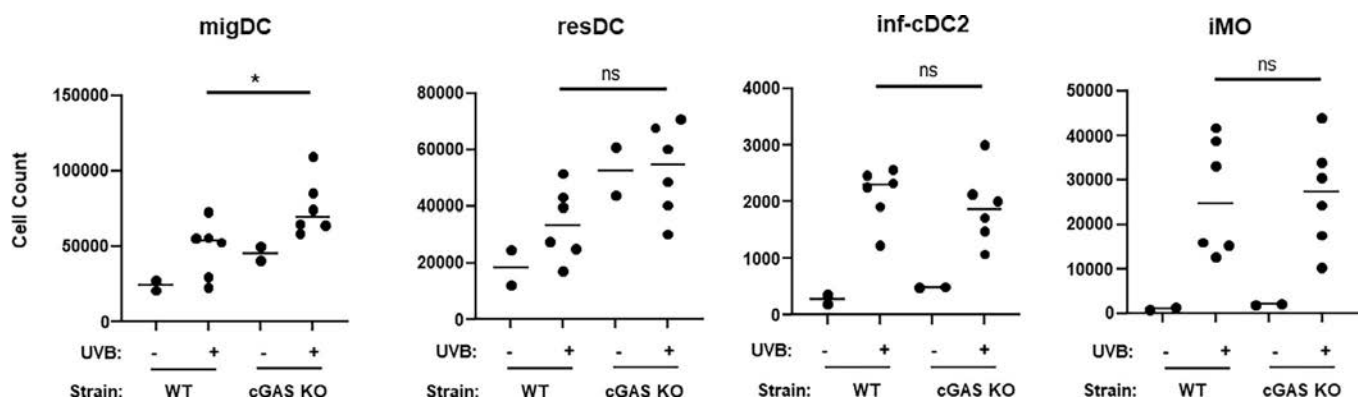


Figure 3. The increase in inf cDC2 and monocyte populations in the dLN are not altered in cGAS-deficient mice. Wild-type B6 or cGAS-deficient B6 mice (cGAS KO) received UVR and the dLN as well as the non-dLN harvested two days post-UVR. * $P < 0.05$, ** $P < 0.01$. cGAS, cyclic GMP-AMP synthase; DC, dendritic cell; dLN, draining lymph node(s); iMO, inflammatory monocyte; inf CDC2, inflammatory cDC2; KO, knockout; mig, migratory; ns, not significant; res, resident; UVR, UV light radiation; WT, wild type.

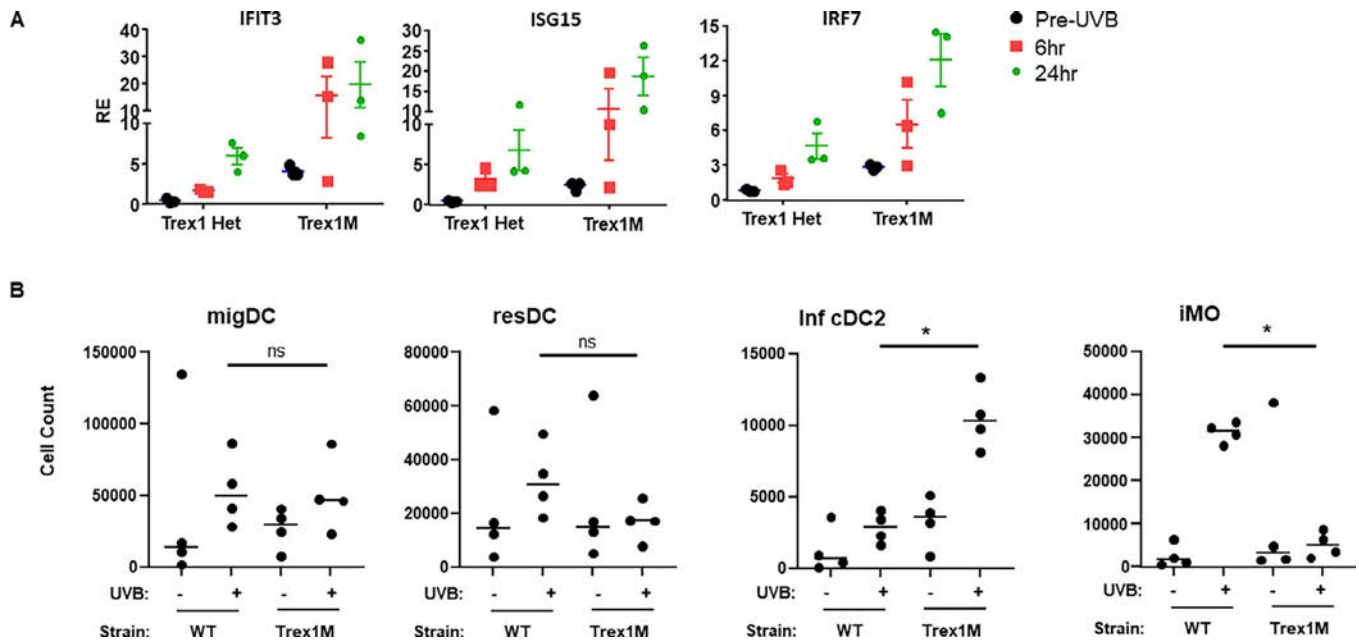


Figure 4. Trex1 D18N mutant (Trex1M) mice demonstrate an exaggerated IFN-I response to UVR and demonstrate an increase in the proportion of inf cDC2 in the dLN. (A) Trex1M homozygous or Trex1M heterozygous mice were exposed to UVR as in Figure 1. At the various time points shown in the figure, skin biopsies were performed and ISG expression determined by qPCR. The results are shown as expression relative to two housekeeping genes as described in the Materials and Methods. (B) Control B6 or Trex1M mice were exposed to UVR and cells harvested from dLN as in Figure 1. The proportions of mig DCs, inf cDC2, and iMO cells were compared among strains. * $P < 0.05$. DC, dendritic cell; dLN, draining lymph node(s); IFN-1, type 1 interferon; iMO, inflammatory monocyte; inf cDC2, inflammatory cDC2; ISG, interferon-stimulated gene; mig, migratory; ns, not significant; qPCR, quantitative polymerase chain reaction; res, resident; UVR, UV light radiation; WT, wild type. Color figure can be viewed in the online issue, which is available at <http://onlinelibrary.wiley.com/doi/10.1002/art.43108/abstract>.

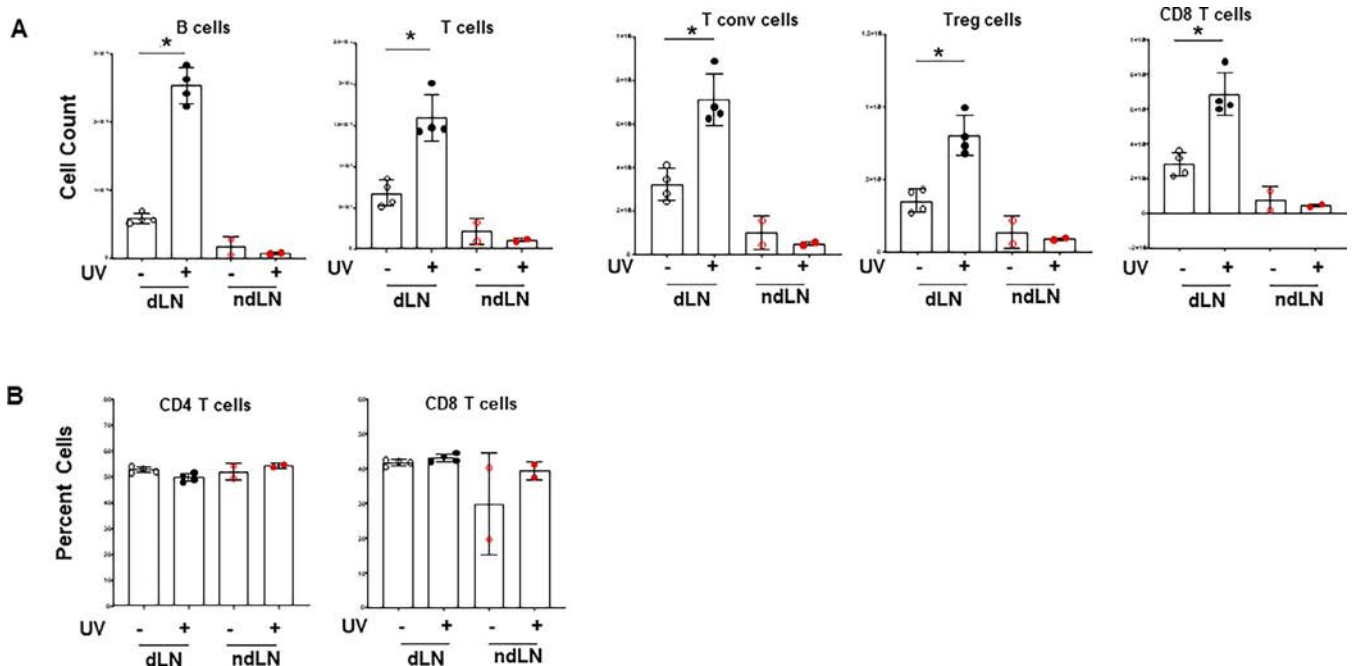


Figure 5. The numbers of adaptive immune cells are increased in the dLN, but not in the non-draining LN (non-dLN), after UVR. B6 mice were exposed to UVR and cells harvested from the draining and non-dLN at two days post-UVR as in Figure 1. B lymphocytes and T cells were quantified by flow cytometry using the antibodies listed in the Materials and Methods. The results are expressed as numbers of cells in (A) and as a percentage in (B). The bars represent the mean, and the SD is shown. * $P < 0.05$. dLN, draining lymph node(s); ndLN, non-draining LN; T conv, conventional T cell; UVR, UV light radiation. Color figure can be viewed in the online issue, which is available at <http://onlinelibrary.wiley.com/doi/10.1002/art.43108/abstract>.

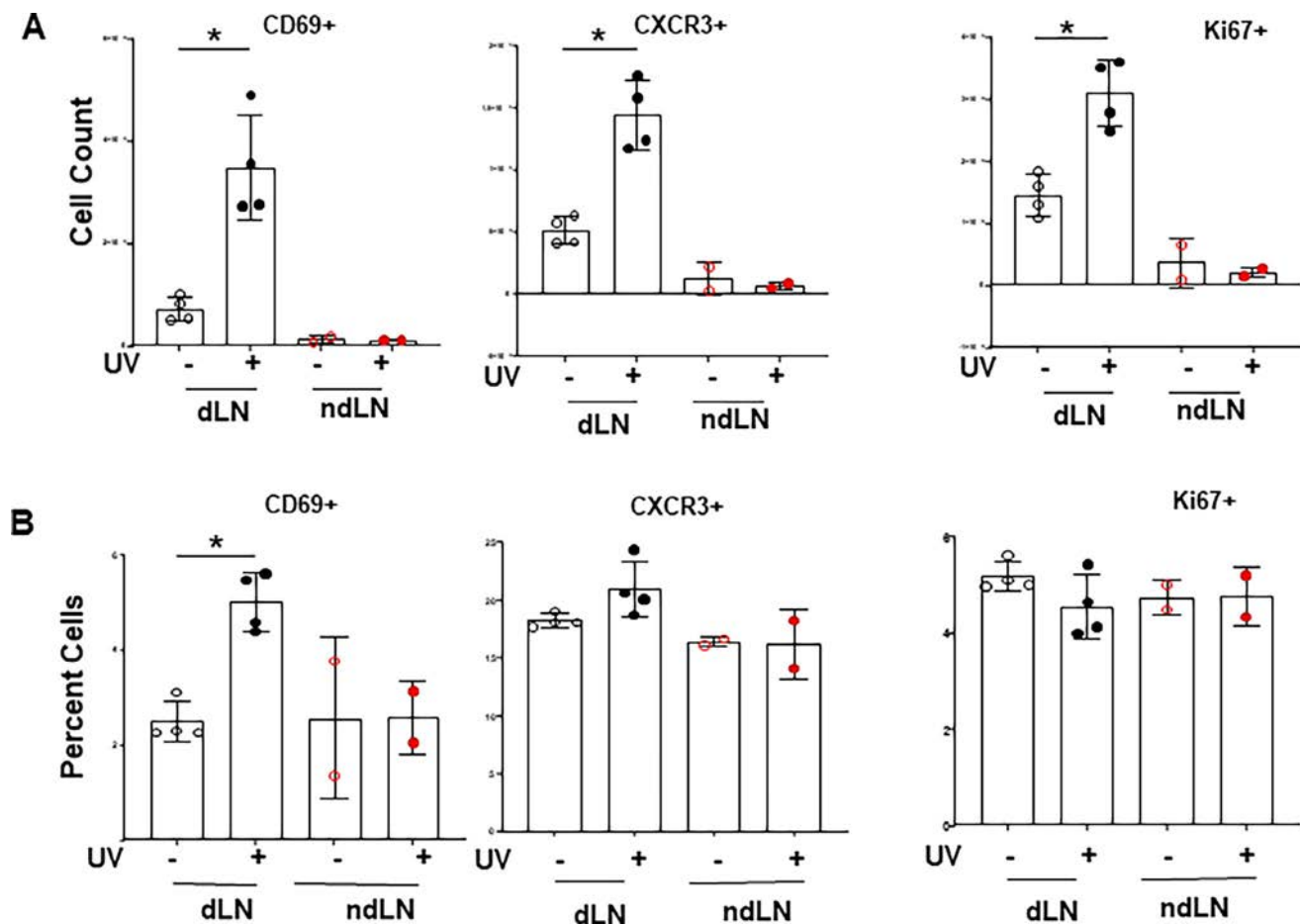


Figure 6. The numbers of CD8+ T cells that express activation, migratory, and proliferation markers are increased, but only the proportion of the activation marker CD69 is increased. CD8+ T cells analyzed in (A) were stained for the markers shown and the results presented as the cell count (A) and percentage (B). * $P < 0.05$. dLN, draining lymph node(s); ndLN, non-draining LN. Color figure can be viewed in the online issue, which is available at <http://onlinelibrary.wiley.com/doi/10.1002/art.43108/abstract>.

depend on the instigating stimulus, DC type activated, localization and other factors.^{25,32–34} Because IFN-I is known to increase MHCII and co-stimulatory molecule expression on APCs,^{35,36} to enhance migration of mig DCs,³⁷ and to suppress Treg cells,³⁸ we explored the trafficking of DCs to dLN after skin exposure to UVB in normal and lupus-prone mice. We observed that trafficking of a unique DC population, inf cDC2,²⁵ to dLN was increased post-UVR and was IFN-I dependent and that the proportion of these DCs in dLN was increased after UVR in a lupus-prone strain, Trex1M mice. UVR was also associated with an early increase in the proportion of activated CD8+ T cells in dLN.

Several studies have shown that microbial stimulation of IFN-I in the skin and other organs generate inflammatory DCs. Min et al³⁹ reported that infection of mouse footpads with *Listeria monocytogenes* stimulated the production of inflammatory CD64+ DCs in dLN and that the maturation of these cells was IFN-1 dependent. Bosteels et al²⁵ observed the generation of inf cDC2 cells (which express CD172a+ and CD11b+ CD26+ CD64+ MAR-1+, but not XCR1, CD103, or CD88) after infection

with a single-stranded RNA virus in the lung. Mice who were deficient in IFNAR did not generate inf cDC2 in response to virus infection.²⁵ In addition to detection of inf cDC2 in lung dLN, this group also showed that microbial infection of skin generated a similar phenotype of inf cDC2 in skin dLN. We and others have observed that UVR stimulates an early IFN-I response in the skin of both mouse and humans,^{4,5} and this response may be exaggerated in human SLE.^{6,40} How IFN-I effects myeloid cell migration to local LNs and subsequent activation of immune cells has not been investigated.

In the present study, we observed that, similar to what has been reported in microbial infections, inf cDC2 are activated by IFN-I in the dLN of B6 mice after UVR. Overall, these findings are significant because, in both studies identifying IFN-I-dependent inf cDC2 in dLN, these inflammatory DCs were shown to be superior to other DCs in antigen presentation to both CD4+ and CD8+ T cells.^{25,39} Furthermore, the inf cDC2 acquired antigen by Fc receptor immune complex uptake, which could be due to engagement of CD64 (FcγR1) and/or FcεR1g. It will be intriguing to see whether, in the context of lupus, the prototypic immune

complex disease, the inf cDC2 are key to boosting autoimmune responses after an encounter with immune complexes.

We have previously shown cGAS to be required for the initial six-hour IFN-I stimulation after UVR in the skin but that, after this, other sensors become activated.⁵ This observation likely explains why cGAS deficiency did not significantly affect inf cDC2 migration at day 2 post-UVR. Li et al⁴¹ recently reported that loss of cGAS in conventional DCs protected Trex1M mice from autoimmunity. Although this study emphasizes the critical importance of DCs in the generation of lupus-like disease associated with high IFN-I production, it also suggests that the mechanisms of spontaneous nucleic acid stimulation versus UVR mediated sensor activation may be somewhat different in Trex1M mice.

Trex1 (DNase III) is a highly abundant Endoplasmic Reticulum-tethered 3'-5' DNA exonuclease that degrades excess or damaged DNA in the cytosol.⁴² Of clinical relevance, Berndt et al⁴³ have shown that, in patients with lupus with Trex1 mutations, UVR causes enhanced photosensitivity in response to phototesting. The increased response in patients was associated with greater DNA damage (increased ROS and generation of photo-products), as well as enhanced IFN-I production by TREX1-deficient cells. Similarly, we found an enhanced IFN-I response in the skin of mice with a knock-in of the same mutation, Trex1N18N, that is detected in 1% to 2% of patients with lupus.^{26,27} The fact that these Trex1M mice also had an increased proportion of inf cDC2 DCs in the dLN after UVR may help to explain how excessive generation of IFN-I in the skin leads to the generation of potent APCs in the dLN and subsequent amplification of the immune response resulting in systemic effects.

Although we did not examine the long-term effects of UVR in our model systems, in this report, others have shown that repetitive lower-dose UVR also caused an increase in the IFN-I response in a lupus-prone mouse strain compared with wild-type mice.⁴⁴ The enhanced IFN-I response in these experiments were associated with suppression of Treg cells in the dLN, which may also contribute to systemic exacerbations of lupus after exposure to UVR. A relationship between reduced LCs in the skin and increased photosensitivity has also been noted.⁴⁵

Although examination of the B cell and T cell response, including Treg cells, to inf cDC2 induced by UV light would require a much more extended duration as well as an analysis of antigen-specific responses in B and T cell transgenic mice, we determined the acute response of adaptive immune cells in our short-term model. We observed that both B cells and T cells, as well as T cell subsets, increased in number in the dLN after skin UVR. These increases could result from either increased recruitment or retention of lymphocytes after UVB. Changes in the numbers of CD69+ activated, chemokine receptor (CXCR3+), and proliferating cells (Ki67+) were proportional to the increase in numbers of B cells and T cells, with the exception of activated CD8+ T cells, which increased both in number and as a percentage of CD8+ T cells. This result could be explained by the increased trafficking

of inflammatory DCs to the dLN and the past observations that these cells are capable of cross-presenting antigens for CD8 T cell priming.²⁵ In a study comparing CD8+ T cells in the skin and kidney of patients with lupus, Dunlap et al⁴⁶ observed that, although the CD8+ T cells in lupus kidneys were activated, those in the skin were not. Whether this reflects migration of the activated CD8+ T cells from skin to dLN and perhaps to the kidneys is an important question that can be determined in future studies.

ACKNOWLEDGMENT

We thank James A. Kuchenbecker, University of Washington, for advice.

AUTHOR CONTRIBUTIONS

All authors contributed to at least one of the following manuscript preparation roles: conceptualization AND/OR methodology, software, investigation, formal analysis, data curation, visualization, and validation AND drafting or reviewing/editing the final draft. As corresponding author, Dr Elkon confirms that all authors have provided the final approval of the version to be published and takes responsibility for the affirmations regarding article submission (eg, not under consideration by another journal), the integrity of the data presented, and the statements regarding compliance with institutional review board/Declaration of Helsinki requirements.






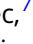


REFERENCES

- Schmidt E, Tony HP, Brocker EB, et al. Sun-induced life-threatening lupus nephritis. *Ann N Y Acad Sci* 2007;1108:35–40.
- Sim JH, Ambler WG, Sollohub IF, et al. Immune cell-stromal circuitry in lupus photosensitivity. *J Immunol* 2021;206(2):302–309.
- Psarras A, Wittmann M, Vital EM. Emerging concepts of type I interferons in SLE pathogenesis and therapy. *Nat Rev Rheumatol* 2022;18(10):575–590.
- Sontheimer C, Liggitt D, Elkon KB. Ultraviolet B irradiation causes stimulator of interferon genes-dependent production of protective type I interferon in mouse skin by recruited inflammatory monocytes. *Arthritis Rheumatol* 2017;69(4):826–836.
- Skopelja-Gardner S, An J, Tai J, et al. The early local and systemic Type I interferon responses to ultraviolet B light exposure are cGAS dependent. *Sci Rep* 2020;10(1):7908.
- Sarkar MK, Hile GA, Tsoi LC, et al. Photosensitivity and type I IFN responses in cutaneous lupus are driven by epidermal-derived interferon kappa. *Ann Rheum Dis* 2018;77(11):1653–1664.
- Morand EF, Furie R, Tanaka Y, et al; TULIP-2 Trial Investigators. Trial of anifrolumab in active systemic lupus erythematosus. *N Engl J Med* 2020;382(3):211–221.
- Skopelja-Gardner S, Tai J, Sun X, et al. Acute skin exposure to ultraviolet light triggers neutrophil-mediated kidney inflammation. *Proc Natl Acad Sci U S A* 2021;118(3).
- Hart PH, Norval M, Byrne SN, et al. Exposure to ultraviolet radiation in the modulation of human diseases. *Annu Rev Pathol* 2019;14:55–81.
- Schwarz T. Mechanisms of UV-induced immunosuppression. *Keio J Med* 2005;54(4):165–171.
- Liu L, Awoyemi AA, Fahy KE, et al. Keratinocyte-derived microvesicle particles mediate ultraviolet B radiation-induced systemic immunosuppression. *J Clin Invest* 2021;131(10):e144963.

12. Kim A, Chong BF. Photosensitivity in cutaneous lupus erythematosus. *Photodermatol Photoimmunol Photomed* 2013;29(1):4–11.
13. Patel J, Vazquez T, Chin F, et al. Multidimensional immune profiling of cutaneous lupus erythematosus in vivo stratified by patient responses to antimalarials. *Arthritis Rheumatol* 2022;74(10):1687–1698.
14. Billi AC, Ma F, Plazyo O, et al. Nonlesional lupus skin contributes to inflammatory education of myeloid cells and primes for cutaneous inflammation. *Sci Transl Med* 2022;14(642):eabn2263.
15. Xu B, Musai J, Tan YS, et al. A critical role for IFN- β signaling for IFN- κ induction in keratinocytes. *Front Lupus* 2024;2:1359714.
16. Maz MP, Reddy AL, Berthier CC, et al. Lupus-prone NZM2328 mice exhibit enhanced UV-induced myeloid cell recruitment and activation in a type I interferon dependent manner. *J Autoimmun* 2024;149:103296.
17. Grieves JL, Fye JM, Harvey S, et al. Exonuclease TREX1 degrades double-stranded DNA to prevent spontaneous lupus-like inflammatory disease. *Proc Natl Acad Sci U S A* 2015;112(16):5117–5122.
18. Griswold SL, Sajja KC, Jang CW, et al. Generation and characterization of iUBC-KikGR photoconvertible transgenic mice for live time-lapse imaging during development. *Genesis* 2011;49(7):591–598.
19. Hor JL, Whitney PG, Zaid A, et al. Spatiotemporally distinct interactions with dendritic cell subsets facilitates CD4+ and CD8+ T cell activation to localized viral infection. *Immunity* 2015;43(3):554–565.
20. An J, Woodward JJ, Lai W, et al. Inhibition of cyclic GMP-AMP synthase using a novel antimalarial drug derivative in Trex1-deficient mice. *Arthritis Rheumatol* 2018;70(11):1807–1819.
21. Leal JM, Huang JY, Kohli K, et al. Innate cell microenvironments in lymph nodes shape the generation of T cell responses during type I inflammation. *Sci Immunol* 2021;6(56):eabb9435.
22. Lyons-Cohen MR, Shamskhov EA, Gerner MY. Site-specific regulation of Th2 differentiation within lymph node microenvironments. *J Exp Med* 2024;221(4):e20231282.
23. Kashem SW, Haniiffa M, Kaplan DH. Antigen-presenting cells in the skin. *Annu Rev Immunol* 2017;35:469–499.
24. Monfrecola G, Lembo S, Cantelli M, et al. The effect of visible blue light on the differentiation of dendritic cells in vitro. *Biochimie* 2014;101:252–255.
25. Bosteels C, Neyt K, Vanheerswynghe M, et al. Inflammatory type 2 cDCs acquire features of cDC1s and macrophages to orchestrate immunity to respiratory virus infection. *Immunity* 2020;52(6):1039–1056.e9.
26. Rice G, Newman WG, Dean J, et al. Heterozygous mutations in TREX1 cause familial chilblain lupus and dominant Aicardi-Goutieres syndrome. *Am J Hum Genet* 2007;80(4):811–815.
27. Namjou B, Kothari PH, Kelly JA, et al. Evaluation of the TREX1 gene in a large multi-ancestral lupus cohort. *Genes Immun* 2011;12(4):270–279.
28. Simpson SR, Rego SL, Harvey SE, et al. T cells produce IFN- α in the TREX1 D18N model of lupus-like autoimmunity. *J Immunol* 2020;204(2):348–359.
29. Celhar T, Hopkins R, Thornhill SI, et al. RNA sensing by conventional dendritic cells is central to the development of lupus nephritis. *Proc Natl Acad Sci U S A* 2015;112(45):E6195–E6204.
30. Dutertre CA, Becht E, Irac SE, et al. Single-cell analysis of human mononuclear phagocytes reveals subset-defining markers and identifies circulating inflammatory dendritic cells. *Immunity* 2019;51(3):573–589.e8.
31. Cuda CM, Misharin AV, Gierut AK, et al. Caspase-8 acts as a molecular rheostat to limit RIPK1- and MyD88-mediated dendritic cell activation. *J Immunol* 2014;192(12):5548–5560.
32. Igyártó BZ, Haley K, Ortner D, et al. Skin-resident murine dendritic cell subsets promote distinct and opposing antigen-specific T helper cell responses. *Immunity* 2011;35(2):260–272.
33. Shklovskaya E, Roediger B, Fazekas de St Groth B. Epidermal and dermal dendritic cells display differential activation and migratory behavior while sharing the ability to stimulate CD4+ T cell proliferation in vivo. *J Immunol* 2008;181(1):418–430.
34. Gerner MY, Kastenmuller W, Ifrim I, et al. Histo-cytometry: a method for highly multiplex quantitative tissue imaging analysis applied to dendritic cell subset microanatomy in lymph nodes. *Immunity* 2012;37(2):364–376.
35. Luft T, Pang KC, Thomas E, et al. Type I IFNs enhance the terminal differentiation of dendritic cells. *J Immunol* 1998;161(4):1947–1953.
36. Blanco P, Palucka AK, Gill M, et al. Induction of dendritic cell differentiation by IFN- α in systemic lupus erythematosus. *Science* 2001;294(5546):1540–1543.
37. Kastenmüller K, Wille-Reece U, Lindsay RWB, et al. Protective T cell immunity in mice following protein-TLR7/8 agonist-conjugate immunization requires aggregation, type I IFN, and multiple DC subsets. *J Clin Invest* 2011;121(5):1782–1796.
38. Srivastava S, Koch MA, Pepper M, et al. Type I interferons directly inhibit regulatory T cells to allow optimal antiviral T cell responses during acute LCMV infection. *J Exp Med* 2014;211(5):961–974.
39. Min J, Yang D, Kim M, et al. Inflammation induces two types of inflammatory dendritic cells in inflamed lymph nodes. *Exp Mol Med* 2018;50(3):e458.
40. Katayama S, Panelius J, Koskenmies S, et al. Delineating the healthy human skin UV response and early induction of interferon pathway in cutaneous lupus erythematosus. *J Invest Dermatol* 2019;139(9):2058–2061.e4.
41. Li T, Yum S, Wu J, et al. cGAS activation in classical dendritic cells causes autoimmunity in TREX1-deficient mice. *Proc Natl Acad Sci U S A* 2024;121(38):e2411747121.
42. Mazur DJ, Perrino FW. Identification and expression of the TREX1 and TREX2 cDNA sequences encoding mammalian 3'→5' exonucleases. *J Biol Chem* 1999;274(28):19655–19660.
43. Berndt N, Wolf C, Fischer K, et al. Photosensitivity and cGAS-dependent IFN-1 activation in patients with lupus and TREX1 deficiency. *J Invest Dermatol* 2022;142(3 Pt A):633–640.e6.
44. Wolf SJ, Estadt SN, Theros J, et al. Ultraviolet light induces increased T cell activation in lupus-prone mice via type I IFN-dependent inhibition of T regulatory cells. *J Autoimmun* 2019;103:102291.
45. Shipman WD, Chyou S, Ramanathan A, et al. A protective Langerhans cell-keratinocyte axis that is dysfunctional in photosensitivity. *Sci Transl Med* 2018;10(454):eaap9527.
46. Dunlap GS, Billi AC, Xing X, et al. Single-cell transcriptomics reveals distinct effector profiles of infiltrating T cells in lupus skin and kidney. *JCI Insight* 2022;7(8):e156341.

BRIEF REPORT

Distinct Pathophysiologic Pathways Support Stratification of Sjögren's Disease Based on Symptoms, Clinical, and Routine Biological Data

Yann Nguyen,¹  Maxime Beydon,²  Jacques-Eric Gottenberg,³  Jacques Morel,⁴  Aleth Perdriger,⁵ Emmanuelle Dernis,⁶ Divi Cornec,⁷  Valérie Devauchelle-Pensec,⁷  Damien Sène,⁸ Philippe Dieudé,⁹ Marion Couderc,¹⁰ Anne-Laure Fauchais,¹¹ Claire Larroche,¹² Olivier Vittecoq,¹³ Carine Salliot,¹⁴  Eric Hachulla,¹⁵ Véronique Le Guern,¹⁶ Xavier Mariette,¹⁷ Raphaële Seror,¹⁷ and Gaëtane Nocturne¹⁷ 

Objective. Recently, three distinct phenotypes of patients with Sjögren disease (SjD) have been described based on cluster analysis: B cell active with low symptoms (BALS), high systemic activity (HSA), and low systemic activity with high symptoms (LSAHS). We aimed to assess whether these clusters were associated with distinct biomarkers and the prognostic value of interferon (IFN) signature.

Methods. The Assessment of Systemic Signs and Evolution in Sjögren's Syndrome cohort is a 20-year prospective cohort of patients with SjD. The following biomarkers were compared: IFN- α 2, IFN- γ , CXCL10, CXCL13, BAFF, interleukin (IL)-7, fms-like tyrosine kinase 3 ligand, CCL19, and tumor necrosis factor receptor 2 (TNF-RII). IFN signature was assessed using transcriptomic analysis. We then compared systemic and symptomatic evolution, and the risk of new immunosuppressant prescription and of lymphoma, according to the IFN signature across the three clusters.

Results. A total of 395 patients (94% female, median age 53 [interquartile range 43–63] years) were included. Higher levels of CXCL13, IL-7, and TNF-RII were found in the BALS and HSA clusters compared with the LSAHS cluster. A high IFN signature was mainly found in the BALS cluster (57%, vs 48% and 38% in the HSA and LSAHS clusters, respectively). This IFN signature was mainly driven by type I IFN, with higher levels of IFN- α 2. In the BALS cluster, a high IFN signature was associated with a higher risk of new immunosuppressant treatment (hazard ratio 9.38; 95% confidence interval 1.22–72.16). All lymphoma occurred in patients with high IFN signature.

Conclusion. The three SjD clusters displayed distinct expressions of IFN signature and markers of T and B cell activation, confirming distinct pathophysiologic mechanisms. High IFN signature could predict systemic evolution in the BALS cluster.

INTRODUCTION

Sjögren disease (SjD) is a common systemic autoimmune disorder, predominantly affecting women at a ratio of 9:1.^{1,2}

The primary symptoms include oral or ocular dryness, fatigue, and joint pain, significantly impacting quality of life. Additionally, systemic manifestations occur in approximately 30% to 50% of patients and can affect all organs. A major complication of SjD is

The Assessment of Systemic Signs and Evolution in Sjögren's Syndrome (ASSESS) national multicenter prospective cohort is supported by the French Ministry of Health (Programme Hospitalier de Recherche Clinique 2005 grant P060228) and the French Society of Rheumatology.

¹Yann Nguyen, MD, PhD: Hôpital Bicêtre, Assistance Publique – Hôpitaux de Paris, Université Paris-Saclay, Le Kremlin-Bicêtre, Hôpital Beaujon, Assistance Publique – Hôpitaux de Paris, Université Paris Cité, Clichy, Centre de Recherche en Épidémiologie et Statistiques, INSERM UMR 1153, Université Paris Cité, Paris, France; ²Maxime Beydon, MD, MPH: Hôpital Bicêtre, Assistance Publique – Hôpitaux de Paris, Université Paris-Saclay, Le Kremlin-Bicêtre, Hôpital Beaujon, Assistance Publique – Hôpitaux de Paris, Université Paris Cité, Clichy, Paris, France; ³Jacques-Eric Gottenberg, MD, PhD: Hôpitaux Universitaires de Strasbourg, Université de Strasbourg, Strasbourg, France; ⁴Jacques Morel, MD, PhD: Centre Hospitalier Universitaire de Montpellier and PhyMedExp, Université de Montpellier, INSERM, CNRS, Montpellier,

France; ⁵Aleth Perdriger, MD, PhD: Centre Hospitalier Universitaire de Rennes, Université de Rennes, Rennes, France; ⁶Emmanuelle Dernis, MD: General Hospital, Le Mans, France; ⁷Divi Cornec, MD, PhD, Valérie Devauchelle-Pensec, MD, PhD: Centre Hospitalier Universitaire de Brest, INSERM 1227, LBAI, Université de Bretagne Occidentale, Centre de Référence des Maladies Auto-Immunes Rares de l'Adulte, Brest, France; ⁸Damien Sène, MD, PhD: Hôpital Lariboisière, Assistance Publique – Hôpitaux de Paris, Paris, France; ⁹Philippe Dieudé, MD, PhD: Hôpital Bichat-Claude Bernard, AP-HP, INSERM UMR 1152, Paris Cité University, Paris, France; ¹⁰Marion Couderc, MD: Centre Hospitalier Universitaire de Clermont-Ferrand and INSERM UMR 1240, Clermont Auvergne University, Clermont-Ferrand, France; ¹¹Anne-Laure Fauchais, MD, PhD: University Hospital of Limoges, Limoges, France; ¹²Claire Larroche, MD: Assistance Publique – Hôpitaux de Paris, Hôpital Avicenne, Bobigny, France; ¹³Olivier Vittecoq, MD, PhD: Rouen University Hospital, Rouen, France; ¹⁴Carine Salliot, MD, PhD: Centre Hospitalier Régional

the substantially increased risk of developing B cell lymphoma.² Therefore, patients with SjD exhibit a wide range of symptoms, systemic manifestations, and associated risks.

Tackling the clinical heterogeneity of SjD is crucial.³ Indeed, despite advances in understanding the disease's pathophysiology, to date, no immunomodulatory drugs have been approved, and symptom management relies on expert opinion. Promising results from early open-label trials have not been replicated in later randomized controlled trials, likely because of disease heterogeneity, inclusion criteria, inappropriate outcome measures, and high placebo response rates.

Recently, efforts have been made to stratify patients with SjD using unsupervised clustering. Different approaches have been proposed, including multiomic strategies allowing the identification of the main biologic pathways involved in SjD pathogeny.^{4,5} Another strategy has been to stratify patients based on subjective symptoms.^{6,7} Our group has performed a cluster analysis of patients with SjD by considering most manifestations of SjD, including subjective symptoms, systemic manifestations, and routine biologic data.⁸ We identified three distinct patient subgroups: those with B cell active disease and low symptom burden (BALS), those with high systemic disease activity and high symptom burdens of dryness and fatigue (HSA), and those with low systemic activity and high symptom burden (LSAHS).⁸ These subgroups showed different symptom trajectories over time and varying risks of lymphoma. Patients from the BALS clusters tended to evolve toward a more systemic and symptomatic disease during the follow-up, with symptoms similar to those of HSA cluster patients. Thus, our findings suggested a heterogeneity in pathophysiologic mechanisms. Herein, we aimed to assess whether these three clusters were associated with distinct pathophysiologic pathways by assessing a panel of biomarkers and evaluating the interferon (IFN) signature and whether a high IFN signature could predict disease evolution across the clusters.

PATIENTS AND METHODS

Study population. The Assessment of Systemic Signs and Evolution of Sjögren's Syndrome (ASSESS) cohort is a French prospective multicenter cohort study in 15 tertiary centers created in 2006. Its primary objective is to identify factors predicting systemic complications and lymphoma in primary SjD during a

prospective 20-year follow-up.^{9–11} All 395 included patients met the 2002 American-European Consensus Group criteria for SjD.^{12,13} Patients with SjD associated with other autoimmune diseases were excluded. The study was promoted by the Assistance Publique-Hôpitaux de Paris and the Société Française de Rhumatologie (French Society of Rheumatology) and was approved by the Ethics Committee of Bichat Hospital and the National Commission for Computing and Liberties in 2006. All patients gave their written consent.

Cluster identification. Cluster identification has been previously described.⁸ Briefly, we used an unsupervised multiple correspondence analysis using 25 selected variables to widely cover SjD manifestations: age at SjD diagnosis, sex, visual analog scales for pain, fatigue, dryness, systemic manifestations as defined by EULAR Sjögren's Syndrome Disease Activity Index (ESSDAI) domains, biologic data (rheumatoid factor; autoantibodies, including anti-SSA, SSB, and RNP; centromere; and DNA antibodies), high gamma globulin or IgG levels (defined by IgG or gammaglobulin levels >15 g/L), monoclonal component, cryoglobulinemia, and low C4 levels. We then performed hierarchical clustering based on the Ward method, followed by k-means algorithms to build homogeneous clusters, and we determined the number of clusters both visually and with the gain in inertia, and the clusters were described and named by their most prominent summary characteristics.

Assessment of serum markers and IFN signature.

Serum samples were obtained at the cohort's enrollment. All biologic samples were immediately frozen, stored, and shipped to the Centre de Ressources Biologiques of Bichat Hospital, which has obtained the French Association for Quality Insurance (certification number 2009/34457) according to norm 96900.

For the present study, we analyzed the biomarkers already available in the ASSESS cohort. The biomarkers were assessed centrally and blindly from any clinical or other biologic data: Eotaxin, CCL2, interleukin (IL)-7, CCL19, TNF-RII, CXCL13, BAFF, fms-like tyrosine kinase 3 ligand (FLT-3), and β 2-microglobulin. Eotaxin, IL-7, CCL19, and CXCL13 were assessed by ProcartaPlex Multiplex Immunoassays from Affymetrix according to the manufacturer's instructions as previously described.^{10,14} β 2-Microglobulin levels (mg/L) were assessed by nephelometry

d'Orléans, Orléans, France; ¹⁵Eric Hachulla, MD, PhD: Referral Centre for Rare Systemic Auto-immune and Auto-inflammatory Diseases North North-West Mediterranean and Guadeloupe (CeRAINOM), INSERM, Centre Hospitalier Universitaire de Lille, U1286 – INFINITE, University of Lille, Lille, France; ¹⁶Véronique Le Guern, MD, MSc: National Referral Centre for Rare Autoimmune and Systemic Diseases, Hôpital Cochin, AP-HP Centre, Université Paris Cité, Paris, France; ¹⁷Xavier Mariette, MD, PhD, Raphaële Seror, MD, PhD, Gaëtane Nocturne, MD, PhD: Hôpital Bichat, Assistance Publique – Hôpitaux de Paris, Université Paris-Saclay, Center for Immunology of Viral Infections and Auto-immune Diseases (IMVA), Institut pour la Santé et la Recherche Médicale (INSERM) UMR 1184, Université Paris-Saclay, Le Kremlin-Bicêtre, Paris, France.

Drs Mariette, Seror, and Nocturne are co-last authors and contributed equally to this work.

Additional supplementary information cited in this article can be found online in the Supporting Information section (<https://acrjournals.onlinelibrary.wiley.com/doi/10.1002/art.43096>).

Author disclosures are available at <https://onlinelibrary.wiley.com/doi/10.1002/art.43096>.

Address correspondence via email to Gaëtane Nocturne, MD, PhD, at Gaetane.nocturne@aphp.fr.

Submitted for publication August 18, 2024; accepted in revised form November 6, 2024.

using the Freelite kit (Binding Site). BAFF, CCL2, and FLT-3 levels were measured using a commercial kit enzyme-linked immunosorbent assay (R&D Systems).^{11,12}

IFN- α 2 and IFN- γ levels were quantified using a Quanterix Homebrew Simoa assay kit in accordance with the manufacturer's instructions.⁴ The IFN signature (high or low) was assessed using whole blood transcriptome through a computed IFN score that represented the aggregate expression of five key IFN genes (*IFI44*, *IFI44L*, *IFIT1*, *IFIT3*, and *MxA*).⁴ Some of these biomarkers can be considered as more T cell related (IL-7 and TNF-RII), B cell related (BAFF, FLT-3, CXCL13, and β 2-microglobulin), or IFN related (CXCL10).

Outcome definition. In the prospective ASSESS cohort during the first 5 years, patients underwent an annual standardized clinical visit with a detailed case report form, enabling yearly assessment of ESSDAI and EULAR Sjögren's Syndrome Patient Reported Index (ESSPRI). Disease activity states were defined according to previously described ESSDAI thresholds¹⁵: low activity (ESSDAI < 5), moderate activity ($5 \leq \text{ESSDAI} \leq 13$) and high activity (ESSDAI ≥ 14). In addition, we defined a "no systemic activity" state (ESSDAI = 0). The patient-acceptable symptom state (PASS) was defined as an ESSPRI < 5 as previously described.¹⁵

We collected the new prescription of immunosuppressant during the 5-year follow-up, which is a good proxy of cumulative activity of the disease and thus of disease progression. We also collected the occurrence of lymphoma during a 15-year period.

Statistical analysis. For descriptive analyses, cytokine levels were presented as medians (interquartile ranges [IQRs]) and were compared across the three clusters with the Kruskal-Wallis rank sum test. We also performed pair-wise Wilcoxon rank sum tests to compare two-by-two clusters. The IFN signature (high or low) was compared with the Pearson chi-square test.

In addition, to describe the disease evolution according to the IFN signature in the subgroup, we presented the proportion of each disease activity state and PASS at each yearly follow-up visit in the first 5 years of follow-up in the ASSESS cohort, according to the IFN signature in each cluster. Changes within different activity states and PASSs were illustrated with alluvial diagrams, and comparisons were made with analyses of variances for repeated measures.

In addition, we assessed in each cluster the associations between the IFN signature and the risk of new immunosuppressant prescription, a surrogate marker of disease activity. We also assessed the risk of incident lymphoma. These risks were calculated with survival analysis and Cox proportional hazards regression models to determine hazard ratios (HRs) and their 95% confidence intervals (CIs). Patients contributed person-time from the date of enrollment in the ASSESS cohort until the date of the occurrence of the lymphoma (or new

immunosuppressant treatment), death, end of follow-up, or loss to follow-up, whichever occurred first. A two-tailed $P \leq 0.05$ was considered statistically significant. All analyses were performed with R (version 4.3.1).

Data availability. Anonymized data from both cohorts, along with the data dictionary, are available on publication. All requests for access must be directed to Dr Mariette. Data transfer will be subject to an access protocol and will require authorization from the scientific board from the Paris-Saclay or the ASSESS cohort. Furthermore, data sharing will be contingent on a data sharing agreement before any transfer to ensure all users of the data adhere to the legal requirements of using personal data.

RESULTS

Study population. We included 385 patients from the ASSESS cohort in the study. Their demographic characteristics, subjective symptoms (according to the ESSPRI), systemic manifestations (according to the ESSDAI domains), biologic data, and data according to the three clusters are presented in Supplementary Table 1. As previously reported, patients in the BALS cluster were younger, had lower ESSPRI scores (median 4.7; IQR 3–7), had higher IgG levels, and more frequently had positive rheumatoid factors, whereas patients from the HSA group were more systemic (median ESSDAI 8; IQR 3–13), and patients from the LSAHS group had lower ESSDAI (median 0; IQR 0–2) but higher ESSPRI (median 6.0; IQR 5.3–7.2) and less frequent anti-SSA antibody positivity (41% vs 68% in the BALS cluster).

Cytokine levels. We evaluated the level of 12 cytokines and chemokines at baseline in all patients included in the ASSESS cohort. Comparisons of cytokine levels among the three groups are presented in Figure 1. Regarding cytokines involved in the T cell pathways, we found higher rates of IL-7 in the BALS (5.9 pg/mL vs 3.8 mg/L; $P < 0.001$) and HSA groups (5.6 pg/mL vs 3.8 mg/L; $P < 0.05$) compared with the LSAHS group without a statistically significant difference between the BALS and HSA groups. Similar results were found regarding TNF-RII levels, which were higher in the BALS (230 ng/mL vs 165 ng/mL; $P < 0.001$) and HSA groups (223 ng/mL vs 165 ng/mL; $P < 0.001$) compared with the LSAHS group, without a difference between the two first clusters. No difference was found in CCL19 levels across the three clusters.

For cytokines associated with B cell activation, we found higher rates of CXCL13 in both the BALS (118 pg/mL) and HSA clusters (114 ng/mL) compared with the LSAHS cluster (79 ng/mL, $P < 0.001$ for both comparisons) without a difference between the two first clusters. However, we found higher rates of FLT-3 in the HSA group compared with the BALS group (103 vs 93 pg/mL; $P = 0.001$) and higher rates of

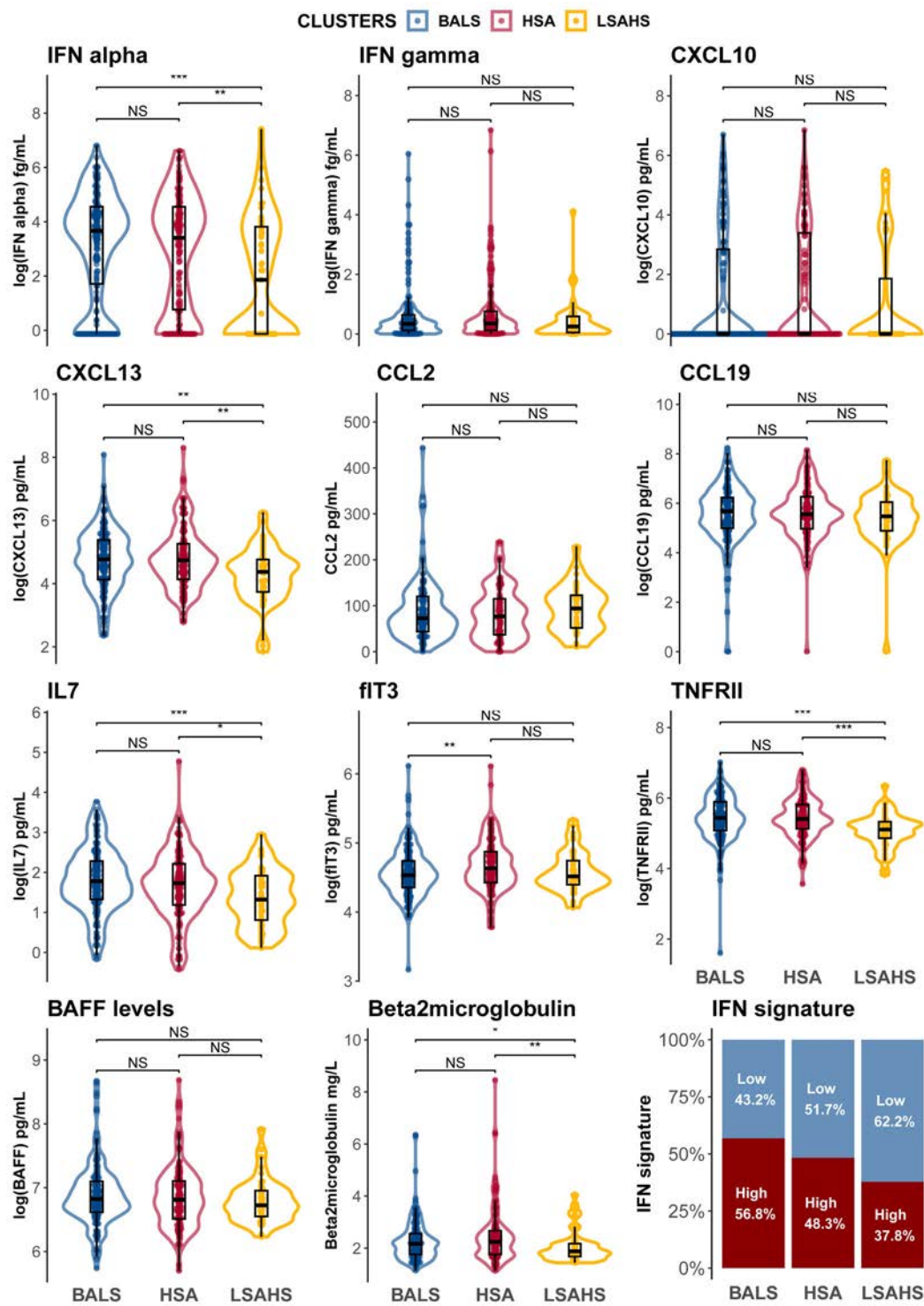


Figure 1. Comparison of cytokine levels and IFN signatures according to the three defined clusters: BALS, HSA, and LSAHS. Wilcoxon rank sum test *P* value intervals: NS *P* > 0.05; **P* value 0.01 to 0.05; ***P* value 0.001 to 0.01; ****P* < 0.001. IFN- α , IFN- γ , CXCL10, CXCL13, CCL19, IL-7, FLT-3, TNF-R11, and BAFF levels have been log-transformed for better visual representation. Log-transformation affects the absolute distance between two points but does not modify rank position, thus not affecting the Wilcoxon rank sum test. BALS, B cell active with low symptoms; FLT-3, fms-like tyrosine kinase 3 ligand; HSA, high systemic activity; IFN, interferon; IL, interleukin; LSAHS, low systemic activity with high symptoms; NS, not significant; TNF-R11, tumor necrosis factor receptor 2. [Correction added on 27 June 2025, after first online publication: Figure 1 has been updated.]

β 2-microglobulin in the HSA cluster (2.24 mg/L) compared with the LSAHS cluster (2.17 mg/L).

A high IFN signature was mainly found in the BALS cluster (57% vs 48% and 38% in the HSA and LSAHS clusters, respectively; $P = 0.05$) (Figure 1). The IFN signature was mainly driven by type I IFN with higher levels of IFN- α 2 in the BALS group (39 fg/mL) compared with the HSA (30 fg/mL) and LSAHS (6 fg/mL) groups (Figure 1).

Evolution of symptoms according to the IFN signature across the three clusters. The 5-year evolution of the proportion of patients with PASSs (ESPPRI < 5) according to the IFN signature in each subgroup is presented in Figure 2. In the BALS group, the proportion of patients with an ESSPRI > 5 increased during the 5 years of follow-up, both in patients with a high IFN signature (57% vs 48% at inclusion; $P < 0.001$) and in those with a low IFN signature (72% vs 54% at inclusion; $P < 0.001$). On the contrary, no substantial changes were found in the HSA and the LSAHS groups according to the IFN signature (Figure 2).

Systemic evolution and risks of new immunosuppressant and lymphoma according to the IFN signature across the three clusters. Changes in disease activity levels according to the IFN signature in each of the three clusters over the 5 years of ASSESS follow-up are presented in Figure 2. Although there were no substantial changes in the HSA and the LSAHS cluster at baseline and across follow-up, patients with a high IFN signature had higher levels of baseline activity in the BALS cluster (20% with moderate-to-high activity in the high IFN signature group vs 14% in the low IFN signature group). In the BALS cluster, there were no substantial changes in systemic activity, defined by the ESSDAI, across follow-up in those with a low IFN signature (23% with moderate-to-high activity at 5 years vs 14%; $P = 0.21$) and a high IFN signature (25% vs 20%; $P = 0.42$). However, in this cluster, a high IFN signature was associated with a higher risk of new immunosuppressant prescription (HR 9.38; 95% CI 1.22–72.16; $P = 0.0032$), which is a good proxy of cumulative activity and thus of disease progression. There were no differences according to the IFN signature in the HSA and the BALS clusters (Figure 3).

Finally, although there was no difference in lymphoma incidence according to the IFN signature in the HSA cluster, all lymphoma in the BALS cluster occurred in patients with a high IFN signature, although the difference was not statistically significant. No lymphoma occurred in the LSAHS cluster.

DISCUSSION

In this study, we found that the stratification of patients with SjD based on symptoms, clinical presentation, and routine biologic data is supported by distinct cytokine profiles. This supports

patients' stratification and consideration of their heterogeneity, particularly in therapeutic trials.

We found that the LSAHS cluster appeared different, with lower anti-SSA positivity rates but also lower levels of cytokines involved in T and B lymphocyte activation and a lower IFN signature. This cluster, which did not develop lymphoma during follow-up and had less systemic progression, thus seems to be a completely distinct profile with less systemic activity both at diagnosis and over time. On the other hand, the other two clusters (BALS and HSA) showed similarities in cytokine expression, with markers of T and B cell activity being higher than in the LSAHS cluster. We found higher levels of FLT-3 in the HSA group, a biomarker that has been previously found to be associated with HSA signs, such as the presence of purpura, low levels of C4, presence of lymphocytopenia, low levels of IgM, high levels of β 2-microglobulin, and a higher ESSDAI score, which are the hallmarks of the HSA group.¹¹ Interestingly, the main difference between BALS and HSA was the level of IFN signature.

Considering that patients in the BALS group were younger and incident lymphoma tended to appear later than in the HSA group, this suggests a potentially common pathophysiologic mechanism between the BALS and HSA groups. The BALS cluster could integrate into a "pre-HSA" cluster, potentially evolving similarly, as described in our study, with more systemic activity (defined by ESSDAI) and symptomatic progression (with an increase in ESSPRI over time). Thus, the challenge was to determine, within the BALS cluster, which patients could evolve into the HSA cluster to potentially consider closer monitoring or early treatment to prevent systemic complications.

We found a higher IFN signature in the BALS cluster compared with the other clusters, particularly mediated by the type I IFN pathway (with higher levels of IFN- α 2). Interestingly, the presence of this more pronounced IFN signature in the BALS group could raise the question of an earlier role for IFN in the immunopathology of SjD. It might raise the question of the opportunity of early anti-IFN strategy in at-risk patients. In addition, this signature was, interestingly, associated only in the BALS cluster with more baseline systemic activity and more systemic progression, reflected by the increased risk of immunosuppressive treatment over time, among BALS patients with a high IFN signature (whereas new prescription of immunosuppressants in the BALS cluster with a low IFN signature was rare). Similarly, in the BALS cluster, lymphomas exclusively occurred among patients with a high IFN signature. Thus, evaluating the IFN pathway could allow for more detailed and supervised stratification of BALS cluster patients and help predict patients at risk of disease evolution.

Previous studies have suggested that the activation of B cells could contribute to systemic complications in SjD, focusing on isolated serum markers (such as β 2-microglobulin, BAFF, or CXCL13) and past or current systemic complications, without concomitant assessment of disease activity and serum markers. Thus, it is not surprising to observe that the levels of these

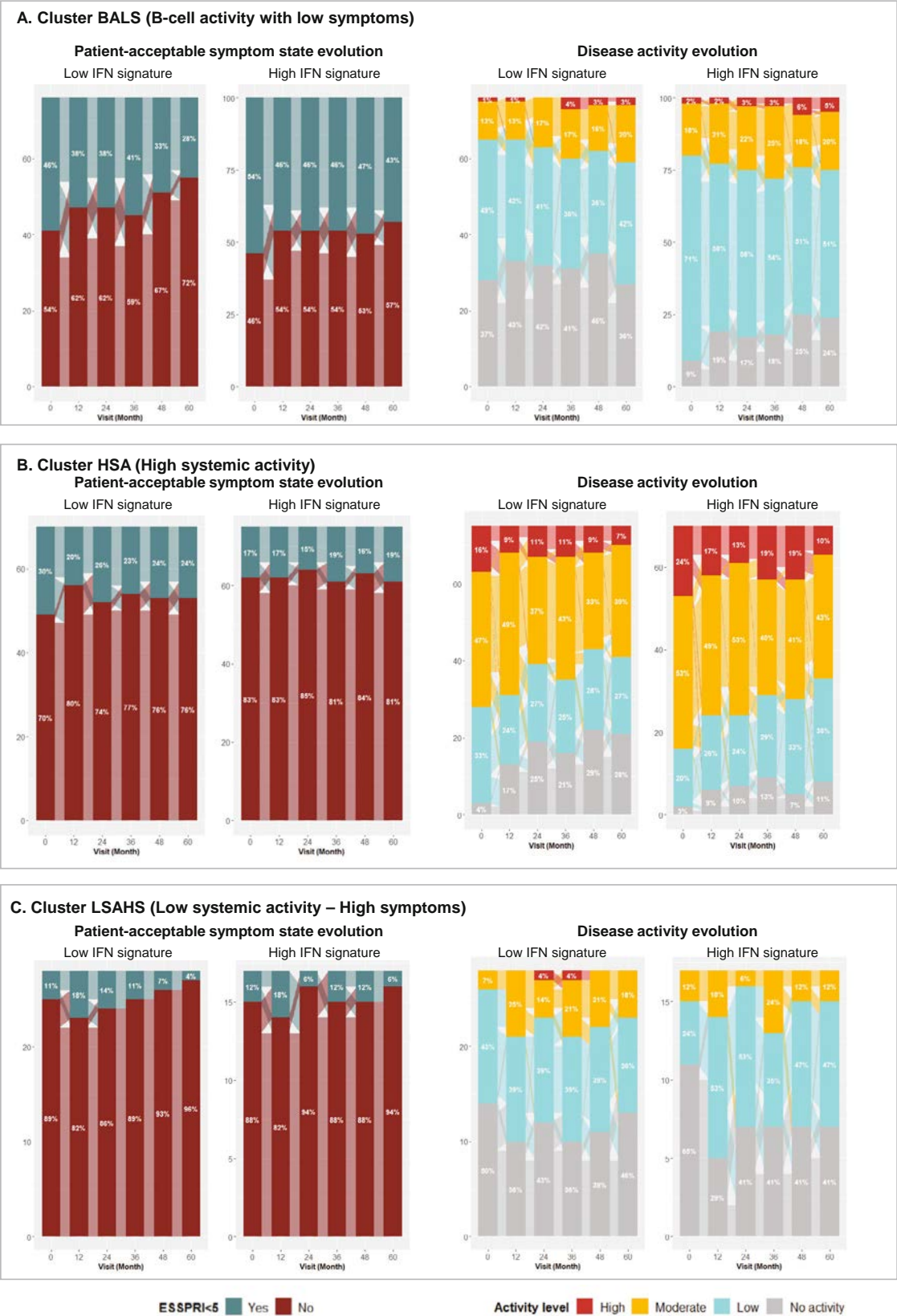


Figure 2. Evolution of patient-acceptable symptom state, defined by ESSPRI <5, and of disease activity level evolution according to the clusters (A, BALS; B, HSA; and C, LSAHS) and the IFN signature (low or high) in the Assessment of Systemic Signs and Evolution in Sjögren's Syndrome cohort (N = 385). Activity levels are defined as follows: no activity (ESSDAI = 0), low activity (ESSDAI < 5), moderate activity (5 ≤ ESSDAI ≤ 13), and high activity (ESSDAI ≥ 14). BALS, B cell active with low symptoms; ESSDAI, EULAR Sjögren's Syndrome Disease Activity Index; ESSPRI, EULAR Sjögren's Syndrome Patient Reported Index; HSA, high systemic activity; IFN, interferon; LSAHS, low systemic activity with high symptoms.

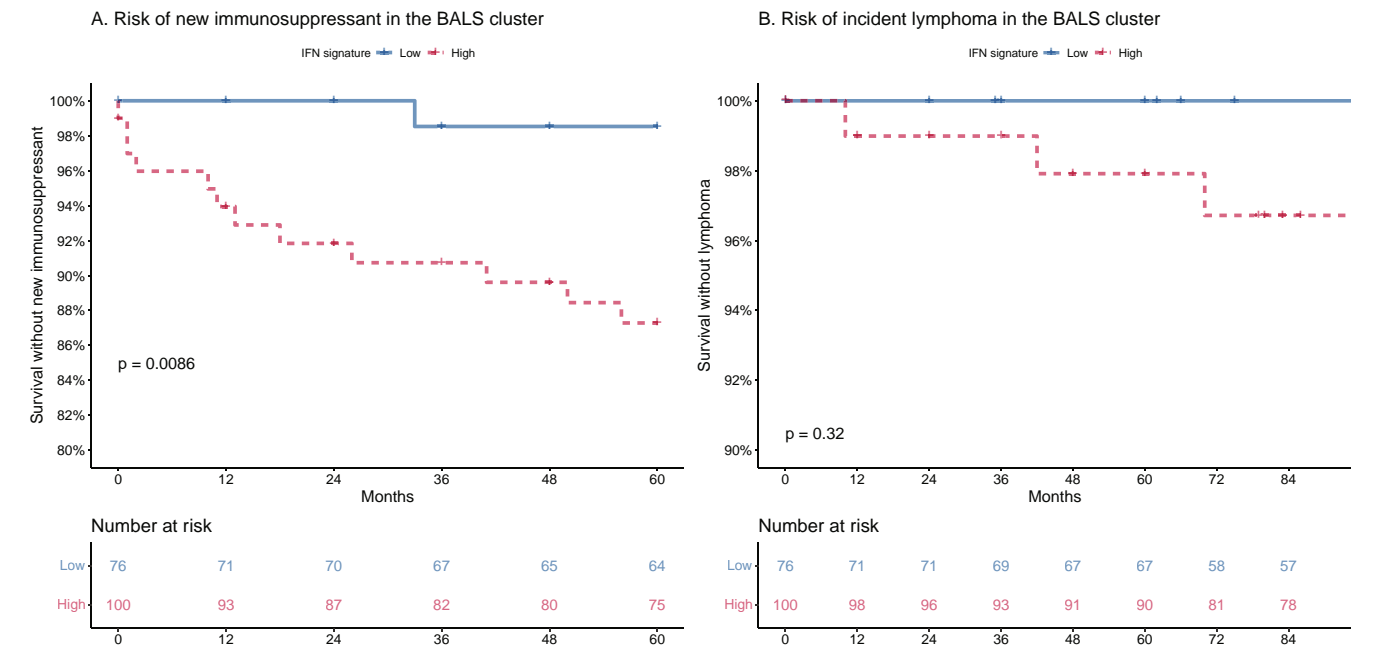


Figure 3. Kaplan-Meier curves estimating the risk of (A) incident lymphoma and of (B) new immunosuppressant prescription according to the IFN signature in the BALS cluster. *P* values were calculated by log-rank test. BALS, B cell active with low symptoms; IFN, interferon.

cytokines were highest in systemic clusters, particularly the HSA cluster, in which ESSDAI was highest. Regarding the IFN signature, evaluated across the entire cohort, it was also associated with a higher systemic activity. However, to our knowledge, this is the first description of the importance of the IFN signature in patients with biologic systemic activity but few symptoms, who are often excluded from therapeutic trials.

There are limitations to our study. Only a few cytokines were available and were evaluated only at inclusion in the ASSESS cohort. Further evaluations, including transcriptomic data, are ongoing, and clusters will be compared, which could lead to a better understanding of the pathophysiology. Nonetheless, this is a large-scale multicenter study, and the cytokines were measured centrally. In addition, we did not find any difference in the evolution of systemic activity in the BALS cluster, defined by ESSDAI, according to the IFN signature. Nevertheless, the evolution of the ESSDAI may be influenced by the treatments received by patients between the different evaluations (made once a year). We therefore assessed the risk of new immunosuppressant as a surrogate marker of systemic evolution.

Overall, our study demonstrated that our stratification, defined by symptoms, systemic clinical signs, and routine biologic data, is based on different pathophysiologic pathways, particularly B and T lymphocyte activation and the IFN α pathway. The latter could help predict the evolution of the BALS cluster, a biologic but minimally symptomatic cluster, to consider closer monitoring and/or early treatments to prevent complications. These findings also push for better stratification of therapeutic trials and contribute to the understanding of the heterogeneity of patients with SjD.

ACKNOWLEDGMENTS

The authors are indebted to all patients for their participation and to all physicians who included patients in the ASSESS cohort. The NECESSITY project has received funding from the Innovative Medicines Initiative 2 Joint Undertaking (IMI 2 JU; NECESSITY grant 806975). J-EG, VD-P, RS, XM, GN, and are members of the NECESSITY consortium.

AUTHOR CONTRIBUTIONS





All authors contributed to at least one of the following manuscript preparation roles: conceptualization AND/OR methodology, software, investigation, formal analysis, data curation, visualization, and validation AND drafting or reviewing/editing the final draft. As corresponding author, Dr Nocturne confirms that all authors have provided the final approval of the version to be published, and takes responsibility for the affirmations regarding article submission (eg, not under consideration by another journal), the integrity of the data presented, and the statements regarding compliance with institutional review board/Declaration of Helsinki requirements.

REFERENCES

1. Mariette X, Criswell LA. Primary Sjögren's syndrome. *N Engl J Med* 2018;379(1):97.
2. Beydon M, McCoy S, Nguyen Y, et al. Epidemiology of Sjögren syndrome. *Nat Rev Rheumatol* 2024;20(3):158–169.
3. The Lancet Rheumatology. Tackling heterogeneity in Sjögren's disease. *Lancet Rheumatol* 2024;6(4):e189.
4. Trutschel D, Bost P, Mariette X, et al; Milieu Intérieur Consortium, ASSESS study investigators, and NECESSITY Consortium. Variability of primary Sjögren's syndrome is driven by interferon- α and interferon- α blood levels are associated with the class II HLA-DQ locus. *Arthritis Rheumatol* 2022;74(12):1991–2002.

5. Soret P, Le Dantec C, Desvaux E, et al; PRECISESADS Clinical Consortium; PRECISESADS Flow Cytometry Consortium. A new molecular classification to drive precision treatment strategies in primary Sjögren's syndrome. *Nat Commun* 2021;12(1):3523.
6. Tam JR, Howard-Tripp N, Lendrem DW, et al; Leeds CTRU; French ASSESS cohort; UK Primary Sjögren's Syndrome Registry. Symptom-based stratification of patients with primary Sjögren's syndrome: multi-dimensional characterisation of international observational cohorts and reanalyses of randomised clinical trials. *Lancet Rheumatol* 2019;1(2):e85–e94.
7. McCoy SS, Woodham M, Bartels CM, et al. Symptom-based cluster analysis categorizes Sjögren's disease subtypes: an international cohort study highlighting disease severity and treatment discordance. *Arthritis Rheumatol* 2022;74(9):1569–1579.
8. Nguyen Y, Nocturne G, Henry J, et al. Identification of distinct subgroups of Sjögren's disease by cluster analysis based on clinical and biological manifestations: data from the cross-sectional Paris-Saclay and the prospective ASSESS cohorts. *Lancet Rheumatol* 2024;6(4):e216–e225.
9. Duret PM, Schleiss C, Kawka L, et al. Association between Bruton's tyrosine kinase gene overexpression and risk of lymphoma in primary Sjögren's syndrome. *Arthritis Rheumatol* 2023;75(10):1798–1811.
10. Nocturne G, Seror R, Fogel O, et al. CXCL13 and CCL11 serum levels and lymphoma and disease activity in primary Sjögren's syndrome. *Arthritis Rheumatol* 2015;67(12):3226–3233.
11. Tobón GJ, Saraux A, Gottenberg JE, et al. Role of Fms-like tyrosine kinase 3 ligand as a potential biologic marker of lymphoma in primary Sjögren's syndrome. *Arthritis Rheum* 2013;65(12):3218–3227.
12. Gottenberg JE, Seror R, Miceli-Richard C, et al; Data at Enrollment in the Prospective ASSESS Cohort. Serum levels of beta2-microglobulin and free light chains of immunoglobulins are associated with systemic disease activity in primary Sjögren's syndrome. Data at enrollment in the prospective ASSESS cohort. *PLoS One* 2013;8(5):e59868.
13. Vitali C, Bombardieri S, Jonsson R, et al; European Study Group on Classification Criteria for Sjögren's Syndrome. Classification criteria for Sjögren's syndrome: a revised version of the European criteria proposed by the American-European Consensus Group. *Ann Rheum Dis* 2002;61(6):554–558.
14. Rivière E, Pascaud J, Virone A, et al. Interleukin-7/interferon axis drives T-cell and salivary gland epithelial cell interactions in Sjögren's syndrome. *Arthritis Rheumatol* 2021;73(4):631–640.
15. Seror R, Bootsma H, Saraux A, et al; EULAR Sjögren's Task Force. Defining disease activity states and clinically meaningful improvement in primary Sjögren's syndrome with EULAR primary Sjögren's syndrome disease activity (ESSDAI) and patient-reported indexes (ESSPRI). *Ann Rheum Dis* 2016;75(2):382–389.

Proteomic Profiling of the Large-Vessel Vasculitis Spectrum Identifying Shared Signatures of Innate Immune Activation and Stromal Remodeling

Robert T. Maughan,¹  Erin Macdonald-Dunlop,¹ Lubna Haroon-Rashid,² Louise Sorensen,³ Natalie Chaddock,² Shauna Masters,⁴ Andrew Porter,¹ Marta Peverelli,¹  Charis Pericleous,¹ Andrew Hutchings,⁵ James Robinson,² Taryn Youngstein,¹ Raashid A. Luqmani,⁴ Justin C. Mason,[†] Ann W. Morgan,³  and James E. Peters¹ 

Objective. Takayasu arteritis (TAK) and giant cell arteritis (GCA), the most common forms of large-vessel vasculitis (LVV), can result in serious morbidity. Understanding the molecular basis of LVV should aid in developing better biomarkers and treatments.

Methods. Plasma proteomic profiling of 184 proteins was performed in two cohorts. Cohort 1 included patients with established TAK (n = 96) and large-vessel GCA (LV-GCA) (n = 35) in addition to healthy control participants (HCs) (n = 35). Cohort 2 comprised patients presenting acutely with possible cranial GCA (C-GCA) in whom the diagnosis was subsequently confirmed (C-GCA, n = 150) or excluded (Not C-GCA, n = 89). Proteomic findings were compared to published transcriptomic data from LVV-affected arteries.

Results. In cohort 1, comparison to HCs revealed 52 differentially abundant proteins (DAPs) in TAK and 72 DAPs in LV-GCA. Within-case analyses identified 16 and 18 disease activity-associated proteins in TAK and LV-GCA, respectively. In cohort 2, comparing C-GCA versus not C-GCA revealed 31 DAPs. Analysis within C-GCA cases suggested the presence of distinct endotypes, with more pronounced proteomic changes in the biopsy-proven subgroup. Cross-comparison of TAK, LV-GCA, and biopsy-proven C-GCA revealed highly similar plasma proteomic profiles, with 26 shared DAPs including interleukin 6 (IL-6), monocyte/macrophage-related proteins (CCL7, CSF1), tissue remodeling proteins (TIMP1, TNC), and novel associations (TNFSF14, IL-7R). Plasma proteomic findings reflected LVV arterial phenotype; for 42% of DAPs, the corresponding gene was differentially expressed in tissue.

Conclusion. These findings suggest shared pathobiology across the LVV spectrum involving innate immunity, lymphocyte homeostasis, and tissue remodeling. Network-based analyses highlighted immune-stromal cross-talk and identified novel therapeutic targets (eg, TNFSF14).

INTRODUCTION

Takayasu arteritis (TAK) and giant cell arteritis (GCA), the most common forms of large-vessel vasculitis (LVV) in adults,

are characterized by granulomatous arterial inflammation. Progressive damage to arterial walls typically results in stenotic remodeling with consequent tissue ischemia and manifestations such as sight loss, stroke, myocardial infarction, and limb

The views expressed herein are those of the authors and do not necessarily represent those of the NIHR or the Department of Health and Social Care.

Supported in part by the Medical Research Council (MRC) Treatment According to Response in Giant Cell Arteritis (TARGET) Partnership award (MR/N011775/1), the Medical Research Foundation (MRF-042-0001-RG-PETE-C0839), Vasculitis UK (V2105), MRC Confidence in Concept (Leeds), the National Institute for Health and Care Research (NIHR) Imperial Biomedical Research Centre (BRC), and the NIHR Leeds BRC (NIHR203331). The Temporal Artery Biopsy Versus Ultrasound in Diagnosis of Giant Cell Arteritis (TABUL) study was funded via an NIHR Health Technology Assessment grant. Dr Chaddock's work was supported by an MRC Discovery Medicine North (DiMeN) award. Dr Pericleous's work was supported by Versus Arthritis (Career Development Fellowship, 21223) and the Imperial College-Wellcome Trust Institutional Strategic Support Fund. Dr Morgan is an NIHR Senior Investigator (NIHR202395) and was supported by the NIHR Leeds BRC and was previously supported by the NIHR Leeds MedTech and Invitro

Diagnostics Co-operative and MRC TARGET Partnership grant. Dr Peters's work was supported by a Medical Research Foundation Fellowship (MRF-057-0003-RG-PETE-C0799).

¹Robert T. Maughan, PhD, Erin Macdonald-Dunlop, PhD, Andrew Porter, PhD, MRCP, Marta Peverelli, MSc, Charis Pericleous, PhD, Taryn Youngstein, MD, MRCP, James E. Peters, PhD, MRCP: Imperial College London, London, United Kingdom; ²Lubna Haroon-Rashid, BSc, Natalie Chaddock, PhD, James Robinson, PhD: University of Leeds, Leeds, United Kingdom; ³Louise Sorensen, PhD, Ann W. Morgan, PhD, FRCP: University of Leeds and NIHR Leeds Biomedical Research Centre, Leeds Teaching Hospitals NHS Trust, Leeds, United Kingdom; ⁴Shauna Masters, RGN, Raashid A. Luqmani, DM, FRCP: University of Oxford, Oxford, United Kingdom; ⁵Andrew Hutchings, MSc: London School of Hygiene & Tropical Medicine, London, United Kingdom.

[†]Dr Mason is deceased.

Drs Maughan and MacDonald-Dunlop contributed equally to this work. Drs Mason, Morgan, and Peters contributed equally to this work.

claudication.¹ Despite phenotypic similarities, TAK and GCA have different demographics, particularly age at onset, and, to a lesser extent, they affect different arterial territories. TAK affects the aorta and its major branches, whereas traditionally GCA was described as involving the cranial arteries such as the temporal artery (a pattern of disease now referred to as cranial GCA [C-GCA]). However, following advances in noninvasive vascular imaging techniques, it became clear that the aorta and other large vessels are frequently affected in GCA, and some patients have a large-vessel-type presentation (large-vessel GCA [LV-GCA]) with non-specific constitutional symptoms and/or limb claudication similar to TAK.^{2,3} Frequent large-vessel involvement in GCA and similar histopathologic changes has led to debate regarding whether TAK and GCA represent varying manifestations of the same disease.^{4,5} This question has important implications for drug development and clinical trial design. However, such comparisons are currently limited by an incomplete understanding of the pathogenic underpinnings of these diseases and a lack of comparative molecular data across LVV phenotypes.

There are several important challenges in the clinical management of TAK and GCA. Both initial diagnosis and recognition of relapse may be delayed and are made more difficult by a lack of effective biomarkers.⁶ Blood tests such as C-reactive protein (CRP) lack specificity, whereas vascular imaging can be insensitive, particularly in glucocorticoid-treated patients, and impractical for frequent serial monitoring.^{7,8} In the era before widespread access to ultrasound scans (USS), the diagnosis of C-GCA was confirmed by performing a temporal artery biopsy (TAB). Although considered the “gold standard” diagnostic test, the presence of skip lesions may lead to false-negative results. Therefore, a negative biopsy does not exclude the diagnosis of GCA. Progress in the treatment of LVV, particularly the development of targeted biologic therapy, lags behind that of other rheumatic diseases. Accordingly, there is an overreliance on long-term glucocorticoids to maintain disease control with resulting iatrogenic harm.^{9,10} Thus, there is a need for better biomarkers and novel therapeutics to improve patient outcomes.

Proteomic profiling has the potential to address these challenges.¹¹ Proteins are the effector molecules of most biologic functions and the targets of most drugs. Given the proximity of arterial tissue to the circulation, blood-based proteomics is likely to be informative in LVV. Specifically, we hypothesized that the levels of inflammation- and cardiovascular-related proteins would provide a read-out of disease activity and arterial pathobiology in patients with LVV and enable the evaluation of molecular similarities and differences between GCA and TAK. To this end, we performed proteomic profiling of 184 circulating proteins in two

independent cohorts that included 281 patients with TAK, LV-GCA, or C-GCA. We identified protein signatures associated with each LVV type and with disease activity. Cross-disease comparison revealed a striking similarity between the proteomic profiles of active LVV types. Our data indicate the shared dysregulation of innate immune and tissue remodeling pathways and highlight the potential for therapeutics targeting immune-stromal cross-talk.

PATIENTS AND METHODS

Cohort 1 study participants. Patients with TAK or LV-GCA were recruited from the Hammersmith Hospital (Imperial College Healthcare NHS Trust, United Kingdom) between 2013 and 2020. Patients with TAK fulfilled EULAR/American College of Rheumatology (ACR) 2022 classification criteria,¹² and they all had typical patterns of arterial involvement in radiologic assessments. Patients with LV-GCA were >50 years old at onset with radiologic evidence of LVV, as defined previously.¹³ Three patients with LV-GCA had concurrent temporal artery involvement (confirmed by temporal artery USS and/or TAB). Healthy control participants (HCs) were recruited locally from hospital and college staff and had no history of inflammatory or cardiovascular disease. Citrate blood samples were centrifuged at 1,000g for 10 minutes within four hours of venipuncture, and plasma was stored at -80°C until use. Disease activity was assessed using the Indian Takayasu Clinical Activity Score (ITAS2010) for TAK¹⁴ and the National Institutes of Health (NIH) score for LV-GCA.¹⁵ Active disease was defined by an ITAS2010 score ≥ 1 or ITAS-CRP score ≥ 2 for TAK and by an NIH score ≥ 2 for LV-GCA. All inactive cases were retrospectively confirmed to be relapse free for one year following sample collection. For the purpose of further investigation within inactive TAK cases, “durable clinical remission” was defined as the following: (1) absence of all signs, symptoms, and laboratory features attributable to active TAK (as per the EULAR definition¹⁶); (2) absence of arterial progression on serial vascular imaging; (3) criteria 1 and 2 sustained for the past three years; and (4) successful cessation of all immunosuppressive treatment. Patients and HCs provided written informed consent, and samples were collected as a subcollection registered with the Imperial College Healthcare Tissue Bank (license: 12275; National Research Ethics Service approval 17/WA/0161).

Cohort 2 study participants. The Temporal Artery Biopsy Versus Ultrasound in Diagnosis of GCA (TABUL) was an international, multicenter, prospective study that compared the

Additional supplementary information cited in this article can be found online in the Supporting Information section (<https://acrjournals.onlinelibrary.wiley.com/doi/10.1002/art.43110>).

Author disclosures are available at <https://onlinelibrary.wiley.com/doi/10.1002/art.43110>.

Address correspondence via email to Robert T. Maughan, PhD, at r.maughan@imperial.ac.uk; to Ann W. Morgan, PhD, FRCP, at a.w.morgan@leeds.ac.uk; or to James E. Peters, PhD, MRCP, at j.peters@imperial.ac.uk.

Submitted for publication October 20, 2024; accepted in revised form January 3, 2025.

sensitivity and specificity of temporal artery ultrasound to biopsy in 381 patients with suspected C-GCA¹⁷ (ClinicalTrials.gov identifier: NCT00974883). Reference diagnosis of C-GCA or Not C-GCA at six months was based on a combination of baseline signs and symptoms, blood tests, TAB, fulfillment of ACR 1990 GCA classification criteria¹⁸, clinical course during the follow-up period, final consultant diagnoses, and verification by an expert review panel, as described previously.¹⁷

Cranial ischemic complications were defined as permanent ocular or nonocular conditions at presentation. Ocular complications included the following: anterior ischemic optic neuropathy, branch retinal artery occlusion, cilioretinal artery occlusion, cranial nerve palsy (third, fourth, or fifth), central retinal artery occlusion, posterior ischemic optic neuropathy, relative afferent pupillary defect, irreversible visual loss, irreversible visual field defect, irreversible ocular motility or irreversible diplopia. Nonocular cranial complications included the following: scalp necrosis, tongue necrosis, and cerebrovascular accident at presentation considered secondary to GCA. Polymyalgic symptoms at presentation are also reported but do not represent a confirmed diagnosis of polymyalgia rheumatica (PMR).

Citrated blood samples were collected as soon as feasible after starting glucocorticoid treatment (median 2 days, interquartile range [IQR] 1–4 days) and were centrifuged at 2,500g for 15 minutes within 1.5 hours of collection, and plasma was stored at -80°C until use. Because of funding constraints and biosample availability, we performed Olink proteomic assays on 239 patient samples of the 381 patients recruited to TABUL. We included all available samples from patients with a diagnosis of C-GCA. We selected a subset of sex- and age- (± 5 years) matched patients without C-GCA such that the ratio of C-GCA to Not C-GCA was approximately 2:1. As part of the study design, we selected an equal proportion of patients with cranial ischemic complications in the Not C-GCA group as in the C-GCA group. Overall study approval was granted by the Berkshire Research Ethics Committee (09/H0505/132), and approval was also granted at local participating clinical sites.

Proteomic analysis. A total of 184 proteins were measured by proximity extension assay using two Olink Target panels, “Inflammation 1” and “Cardiometabolic,” at the Leeds Immunogenomics Facility, University of Leeds. To provide a succinct and standardized nomenclature, we report proteins by the symbols of the genes encoding them (see Supplementary Data 1 for a full list of proteins and associated full names and accession numbers). Cohort 1 and 2 samples were processed and analyzed independently, but proteomic measurements were performed in the same facility. We designed assay plates such that samples were balanced across plates according to disease grouping and disease activity status, with randomization to determine well position within plates. Proteomic data were normalized using

standard Olink workflows, which includes interplate normalization, to produce measures of relative protein abundance (“Normalised Protein eXpression [NPX]”) (\log_2 scale). For visualization, we transformed to Z scores (mean = 0, SD = 1). Because of a technical fault with a PCR machine during the running of one plate on the Inflammation 1 panel for cohort 2, it was necessary to rerun this plate as a separate batch. Principal component analysis (PCA) revealed a batch effect, with samples from this plate separated from samples on the other three plates run as part of the first batch. We therefore adjusted for this batch effect for proteins measured on the Inflammation 1 panel in cohort 2, using batch (a binary variable) as a covariate in linear model based differential abundance analyses. For situations requiring batch-correction outside of differential abundance testing (eg, visualization of protein levels using violin plots and heatmaps and network analyses), the residuals from the linear model (in Wilkinson notation) $\text{NPX} \sim \text{batch}$ were used to generate batch-corrected protein values. Further PCA of these residuals confirmed that the batch effect had been removed. The residuals were then converted to Z scores before visualization or other downstream analyses. Cardiometabolic panels for cohort 1 were not affected by this issue and were analyzed as a single batch.

Proteins with >75% of samples below the lower limit of detection were removed, resulting in 158 and 167 protein measurements for cohort 1 and 2, respectively. Sample-level quality control (QC) was performed using internal assay controls, boxplots of relative protein abundance values and PCA for outlier detection. In cohort 1, three samples (1 HC sample and 2 TAK samples) were excluded from Inflammation 1 panel measurements because of amplification failures. In cohort 2, 15 samples (9 C-GCA samples and 6 not C-GCA samples) were excluded from the Inflammation 1 panel measurements, and 3 samples (all C-GCA) were excluded from the Cardiometabolic panel measurements because of amplification failures and flagged status in internal QC checks. When possible, all available data were analyzed (eg, differential abundance analyses), but some analyses (eg, hierarchical clustering, PCA, multiple linear regression vs clinical parameters) necessitated using only complete data.

Differential protein abundance was performed using linear models (*lm* function in R). For a given protein, protein abundance was regressed on disease status (encoded as 0 or 1). The beta coefficient for the disease status term represents the estimated \log_2 fold change ($\log_2\text{FC}$) in the protein level between groups under comparison. For example, for the analysis of TAK versus HCs, the regression model was $\text{NPX} \sim \text{D}$, in which NPX was \log_2 protein level (continuous variable) and D was a binary variable, encoded as 0 for HC and 1 for TAK. Correction for multiple testing (multiple proteins) was performed using the Benjamini-Hochberg method (via the *p.adjust* function in R), and an adjusted *P* value of <0.05 (ie, false-discovery rate <5%) was defined as significant.

Protein annotation. The 184 proteins measured were highly enriched for pathways related to immune function and the cardiovascular system, as demonstrated by Reactome pathway overrepresentation analysis (Supplementary Data 2). Because of this enrichment, proteins were manually classified as “cytokine related,” “growth factor related,” “chemokine, other immune/inflammatory related protein,” “extracellular matrix related,” or “other function” to facilitate the annotation of differential abundance results. This was done using a combination of public resources including Gene Ontology terms, pathway, and functional databases. The full list of proteins and associated classifications is provided in Supplementary Data 1.

Network analysis. The protein–protein interaction network between LVV-associated proteins with directionally concordant changes across LVV types was constructed using high-confidence interactions (confidence ≤ 0.9) sourced from the Search Tool for the Retrieval of Interacting Genes/Proteins (STRING).¹⁹ No additional filtering of interactions was performed. The protein coexpression network was created using interprotein correlation of abundance values. Node edges were defined as Pearson $r \geq 0.6$. Cohort 1 (TAK and LV-GCA) and cohort 2 (C-GCA) networks were computed individually and then intersected so that only correlations present in both networks feature in the final network. Both networks were plotted using the igraph package in R.²⁰

Tissue gene expression of LVV-associated proteins.

Bulk RNA sequencing (RNA-seq) data from human tissues were accessed from the Genotype-Tissue Expression (GTEx) database as median transcripts per million values per tissue.²¹ Data preprocessing included the following: removal of sex-specific organ data (ie, cervix, breast, vagina, testis, fallopian tubes), removal of purified cell data (eg, cultured fibroblasts), and when there were multiple sample types per tissue group (eg, artery-coronary or artery-aorta), the highest expression value was used for that tissue type. Enhanced tissue expression was defined as more than four-fold higher than the average expression in other tissues, as done previously by the Human Protein Atlas.²²

RNA-seq analysis of LVV arterial tissue. A previous study compared the transcriptomic profile of inflammatory and noninflammatory aortic aneurysms using bulk RNA-seq.²³ Gene-level count data were accessed and filtered for cases of inflammatory aneurysm associated with GCA ($n = 8$) for comparison with noninflammatory cases ($n = 25$). Data were normalized, genes with low expression were removed, and groups were compared using the standard edgeR package methodology.²⁴ Differentially expressed genes (DEGs) were defined using Benjamini-Hochberg adjusted $P < 0.05$. DEGs were then compared with LVV-associated plasma proteins regarding overlap and Pearson correlation of \log_2 FC in each disease.

Supervised learning. Predictive models to develop disease activity biomarkers in TAK and diagnostic markers in C-GCA were constructed using the *glmnet*²⁵ and *caret*²⁶ R packages. For these analyses, data were split into training and test sets. Modeling fitting was performed on the training set using five-fold cross-validation and performance and then evaluated in the test set. Full details are provided in the Supplementary Methods.

Other analyses and data and code availability.

Details of additional analyses are provided in the Supplementary Information File. The post QC proteomic data are available from figshare (<https://doi.org/10.6084/m9.figshare.26928211.v1>). The raw proteomic data and the R code for QC and differential abundance analysis are available from Github (https://github.com/r-maughan/LVV_Olink).

RESULTS

To identify proteins associated with LVV and to evaluate the presence of shared or distinct molecular signatures across TAK, LV-GCA, and C-GCA, we measured plasma levels of 184 inflammation- and cardiovascular-related proteins (Supplementary Data 1) in two independent cohorts using the Olink Target antibody-based proximity extension assay (Figure 1). To provide a standardized nomenclature, we report proteins using the nonitalicized Human Genome Organisation gene symbol of the encoding gene.

Shared plasma proteomic profiles in TAK and LV-GCA.

Cohort 1 included 96 patients with TAK, 35 patients with LV-GCA, and 35 HCs (Supplementary Table 1). Patient characteristics were typical for TAK and LV-GCA regarding age and sex, with younger onset and greater female to male ratio in TAK. HCs were well matched in terms of demographics to the patients with TAK. Patients with LV-GCA were older and had a higher proportion of individuals of White European ancestry. The patient samples analyzed encompassed a broad range of disease activity, disease duration, and treatment status, particularly in TAK, in which sample size was greater. Patients with active disease tended to have shorter disease durations and were receiving higher glucocorticoid doses, as might be expected (Supplementary Data 3). In cohort 1, 158 proteins (86%) passed QC parameters (see the Methods section) and were available for analysis.

Comparison of proteomic profiles between patients with TAK and HCs identified 52 differentially abundant proteins (DAPs), with 42 up-regulated and 10 down-regulated (Figure 2A and Supplementary Data 4). Cross-referencing of our results to those of a previous study,²⁷ which used a different proteomic platform, demonstrated that many of our proteomic associations were novel (Supplementary Figure S1, Supplementary Data 4). We next compared LV-GCA to HCs, revealing 72 DAPs, with 60 increased

Cohort 1

Cohort 2

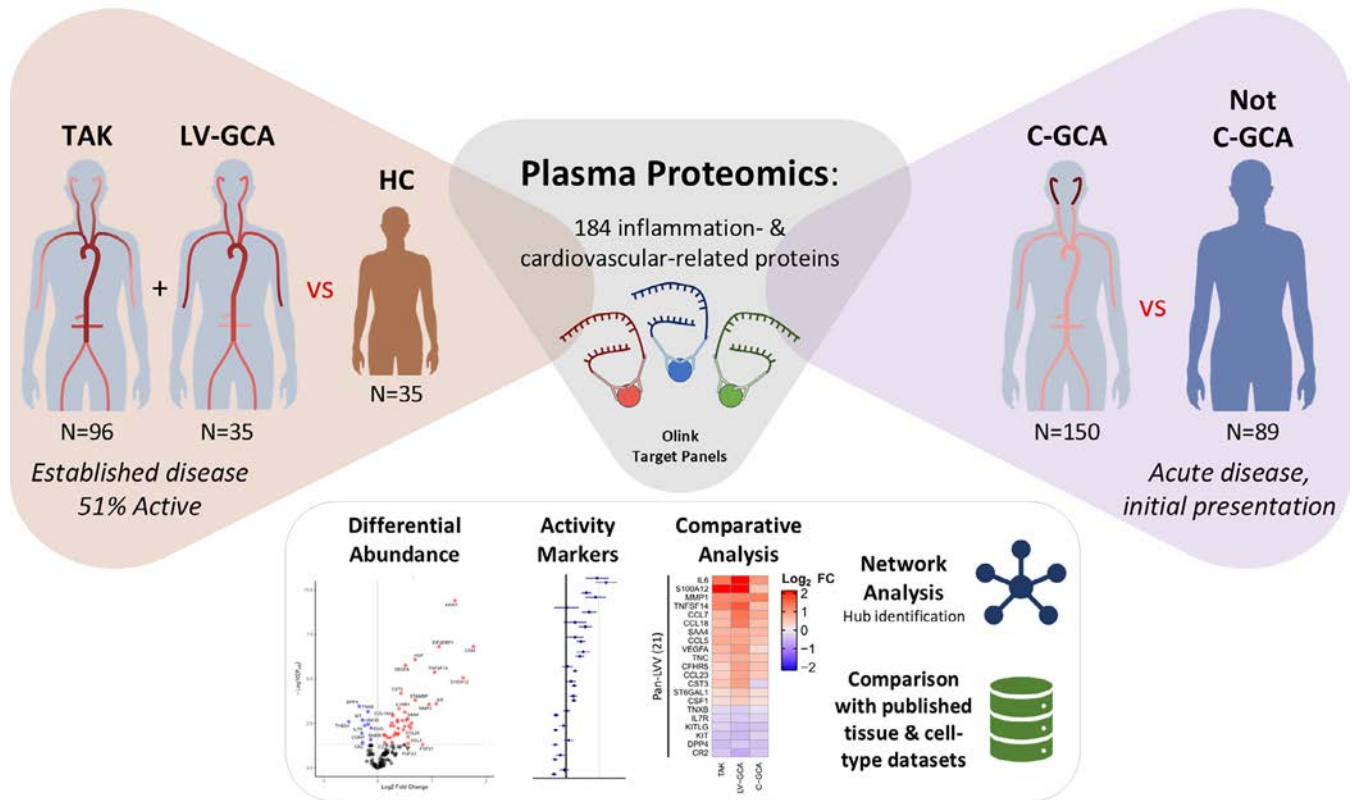


Figure 1. Study overview. Schematic overview of study to investigate the plasma proteomic changes associated with each form of LVV in two independent cohorts. Cohort 1: patients with established TAK and LV-GCA and HC participants. Cohort 2: patients presenting acutely with possible cranial giant cell arteritis in whom the diagnosis was subsequently confirmed (C-GCA) or ruled out (Not C-GCA). Disease-specific proteomic profiles defined by differential abundance analysis were compared. Network-based analysis of LVV-associated proteins and integrated analysis with published tissue and cell-type data sets was also conducted. C-GCA, cranial giant cell arteritis; HC, healthy control participant; ILV-GCA, large-vessel giant cell arteritis; LVV, large-vessel vasculitis; TAK, Takayasu arteritis.

and 12 decreased (Figure 2B and Supplementary Data 5). The proteomic changes in TAK and LV-GCA in comparison to HCs were highly similar; 40 proteins were significantly altered in both diseases, and 85% of all proteins had directionally concordant changes with respect to HCs (Figure 2C and D). Proteomic similarity of TAK and LV-GCA was also reflected in PCA, with TAK and LV-GCA clustering together and separated from HCs (Supplementary Figure S2A).

As expected, many up-regulated proteins in TAK and LV-GCA indicated immune activation including cytokines, chemokines, and growth factors (Supplementary Figure S2B). Plasma interleukin 6 (IL-6), the pleiotropic cytokine of known importance to LVV pathogenesis,¹³ was significantly up-regulated in both TAK and LV-GCA (Figure 2E), together with liver-derived inflammatory proteins such as SAA4 and FCN2. Prominent innate immune involvement in both TAK and LV-GCA was indicated by increased levels of neutrophil-derived proteins (S100A12, LCN2, DEFA1) and monocyte/macrophage activation and chemotactic factors (CSF1, CCL3, CCL5, CCL7, CCL14). Plasma levels of

tumor necrosis factor (TNF), IL-12B, and interferon γ were not significantly altered despite previous links to TAK pathogenesis.²⁸ In contrast, we observed large increases in oncostatin M (OSM) and TNF superfamily 14 (TNFSF14) (LIGHT), cytokines not previously associated with LVV (Figure 2E). In addition to the dysregulation of immune-related proteins, we observed the up-regulation of proteins with functions related to the extracellular matrix (TIMP1, MMP-1, CST3, TNC), fibrosis (TGFB1) and angiogenesis (VEGF-A, HGF, ANG, COL18A1) in both diseases, likely reflecting a signature of arterial injury and remodeling. Six proteins were consistently down-regulated in both diseases, including IL-7R, KIT, TNXB, and THBS4 (both extracellular matrix [ECM]-related glycoproteins), DPP4 (a glucose metabolism and T cell activation factor), and CR2 (the complement C3d receptor).

To evaluate whether there were disease-specific effects, we performed a direct comparison of TAK versus LV-GCA, which revealed six significant DAPs (Supplementary Data 6). Visualizing the relative abundance of these proteins in each group demonstrated that the dysregulation of these proteins

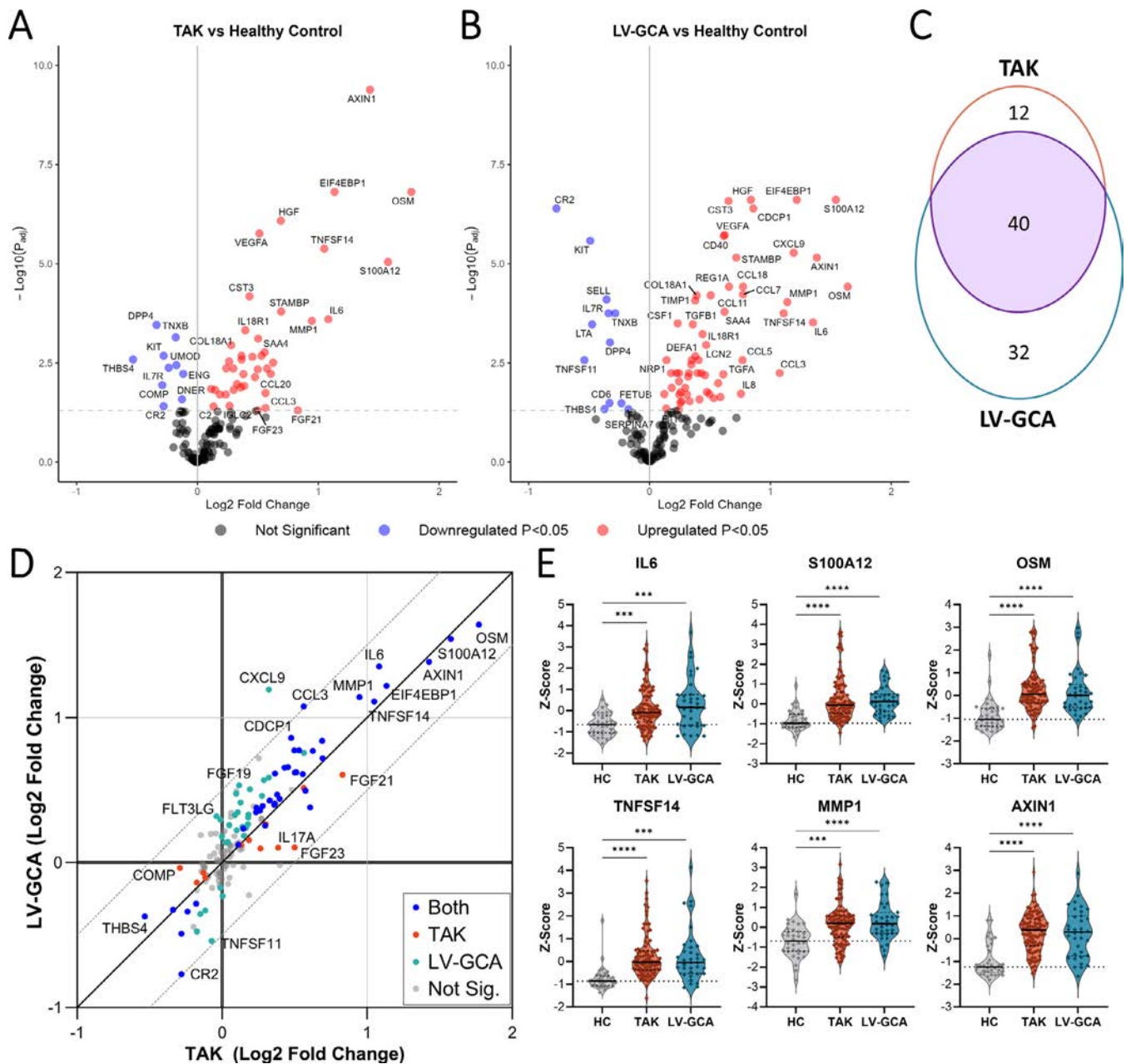


Figure 2. Plasma proteomic changes in TAK and LV-GCA compared to HCs. Volcano plots showing results of differential protein abundance analyses: (A) patients with TAK ($n = 96$) versus HCs ($n = 35$), (B) patients with LV-GCA ($n = 35$) versus HC. $-\log_{10}(P_{\text{adj}}) = -\log_{10}$ Benjamini-Hochberg adjusted P value. Red and blue indicate proteins that are significantly ($P_{\text{adj}} < 0.05$) up-regulated and down-regulated, respectively. (C) Venn diagram showing the overlap in proteins significantly altered in TAK versus HC compared to LV-GCA versus HC analyses. (D) Comparison of \log_2 fold changes in all proteins for TAK versus HC and LV-GCA versus HC analyses, diagonal lines represent line of identity and $\pm 0.5 \log_2$ fold change. Blue represents proteins that are significant in both analyses; orange represents proteins that are significant only in TAK versus HC; teal represents proteins that are significant only in LV-GCA versus HC; gray represents proteins that are nonsignificant in both analyses. (E) Violin plots showing scaled protein levels (as Z scores) for selected proteins with prominent changes in both TAK and LV-GCA. $P_{\text{adj}} < 0.05$: *, $P \leq 0.01$: **, $P \leq 0.001$: ***, $P \leq 0.0001$: ****. HC, healthy control; LV-GCA, large-vessel giant cell arteritis; Sig., significant; TAK, Takayasu arteritis. Color figure can be viewed in the online issue, which is available at <http://onlinelibrary.wiley.com/doi/10.1002/art.43110/abstract>.

appeared to be LV-GCA specific (Supplementary Figure S3A). For example, in LV-GCA, but not TAK, CXCL9, CCL11, and CA3, levels were elevated compared to HCs. Similarly, CR2 and TNFSF11 (RANKL) were significantly reduced in LV-GCA but not in TAK. Changes specific to TAK were less prominent,

with no proteins that had significant changes in TAK versus both HCs and LV-GCA. However, we observed that FGF23 and IL-17A were significantly increased in TAK compared to HCs but were not significantly increased in LV-GCA versus HC (Supplementary Figure S3B).

Signatures of active disease in patients with TAK and LV-GCA. To identify proteins associated with disease activity in TAK and LV-GCA, we next compared the proteomic profile of active and inactive patients within each disease. In TAK samples, 16 proteins were significantly altered in active disease, with 11 up-regulated and 5 down-regulated (Figure 3A and Supplementary Data 7). Up-regulated proteins included neutrophil-related factors (S100A12, CXCL5, CXCL1), liver-derived proteins (SAA4, CFHR5), ECM components (TNC, NID1, CRTAC1, COMP), and angiogenic factors (VEGF-A, ANG), indicating innate immune activation and vascular remodeling (Figure 3B). To corroborate the results of the active versus inactive patient analysis and identify proteins whose levels vary with the degree of disease activity, we tested for association with the numerical ITAS2010 disease activity score.¹⁴ Eight of the 158 proteins measured were significantly correlated (adjusted $P < 0.05$) with the ITAS2010 score (Supplementary Figure S4A and C), and 7 of these 8 were differentially abundant in the active versus inactive analysis.

Assessment of disease activity in TAK is currently based on the evaluation of clinical features, imaging, and clinical laboratory measures of inflammation, particularly CRP levels. However, CRP lacks both sensitivity and specificity for active TAK.⁷ In keeping with this, 20 patients with active TAK had normal CRP levels (<5 mg/L). We found that six proteins (NID1, TNC, S100A12, CD274 [soluble programmed death ligand 1], DEFA1, and DPP4) were more strongly correlated with ITAS2010 than CRP (Supplementary Figure S4). Motivated by this finding, we formally evaluated whether we could develop a multimarker protein signature using supervised learning to improve classification of disease activity (Supplementary Material). Using Least Absolute Shrinkage and Selection Operator (LASSO) regression, we generated a 10-protein signature that outperformed CRP (area under the curve [AUC] 0.8 vs 0.72, respectively; Supplementary Figure S5A and B). However, a simpler two-protein logistic regression model comprising CRP and COMP performed even better (AUC 0.9; Supplementary Figure S5C), demonstrating proof-of-principle that the addition of a single protein could provide improved and clinically tractable biomarker-based assessment of disease activity in TAK.

In LV-GCA, 18 proteins were significantly associated with active disease, with 17 increased and 1 decreased (Figure 3A, Supplementary Data 8). Although two proteins (CFHR5 and VEGF-A) were increased in active disease in both LV-GCA and TAK, the LV-GCA activity signature was mostly distinct to that of TAK (Figure 3A and C). A more prominent acute phase response was evident in active LV-GCA compared to TAK with large increases in IL-6 and multiple liver-derived inflammatory proteins (MBL2, ST6GAL1, C2) (Figure 3D). There were also differences in the chemokines and other immunoregulatory proteins affected; CXCL5 and CXCL1 levels were not significantly changed in active LV-GCA (Figure 3E), but there were increases in the monocyte-attracting chemokines (CCL7, CCL14, CCL23) and the T cell

recruitment and activation factors (CCL18, GNLy, TIMD4). Lastly, there were activity-associated increases in remodeling-associated proteins TIMP1, COL18A1, and NRP1 in LV-GCA but not TAK.

To determine whether proteomic differences persist despite clinically quiescent disease, we compared patients with inactive TAK and LV-GCA to HCs. This analysis identified 22 and 61 DAPs in inactive TAK and LV-GCA, respectively, with 18 DAPs being common to both diseases (Supplementary Figure S6A–C, Supplementary Data 9 and 10). Examples of proteins that remained elevated in inactive disease include OSM, S100A12, TNFSF14, and AXIN1 (Supplementary Figure S6D). Importantly, these proteins remained chronically elevated regardless of disease duration (Supplementary Figure S6E), even in patients with TAK who had withdrawn all treatment following durable clinical remission (Supplementary Figure S6D; median time off treatment 2 years [IQR 1.5–5.1 years], further details in Supplementary Data 11). Thus, our data indicate that some proteomic changes observed in patients with TAK and LV-GCA represent persistent molecular derangements that do not normalize with clinical remission.

Biopsy-proven C-GCA has a distinct proteomic endotype. We next performed proteomic profiling of an independent cohort of 239 patients presenting acutely with possible C-GCA (cohort 2), recruited to the TABUL study.¹⁷ Blood samples were taken rapidly following initiation of high-dose glucocorticoids; median treatment duration was 2 days (IQR 1–4 days). All patients underwent both TAB and USS, and a diagnosis of C-GCA was subsequently confirmed or excluded (Not C-GCA) as described in the Methods. Patient characteristics were typical for suspected C-GCA, with the majority of patients being more than 60 years old (87.4%), female (72%), and having White European ancestry (99.3%) (Supplementary Table 2). Of patients diagnosed with C-GCA, 56 patients (37.3%) had a positive TAB, 78 patients (52%) had an abnormal USS, and 53 patients (35.3%) were negative for both TAB and USS. Compared to the Not C-GCA group, patients with C-GCA were slightly older (median age 4 years greater) and had higher erythrocyte sedimentation rates (ESRs), CRP levels, and platelet levels (Supplementary Table 2). Proteomic profiling was performed using the same Olink platform as for cohort 1. A total of 167 proteins (91%) passed QC parameters, and data from a minimum of 225 patients were available for analysis (see the Methods section).

Proteomic comparison of C-GCA ($n = 150$) to Not C-GCA ($n = 89$) revealed 31 DAPs (Figure 4A and Supplementary Data 12). Further investigation revealed heterogeneity of these protein profiles within C-GCA and that differences compared to the Not C-GCA group were mostly driven by the TAB-positive (TAB+) C-GCA subgroup (Supplementary Methods, Supplementary Figure S7). In analyses stratified by TAB result, comparison of TAB+ C-GCA ($n = 56$) to Not C-GCA identified 62 DAPs (Figure 4B, Supplementary Data 13), whereas only 1 DAP was

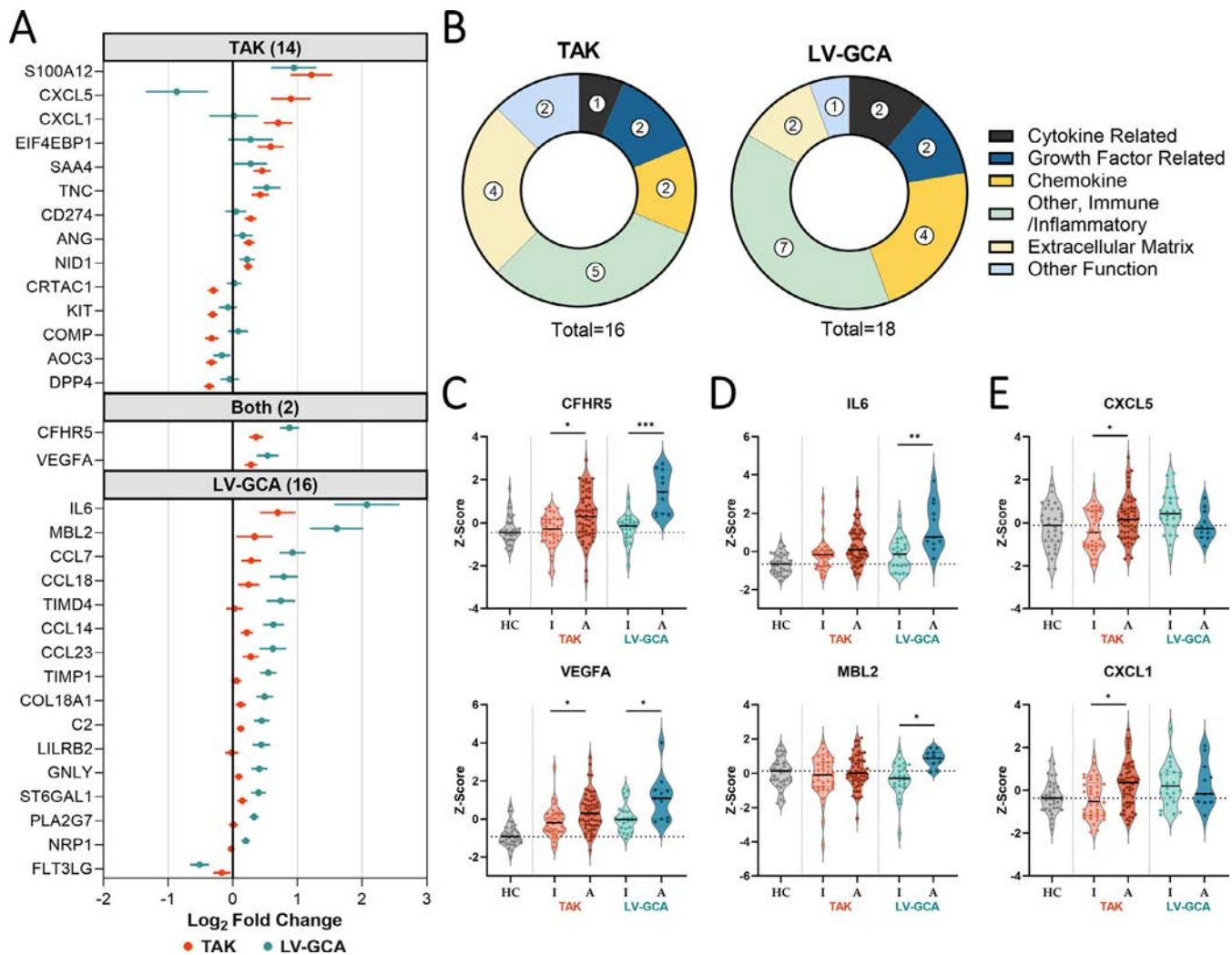


Figure 3. Proteins associated with active disease in TAK and LV-GCA. (A) Points indicating log₂ fold change estimate \pm SE (horizontal bars) for proteins that were significantly (adjusted $P < 0.05$) differentially abundant in the active versus inactive patient analysis for TAK only ($n = 56$ vs $n = 40$) (top panel), both diseases (middle panel) and LV-GCA only ($n = 11$ vs $n = 24$) (bottom panel). (B) Functional categories of differentially abundant proteins from TAK and LV-GCA activity analyses. Violin plots depict the scaled abundance values (Z scores) for proteins associated with disease activity in (C) both diseases and (D and E) for the proteins that had divergent associations with disease activity in TAK and LV-GCA. P values adjusted using Benjamini-Hochberg method; no symbol: nonsignificant, adjusted $*P < 0.05$, $**P \leq 0.01$, $***P \leq 0.001$. HC, healthy control; LV-GCA, large-vessel giant cell arteritis; TAK, Takayasu arteritis. Color figure can be viewed in the online issue, which is available at <http://onlinelibrary.wiley.com/doi/10.1002/art.43110/abstract>.

identified in the TAB-negative (TAB-) C-GCA ($n = 89$) versus Not C-GCA comparison (Supplementary Data 14). The increase in significant associations when limiting to biopsy-proven cases, despite reduction in sample size and statistical power, indicates that TAB+ C-GCA is enriched for proteomic signal and that the TAB- C-GCA group was diluting this signal in the analysis of all C-GCA versus not C-GCA. Comparison of the estimated log₂FCs and protein abundances from the TAB+ and TAB- stratified analyses confirmed larger magnitudes of effect in the former (Figure 4D and F). We additionally found that patients with TAB+ C-GCA had higher levels of CRP, ESR, platelets, and presence of polymyalgic symptoms compared to patients with TAB- C-GCA (Figure 4C and Supplementary Data 15). Moreover, PCA of

all proteins assayed indicated separation of TAB+ C-GCA from TAB- C-GCA (Supplementary Figure S7C). Together, these findings indicate that C-GCA can be stratified into biologically and clinically distinct subsets by TAB result.

Further exploration using hierarchical clustering revealed that although most TAB- C-GCA patients were proteomically distinct from patients with TAB+ C-GCA, 18 TAB- C-GCA patients displayed a similar profile to the TAB+ C-GCA group (Supplementary Figure S8). However, this pattern had no significant association with demographic or clinical parameters. Relatedly, the comparison of patients with TAB- C-GCA who had abnormal USS ($n = 36$) to patients without C-GCA did not identify any significant proteins. Together, these results

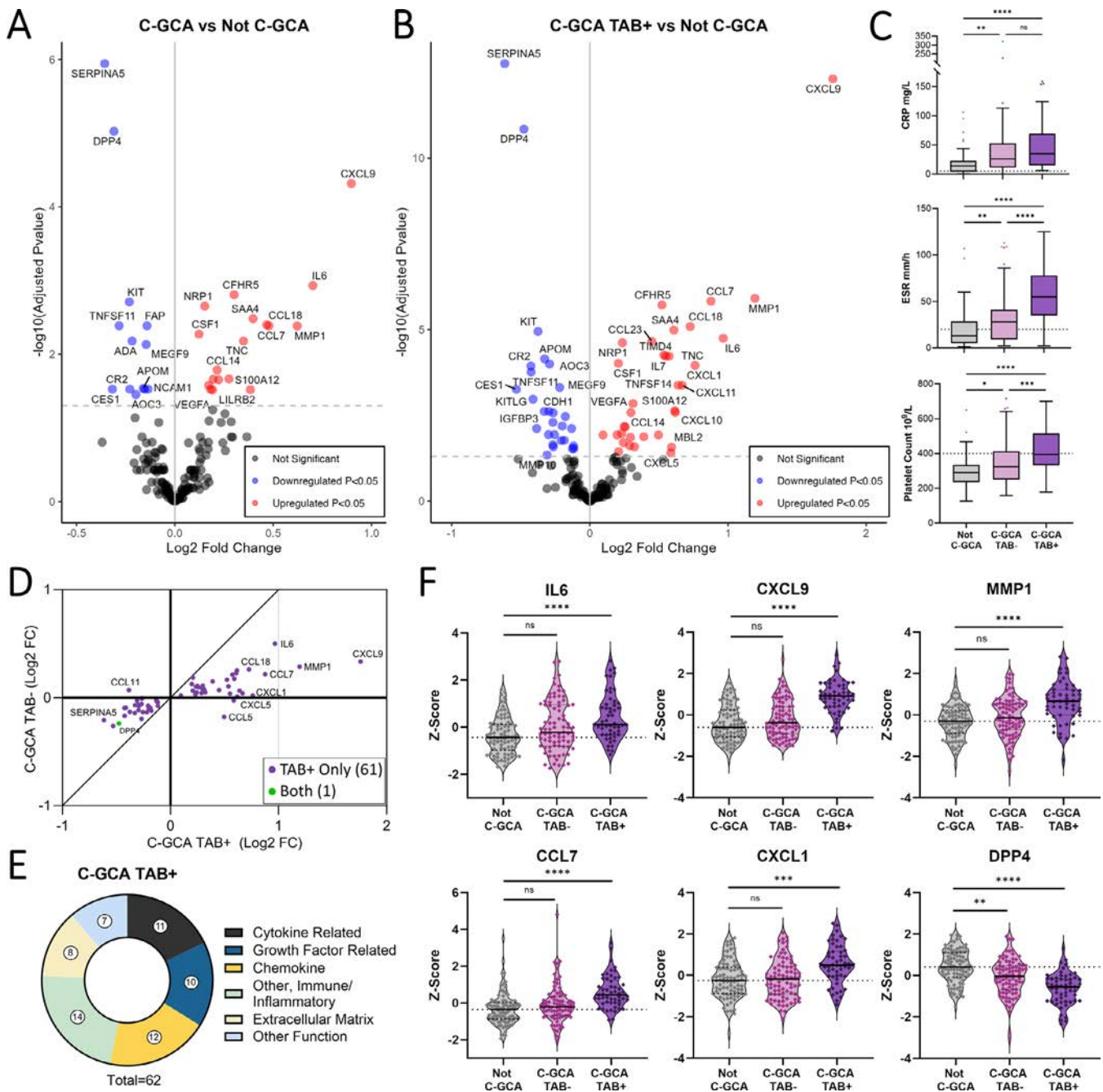


Figure 4. Proteomic changes associated with C-GCA are most pronounced in biopsy-proven disease. (A) Volcano plots for the differential protein abundance comparisons of C-GCA ($n = 150$) versus Not C-GCA ($n = 89$) and (B) for the comparison of TAB positive C-GCA (C-GCA TAB+, $n = 56$) versus Not C-GCA ($n = 89$). $-\log_{10}(P_{adj}) = -\log_{10}$ Benjamini-Hochberg adjusted P value. Red and blue indicate proteins that are significantly ($P_{adj} < 0.05$) up-regulated and down-regulated, respectively. (C) Boxplot showing CRP, ESR, and platelet count in Not C-GCA, TAB- C-GCA, and TAB+ C-GCA. Median and IQR represented by line and box edges respectively, upper whisker represents the upper quartile plus 1.5 times the IQR, lower whisker represents lower quartile minus 1.5 times IQR. Statistical comparisons made with Kruskal-Wallis and Dunn's post hoc tests. (D) Comparison of \log_2 fold changes for differentially abundant proteins in C-GCA TAB+ versus Not C-GCA and C-GCA TAB- versus Not C-GCA, diagonal line represents line of identity. (E) Functional categories of differentially abundant proteins in C-GCA TAB+ versus Not C-GCA comparison. (F) Violin plots showing scaled protein levels (Z score) for selected proteins with prominent changes in C-GCA TAB+ cases. Adjusted $**P < 0.05$, $****P \leq 0.0001$. C-GCA, cranial giant cell arteritis; CRP, C-reactive protein; ESR, erythrocyte sedimentation rate; IQR, interquartile range; ns, nonsignificant; TAB, temporal artery biopsy. Color figure can be viewed in the online issue, which is available at <http://onlinelibrary.wiley.com/doi/10.1002/art.43110/abstract>.

suggest that TAB rather than USS positivity more closely reflects the proteomic phenotype.

The 62 proteins associated with TAB+ C-GCA suggest both innate and adaptive immune activation with dysregulation of cytokines, growth factors, chemokines, and other immune-related proteins (Figure 4E). In a previous proteomic study,²⁹ five of these proteins were identified as significantly altered in C-GCA (Supplementary Figure S9 and Supplementary Data 13). Similar to TAK and LV-GCA, many proteins involved in innate immune function were up-regulated including acute phase response mediators (IL-6, MBL2, SAA4, CFHR5, ST6GAL1) and factors involved in neutrophil and monocyte migration and activation (CXCL1, CCL14, CCL7, S100A12, CSF-1). Several chemokines involved in T and B cell recruitment were also increased (CXCL9, CXCL10, CXCL11, CCL18) together with altered levels of lymphocyte survival and proliferation factors (increased: IL-7; decreased: IL-7R, KITLG, TNFSF11). In addition, increases in ECM (MMP-1, TIMP1, TNC, LTBP2), fibrosis (TGFB1) and angiogenesis-related proteins (VEGF-A, HGF, NRP1) were indicative of vascular remodeling. The down-regulated proteins with the lowest *P* values were SERPINA5 and DPP4 (Figure 4F). In secondary analyses, we did not identify any proteins that were significantly associated with cranial ischemic complications or polymyalgic symptoms within patients with C-GCA when analyzed both as a single group and when separated by TAB result.

Supervised learning to identify protein-based diagnostics for C-GCA. There are no specific diagnostic blood tests for C-GCA. Although ESR and CRP are typically elevated, they are nonspecific. For example, CRP was elevated (>5 mg/L) in 69% of patients in the Not C-GCA group in this study. We therefore tested whether a blood-based protein or proteomic biomarker could aid diagnosis of C-GCA, randomly splitting the data into training and test sets (Supplementary Material). Using logistic regression models, the best predictive univariate markers for biopsy-proven C-GCA were CXCL9, DPP4, and SERPINA5 (Supplementary Figure S10A, Supplementary Table 3). Despite having one of the larger estimated \log_2 FCs in the differential abundance analyses (Figure 4A and B), IL-6 was less effective as a predictor (Supplementary Table 3). We then explored whether predictive performance could be enhanced through a more sophisticated multivariate modeling approach. We supplied all proteins measured as input variables and trained a model using LASSO regression (which performs variable selection) and cross-validation. This resulted in an 11-protein model that provided improved diagnostic performance compared to the univariate models (accuracy 0.87, AUC 0.94) (Supplementary Figure S10B, Supplementary Tables 3 and 4). The most important features in the LASSO model were CXCL9, DPP4, and SERPINA5 (Supplementary Figure S10B), consistent with the findings of the univariate logistic regression analyses.

Correlated proteomic changes in active TAK, LV-GCA, and biopsy-proven C-GCA with IL-6 and VEGF-A identified as key hub proteins.

We next explored similarities and differences in the plasma proteomic signatures associated with each form of LVV. We considered the possibility that our results might be impacted by differences in study design. In cohort 2, patients with C-GCA were sampled with active disease at the time of diagnosis, whereas in cohort 1, patients were sampled during both active and inactive disease over a range of disease durations. To mitigate against this, we reanalyzed cohort 1 restricting patient samples to active disease only. These analyses revealed 68 and 69 DAPs for active TAK versus HCs and active LV-GCA versus HCs, respectively, of which the majority had also been significantly altered in the corresponding previous analyses using all cases (80.9% and 81.6% respectively, Supplementary Data 16 and 17). We then compared the results of these TAK and LV-GCA analyses to the proteomic associations identified in the TAB+ C-GCA versus not C-GCA comparison in cohort 2.

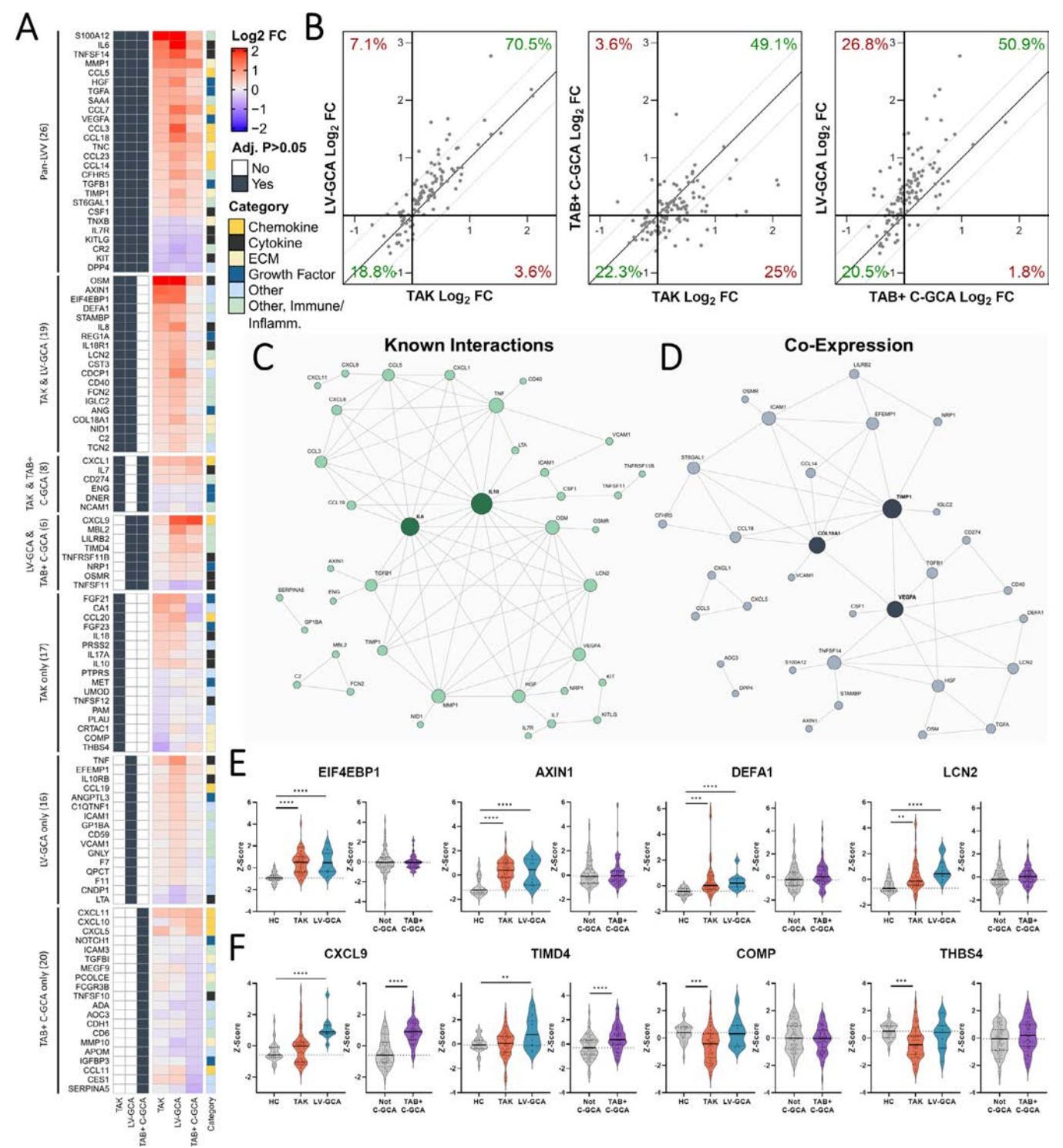
A total of 112 DAPs were identified in one or more LVV type (subsequently referred to as LVV-associated proteins, Figure 5A, Supplementary Data 18). Directional changes were highly similar with 74 (66.1%) having concordant changes (Figure 5B) and significant correlation between both TAK and LV-GCA profiles with that of TAB+ C-GCA (Pearson $r = 0.49$ and $r = 0.69$, respectively, both $P < 0.0001$). Twenty-six proteins (23.2%) were dysregulated in all three diseases and 33 proteins (29.5%) were dysregulated in two. Of the 26 shared DAPs, all had directionally concordant changes, including 20 up-regulated and 6 down-regulated proteins. We define these 26 proteins as the “pan-LVV signature” (Supplementary Data 18). Up-regulated proteins included IL-6, acute phase proteins (SAA4, CFHR5, ST6GAL1), monocyte and neutrophil factors (S100A12, CSF-1), monocyte and lymphocyte chemokines (CCL5, CCL7, CCL3, CCL18, CCL23), and TNFSF14. Levels of proteins related to arterial remodeling were also increased, including VEGF-A, HGF, MMP-1, TIMP1, and the ECM glycoprotein TNC. Down-regulated proteins included IL-7R, KIT, and KITLG, each involved in lymphocyte differentiation and proliferation, DPP-4, CR2, and TNXB (another ECM tenascin).

Using the GTEx tissue transcriptome database,²¹ we explored the global tissue expression profile of each LVV-associated protein, defining enhanced expression as more than four-fold higher than average tissue level as per Human Protein Atlas methodology.²² A total of 83 proteins (74.1%) had enhanced expression in ≥ 1 tissue. The most represented tissues were liver, spleen, and whole blood (Supplementary Figure S11). A total of 11 proteins had enhanced arterial expression including TNC, TIMP1, COL18A1, and TNFRSF11B (osteoprotegerin), thereby indicating the possibility of blood-based measurement of arterial biomarkers in LVV.

To infer relationships between proteins, we constructed two networks using the 74 proteins with concordant changes using

(1) annotated protein–protein interactions from STRING¹⁹ (Figure 5C) and (2) coexpression (Pearson $r \geq 0.6$) (Figure 5D). The network of annotated interactions identified IL-6 and IL-10 as the central hubs with connections to proteins with distinct functions including chemotaxis (eg, CCL5, CCL3), angiogenesis (eg, VEGF-A, HGF) and tissue remodeling (eg, MMP-1, TIMP1,

TGFB1). In the network constructed using protein coexpression data, TIMP1 and VEGF-A displayed even greater connectivity, appearing as central nodes with edges connecting both to other remodeling-related proteins (eg, COL18A1, NRP1) and multiple immune-associated proteins (eg, CSF1, TNFSF14, CCL14). These networks indicate the coordinated regulation of immune



(Figure legend continues on next page.)

and vascular remodeling processes, highlighting immune-stromal cross-talk in LVV.

The most prominent inter-disease differences were between TAK and LV-GCA profiles compared to TAB+ C-GCA (Figure 5A). In particular, the large increases in EIF4EBP1 and AXIN1 observed in TAK and LV-GCA were not seen in C-GCA. Similarly, increases in the neutrophil proteins DEFA1 and LCN2 were observed exclusively in TAK and LV-GCA (Figure 5E). There were also differences between LV-GCA and TAB+ C-GCA profiles compared to TAK, which indicate some degree of divergence between diseases. For example, increases in CXCL9 and TIMD4 were seen only in the GCA groups, whereas decreases in the ECM-related proteins COMP and THBS4 were only found in TAK (Figure 5F).

Plasma proteomic signatures reflect LVV arterial tissue phenotype. Plasma proteins arise not only from blood cells but also from a wide range of tissues and organs, including the vasculature, which is in direct contact with the blood. We therefore sought to evaluate whether changes in patient plasma (Figure 5A) reflect the phenotype of arterial tissue affected by LVV. Using bulk RNA-seq data from a study that compared surgically resected aortic tissue of LV-GCA to noninflammatory aortic aneurysms (NI-AA),²³ we found that for 47 (42%) of the LVV-associated plasma proteins, the corresponding gene was differentially expressed in LVV arterial tissue (Figure 6A and Supplementary Data 19). Moreover, the \log_2 FCs of these 47 plasma proteins correlated with the \log_2 FC of the corresponding gene in LVV tissue versus NI-AA (Figure 6B), and 28 plasma proteins (59.6%) had directionally concordant changes across the transcriptomic analysis of LVV arterial tissue and the plasma proteomic analyses of all the three LVV types.

Using the blueprint and GTEx bulk RNA-seq data sets,^{21,30} we explored the cell type and arterial expression profile of the 47 genes and proteins dysregulated in both plasma and arterial tissue (Supplementary Figure S12A). Macrophage and neutrophil expressed genes and proteins made up the largest subset (34%); this included *CCL7*, *CSF1*, *CXCL9*, and *CDCP1*, which

were increased in both tissue and plasma (Figure 6C). Genes and proteins expressed by nonimmune stromal cells, such as *TNC*, *MMP1*, *TIMP1*, and *NRP1*, were also prominent (Figure 6D). This latter cluster was enriched for genes of high arterial expression (GTEx) and could be useful as markers of arterial remodeling. The remainder were lymphocyte-derived (Figure 6E) or had mixed expression profiles. Of note, despite the significant decreases in plasma protein DPP4, CR2, and IL-7R in LVV, the expression of the corresponding genes was significantly increased in LVV arterial tissue (Figure S12B), emphasizing that there may be directionally discordant effects between different tissue compartments and/or between intracellular messenger RNA (mRNA) expression and plasma protein levels. Overall, these findings indicate that plasma proteomic signatures can reflect aspects of LVV tissue phenotype and could provide a valuable noninvasive read-out of pathogenic processes occurring in diseased arteries.

DISCUSSION

TAK and GCA are currently classified as separate diseases,^{12,31} but some investigators have proposed that they could represent varying manifestations of the same disease spectrum.^{4,5} This debate has largely focused on phenotypic similarities, reflecting patterns of arterial injury.³ Genome-wide association studies reveal differences in the genetic risk factors associated with TAK or GCA.³² However, a key unanswered question is whether the molecular effector pathways acting in these diseases are shared or distinct. This information is important for the rational selection of new therapeutic strategies that target specific proteins.

Here, we address this by comparing the plasma proteomic profile of TAK, LV-GCA, and C-GCA. In 281 patients with LVV, we measured 184 inflammation- and vascular-associated proteins to characterize the plasma proteome of each major LVV type and evaluate changes associated with disease activity states. We found that the proteomic profiles associated with active TAK, LV-GCA, and biopsy-proven C-GCA were similar and identified a

(Figure legend continued from previous page.)

Figure 5. Comparison of active TAK, LV-GCA and biopsy-proven C-GCA proteomic profiles. (A) Heatmap showing \log_2 FCs of the 112 DAPs identified in active TAK versus HC, active LV-GCA vs HC, and TAB+ C-GCA versus not C-GCA comparisons. Left: navy boxes represent proteins with statistically significant changes (adjusted $P < 0.05$) in each disease. Right: annotated functional category for each protein. (B) Comparison of disease vs HC \log_2 FCs for 112 DAPs. Diagonal lines represent the line of identity. Network plots of (C) known protein–protein interactions and (D) protein–protein coexpression for 74 proteins with directionally concordant changes across diseases. Node size corresponds to number of edges. For C, high confidence interactions (≥ 0.9) were sourced from STRING¹⁹ and for D, protein coexpression was defined as a Pearson correlation ≥ 0.6 in both patients with active TAK/LV-GCA and patients with TAB+ C-GCA. (E) Violin plots showing scaled abundance values (Z scores) for selected proteins associated with active TAK and LV-GCA but not C-GCA and (F) those identified as different between active LV-GCA and C-GCA versus active TAK. P values adjusted using Benjamini-Hochberg method; no symbol: nonsignificant, Adjusted $^*P < 0.05$, $^{**}P \leq 0.01$, $^{***}P \leq 0.001$, $^{****}P \leq 0.0001$. C-GCA, cranial giant cell arteritis; CRP, C-reactive protein; DAP, differentially abundant protein; ESR, erythrocyte sedimentation rate; HC, healthy control participant; IQR, interquartile range; \log_2 FC, log 2 fold change; LV-GCA, large-vessel giant cell arteritis; ns, nonsignificant; TAB, temporal artery biopsy; TAK, Takayasu arteritis. Color figure can be viewed in the online issue, which is available at <http://onlinelibrary.wiley.com/doi/10.1002/art.43110/abstract>.

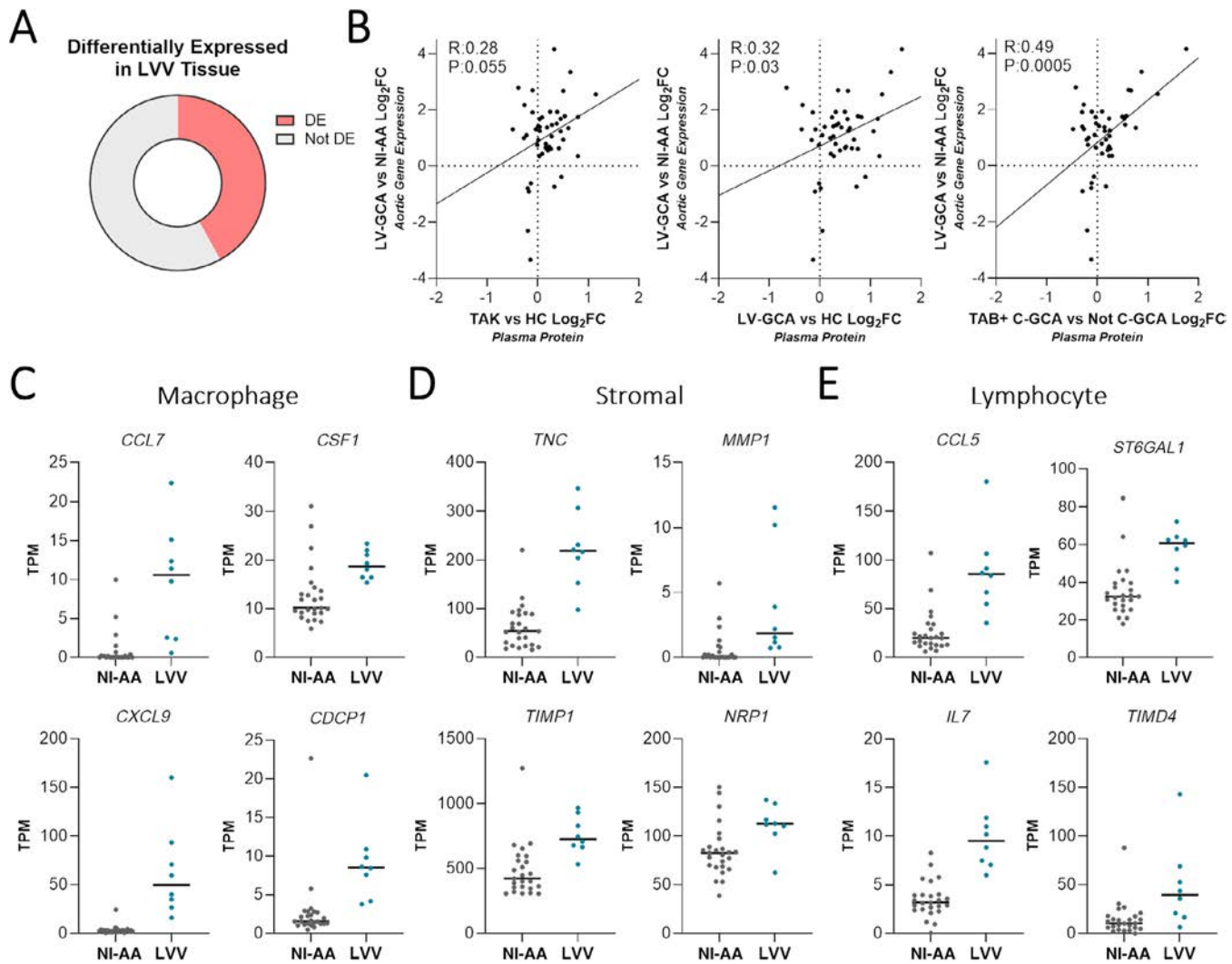


Figure 6. Correspondence of LVV plasma profile to arterial tissue phenotype. Comparison of plasma proteomic profiles associated with LVV and gene expression changes identified in aortic tissue affected by LVV.²³ (A) Pie chart showing the proportion of 112 LVV-associated plasma proteins (Supplementary Data 18) that were also differentially expressed (adjusted $P < 0.05$) in LV-GCA-related aortic aneurysm ($n = 8$) versus NI-AA ($n = 25$) by bulk RNA sequencing. (B) Comparison of plasma protein and aortic gene expression \log_2 FCs for the 47 proteins and corresponding genes that had significant changes in both LVV plasma and aortic tissue, each point represents a gene/protein pair. For proteomics (Y axes), \log_2 FCs represent active TAK versus HC, active LV-GCA versus HC, and TAB positive C-GCA (TAB+ C-GCA) versus Not C-GCA comparisons. For transcriptomics (X axes), \log_2 FCs represent LV-GCA associated aortitis versus NI-AA. (C–E) Dot plots showing aortic gene expression of genes/proteins differentially expressed/abundant in both LVV plasma and aortic tissue. Aortic gene expression in LVV versus NI-AA for genes typically expressed by (C) macrophages, (D) nonhematopoietic stromal cells, and (E) lymphocytes. Gene expression measured in TPM, cell-type expression classified using blueprint data (Figure S8). P values were adjusted using Benjamini-Hochberg method. C-GCA, cranial giant cell arteritis; HC, healthy control participant; \log_2 FC, \log_2 fold change; LV-GCA, large-vessel giant cell arteritis; LVV, large-vessel vasculitis; NI-AA, noninflammatory aortic aneurysm; TAB, temporal artery biopsy; TAK, Takayasu arteritis; TPM, transcripts per million. Color figure can be viewed in the online issue, which is available at <http://onlinelibrary.wiley.com/doi/10.1002/art.43110/abstract>.

26-protein “pan-LVV” signature common to all three groups. This signature primarily included proteins of immunologic function, but it also comprised proteins arising from or acting on the stroma, indicative of arterial injury, and/or repair. Some of these proteins have well-established roles in LVV (eg, IL-6 and VEGF-A),^{13,28} but others have not been previously linked to LVV.

The signature reflected prominent innate immune activation, particularly with increases in several proteins related to monocyte

and macrophage function. Coexpression analysis revealed coordinated regulation of such proteins (eg, CSF1, CCL18, CCL14) with multiple proteins involved in tissue remodeling (eg, VEGF-A, TIMP1, and TGFB1) thereby highlighting innate immune-stromal cross-talk in LVV. This is consistent with recent reports implicating profibrotic macrophage subsets in the fibrotic and stenotic remodeling of arteries in TAK and GCA, cell types that are less affected by current treatments.^{33,34} These findings underscore

the importance of macrophages in TAK and GCA pathogenesis and illustrate the need for therapeutics which target macrophages beyond proinflammatory functions alone.

We also observed evidence for adaptive immune involvement, with changes in lymphocyte-related proteins such as IL-7R and TNFSF14. Plasma IL-7R was decreased in all LVV groups irrespective of disease activity status. Its ligand IL-7 was also significantly increased in TAK and C-GCA. IL-7 is essential for T cell development and homeostasis while soluble IL-7R (sIL-7R) potentiates IL-7 activity by enhancing bioavailability.³⁵ The pattern observed is similar to findings in antineutrophil cytoplasmic antibody (ANCA)-associated vasculitis and tuberculosis infection but contrasts with rheumatoid arthritis and lupus in which sIL-7R levels are increased.^{36–38} Interestingly, the mRNA expression of IL-7R was increased in the transcriptomic analysis of LV-GCA aortitis, and a recent study reported that IL-7R expressing T cells are involved in the persistence of vasculitic lesions in a mouse chimeric model.³⁹ Decreased IL-7R in the plasma of patients with LVV may therefore reflect the recruitment of specific T cell subsets from the circulation to vasculitic lesions. As another example, TNFSF14 (LIGHT) was prominently elevated. TNFSF14 acts as a T cell costimulatory factor and triggers T cell activation and proliferation.⁴⁰ TNFSF14 promotes systemic immunopathology, as demonstrated by transgenic animals with constitutive TNFSF14 expression in T cells.⁴¹ Moreover, TNFSF14 can also act on non-hematopoietic structural cells including fibroblasts, endothelial, and smooth muscle cells to drive tissue fibrosis.⁴² Consistent with this, our coexpression network analysis identified an edge connecting TNFSF14 to VEGF-A, a central hub node. Current treatment strategies in LVV are limited to suppression of inflammation and do not target fibrosis directly. Thus, TNFSF14 antagonism may be a novel therapeutic approach in LVV that provides dual targeting of both the immune response and the consequent stromal reaction.

Lastly, the signature included tissue remodeling proteins expressed by immune cells (eg, VEGF-A) or stromal cells (eg, TNC, TIMP1, MMP-1); the latter may represent useful markers of arterial damage independent of inflammation. Increased plasma TNC in LVV is relevant given its enrichment in normal arteries and increased expression in arteries affected by LVV. TNC is an ECM protein primarily expressed by fibroblasts at sites of tissue damage where it supports repair. It gained interest as a candidate marker of vascular injury, but its levels are also elevated in other disease states.⁴³ Although this lack of specificity to LVV may preclude its use as a diagnostic marker, TNC, and other ECM proteins could be useful for monitoring arterial injury during follow-up and should be evaluated in longitudinal studies.

Despite the overall similarity in LVV proteomic profiles, we identified differences that suggest some immunologic divergence between diseases. For example, the chemokine CXCL9 was higher in LV-GCA and C-GCA compared to TAK. CXCL9 is produced by macrophages and other cell types in response to

interferon γ and typically reflects activation of the Th1 pathway.⁴⁴ Increased plasma CXCL9 has been reported previously in GCA and is associated with CXCR3+ cell infiltration into diseased arteries.⁴⁵ Previous studies speculated that TAK and GCA differ in the susceptibility of T cell pathways to glucocorticoids whereby Th1 responses persist in GCA and Th17 responses persist in TAK after treatment initiation.^{46,47} Our observation that CXCL9 was exclusively increased in GCA while IL-17A was exclusively increased in TAK may support this theory.

Beyond comparing LVV types, this study provided several disease-specific insights. We identified novel markers of active disease in TAK and in LV-GCA. Disease activity assessment is challenging in LVV, in which existing markers such as CRP have well-recognized limitations, and there can be practical constraints regarding the frequent use of vascular imaging.^{7,8} In a proof-of-principle analysis, we demonstrate that a single additional marker, the ECM glycoprotein COMP, used in combination with CRP markedly increases the accuracy of disease activity detection when compared to the use of CRP alone. Although further study is required to validate the novel markers identified here in independent cohorts, our findings suggest that significant improvements can be made with simple additions to the laboratory testing regimens used for monitoring LVV. Importantly, we also found that many proteins remained altered in patients with TAK and LV-GCA despite clinically quiescent disease. OSM and AXIN1 were elevated regardless of disease activity, whereas activity markers such as S100A12 and VEGF-A were highest in active disease but remained increased despite clinical disease quiescence. These findings may parallel the inaccuracy of clinical disease activity assessment compared to histopathologic or radiologic evaluations of arterial inflammation.^{48–50} However, we observed similar derangements in patients with TAK who had achieved durable clinical remission (defined here as the absence of any symptom, sign, laboratory feature or radiographic evidence for active TAK over the last three years of monitoring and the safe cessation of all immunosuppressive treatments). Therefore, although the persistent changes observed likely indicate subclinical inflammation, future studies are required to determine whether they are associated with clinically important outcomes.

Our results suggest that biopsy-positive and -negative C-GCA are proteomically distinct. There are two possibilities that could explain our findings. First, despite a careful clinical phenotyping algorithm, which included external expert review, there may be instances of misclassification within the TAB- C-GCA group, such that some patients were erroneously labeled as C-GCA. However, this cannot fully explain our findings because the TAB- C-GCA group included some patients with a positive USS. Alternatively, TAB positivity may reflect the burden of arterial disease. Skip lesions, with discontinuous segments of arterial inflammation, can occur in GCA, and so a patient with lower burden of arterial disease is more likely to have a negative biopsy on the small biopsy section of artery sampled. Thus, it is possible that

the proteomic read-out may reflect quantitative differences in the extent of arteritis. Our clinical laboratory data provided additional evidence of differences between TAB+ and TAB− patients, with higher ESR, CRP, and platelet count in the former group, in keeping with previous studies.^{51–53} Other clinical differences in TAB+ and TAB− C-GCA have been described, including greater risk of visual loss^{53,54} and higher prevalence of PMR in TAB+ patients,⁵¹ although these findings have not replicated in all case series.⁵⁵ Our data support the concept that C-GCA can be stratified by biopsy into biologically distinct endotypes, which may have implications for future trial design and precision medicine strategies.

Our study had limitations. We used a targeted proteomic panel that was enriched for inflammatory and vascular proteins and thus our ability to compare between LVV groups is limited to the proteins measured. The HCs in cohort 1 were well matched to patients with TAK but were younger than patients with LV-GCA. Differences in study design between cohort 1 and cohort 2 mean that proteomic differences between C-GCA and the other LVV groups may be confounded by differences in disease duration and treatment history. In addition, the controls in cohort 2 (“Not GCA”) were individuals who presented with symptoms for which a diagnosis of C-GCA was considered but ultimately excluded, whereas the controls in cohort 1 were healthy participants with no symptoms. In cohort 1, there was heterogeneity in treatment, with varying administration of steroids and other immunosuppressants, which could potentially impact the plasma proteome. However, treatment (particularly glucocorticoid dose) is given in response to disease activity, reflected in the correlation between disease activity scores and prednisolone dose in cohort 1. Thus, attempting to statistically adjust for treatment risks over-adjustment.^{56,57} For supervised learning, we split the data into training and test sets, but the relatively modest sample sizes mean that estimates of model performance are more vulnerable to stochastic variation. We mitigated this by also estimating model performance through cross-validation in the larger training set. Finally, in the case of membrane-bound proteins that undergo cleavage to produce a soluble form, it is not always clear whether plasma protein measurements are exclusively capturing the latter or also protein from cell membranes (for example, arising from in vivo sources such as exo- or ectosomes or ex vivo processes such as venepuncture or sample processing), complicating interpretation.

In conclusion, similarities in the plasma proteomic profiles of active TAK and GCA indicate common effector pathways resulting in inflammatory arterial damage despite differences in genetic etiology. Our integrated analysis of plasma and arterial tissue highlight the role played by macrophages and their protein products in LVV and indicate significant potential for their targeting in novel treatments and biomarkers. Future work should expand the molecular characterization of the LVV disease spectrum by extending the number of proteins measured via use of complementary proteomic platforms and by concurrent measurement

of other -omic layers (eg, RNA-seq of immune cells). Longitudinal studies characterizing the temporal changes in the molecular profile across the disease course will be valuable in delineating acute from chronic changes and allowing intraindividual assessment of putative biomarkers identified here.

ACKNOWLEDGMENTS

We thank Professor Marina Botto and Professor Matthew Pickering for helpful comments on the article. We thank the patients and healthy volunteers who participated in this study, along with the clinical research teams who recruited patients. We thank Surjeet Singh as the chief study coordinator for TABUL, and Bhaskar Dasgupta as a coinvestigator on TABUL, who played a leading role in the study recruitment. Dr Mason tragically passed away during the study, and we dedicate this article to his memory.

AUTHOR CONTRIBUTIONS

All authors contributed to at least one of the following manuscript preparation roles: conceptualization AND/OR methodology, software, investigation, formal analysis, data curation, visualization, and validation AND drafting or reviewing/editing the final draft. As corresponding author, Drs Maughan, Morgan, and Peters confirm that all authors have provided the final approval of the version to be published and take responsibility for the affirmations regarding article submission (eg, not under consideration by another journal), the integrity of the data presented, and the statements regarding compliance with institutional review board/Declaration of Helsinki requirements.




REFERENCES

- Pugh D, Karabayas M, Basu N, et al. Large-vessel vasculitis. *Nat Rev Dis Primers* 2022;7(1):93.
- Koster MJ, Matteson EL, Warrington KJ. Large-vessel giant cell arteritis: diagnosis, monitoring and management. *Rheumatology (Oxford)* 2018;57(suppl 2):ii32–ii42.
- Gribbons KB, Ponte C, Carette S, et al. Patterns of arterial disease in Takayasu arteritis and giant cell arteritis. *Arthritis Care Res (Hoboken)* 2020;72(11):1615–1624.
- Grayson PC. Lumpers and splitters: ongoing issues in the classification of large vessel vasculitis. *J Rheumatol* 2015;42(2):149–151.
- Maksimowicz-McKinnon K, Clark TM, Hoffman GS. Takayasu arteritis and giant cell arteritis: a spectrum within the same disease? *Medicine (Baltimore)* 2009;88(4):221–226.
- Watanabe Y, Miyata T, Tanemoto K. Current clinical features of new patients with Takayasu arteritis observed from cross-country research in Japan: age and sex specificity. *Circulation* 2015;132(18):1701–1709.
- Tombetti E, Hysa E, Mason JC, et al. Blood biomarkers for monitoring and prognosis of large vessel vasculitides. *Curr Rheumatol Rep* 2021;23(3):17.
- O'Connor TE, Carpenter HE, Bidari S, et al. Role of inflammatory markers in Takayasu arteritis disease monitoring. *BMC Neurol* 2014;14(1):62.
- Broder MS, Sarsour K, Chang E, et al. Corticosteroid-related adverse events in patients with giant cell arteritis: a claims-based analysis. *Semin Arthritis Rheum* 2016;46(2):246–252.
- Pujades-Rodriguez M, Morgan AW, Cubbon RM, et al. Dose-dependent oral glucocorticoid cardiovascular risks in people with immune-mediated inflammatory diseases: a population-based cohort study. *PLoS Med* 2020;17(12):e1003432.

11. Joshi A, Rienks M, Theofilatos K, et al. Systems biology in cardiovascular disease: a multiomics approach. *Nat Rev Cardiol* 2021;18(5):313–330.
12. Grayson PC, Ponte C, Suppiah R, et al; DCVAS Study Group. 2022 American College of Rheumatology/EULAR Classification Criteria for Takayasu Arteritis. *Arthritis Rheumatol* 2022;74(12):1872–1880.
13. Stone JH, Tuckwell K, Dimonaco S, et al. Trial of tocilizumab in giant-cell arteritis. *N Engl J Med* 2017;377(4):317–328.
14. Misra R, Danda D, Rajappa SM, et al. Development and initial validation of the Indian Takayasu Clinical Activity Score (ITAS2010). *Rheumatology (Oxford)* 2013;52(10):1795–1801.
15. Kerr GS, Hallahan CW, Giordano J, et al. Takayasu arteritis. *Ann Intern Med* 1994;120(11):919–929.
16. Hellmich B, Agueda A, Monti S, et al. 2018 Update of the EULAR recommendations for the management of large vessel vasculitis. *Ann Rheum Dis* 2020;79(1):19–30.
17. Luqmani R, Lee E, Singh S, et al. The role of ultrasound compared to biopsy of temporal arteries in the diagnosis and treatment of giant cell arteritis (TABUL): a diagnostic accuracy and cost-effectiveness study. *Health Technol Assess* 2016;20(90):1–238.
18. Hunder, G. G., Bloch, D. A., Michel, B. A., Stevens, M. B., Arend, W. P., Calabrese, L. H., Edworthy, S. M., Fauci, A. S., Leavitt, R. Y., Lie, J. T., Lightfoot, R. W., Masi, A. T., McShane, D. J., Mills, J. A., Wallace, S. L., & Zvaifler, N. J. (1990). The American College of Rheumatology 1990 criteria for the classification of giant cell arteritis. *Arthritis & Rheumatism*, 33(8), 1122–1128. Portico. <https://doi.org/10.1002/art.1780330810>
19. Szklarczyk D, Kirsch R, Koutrouli M, et al. The STRING database in 2023: protein-protein association networks and functional enrichment analyses for any sequenced genome of interest. *Nucleic Acids Res* 2023;51(D1):D638–D646.
20. Csárdi G, Nepusz T. The igraph software package for complex network research. 2006. Accessed July 11, 2024. Available from <https://www.semanticscholar.org/paper/The-igraph-software-package-for-complex-network-Cs%C3%A1rdi-Nepusz/1d2744b83519657f5f2610698a8ddd177ced4f5c>.
21. Lonsdale J, Thomas J, Salvatore M, et al; GTEx Consortium. The Genotype-Tissue Expression (GTEx) project. *Nat Genet* 2013;45(6):580–5.
22. Uhlén M, Fagerberg L, Hallström BM, et al. Proteomics. Tissue-based map of the human proteome. *Science* 2015;347(6220):1260419.
23. Hur B, Koster MJ, Jang JS, et al. Global transcriptomic profiling identifies differential gene expression signatures between inflammatory and noninflammatory aortic aneurysms. *Arthritis Rheumatol* 2022;74(8):1376–1386.
24. Chen Y, Lun ATL, Smyth GK. From reads to genes to pathways: differential expression analysis of RNA-seq experiments using Rsubread and the edgeR quasi-likelihood pipeline. *F1000 Res* 2016;5:1438.
25. Friedman J, Hastie T, Tibshirani R. Regularization paths for generalized linear models via coordinate descent. *J Stat Softw* 2010;33(1):1–22.
26. Kuhn M. Building predictive models in R using the caret package. *J Stat Softw* 2008;28(5):1–26.
27. Cui X, Qin F, Song L, et al. Novel biomarkers for the precise diagnosis and activity classification of Takayasu arteritis. *Circ Genom Precis Med* 2019;12(1):e002080.
28. Robinette ML, Rao DA, Monach PA. The immunopathology of giant cell arteritis across disease spectra. *Front Immunol* 2021;12:623716.
29. Burja B, Feichtinger J, Lakota K, et al. Utility of serological biomarkers for giant cell arteritis in a large cohort of treatment-naïve patients. *Clin Rheumatol* 2019;38(2):317–329.
30. Fernández JM, de la Torre V, Richardson D, et al. The BLUEPRINT data analysis portal. *Cell Syst* 2016;3(5):491–495.e5.
31. Ponte C, Grayson PC, Robson JC, et al; DCVAS Study Group. 2022 American College of Rheumatology/EULAR classification criteria for giant cell arteritis. *Arthritis Rheumatol* 2022;74(12):1881–1889.
32. Carmona FD, Coit P, Saruhan-Direskeneli G, et al; Spanish GCA Study Group; Italian GCA Study Group; Turkish Takayasu Study Group; Vasculitis Clinical Research Consortium. Analysis of the common genetic component of large-vessel vasculitides through a meta-immunochip strategy. *Sci Rep* 2017;7(1):43953.
33. Kong X, Xu M, Cui X, et al. Potential role of macrophage phenotypes and CCL2 in the pathogenesis of Takayasu arteritis. *Front Immunol* 2021;12:646516.
34. Jiemy WF, van Sleen Y, van der Geest KS, et al. Distinct macrophage phenotypes skewed by local granulocyte macrophage colony-stimulating factor (GM-CSF) and macrophage colony-stimulating factor (M-CSF) are associated with tissue destruction and intimal hyperplasia in giant cell arteritis. *Clin Transl Immunology* 2020;9(9):e1164.
35. Aloufi NA, Ali AK, Burke Schinkel SC, et al. Soluble CD127 potentiates IL-7 activity in vivo in healthy mice. *Immun Inflamm Dis* 2021;9(4):1798–1808.
36. Yoon T, Pyo JY, Ahn SS, et al. Serum soluble interleukin-7 receptor alpha levels are negatively correlated with the simultaneous activity of antineutrophil cytoplasmic antibody-associated vasculitis. *Clin Exp Rheumatol* 2023;41(4):879–886.
37. Lundtoft C, Afum-Adjei Awuah A, Rimpler J, et al. Aberrant plasma IL-7 and soluble IL-7 receptor levels indicate impaired T-cell response to IL-7 in human tuberculosis. *PLoS Pathog* 2017;13(6):e1006425.
38. Meyer A, Parmar PJ, Shahrara S. Significance of IL-7 and IL-7R in RA and autoimmunity. *Autoimmun Rev* 2022;21(7):103120.
39. Sato Y, Jain A, Ohtsuki S, et al. Stem-like CD4+ T cells in perivascular tertiary lymphoid structures sustain autoimmune vasculitis. *Sci Transl Med* 2023;15(712):eadh0380.
40. Ware CF, Croft M, Neil GA. Realignment of the LIGHT signaling network to control dysregulated inflammation. *J Exp Med* 2022;219(7):e20220236.
41. Shaikh RB, Santee S, Granger SW, et al. Constitutive expression of LIGHT on T cells leads to lymphocyte activation, inflammation, and tissue destruction. *J Immunol* 2001;167(11):6330–6337.
42. Herro R, Croft M. The control of tissue fibrosis by the inflammatory molecule LIGHT (TNF Superfamily member 14). *Pharmacol Res* 2016;104:151–155.
43. Golledge J, Clancy P, Maguire J, et al. The role of tenascin C in cardiovascular disease. *Cardiovasc Res* 2011;92(1):19–28.
44. Berthoud TK, Dunachie SJ, Todryk S, et al. MIG (CXCL9) is a more sensitive measure than IFN- γ of vaccine induced T-cell responses in volunteers receiving investigated malaria vaccines. *J Immunol Methods* 2009;340(1):33–41.
45. Graver JC, Abdulahad W, van der Geest KSM, et al. Association of the CXCL9-CXCR3 and CXCL13-CXCR5 axes with B-cell trafficking in giant cell arteritis and polymyalgia rheumatica. *J Autoimmun* 2021;123:102684.
46. Deng J, Younge BR, Olshen RA, et al. Th17 and Th1 T-cell responses in giant cell arteritis. *Circulation* 2010;121(7):906–915.
47. Saadoun D, Garrido M, Comarmond C, et al. Th1 and Th17 cytokines drive inflammation in Takayasu arteritis. *Arthritis Rheumatol* 2015;67(5):1353–1360.
48. Kaymakci MS, Boire NA, Bois MC, et al. Persistent aortic inflammation in patients with giant cell arteritis. *Autoimmun Rev* 2023;22(9):103411.
49. Uy CP, Tarkin JM, Gopalan D, et al. The impact of integrated noninvasive imaging in the management of Takayasu arteritis. *JACC Cardiovasc Imaging* 2021;14(2):495–500.
50. Grayson PC, Alehashemi S, Bagheri AA, et al. 18 F-fluorodeoxyglucose-positron emission tomography as an imaging biomarker in a

- prospective, longitudinal cohort of patients with large vessel vasculitis. *Arthritis Rheumatol* 2018;70(3):439–449.
51. Koster MJ, Yeruva K, Crowson CS, et al. Giant cell arteritis and its mimics: a comparison of three patient cohorts. *Semin Arthritis Rheum* 2020;50(5):923–929.
52. Gonzalez-Gay MA, Garcia-Porrúa C, Llorca J, et al. Biopsy-negative giant cell arteritis: clinical spectrum and predictive factors for positive temporal artery biopsy. *Semin Arthritis Rheum* 2001;30(4):249–256.
53. Duhaut P, Pinède L, Bornet H, et al. Biopsy proven and biopsy negative temporal arteritis: differences in clinical spectrum at the onset of the disease. *Groupe de Recherche sur l'Artérite à Cellules Géantes. Ann Rheum Dis* 1999;58(6):335–341.
54. Chatelain D, Duhaut P, Schmidt J, et al; Groupe de Recherche sur l'Artérite à Cellules Géantes. Pathological features of temporal arteries in patients with giant cell arteritis presenting with permanent visual loss. *Ann Rheum Dis* 2009;68(1):84–88.
55. Putman MS, Gribbons KB, Ponte C, et al. Clinicopathologic associations in a large international cohort of patients with giant cell arteritis. *Arthritis Care Res (Hoboken)* 2022;74(6):1013–1018.
56. Westreich D, Greenland S. The table 2 fallacy: presenting and interpreting confounder and modifier coefficients. *Am J Epidemiol* 2013; 177(4):292–298.
57. Schisterman EF, Cole SR, Platt RW. Overadjustment bias and unnecessary adjustment in epidemiologic studies. *Epidemiology* 2009;20 (4):488–495.

Absence of Functional Autoantibodies Targeting Angiotensin II Receptor Type 1 and Endothelin-1 Type A Receptor in Circulation and Purified IgG From Patients With Systemic Sclerosis

Wieke M. van Oostveen,¹  Eva M. Hoekstra,¹  E. W. Nivine Levarht,¹ Ilana B. Kotliar,² Thomas P. Sakmar,³ René E. M. Toes,¹ Jeska K. de Vries-Bouwstra,¹ Laura H. Heitman,⁴ and Cynthia M. Fehres¹ 

Objective. Systemic sclerosis (SSc) is a rare but severe autoimmune disease characterized by immune dysregulation, fibrosis, and vasculopathy. Although previous studies have highlighted the presence of functional autoantibodies targeting the angiotensin II receptor type 1 (AT₁) and endothelin-1 type A receptor (ET_AR), leading to autoantibody-mediated receptor stimulation and subsequent activation of endothelial cells (ECs), a comprehensive understanding of the direct interaction between these autoantibodies and their receptors is currently lacking. Moreover, existing data confirming the presence of these autoantibodies in SSc often rely on similar methodologies and assays. Our aim was to replicate previous findings and to investigate the functional effects of IgG derived from patients with SSc (SSc IgG) on AT₁ and ET_AR signaling, the downstream EC response, and the presence of AT₁-binding autoantibodies in circulation.

Methods. Quantitative polymerase chain reaction and cytokine enzyme-linked immunosorbent assay, alongside a real-time cell analyzer, were used to assess receptor-specific functional characteristics of purified SSc IgG (n = 18). Additionally, a novel protein capture assay using solubilized epitope-tagged AT₁ was developed to detect AT₁-binding autoantibodies in plasma samples from patients with SSc (n = 28) and healthy donors (n = 14).

Results. No evidence for EC activation in an AT₁- or ET_AR-dependent manner was revealed. Furthermore, stimulation with SSc IgG did not induce receptor activation or alter G protein-coupled receptor signaling on agonist stimulation in a model with receptor overexpression. Lastly, no AT₁-binding autoantibodies were detected in plasma samples from patients with SSc when using epitope-tagged solubilized AT₁.

Conclusion. Overall, our study did not provide evidence to support the presence of AT₁- or ET_AR-activating autoantibodies in purified SSc IgG or AT₁-binding autoantibodies in the circulation of patients with SSc.

INTRODUCTION

Systemic sclerosis (SSc) is a rheumatic autoimmune disorder characterized by microangiopathy, including Raynaud phenomenon (RP), immune dysregulation, and fibrosis of the skin and internal organs.¹ Clinical presentation of SSc vary from an indolent form with limited deterioration to rapidly progressive disease, associated with irreversible organ damage and relatively high mortality rates.² Despite its rarity, SSc poses a significant clinical

challenge because of its clinical heterogeneity and potential for a high mortality rate.³ More than 95% of patients with SSc test positive for antinuclear antibodies (ANAs) including anti-topoisomerase I antibodies (ATA) and anticentromere antibodies (ACA). The presence of ATA and ACA is disease specific. The two antibodies rarely co-occur and are associated with distinct clinical phenotypes.⁴ Although the underlying pathologic mechanisms in SSc subtypes remain largely elusive, the presence of ANA and RP precedes clinical disease and fibrosis onset, indicating a potential link between

¹Wieke M. van Oostveen, MSc, Eva M. Hoekstra, MD, MSc, E. W. Nivine Levarht, BSc, René E. M. Toes, PhD, Jeska K. de Vries-Bouwstra, MD, PhD, Cynthia M. Fehres, PhD: Leiden University Medical Center, Leiden, The Netherlands;

²Ilana B. Kotliar, PhD: The Rockefeller University and Tri-Institutional PhD Program in Chemical Biology, New York, New York; ³Thomas P. Sakmar, MD: The Rockefeller University, New York, New York; ⁴Laura H. Heitman, PhD: Leiden University and Oncode Institute, Leiden, The Netherlands.

Additional supplementary information cited in this article can be found online in the Supporting Information section (<http://onlinelibrary.wiley.com/doi/10.1002/art.43099>).

Author disclosures are available at <https://onlinelibrary.wiley.com/doi/10.1002/art.43099>.

Address correspondence via email to Cynthia M. Fehres, PhD, at c.m.fehres@lumc.nl.

Submitted for publication September 12, 2024; accepted in revised form December 11, 2024.

autoimmunity and vasculopathy. A deeper understanding of disease pathogenesis could facilitate early intervention to halt fibrosis and disease progression.

RP, an early but nonspecific sign of SSc, is characterized by restricted blood flow to the extremities due to endothelial cell (EC) dysregulation and exaggerated vasoconstriction.⁵ This vasoconstrictive response, along with vasodilation, is regulated by the renin-angiotensin-system, with angiotensin II (AngII) and its receptor angiotensin II type 1 (AT₁) playing pivotal roles.^{6,7} Additionally, endothelin-1 (ET-1), a proinflammatory peptide, contributes to vasoconstriction by activating endothelin-1 type A receptor (ET_AR), implying potential involvement for AngII and ET-1 in SSc pathogenesis.⁸ Indeed, the use of angiotensin-converting enzyme inhibitors in SSc has been associated with reduced death from renal crisis, although no effect on RP was found.^{9,10} Furthermore, several clinical trials have investigated the effects of AT₁ and ET_AR inhibitors to reduce disease manifestations, such as fibrosis, pulmonary arterial hypertension, and digital ulcers. Although these blockers alleviated vascular complications, no effect on fibrosis in skin or other organs was observed, thereby highlighting the need for further research into the role of AT₁ and ET_AR in SSc pathophysiology.^{11–15}

Previous studies have reported the presence of autoantibodies against AT₁ and ET_AR in SSc,^{16–19} as well as in other diseases, including preeclampsia and renal-allograft rejection.^{20–22} In SSc, high autoantibody levels predicted disease-related death and thus were proposed as biomarkers for risk assessment for disease progression.¹⁹ These autoantibodies are defined to act as agonists, as they activate the receptor and its downstream signaling cascade.^{20–23} Both AT₁ and ET_AR are members of the G protein-coupled receptor (GPCR) family, which are membrane-bound proteins characterized by seven transmembrane helices and intracellular coupling to heterotrimeric G proteins composed of α , β , and γ subunits.²⁴ On agonist ligand stimulation, GPCRs activate various downstream signaling pathways through coupling to G proteins or via β -arrestins.²⁵ Activated AT₁ and ET_AR primarily couple to G $\alpha_{q/11}$ leading to increased cytosolic Ca²⁺ and subsequent vasoconstriction.^{26–28}

The contribution of AT₁ and ET_AR activation to vasoconstriction and the reported presence of autoantibodies targeting AT₁ and ET_AR in SSc suggest a potential contribution of agonistic anti-AT₁- and anti-ET_AR autoantibodies to vasculopathy in SSc. However, detailed studies examining the direct interaction between these autoantibodies and their receptors are currently lacking.^{18,28} Therefore, the present study aimed to investigate the functional effects of IgG derived from patients with SSc (SSc IgG) on AT₁ and ET_AR signaling, as well as its downstream EC response. To this end, in addition to conventional techniques such as quantitative polymerase chain reaction (qPCR) and cytokine enzyme-linked immunosorbent assay (ELISA), a real-time cell analyzer (RTCA), well-validated for studying GPCR pharmacology, was used to assess functional characteristics of SSc IgG in

a direct and receptor-specific manner. Additionally, a novel protein capture assay using solubilized receptors was established to evaluate the presence of anti-AT₁ autoantibodies in the circulation of patients with SSc.

MATERIALS AND METHODS

Patients and healthy individuals. Plasma and serum samples were collected from patients with SSc who were part of a prospective cohort study (the Leiden Combined Care in Systemic Sclerosis cohort) at the Leiden University Medical Center's Rheumatology outpatient clinic. Patient characteristics are detailed in Supplementary Table 1. Patients with both low and high levels of anti-AT₁ (cutoff = 9.5) and anti-ET_AR antibodies (cutoff = 10.4) were included, as measured in serum by Riemekasten et al,¹⁹ as previously reported. All patients met the American College of Rheumatology/EULAR 2013 criteria for the classification of SSc and had not undergone hematopoietic stem cell transplantation.²⁹ The study was approved by the Leiden University Medical Center ethical review board (protocol P17.151). Written informed consent was obtained from both patients and healthy donors (HDs).

Purification of IgG antibodies. IgG antibodies were purified from plasma using a 1-mL HiTrap Protein G HP affinity column (GE29-0485-81; Cytiva), followed by a direct buffer exchange using a 53-mL HiPrep 26/10 desalting column (GE17-5087-01; Cytiva). Isolated IgG was concentrated to 4 to 26 mg/mL using Amicon Ultra-15 50 kDa filter devices (UFC9050; Merck) and potential endotoxins were removed with Pierce High-Capacity Endotoxin Removal Spin Columns (88274; ThermoFisher Scientific). Aliquots were stored at –20°C for subsequent experiments.

Stable transfection Chinese hamster ovary cells. Chinese hamster ovary (CHO)–K1 (ATCC, CCL-61) cells were transfected with human ET_AR (EDNRA, NM_001957) Ohu22257C; GenScript Biotech) cloned into a pcDNA3.1⁺N-6His vector using PolyJet DNA Transfection Agent (SL100688; SigmaGen) according to manufacturer's protocol. Briefly, 1 μ g of plasmid was added to cells (0.1 million cells/well) at low passage number in a 24-well plate. After seven days, cells were selected with geneticin (11811-064; Gibco) and single-cell sorted using a His-tag antibody (OAEA00010; Aviva). Functional expression of ET_AR on clones was confirmed using ET-1 (HY-P0202; MedChemExpress).

Cell culture. Human telomerase reverse transcriptase (TERT)–immortalized human umbilical vein ECs (HUVETs/TERT2, CRL-4053, ATCC) were cultured on gelatin-coated dishes in vascular cell basal medium (ATCC-PCS-100-030, ATCC) supplemented with endothelial cell growth kit-VEGF (ATCC-PCS-100-041, ATCC), glutamax, 100 U/mL penicillin-streptomycin

(Pen-Strep), and 5% fetal calf serum (FCS). Medium was refreshed every two days, and cells were maintained at 37°C with 5% CO₂ until 80% to 90% confluence. CHO-K1 cells, CHO-ET_AR, and commercially acquired CHO-AT₁ (ES-072-C; PerkinElmer) were cultured in Ham's F12 medium (21765029; Gibco) with 10% FCS and 100 U/mL of Pen-Strep. Additionally, for CHO-AT₁ and CHO-ET_AR cells, 0.4 mg/mL of geneticin was added to maintain selection pressure. Cells were grown at 37°C under 5% CO₂ until 70% to 80% confluence.

Stimulation of HUVEC for qPCR and ELISA. HUVECs (p5–15) were seeded in gelatin-coated 12-well plates (0.1 million cells/well) and cultured overnight. Cells were serum-starved for one hour before pretreatment with 2 μ M of valsartan (AT₁ antagonist, HY-18204; MedChemExpress) and 2 μ M of BQ-123 (ET_AR antagonist, HY-12378; MedChemExpress) or a vehicle (0.02% DMSO/phosphate buffered saline [PBS]) for one hour. Cells were then treated with 200 μ g/mL of IgG, 10 μ M of AngII (A9525; Sigma-Aldrich) with 10 μ M of ET-1 (HY-P0202; MedChemExpress), 10 ng/mL of recombinant human tumor necrosis factor α (rhTNF α) (210-TA; R&D Systems), or medium. After 1 hour, a medium with FCS was added leading 1% FCS followed by incubation for 48 hours.

RNA isolation and qPCR. After 48 hours, HUVEC supernatant was collected, and cells were lysed in TRIzol (15596026; Invitrogen). RNA was isolated using the RNA Microprep Kit (R2063; Zymo Research) following the manufacturer's protocol. RNA concentration and purity were assessed using NanoDrop (Thermo Scientific). Next, 500 ng of RNA from each condition was mixed with the iScript complementary DNA (cDNA) Synthesis Kit (1708891; Bio-Rad) and supplemented to 20 μ L with nuclease-free water (11538646; Invitrogen). qPCR was performed using 3 μ L of diluted cDNA and 5 μ L of master mix containing 2.5 pmol of forward and reverse primer, double distilled H₂O, and SensiFAST SYBR No-ROX Kit (BIO-98005; Meridian Bioscience). Primer sequences are listed in Supplementary Table 2. The cDNA dilutions, primer concentrations, and standards were optimized according to the literature.³⁰ Mean cycle quantification (Cq) values were determined from technical replicates ($n = 3$). Relative quantity was calculated using $(1+E)^{\Delta Cq}$, in which E is the PCR efficiency from the standard curve, and ΔCq is the difference between the sample and the medium control. Relative normalized expression was obtained by dividing the relative quantity of the target (intercellular adhesion molecule 1 [*ICAM1*], selectin E (*SELE*), C-C Motif Chemokine Ligand 2 [*CCL2*]) by the reference (beta-2-microglobulin [*B2M*]). Data were exported from CFX Maestro 3.2 (version 5.2; Bio-Rad) for statistical analysis.

Cytokine ELISA. Supernatants from IgG-stimulated HUVECs were analyzed for interleukin-6 (IL-6) (88-7066-88), IL-8 (88-8086-88), and TNF α (88-7346-88) using ELISA kits (Invitrogen) following the manufacturer's protocol. Briefly,

384-well plates (3700; Corning) were coated with 15 μ L of antigen and blocked with 75 μ L of 1% bovine serum albumin [BSA]/PBS. Diluted supernatant (IL-6, TNF α : 2 \times ; IL-8: 10 \times), detection antibody, horseradish peroxidase (HRP)-labeled avidin antibody, and tetramethylbenzidine substrate (555214; BD Biosciences) were sequentially added (15 μ L each). Reactions were stopped with 15 μ L 1 *M* H₂SO₄, and absorbance was measured at 450 nm using a Multiskan Fc reader (Thermo Scientific). Cytokine standards (IL-6, IL-12: kit components; TNF α : 51-26376E; BD Biosciences) were used to calculate cytokine production when within the linear range.

Real-time cell analysis. Label-free, functional experiments were conducted using an xCELLigence RTCA (Agilent), which measures changes in impedance due to whole-cell responses, reflecting changes in cell number, proliferation rate, adhesion, and morphology expressed as the dimensionless parameter cell index (CI). This method is well-validated to study compound-receptor interactions.^{31–35} All assays were performed at 37°C and 5% CO₂ in 96-well E-plates (300600900; Agilent) with 100 μ L/well final volume. Background impedance was measured in 35 to 45 μ L medium followed by the seeding of 40,000 cells/well. CI values were recorded every 15 minutes overnight. Cells were pretreated for one hour with 1 μ M of an antagonist, 100 μ g/mL of IgG, or a vehicle. Next, responses to 100 μ M ATP, agonist, 200 μ g/mL IgG or PBS were measured for 30 to 120 minutes. Compounds and IgG were added simultaneously to the E-plate using a VIAFLO 96-channel Handheld Electronic pipette (INTEGRA Biosciences). Experimental data were acquired using RTCA Software (version 2.2.1; Agilent). CI values were normalized just before compound or IgG addition to obtain normalized CI (nCI) values. Baseline corrections were made by subtracting vehicle control nCI values from each data point. Absolute net area under the curve (AUC) was calculated for the initial 60 minutes after stimulation (30 minutes for IgG pretreatment on CHO-ET_AR cells). Net AUC data were analyzed with nonlinear regression in GraphPad Prism (version 9.3.1).

Protein capture assay. A novel protein assay using solubilized AT₁ was established to measure AT₁-binding autoantibodies in SSC plasma. Solubilized GPCRs were obtained as described previously.³⁶ Briefly, epitope-tagged human GPCR constructs (AT₁, CXCR3 [C-X-C motif chemokine receptor 3], cholinergic receptor muscarinic 3 [CHRM3]) with an N-terminal FLAG tag (DYKDDDDK) and C-terminal 1D4 tag (TETSQVAPA) were encoded in a pcDNA3.1⁺ mammalian expression vector. HEK293 FreeStyle cells were cultured according to manufacturer's instructions. One day before transfection, HEK293FS cells were diluted to 0.5 million cells/mL. The following day, 100 mL of cell suspension was transfected with plasmid DNA encoding CXCR3, CHRM3, or AT₁ using OptiMEM (12559099; Gibco) and 293fectin transfection reagent (10553283; Gibco).

Help vectors (p33-SV40LT, pORF-hp21V.16, pORF-hp27V02) were added to stop cell cycle and boost protein production, resulting in a final DNA concentration of 1 $\mu\text{g/mL}$. For mock-transfected cells, only help vectors were added. After 24 hours, cells were harvested and washed with cold PBS. For each transfection, 500 μL of cells was stained with anti-FLAG M2-fluorescein isothiocyanate (FITC) mouse monoclonal antibody (mAb) (1:200, F4049; Sigma-Aldrich) followed by flow cytometry to validate successful transfection. Remaining cells were solubilized using n-dodecyl- β -D-maltoside (DDM) detergent (850520; Avanti) to form micelles to maintain GPCR conformation. Cells were incubated in solubilization buffer (50 mM HEPES, 1 mM EDTA, 150 mM NaCl, and 5 mM MgCl_2 [pH 7.4]) with 1% (weight/volume) DDM and complete protease inhibitor (11836170001; Roche) for two hours at 4°C with head-over-head rotation. Lysates were clarified by centrifugation at 22,000g for 20 minutes at 4°C. Clarified solubilized membrane proteins were snap frozen in liquid nitrogen and stored at -80°C. Total protein concentration was determined using Pierce BCA protein assay (23227; Thermo Scientific) according to the manufacturer's protocol.

Plasma samples from 14 HDs and 28 patients with SSc were selected. Nunc MaxiSorp 96-well plate (430341; Thermo Scientific) were coated with 1 $\mu\text{g/mL}$ of rhodopsin monoclonal antibody (1D4) (MA1-722; Invitrogen) to capture solubilized GPCRs via their 1D4 epitope tag. After blocking with 1% BSA/PBS, solubilized GPCRs in solubilization buffer (with 1% BSA) were incubated for 30 minutes while shaking. Fractions of mock-transfected cells were included as negative control. Diluted plasma samples (1:100), anti-CXCR3 antibody (0.4 $\mu\text{g/mL}$, HPA045942; Atlas Antibodies), anti-CHRM3 antibody (0.4 $\mu\text{g/mL}$, HPA048036; Atlas Antibodies) and anti-DYKDDDDK tag (D6W5B) (2 $\mu\text{g/mL}$, 14793S; Cell Signaling) were diluted in same buffer as solubilized GPCRs and incubated for one hour followed by incubation with 1:1,000 anti-human IgG/HRP (P0214; DAKO) or 1:7,500 anti-rabbit Ig/HRP (P0448; DAKO). Following extensive washing, plates were incubated with H_2O_2 /ABTS. Absorbance at 415 nm was measured every 30 minutes.

Statistical analysis. Statistical analysis was performed with GraphPad Prism software (version 9.3.1). Variables are expressed as means \pm SEMs of three individually performed experiments with technical duplicates, unless otherwise specified. Statistical analysis was performed using Kruskal-Wallis test with Dunn's correction for nonparametric values, unless otherwise specified. $P < 0.05$ was considered as statistically significant.

RESULTS

No EC activation upon stimulation with SSc IgG.

Because previous studies described a potential role for autoantibodies targeting AT_1 and ET_AR resulting in EC

activation,^{13,18,37,38} we set out to study the effect of SSc antibodies on endothelium by stimulation of human ECs with HD-derived IgG (HD IgG) and SSc IgG. Immortalized HUVECs were used to eliminate HUVEC donor-specific effects. First, as positive control, HUVECs were stimulated with 10 ng/mL of $\text{TNF}\alpha$ for 48 hours to evaluate the up-regulation of *SELE*, *ICAM1*, and *CCL2*, all genes associated with EC activation. A fold change of 43.8 for *SELE*, 25.6 for *ICAM1*, and 13.1 for *CCL2* following $\text{TNF}\alpha$ stimulation indicated the suitability of HUVEC as a model to study EC activation (Supplementary Figure 1). Next, isolated IgG from plasma samples from patients and HDs were used to minimize the potential influence of plasma components on vasculature, given the elevated levels of AngII and ET-1 in patients with SSc.^{11,12} Although the addition of IgG fractions to HUVECs did induce a slight up-regulation of *SELE*, *ICAM1*, and *CCL2*, no differences were observed for SSc IgG ($n = 5$ –10) compared to HD IgG ($n = 3$) (Figure 1A). Furthermore, stimulation with agonists AngII and ET-1 did not lead to EC activation. Likewise, pretreatment with AT_1 -specific antagonist valsartan and ET_AR -specific antagonist BQ-123 did not attenuate the up-regulation of these markers.

Next, cytokine production by EC after stimulation with SSc and HD IgG was assessed. Although $\text{TNF}\alpha$ stimulation of EC as positive control led to high cytokine production with optical density values outside the linear range (data not shown), no significant up-regulation of the proinflammatory cytokines IL-6, IL-8, or $\text{TNF}\alpha$ was observed on stimulation with SSc IgG (Figure 1B). Altogether, these data suggest limited contribution of SSc IgG in EC activation.

Because the up-regulation of activation markers and proinflammatory cytokine production has been reported as a consequence of SSc IgG-induced AT_1 - and/or ET_AR -mediated EC activation, we next aimed to study the potential direct effects of SSc IgG using another read-out. To this end, we took advantage of RTCA, a method to study cell morphologic effects of GPCR activation and previously applied to study EC responses.³⁹ HUVECs were stimulated with 100 μM of ATP to define their non- AT_1 - or ET_AR -specific response window (Figure 1C), resulting in an average net AUC of 18.6. To study receptor-specific activation, HUVECs, either pretreated with specific antagonists or a vehicle, were stimulated with 10 μM of AngII, 10 μM of ET-1, or both. No effect of agonist stimulation was observed, both with and without antagonist pretreatment (Figure 1D). These results confirm our findings in Figure 1B showing limited effect of AngII with ET-1 stimulation on EC. To exclude differences in signaling between agonists and IgG, isolated IgG of HDs ($n = 3$) and patients with SSc ($n = 5$) was tested using RTCA. Similar to agonist stimulation, no activation of EC was observed on incubation with IgG (Figure 1E). Quantification of responses induced by HD IgG ($n = 3$) and SSc IgG ($n = 5$) showed no EC activation in an AT_1 - or ET_AR -dependent manner (Figure 1F). In summary, stimulation of EC with SSc IgG did not provide evidence for EC activation in an AT_1 - or ET_AR -dependent manner.

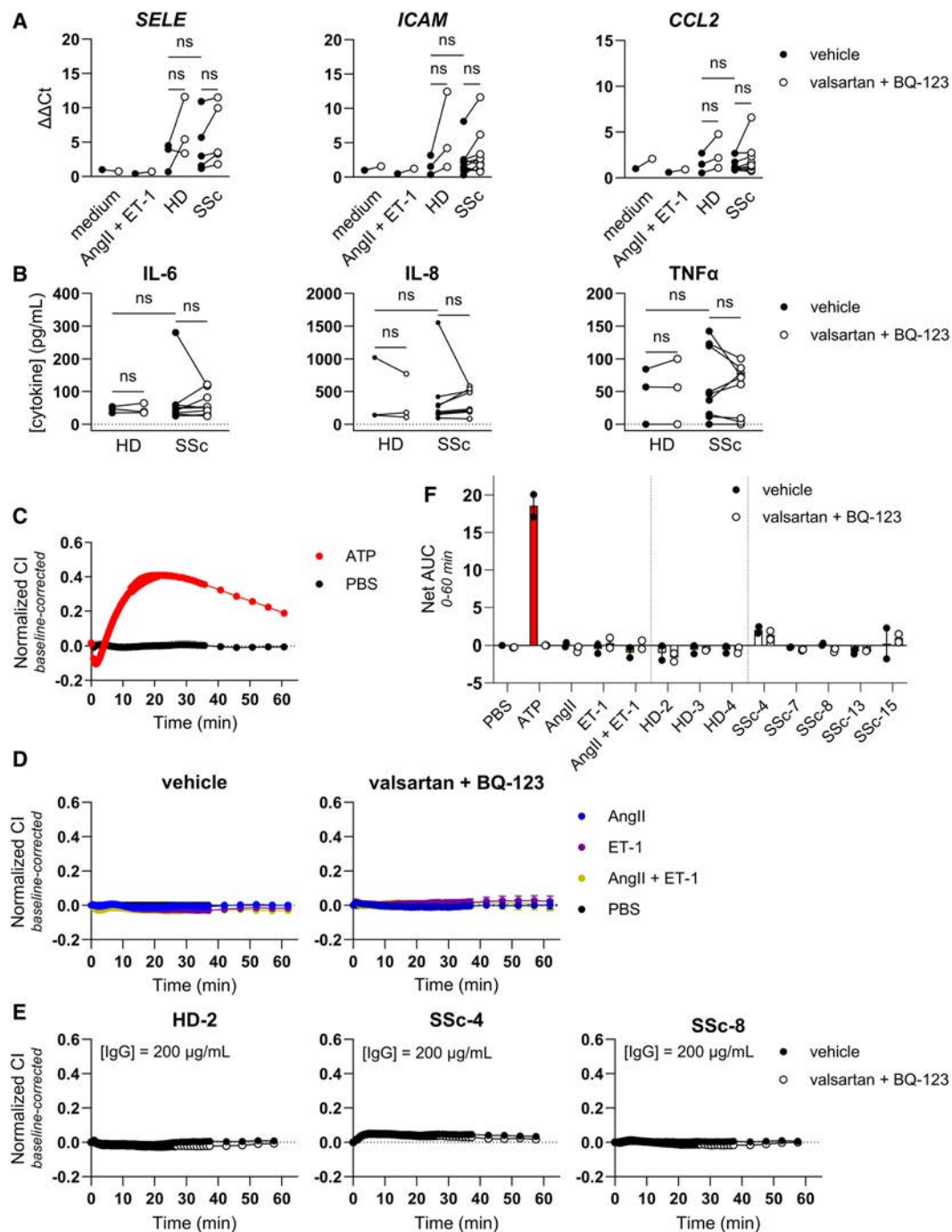


Figure 1. SSc IgG does not activate HUVECs in an AT₁- or ET_AR-mediated manner. (A) $\Delta\Delta Ct$ of *SELE*, *ICAM1*, and *CCL2* in HUVECs pretreated with vehicle or 1 μM of AT₁ antagonist valsartan plus ET_AR antagonist BQ-123 followed by stimulation with 10 μM of AngII plus ET-1 or 200 $\mu g/mL$ of IgG. Data points represent mean $\Delta\Delta Ct$ measured in technical triplicates. (B) Cytokine ELISA for IL-6, IL-8, and TNF α with supernatant of HUVECs stimulated with 200 $\mu g/mL$ of IgG for 48 hours. Data points represent mean cytokine concentration measured in technical triplicates. (C) Representative graph of baseline-corrected real-time nCI traces of HUVECs stimulated with 100 μM of ATP. (D) Representative graphs of baseline-corrected nCI traces of HUVECs pretreated with a vehicle or 1 μM of valsartan plus BQ-123 before stimulation with 10 μM of AngII, 10 μM of ET-1, or both agonists. (E) Representative graphs of baseline-corrected nCI traces of HUVECs pretreated with a vehicle or 1 μM antagonist before stimulation with 200 $\mu g/mL$ of IgG. (F) Net AUC (mean \pm SEM, n = 2) of HUVECs 0- to 60-minute baseline-corrected nCI traces pretreated with a vehicle or antagonist before stimulation with 10 μM agonists or 200 $\mu g/mL$ of IgG. AngII, angiotensin II; AT₁, angiotensin II receptor type 1; AUC, area under the curve; CI, cell index; $\Delta\Delta Ct$, gene expression fold change; *CCL2*, CC chemokine ligand 2; ET-1, endothelin-1; ET_AR, endothelin-1 type A receptor; HD, healthy donor; HUVEC, human umbilical vein endothelial cell; *ICAM1*, intercellular adhesion molecule 1; IL-6, interleukin-6; nCI, normalized cell index; ns, not specific; PBS, phosphate buffered saline; *SELE*, selectin E; SSc, systemic sclerosis; TNF α , tumor necrosis factor α . Color figure can be viewed in the online issue, which is available at <http://onlinelibrary.wiley.com/doi/10.1002/art.43099/abstract>.

SSc IgG and the activation of AT₁ using an AT₁-overexpressing CHO model. Next, model cell lines overexpressing either human AT₁ (CHO-AT₁) and human ET_AR (CHO-ET_AR) were established. These cell lines were characterized using RTCA to ensure potent and specific AngII- and ET-1-mediated activation of AT₁ and ET_AR, respectively (Supplementary Figures 2 and 3).

Specificity of AngII for AT₁ was tested by stimulating parental (ie, nontransfected) CHO and CHO-AT₁ cells with 1 nM AngII (Figure 2A). No response was detected in the parental cells following AngII stimulation, whereas CHO-AT₁ exhibited an increasing response within the initial five minutes, indicating a potent and

functional AT₁ response. Pretreatment with 1 μ M AT₁ antagonist valsartan decreased net AUC by 74% compared to the response of vehicle-pretreated cells (Figure 2B), indicating the suitability of this model for studying selective AT₁ activation. Next, CHO-AT₁ cells were stimulated for 60 minutes with 200 μ g/mL of purified IgG of 4 HDs and 18 patients with SSc. As presented in Figure 2C, baseline-corrected nCI values did not reveal any response to IgG. Additionally, no discernible differences between HD and SSc IgG or in curve traces between cells pretreated with valsartan and those pretreated with vehicle could be observed. Quantification of responses into Net AUC showed no stimulatory effect of IgG, whereas stimulation with 1 nM AngII led to a potent

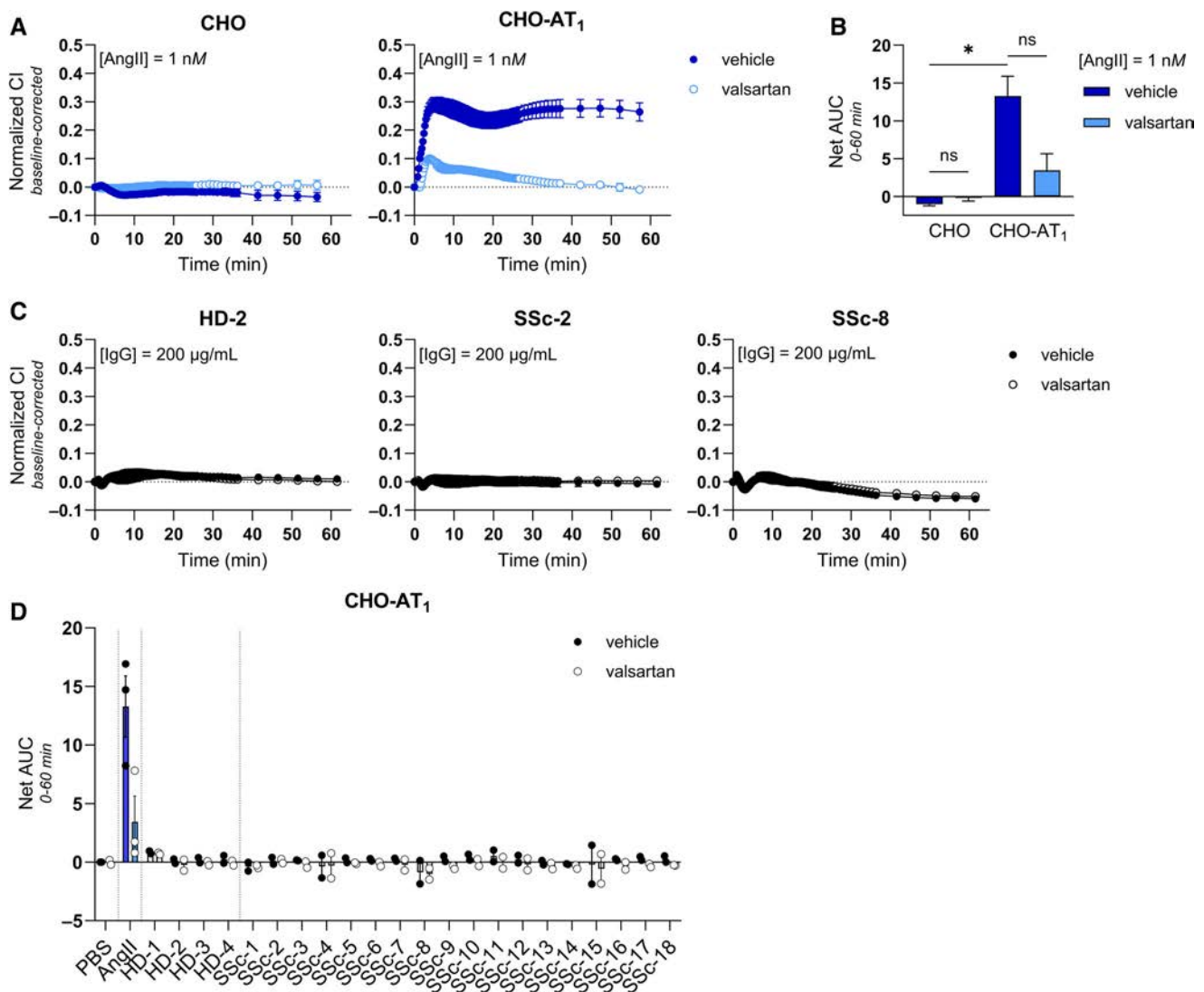


Figure 2. No observed effect of SSc IgG on CHO-AT₁ cells in an AT₁-mediated manner. (A) Representative graphs of baseline-corrected nCI traces of CHO and CHO-AT₁ cells pretreated with vehicle or 1 μ M valsartan before stimulation with 1 nM AngII. (B) Net AUC (mean \pm SEM, $n = 2-3$) of CHO and CHO-AT₁ 0- to 60-minute baseline-corrected nCI traces to 1 nM AngII. (C) Representative graphs of baseline-corrected nCI traces of CHO-AT₁ cells pretreated with vehicle or 1 μ M valsartan before stimulation with 200 μ g/mL of HD IgG or SSc IgG. (D) Net AUC (mean \pm SEM, $n = 2-3$) of CHO-AT₁ 0- to 60-minute baseline-corrected nCI traces to 1 nM of AngII or 200 μ g/mL of IgG in absence and presence of 1 μ M valsartan on the individual level. AngII, angiotensin II; AT₁, angiotensin II receptor type 1; AUC, area under the curve; CHO, Chinese hamster ovary; CI, cell index; HD, healthy donor; nCI, normalized cell index; ns, not specific; PBS, phosphate buffered saline; SSc, systemic sclerosis. Color figure can be viewed in the online issue, which is available at <http://onlinelibrary.wiley.com/doi/10.1002/art.43099/abstract>.

AT₁-mediated response (Figure 2D). Taken together, we did not obtain evidence for AT₁-mediated activation by SSc IgG in the highly sensitive CHO-AT₁ cells.

SSc IgG and the activation of ET_AR using an ET_AR-overexpressing CHO model. Similarly, the specificity of the endogenous ligand ET-1 for ET_AR was confirmed by stimulating CHO and CHO-ET_AR with 10 nM of ET-1 (Figure 3A). No response was observed in parental CHO cells on ET-1 stimulation, whereas CHO-ET_AR displayed an increasing response in the first five minutes indicating functional expression of ET_AR

in transfected cells. Pretreatment with specific ET_AR antagonist BQ-123 decreased Net AUC by approximately 65% compared to the response of vehicle-pretreated cells (Figure 3B). Subsequently, isolated IgG from the same 4 HDs and 18 patients with SSc was used to stimulate CHO-ET_AR cells. Analogous to the curve traces obtained with HUVEC and CHO-AT₁R, no stimulatory effect of IgG on CHO-ET_AR cells was revealed (Figure 3C). Additionally, no observable differences between HD and SSc IgG or in curve traces between cells pretreated with valsartan and those pretreated with a vehicle could be observed. Quantification of responses into net AUC showed no stimulatory effect

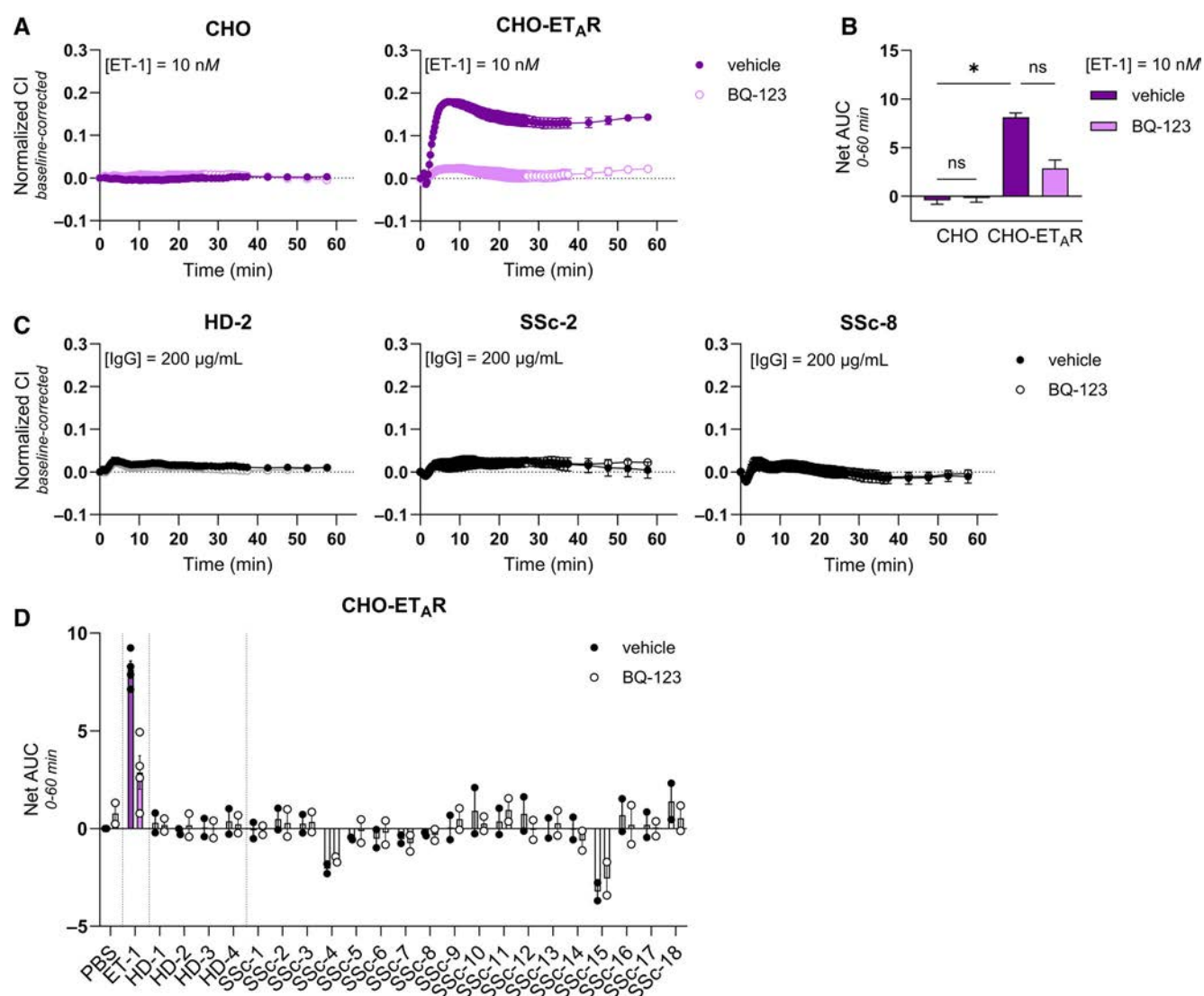


Figure 3. No observed effect of SSc IgG on CHO-ET_AR cells in an ET_AR-mediated manner. (A) Representative graphs of baseline-corrected nCI traces of CHO and CHO-ET_AR cells pretreated with a vehicle or 1 μ M of BQ-123 before stimulation with 10 nM of ET-1. (B) Net AUC (mean \pm SEM, $n = 2-4$) of CHO and CHO-ET_AR 0- to 60-minute baseline-corrected nCI traces to 10 nM ET-1. (C) Representative graphs of baseline-corrected nCI traces of CHO-ET_AR cells pretreated with a vehicle or 1 μ M BQ-123 before stimulation with 200 μ g/mL of HD IgG or SSc IgG. (D) Net AUC (mean \pm SEM, $n = 2-4$) of CHO-ET_AR 0- to 60-minute baseline-corrected nCI traces to 10 nM ET-1 or 200 μ g/mL of IgG in the absence and presence of 1 μ M BQ-123 on an individual level. AUC, area under the curve; CHO, Chinese hamster ovary; CI, cell index; ET-1, endothelin-1; ET_AR, endothelin-1 type A receptor; HD, healthy donor; nCI, normalized cell index; ns, not specific; PBS, phosphate buffered saline; SSc, systemic sclerosis. Color figure can be viewed in the online issue, which is available at <http://onlinelibrary.wiley.com/doi/10.1002/art.43099/abstract>.

of IgG whereas stimulation with 10 nM ET-1 led to an ET_AR-mediated response (Figure 3D). Overall, similar to results obtained in CHO-AT₁ cells, there was no observed evidence for ET_AR activation by SSc IgG on CHO-ET_AR cells.

No evidence for allosteric effect of SSc IgG on AngII response in CHO-AT₁ model. To test for allosteric modulation by SSc IgG, CHO-AT₁ cells were stimulated with AngII ($10^{-9.5}$, $10^{-8.5}$, and $10^{-7.5}$ M) to obtain response curves without any IgG pretreatment (Figure 4A). Selected AngII concentrations are within the linear range of the concentration-response curve (Supplementary Figure 2) to ensure detectability of changes in agonistic response. Next, CHO-AT₁ cells were pretreated with 100 µg/mL of HD or SSc IgG followed by stimulation with AngII ($10^{-9.5}$, $10^{-8.5}$, and $10^{-7.5}$ M) for 60 minutes. No evident differences in curve traces were observed between cells without IgG pretreatment and those with IgG pretreatment (Figure 4B). Furthermore, IgG isolated from patients with SSc did not alter the response to AngII compared to cells pretreated with HD IgG. Quantification of the responses into the net AUC confirmed no significant difference in AngII response between HD and SSc IgG-pretreated cells (Figure 4C). Altogether, these data do not provide evidence for altered AT₁ signaling on AngII stimulation after pretreatment with SSc IgG.

No evidence for allosteric effect of SSc IgG on ET-1 response in CHO-ET_AR model. Similarly, CHO-ET_AR cells were stimulated with ET-1 (10^{-9} , 10^{-8} , and 10^{-7} M) to obtain responses without any IgG pretreatment (Figure 5A). Next, cells were pretreated with 100 µg/mL of HD or SSc IgG pretreatment followed by ET-1 (10^{-9} , 10^{-8} , and 10^{-7} M) stimulation for 30 minutes. IgG-pretreated cells showed no observable differences in curve traces compared to vehicle-pretreated cells (Figure 5B). Additionally, SSc IgG pretreatment did not affect the response to ET-1 compared to pretreatment with HD IgG. Quantification of the responses into the net AUC confirmed no significant difference in net AUC between HD and SSc IgG-pretreated cells (Figure 5C). Altogether, these data do not provide evidence for altered ET_AR signaling on ET-1 stimulation after pretreatment with SSc IgG.

No AT₁-binding IgG detected in SSc plasma using solubilized membrane proteins. Given the absence of direct functional or response-modifying effects of SSc IgG in an AT₁- or ET_AR-dependent manner, a new protein capture assay independent of receptor activation was established to detect the potential presence GPCR-binding autoantibodies. In this assay, the GPCRs retain their 3D-conformational integrity in detergent micelles. Epitope-tagged AT₁ was expressed and solubilized into

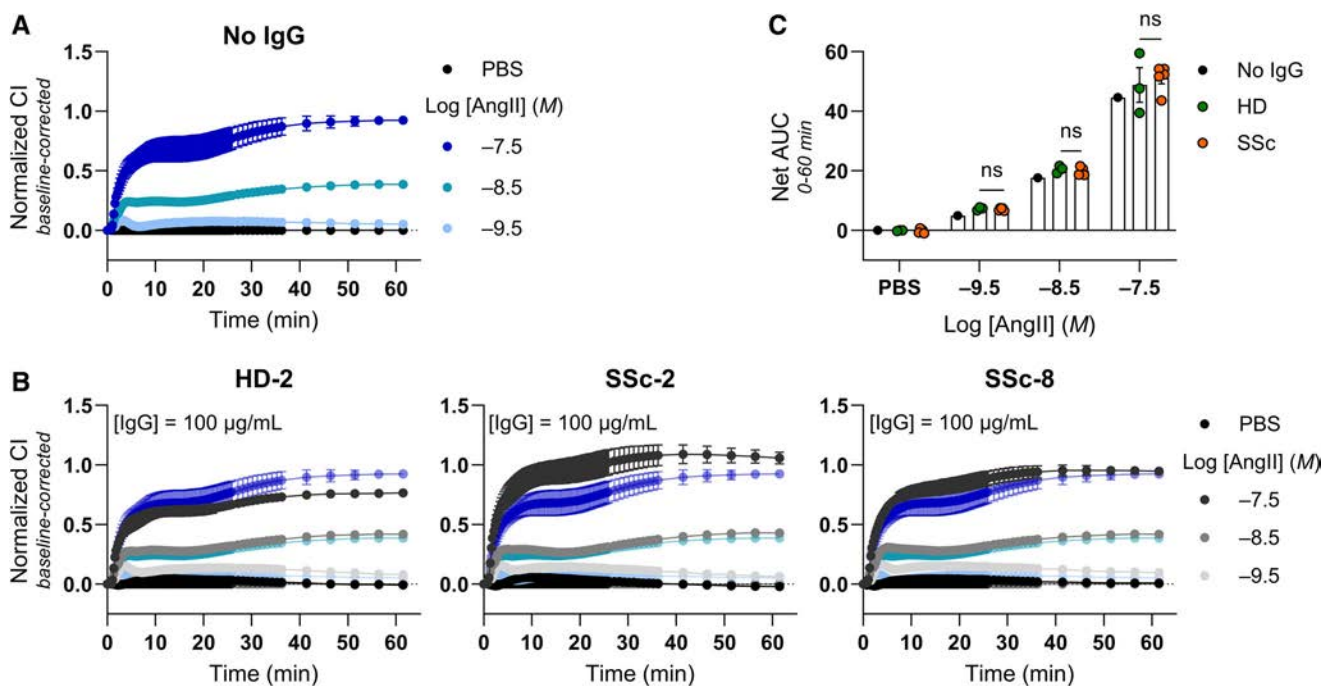


Figure 4. Pretreatment with SSc IgG does not alter AngII responses in CHO-AT₁ cells. (A) Representative graph of baseline-corrected normalized CI traces of CHO-AT₁ cells stimulated with $10^{-9.5}$ to $10^{-7.5}$ M AngII without any IgG pretreatment. (B) Representative graphs of CHO-AT₁ cells pretreated with 100 µg/mL of HD IgG or IgG derived from patients with SSc before stimulation with $10^{-9.5}$ to $10^{-7.5}$ M AngII. (C) Net AUC (mean ± SEM) of CHO-AT₁ cells pretreated with 100 µg/mL of IgG before stimulation with AngII. Dots represent mean net AUC of two individual performed experiments with technical duplicates. Statistical analysis using the Mann-Whitney U-test with Dunn's correction for multiple testing. AngII, angiotensin II; AT₁, angiotensin II receptor type 1; AUC, area under the curve; CHO, Chinese hamster ovary; CI, cell index; HD, healthy donor; ns, not significant; PBS, phosphate buffered saline; SSc, systemic sclerosis.

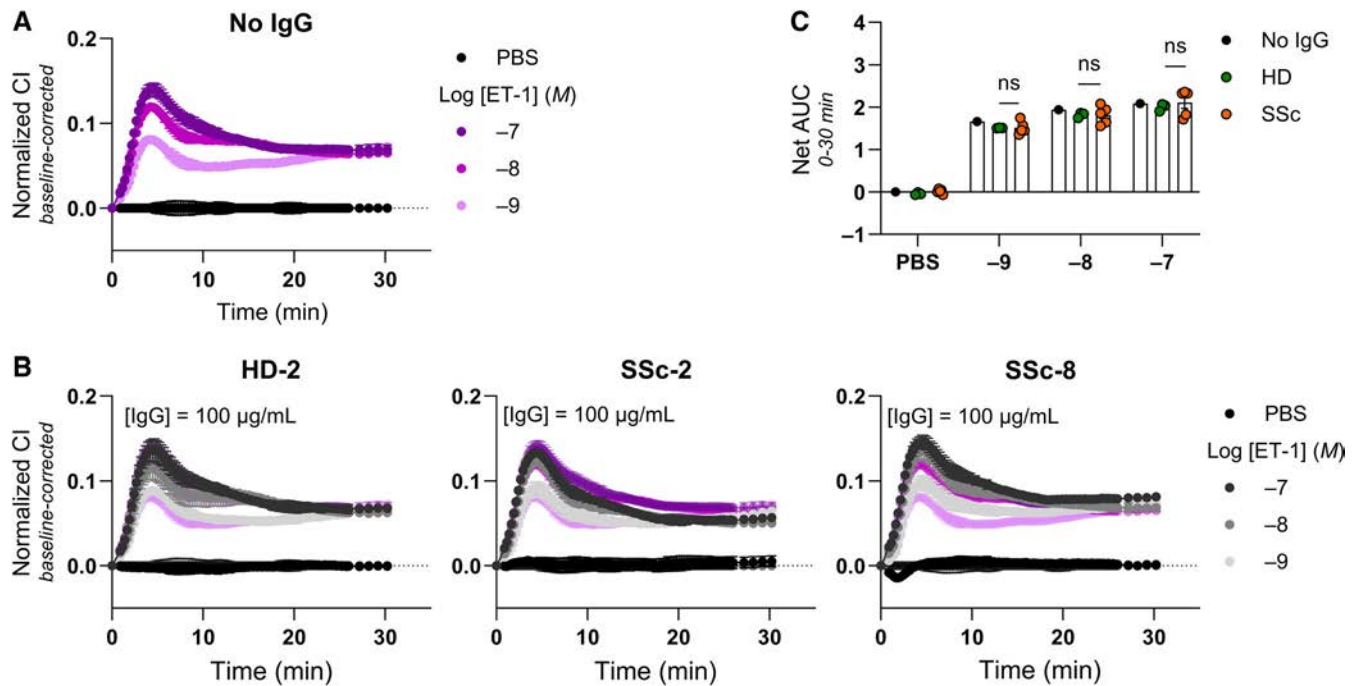


Figure 5. Pretreatment with SSc IgG does not alter ET-1 responses in CHO-ET_AR cells. (A) Representative graph of baseline-corrected normalized CI traces of CHO-ET_AR cells stimulated with 10⁻⁹ to 10⁻⁷ M ET-1 without any IgG pretreatment. (B) Representative graphs of CHO-ET_AR cells pretreated with 100 μg/mL of HD IgG or SSc IgG before stimulation with 10⁻⁹ to 10⁻⁷ M ET-1. (C) Net AUC (mean ± SEM) of CHO-ET_AR cells pretreated with 100 μg/mL of IgG before stimulation with ET-1. Dots represent mean net AUC of two individual performed experiments with technical duplicates. Statistical analysis using the Mann-Whitney U-test with Dunn's correction for multiple testing. AUC, area under the curve; CHO, Chinese hamster ovary; CI, cell index; ET-1, endothelin-1; ET_AR, endothelin-1 type A receptor; HD, healthy donor; ns, not significant; PBS, phosphate buffered saline; SSc, systemic sclerosis.

micelles as described in the material and methods section. Before solubilization, the presence of AT₁ in transfected cells was confirmed via the N-terminal FLAG tag using flow cytometry (Supplementary Figure 4). Solubilized GPCRs were added to anti-1D4-coated wells to capture GPCRs via their C-terminal

1D4 tag (Figure 6A). Solubilized membrane fractions from non-transfected cells (MOCK) were used as negative controls. None of the antibodies exhibited reactivity toward MOCK, whereas anti-CXCR3 and anti-CHRM3 antibodies displayed binding only to their respective solubilized GPCRs, confirming the specificity

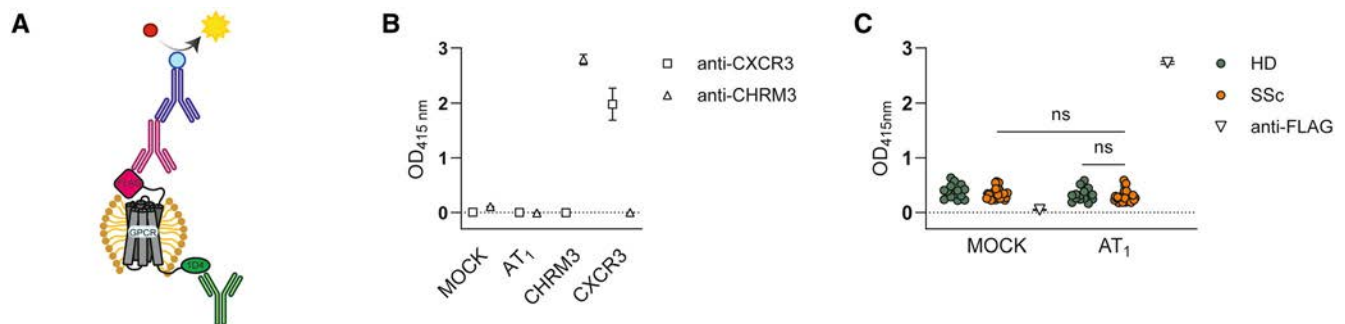


Figure 6. Detection of AT₁-binding IgG in circulation using protein capture assay. (A) Schematic figure of the protein capture assay using wells coated with 1 μg/mL of anti-1D4 tag antibody to capture solubilized GPCRs followed by detection with anti-FLAG tag antibody as positive control. (B) OD_{415 nm} values (mean ± SEM) of 0.4 μg/mL of anti-CXCR3 and 0.4 μg/mL of anti-CHRM3 antibodies toward 100 μg/mL of solubilized AT₁, CHRM3, and CXCR3. MOCK as negative control. (C) OD_{415 nm} values (mean ± SEM) of 1:100 diluted plasma samples towards 100 μg/mL solubilized membrane proteins of MOCK- or AT₁-transfected HEK293-FreeStyle cells. 2 μg/mL of anti-FLAG tag antibody was included as positive control. Dots represent average OD value of SSc plasma (n = 28) or HD plasma (n = 14) measured in duplicate. AT₁, angiotensin II receptor type 1; CHRM3, cholinergic receptor muscarinic 3; CXCR3, CXC Motif Chemokine Receptor 3; GPCR, G protein-coupled receptor; HD, healthy donor; MOCK, nontransfected cells; SSc, systemic sclerosis.

and sensitivity of this assay as well as the feasibility detection of the GPCRs (Figure 6B). Next, plasma samples from 28 patients with SSc, along with plasma samples of 14 HDs, were analyzed for AT₁-binding IgG using HRP-labeled anti-human IgG. Compared to MOCK, OD values for solubilized AT₁ did not increase for both HD and SSc plasma, whereas for anti-FLAG OD values increased from 0.05 to 2.7 (Figure 6C). Furthermore, no differences in AT₁-binding between HD and SSc plasma samples were detected. These findings do not provide evidence for the presence of AT₁-binding autoantibodies in circulation of patients with SSc and are in line with the other performed experiments.

DISCUSSION

SSc is a severe autoimmune disease marked by dysregulated immunity, fibrosis, and vasculopathy, with no existing cure. Given the early occurrence of vasculopathy in disease pathogenesis, it is essential for early intervention to understand the factors contributing to EC dysregulation and exaggerated vasoconstriction. Previous studies have described autoantibodies targeting AT₁ and ET_AR, two receptors pivotal to blood pressure homeostasis, as relevant contributors to the pathogenesis of SSc. These autoantibodies are described to activate their respective receptors, which leads to abnormal vasoconstriction and subsequent microangiopathy, implying potential involvement of anti-AT₁- and anti-ET_AR autoantibodies in SSc pathogenesis.^{16,37} However, the functional effects of anti-AT₁- and anti-ET_AR autoantibodies have primarily been explored through nonspecific markers situated downstream in the GPCR signaling cascade, leaving their receptor-specific effects unclear.^{19,38} In this study, we employed a combination of conventional techniques such as qPCR and ELISA, alongside a robust platform measuring morphologic changes on GPCR activation to investigate the functional effects of SSc IgG. Additionally, we established a novel protein capture assay using solubilized AT₁ in micelles to screen for anti-AT₁-binding autoantibodies in circulation. Despite using various techniques and different cell lines, our results do not provide evidence supporting the presence or functional role of AT₁- or ET_AR-binding autoantibodies in SSc IgG or the presence of AT₁-binding autoantibodies in the circulation of patients with SSc.

The absence of a “positive” SSc-derived autoantibody-mediated signal could be a consequence of multiple factors. Our observations revealed no evidence of EC activation following incubation with SSc IgG, regardless of pretreatment with AT₁- and ET_AR-specific antagonists. Previous studies reported increased messenger RNA and protein levels of IL-8 and vascular cell adhesion molecule 1 after the incubation of ECs with SSc IgG in an AT₁- and ET_AR-dependent manner.¹⁸ However, these effects displayed high levels of variability and varied between EC donors. Therefore, possible EC donor-specific effects and a contribution of autoantibodies other than anti-AT₁ and anti-ET_AR to EC activation cannot be excluded, potentially

explaining differences in outcome. Another study reported EC proliferation and coagulation on stimulation with SSc IgG, resulting in extracellular signal-regulated kinase (ERK)1/2 phosphorylation in an AT₁- and ET_AR-dependent manner.³⁸ In the same study, stimulation with AngII and ET-1 did not show up-regulated ERK1/2 phosphorylation, which argues for AT₁- and ET_AR-independent effects. Similar findings were observed in another study,⁴⁰ in which no up-regulation of pERK1/2, mechanistic target of rapamycin complex 1 (mTORC1), or mTORC2 was detected following stimulation with AngII or ET-1. These findings align with our results, in which stimulation with AngII or ET-1 did not result in the up-regulation of markers for EC activation or a direct AT₁- or ET_AR-mediated response, as measured with RTCA. Overall, our data indicate no AT₁- or ET_AR-dependent activation of EC by SSc IgG, and neither could agonist-mediated activation of EC be detected. This raises questions regarding the suitability of EC to study the presence and effects of AT₁- and ET_AR-activating autoantibodies in total IgG derived from patients with SSc.

Considering the reported low endogenous expression levels of GPCRs on human cells,^{24,41–44} it is possible that AT₁ and ET_AR expression on HUVECs might be insufficient to detect activation of these receptors by SSc IgG. Therefore, we established models using CHO cells that overexpress the human AT₁ and ET_AR, respectively to study these receptors. Agonist-mediated responses were measured in real-time, which could be effectively blocked with receptor-specific antagonists, confirming the suitability of this method to study AT₁ and ET_AR activation specifically and sensitively. However, while activation of AT₁ and ET_AR was observed upon stimulation with AngII and ET-1 respectively, no such effects were detected when using SSc IgG. Although some individuals displayed minimal changes in net AUC compared to control, the curve traces remained comparable irrespective of antagonist pretreatment. This suggests that any observed changes in impedance are likely not attributable to AT₁- or ET_AR activation.

Instead of direct activation, autoantibodies may alter the affinity of the natural agonist for the orthosteric binding pocket through allosteric modulation, a phenomenon previously described⁴⁵ for AT₁. Allosteric ligands blocked the binding of rat polyclonal IgG to extracellular loop 2, thereby attenuating AngII-mediated signaling. While previous studies detected changes in intracellular Ca²⁺ levels when incubating CHO cells transiently expressing AT₁ with precipitated SSc IgG before stimulation with AngII,⁴⁶ our study did not observe changes in net AUC values following the incubation of CHO-AT₁ or CHO-ET_AR with SSc IgG compared to controls. Differences in outcome could potentially be explained by discrepancies in preparation methods of IgG fractions, the concentration of AngII used for stimulation, and the use of transiently transfected cells.

We developed a novel protein capture assay to screen for AT₁-binding autoantibodies in SSc plasma to distinguish between

the functionality and binding characteristics of autoantibodies. To minimize interference of nuclear antigens, AT₁ was solubilized into micelles and captured via their 1D4-tag using antibody-coated wells. Micelles containing solubilized, epitope-tagged CXCR3 and CHRM3 were included as technical controls for GPCR conformation after solubilization, as well-validated antibodies are available for these two GPCRs, unlike AT₁ and ET_AR.⁴⁷ Despite the presence of AT₁, OD values of all plasma samples toward solubilized AT₁ were consistently low and comparable to values using solubilized membrane fractions of nontransfected cells, in which tag-specific capturing is not applicable. Furthermore, OD values of plasma samples from patients with SSC toward AT₁ did not differ from those of plasma from HDs. These observations argue against the presence of AT₁-binding autoantibodies in the circulation of patients with SSC. It would, therefore, be of relevance to scrutinize whether the commercially available assays used for detecting anti-AT₁ and anti-ET_AR reactivity could effectively detect antibodies against other antigens such as nuclear or cytoplasmic proteins. Unfortunately, protocols and reagents for these assays have not been shared, complicating such endeavors. Previous studies reported a strong correlation between ATA and anti-AT₁ and anti-ET_AR autoantibodies. Additionally, high prevalence of positive reactivity was observed in plasma samples from other diseases associated with ANA, whereas samples from diseases with no known ANA levels were nearly negative.⁴⁶ Further research into the specificity of these commercial assays is needed to exclude the possibility of detected ANA instead of the presumed AT₁- and ET_AR-binding autoantibodies in plasma derived from patients with SSC.

Finally, while multiple reports described the presence of AT₁- and ET_AR-binding autoantibodies in association with clinical manifestations in SSC,^{16,19,38,40,48} other reports found no correlation between the presence of these autoantibodies and clinical disease manifestations.^{2,49} This discrepancy raises questions about the clinical relevance of these autoantibodies in to identify and discriminate patients with SSC, leaving their role in SSC pathogenesis unclear. Similar observations have been described for autoantibodies targeting platelet-derived growth factor receptor (PDGFR). Initial reports suggested that stimulatory anti-PDGFR autoantibodies were a disease-specific hallmark of SSC.⁵⁰ Later studies detected these autoantibodies in the sera of HDs and without agonistic activity, highlighting the uncertain clinical significance and technical challenges in determining the role of functional autoantibodies in SSC pathogenesis.^{51,52}

It is essential to acknowledge certain limitations in our study. Firstly, the sample size employed in functional studies, comprising 4 HDs and 18 patients with SSC, may be considered relatively small, particularly given the heterogeneous nature of SSC. Moreover, the use of cell lines to investigate AT₁ and ET_AR activation by autoantibodies could be considered artificial compared to the natural physiologic environment. Another limitation of our study is the absence of an anti-AT₁ or anti-ET_AR agonistic antibody,

which could have served as positive control to further validate the assays used in our study. Although in one study an anti-AT₁-activating mAb was described, it was generated by immunizing mice with membrane extracts of human AT₁-expressing CHO cells, making it disease unspecific.⁵³ Furthermore, its production relied on the screening of mouse hybridoma culture supernatants for anti-AT₁ antibodies using the commercially available anti-AT₁ ELISA, of which the specificity has been questioned in this article.⁵³ Although our study did not observe changes in AngII- or ET-1-mediated signaling on incubation with SSC IgG using RTCA, it is possible that long-lasting effects targeting different pathways been overlooked. However, the lack of responses observed in HUVECs over a 48-hour time interval on incubation with SSC IgG does not support a major role for long-lasting signaling pathways. Lastly, while we assessed presence of AT₁-binding autoantibodies in circulation was assessed, there is currently no data available regarding ET_AR-binding autoantibodies.

In summary, our study did not yield evidence supporting the presence of AT₁- or ET_AR-activating autoantibodies in purified SSC IgG. Both direct agonistic effect as well as modulated responses of the natural agonist were assessed. Furthermore, we did not detect AT₁-binding IgG in circulation of patients with SSC. Because the correlation to disease manifestations and specificity to SSC pathogenesis remains controversial, the clinical relevance of using anti-AT₁ and anti-ET_AR autoantibodies as biomarkers in SSC becomes unclear.

ACKNOWLEDGMENTS

The authors thank Dr Riemekasten and her colleagues for measuring the anti-AT₁ and anti-ET_AR antibody levels in serum with their solid phase ELISA, as published previously.¹⁹

AUTHOR CONTRIBUTIONS

All authors contributed to at least one of the following manuscript preparation roles: conceptualization AND/OR methodology, software, investigation, formal analysis, data curation, visualization, and validation AND drafting or reviewing/editing the final draft. As corresponding author, Dr Fehres confirms that all authors have provided the final approval of the version to be published, and takes responsibility for the affirmations regarding article submission (eg, not under consideration by another journal), the integrity of the data presented, and the statements regarding compliance with institutional review board/Declaration of Helsinki requirements.

REFERENCES

1. Denton CP, Khanna D. Systemic sclerosis. *Lancet* 2017;390(10103):1685–1699.
2. Lemmers JM, van Caam AP, Kersten B, et al. Nailfold capillaroscopy and candidate-biomarker levels in systemic sclerosis-associated pulmonary hypertension: a cross-sectional study. *J Scleroderma Relat Disord* 2023;8(3):221–230.
3. van Leeuwen NM, Liem SIE, Maurits MP, et al. Disease progression in systemic sclerosis. *Rheumatology (Oxford)* 2021;60(3):1565–1567.

4. Wortel CM, Liem SI, van Leeuwen NM, et al. Anti-topoisomerase, but not anti-centromere B cell responses in systemic sclerosis display active, Ig-secreting cells associated with lung fibrosis. *RMD Open* 2023;9(3):e003148.
5. Wigley FM. Clinical practice. Raynaud's phenomenon. *N Engl J Med* 2002;347(13):1001–1008.
6. Weir MR, Dzau VJ. The renin-angiotensin-aldosterone system: a specific target for hypertension management. *Am J Hypertens* 1999;12(12 Pt 3):205S–213S.
7. Dziadzio M, Denton CP, Smith R, et al. Losartan therapy for Raynaud's phenomenon and scleroderma: clinical and biochemical findings in a fifteen-week, randomized, parallel-group, controlled trial. *Arthritis Rheum* 1999;42(12):2646–2655.
8. Böhm F, Pernow J. The importance of endothelin-1 for vascular dysfunction in cardiovascular disease. *Cardiovasc Res* 2007;76(1):8–18.
9. Steen VD, Costantino JP, Shapiro AP, et al. Outcome of renal crisis in systemic sclerosis: relation to availability of angiotensin converting enzyme (ACE) inhibitors. *Ann Intern Med* 1990;113(5):352–357.
10. Bütikofer L, Varisco PA, Distler O, et al; EUSTAR collaborators. ACE inhibitors in SSc patients display a risk factor for scleroderma renal crisis—a EUSTAR analysis. *Arthritis Res Ther* 2020;22(1):59.
11. Matucci-Cerinic M, Denton CP, Furst DE, et al. Bosentan treatment of digital ulcers related to systemic sclerosis: results from the RAPIDS-2 randomised, double-blind, placebo-controlled trial. *Ann Rheum Dis* 2011;70(1):32–38.
12. Kawaguchi Y, Takagi K, Hara M, et al. Angiotensin II in the lesional skin of systemic sclerosis patients contributes to tissue fibrosis via angiotensin II type 1 receptors. *Arthritis Rheum* 2004;50(1):216–226.
13. Seibold JR, Denton CP, Furst DE, et al. Randomized, prospective, placebo-controlled trial of bosentan in interstitial lung disease secondary to systemic sclerosis. *Arthritis Rheum* 2010;62(7):2101–2108.
14. Khanna D, Denton CP, Merkel PA, et al; DUAL-1 Investigators; DUAL-2 Investigators. Effect of macitentan on the development of new ischemic digital ulcers in patients with systemic sclerosis: Dual-1 and Dual-2 randomized clinical trials. *JAMA* 2016;315(18):1975–1988.
15. Galiè N, Barberà JA, Frost AE, et al; AMBITION Investigators. Initial use of ambrisentan plus tadalafil in pulmonary arterial hypertension. *N Engl J Med* 2015;373(9):834–844.
16. Becker MO, Kill A, Kutsche M, et al. Vascular receptor autoantibodies in pulmonary arterial hypertension associated with systemic sclerosis. *Am J Respir Crit Care Med* 2014;190(7):808–817.
17. Reinsmoen NL, Lai CH, Heidecke H, et al. Anti-angiotensin type 1 receptor antibodies associated with antibody mediated rejection in donor HLA antibody negative patients. *Transplantation* 2010;90(12):1473–1477.
18. Kill A, Tabeling C, Undeutsch R, et al. Autoantibodies to angiotensin and endothelin receptors in systemic sclerosis induce cellular and systemic events associated with disease pathogenesis. *Arthritis Res Ther* 2014;16(1):R29.
19. Riemekasten G, Philippe A, Näther M, et al. Involvement of functional autoantibodies against vascular receptors in systemic sclerosis. *Ann Rheum Dis* 2011;70(3):530–536.
20. Wallukat G, Homuth V, Fischer T, et al. Patients with preeclampsia develop agonistic autoantibodies against the angiotensin AT₁ receptor. *J Clin Invest* 1999;103(7):945–952.
21. Dragun D, Müller DN, Bräsen JH, et al. Angiotensin II type 1-receptor activating antibodies in renal-allograft rejection. *N Engl J Med* 2005;352(6):558–569.
22. Bian J, Lei J, Yin X, et al. Limited AT₁ receptor internalization is a novel mechanism underlying sustained vasoconstriction induced by AT₁ receptor autoantibody from preeclampsia. *J Am Heart Assoc* 2019;8(6):e011179.
23. Pearl MH, Chen L, ElChaki R, et al. Endothelin type A receptor antibodies are associated with angiotensin II type 1 receptor antibodies, vascular inflammation, and decline in renal function in pediatric kidney transplantation. *Kidney Int Rep* 2020;5(11):1925–1936.
24. Rosenbaum DM, Rasmussen SGF, Kobilka BK. The structure and function of G-protein-coupled receptors. *Nature* 2009;459(7245):356–363.
25. Yang D, Zhou Q, Labroska V, et al. G protein-coupled receptors: structure- and function-based drug discovery. *Signal Transduct Target Ther* 2021;6(1):7.
26. Speck D, Kleinau G, Szczepek M, et al. Angiotensin and endothelin receptor structures with implications for signaling regulation and pharmacological targeting. *Front Endocrinol (Lausanne)* 2022;13:880002.
27. Li Y, Li B, Chen W-D, et al. Role of G-protein coupled receptors in cardiovascular diseases. *Front Cardiovasc Med* 2023;10:1130312.
28. Higuchi S, Ohtsu H, Suzuki H, et al. Angiotensin II signal transduction through the AT₁ receptor: novel insights into mechanisms and pathophysiology. *Clin Sci (Lond)* 2007;112(8):417–428.
29. van den Hoogen F, Khanna D, Fransen J, et al. Classification criteria for systemic sclerosis: an American College of Rheumatology/European League against Rheumatism collaborative initiative. *Arthritis Rheum* 2013;65(11):2737–2747.
30. Taylor SC, Nadeau K, Abbasi M, et al. The ultimate qPCR experiment: producing publication quality, reproducible data the first time. *Trends Biotechnol* 2019;37(7):761–774.
31. Doornbos MLJ, Heitman LH. Label-free impedance-based whole cell assay to study GPCR pharmacology. *Methods Cell Biol* 2019;149:179–194.
32. Doornbos MLJ, Van der Linden I, Vereyken L, et al. Constitutive activity of the metabotropic glutamate receptor 2 explored with a whole-cell label-free biosensor. *Biochem Pharmacol* 2018;152:201–210.
33. Ke N, Nguyen K, Irelan J, et al. Multidimensional GPCR profiling and screening using impedance-based label-free and real-time assay. *Methods Mol Biol* 2015;1272:215–226.
34. Chen ANY, Malone DT, Pabreja K, et al. Detection and quantification of allosteric modulation of endogenous m4 muscarinic acetylcholine receptor using impedance-based label-free technology in a neuronal cell line. *J Biomol Screen* 2015;20(5):646–654.
35. Hillger JM, le Roy B, Wang Z, et al. Phenotypic screening of cannabinoid receptor 2 ligands shows different sensitivity to genotype. *Biochem Pharmacol* 2017;130:60–70.
36. Lorenzen E, Dodig-Crnković T, Kotliar IB, et al. Multiplexed analysis of the secretin-like GPCR-RAMP interactome. *Sci Adv* 2019;5(9):eaaw2778.
37. Berger M, Steen VD. Role of anti-receptor autoantibodies in pathophysiology of scleroderma. *Autoimmun Rev* 2017;16(10):1029–1035.
38. Catar R, Herse-Naether M, Zhu N, et al. Autoantibodies targeting AT₁- and ET_A-receptors link endothelial proliferation and coagulation via Ets-1 transcription factor. *Int J Mol Sci* 2021;23(1):244.
39. Mocking TAM, van Oostveen WM, van Veldhoven JPD, et al. Label-free detection of prostaglandin transporter (SLCO2A1) function and inhibition: insights by wound healing and TRACT assays. *Front Pharmacol* 2024;15:1372109.
40. Catar RA, Wischnewski O, Chen L, et al. Non-HLA antibodies targeting angiotensin II type 1 receptor and endothelin-1 type A receptors induce endothelial injury via β 2-arrestin link to mTOR pathway. *Kidney Int* 2022;101(3):498–509.
41. Fredriksson R, Schiöth HB. The repertoire of G-protein-coupled receptors in fully sequenced genomes. *Mol Pharmacol* 2005;67(5):1414–1425.
42. Regard JB, Sato IT, Coughlin SR. Anatomical profiling of G protein-coupled receptor expression. *Cell* 2008;135(3):561–571.

43. Okuno K, Torimoto K, Cicalese SM, et al. Angiotensin II type 1A receptor expressed in smooth muscle cells is required for hypertensive vascular remodeling in mice infused with angiotensin II. *Hypertension* 2023;80(3):668–677.
44. Davenport AP, Hyndman KA, Dhaun N, et al. Endothelin. *Pharmacol Rev* 2016;68(2):357–418.
45. Singh KD, Jara ZP, Harford T, et al. Novel allosteric ligands of the angiotensin receptor AT1R as autoantibody blockers. *Proc Natl Acad Sci USA* 2021;118(33):e2019126118.
46. Bankamp L, Preuß B, Pecher AC, et al. Functionally active antibodies to the angiotensin II type 1-receptor measured by a luminometric bioassay do not correlate with clinical manifestations in systemic sclerosis: a comparison with antibodies to vascular receptors and topoisomerase I detected by ELISA. *Front Immunol* 2021;12:786039.
47. Dahl L, Kotliar IB, Bendes A, et al. Multiplexed selectivity screening of anti-GPCR antibodies. *Sci Adv* 2023;9(18):eadf9297.
48. Günther J, Kill A, Becker MO, et al. Angiotensin receptor type 1 and endothelin receptor type A on immune cells mediate migration and the expression of IL-8 and CCL18 when stimulated by autoantibodies from systemic sclerosis patients. *Arthritis Res Ther* 2014;16(2):R65.
49. İlgen U, Yayla ME, Düzgün N. Anti-angiotensin II type 1 receptor autoantibodies (AT₁R-AAs) in patients with systemic sclerosis: lack of association with disease manifestations. *Rheumatol Int* 2017;37(4):593–598.
50. Baroni SS, Santillo M, Bevilacqua F, et al. Stimulatory autoantibodies to the PDGF receptor in systemic sclerosis. *N Engl J Med* 2006;354(25):2667–2676.
51. Balada E, Simeón-Aznar CP, Ordi-Ros J, et al. Anti-PDGFR- α antibodies measured by non-bioactivity assays are not specific for systemic sclerosis. *Ann Rheum Dis* 2008;67(7):1027–1029.
52. Loizos N, Lariccia L, Weiner J, et al. Lack of detection of agonist activity by antibodies to platelet-derived growth factor receptor α in a subset of normal and systemic sclerosis patient sera. *Arthritis Rheum* 2009;60(4):1145–1151.
53. Yue X, Yin J, Wang X, et al. Induced antibodies directed to the angiotensin receptor type 1 provoke skin and lung inflammation, dermal fibrosis and act species overarching. *Ann Rheum Dis* 2022;81(9):1281–1289.

Critical Role for Transglutaminase 2 in Scleroderma Skin Fibrosis and in the Development of Dermal Sclerosis in a Mouse Model of Scleroderma

Angela Y. Y. Tam,¹ Korsia Khan,¹ Shiwen Xu,¹ Marianne Bergin,² Linghong Huang,² Erik Arroyo Colon,¹ Danyi Cheng,¹ Elisabetta A. M. Verderio,³ Voon Ong,¹ Christopher P. Denton,¹ John Atkinson,² Tim S. Johnson,² and David J. Abraham¹

Objective. Scleroderma is a life-threatening autoimmune disease characterized by inflammation, tissue remodeling, and fibrosis. This study aimed to investigate the expression and function of transglutaminase 2 (TGM2) in scleroderma skin and experimentally induced dermal fibrosis to determine its potential role and therapeutic implications.

Methods. We performed immunohistochemistry on skin sections to assess TGM2 expression and localization, and protein biochemistry of both systemic sclerosis-derived and healthy control dermal fibroblasts to assess TGM2 expression, function, and extracellular matrix deposition in the presence of TGM2 inhibiting and transforming growth factor (TGF)- β neutralizing antibodies and a small-molecule inhibitor of the TGF- β RI kinase. Mice with a complete deficiency of TGM2 (*Tgm2*^{-/-}) were investigated in the bleomycin-induced model of skin fibrosis.

Results. TGM2 was found to be widely expressed in both control and scleroderma skin samples, as well as in cultured fibroblasts. Scleroderma fibroblasts exhibited elevated TGM2 expression, which correlated with increased expression of fibrosis markers (Col-1, α SMA, and CCN2). Inhibition of TGM2 using an inhibiting antibody reduced the expression of key markers of fibrosis. The effects of TGM2 inhibition were similar to those observed with TGF- β neutralization, suggesting a potential crosstalk between TGM2 and TGF- β signaling. Moreover, *TGM2* knockout mice showed significantly reduced dermal fibrosis compared with wild type mice. In vitro experiments with *TGM2*-deleted fibroblasts demonstrated impaired cell migration and collagen matrix contraction, which could be partially restored by exogenous TGF- β .

Conclusion. TGM2 can regulate several key profibrotic activities of TGF- β suggesting that attenuating TGM2 function may be of benefit in severe forms of connective tissue disease with skin fibrosis.

INTRODUCTION

The connective tissue disease scleroderma (systemic sclerosis [SSc]) is associated with significant morbidity and mortality, with survival dependent on disease subset and organ involvement.^{1,2} Despite some advances in treatments,³ there is an unmet need to develop more effective therapies. Elucidation of the pathobiology of scleroderma has been

extensively studied^{4,5} and characterized by vasculopathy and persistent inflammation promoting autoimmunity and excessive tissue remodeling and scarring leading to organ-based replacement fibrosis.^{6,7}

In scleroderma and other remodeling diseases, inflammation drives fibrosis, causing excessive scarring.⁸ Fibroblasts play a crucial role in fibrosis, exhibiting functional heterogeneity and undergoing phenotypic switching during fibrosis

Supported by UCB.

¹Angela Y. Y. Tam, BSc, PhD, Korsia Khan, BSc, Shiwen Xu, MD, PhD, Erik Arroyo Colon, BS, MSc, Danyi Cheng, BS, MS, Voon Ong, MD, PhD, Christopher P. Denton, MD, PhD, David J. Abraham, BSc, PhD: University College London, London, United Kingdom; ²Marianne Bergin, BSc, MS, Linghong Huang, BSc, PhD, John Atkinson, PhD, Tim S. Johnson, BSc, PhD: UCB, Slough, United Kingdom; ³Elisabetta A. M. Verderio, PhD: Nottingham Trent University, Nottingham, United Kingdom, and University of Bologna, Bologna, Italy.

Present address: Linghong Huang and Tim S. Johnson, Mestag Therapeutics Limited, Cambridge, and University of Sheffield, Sheffield, United Kingdom; John Atkinson, Gilead Sciences, Oxford, United Kingdom.

Dr Tam, Ms Khan, and Dr Xu contributed equally to this work. Drs Atkinson, Johnson, and Abraham contributed equally to this work.

Additional supplementary information cited in this article can be found online in the Supporting Information section (<https://acrjournals.onlinelibrary.wiley.com/doi/10.1002/art.43104>).

Author disclosures and graphical abstract are available at <https://onlinelibrary.wiley.com/doi/10.1002/art.43104>.

Address correspondence via email to David J. Abraham, BSc, PhD, at david.abraham@ucl.ac.uk; or to Tim S. Johnson, BSc, PhD, at T.Johnson@sheffield.ac.uk.

Submitted for publication October 5, 2023; accepted in revised form December 10, 2025.

development. In patients with scleroderma, skin sections reveal abundant fibroblast-like cells, including myofibroblasts, responsible for excessive production and deposition of extracellular matrix (ECM) proteins.⁹

Transforming growth factor (TGF)- β is a key driver of fibroblast activation to myofibroblasts in scleroderma.^{10,11} The TGF- β pathway has been extensively studied at the molecular level and in various fibrotic conditions, including renal and lung fibrosis.^{8,12}

Transglutaminases (TGMs) are a family of proteins with structural and functional homology that are enzymatically active and catalyze the formation of post-translational bonds between proteins.¹³ TGM2, one of the most studied members of the family, is expressed by many cell types and tissues.¹⁴ In addition to its catalytic function, TGM2 exhibits other functional activities, such as a mediating signaling via G-coupled protein receptors, as a coreceptor for integrin, a regulator of protein kinases, and an interactor with several proteins presenting adhesion or scaffold-like properties.^{14,15} Found mainly intracellularly, TGM2 can also be localized to the plasma membrane and found extracellularly.¹⁶ Within the extracellular environment, TGM2 can become active leading to the extensive crosslinking between many distinct ECM proteins (eg, collagens and fibronectin). Therefore, TGM2 is considered to play a key role in the regulation and homeostasis of the ECM in wound healing¹⁷ and other critical biologic processes such as cell adhesion, motility, and survival.^{14,18}

TGM2 has also been associated with a number of human diseases including inflammatory disorders, renal disease, pulmonary disorders, cancer, cardiovascular disease, and dementia.^{14,15} Indeed, there has been a recent focus on the role of TGM2 in aberrant tissue remodeling and function in scarring and fibrotic diseases.^{19–23} Because of the inherent complex functional activities, there are a number of ways that TGM2 may promote tissue scarring and fibrosis.¹⁵ For instance, the crosslinking of several common ECM proteins by TGM2 renders them more resistant to degradation, enhancing accumulation and dramatically altering the tissue stiffness and fibroblast cell-ECM biomechanics.^{16,17} An altered tissue biomechanical environment has been shown to be fundamental in regulating fibroblast function and the myofibroblast phenotype in fibrosis and scleroderma.¹¹ Furthermore, TGM2 impacts upon cell survival and enhances cell adhesion and migration,²⁴ which are all important aspects of scarring and fibrosis. Importantly TGM2 has been shown to play a crucial role in the activation of TGF- β 1 by crosslinking the large latent TGF- β 1 complex to the ECM initiating release of the active TGF- β 1 dimer.²⁵ This has been shown to be a rate-limiting step in TGF- β 1 activation in fibrotic models.²⁶ TGM2 has been shown to be important in studies using in vitro and in vivo models of kidney and lung fibrosis. In the in vitro investigations, TGM2 expression associated with markers of scarring and fibrosis and inhibition of TGM2 reduced myofibroblast formation.²³ In vivo studies showed that TGM2 knockout (KO) mice exhibited attenuated lung fibrosis following bleomycin

challenge²¹ and in a unilateral ureteral obstruction model of chronic kidney disease,²⁷ and the addition of a small-molecule TGM2 inhibitor reduced both glomerular and tubulointerstitial fibrosis in a rodent model of diabetic nephropathy.²⁰

A recent study has begun to dissect the intricate role of TGM2 in the activation of SSc fibroblasts and role of TGM2 in fibrosis.¹⁹ Here we deepen our understanding of TGM2 in the context of scleroderma. Investigations encompassing both skin sections and primary fibroblasts obtained from patients with scleroderma, alongside the bleomycin-induced skin injury model of sclerosis, sought to unravel the expression and activity of TGM2. These revealed that TGM2 is not only expressed by both control and scleroderma fibroblasts but also exhibits heightened expression levels in scleroderma, thus shedding light on a potentially key role in the pathogenesis of this complex disorder.

In control human dermal fibroblasts, TGM2 could be induced by TGF- β 1 treatment. The presence of a TGM2-inhibiting antibody²⁸ reduced the expression of fibrotic markers in scleroderma cells that were observed with a pan-TGF- β neutralizing antibody and an ALK5 inhibitor. TGF- β bioactivity and Smad2/3 phosphorylation were also reduced in TGM2 inhibited scleroderma cells. TGM2 KO mice were protected from skin sclerosis. Our data suggest that TGM2 plays a role in skin fibrosis in scleroderma involving interactions between TGM2 and TGF- β 1 in dermal fibroblasts leading to enhanced ECM production and a profibrotic phenotype.

MATERIALS AND METHODS

Cell culture. Human dermal fibroblast cultures were established from skin biopsies of patients with diffuse cutaneous SSc (dcSSc), and healthy control (HC) volunteers, as described previously.²⁹ All patients met the 2013 American College of Rheumatology/European League Against Rheumatism criteria for SSc.³⁰ Informed consent and ethical approval were obtained for all procedures. Fibroblasts were cultured until confluence, and all cell lines were used between passages 2 and 6 for experiments. Confluent monolayers were quiesced in 0.5% bovine serum albumin supplemented Dulbecco's Modified Eagle Medium for 24 hours before lysis for Western blotting. The study was approved by the Health Research Authority, National Research Ethics Service Committee London (Research Ethics Committee reference: 6398). For growth factor treatment, cells were incubated with TGF- β 1 (2 ng/mL; R&D Systems; Cat-7754-BH) and incubated for a further 24 hours before being lysed for Western blot analysis. The mature ECM deposited by cultured HC and scleroderma fibroblasts was assessed using a 384-well immunofluorescence assay.³¹ In some experiments, fibroblasts were cultured in the presence of a TGM2 inhibiting antibody,²⁸ a potent and selective TGF- β Type I receptor/ALK5 inhibitor (10 μ M; Tocris Cat1614), or inhibitory antibodies capable of neutralizing all forms of TGF- β (10 μ g/mL; 1D11 Cat - MAB1835).^{32,33}

Immunohistochemistry, activity, and antigen staining for TGM2.

Formalin-fixed 3 μ m paraffin sections were used for immunostaining following the blockade of the endogenous peroxidase using 3% hydrogen peroxide. Optimally diluted anti-TGM2 antibody (1.0 μ g/mL)²⁸ and anti-GAPDH (0.2 μ g/mL; Sigma; Cat -SAB4300645) were used in this series. Specificity of staining was confirmed in control sections incubated with an isotype-matched irrelevant control antibody. Antibodies were detected using the NovoLink polymer kit (Leica Microsystems Cat No: RE7150-K). Sections were viewed and photographed using a Zeiss Axioscope brightfield microscope using AxioVision software, digitalized using a Hamamatsu NanoZoomer 2.0-HT Slide Scanner, and visualized using the NDP viewer software. Staining intensity was assessed using semiquantitative assessment of epidermal, dermal, and perivascular staining by an experienced observer blinded to sample identity during scoring. The expression of TGM2 was assessed in whole skin biopsies examining global staining, epidermis, and dermis, infiltrating inflammatory cells when present and in and around vascular structures. Expression was assessed using a semiquantitative grading of the expression, and distribution of staining as assessed by five independent observers trained by a histopathologist and scored between 0 and 3 with 0 (no staining) and 3 (maximal staining) in 0.5 increments. Scoring was performed at $\times 40$ magnification using a global score across the section and three dermal areas for HC (n = 5): dcSSc lesional (n = 5), dcSSc nonlesional (NL; n = 5), established SSc (n = 5), and limited cutaneous SSc (lcSSc; n = 5). Total scores were obtained and average expression values calculated. Graphical data are presented as average staining score \pm SD. TGM2 activity was measured by the incorporation of biotinylated cadaverine or T26 peptide,²⁶ and TGM2 antigen staining was performed using TGM2 epitope-specific antibodies as described previously.²⁸

Western blot analysis and ECM deposition.

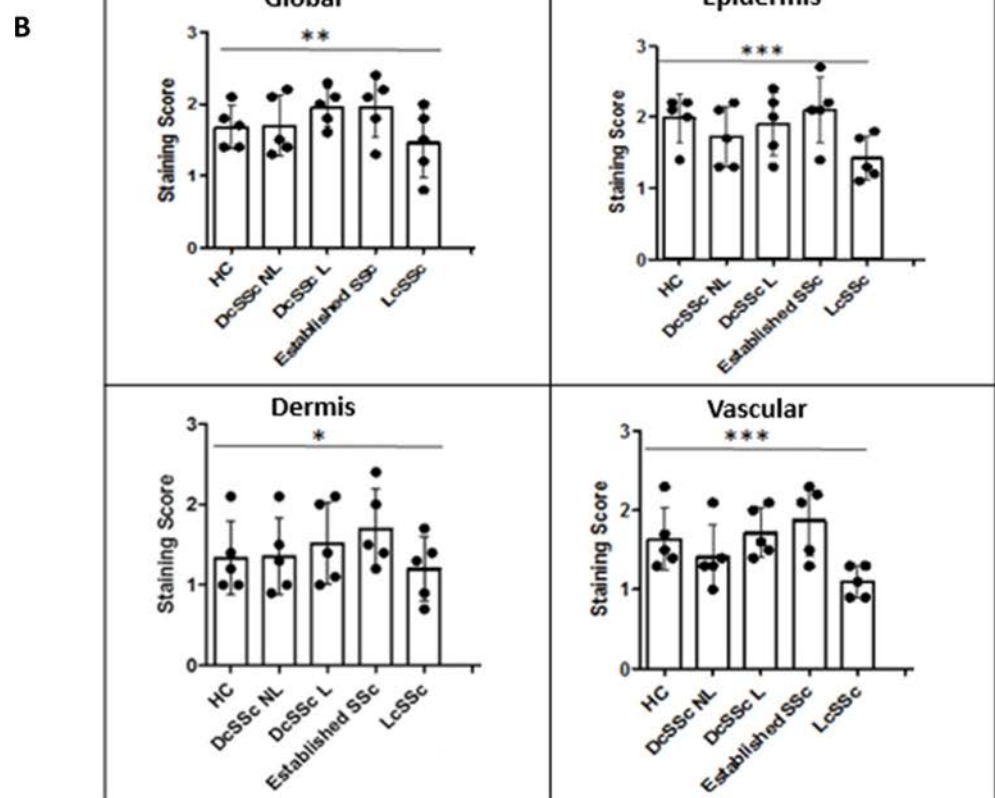
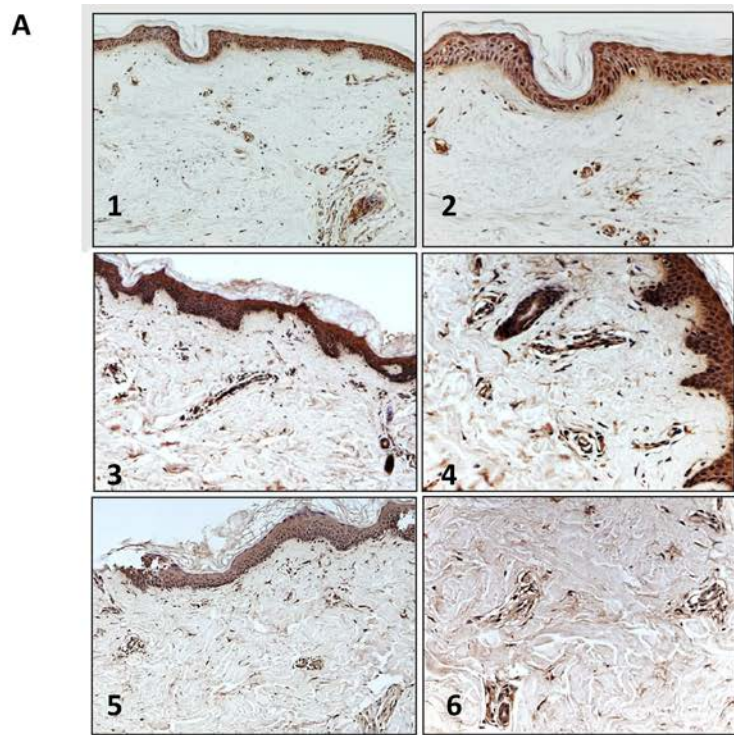
Fibroblasts were lysed in radioimmunoprecipitation assay buffer (Sigma) with protease inhibitors (Roche). Total protein concentration was determined by bicinchoninic acid assay (Pierce). Samples were heat denatured under reducing conditions with NuPAGE reducing agent (Invitrogen) and subjected to the NuPAGE electrophoresis system (Invitrogen). Protein bands were transferred onto nitrocellulose membranes (GE Healthcare), which were incubated in block buffer (5% nonfat dry milk, 0.1% Tween-20 [Sigma] in phosphate-buffered saline) for 1 hour, followed by incubation at 4°C overnight with primary antibodies against TGM2 (IA12, UCB Pharma), α -SMA (71 ng/mL, Dako; Cat M0851/1A4), Col-1 (0.4 μ g/mL, Millipore; Cat AB78), CCN2 (0.1 μ g/mL, Santa Cruz Biotechnology; Cat SC-14939), TNC2 μ g/mL (Proteintech; Cat 67710-1), Shad 2 (Cell signaling; Cat 5678), pSmad2/3 (Cell signaling; Cat 8828), and GAPDH (0.2 μ g/mL, Abcam; Cat Ab8245/6C5), diluted in block buffer. Blots were developed by incubation with horseradish

peroxidase-conjugated secondary antibodies (1:5000, for mouse -Cell Signaling; Cat 7076S, for rabbit -Cat 7074S). The signal was detected using enhanced chemiluminescence (Pierce) and exposure to Hyperfilm (GE Healthcare). For proteins of similar MW (CCN2, α -SMA, and GAPDH), equal amounts of protein were loaded, and samples were run simultaneously on separate blots and probed with antibodies, for proteins significantly different in MW (Col-1, TGM2, TNC2, GAPDH); the same blot was used and probed simultaneously with different antibodies. Densitometry was performed on the bands using Visionworks LS software and displayed in arbitrary densitometry units. For analysis of ECM deposition, dermal fibroblasts from HC and patients with SSc were cultured alone, with TGM2 inhibitory antibody BB7 or IgG control²⁸ for 7 days in black wall 384 well imaging plates (BD Biosciences). Cells were removed by lysis with ammonium hydroxide, and deposited proteins were fixed with ice-cold methanol. ECM accumulation was measured by immunofluorescence staining of individual matrix proteins. Cellomics Arrayscan analysis under the "Cellomics Cell Health" profiling bioapplication used a 10 \times objective and 2 \times 2 binning (1104 \times 1104 pixels/field) with "low pass filter" background correction. Matrix was stained with antibodies to fibronectin and collagens I, III, and IV.³¹

TGM2 KO mice. All mice used for experiments were aged 4 to 15 weeks at the beginning of the study, including male and female mice. Animals were genotyped by polymerase chain reaction. Mice harboring the *TGM2* null allele have been described previously.^{34,35}

Bleomycin murine model of dermal fibrosis. The bleomycin-induced murine model was performed by administration of bleomycin (2 units/mL; 0.5mg in 100 μ L sterile saline) or saline alone via subcutaneous injection into the dermis as described previously.³⁶ After 30 days (treatment time as indicated in each figure), skin tissue was harvested for histology and protein analysis and was fixed with neutral buffered formalin (10%; CellStor).

Skin histology and advanced microscopy. Mouse dermal samples were fixed in formalin and embedded in paraffin. These tissue blocks were sectioned (4–6 μ m) and mounted on glass slides for hematoxylin and eosin (Surgipath and Sigma), Picro Sirius Red (PSR) staining (WVR and Raymond Lab), or Goldner trichrome (MT), for general morphologic analysis and collagen deposition, respectively. The sections were imaged using the NanoZoomer (Hamamatsu) and analyzed using 10 \times magnification in the NDP View software or imaged using a Zeiss Axio Observer apotome microscope and Axio Cam MR R3 camera and viewed in ZEN Blue microscopy software. For polarized light microscopy,³⁷ samples were stained with PSR and observed using a polarized light microscope (Zeiss, Axioskop 2, mot plus). Quantification of collagen fibers under polarized light color



(Figure legend continues on next page.)

threshold analysis was assessed according to published protocols³⁸ to assess fibrillar hue and spatial distribution. Data are presented as percentage of stained fibrillar collagen fiber color. For scanning electron microscopy (SEM) of Col-1 fibrils, samples were prepared by fixation, followed by dehydration, mounting, sputter coated with gold, and images assessed for collagen fiber composition and morphology using a Philips (FEI) 501 Scanning Electron Microscope.³⁹ Wound closure and collagen gel contraction assays with fibroblasts were performed and assessed as previously described.^{40,41}

Statistical analysis. Statistical significance to compare groups was calculated by one way analysis of variance or unpaired student two-tailed *t*-test, as indicated, using Microsoft Excel or GraphPad Prism V8.43. A value of *P* < 0.05 was considered significant.

RESULTS

TGM2 expression in control and scleroderma skin and fibroblasts cultured in vitro. TGM2 expression in human skin biopsies was investigated using immunohistochemistry with the IA12 antibody. TGM2 staining was observed in all skin compartments (epidermis, dermis, vascular, and inflammatory infiltrates) in both HC and scleroderma samples (Figure 1A). In HC samples, prominent levels were found in the epidermis and vascular compartments, with lower levels in the dermis and inflammatory cells. TGM2 staining was distributed throughout the skin samples, with increased expression observed in inflammatory infiltrates and the dermis. Staining was also visible in secondary dermal structures. TGM2 expression in keratinocytes was evenly distributed in both HC and scleroderma tissue, with a slight decrease in NL samples and in lcSSc (Figure 1B). Elevated expression in dermal fibroblasts was observed in lesional dcSSc, whereas expression levels appeared unchanged in lcSSc and NL dcSSc. Vascular and perivascular staining levels of TGM2 remained unchanged across the scleroderma disease spectrum. Decreased staining

levels were observed in lcSSc samples. Elevated TGM2 staining in inflammatory infiltrates was prominent in NL and lesional dcSSc tissue, whereas lcSSc showed unaltered staining in inflammatory infiltrates (Figure 1B). The IA12 antibody used detected an approximately 80Kda protein band of TGM2 in all primary fibroblast lines (Figure 2A). TGM2 expression was higher in SSc fibroblasts compared with normal control counterparts (Figure 2A). Treatment with TGF- β 1 for 24 hours increased TGM2 levels in HC dermal fibroblasts, resembling the levels in SSc dermal cells (Figure 2B). In dermal biopsies, TGM2 insitu-activity was observed in the epidermis, hair follicles, dermis, and around blood vessels (Supplemental Figure 1A and 1B). Among the eight SSc skin samples examined, one showed increased extracellular TGM2 expression in the dermis, whereas two samples exhibited similar but lower expression levels. The remaining five samples had similar TGM2 staining as healthy volunteers. The three SSc skin biopsies with elevated extracellular TGM2 showed reduced TG activity in the dermis after zampilimab treatment, indicating TGM2-specific activity (Supplemental Figure 1E and F).

Inhibition of TGM2 attenuates the expression of fibrotic protein markers in SSc dermal fibroblasts in vitro. To examine the impact of TGM2 inhibition on fibrosis, the levels of Col-1, CCN2, and α SMA were assessed using specific antibodies and Western blotting (Figure 2C). HC and scleroderma fibroblasts were cultured alone and in the presence of increasing concentrations of TGM2 inhibitory antibody.²⁸ Scleroderma fibroblasts exhibited significantly elevated Col-1, α SMA, and CCN2 compared with HC. The presence of BB7 resulted in a decrease in Col-1, α SMA, and CCN2 in both cell types, first apparent at a concentration of approximately 500 nM. The BB7 dose-dependent decrease in Col-1, α SMA, and CCN2 was more pronounced with the scleroderma cells (Figure 2C). These results were further validated using three different HC and scleroderma cells lines at a dose of 1000 nM, which showed a maximum response in the dose response study (Figure 2D), where the level of expression of the three markers in scleroderma-derived

(Figure legend continued from previous page.)

Figure 1. TGM2 expression in control and scleroderma skin and the comparison of TGM2 expression patterns across the scleroderma disease spectrum. (A) Derma biopsies from HC patients with scleroderma (dcSSc; lesional and NL⁴²; lcSSc; and established SSc [>5 years duration]) were stained for TGM2 expression using immunohistochemistry (HC: panels 1 and 2; scleroderma NL skin: panels 3 and 4; scleroderma lesional skin: panels 5 and 6; magnification $\times 10$: left; magnification $\times 20$: right). (B) Comparison of expression patterns of TGM2 globally and within specific dermal compartments were made. Expression patterns of cross-sectional TGM2 and within specific dermal compartments were scored by five blinded observers experienced in examining skin tissue. A semiquantitative grading of the total expression and distribution of staining was employed. Staining was graded between 0 and 3 with 0 (no staining) and 3 (highest staining) in 0.5 increments. Examination was performed at $\times 40$ magnification on five randomly selected areas by each observer per control and disease biopsy. Total scores and average values were determined. Data represent mean staining score \pm SD from five biopsy samples. Total score values were used to assess relevance of the differences using statistical significance as determined by *t*-test **P* = 0.05. ***P* < 0.01, ****P* < 0.001. DcSSc, diffuse cutaneous systemic sclerosis; HC, healthy control, lcSSc, limited systemic sclerosis; NL, nonlesional; SSc, systemic sclerosis; TGM2, transglutaminase 2.

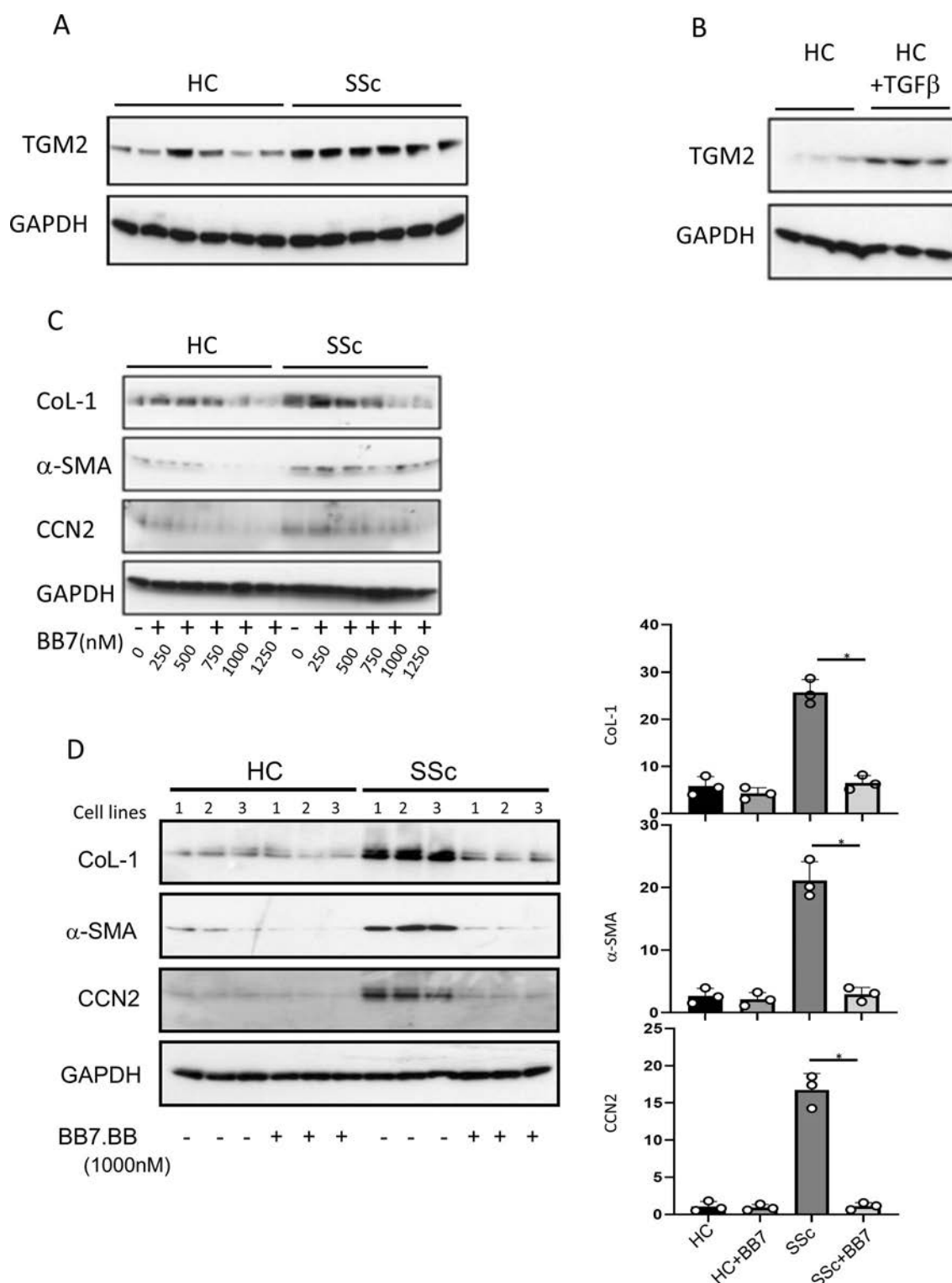
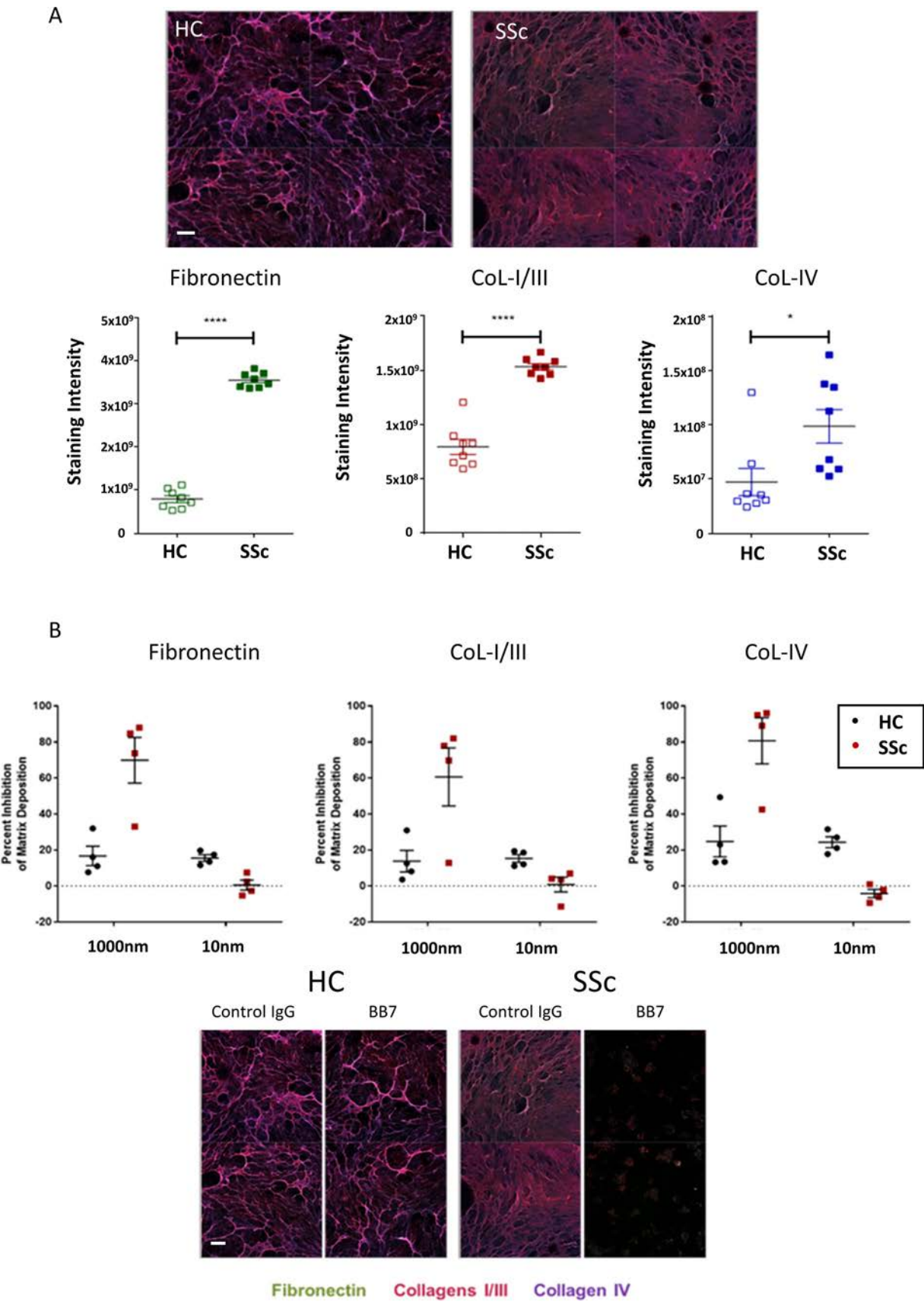


Figure 2. Increased expression of TGM2 by SSc fibroblasts and inhibition of TGM2 attenuates the expression of fibrotic protein markers in SSc dermal fibroblasts in vitro. (A) Expression of TGM2 (IA12 antibody) in primary HC fibroblasts ($n = 6$) and scleroderma fibroblasts ($n = 6$) was analyzed by Western blotting and normalized to expression of GAPDH. (B) TGM2 expression in primary HC fibroblasts ($n = 3$) was determined following fibroblast treatment with TGF- β 1 (4 ng/mL) for 24 hours. (C) Dermal fibroblasts isolated from HC and patients with SSc were cultured with TGM2 neutralizing antibody BB7.BB over a dose response range 0–1250 nM. (D) Survey of three HC and scleroderma fibroblasts cell lines culture in the presence of 1000 nM of BB7.BB. Expression of Col-1, α SMA, and CCN2 were analyzed by Western blotting and normalized to expression of GAPDH. Densitometry analysis of Western blots (D; right) is shown. Bars show mean \pm standard error of the mean. Statistical significance was tested using the t -test, $*P < 0.05$. HC, healthy control; SEM, scanning electron microscopy; SSc, scleroderma; TGF, transforming growth factor; TGM2, transglutaminase 2.



(Figure legend continues on next page.)

fibroblasts was found to be significantly reduced to between 70% and 90% of that present in the absence of BB7.

Deposition of ECM and impact of TGM2 inhibitory and TGF- β -neutralizing antibodies. The deposition of ECM by primary fibroblast cell lines was measured using a 384 well assay format and high-content image acquisition using Cellomics software as previously described.³¹ Significantly higher levels of all four ECM components, Fibronectin and collagens types I, III, and IV, were found to be accumulated by SSc fibroblasts compared with the HC cells (Figure 3A). This observation was particularly apparent when examining fibronectin and collagens Type I/III. The presence of the TGM2 inhibitory antibody (BB7;1000nM) resulted in a decrease in the amount of ECM deposited (Figure 3B); this observation was more evident when examining the SSc fibroblasts. Although TGM2 inhibition lowers the ECM levels deposited by SSc cells, it had little impact on the amount of ECM made by normal fibroblasts. At the lower concentration of BB7 (10nM), ECM accumulation in SSc cells was not reduced. Levels of Col-1 and α SMA were also assessed by immune probing Western blots using specific antibodies and total protein isolated from explanted and cultured fibroblasts from HC and patients with scleroderma (SSc).

Using a panel of TGF- β -responsive proteins, in the presence of TGF β 1, addition of anti-TGM2 antibody (BB7) blocked Col-1, Tenascin C (TNC), CCN2, and α SMA induction to a similar level to a pan TGF- β blocking antibody and ALK5 inhibitor (Figure 4A). Treatment with irrelevant IgG control had no effect on either HC or scleroderma cells. Studies using scleroderma cells revealed that treatment with TGF- β 1, in combination with antibodies BB7 and a pan-TGF- β blocking antibody, or in the presence of an ALK5 inhibitor for 48 hours, resulted in a reduction of Col-1, TNC, CCN2, and α SMA to levels comparable with control cells (Figure 4A).

The impact of BB7 on cellular levels of Col-1, TNC, CCN2, and α SMA (similar to specific anti-TGF- β 1 treatments) is intriguing based on blocking just TGM2s extracellular post-translational modification of the ECM affecting ECM turnover and is more suggestive of a predominant role in TGM2 activation in these cells. This was subsequently investigated by looking at Smad phosphorylation and active TGF- β 1 levels.

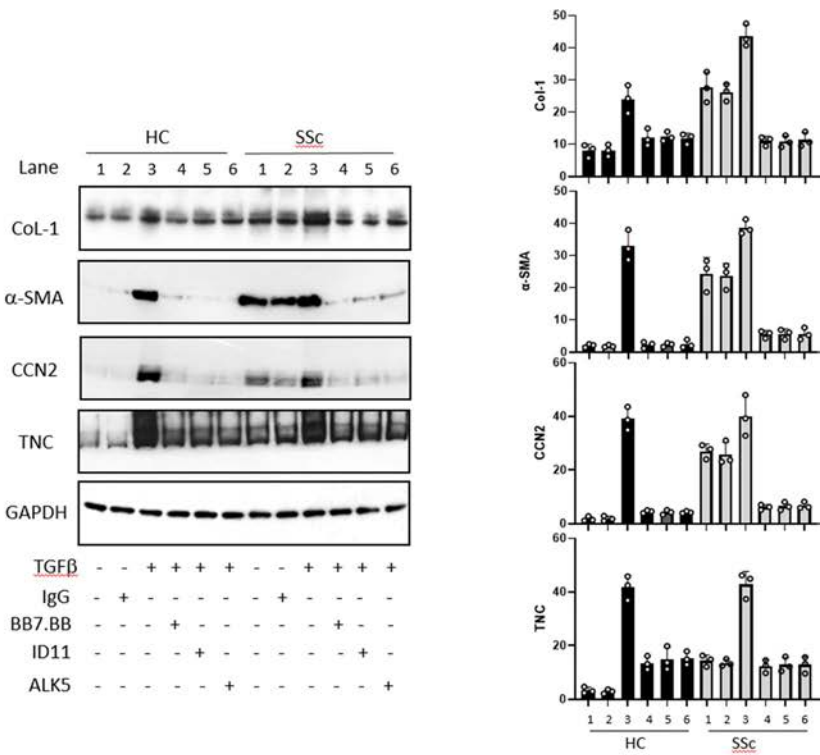
Influence of TGM2 inhibition on Smad 2/3 phosphorylation in dermal fibroblasts. To explore the role of TGM2 in scleroderma fibroblasts, studies were performed to examine whether TGM2 exerted any influence on TGF- β signaling by examining the Smad pathway. pSmad2/3 levels were readily detected at baseline in all three scleroderma fibroblast lines studied. The elevation in pSmad2/3 was mirrored by high levels of both Col-1 and α SMA within these cells (Figure 4B). When cultured in the presence of BB7, a pan-TGF- β blocking antibody or the ALK5 inhibitor, SB431542, a significant reduction in phosphorylation of Smad2/3, was observed (Figure 4B). Although there was some variation between the three primary SSc cell lines, there was a profound decrease in Col-1 and α SMA (of between 60% and 80%) in the presence of BB7, a pan-TGF- β blocking antibody or the ALK5 inhibitor. This was suggestive of a change in TGF- β 1 driven Smad signaling by blocking TGM2 activity. To confirm this, the levels of active TGF- β 1 were measured in the media of cells exposed to BB7 using the mink lung bioassay and were shown to be reduced by more than 80% (Figure 4C).

TGM2 gene deletion attenuates dermal tissue fibrosis in vivo. In order to investigate the effect of TGM2 deletion on the development of dermal fibrosis in vivo, we examined the extent of bleomycin-induced skin remodeling in global TGM2 KO mice. Figure 5A shows representative skin sections from wild type (WT) and TGM2 null mice treated with saline and bleomycin. Dermal thickness was measured from both MT- and PSR-stained sections. As shown in Figure 5A, bleomycin treatment caused a significant increase ($P \leq 0.05$) in the dermal thickness of the WT mice. TGM2 null mice following treatment with bleomycin showed no changes and were not significantly different from the TGM2 null mice treated with saline alone. By employing the Sircol assay to assess collagen content, a statistically significant increase ($P \leq 0.001$) in collagen was observed in the skin of WT mice treated with bleomycin compared with saline alone. In contrast, the TGM2 null mice exhibited no significant difference or changes in dermal collagen content when treated with saline or bleomycin (Figure 5A). To determine why the TGM2 KO mice were protected from bleomycin-induced skin fibrosis, we examined the skin of mice following PSR staining under polarized light and using high resolution SEM. Under polarized light, thick collagen

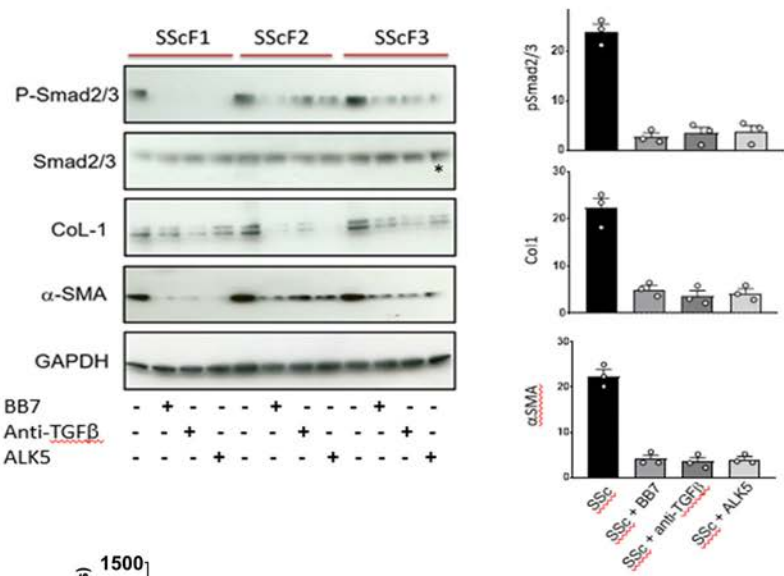
(Figure legend continued from previous page.)

Figure 3. TGM2 antibody attenuates extracellular matrix deposition of fibroblasts in vitro. In (A), the readout is mean total intensity for each fluorophore. Data for fibronectin (left), collagens I and III (middle), and collagen IV (right), compare seven cultures derived from HC and seven from patients with SSc. In (B), cells were culture as in (A), but in the presence of BB7, and matrix was stained with antibodies to fibronectin (green) and collagens I, III (purple), and IV (blue). The data show responses from four cultures derived from HC and four from patients with SSc run in 2 independent experiments in the presence of BB7 (10 nM or 1000 nM) relative to 1000nM IgG control and given as percentage reduction in the amount of deposited extracellular matrix.³¹ All images shown are representative merged images. Statistical significance was determined by *t*-test * $P = 0.05$, *** $P < 0.001$. Scale bar = 100 nm. HC, healthy control; SSc, systemic sclerosis. Color figure can be viewed in the online issue, which is available at <http://onlinelibrary.wiley.com/doi/10.1002/art.43104/abstract>.

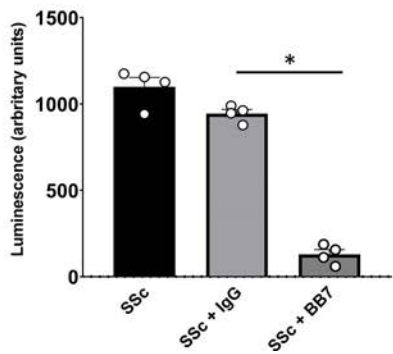
A



B



C



(Figure legend continues on next page.)

fibers appear red and then progressively thinner through orange, yellow, to green. WT skin appears predominantly red and orange, whereas the *TGM2* KO mouse skin is predominantly green and yellow (Supplemental Figure 2A). This was quantified using Image J software clearly demonstrating a shift toward smaller collagen fibers in the *TGM2* KO (Supplemental Figure 2B). This observation was confirmed using SEM where the thicker “bright” collagen fibers that are most common in WT skin are all but absent in the *TGM2* KO mice (Supplemental Figure 2C).

Functional assessment of TGM2 deletion in primary dermal fibroblasts. We next performed an in vitro analysis using primary WT and *TGM2* KO dermal fibroblasts. Following the injury to the monolayer, although WT mouse fibroblasts were able to effectively repair the wound gap in the injured cell monolayer, at 48-hours post-injury only a few *TGM2* null fibroblasts were observed to enter the wound site, exhibiting a defect in migratory capacity (Figure 5B). Furthermore, compared with WT cells, the *TGM2* null fibroblast exhibited a reduced ability to contract 3-D Col-1 matrixes (Figure 5C). Addition of TGF- β 1 is able to stimulate a slight increase in contraction in the WT group and significantly increase contraction by *TGM2* null cells. These data indicate that the KO of the *TGM2* gene impacts cell migration and differentiation and that exogenous TGF- β 1 can partially restore and rescue the procontractile behavior.

DISCUSSION

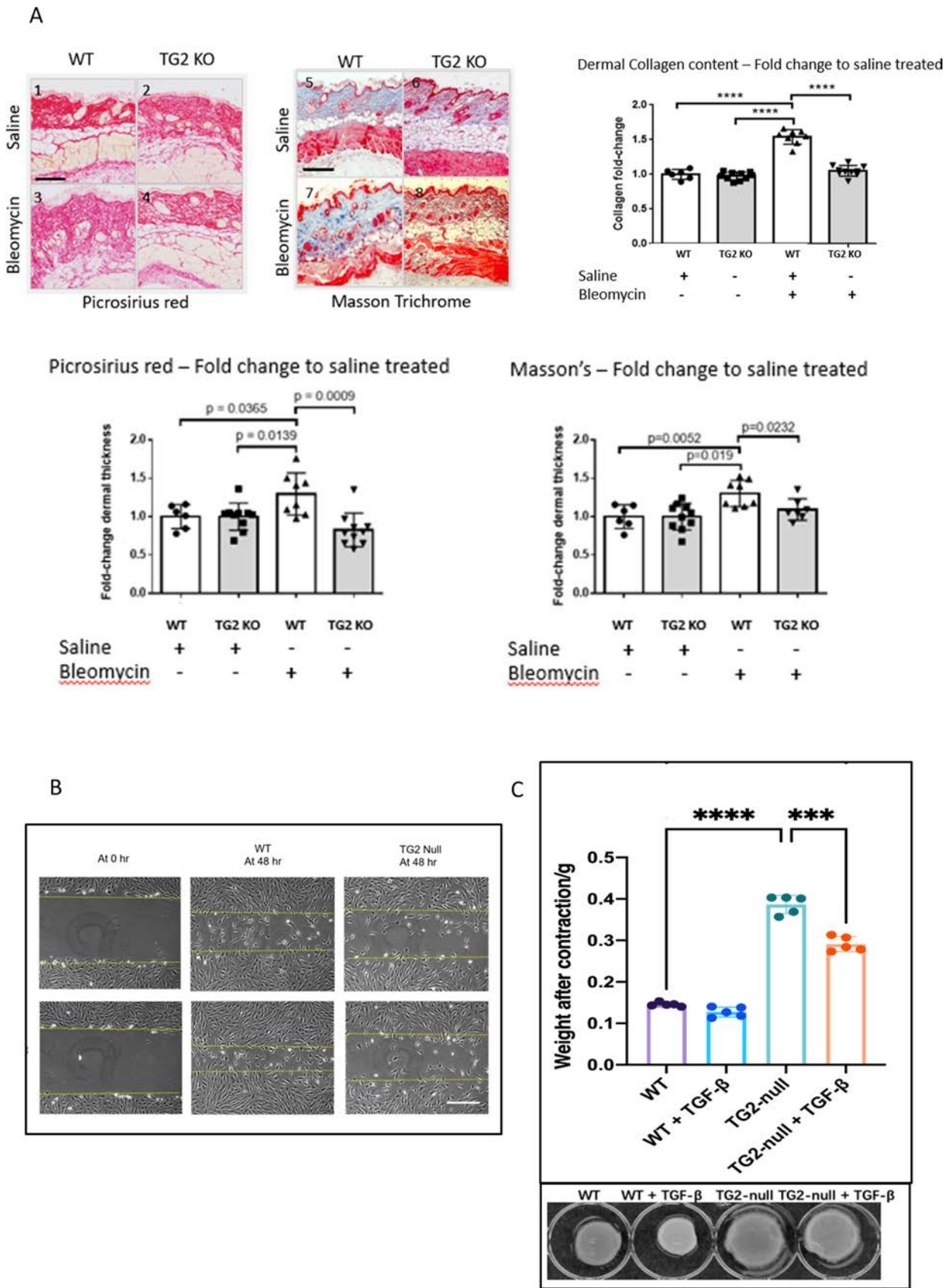
Our study has shown that TGM2 is highly expressed in scleroderma skin where it is widely distributed and associated with many cell types. Previous studies in renal and pulmonary fibrosis have similarly observed extensive TGM2 expression and activity within a number of cells in fibrotic lesions.^{20,21,26,27} Differences in the temporal expression of TGM2 antigen and activity have also been described⁴³ and may be related to the local microenvironment, the allosteric conformational changes in TGM2 that regulate activity and function, and the catalytic dependencies of TGM2 including cofactor availability, sequestration into the extracellular matrix, and secretion.¹⁴ Our study did not specifically phenotype the TGM2 expressing cells

in the dermis, but suggest that in scleroderma several cell types are contributing to TGM2 expression and release, including fibroblasts. Further studies extending the localization of TGM2 to defined cell types within the skin would be beneficial and could encompass spatial analysis critical to determine cell phenotypes and interactions that impact upon the functional role of TGM2 in skin fibrosis.

The TGM2-TGF- β axis has been previously studied and several key reciprocal functional relationships have been elucidated. TGF- β regulates *TGM2* messenger RNA.^{23,25} Equally, TGM2 is able to modulate TGF- β levels, activation, and signaling.^{25,26,43,44} Our studies employed primary dermal fibroblast grown in vitro, and in order to minimize activation associated with 2-D culture, cells were preconditioned in low-serum to induce quiescence. We also matched HC and SSc fibroblasts for passage and cultured under identical conditions, ensuring differences reflect intrinsic properties. Nonetheless, our experimental conditions appear to have tissue-culture activated our fibroblasts, as illustrated by the expression of α SMA and CCN2 in our healthy dermal fibroblast populations. We show enhanced levels of TGM2 in scleroderma fibroblasts; observations consistent with previous studies of idiopathic pulmonary fibrosis lung fibroblasts which also showed raised TGM2 levels.²¹ Our findings also confirm and extend previous studies that overexpression of TGM2 is associated with elevated ECM production by fibrotic fibroblasts.^{21,23} Furthermore, our data suggest a direct role for TGM2 as selective inhibition using BB7, an antibody directed toward the catalytic core of TGM2,²⁸ which reverses the scleroderma phenotype, reduced the expression of Col-1, CCN2, fibronectin, and α SMA. This suggests a prominent role for TGM2 in myofibroblast formation.¹¹ These studies highlight important interactions between TGM2 and TGF- β influencing TGF- β activation and signalling^{45,46} and are relevant to our studies exploring fibroblast and myofibroblast formation and function including ECM production, migration, and matrix contraction. Exogenous TGM2 activates lung fibroblasts, which is relevant to idiopathic pulmonary fibrosis.²³ Furthermore, TGM2 mediated interaction are also known to inhibit Hippo signaling and lead to accumulation of YAP, thereby having the ability to profoundly alter mechanotransduction.⁴⁷

(Figure legend continued from previous page.)

Figure 4. TGM2 inhibition attenuates TGF- β -induced expression of fibrotic protein markers and alters Smad 2/3 phosphorylation and TGF- β levels in control and SSc dermal fibroblasts. (A) Dermal fibroblasts isolated from HC ($n = 3$) and SSc cell lines ($n = 3$) were cultured alone or with recombinant TGF- β 1 (4 ng/mL), and then treated with combinations of control IgG, antibody BB7 (anti-TGM2; 1000 nM), a pan-TGF- β blocking antibody (10 μ g/mL), or in the presence of a small-molecule inhibitor of ALK5/TGF- β RI (SB431542; 10 μ M) for a further 48 hours. Expression of Col-1, TNC, and α SMA were analyzed by Western blotting; blots shown are representative of $n = 3$. (B) Levels of SMAD2/3, phospho-SMAD2/3, collagen I, and α SMA were assessed in SSc cell lines cultured alone or treated with BB7, a pan-TGF- β blocking antibody or with the ALK5 inhibitor. (C) Primary SSc dermal fibroblasts were grown in culture and then treated for 48 hours with either of BB7 or control IgG (1000nM). The media was then removed and the level of active TGF- β measured using the mink lung cell bioassay. Data represent mean \pm standard error of the mean for luminescence. * $P < 0.05$. HC, healthy control; SSc, scleroderma; TGF, transforming growth factor; TGM2, transglutaminase 2. Color figure can be viewed in the online issue, which is available at <http://onlinelibrary.wiley.com/doi/10.1002/art.43104/abstract>.



(Figure legend continues on next page.)

A number of in vitro studies have highlighted some of the essential requirements needed for the differentiation of fibroblasts into myofibroblasts.⁴⁸ The three key factors widely regarded as required are the presence of growth factors (eg, TGF- β), an appropriate ECM substrate (such as Fibronectin containing extra domain A/collagen), and the ability of the cells to respond to and develop biomechanical stress. We and others have shown that TGF- β signaling through the canonical Smad pathway plays a major role in the formation of myofibroblasts.¹¹ We demonstrate here that TGF- β treatment leads to elevated ECM production and deposition and increased myofibroblast transition (as assessed by α SMA expression). The presence of a TGF- β -neutralizing antibody or inhibition of TGF- β receptor signaling using a small-molecule ALK5 inhibitor prevented increases in both ECM and α SMA expression. Previous studies using different selective ALK5 inhibitors at varying concentrations have reported differing effects on fibroblast α SMA levels and contractile function. These differences in inhibitor selectivity and potency, along with the observations regarding fibroblast activation on different substrates highlighted above, underscore the importance of using appropriate controls, ensuring effective inhibitor potency, and defining fibroblast environments to achieve consistent and robust results.^{49,50}

Surprisingly, treatment of TGF- β -activated fibroblasts with BB7 also prevented the TGF- β -induced increase in Col-1 and α SMA. Moreover, the presence of BB7 was able to inhibit the levels or activity of TGF- β secreted by scleroderma fibroblasts, thus attenuating the endogenous Smad signaling observed in these cells thereby preventing the increase in Col-1 expression and reducing the level of myofibroblast marker α SMA in the cells. These data strongly suggest that in dermal fibroblasts and prominently in scleroderma there is a close biologic interaction between TGM2 and TGF- β . TGM2 directly influences the level of active TGF- β and is able to modulate TGF- β signaling. These data provide evidence to support the notion of a functional relationship between TGM2 and TGF- β involving coregulation of

ECM production and myofibroblast transition. Previous studies have suggested that similar biologic pathways are active in renal disease,²⁶ lung fibrosis,²³ mesenchymal transition involving both endothelial cells⁴³ and epithelial cells,^{13,15} and in fibroblast wound healing responses.¹⁸

To examine the role of TGM2 in vitro and in vivo in tissue fibrosis, a number of studies have been reported and have employed small-molecule inhibitors,^{20,51} RNA interference,²² and *TGM2* null mice.^{21,34,35} As part of our multifaceted approach to studying TGM2 in dermal fibrosis, we used a mouse model of experimentally induced skin fibrosis in the setting of the *TGM2* KO mouse. We studied the extent of tissue remodeling at 28 days following bleomycin treatment, a timepoint giving maximum fibrotic response. We show that *TGM2* null mice were protected from skin fibrosis, exhibiting reduced scar formation when determined histologically and showing no significant increase in dermal collagen content following bleomycin treatment. Our results are in line with other reports examining TGM2 function in several tissues using in vivo models of cardiac,⁵¹ pulmonary, and renal fibrosis,^{21,27} in which TGM2 inhibition or gene deletion resulted in reduced tissue remodeling and scarring. To further investigate mechanistically why the *TGM2* null mice were resistant to bleomycin treatment and protected from fibrosis, we examined the structure of the dermis in more detail and obtained explanted *TGM2*-null dermal fibroblasts (fibrotic and controls) in order to study their behavior in vitro and functional activity. Interestingly our work revealed that the skin of *TGM2* null animals was characterized by thinner, newly formed, and less crosslinked collagen fibers. The absence of TGM2 is likely to result in decreased formation of protease-resistant crosslinks in the dermal ECM fibrils, reduced tissue stiffness, and an increased ECM proteolytic degradation.⁵² Moreover, the ECM reservoir of TGF- β may also be compromised with less binding of latent TGF- β binding protein to the matrix.²⁵ Together, the more compliant matrix, coupled with depressed bioavailable TGF- β , may cause a loss in the functional response to stimuli that promote tissue remodeling and fibrosis. Thus, the

(Figure legend continued from previous page.)

Figure 5. TGM2 gene deletion protects mice from bleomycin-induced skin fibrosis and impacts upon primary dermal fibroblast functional activities. In (A), skin sections were stained with Masson's Trichrome and picrosirius red and dermal thickness measured using the NanoZoomer NDP software. Three measurements were taken across the skin sections and the averages skin thickness given as fold change relative to saline treated control mice. Stained sections were scanned using a NanoZoomer and viewed with the NDP viewer ($\times 10$ magnification). Data are presented as fold change in dermal thickness. * $P \leq 0.05$; ** $P \leq 0.01$; *** $P \leq 0.001$. Bar = 200 microns. (B) Primary dermal fibroblasts were culture to confluence, and the monolayers scratched to induce a single injury in the monolayer. A zero time point following wounding (left), scratch repair after 48 hours for WT (middle), and TG2 null (right) fibroblast populations are shown. The upper panel shows migration of fibroblast after 48 hours in the absence and presence (lower panels) of TGF- β . (C) Dermal biopsies (4 mm) were taken from 6 to 10 mice and snap frozen ready for use. Collagen content was measured using the Sircoll as per the manufacturer's instructions. The Sircoll assay is a colorimetric assay for tissue collagen against a curve of collagen reference standards. Measurements are presented as fold change relative to the saline treated controls **** $P = 0.0001$. Average collagen content per biopsy were WT/saline ($n = 6/27.3$ ug), WT/bleomycin ($n = 8/41.9$ ug), TG2 null/saline ($n = 10/40.8$ ug), and TG2 null/bleomycin ($n = 10/43.95$ ug). Fibroblast populations derived from explant skin cultures, which were placed with 3D collagen gels (left panel), and their level of contraction was assessed at 48 hours (right panel). Contraction was determined by quantification of gel weight after contraction. Statistical significance was tested by one way ANOVA with Tukey's multiple comparison, * $P < 0.05$, *** $P < 0.0001$. Scale bar = 200 μ m. ANOVA, analysis of variance; KO, knockout; TGM2, transglutaminase 2; TGF, transforming growth factor; WT, wild type. Color figure can be viewed in the online issue, which is available at <http://onlinelibrary.wiley.com/doi/10.1002/art.43104/abstract>.

more rapid turnover of the dermal ECM in the *TGM2* KO mice along with the inability to crosslink the matrix and incorporate and activate latent TGF- β represents a plausible hypothesis that underlies the failure to progress scar formation and develop fibrosis.

Our studies note that *TGM2* gene deletion imparts a profound influence on fibroblast function, with a severe impact on cell migration and the ability of *TGM2* null cells to remodel Col-1 3-D matrixes. The significantly reduced migration of these fibroblasts following scratch wounding and inability to effectively contract collagen gels suggests alterations in cell adhesion, attachment and motility, and an impairment in the transition of fibroblasts to their activated contractile myofibroblasts counterparts. In support of these observations, cell-surface TGM2 has been reported to be essential for the organization of cell adhesion foci involving integrins, fibronectin, and matricellular proteins and is therefore pivotal for fibroblast adhesion and migration.^{13–15,35} TGM2 is also known to facilitate the regulation of signaling pathways that govern stress fiber formation and myofibroblast differentiation,^{53–56} and which results in the expression of potent profibrotic genes such as *CCN2* and collagen.⁵⁴ These studies are consistent with what we show in our current study, that the absence of TGM2 expression by fibroblasts results in several key functional deficits that are crucial to scarring and fibrosis, thereby increasing our understanding of the role of TGM2 in fibrogenesis.

It is important to note that these current studies, along with the recent report by Zhou et al,¹⁹ are the first to begin to explore in detail and understand the role of TGM2 in scleroderma. Although we find a substantial agreement between the findings of Zhou et al and our own in the current study, especially evident in 3-D and in vivo models, there are notable disparities with the 2-D cell culture systems. Our study uses low passage fibroblasts obtained from patients with early dcSSc derived by whole tissue explant culture and not enzymic-treatment yielding cells with a pronounced fibrotic phenotype and HCs, an experimental design that contrasts with that of Zhou et al, as their reported data in 2-D primarily involves TGF- β -treated fibroblasts cultured in 2-D, enabling direct comparisons that are inherently limited. Plausible explanations for this disparity are that 2-D culture environment is likely to induce alterations in fibroblast behavior, although this effect would likely impact both SSc and HC cells alike and the potential confounding impact of the passage dependency phenomenon, wherein the disease phenotype diminishes with prolonged in vitro culture. Our data (unpublished) corroborate this phenomenon, notably illustrating a marked reduction in TGM2 expression and responsiveness to inhibition with advancing passage. The observed loss of disease phenotype in 2-D culture may potentially be mitigated or unmasked when cells are cultured within a 3-D environment. Additionally, considering the inherent plasticity and adaptability of fibroblasts, further investigation into the impact of culture conditions and passage number on disease phenotype maintenance is warranted, particularly in this context.

Nonetheless, together these data provide strong evidence for the involvement of TGM2 in dermal fibrosis in scleroderma through the regulation of TGF- β and the reciprocal modulation by TGM2 of TGF- β functional activity, thus revealing that there are several ways by which TGM2 can promote fibrosis. Although this current study did not assess scleroderma lung, TGM2 is expressed by pulmonary fibroblasts.²¹ In view of the previous persuasive data concerning the role of TGM2 in interstitial lung diseases,^{21,23} it is likely that TGM2 would exert an important influence in the pulmonary complications in scleroderma. The availability of a human specific monoclonal antibody for TGM2²⁸ provides extra impetus toward the potential use of TGM2 blockade in scleroderma and would significantly add to the increasing number of antifibrotic therapies available or currently under investigation for this scleroderma.

AUTHOR CONTRIBUTIONS

All authors contributed to at least one of the following manuscript preparation roles: conceptualization AND/OR methodology, software, investigation, formal analysis, data curation, visualization, and validation AND drafting or reviewing/editing the final draft. As corresponding author, Dr Abraham confirms that all authors have provided the final approval of the version to be published, and takes responsibility for the affirmations regarding article submission (eg, not under consideration by another journal), the integrity of the data presented, and the statements regarding compliance with institutional review board/Declaration of Helsinki requirements.

ROLE OF THE STUDY SPONSOR

UCB had no role in the study design or in the collection, analysis, or interpretation of the data, the writing of the manuscript, or the decision to submit the manuscript for publication. Publication of this article was not contingent upon approval by UCB.

REFERENCES

1. Denton CP, Khanna D. Systemic sclerosis. *Lancet* 2017;390(10103):1685–1699.
2. Nihtyanova SI, Denton CP. Pathogenesis of systemic sclerosis associated interstitial lung disease. *J Scleroderma Relat Disord* 2020;5(2 suppl):6–16.
3. Pope JE, Denton CP, Johnson SR, et al. State-of-the-art evidence in the treatment of systemic sclerosis. *Nat Rev Rheumatol* 2023;19:212–226.
4. Allanore Y, Simms R, Distler O, et al. Systemic sclerosis. *Nat Rev Dis Primers* 2015;23:15002.
5. Volkman ER, Varga J. Emerging targets of disease-modifying therapy for systemic sclerosis. *Nat Rev Rheumatol* 2019;15:208–224.
6. Gabrielli A, Avvedimento EV, Krieg T. Scleroderma. *N Engl J Med* 2009;360:1989–2003.
7. Distler JHW, Riemekasten G, Denton CP. The exciting future for scleroderma: what therapeutic pathways are on the horizon? *Rheum Dis Clin North Am* 2023;49:445–462.
8. Henderson NC, Rieder F, Wynn TA. Fibrosis: from mechanisms to medicines. *Nature* 2020;587:555–566.

9. Tabib T, Huang M, Morse N, et al. Myofibroblast transcriptome indicates SFRP2^{hi} fibroblast progenitors in systemic sclerosis skin. *Nat Commun* 2021;19:12:4384.
10. Romano E, Rosa I, Fioretto BS, et al. the role of pro-fibrotic myofibroblasts in systemic sclerosis: from origin to therapeutic targeting. *Curr Mol Med* 2022;22:209–239.
11. Gyftaki-Venieri DA, Abraham DJ, Ponticos M. Insights into myofibroblasts and their activation in scleroderma: opportunities for therapy? *Curr Opin Rheumatol* 2018;30:581–587.
12. Christian JL, Hill CS. Transforming growth factor- β family biology: from basic mechanisms to roles in development and disease. *Dev Dyn* 2022;251:6–9.
13. Lorand L, Graham RM. Transglutaminases: crosslinking enzymes with pleiotropic functions. *Nat Rev Mol Cell Biol* 2003;4:140–156.
14. Tatsukawa H, Furutani Y, Hitomi K, et al. Transglutaminase 2 has opposing roles in the regulation of cellular functions as well as cell growth and death. *Cell Death Dis* 2016;7:e2244.
15. Szondy Z, Korponay-Szabo I, Kiraly R, et al. Transglutaminase 2 in human diseases. *Biomedicine (Taipei)* 2017;7:15.
16. Johnson TS, Skill NJ, El Nahas AM, et al. Transglutaminase transcription and antigen translocation in experimental renal scarring. *J Am Soc Nephrol* 1999;10:2146–2157.
17. Fisher M, Jones RA, Huang L, et al. Modulation of tissue transglutaminase in tubular epithelial cells alters extracellular matrix levels: a potential mechanism of tissue scarring. *Matrix Biol* 2009;28:20–31.
18. Verderio EA, Johnson TS, Griffin M. Transglutaminases in wound healing and inflammation. *Prog Exp Tumor Res* 2005;38:89–114.
19. Zhou X, Trinh-Minh T, Matei AE, et al. Amelioration of fibrotic remodeling of human 3-dimensional full-thickness skin by transglutaminase 2 inhibition. *Arthritis Rheumatol* 2023;75:1619–1627.
20. Johnson TS, Fisher M, Haylor JL, et al. Transglutaminase inhibition reduces fibrosis and preserves function in experimental chronic kidney disease. *J Am Soc Nephrol* 2007;18:3078–3088.
21. Olsen KC, Sapinoro RE, Kottmann RM, et al. Transglutaminase 2 and its role in pulmonary fibrosis. *Am J Respir Crit Care Med* 2011;184:699–707.
22. Zhao G, Zhang ZQ, Zhang B, et al. Down-regulation of tTG expression by RNAi inhibits HSC proliferation and attenuates liver fibrosis. *Int J Clin Exp Pathol* 2011;20:4:513–520.
23. Fell S, Wang Z, Blanchard A, et al. Transglutaminase 2: a novel therapeutic target for idiopathic pulmonary fibrosis using selective small molecule inhibitors. *Amino Acids* 2021;53:205–217.
24. Belkin AM. Extracellular TG2: emerging functions and regulation. *FEBS J* 2011;278:4704–4716.
25. Nunes I, Gleizes PE, Metz CN, et al. Latent transforming growth factor-beta binding protein domains involved in activation and transglutaminase-dependent cross-linking of latent transforming growth factor-beta. *J Cell Biol* 1997;136:1151–1163.
26. Huang L, Haylor JL, Fisher M, et al. Do changes in transglutaminase activity alter latent transforming growth factor beta activation in experimental diabetic nephropathy? *Nephrol Dial Transplant* 2010;25:3897–3910.
27. Shweke N, Boulos N, Jouanneau C, et al. Tissue transglutaminase contributes to interstitial renal fibrosis by favoring accumulation of fibrillar collagen through TGF-beta activation and cell infiltration. *Am J Pathol* 2008;173:631–642.
28. Maamra M, Benayad OM, Matthews D, et al. Transglutaminase 2: development of therapeutic antibodies reveals four inhibitory epitopes and confirms extracellular function in fibrotic remodelling. *Br J Pharmacol* 2022;179:2697–2712.
29. Abraham D, Lupoli S, McWhirter A, et al. Expression and function of surface antigens on scleroderma fibroblasts. *Arthritis Rheum* 1991;34:1164–1172.
30. van den Hoogen F, Khanna D, Fransen J, et al. Classification criteria for systemic sclerosis: an American college of rheumatology/European league against rheumatism collaborative initiative. *Ann Rheum Dis* 2013;72:1747–1755.
31. Qureshi OS, Bon H, Twomey B, et al. An immunofluorescence assay for extracellular matrix components highlights the role of epithelial cells in producing a stable, fibrillar extracellular matrix. *Biol Open* 2017;15:6:1423–1433.
32. Dasch JR, Pace DR, Waegell W, et al. Monoclonal antibodies recognizing transforming growth factor-beta. Bioactivity neutralization and transforming growth factor beta 2 affinity purification. *J Immunol* 1989;142:1536–1541.
33. Rice LM, Padilla CM, McLaughlin SR, et al. Fresolimumab treatment decreases biomarkers and improves clinical symptoms in systemic sclerosis patients. *J Clin Invest* 2015;125:2795–2807.
34. De Laurenzi V, Melino G. Gene disruption of tissue transglutaminase. *Mol Cell Biol* 2001;21:148–155.
35. Scarpellini A, Huang L, Burhan I, et al. Syndecan-4 knockout leads to reduced extracellular transglutaminase-2 and protects against tubulointerstitial fibrosis. *J Am Soc Nephrol* 2014;25:1013–1027.
36. Liu S, Shi-wen X, Abraham DJ, et al. CCN2 is required for bleomycin-induced skin fibrosis in mice. *Arthritis Rheum* 2011;63:239–246.
37. Rittié L. Method for picrosirius red-polarization detection of collagen fibers in tissue sections. *Methods Mol Biol* 2017;1627:395–407.
38. Rich L, Whitaker P. Collagen and picrosirius red staining: a polarized light assessment of fibrillar hue and spatial distribution. *J Morphol Sci* 2005;22:97–104.
39. Gupta A, Vara DS, Punshon G, et al. In vitro small intestinal epithelial cell growth on a nanocomposite polycaprolactone scaffold. *Biotechnol Appl Biochem* 2009;54:221–229.
40. Rajkumar VS, Shiwen X, Bostrom M, et al. Platelet-derived growth factor-beta receptor activation is essential for fibroblast and pericyte recruitment during cutaneous wound healing. *Am J Pathol* 2006;169:2254–2265.
41. Donovan J, Shiwen X, Norman J, et al. Platelet-derived growth factor alpha and beta receptors have overlapping functional activities towards fibroblasts. *Fibrogenesis Tissue Repair* 2013;6:10.
42. Rajkumar VS, Howell K, Csiszar K, et al. Shared expression of phenotypic markers in systemic sclerosis indicates a convergence of pericytes and fibroblasts to a myofibroblast lineage in fibrosis. *Arthritis Res Ther* 2005;7:R1113–R1123.
43. Telci D, Collighan RJ, Basaga H, et al. Increased TG2 expression can result in induction of transforming growth factor beta1, causing increased synthesis and deposition of matrix proteins, which can be regulated by nitric oxide. *J Biol Chem* 2009;284:29547–29558.
44. Wang Y, Lin C, Han R, et al. Metformin attenuates TGF- β 1-induced pulmonary fibrosis through inhibition of transglutaminase 2 and subsequent TGF- β pathways. *3 Biotech* 2020;10:287.
45. Wang Z, Perez M, Lee ES, et al. The functional relationship between transglutaminase 2 and transforming growth factor β 1 in the regulation of angiogenesis and endothelial-mesenchymal transition. *Cell Death Dis* 2017;8:e3032.
46. Lockhart-Cairns MP, Cain SA, Dajani R, et al. Latent TGF β complexes are transglutaminase cross-linked to fibrillin to facilitate TGF β activation. *Matrix Biol* 2022;107:24–39.
47. Fisher ML, Kerr C, Adhikary G, et al. Transglutaminase interaction with α 6 β 4-integrin stimulates YAP1-dependent Δ Np63 α stabilization and leads to enhanced cancer stem cell survival and tumor formation. *Cancer Res* 2016;76:7265–7276.
48. Hinz B, Lagares D. Evasion of apoptosis by myofibroblasts: a hallmark of fibrotic diseases. *Nat Rev Rheumatol* 2020;16:11–31.

49. Ishida W, Mori Y, Lakos G, et al. Intracellular TGF- β receptor blockade abrogates Smad-dependent fibroblast activation in vitro and in vivo. *J Invest Dermatol* 2006;126:1733–1744.
50. Chen Y, Shi-wen X, Eastwood M, et al. Contribution of activin receptor-like kinase 5 (transforming growth factor β receptor type I) signaling to the fibrotic phenotype of scleroderma fibroblasts. *Arthritis Rheum* 2006;54:1309–1316.
51. Wang Z, Stuckey DJ, Murdoch CE, et al. Cardiac fibrosis can be attenuated by blocking the activity of transglutaminase 2 using a selective small-molecule inhibitor. *Cell Death Dis* 2018;9:613.
52. Katt WP, Antonyak MA, Cerione RA. Opening up about tissue transglutaminase: when conformation matters more than enzymatic activity. *Med One* 2018;3:e180011.
53. Janiak A, Zemskov EA, Belkin AM. Cell surface transglutaminase promotes RhoA activation via integrin clustering and suppression of the Src-p190RhoGAP signaling pathway. *Mol Biol Cell* 2006;17:1606–1619.
54. Kennedy L, Shi-Wen X, Carter DE, et al. Fibroblast adhesion results in the induction of a matrix remodeling gene expression program. *Matrix Biol* 2008;27:274–281.
55. Panciera T, Azzolin L, Cordenonsi M, et al. Mechanobiology of YAP and TAZ in physiology and disease. *Nat Rev Mol Cell Biol* 2017;18:758–770.
56. Benn MC, Weber W, Klotzsch E, et al. Tissue transglutaminase in fibrosis-more than an extracellular matrix cross-linker. *Curr Opin Biomed Eng* 2019;10:156–164.

Serum Type I Interferon Score for Prediction of Clinically Meaningful Disease Progression in Limited Cutaneous Systemic Sclerosis

Stefano Di Donato,¹  Rebecca Ross,²  Ranjitha Karanth,² Vishal Kakkar,¹ Enrico De Lorenzis,³ 
Lesley-Anne Bissell,¹ Kristina Clark,⁴ Philip Yee,⁴ Christopher P. Denton,⁴  and Francesco Del Galdo¹ 

Objective. To assess the value of serum type I interferon (IFN) score in predicting clinically meaningful progression in limited cutaneous systemic sclerosis (lcSSc) using a novel composite endpoint adopted from the MINIMISE clinical trial.

Methods. A retrospective, longitudinal lcSSc cohort was identified within a national, multicenter observational cohort. The MINIMISE trial combined Morbi-mortality endpoint was used as the clinical outcome for a time to clinical worsening (TTCW) design. The IFN score was calculated from the serum concentration of chemokine C-C motif ligand (CCL) 2, CCL8, CCL19, C-X-C motif chemokine ligand (CXCL) 9, CXCL10, and CXCL11 on patients and age- and sex-matched healthy controls (HCs). A “high” IFN score was defined as 2 SDs above the HC mean. The association of the IFN score with TTCW was assessed using Cox proportional hazard regressions and Kaplan-Meier curves. The potential improvement in risk stratification when combining IFN score with lcSSc clinical features was explored.

Results. A total of 149 patients were included in the analysis: 67 “high” IFN and 82 “low.” High IFN patients presented a shorter TTCW (74.7 months [95% confidence interval (CI) 70.1–79.3] vs 110.6 months [95% CI 107.2–114.0]; $P < 0.001$) and met the endpoint in higher proportion compared with low IFN (55% vs 12%; $P < 0.001$). A high IFN score conferred hazard ratio (HR) 5.5 (95% CI 2.7–11.3) for TTCW compared with low IFN, and IFN score as a continuous variable conferred HR 2.38 (95% CI 1.4–4.0) for TTCW independently of clinical variables. Pulmonary arterial hypertension, interstitial lung disease, digital ulcers, and modified Rodnan skin score were associated with TTCW. An exploratory analysis showed that these clinical features improve risk stratification over time in combination with IFN score.

Conclusion. Serum assessment of type I IFN activity is a valuable predictor of clinically meaningful outcomes in lcSSc. The combination of serum IFN score with sentinel clinical features can improve stratification strategies in clinical trials and patient management.

INTRODUCTION

Patients with limited cutaneous systemic sclerosis (lcSSc) represent more than 60% of the SSc population and often experience a slower disease progression with reduced extent of fibrotic organ damage compared to patients within the diffuse cutaneous (dc) subset. Nonetheless, the lcSSc subset is still burdened by a

considerable morbidity accrual over time, evident through various indicators such as esophageal dysfunction (62%), interstitial lung disease (ILD; 35%), digital ulcers (DUs; 37%), cardiac diastolic dysfunction (20%), and joint synovitis (13%).^{1,2} Furthermore, lcSSc still carries a considerable overall mortality at 10 years of 22%,³ with 55% 3-year mortality in patients developing pulmonary artery hypertension (PAH).⁴

Supported by the Leeds Biomedical Research Centre, National Institute for Health Research (grant NIHR213331).

¹Stefano Di Donato, MD, Vishal Kakkar, MD, Lesley-Anne Bissell, MD, PhD, Francesco Del Galdo, MD, PhD: Leeds Institute of Rheumatic and Musculoskeletal Medicine, University of Leeds and Leeds Biomedical Research Centre, National Institute for Health Research, Leeds Teaching Hospitals NHS Trust, Leeds, United Kingdom; ²Rebecca Ross, PhD, Ranjitha Karanth, MD: Leeds Institute of Rheumatic and Musculoskeletal Medicine, University of Leeds, Leeds, United Kingdom; ³Enrico De Lorenzis, MD, PhD: Catholic University of the Sacred Heart, Fondazione Policlinico Universitario Agostino Gemelli IRCCS, Rome, Italy; ⁴Kristina Clark, MD, PhD, Philip Yee, MD, Christopher P. Denton, MD, PhD: University College London, London, United Kingdom.

Additional supplementary information cited in this article can be found online in the Supporting Information section (<https://acrjournals.onlinelibrary.wiley.com/doi/10.1002/art.43120>).

Author disclosures and graphical abstract are available at <https://onlinelibrary.wiley.com/doi/10.1002/art.43120>.

[Correction added on 7 April 2025, after first online publication: The copy-right line and legal statement were changed.]

Address correspondence via email to Francesco Del Galdo, MD, PhD, at f.delgaldo@leeds.ac.uk; or to Christopher P. Denton, MD, PhD, at c.denton@ucl.ac.uk.

Submitted for publication May 18, 2024; accepted in revised form December 10, 2024.

The slower rate of progression in this subset and the need to observe and measure the efficacy of investigational drugs within a constrained timeframe of a clinical trial have led to a deep underrepresentation of patients with lcSSc in intervention studies, defining a highly unmet need in the field.⁵ Time-to-event trials allow the combination of multiple events, all defined as endpoints, and have been used successfully to measure the efficacy of interventions in complex populations with challenging outcome measures, including important examples of connective tissue disease-associated PAH.⁶ The analysis of the Royal Free cohort of patients with lcSSc has led to the identification of clinically significant events in patients with lcSSc and their relative accrual over time.⁷ Building on this analysis, Denton et al have proposed the design of an intervention study for mycophenolate mofetil (MMF) employing a time-to-combined event endpoint (MINIMISE trial; EudraCT: 2019-004139-21; [ClinicalTrials.gov](https://clinicaltrials.gov/ct2/show/study/NCT04927390): NCT04927390).⁸ The events considered in the MINIMISE combined endpoint included SSc-related mortality and SSc-related organ manifestations, such as new onset of PAH, new ILD or ILD progression, clinically significant worsening of the modified Rodnan skin score (mRSS), new onset of SSc-related cardiac disease, new DUs requiring hospitalization, and significant gastrointestinal (GI) tract disease.

The composite “Morbi-mortality” MINIMISE trial endpoint of “time to clinical worsening” (TTCW) reflected expert consensus of the most clinically relevant events that would be robustly captured during follow-up in a clinical trial or observational cohort and that might reasonably be expected to be influenced by immunosuppressive disease-modifying therapy such as MMF. Content validity is supported by several component endpoints showing reduced frequency in the Royal Free SSc Cohort in dcSSc from 2000 to 2003, when MMF was generally used for treating skin disease, compared with 1990 to 1993, when MMF was not routinely available.⁹ Type I interferon (IFN) activation has been linked to several aspects of SSc disease progression,¹⁰ including skin involvement,^{11–13} ILD,^{14,15} DUs,¹⁶ and PAH.¹⁷ In this context, given that all these aspects are included in the MINIMISE endpoint, we aimed to analyze the TTCW of patients with lcSSc in a single-center observational study and to determine the value of type I IFN activation in identifying risk strata for TTCW accrual over time.

Bauer et al identified that several chemokines, known to be induced in vitro by type I IFN, were most significantly up-regulated in the serum of patients with systemic lupus erythematosus with high IFN signature as measured by peripheral blood transcriptome.¹⁸ In their work they indicated that the top six chemokines for concentration and significance were chemokine C-C motif ligand (CCL) 2, also referred to as monocyte chemoattractant protein 1; CCL8, also known as monocyte chemoattractant protein 2; CCL19, also known as macrophage inflammatory protein-3 β ; C-X-C motif chemokine ligand (CXCL) 10, also known as IFN γ -induced protein 10; CXCL9, also known as IFN γ -induced

protein 9; and CXCL11, also known as IFN γ -induced protein 11. Significantly, previous data highlighted that a score based on these six chemokines effectively stratifies clinical outcomes in dcSSc.¹⁹ Building upon this foundation, we developed a TTCW analysis to tailor this stratification approach to lcSSc, considering its distinct natural history.

PATIENTS AND METHODS

Study design and patients. The study was designed as a longitudinal retrospective study of incident patients aged ≥ 18 years fulfilling the 2013 ACR/EULAR classification criteria for SSc²⁰ and presenting with the lcSSc subset as defined by LeRoy et al.²¹ All patients were enrolled from a single-center observational cohort attending the Leeds Teaching Hospital Trust Rheumatology outpatient from December 1, 2013, until November 30, 2019. All patients provided informed consent, and the research was undertaken in compliance with the Declaration of Helsinki. Study protocol and relative informed consent were approved by the Human Research Ethics committee (“Leeds Teaching Hospitals Connective Tissue Disease and Vasculitis Cohort Cross-sectional and Longitudinal Clinical and Basic Science Evaluation (CONVAS),” Research Ethics Committee reference: RR10/9608 from December 1, 2013, until January 1, 2015; and “Stratification for Risk of Progression in Systemic Sclerosis (STRIKE),” Research Ethics Committee reference 15/NE/0211, ID 178638 from January 1, 2015, to ongoing). Patients or the public were not involved in the design, conduct, reporting, and dissemination plans of this research.

The characterization at baseline of patients included sex, age, antinuclear antibody (ANA) positivity, antitopoisomerase I (Scl70) and anticentromere (ACA) positivity, pharmacologic treatment, disease duration defined from the first non-Raynaud Phenomenon SSc symptom, history or presence of DUs (referred as DU disease), presence of PAH, presence of calcinosis, mRSS, symptomatic gastroesophageal reflux disease, diagnosis of ILD, forced vital capacity (FVC), and diffusing capacity of the lungs for carbon monoxide (DLco) percent predicted. All patients received at least one follow-up every 6 months until event development or censoring. Database extract and chart review were employed for the identification of clinically meaningful events qualifying for the study endpoint and relative clinical validation, when needed.

IFN score calculations and threshold definition. The IFN score was calculated as the average of the natural logarithm of the concentration of CCL2, CCL8, CCL19, CXCL10, CXCL9, and CXCL11 based on the work from Bauer et al.¹⁸ Using the methodology previously established in dcSSc, the threshold for the definition of a “high” IFN score was set as the mean of the IFN score calculated on 72 healthy volunteers matched for sex and age (data not shown) plus 2 standard deviations (SDs).¹⁹

Objective of the study and endpoint definition. The objective of the study was to explore the value of IFN score in predicting the risk of clinically significant events over time in patients affected by lcSSc and enrolled in our observational cohort. Patients were included in the analysis if they fulfilled the 2013 ACR/EULAR classification criteria for SSc within the lcSSc subset at baseline and had an available serum sample within 3 months from the baseline, with at least 48 months of observation.

For the assessment of the MINIMISE endpoint, we analyzed the cohort for the occurrence of the first of the following “Morbidity” events: SSc-related death, new diagnosis or progressive lung fibrosis as defined by an absolute FVC% drop of $\geq 10\%$ in 12 months or between 5% and 9% with a 15% DLco reduction, new right heart catheter-diagnosed PAH according to the current definition at the time of the diagnosis, new onset of scleroderma renal crisis, new onset of major cardiac complication related to SSc as defined by systolic ejection fraction drop to $< 45\%$ or pericardial effusion impairing cardiac function or arrhythmia requiring antiarrhythmic therapy (cardioversion or medical) or need for a cardiac device, new onset of SSc-related GI disease requiring enteral nutrition supplementation for at least 3 weeks or any parenteral feeding or hospital admission for intestinal obstruction or pseudo-obstruction, severe digital vasculopathy requiring hospitalization (including gangrene, amputation, osteomyelitis, or septic arthritis, and excluding elective hospitalization for vasodilator treatment), and an mRSS absolute increase of ≥ 5 units and a 25% increase from baseline (Supplementary File 1).

Power analysis and sample size considerations. To inform an effect size for our event-free survival analysis sample calculation, we used previous data from a large longitudinal SSc cohort that showed a combined cumulative incidence of clinically meaningful significant events (namely ILD, PAH, cardiac SSc involvement, and mRSS worsening) of approximately 40% over a period of 5 years in patients with lcSSc and of approximately 73% in patients with dcSSc.⁷ Prior analysis indicated that 50% of patients had a high IFN score; hence, we set a ratio between the IFN high and IFN low arms of 1 to 1. We hypothesized a hazard ratio (HR) for IFN high versus IFN low of 2.0. For this analysis, we set a maximum accrual duration of 10 years, a power of 80%, and an alpha of 5%, all with a two-sided hypothesis test. Using the R package ‘gsDesign,’ a sample size of 56 patients for each group and 42 required events were needed. Adjusting the overall 112 patients required for a censoring up to 25%, we set 140 patients as the minimum sample size for our study. Based on these assumptions, we analyzed the serum IFN score on the first 150 consecutive patients with lcSSc enrolled in the observational study with at least 4 years of observation.

Statistical analysis. Categorical data were reported as counts and percentages and comparisons of categorical data were performed using Fisher exact test or Pearson chi-square

test, as appropriate. Continuous data were reported as mean (SD) or medians (interquartile range [IQR]), and normality was assessed with the Shapiro-Wilk significance test, with a graphical check through density plots and QQ plots. The homogeneity of variance for continuous variables was assessed using an F test, and comparisons of continuous data were performed with Student's *t*-test or Wilcoxon test, as appropriate. The date of serum sample collection was considered as the formal baseline in the time-to-event analysis. Event-free survival for IFN groups was plotted using Kaplan-Meier (KM) curves, and the comparison between the two restricted mean TTCW was computed non-parametrically as the area under the KM curve, using the smaller of the maximum observed times in the two groups. Confidence intervals (CIs) and statistical significance for the comparisons were derived using the Greenwood plug-in estimator for variance. The event-free survival probabilities across the two groups were compared at three timepoints potentially relevant for clinical trial design and clinical management (12, 24, and 36 months) using the difference in KM estimates of survival. Because SSc-related death was included in the composite Morbidity event, we did not need to account for this as a competing risk before clinical worsening.

To investigate the association between IFN score and the risk over time of meeting the endpoint and to account for known disease domains that prognostically affect the development of disease complications included in the endpoint, univariable and multivariable Cox proportional hazard (CPH) regressions were performed. To account for potential nonlinear relationships between the IFN score and the outcome, we employed a penalized spline function when modeling the IFN score as a continuous variable. The proportional hazards assumption was tested via complementary log-log plot. To visually assess the multivariable Cox regressions using the IFN score, we chose time-dependent receiver operating characteristic (ROC) curves that change over time to provide a fuller description of the models.^{22,23} The event-free survival prediction accuracy of the models was assessed using bootstrap resampling with 1,000 iterations. We then calculated the concordance index (C-index) and area under the curve (AUC) of the models at three timepoints (12 months, 24 months, and 36 months).

The relationship between clinical features and IFN score on patient outcomes was explored using both visual and statistical methods. Clinical variables such as mRSS, PAH, ILD, DUs, and IFN score were dichotomized. UpSet plots were employed to visualize the intersections of various clinical and IFN score combinations and their associated event rates. KM curves were generated for newly identified high-risk and low-risk groups, with survival differences assessed using the log-rank test. Additionally, a forest plot was used to compare the relative risks (RRs) of different feature combinations over multiple time points, offering a clear comparison between high-risk and low-risk groups. Data analysis was conducted using R core team software (RStudio) and the

packages ‘anytime,’ ‘survival,’ ‘survminer,’ ‘ComparisonSurv,’ ‘survRM2,’ ‘ggsurvfit,’ ‘gtsummary,’ ‘moonBook,’ ‘survivalROC,’ ‘risksetROC,’ and ‘ggplot2.’

RESULTS

Complete data were available for 149 patients, 143 (96%) of whom were women. The mean \pm SD age at baseline was 60 ± 16 years, and the median (IQR) disease duration from the first non-Raynaud Phenomenon symptom was 8 (IQR 10) years. A total of 141 (95%) patients were ANA positive, 100 (67%) were ACA positive, 12 (8.1%) were Scl70 positive, and 35 (23%) patients were anti-Ro52 positive. At baseline, 36 (24%) patients had ILD, 58 (39%) had DU disease, 53 (36%) had calcinosis, 9 (6%) had right heart catheter-diagnosed PAH, and 127 (85%) were receiving proton pump inhibitor treatment for upper GI involvement. Mean \pm SD mRSS was 2.09 ± 2.63 , the mean \pm SD FVC% was $109\% \pm 20\%$, and the mean \pm SD DLco% was $67\% \pm 15\%$. Of the nine patients with PAH at baseline, six were receiving combination therapy (four with phosphodiesterase 5 inhibitors [PDE5is] combined with endothelin receptor antagonists [ERAs], one with calcium channel blockers combined with PDE5is and ERAs, and one with angiotensin-converting enzyme inhibitors combined with PDE5is) and three single therapy (two receiving ERAs and one receiving intravenous iloprost) based on patients’ tolerability and in line with the current standard of care in the United Kingdom at the time of the analysis. The remaining treatments are reported in Table 1.

Event accrual clinical analysis. The study was structured to ensure a minimum intended follow-up duration of 4 years for each participant, extending up to a maximum of 10 years. The consecutive patients planned were recruited between December 2013 and December 2019; hence, we completed the 4-year follow-up of the last recruited patient in December 2023. The median (IQR) follow-up of the cohort was 88 (IQR 48) months. A total of 77 patients were censored before 10 years follow-up with a median (IQR) censoring time of 89 (IQR 9) months. A total of 47 (32.5%) patients developed the Morbi-mortality endpoint by the time of the analysis with a restricted mean time to event of 94.5 (95% CI 78.4–111.3) months. The most common event was represented by new diagnosis of PAH ($n = 13$; 27.3%), followed by SSc-related mortality ($n = 9$; 19%), progression of ILD ($n = 6$; 13%), SSc-related cardiac events ($n = 6$; 13%), mRSS worsening ($n = 5$; 11%), GI complications ($n = 4$; 8.5%), severe digital vasculopathy requiring hospitalization ($n = 3$; 6.4%), and scleroderma renal crisis ($n = 1$; 2.1%).

Participants were censored at the time of first event. Subsequent events are reported in the Supplementary Material by IFN score group (Supplementary Table 1). The KM analysis for the overall cohort showed an event probability of 5.4% (95% CI 1.7%–8.9%) at 12 months, 10.1% (95% CI 5.1%–14.8%) at

24 months, 15.4% (95% CI 9.4%–21.0%) at 36 months, 21.5% (95% CI 14.6%–27.8%) at 60 months, and 34.9% (95% CI 25.6%–43.0%) at 120 months (Figure 1; Supplementary Table 2).

Patients who did not develop an event of interest had a significantly lower mean \pm SD age at baseline compared with those who did (60 ± 17 vs 64 ± 16 ; $P = 0.035$) and a tendency toward higher prevalence of isolated ACA positivity (46% vs 26%; $P = 0.053$). Conversely, patients who developed the Morbi-mortality endpoint presented a higher baseline mean \pm SD mRSS (3.2 ± 3.4 vs 1.6 ± 2.1 ; $P < 0.001$) and a higher prevalence at baseline of DU disease (53% vs 32%; $P = 0.015$), ILD (40% vs 17%; $P = 0.002$), and PAH (15% vs 2%; $P = 0.005$). Accordingly, they also had a significantly lower mean \pm SD FVC ($100\% \pm 21\%$ vs $113\% \pm 18\%$; $P < 0.001$), and DLco percent-age predicted ($58\% \pm 13\%$ vs $72\% \pm 14\%$; $P < 0.001$).

IFN score analysis. The concentration of the serum chemokines included in the IFN score was significantly higher in the lcSSc cohort compared with a reference healthy control (HC) cohort matched for age and sex. Specifically, the natural logarithm (ln) of CXCL9 serum concentration was 6.93 ± 1.09 pg/mL (vs 6.11 ± 0.79 pg/mL; $P < 0.001$), ln CXCL10 was 5.99 ± 0.77 pg/mL (vs 5.43 ± 0.47 pg/mL; $P < 0.001$), ln CXCL11 was 3.89 ± 0.71 pg/mL (vs 3.40 ± 0.32 pg/mL; $P < 0.001$), ln CCL8 was 3.78 ± 0.46 pg/mL (vs 3.43 ± 0.43 pg/mL; $P < 0.001$), and ln CCL19 was 5.82 ± 0.83 pg/mL (vs 5.20 ± 0.53 pg/mL; $P < 0.001$). A numerical but not statistically significant difference was also observed for ln CCL2 (6.14 ± 0.57 pg/mL vs 6.00 ± 0.75 pg/mL) (Figure 2A). The IFN score presented a normal distribution in the lcSSc cohort with a mean \pm SD value of 5.50 ± 0.44 , which was significantly higher than that of the HCs (4.97 ± 0.27 ; $P < 0.001$) (Figure 2B). Sixty-seven (45%) patients had an IFN score above two upper SDs of the matched HC mean (5.50) and were classified as high, whereas 82 (55%) were below this boundary and classified as “low” (Figure 2C). The distribution of the baseline clinical features across IFN groups is shown in Table 2.

Patients within the IFN high group presented a greater incidence of Morbi-mortality events compared with those in the IFN low (37 [55%] vs 10 [12%]; $P < 0.001$) (Figure 2D). IFN high patients had a higher median (IQR) age compared with IFN low patients (66 [IQR 16] vs 58 [IQR 15]; $P = 0.01$) and had a significantly higher prevalence of anti-Ro52 antibodies (34% vs 15%; $P = 0.025$). No statistically significant difference was found across the two groups in terms of median (IQR) disease duration (8 [IQR 8] vs 5 [IQR 9]; $P = 0.39$), sex distribution, ethnicity, ANA positivity, ACA, antitopoisomerase I antibody status, and treatments (Table 1). Similarly, no statistically significant differences were present between the two subgroups for baseline organ-specific manifestations, namely, ILD, DU disease, skin calcinosis history, PAH, mRSS, FVC%, DLco%, and upper GI involvement (Table 1).

Table 1. Overall cohort demographic and clinical characteristics divided by event onset during follow-up*

Characteristic	Overall (N = 149)	Cohort by event				Cohort by IFN group			
		No event (n = 102)	Event (n = 47)	P value ^a	Q value ^b	IFN low (n = 82)	IFN high (n = 67)	P value ^a	Q value ^b
Age, mean (SD), y	60 (16)	60 (17)	64 (16)	0.035	0.087	58 (15)	66 (16)	0.002	0.013
Sex, n (%)				0.4	0.6			0.4	0.6
Female	143 (96)	99 (97)	44 (94)	–	–	80 (98)	63 (94)	–	–
Male	6 (4.0)	3 (2.9)	3 (6.4)	–	–	2 (2.4)	4 (6.0)	–	–
Disease duration, median (IQR), y	8 (10)	8 (10)	8 (11)	0.9	>0.9	8 (10)	5 (9)	0.4	0.6
ANA positive, n (%)	141 (95)	96 (94)	45 (96)	>0.9	>0.9	76 (93)	65 (97)	0.3	0.6
ACAs, n (%)	100 (67)	70 (69)	30 (64)	0.6	0.8	56 (68)	44 (66)	0.7	0.8
Isolated ACA positivity, n (%)				0.009	0.052			0.086	0.4
ACA only	59 (40)	47 (46)	12 (26)	–	–	37 (45)	22 (33)	–	–
Non-ACA only	90 (60)	55 (54)	35 (74)	–	–	45 (55)	45 (67)	–	–
Anti topoisomerase I antibodies, n (%)	12 (8.1)	8 (7.8)	4 (8.5)	>0.9	>0.9	8 (9.8)	4 (6.0)	0.4	0.6
Anti-Ro52 antibodies, n (%)	35 (23)	20 (20)	15 (32)	0.1	0.2	12 (15)	23 (34)	0.005	0.027
Anti-RNA polymerase III antibodies, n (%)	4 (2.7)	2 (2.0)	2 (4.3)	0.6	0.8	1 (1.2)	3 (4.5)	0.3	0.6
Anti U1-RNP1 antibodies, n (%)	8 (5.4)	6 (5.5)	2 (4.3)	>0.9	>0.9	3 (3.7)	5 (7.5)	0.5	0.6
mRSS, mean (SD)	2.09 (2.63)	1.59 (2.05)	3.17 (3.36)	<0.001	0.005	1.93 (2.15)	2.28 (3.12)	0.7	0.9
FVC, median (IQR), %	109 (20)	113 (18)	100 (21)	<0.001	0.005	109 (20)	108 (20)	0.5	0.6
DLco, median (IQR), %	67 (15)	72 (14)	58 (13)	<0.001	<0.001	69 (15)	64 (14)	0.028	0.13
Upper gastrointestinal symptoms, n (%)	96 (64)	62 (61)	34 (72)	0.2	0.3	51 (62)	45 (67)	0.5	0.6
Calcinosis, n (%)	53 (36)	35 (34)	18 (38)	0.6	0.8	27 (33)	26 (39)	0.5	0.6
Interstitial lung disease, n (%)	36 (24)	17 (17)	19 (40)	0.002	0.007	18 (22)	18 (27)	0.5	0.6
Digital ulcers disease, n (%)	58 (39)	33 (32)	25 (53)	0.015	0.052	30 (37)	28 (42)	0.5	0.6
Pulmonary artery hypertension, n (%)	9 (6.0)	2 (2.0)	7 (15)	0.005	0.018	3 (3.7)	6 (9.0)	0.3	0.6
Sjögren syndrome overlap, n (%)	15 (10)	11 (11)	4 (8.5)	0.8	>0.9	6 (7.3)	9 (13)	0.2	0.6
Mycophenolate mofetil, n (%)	13 (8.7)	9 (8.8)	4 (8.5)	>0.9	>0.9	9 (11)	4 (6.0)	0.3	0.6
Aspirin, n (%)	30 (20)	20 (20)	10 (21)	0.8	>0.9	15 (18)	15 (22)	0.5	0.6
Calcium channel blockers, n (%)	94 (63)	67 (66)	27 (57)	0.3	0.6	54 (66)	40 (60)	0.4	0.6
Hydroxychloroquine, n (%)	26 (17)	19 (19)	7 (15)	0.6	0.7	17 (21)	9 (13)	0.2	0.6
Endothelin receptor antagonists, n (%)	7 (4.7)	2 (2.0)	5 (11)	0.032	0.087	3 (3.7)	4 (6.0)	0.7	0.8
Phosphodiesterase 5 inhibitors, n (%)	24 (16)	14 (14)	10 (21)	0.2	0.4	16 (20)	8 (12)	0.2	0.6
Intravenous iloprost, n (%)	26 (17)	14 (14)	12 (26)	0.078	0.2	16 (20)	10 (15)	0.5	0.6
ACE inhibitors, n (%)	51 (34)	33 (32)	18 (38)	0.5	0.7	23 (28)	28 (42)	0.079	0.3
IFN score, mean (SD)	5.45 (0.46)	5.34 (0.38)	5.67 (0.37)	<0.001	<0.001	5.24 (0.27)	5.70 (0.34)	<0.001	<0.001
Event, n (%)								<0.001	<0.001
Cardiac event	6 (4.0)	–	6 (13)	–	–	2 (2.4)	4 (6.0)		
Gastrointestinal failure	4 (2.7)	–	4 (8.5)	–	–	0 (0)	4 (6.0)		
SSc-related mortality	9 (6.0)	–	9 (19)	–	–	1 (1.2)	8 (12)		
No event	102 (68)	102 (100)	–	–	–	72 (88)	30 (45)		
Pulmonary artery hypertension	13 (8.7)	–	13 (28)	–	–	4 (4.9)	9 (13)		
Interstitial lung disease progression	6 (4.0)	–	6 (13)	–	–	2 (2.4)	4 (6.0)		
Renal crisis	1 (0.7)	–	1 (2.1)	–	–	0 (0)	1 (1.5)		
Severe digital vasculopathy	3 (2.0)	–	3 (6.4)	–	–	1 (1.2)	2 (3.0)		
Skin worsening (mRSS)	5 (3.4)	–	5 (11)	–	–	0 (0)	5 (7.5)		

* ACA, anticentromere antibody; ACE, angiotensin-converting enzyme; ANA, antinuclear antibody; DLco, diffusing capacity of the lungs for carbon monoxide; FVC, forced vital capacity; IFN, interferon; IQR, interquartile range; mRSS, modified Rodnan skin score; SSc, systemic sclerosis.

^a Wilcoxon rank sum test, Fisher exact test, or Pearson chi-square test.

^b False discovery rate correction for multiple testing.

Parameters associated with the risk of event over time. At univariable CPH regression, the baseline clinical and demographics characteristics associated with an increased hazard of developing the endpoint over time were presence of

PAH (HR 4.78, 95% CI 2.12–10.80; $P = 0.001$), presence of ILD (HR 2.73, 95% CI 1.52–4.89; $P = 0.002$), presence of DU disease (HR 2.12, 95% CI 1.20–3.77; $P = 0.026$), mRSS (HR 1.13, 95% CI 1.05–1.21; $P = 0.002$), age (HR 1.03, 95%

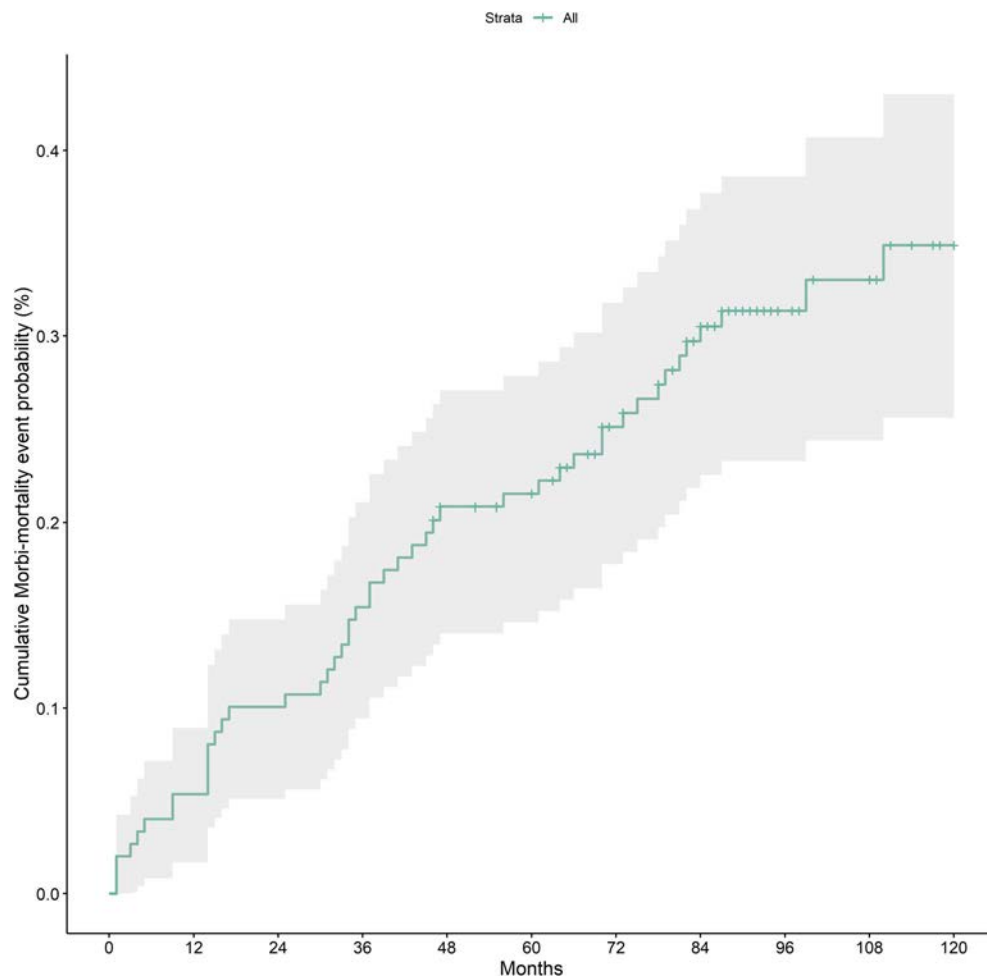


Figure 1. Kaplan-Meier curve showing the overall cohort cumulative time to clinical worsening incidence probability. Color figure can be viewed in the online issue, which is available at <http://onlinelibrary.wiley.com/doi/10.1002/art.43120/abstract>.

CI 1.01–1.06; $P = 0.044$), FVC% (HR 0.98, 95% CI 0.96–0.99; $P = 0.002$), DLco% (HR 0.94, 95% CI 0.92–0.96; $P < 0.001$), and use of ERAs (HR 5.45, 95% CI 2.10–14.20; $P = 0.002$). In this context, IFN score, modeled using a penalized spline, was significantly associated with an increased hazard of developing the endpoint over time. The linear component showed a strong association (HR 2.82, 95% CI 1.58–4.69; $P < 0.001$), and its nonlinear component also contributed significantly ($P = 0.008$). When using a dichotomous model, being in the IFN high group at baseline conferred more than six-fold hazard of Morbi-mortality events over time compared with being in the IFN low group (HR 6.20, 95% CI 3.07–12.5; $P < 0.001$) (Table 2).

A total of 37 deaths occurred during follow-up, 16 of which were directly attributed to scleroderma. Of these, 9 were included in the TTCW analysis as the first event for the patients, whereas the remaining 7 occurred after other outcome events. After adjusting for age, IFN score was not significantly associated with overall survival in the CPH model, as expected when most of the deaths were not related to SSc. In contrast, age emerged as a significant predictor of all-cause mortality, with an HR of 1.16 ($P < 0.001$) (data not shown). Conversely, when considering

deaths attributed to scleroderma ($n = 16$), after adjusting for age, IFN score had a significant positive association with SSc mortality in its linear component (HR 2.83, 95% CI 1.18–6.75; $P = 0.019$), whereas the nonlinear component did not reach statistical significance ($P = 0.230$). Age was also independently associated with SSc mortality (HR 1.12, 95% CI 1.04–1.20; $P = 0.001$).

A multivariable CPH regression model was built to test for the independence of the associations found at univariable analysis. We built two multivariable CPH models using the IFN score either as a continuous or a categorical variable, along with the other clinical features significantly associated with event accrual, namely mRSS, presence of baseline ILD, FVC, presence of baseline PAH, DLco, use of ERAs, DU disease, and age. Notably, informed by clinical plausibility and known collinearity, we opted to exclude DLco and FVC from our analysis, given their significant overlap with PAH and ILD, respectively, as well as the use of ERA because of its indication in DU disease and PAH. All the clinical features except for age retained statistical significance in both models, and IFN score was independently associated with an increased risk of events as both a continuous and a dichotomous variable (Table 3).

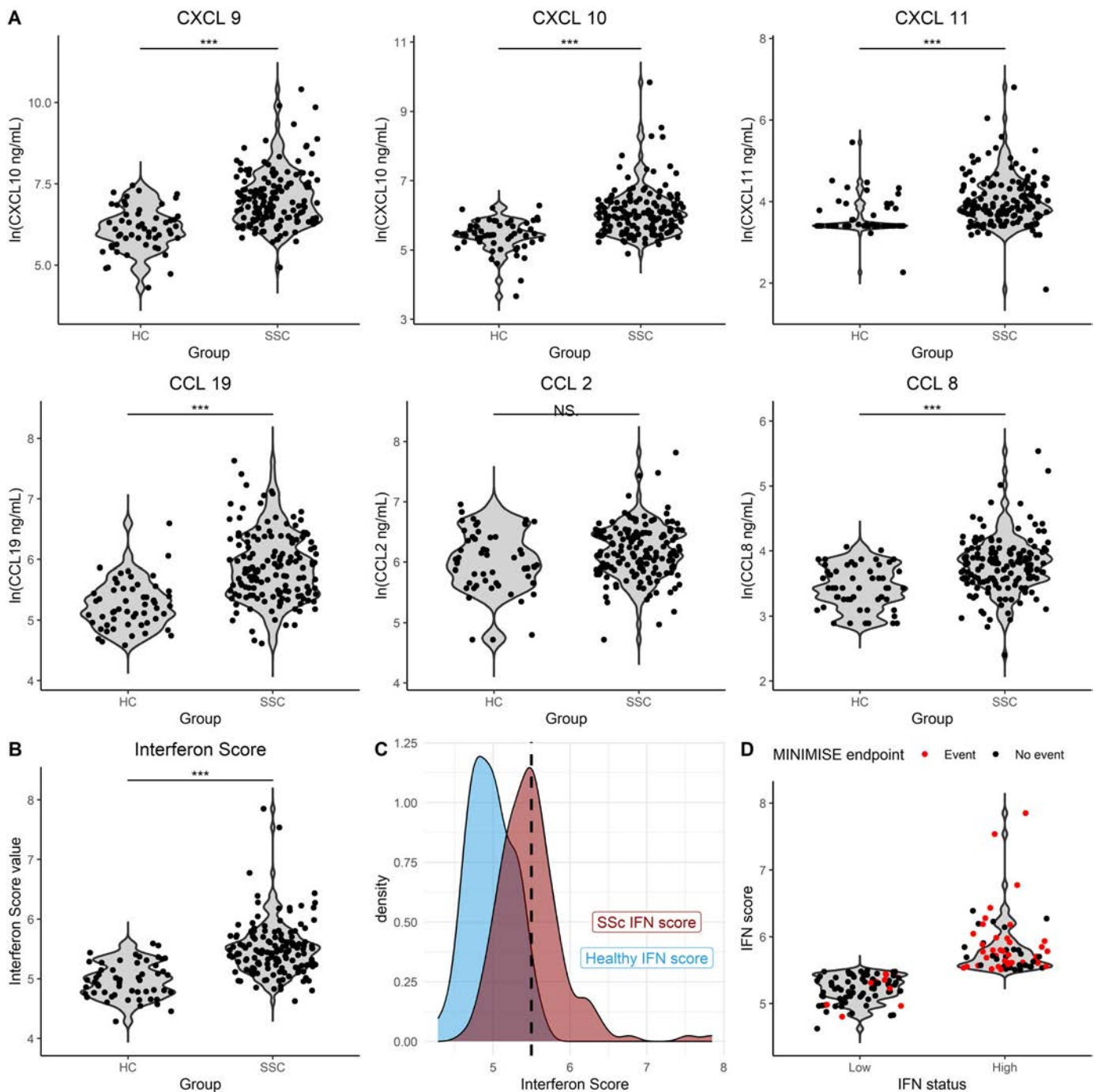


Figure 2. Type I IFN serum score in limited cutaneous SSc. (A) The concentration of the serum chemokines included in the IFN score was significantly higher in the limited cutaneous SSc cohort compared with a reference HC cohort matched for age and sex, except for CCL2 (Student's *t*-tests with Bonferroni correction). (B) Violin plots with jittering showing the values of IFN scores of HCs and patients with SSc (Student's *t*-test). (C) Density distributions of the IFN scores of HCs are in light blue and patients with SSc are in red. The dotted line represents the +2 SDs threshold from HC mean marking the IFN "high" and "low" categories. (D) Violin plots with jittering representing the individual IFN score values in the low (left pane) and high (right pane) groups; red dots represent the IFN scores of patients experiencing the outcome during follow-up. ****P* < 0.001. CCL, chemokine C-C motif ligand; CXCL, C-X-C motif chemokine ligand; HC, healthy control; IFN, interferon; NS, not significant; SSc, systemic sclerosis.

ROC curve analysis of models' performance. The performance of the multivariable CPH models containing IFN score as a continuous or categorical variable was assessed at three

different time points. A time-dependent incident case/dynamic control ROC curve approach was chosen mapping the risk score against the presence or absence of the event over time. The two

Table 2. Univariable Cox proportional hazard regressions for Morbi-mortality event occurrence*

Characteristic	HR	95% CI	P value	Q value ^a
Age	1.03	1.01–1.06	0.02	0.044
Sex				
Female	–	–	–	–
Male	1.50	0.47–4.84	0.5	0.7
Anticentromere	0.84	0.46–1.52	0.6	0.7
Antitopoisomerase I	1.03	0.37–2.88	>0.9	>0.9
Anti-Ro52	1.51	0.82–2.79	0.2	0.3
Disease duration	1.00	0.97–1.04	0.8	>0.9
Isolated ACA positivity				
ACA only	–	–	–	–
Non-ACA only	2.01	1.04–3.88	0.037	0.073
mRSS	1.13	1.05–1.21	<0.001	0.002
FVC	0.98	0.96–0.99	<0.001	0.002
DLco	0.94	0.92–0.96	<0.001	<0.001
Upper GI	1.43	0.75–2.70	0.3	0.4
Interstitial lung disease	2.73	1.52–4.89	<0.001	0.002
Digital ulcers disease	2.12	1.20–3.77	0.01	0.026
Calcinosis	1.19	0.66–2.14	0.6	0.7
Pulmonary artery hypertension	4.78	2.12–10.8	<0.001	0.001
Mycophenolate use	0.94	0.34–2.62	>0.9	>0.9
ET1 inhibitor use	5.45	2.10–14.2	<0.001	0.002
Interferon score			<0.001	<0.001
Linear component	2.82	1.58–4.69	<0.001	–
Nonlinear component	–	–	0.008	–
Interferon score group				
Low	–	–	–	–
High	6.20	3.07–12.5	<0.001	<0.001

* ACA, anticentromere antibody; CI, confidence interval; DLco, diffusing capacity of the lungs for carbon monoxide; ET1, endothelin 1; FVC, forced vital capacity; GI, gastrointestinal; HR, hazard ratio; mRSS, modified Rodnan skin score.

^a False discovery rate correction for multiple testing.

models including the presence of baseline ILD, presence of baseline PAH, baseline mRSS, age, and IFN score showed an excellent AUC for all timepoints. In particular, the model built using the continuous IFN score modeled as a penalized spline showed an AUC \pm SE of 0.799 ± 0.028 , 0.803 ± 0.028 , and 0.801 ± 0.029 for 12 months, 24 months, and 36 months, respectively, and a C-index \pm SE of 0.806 ± 0.029 , whereas the model built using

the categorical IFN score showed an AUC \pm SE of 0.798 ± 0.029 , 0.804 ± 0.030 , and 0.805 ± 0.029 for 12 months, 24 months, and 36 months, respectively, with a C-index \pm SE of 0.794 ± 0.030 . For the same timepoints, an exploratory model built including only the baseline presence of ILD, baseline presence of PAH, mRSS, and age showed an AUC \pm SE of 0.723 ± 0.036 , 0.716 ± 0.034 , and 0.716 ± 0.033 , respectively, and a

Table 3. Multivariate Cox proportional hazard regression models for IFN score as a continuous and categorical variable correcting for significantly associated clinical predictors of event in univariate analysis*

Characteristic	Model 1: IFN continuous			Model 2: IFN categorical		
	HR	95% CI	P value	HR	95% CI	P value
ILD	3.10	1.68–5.75	<0.001	3.13	1.69–5.77	<0.001
PAH	3.81	1.60–9.08	0.003	3.15	1.29–7.69	0.012
mRSS	1.14	1.04–1.25	0.006	1.12	1.03–1.21	0.005
DUs disease	1.77	0.98–3.22	0.059	2.06	1.13–3.74	0.018
Age	1.02	1.00–1.05	0.10	1.03	1.00–1.06	0.043
IFN score						
Linear component	2.38	1.41–4.01	0.004	–	–	–
Nonlinear component	–	–	0.005	–	–	–
IFN score group						
Low	–	–	–	–	–	–
High	–	–	–	5.53	2.70–11.3	<0.001

* CI, confidence interval; DU, digital ulcer; HR, hazard ratio; IFN, interferon; ILD, interstitial lung disease; mRSS, modified Rodnan skin score; PAH, pulmonary artery hypertension.

C-index \pm SE of 0.713 ± 0.040 , whereas a model built with IFN score alone had an AUC \pm SE of 0.728 ± 0.032 , 0.730 ± 0.032 , and 0.730 ± 0.032 , respectively, with a C-index \pm SE of 0.733 ± 0.032 (Supplementary Figure 1).

Event-free survival analysis. Patients in the IFN low group had a significantly higher 10-year event-free survival probability compared to the IFN high group, with a restricted mean TTCW of 110.6 months (95% CI 107.2–114.0) versus 74.7 months (95% CI 70.1–79.3) in IFN high ($P < 0.001$) (Supplementary Figure 2). The event probability of the IFN low group was significantly lower compared with the IFN high group at 12 months (1.2% [95% CI 0.0%–3.6%] vs 10.4% [95% CI 2.8%–17.5%]; $P = 0.018$), 24 months (4.9% [95% CI 0.1%–9.4%] vs 16.4% [95% CI 7.1%–24.8%]; $P = 0.024$), 36 months (4.9% [95% CI 0.1%–9.4%] vs 28.4% [95% CI 16.7%–38.4%]; $P < 0.001$), 60 months (7.4% [95% CI 1.5%–12.9%] vs 38.8% [95% CI 26.0%–49.4%]; $P < 0.001$), and 120 months (13.0% [95% CI 5.1%–20.2%] vs 62.3% [95% CI 44.3%–74.5%]; $P < 0.001$) (Supplementary Table 3 and Supplementary Figure 2). No significant difference in the median (IQR) censoring time in months was detected across IFN high and low groups (89 [IQR 9] vs 89 [IQR 8], respectively, $P = 0.866$). To further account for the possible influence of censoring, a KM analysis based on cases who had at least 5-year follow-up without censoring was performed. To do so, we filtered only patients who either developed an event in the first 5 years of follow-up or had an event-free follow-up of at least 5 years. Using this approach, 136 patients were included in a 5-year KM analysis, of whom there were 59 in the IFN high and 77 in the IFN low groups. IFN low patients maintained a higher restricted mean TTCW compared with IFN high patients (103.5 months [95% CI 97.4–110.2] vs 74.1 [95% CI 62.8–85.3]; $P < 0.001$) (Supplementary Table 4 and Supplementary Figure 3).

Combination of clinical and IFN score parameters identifies subsets of patients with distinct clinical outcomes over time. Based on the significant predictors in the multivariate CPH regression (namely, IFN score, mRSS, DU disease, ILD, and PAH), we built upset plots depicting the prevalence and clinical outcome of these features alone or in combination in our population (Figure 3A). To allow a meaningful visualization of subgroups, patients fulfilling the mRSS >4 or baseline DU disease criteria were grouped as having “acral involvement,” whereas patients with PAH or ILD at baseline were classified as presenting “cardiopulmonary involvement.” Patients meeting the criteria for both acral and cardiopulmonary involvements were recognized as having dual involvement. Conversely, patients showing no clinical involvement at baseline were categorized as having none. The four clinical groups were further stratified based on IFN high or low categories leading to eight strata. The upset plot distinctly highlighted that only the strata

characterized by high IFN in combination with acral and/or cardiopulmonary manifestations notably exceeded the 50% threshold for event occurrence. In contrast, other patient subsets fell below the 50% threshold, indicating a lower incidence of events. Notably, among the incident cases without acral or cardiopulmonary manifestations at baseline, 2 of 36 low IFN patients developed the outcome (5.6%) compared with 5 of 25 high IFN patients (20.0%), reflecting a nearly four-fold higher incidence rate despite the low numbers. Accordingly, when comparing these two groups without baseline clinical manifestations, the restricted mean TTCW was shorter for the high IFN group compared with the low IFN group (104.5 months, 95% CI 92.0–117.1 vs 116.7 months, 95% CI 112.0–121.3) with a between-group difference of –12.1 months (95% CI –25.5 to 1.3; $P = 0.076$).

On this basis, patients fulfilling at least one clinical criterion (acral and/or cardiopulmonary) and the serologic criterion of high IFN were classified as being “high risk,” whereas those not fulfilling both criteria were deemed to be “low risk.” The 10-year event-free survival curve of these two groups highlighted a major difference in restricted mean TTCW (55.7 months [95% CI 43.6–67.9] vs 105.8 months [95% CI 100.4–111.3] for high risk vs low risk, respectively, $P < 0.001$) (Figure 3B; Supplementary Table 5). Forest plots of the RR of each group at 24, 36, and 48 months relative to the overall cohort (Figure 3C) indicated that at 24 months the RR for the IFN high group is 1.62 (95% CI 1.07–2.48), whereas for the IFN low group it is 1.22 (95% CI 0.81–1.83). The high-risk (at least one clinical criterion and a high IFN score) group’s RR is 2.20 (95% CI 1.84–2.66), contrasting with the low-risk group at 1.10 (95% CI 0.99–1.21). Patients with acral and/or cardiopulmonary manifestations had an RR of 1.56 (95% CI 1.11–2.01) against 0.90 (95% CI 0.75–1.05) for those without. At 36 months, the RR of the IFN high group was 2.35 (95% CI 1.88–2.92), and the IFN low one was 1.31 (95% CI 0.98–1.74). The high-risk group’s RR was 2.75 (95% CI 2.31–3.19), whereas the low-risk group remained relatively stable at 1.15 (95% CI 1.02–1.28). The presence of acral and/or cardiopulmonary manifestations resulted in an RR of 1.75 (95% CI 1.39–2.11), with the absence of these manifestations showing an RR of 0.95 (95% CI 0.80–1.10). At 48 months, data consolidation occurs with increases in RR for long-term follow-ups in the high-risk and IFN high groups, indicating a sustained risk over time.

DISCUSSION

Our study shows for the first time that patients with lcSSc show a high IFN activation in their serum in a proportion even higher than the one observed in dcSSc. Given the effect of standard immune suppression on serum IFN score shown in the Scleroderma Lung Study II cohort, it is plausible to speculate that the increased proportion observed in patients with lcSSc may be driven by a lower prevalence of immune-suppressant medications in this cohort (17.4% vs 70% of dcSSc).²⁴ Herein we show

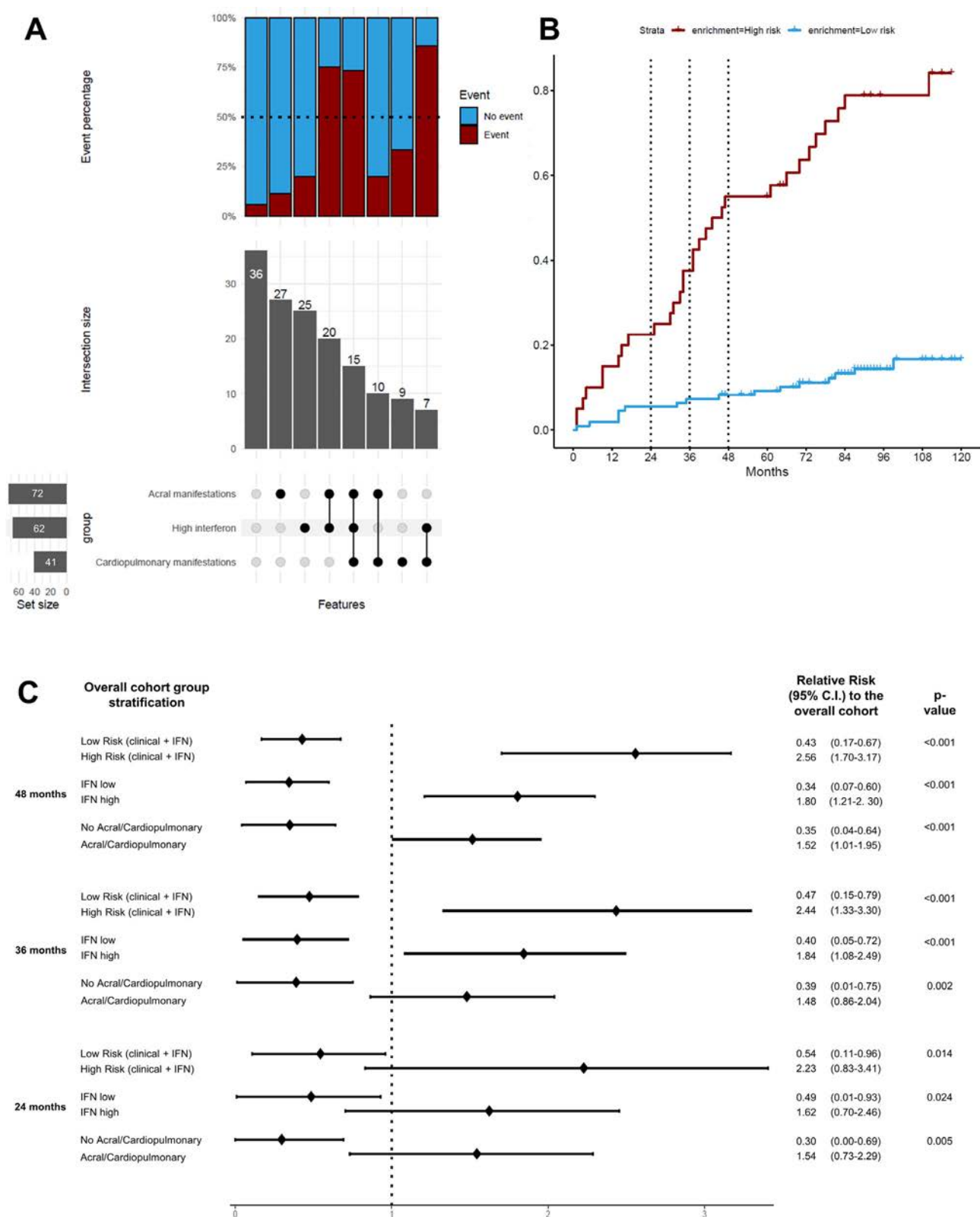


Figure 3. Combinations of clinical and serum IFN score groups. (A) Upset plots of clinical and serological subgroups with relative numerosity, prevalence, and intersection size. (B) Kaplan-Meier curves for cumulative events for patients in the high-risk and low-risk groups for 120-month follow-up. (C) Forest plot for three time points relevant for clinical trials showing the relative risk for time to clinical worsening compared with the overall cohort for different stratification groups. The dotted line on 1 represents the risk of the unselected population for that relative time point. C.I., confidence interval; IFN, interferon.

that patients with high IFN activity at baseline have a worse clinical outcome as assessed by an increased proportion of patients meeting the combined event (57% vs 12%) and a shorter restricted mean TTCW (74.4 [95% CI 70.1–79.3] months in IFN high vs 110.6 [95% CI 107.2–114.0] months in IFN low).

It is intriguing to observe that despite this negative prognostic value, there was no difference at baseline in the prevalence of clinically meaningful organ manifestations. This observation supports the notion that type I IFN signature may reflect biologic disease activity before clinically detectable damage.²⁵ Although this was an analysis of a prevalent cohort with highly variable disease duration at time of enrollment, we did not observe a significant difference in disease duration across IFN groups or event groups. The observation that disease duration did not differ in patients with or without events may support that the concept of accumulation of disease damage over time, true for most inflammatory conditions, may not entirely apply to lcSSc and/or may be mitigated by survival bias. In this context, the value of a specific type of disease activity (eg, type I IFN) may play a more important role than disease duration. Longitudinal studies are ongoing to determine the effect of disease duration or immunomodulatory treatments on type I IFN score and how this can modulate its value in predicting for clinically meaningful events.

Our results, identifying the baseline presence of ILD, PAH, and more severe skin involvement as predictive of disease complications, align with the established literature regarding prognostic factors in SSc, affirming known associations between baseline organ involvement, namely ILD, PAH, and skin fibrosis, and SSc-related events.^{7,26,27} These associations likely stem from the intrinsic risk of SSc-related mortality inherent in these conditions, specifically with regard to PAH and ILD, but they also potentially signify a more severe disease phenotype that elevates the risk of other organ failures and clinically significant events. Additionally, consistent with prior multicenter studies,^{28–30} a history of DUs in our cohort increased the risk of severe vascular events, worse disease progression, and survival outcomes. The MINIMISE composite endpoint of disease progression includes change in mRSS. We consider this to be an important and novel aspect of our work but appreciate that the threshold for clinically meaningful progression is extrapolated from previous studies of dcSSc. This is a limitation, and future work examining other independent SSc cohorts will determine if this threshold may be adjusted for application to lcSSc. Using similar clinical features, the revised European Scleroderma Trials and Research Activity Index (EUSTAR-AI) has been proposed as a score to enrich for poor outcome in dcSSc.³¹ In our cohort, only 7 of 149 patients had EUSTAR-AI scores above 2.5 (ie, active disease), as one would expect in the lc subset; nonetheless, the IFN score did correlate with EUSTAR-AI, although weakly (Spearman $\rho = 0.230$; $P = 0.006$).

Our findings further support the significance of antibody profiles known to exhibit both positive and negative prognostic implications. Specifically, the observed lower incidence of

Morbi-mortality events in patients solely positive for ACA resembles trends from other incident SSc cohorts.⁷ Notably, we observed a numerically higher proportion of patients with low IFN score presenting an isolated ACA positivity (45% vs 33%) with a trend toward significance. This latter observation may explain the loss of significance of ACA positivity in multivariate analysis with IFN score. Further, our investigation revealed a significantly higher prevalence of anti-Ro52 antibodies in the IFN high group, suggesting a potential relationship between autoantibody profiles and differential IFN expression. The prevalence of the Ro-52 autoantibody in our cohort mirrors findings from significant multicentric studies,³² with its positivity previously linked to markedly worse survival rates, PAH, and ILD progression.^{33,34} Nonetheless, in our lcSSc cohort, anti-Ro52 failed to confer a significantly increased risk of events, likely because of the inclusion of a small subset of patients with overlapping Sjögren disease. Notably, the presence of another autoimmune disease overlap has been shown to confer a milder phenotype in SSc,³⁵ which may mask the potential impact of anti-Ro52 antibodies on disease severity.

Furthermore, we showed that the integration of established clinical features such as ILD, PAH, and mRSS with the IFN score improved the prediction of trial-relevant events. This fosters a paradigm shift toward personalized medicine in lcSSc trials. In fact, this composite model not only enables the identification of patients at higher risk of specific complications but also facilitates the evaluation of therapeutic interventions tailored to individual risk profiles.^{36,37} Lastly, the inclusion of antibody profiles, with anti-Ro52 indicating a higher risk of adverse outcomes and, even more so, the exclusion of the isolated ACA-positive profile showcasing a protective association, could refine even further lcSSc trial cohorts, enabling a more effective evaluation of therapeutic efficacy in intervention studies.

Our study retains inherent limitations because of its retrospective nature, which is primarily susceptible to information bias and nonparticipation bias, the latter potentially censoring patients with milder phenotypes and thus underpowering the analysis. In the attempt to mitigate this limitation, we have performed an analysis on the patients with complete 5-year follow-up data available, and we have observed a very similar effect on type I IFN score. An additional limitation is that although our sample size was calculated for detecting differences in event-free survival between lcSSc groups, the validation of our proposed multivariable model metrics necessitates a larger confirmatory cohort, as our current numbers of events precluded cross-validation approaches. Future, larger-scale, multicentric studies will be instrumental in refining potential patient-selection tools.

Another aspect of interest regarding the utility of IFN score lies in understanding its temporal dynamics. Given its demonstrated dysregulation across various autoimmune conditions,¹⁸ elucidating its temporal kinetics is pivotal to portray IFN score as a dynamic biomarker, revealing SSc disease flares and

progression, or potentially establishing this biomarker as a stable pathogenetic signature, akin to antibody profiles. Assessing the longitudinal change in IFN score over time is therefore warranted for identifying a time-dependent association with the onset of clinically apparent organ damage. In this sense, comparing the trajectories of IFN scores in patients with differing outcomes over time could be very useful to understand the effect of molecular heterogeneity in a longitudinal setting. Moreover, it remains to be assessed whether, similarly to what has been observed in the Scleroderma Lung Study II,²⁴ serum IFN score may change following immune suppression in lcSSc. Longitudinal studies are ongoing to determine the effect of disease duration or immunomodulatory treatments on type I IFN score and how this can modulate its value in predicting for clinically meaningful events.

In conclusion, our data demonstrate that type I IFN activation is common in SSc, extending to both cutaneous subsets. Our data also demonstrate that the IFN score may aid in the assessment of disease activity and in enrichment for a higher probability of clinically meaningful events over time in lcSSc trials.

AUTHOR CONTRIBUTIONS

All authors contributed to at least one of the following manuscript preparation roles: conceptualization AND/OR methodology, software, investigation, formal analysis, data curation, visualization, and validation AND drafting or reviewing/editing the final draft. As corresponding author, Drs Del Galdo and Denton confirm that all authors have provided the final approval of the version to be published, and take responsibility for the affirmations regarding article submission (eg, not under consideration by another journal), the integrity of the data presented, and the statements regarding compliance with institutional review board/Declaration of Helsinki requirements.

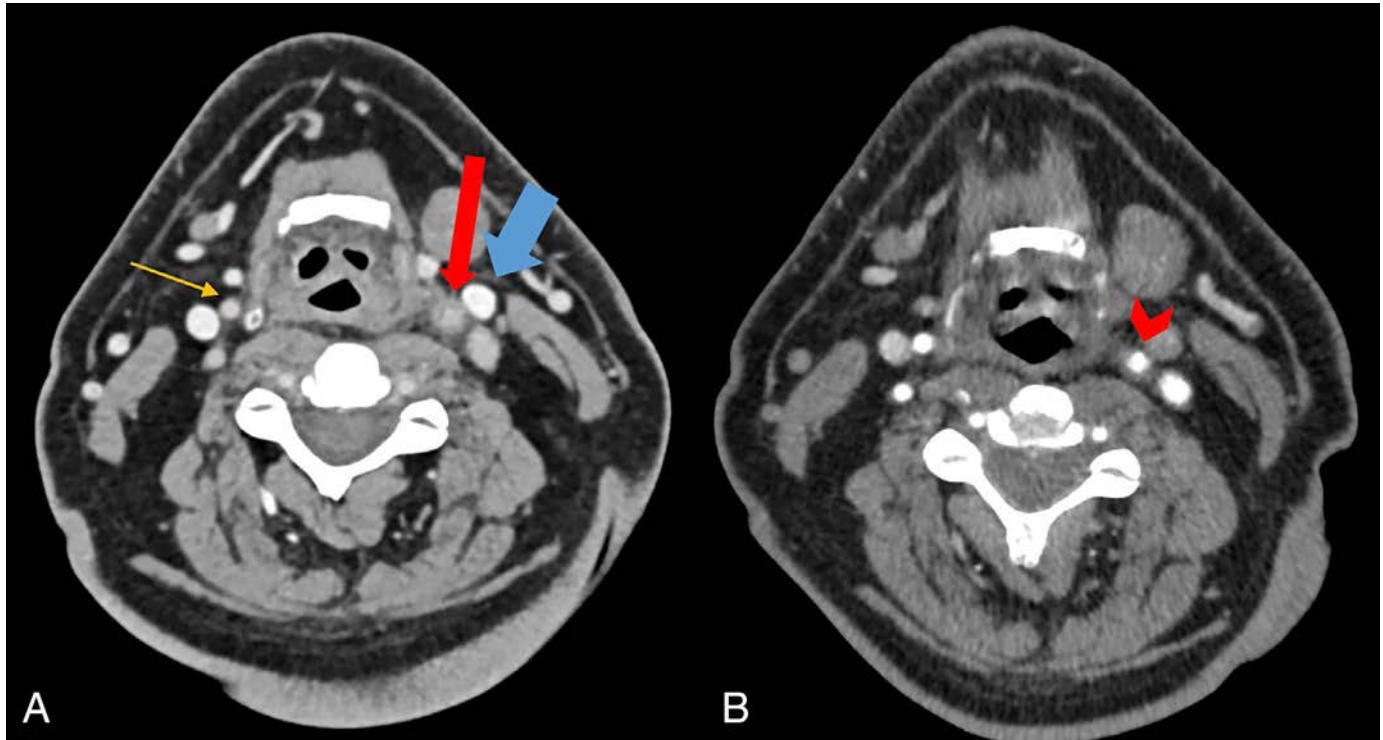
REFERENCES

- Lescoat A, Murphy SL, Roofeh D, et al. Considerations for a combined index for limited cutaneous systemic sclerosis to support drug development and improve outcomes. *J Scleroderma Relat Disord* 2021;6(1):66–76.
- Frantz C, Huscher D, Avouac J, et al; EUSTAR co-authors. Outcomes of limited cutaneous systemic sclerosis patients: results on more than 12,000 patients from the EUSTAR database. *Autoimmun Rev* 2020;19(2):102452.
- De Almeida Chaves S, Porel T, Mounié M, et al. Sine scleroderma, limited cutaneous, and diffused cutaneous systemic sclerosis survival and predictors of mortality. *Arthritis Res Ther* 2021;23(1):295.
- Lefèvre G, Dauchet L, Hachulla E, et al. Survival and prognostic factors in systemic sclerosis-associated pulmonary hypertension: a systematic review and meta-analysis. *Arthritis Rheum* 2013;65(9):2412–2423.
- Lescoat A, Roofeh D, Townsend W, et al. Domains and outcome measures for the assessment of limited cutaneous systemic sclerosis: a scoping review protocol. *BMJ Open* 2021;11(3):e044765.
- Galiè N, Barberà JA, Frost AE, et al; AMBITION Investigators. Initial use of ambrisentan plus tadalafil in pulmonary arterial hypertension. *N Engl J Med* 2015;373(9):834–844.
- Nihtyanova SI, Sari A, Harvey JC, et al. Using autoantibodies and cutaneous subset to develop outcome-based disease classification in systemic sclerosis. *Arthritis Rheumatol* 2020;72(3):465–476.
- Mycophenolate in limited cutaneous systemic sclerosis (MINIMISE-Pilot). [ClinicalTrials.gov](https://clinicaltrials.gov/identifiers/NCT04927390) identifier NCT04927390. 2023. Accessed July 27, 2023. <https://clinicaltrials.gov/study/NCT04927390>
- Nihtyanova SI, Tang EC, Coghlan JG, et al. Improved survival in systemic sclerosis is associated with better ascertainment of internal organ disease: a retrospective cohort study. *QJM* 2010;103(2):109–115.
- Kakkar V, Assassi S, Allanore Y, et al. Type 1 interferon activation in systemic sclerosis: a biomarker, a target or the culprit. *Curr Opin Rheumatol* 2022;34(6):357–364.
- Delaney TA, Morehouse C, Brohawn PZ, et al. Type I IFNs regulate inflammation, vasculopathy, and fibrosis in chronic cutaneous graft-versus-host disease. *J Immunol* 2016;197(1):42–50.
- Ruzek MC, Jha S, Ledbetter S, et al. A modified model of graft-versus-host-induced systemic sclerosis (scleroderma) exhibits all major aspects of the human disease. *Arthritis Rheum* 2004;50(4):1319–1331.
- Ross RL, Corinaldesi C, Migneco G, et al. Targeting human plasmacytoid dendritic cells through BDCA2 prevents skin inflammation and fibrosis in a novel xenotransplant mouse model of scleroderma. *Ann Rheum Dis* 2021;80(7):920–929.
- Tiev KP, Hua-Huy T, Kettaneh A, et al. Serum CC chemokine ligand-18 predicts lung disease worsening in systemic sclerosis. *Eur Respir J* 2011;38(6):1355–1360.
- Valenzi E, Tabib T, Papazoglou A, et al. Disparate interferon signaling and shared aberrant basaloid cells in single-cell profiling of idiopathic pulmonary fibrosis and systemic sclerosis-associated interstitial lung disease. *Front Immunol* 2021;12:595811.
- Yin H, Distler O, Shen L, et al. Endothelial response to type I interferon contributes to vasculopathy and fibrosis and predicts disease progression of systemic sclerosis. *Arthritis Rheumatol* 2024;76(1):78–91.
- George PM, Oliver E, Dorfmueller P, et al. Evidence for the involvement of type I interferon in pulmonary arterial hypertension. *Circ Res* 2014;114(4):677–688.
- Bauer JW, Baechler EC, Petri M, et al. Elevated serum levels of interferon-regulated chemokines are biomarkers for active human systemic lupus erythematosus. *PLoS Med* 2006;3(12):e491.
- Hinchcliff M, Huang S, Assassi S, et al. Serum interferon score is a biomarker of active disease in patients with early diffuse cutaneous systemic sclerosis enrolled in the prospective registry of early systemic sclerosis (PRESS) cohort. *Lancet Rheum* 2024;24(12):000403.
- van den Hoogen F, Khanna D, Fransen J, et al. 2013 classification criteria for systemic sclerosis: an American College of Rheumatology/European League Against Rheumatism collaborative initiative. *Ann Rheum Dis* 2013;72(11):1747–1755.
- LeRoy EC, Black C, Fleischmajer R, et al. Scleroderma (systemic sclerosis): classification, subsets and pathogenesis. *J Rheumatol* 1988;15(2):202–205.
- Heagerty PJ, Lumley T, Pepe MS. Time-dependent ROC curves for censored survival data and a diagnostic marker. *Biometrics* 2000;56(2):337–344.
- Heagerty P, Zheng Y. Survival model predictive accuracy and ROC curves. *Biometrics* 2005;61(1):92–105.
- Assassi S, Li N, Volkmann ER, et al. Predictive significance of serum interferon-inducible protein score for response to treatment in systemic sclerosis-related interstitial lung disease. *Arthritis Rheumatol* 2021;73(6):1005–1013.
- Brkic Z, van Bon L, Cossu M, et al. The interferon type I signature is present in systemic sclerosis before overt fibrosis and might contribute to its pathogenesis through high BAFF gene expression and high collagen synthesis. *Ann Rheum Dis* 2016;75(8):1567–1573.

26. Becker M, Graf N, Sauter R, et al; EUSTAR Collaborators; EUSTAR Collaborators (numerical order of centres). Predictors of disease worsening defined by progression of organ damage in diffuse systemic sclerosis: a European Scleroderma Trials and Research (EUSTAR) analysis. *Ann Rheum Dis* 2019;78(9):1242–1248.
27. Distler O, Assassi S, Cottin V, et al. Predictors of progression in systemic sclerosis patients with interstitial lung disease. *Eur Respir J* 2020;55(5):55.
28. Mihai C, Landewé R, van der Heijde D, et al; EUSTAR co-authors. Digital ulcers predict a worse disease course in patients with systemic sclerosis. *Ann Rheum Dis* 2016;75(4):681–686.
29. Mihai C, Distler O, Gheorghiu AM, et al; EUSTAR collaborators. Incidence and risk factors for gangrene in patients with systemic sclerosis from the EUSTAR cohort. *Rheumatology (Oxford)* 2020; 59(8):2016–2023.
30. Blagojevic J, Abignano G, Avouac J, et al; EUSTAR co-workers. Use of vasoactive/vasodilating drugs for systemic sclerosis (SSc)-related digital ulcers (DUs) in expert tertiary centres: results from the analysis of the observational real-life DeSSciphre study. *Clin Rheumatol* 2020;39(1):27–36.
31. Fasano S, Riccardi A, Messiniti V, et al. Revised European Scleroderma Trials and Research Group Activity Index is the best predictor of short-term severity accrual. *Ann Rheum Dis* 2019; 78(12):1681–1685.
32. Parker JC, Burlingame RW, Bunn CC. Prevalence of antibodies to Ro-52 in a serologically defined population of patients with systemic sclerosis. *J Autoimmune Dis* 2009;6:2.
33. Lee A, Patterson KA, Tan DJ, et al. Anti-Ro52/TRIM21 is independently associated with pulmonary arterial hypertension and mortality in a cohort of systemic sclerosis patients. *Scand J Rheumatol* 2021; 50(6):469–474.
34. Hamberg V, Sohrabian A, Volkmann ER, et al. Anti-Ro52 positivity is associated with progressive interstitial lung disease in systemic sclerosis-an exploratory study. *Arthritis Res Ther* 2023; 25(1):162.
35. Avouac J, Airò P, Dieude P, et al. Associated autoimmune diseases in systemic sclerosis define a subset of patients with milder disease: results from 2 large cohorts of European Caucasian patients. *J Rheumatol* 2010;37(3):608–614.
36. Del Galdo F, Hartley C, Allanore Y. Randomised controlled trials in systemic sclerosis: patient selection and endpoints for next generation trials. *Lancet Rheumatol* 2020;2(3):e173–e184.
37. Hinchcliff M, Garcia-Milian R, Di Donato S, et al. Cellular and molecular diversity in scleroderma. *Semin Immunol* 2021;58:101648.

DOI 10.1002/art.43093

Clinical Images: Transient perivascular inflammation of the carotid artery syndrome



The patient, a 53-year-old man, presented to the emergency department with acute left-sided neck pain for three days. He had a medical history of pT3N0 pancreatic acinar cell carcinoma with distal pancreatectomy and splenectomy eight months prior. He was treated with a course of adjuvant chemotherapy, with the last cycle two weeks before presentation. On examination, the neck appeared normal but was exquisitely tender to palpation. Serum markers of inflammation were elevated, with a white blood cell (WBC) count of $10.1 \times 1,000/\mu\text{L}$ (reference $4.0\text{--}11.0 \times 1,000/\mu\text{L}$), a C-reactive protein (CRP) level of 5.9 mg/L (reference $<3.1 \text{ mg/L}$), and an erythrocyte sedimentation rate (ESR) of 67 mm/hr (reference $0\text{--}20 \text{ mm/hr}$). A computed tomography (CT) scan of the neck revealed focal circumferential soft tissue thickening around the left carotid bifurcation (A; red arrow) with trace adjacent fat stranding and trace fluid. The left internal jugular vein is brighter (blue arrow) as it is in the venous phase. The contralateral right internal carotid artery is unremarkable (yellow arrow). Based on the clinical history and radiologic findings, the patient was diagnosed with transient perivascular inflammation of the carotid artery (TIPIIC) syndrome. He was discharged from the emergency department and took ibuprofen for five days, and symptoms improved. Laboratory tests performed two days later revealed a down-trending WBC count of $8.9 \times 1,000/\mu\text{L}$, CRP level of 1.8 mg/L , and ESR of 40 mm/hr . A repeat CT scan of the neck one month later (B) showed an interval decrease of circumferential soft tissue thickening surrounding the left carotid bifurcation, and the lumen showing improvement in the uniform wall thickening (small red arrow). This patient's neck pain at the carotid bifurcation in the past may have been described as "carotidynia," which is a nonspecific term because it encompasses multiple possible underlying pathologies to explain this clinical phenomenon.¹ The new terminology of TIPIIC syndrome has been established to identify rare cases of neck pain in association with radiologic findings of perivascular inflammation of the carotid artery. TIPIIC syndrome often resolves spontaneously within two weeks or with anti-inflammatory medication.² The underlying pathophysiology is poorly understood, and further research is needed in this area.

Author disclosures are available at <https://onlinelibrary.wiley.com/doi/10.1002/art.43093>.

1. Jud P, Struger J, Gattringer T, et al. Retrospective analysis of long-term clinical, diagnostic and outcome parameters in patients with TIPIC syndrome. *Vasc Med* 2023;28(4):345–347.
2. Micieli E, Voci D, Mumoli N, et al. Transient perivascular inflammation of the carotid artery (TIPIC) syndrome. *Vasa* 2022;51(2):71–77.


Neeharika Namineni, MD 

neeha@namineni.com

Stanford University

Palo Alto, CA

Sowmya Mahalingam, MBBS, MD

Abhijeet Danve, MBBS, MD, MHS 

Yale School of Medicine

New Haven, CT

DOI 10.1002/art.43116


Clinical Images: A treatable cause of bilateral leg edema and pleural effusion: yellow nail syndrome with IgG4-related disease



The patient, a 78-year-old man with bronchiectasis and recurrent bronchial infections, presented with dyspnea persisting for 3 months. Physical examination revealed decreased right-sided breath sounds, marked bilateral pitting edema of the lower extremities, (A) thickened yellow nails, and submandibular gland swelling. Laboratory test results were unremarkable except for elevated serum IgG and IgG4 concentrations (1,766 and 563 mg/dL; reference ranges: 870–1,700 and 11–121 mg/dL, respectively). Potassium hydroxide and bacterial culture results were negative, ruling out nail infection. (B) Chest x-ray and computed tomography scan showed a right pleural effusion, which was an exudate with lymphocytic predominance, no malignant cells, and negative findings for bacteria or mycobacteria. Echocardiography confirmed normal cardiac function. Lymphoscintigraphy demonstrated delayed lymphatic transport and dermal back-flow, consistent with lymphedema. Yellow nail syndrome (YNS) was diagnosed based on the triad of yellow nails, lymphedema, and pulmonary disease. (C) Pleural biopsy revealed lymphoid follicles surrounded by numerous IgG4-positive plasma cells with an IgG4/IgG ratio of 90%. Therefore, IgG4-related disease was identified as the underlying cause of YNS. The patient did not respond to diuretics but showed significant improvement with oral prednisolone (0.6 mg/kg) and compression therapy. At 6- and 12-month follow-ups, pleural effusion resolved, nails normalized, and lymphedema improved. YNS is a rare disorder associated with various malignancies or autoimmune diseases.^{1,2} However, the etiology of the yellow nails in this disorder is not presently understood. Long-term prognosis depends on the severity of recurrent pleural effusion and underlying etiology.³ Although supportive care remains the primary approach in YNS management, recognizing IgG4-related disease as a treatable underlying disease is crucial for optimal patient care.

Author disclosures are available at <https://onlinelibrary.wiley.com/doi/10.1002/art.43116>.

1. Abdalla A, Jamous F. Yellow nail syndrome: a case presentation and a review of management options. *S D Med* 2021;74(8):368–371.
2. Gupta S, Samra D, Yel L, et al. T and B cell deficiency associated with yellow nail syndrome. *Scand J Immunol* 2012;75(3):329–335
3. Iqbal M, Rossoff LJ, Marzouk KA, et al. Yellow nail syndrome: resolution of yellow nails after successful treatment of breast cancer. *Chest* 2000;117(5):1516–1518.

Seiya Oba, MD, PhD 
oba.rheu@tmd.ac.jp
Yusuke Matsuo, MD, PhD
Institute of Science Tokyo
Tokyo, Japan
Tokyo Kyosai Hospital
Tokyo, Japan

LETTER

DOI 10.1002/art.43101

Targeting long noncoding RNA H19 in subchondral bone osteocytes and cartilage degradation in osteoarthritis: comment on the article by Wang et al

To the Editor:

Recently, a study published in *Arthritis & Rheumatology* showed that patients with osteoarthritis (OA) and mice models have high subchondral bone mass, along with much long noncoding RNA (lncRNA) H19⁺ osteocytes.¹ Mice with H19 gene-deficient osteocytes were less susceptible to destabilization of medial meniscus (DMM)-induced OA features. Moreover, suppression of H19 alleviated subchondral bone remodeling and OA progression.¹ Collectively, the findings showed that H19 was highly expressed in OA, and H19 contributed to OA pathogenesis.

OA is a chronic degenerative joint disorder characterized by cartilage loss and pain in multiple joints. This disease is highly prevalent in the older population all over the world. To date, it is estimated that more than 500 million people may be affected by OA. There is no method to fully cure the disease. Therefore, OA takes a significant part in economic burden and needs more resources in the health care system. Finding out targets related to OA is urgent. There are several studies about the role of H19 in OA. However, the findings were inconsistent. A study of the Chinese Han population indicated that the H19 gene rs217727 polymorphism (A allele) was related to a higher risk of OA (odds ratio 1.27; $P = 0.001$), and rs217727 of the H19 gene was positively related to plasma levels of lncRNA H19 in patients with OA.² Similarly, expression of H19 was elevated in the cartilage tissue of patients with OA.³ Knockdown H19 in chondrocytes inhibited chondrocyte apoptosis and matrix metalloproteinase 1 (MMP-1) and MMP-13 expression but contributed to chondrocyte proliferation and up-regulated collagen type II $\alpha 1$ -chain (COL2A1) and microRNA-140-5p (miR-140-5p) expression. Interestingly, H19 promoted matrix degradation in chondrocytes by inhibiting miR-140-5p.³ Moreover, H19 expression was elevated in interleukin-1 β (IL-1 β)-treated chondrocytes and was negatively related to the expression of miR-106a-5p in IL-1 β -treated chondrocytes.⁴


Overexpression of H19 in IL-1 β -treated chondrocytes suppressed proliferation but promoted apoptosis of the cells. On the contrary, overexpression of miR-106a-5p in IL-1 β -treated

chondrocytes resulted in proliferation but inhibited apoptosis of the cells in the presence of the H19 addition.⁴ These data suggested that H19 may promote OA development by inhibiting miR-140-5p and miR-106a-5p. Recently, H19 was also found to inhibit OA development. In DMM-induced OA mice, there was high expression of IL-38, and injection of IL-38 into OA mice significantly alleviated inflammatory responses.⁵ H19 bound to transcription factor tumor protein p53 (TP53) and then up-regulated IL-38 expression. OA mice injected with overexpressed H19 lentivirus vector up-regulated IL-38 expression, whereas the expression of IL-38 was reduced when OA mice were injected with overexpressed H19 and inhibited TP53 lentivirus vectors.⁵ Interestingly, expression of synovial fluid inflammatory cytokines IL-6, IL-8, IL-17, IL-22, and tumor necrosis factor- α and cartilage damage were reduced after injection of overexpressed H19 in OA mice but were increased by a combined injection of overexpressed H19 and inhibited IL-38 lentivirus vectors, overexpressed H19, and inhibited TP53 lentivirus vectors.⁵ Furthermore, Tan et al reported that H19 was lower in the cartilage of patients with OA compared with controls.⁶ Coculturing fibroblast-like synoviocytes (FLSs) with overexpressed H19 and chondrocytes promoted proliferation and migration of chondrocytes. When chondrocytes were stimulated with IL-1 β , the expression of MMP-13 and ADAMTS5 was increased, and expression of COL2A1 and aggrecan was reduced. The addition of H19 overexpressed FLSs to IL-1 β -treated chondrocytes significantly inhibited the inflammatory components production and up-regulated expression of sulfated glycosaminoglycans.⁶

Based on the above findings, it is still difficult to say whether H19 contributes to OA development or inhibits OA risk. In the future, several questions need clarification. First, different findings may relate to different study designs.^{3–6} To better clarify the role of H19 in OA development, the same design may be needed. For instance, H19 gene-deficient mice need conduction and will be treated with DMM. Second, a different role of H19 in OA may correlate with the effects of H19 on downstream signaling, such as interaction with miR-140-5p, miR-106a-5p, TP53, and IL-38. In the future, more in vivo studies are needed to confirm the effects of both interfering H19 and downstream signaling, for example, both knocking out H19 and miR-140-5p genes in OA mice.


Supported by the National Natural Science Foundation of China (grant 81701606).

Author disclosures are available at <https://onlinelibrary.wiley.com/doi/10.1002/art.43101>.

An-Fang Huang, MM 

louch211@163.com

Affiliated Hospital of Southwest Medical University
Sichuan, China

Wang-Dong Xu, MD 

Southwest Medical University
Sichuan, China

1. Wang R, Mehrjou B, Dehghan-Banian D, et al. Targeting long non-coding RNA H19 in subchondral bone osteocytes alleviates cartilage degradation in osteoarthritis. *Arthritis Rheumatol* 2025;77(3): 283–297.
2. Wang H, Li J, Cheng Y, Yao J. Association of long-chain noncoding RNA H19 and MEG3 gene polymorphisms and their interaction with risk of osteoarthritis in a Chinese Han population. *Genet Test Mol Biomarkers* 2020;24(6):328–337.
3. Yang B, Xu L, Wang S. Regulation of lncRNA-H19/miR-140-5p in cartilage matrix degradation and calcification in osteoarthritis. *Ann Palliat Med* 2020;9(4):1896–1904.
4. Zhang X, Liu X, Ni X, et al. Long non-coding RNA H19 modulates proliferation and apoptosis in osteoarthritis via regulating miR-106a-5p. *J Biosci* 2019;44(6):128.
5. Zhou Y, Li J, Xu F, et al. Long noncoding RNA H19 alleviates inflammation in osteoarthritis through interactions between TP53, IL-38, and IL-36 receptor. *Bone Joint Res* 2022;11(8):594–607.
6. Tan F, Wang D, Yuan Z. The fibroblast-like synoviocyte derived exosomal long non-coding RNA H19 alleviates osteoarthritis progression through the miR-106b-5p/TIMP2 axis. *Inflammation* 2020;43(4): 1498–1509.

DOI 10.1002/art.43100

Reply

To the Editor:

We appreciate the opportunity to address the thoughtful comments raised regarding our recently published manuscript “Targeting Long Noncoding RNA H19 in Subchondral Bone Osteocytes and the Alleviation of Cartilage Degradation in Osteoarthritis.”¹ In response to the remarks on the inconsistent findings concerning the role of H19 in osteoarthritis (OA), we acknowledge the complexity in this heterogeneous disease as discussed in our previous review paper,² which was published before the current study focusing on subchondral bone osteocytes. Despite these discrepancies, to the best of our understanding, the majority of evidence supports elevated H19 expression in OA cartilage.

Unlike earlier studies, including those referenced in the comment, our research specifically examined subchondral bone osteocytes, an underexplored component in OA and their role in subchondral bone remodeling and cartilage degradation in OA. In both clinical OA samples and destabilization of the medial meniscus-induced OA mouse model, we observed elevated H19 expression in subchondral bone osteocytes of the OA side.

By using osteocyte-specific H19 knockout mice and an osteocyte cellular model exposed to shear stress, we demonstrated the causal relationship between osteocyte function and OA progression, which is partly attributed to the phosphatidylinositol 3-kinase/protein kinase B/glycogen synthase kinase 3 signaling pathway. The translational potential of our findings is illustrated by employing antisense oligonucleotides delivered via magnetic metal-organic frameworks, which effectively mitigate OA progression via inhibiting H19 expression in vivo. Although cartilage remains central to OA pathology, our study provides solid evidence that the elevated H19 expression in osteocytes contributes to aberrant subchondral bone remodeling and OA progression, which is supported by a more comprehensive study design compared with similar research in the field. However, given the multifactorial nature of OA, we agree that further investigations are necessary to address the role of H19 and other long noncoding RNAs across different OA stages, phenotypes, and mechanical environments to enhance our understanding of OA development and progression.^{3,4}

Wayne Y. W. Lee, PhD 

waynelee@cuhk.edu.hk

Department of Orthopaedics and Traumatology, Faculty of
Medicine

The Chinese University of Hong Kong, Hong Kong, China; Li Ka Shing Institute of Health Sciences, The Chinese University of Hong Kong, Hong Kong, China; SH Ho Scoliosis Research Laboratory, Joint Scoliosis Research Center of the Chinese University of Hong Kong and Nanjing University, The Chinese University of Hong Kong, Hong Kong, China; and Center for Neuromusculoskeletal Restorative Medicine, CUHK InnoHK Centres, Hong Kong Science Park

Hong Kong, China

Rongliang Wong, PhD



Department of Orthopaedics and Traumatology, Faculty of
Medicine

The Chinese University of Hong Kong, Hong Kong, China; Li Ka Shing Institute of Health Sciences, The Chinese University of Hong Kong, Hong Kong, China; SH Ho Scoliosis Research Laboratory, Joint Scoliosis Research Center of the Chinese University of Hong Kong and Nanjing University, The Chinese University of Hong Kong, Hong Kong, China; and State Key Laboratory of Pharmaceutical Biotechnology, Division of Sports Medicine and Adult Reconstructive Surgery, Nanjing Drum Tower Hospital, The Affiliated Hospital of Nanjing University Medical School

Nanjing, China

1. Wang R, Mehrjou B, Dehghan-Banian D, et al. Targeting long non-coding RNA H19 in subchondral bone osteocytes alleviates cartilage degradation in osteoarthritis. *Arthritis Rheumatol* 2025;77(3): 283–297.
2. Wang R, Shiu HT, Lee WYW. Emerging role of lncRNAs in osteoarthritis: an updated review. *Front Immunol* 2022;13:982773.
3. Chen D, Shen J, Zhao W, et al. Osteoarthritis: toward a comprehensive understanding of pathological mechanism. *Bone Res* 2017;5(1): 16044.

Author disclosures are available at <https://onlinelibrary.wiley.com/doi/10.1002/art.43101>.

An-Fang Huang, MM 
louch211@163.com
 Affiliated Hospital of Southwest Medical University
 Sichuan, China
 Wang-Dong Xu, MD 
 Southwest Medical University
 Sichuan, China

1. Wang R, Mehrjou B, Dehghan-Banian D, et al. Targeting long non-coding RNA H19 in subchondral bone osteocytes alleviates cartilage degradation in osteoarthritis. *Arthritis Rheumatol* 2025;77(3): 283–297.
2. Wang H, Li J, Cheng Y, Yao J. Association of long-chain noncoding RNA H19 and MEG3 gene polymorphisms and their interaction with risk of osteoarthritis in a Chinese Han population. *Genet Test Mol Biomarkers* 2020;24(6):328–337.
3. Yang B, Xu L, Wang S. Regulation of lncRNA-H19/miR-140-5p in cartilage matrix degradation and calcification in osteoarthritis. *Ann Palliat Med* 2020;9(4):1896–1904.
4. Zhang X, Liu X, Ni X, et al. Long non-coding RNA H19 modulates proliferation and apoptosis in osteoarthritis via regulating miR-106a-5p. *J Biosci* 2019;44(6):128.
5. Zhou Y, Li J, Xu F, et al. Long noncoding RNA H19 alleviates inflammation in osteoarthritis through interactions between TP53, IL-38, and IL-36 receptor. *Bone Joint Res* 2022;11(8):594–607.
6. Tan F, Wang D, Yuan Z. The fibroblast-like synovial cell derived exosomal long non-coding RNA H19 alleviates osteoarthritis progression through the miR-106b-5p/TIMP2 axis. *Inflammation* 2020;43(4): 1498–1509.

DOI 10.1002/art.43100

Reply

To the Editor:

We appreciate the opportunity to address the thoughtful comments raised regarding our recently published manuscript “Targeting Long Noncoding RNA H19 in Subchondral Bone Osteocytes and the Alleviation of Cartilage Degradation in Osteoarthritis.”¹ In response to the remarks on the inconsistent findings concerning the role of H19 in osteoarthritis (OA), we acknowledge the complexity in this heterogeneous disease as discussed in our previous review paper,² which was published before the current study focusing on subchondral bone osteocytes. Despite these discrepancies, to the best of our understanding, the majority of evidence supports elevated H19 expression in OA cartilage.

Unlike earlier studies, including those referenced in the comment, our research specifically examined subchondral bone osteocytes, an underexplored component in OA and their role in subchondral bone remodeling and cartilage degradation in OA. In both clinical OA samples and destabilization of the medial meniscus-induced OA mouse model, we observed elevated H19 expression in subchondral bone osteocytes of the OA side.

By using osteocyte-specific H19 knockout mice and an osteocyte cellular model exposed to shear stress, we demonstrated the causal relationship between osteocyte function and OA progression, which is partly attributed to the phosphatidylinositol 3-kinase/protein kinase B/glycogen synthase kinase 3 signaling pathway. The translational potential of our findings is illustrated by employing antisense oligonucleotides delivered via magnetic metal-organic frameworks, which effectively mitigate OA progression via inhibiting H19 expression in vivo. Although cartilage remains central to OA pathology, our study provides solid evidence that the elevated H19 expression in osteocytes contributes to aberrant subchondral bone remodeling and OA progression, which is supported by a more comprehensive study design compared with similar research in the field. However, given the multifactorial nature of OA, we agree that further investigations are necessary to address the role of H19 and other long noncoding RNAs across different OA stages, phenotypes, and mechanical environments to enhance our understanding of OA development and progression.^{3,4}

Wayne Y. W. Lee, PhD 
waynelee@cuhk.edu.hk

Department of Orthopaedics and Traumatology, Faculty of Medicine

The Chinese University of Hong Kong, Hong Kong, China; Li Ka Shing Institute of Health Sciences, The Chinese University of Hong Kong, Hong Kong, China; SH Ho Scoliosis Research Laboratory, Joint Scoliosis Research Center of the Chinese University of Hong Kong and Nanjing University, The Chinese University of Hong Kong, Hong Kong, China; and Center for Neuromusculoskeletal Restorative Medicine, CUHK InnoHK Centres, Hong Kong Science Park

Hong Kong, China

Rongliang Wong, PhD

Department of Orthopaedics and Traumatology, Faculty of Medicine

The Chinese University of Hong Kong, Hong Kong, China; Li Ka Shing Institute of Health Sciences, The Chinese University of Hong Kong, Hong Kong, China; SH Ho Scoliosis Research Laboratory, Joint Scoliosis Research Center of the Chinese University of Hong Kong and Nanjing University, The Chinese University of Hong Kong, Hong Kong, China; and State Key Laboratory of Pharmaceutical Biotechnology, Division of Sports Medicine and Adult Reconstructive Surgery, Nanjing Drum Tower Hospital, The Affiliated Hospital of Nanjing University Medical School

Nanjing, China

1. Wang R, Mehrjou B, Dehghan-Banian D, et al. Targeting long non-coding RNA H19 in subchondral bone osteocytes alleviates cartilage degradation in osteoarthritis. *Arthritis Rheumatol* 2025;77(3): 283–297.
2. Wang R, Shiu HT, Lee WYW. Emerging role of lncRNAs in osteoarthritis: an updated review. *Front Immunol* 2022;13:982773.
3. Chen D, Shen J, Zhao W, et al. Osteoarthritis: toward a comprehensive understanding of pathological mechanism. *Bone Res* 2017;5(1): 16044.

4. Lv Z, Yang YX, Li J, et al. Molecular classification of knee osteoarthritis. *Front Cell Dev Biol* 2021;9:725568.

DOI 10.1002/art.43102

Limitations in the real-world emulation of the HORIZON-Pivotal Fracture Trial: comment on the article by D'Andrea et al

To the Editor:

We read with great interest the article by D'Andrea et al¹ that emulated the HORIZON-Pivotal Fracture Trial (PFT) using real-world data from US claims databases. This study adds valuable insights into the effectiveness of zoledronic acid in reducing hip fractures in postmenopausal women with osteoporosis under routine clinical practice, particularly addressing the efficacy–effectiveness gap. Although the authors acknowledge several limitations, we believe that certain important aspects were left unaddressed, which could further influence the interpretation of the study results.

First, the potential for residual confounding despite propensity score matching cannot be entirely ruled out. Although the authors balanced 85 baseline covariates among treatment groups, critical unmeasured variables, such as body mass index or specific bone mineral density scores, were not captured in the claims data. These factors are known to influence fracture risk and could confound the observed associations between zoledronic acid and fracture outcomes. Excluding these variables may result in incomplete adjustment for differences in baseline risk among treatment groups.

Second, using claims data for emulation inherently introduces limitations in the accuracy of outcome assessment, particularly for events such as vertebral fractures, which are known to be underreported in administrative databases. The authors rightly chose to exclude vertebral fractures due to concerns about misclassification. Still, the underdiagnosis of such fractures in routine clinical practice limits our ability to fully evaluate the impact of zoledronic acid on all osteoporotic fractures.² This selective outcome assessment may have contributed to the observed attenuation in the effect of zoledronic acid compared to the randomized controlled trial.

Third, treatment patterns and adherence may vary significantly across health care systems and geographic regions.³ The data used in this study were derived from US claims databases, and the generalizability of the findings to other settings may be limited. Differences in health care infrastructure, physician prescribing habits, and patient preferences can all influence adherence to osteoporosis therapies and, consequently, the effectiveness of zoledronic acid in preventing fractures. This variability could limit the external validity of the study results when applied to populations outside the United States.

Finally, the relatively short follow-up period of 18 months in the real-world study compared to the 36-month follow-up in the HORIZON-PFT raises concerns about the long-term sustainability of the treatment effect. The authors acknowledge that poor adherence in clinical practice may have diminished the observed effectiveness, but longer follow-up would be necessary to assess whether the beneficial effects of zoledronic acid persist over time, particularly for nonvertebral fractures. In conclusion, although the real-world emulation of the HORIZON-PFT provides valuable insights, it is crucial to consider the limitations inherent in using claims data, the potential for residual confounding, and the influence of treatment patterns across different health care settings. We hope that future studies will address these gaps to provide a more comprehensive understanding of the real-world effectiveness of osteoporosis treatments.

Author disclosures are available at <https://onlinelibrary.wiley.com/doi/10.1002/art.43102>.

Peng Shih-Kuei 
 Poi Kuo
 James Cheng-Chung Wei, MD, PhD 
jccwei@gmail.com
 Chung Shan Medical University Hospital
 Taichung, Taiwan

1. D'Andrea E, Schneeweiss S, Franklin JM, et al. Efficacy versus effectiveness: the HORIZON-Pivotal Fracture Trial and its emulation in claims data. *Arthritis Rheumatol* 2025;77:12–21.
2. Reid IR, Horne AM, Mihov B, et al. Fracture prevention with zoledronate in older women with osteopenia. *N Engl J Med* 2018;379:2407–2416.
3. Curtis JR, Yun H, Matthews R, et al. Adherence with intravenous zoledronate and intravenous ibandronate in the United States Medicare population. *Arthritis Care Res (Hoboken)* 2012;64(7):1054–1060.

DOI 10.1002/art.43103

Reply

To the Editor:

We appreciate the thoughtful commentary by Shih-Kuei et al regarding our study that emulated the HORIZON-Pivotal Fracture Trial (PFT) using real-world data from two large US claims-based databases.¹ We recognize the importance of the points raised and provide a detailed response. We acknowledged in our manuscript that residual confounding cannot be entirely ruled out, which is an inherent limitation of observational studies. Although we balanced 85 baseline covariates between treatment groups, specific variables such as body mass index (BMI) and bone mineral density (BMD) scores were not captured. Nonetheless, we

used a robust propensity score-matching technique to minimize confounding by measurable factors. Including numerous covariates related to demographics, overall health status, comorbidities, use of health care services, filled drug prescriptions, and osteoporosis-specific treatments enhance our control of confounding variables because these collectively act as proxies for unobserved factors.² However, we encourage future studies to control for clinical data, such as BMI and BMD scores, when available.

As stated in our study, we deliberately excluded vertebral fractures as an outcome due to the high risk of misclassification. Underdiagnosis and underreporting of vertebral fractures in US administrative databases limit the reliability of evaluating these outcomes because 65% to 75% of vertebral fractures in postmenopausal women with osteoporosis are clinically silent and often undetected.³ Consequently, our primary focus was on hip fractures, which are well-documented and validated within claims data. Notably, this exclusion does not explain the attenuated effect of zoledronic acid on hip fracture risk observed in our study compared to the HORIZON-PFT study because each trial outcome was evaluated independently. We encourage exploring a broader range of fracture outcomes in settings in which they can be accurately captured.

We recognize that treatment patterns and adherence may vary across health care systems and geographic regions. Differences in health care infrastructure, physician prescribing habits, and patient preferences indeed influence adherence and the overall effectiveness of therapies. We concur with Shih-Kuei et al that further studies across different health care systems outside the United States could evaluate the generalizability of our findings.


The relatively short follow-up period of 18 months reflects adherence patterns in the real-world setting, in which many patients struggle to maintain long-term adherence to annual zoledronic acid infusions. Although the 36-month follow-up in the HORIZON-PFT provided a broader view of long-term efficacy, our study aimed to reflect real-world treatment effectiveness, often limited by adherence issues. We share the concern about the sustainability of the treatment effect and believe measures should be taken to increase adherence in clinical practice, enabling longer follow-up studies to better evaluate the effects of osteoporosis drugs.

In conclusion, our study provides valuable insights into the real-world effectiveness of zoledronic acid compared to the efficacy shown in the trial. These findings should be interpreted considering the inherent limitations discussed in our manuscript, such as residual confounding and duration of follow-up.¹ Future research addressing the effect of zoledronic acid on hip and vertebral fractures in other health care

settings will enhance our understanding of its real-world effectiveness.

We thank the authors for contributing to this discussion.

Author disclosures are available at <https://onlinelibrary.wiley.com/doi/10.1002/art.43103>.

Elvira D'Andrea, MD, PhD, MPH 
elvira.dandrea@mail.harvard.edu
AbbVie, Inc
North Chicago, IL
Brigham and Women's Hospital
and Harvard Medical School
Boston, MA
Shirley Wang, PhD, ScM
Brigham and Women's Hospital
and Harvard Medical School
Boston, MA

1. D'Andrea E, Schneeweiss S, Franklin JM, et al. Efficacy versus effectiveness: the HORIZON-Pivotal Fracture Trial and its emulation in claims data. *Arthritis Rheumatol* 2025;77:12–21.
2. Greenland S. Invited commentary: variable selection versus shrinkage in the control of multiple confounders. *Am J Epidemiol* 2008;167(5): 523–529.
3. Lems WF, Paccou J, Zhang J, et al; International Osteoporosis Foundation Fracture Working Group. Vertebral fracture: epidemiology, impact and use of DXA vertebral fracture assessment in fracture liaison services. *Osteoporos Int* 2021;32(3):399–411.

DOI 10.1002/art.43107

Avoiding placebo as control treatment in rheumatology trials: can we do better? Comment on the article by Kivitz et al

To the Editor:

Kivitz et al¹ describe the results of a randomized placebo-controlled trial on the efficacy and safety of intravenous secukinumab compared to placebo in patients with active psoriatic arthritis. Eligible patients had both active joints and active skin disease or a history of it:

Patients aged ≥ 18 years who fulfilled the Classification Criteria for Psoriatic Arthritis, had a diagnosis of PsA for six months or longer, and had active PsA (defined by three or more swollen and three or more tender joints despite current or past treatment with nonsteroidal anti-inflammatory drugs, disease-modifying antirheumatic drugs, or tumor necrosis factor [TNF] inhibitors) were enrolled in the study. Enrolled patients were required to have either signs of skin manifestations of plaque psoriasis or nail changes consistent with psoriasis or to have a documented history of plaque psoriasis.

Patients randomized to placebo received 16 weeks of placebo before switching to active treatment. Although the results are of interest, I really wonder whether there was sufficient equipoise, that is, uncertainty of which treatment arm would be better off to allow a placebo control group. Before the start of this trial (in 2020 as recorded on [ClinicalTrials.gov](https://clinicaltrials.gov)), the sponsor (Novartis) had already amply demonstrated that secukinumab administered subcutaneously is effective and safe in the target population. So in the 190 placebo patients, effective (subcutaneous) treatment was delayed for 16 weeks, whereas the a priori expectation for efficacy of intravenous secukinumab was of course quite high. The design implicitly acknowledges this because placebo patients were switched to intravenous treatment after 16 weeks, which would be unethical if any efficacy of intravenous treatment were completely unknown.

I know placebo-controlled designs are the default option in registration trials for the regulatory authorities as an efficient way to document efficacy. And thankfully the period of placebo treatment has now been shortened to three months or 16 weeks in many rheumatologic conditions.² However, testing a new mode of administration for a drug already proved to be effective is a different scenario. So, I wonder why the researchers did not opt for a noninferiority design with a control group receiving subcutaneous secukinumab. This would have had the added benefit of a direct comparison of the two modes of administration. But the key benefit would have been the avoidance of unnecessary suffering in a substantial group of patients.

Author disclosures are available at <https://onlinelibrary.wiley.com/doi/10.1002/art.43107>.

Maarten Boers, MSc, MD, PhD 
eds@amsterdamumc.nl
 Amsterdam University Medical Centers
 Amsterdam, The Netherlands

1. Kivitz A, Sedova L, Churchill M, et al. Efficacy and safety of intravenous secukinumab for the treatment of active psoriatic arthritis: results from a randomized, placebo-controlled phase 3 study. *Arthritis Rheumatol* 2025;77(2):171–179.
2. Boers M. The time has come to limit the placebo period in rheumatoid arthritis trials to 3 months: a systematic comparison of 3- and 6-month response rates in trials of biological agents. *Ann Rheum Dis* 2010;69(1):186–192.

DOI 10.1002/art.43106

2023 American College of Rheumatology/American College of Chest Physicians guideline for the screening and monitoring of interstitial lung disease in people with systemic autoimmune rheumatic diseases: comment on the article by Johnson et al

To the Editor:

We read with great interest the recently published 2023 American College of Rheumatology (ACR)/American College of

Chest Physicians (CHEST) guideline for the screening and monitoring of interstitial lung disease (ILD) in people with systemic autoimmune rheumatic diseases (SARDs).¹ We would like to acknowledge the importance of this effort and commend the authors for addressing an issue of this magnitude. However, we feel obliged to express concerns regarding some of the recommendations.

The most striking feature of these guidelines was a consistent inclination toward additional screening, regardless of uncertainty. The authors of the guidelines explicitly stated this preference when they wrote, “Where there is uncertainty regarding whom to screen, clinicians should proceed with screening.” This perspective led to the creation of a “high-risk” group, which across diseases includes patients who previously would not have been screened. For rheumatoid arthritis (RA), for instance, it includes patients with high antibody titers, older age at onset, higher body mass index, and male sex, a substantial increase from current screening practice. For mixed connective tissue disease and Sjögren disease, many of the listed risk factors are unsubstantiated, and the accompanying literature review explicitly placed defining the magnitude of risk these factors confer as outside of scope.

An inclination toward screening regardless of uncertainty also affected recommendations for how to screen for ILD. The guidelines recommend both pulmonary function tests (PFTs; including spirometry, lung volumes, and diffusion capacity) and screening with a high-resolution computed tomography (HRCT) scan. Such an approach would identify the maximal amount of preclinical disease, including that which may never progress or affect a patient’s quality of life, and that which is unrelated to rheumatic diseases (incidentalomas, such as benign nodules). They also recommend against screening with conventional chest radiography, which would be less likely to identify incidentalomas and would provide lower radiation exposure. None of the cited literature demonstrated improved outcomes with such an expansive approach.

Monitoring of SARD-ILD presents similar problems. The natural history of patients who screen negative up front and initiate effective therapies for SARDs is currently uncertain. Yet, the guidelines recommend ongoing follow-up for asymptomatic patients and recommend both HRCT and PFTs based on no available evidence. The recommended interval for screening remains somewhat nebulous (every 3–12 months initially then “less frequently once stable”) depending on disease, but the provided flowchart that most physicians will reference recommends rheumatologists “consider yearly re-screening in high-risk patients.” In practice this would amount to yearly screening with HRCT and PFTs for most patients with SARDs *despite negative initial testing*.

Acknowledging these concerns, proponents of screening may reasonably ask, “What is the harm?” We would suggest rheumatologists consider the widely acknowledged harms of screening in general, which will apply to these recommendations as well. These include the risks of overdiagnosis (ie, detecting disease that would not have otherwise harmed a patient during their lifetime), subsequent testing of incidental findings (often triggering a

cascade of further tests and potentially harmful interventions), radiation exposure, and the looming specter of overtreatment (ie, unnecessary or overly aggressive treatment that does not benefit a patient).

Given the expansive approach of these recommendations, harms will be inevitable. For RA, for instance, the authors acknowledge a low frequency of progressive ILD (“3–5%”) and a “a larger proportion [who] have asymptomatic or stable disease.” How many patients may have asymptomatic or stable disease? Estimates in the literature vary widely, ranging between 2% and 58% in different cohorts.^{2–5} This suggests that a substantial fraction of those identified as having “RA-ILD” may never have progressed or gone on to experience harm from their underlying disease.

Recommendations for screening should be limited when key appropriateness criteria are not met. These include the presence of a preclinical period during which disease can be detected, the existence of an effective intervention, a favorable risk-benefit profile, and cost effectiveness (both to the patient and to the health care system). There is substantial uncertainty that these recommendations meet those criteria, and we suspect they will not be met as additional information arises. Indeed, all but one recommendation was based on “very low” certainty of evidence by the GRADE approach (the Grading of Recommendations, Assessment, Development and Evaluation). The authors provided appropriate caveats to acknowledge this, but unfortunately this will do little to blunt the imprimatur of the phrase “guideline recommendations,” which have been endorsed by two of the foremost professional societies in rheumatology and pulmonology: ACR and CHEST.

Despite these concerns, we commend the authors for their efforts to provide guidance for these uncommon and difficult diseases. We would reaffirm that proponents of screening have the best of intentions and would acknowledge that some patients would clearly benefit from additional screening. We are also concerned about the widespread uptake of these recommendations and the underlying bias toward screening despite uncertainty, which will result in overtesting, overdiagnosis, overtreatment, and complications. Whether the benefits of this approach outweigh these risks remains to be seen and should be the focus of subsequent research.


Author disclosures are available at <https://onlinelibrary.wiley.com/doi/10.1002/art.43106>.

Julian Segan, MBBS (hons)

j.segan@alfred.org.au

Alfred Health

Melbourne, Victoria, Australia

Michael Putman, MD, MSCI 

Medical College of Wisconsin

Milwaukee

Richard Conway, MBBChBAO, PhD 

Trinity College Dublin, The University of Dublin Trinity College and St. James's Hospital

Dublin, Ireland

1. Johnson SR, Bernstein EJ, Bolster MB, et al. 2023 American College of Rheumatology (ACR)/American College of Chest Physicians (CHEST) guideline for the screening and monitoring of interstitial lung disease in people with systemic autoimmune rheumatic diseases. *Arthritis Care Res (Hoboken)* 2024;76(8):1070–1082.
2. Gabbay E, Tarala R, Will R, et al. Interstitial lung disease in recent onset rheumatoid arthritis. *Am J Respir Crit Care Med* 1997;156(2 Pt 1): 528–535.
3. Dawson JK, Fewins HE, Desmond J, et al. Fibrosing alveolitis in patients with rheumatoid arthritis as assessed by high resolution computed tomography, chest radiography, and pulmonary function tests. *Thorax* 2001;56(8):622–627.
4. Bartels CM, Bell CL, Shinki K, et al. Changing trends in serious extra-articular manifestations of rheumatoid arthritis among United States veterans over 20 years. *Rheumatology (Oxford)* 2010;49(9): 1670–1675.
5. Raimundo K, Solomon JJ, Olson AL, et al. Rheumatoid arthritis-interstitial lung disease in the United States: prevalence, incidence, and healthcare costs and mortality. *J Rheumatol* 2019;46(4): 360–369.

DOI 10.1002/art.43111

Reply

To the Editor:

We thank the authors for their letter to the editor in response to the publication of the ACR/CHEST guidelines for the screening,^{1,2} monitoring,^{1,2} and treatment^{3,4} of ILD in people with SARDs. The ACR prioritizes the development of methodologically sound, evidence-based clinical practice guidelines that incorporate a range of perspectives, expertise, and experiences, including those of patients.⁵ Patient input is especially crucial when guidelines are based on low-certainty evidence, as these recommendations are particularly influenced by patients' values and preferences.^{5,6}

Clinical practice guidelines fulfill several objectives.⁵ Although the purpose of clinical practice guidelines is to provide guidance to clinicians, they are not intended to be doctrine.⁵ Secondary objectives of clinical practice guidelines are to promote awareness and be used for advocacy to improve access to tests or treatments.⁵ There is considerable diagnostic delay with regard to ILD. Cosgrove et al found a diagnostic delay in ILD of 3 or more years in 19% of patients studied, and most patients were misdiagnosed.⁷ Diagnostic delay may be reduced if the importance of early diagnosis were more widely recognized.⁸ The SARD-ILD guidelines increase awareness of the need for screening and provide guidance for monitoring. By identifying SARD-ILD and tailoring evaluation and management to each patient, there is an opportunity for earlier treatment, which could potentially improve patient outcomes. For those individuals who develop progressive disease, there is evidence to support the benefit of early treatment intervention. Clinical practice guidelines highlight areas of needed research. Very little is known about the natural history of ILD

across the SARDs. In the guidelines, we highlight several areas where more data are needed. We agree with the authors that research on screening and monitoring of ILD, including optimal frequency and cost-benefit analysis, is needed. These guidelines will be updated as new data emerge.

The SARD-ILD guideline patient panel expressed a preference for identifying ILD early, even if there was a risk for identifying either subclinical disease that might not progress or incidental findings requiring additional testing.⁹ Patients generally favored screening as an opportunity to learn more about their disease and identify ILD early, even ILD that might never cause symptoms. The screening and monitoring recommendations are conditional recommendations, except for the strong recommendation against surgical lung biopsy. A conditional recommendation indicates that the recommended course of action is likely to be preferred by most people but many may not. This is because of the uncertainty regarding the balance of benefits and harms, or because individuals may value the outcomes differently.¹⁰ Screening and monitoring for ILD should be performed in shared decision-making with the rheumatologist and/or pulmonologist and the patient. The inclusion of patient perspectives in these guidelines is unique and should not be undervalued. Taking care of the patient on the patient's terms should be a transcendent principle. The current SARD-ILD guidelines synthesize the best available evidence with expert experience and align with patient preferences.

Supported by the American College of Rheumatology.

Author disclosures are available at <https://onlinelibrary.wiley.com/doi/10.1002/art.43111>.

Sindhu R. Johnson, MD, PhD 
Sindhu.Johnson@uhn.ca
 University of Toronto
 and Schroeder Arthritis Institute, Toronto Western Hospital
 Toronto, Ontario, Canada
 and Mount Sinai Hospital
 New York, NY

Marcy B. Bolster, MD 
 Massachusetts General Hospital
 Boston

Sonye K. Danoff, MD, PhD
 Johns Hopkins University School of Medicine
 Baltimore, MD

Michael George, MD, MSCE 
 University of Pennsylvania
 Philadelphia

Gordon Guyatt, MD
 Reza D. Mirza, MD, MSc 
 McMaster University
 Hamilton, Ontario, Canada

Dinesh Khanna, MD, MS 
 University of Michigan
 Ann Arbor
 Aberdeen Allen Jr PhD
 Parlin, NJ

Amy Turner 
 American College of Rheumatology
 Atlanta, GA

Elana J. Bernstein, MD, MSc
 Columbia University Vagelos College of Physicians and Surgeons
 and Columbia University Irving Medical Center
 New York, NY

1. Johnson SR, Bernstein EJ, Bolster MB, et al. 2023 American College of Rheumatology (ACR)/American College of Chest Physicians (CHEST) guideline for the screening and monitoring of interstitial lung disease in people with systemic autoimmune rheumatic diseases. *Arthritis Care Res (Hoboken)* 2024;76(8):1070–1082.
2. Johnson SR, Bernstein EJ, Bolster MB, et al. 2023 American College of Rheumatology (ACR)/American College of Chest Physicians (CHEST) guideline for the screening and monitoring of interstitial lung disease in people with systemic autoimmune rheumatic diseases. *Arthritis Rheumatol* 2024;76(8):1201–1213.
3. Johnson SR, Bernstein EJ, Bolster MB, et al. 2023 American College of Rheumatology (ACR)/American College of Chest Physicians (CHEST) guideline for the treatment of interstitial lung disease in people with systemic autoimmune rheumatic diseases. *Arthritis Care Res (Hoboken)* 2024;76(8):1051–1069.
4. Johnson SR, Bernstein EJ, Bolster MB, et al. 2023 American College of Rheumatology (ACR)/American College of Chest Physicians (CHEST) guideline for the treatment of interstitial lung disease in people with systemic autoimmune rheumatic diseases. *Arthritis Rheumatol* 2024;76(8):1182–1200.
5. Johnson SR, Turner AS, Goodman SM. How the American College of Rheumatology develops guidelines. *Rheum Dis Clin North Am* 2022; 48(3):579–588.
6. Fraenkel L, Miller AS, Clayton K, et al. When patients write the guidelines: patient panel recommendations for the treatment of rheumatoid arthritis. *Arthritis Care Res (Hoboken)* 2016;68(1):26–35.
7. Cosgrove GP, Bianchi P, Danese S, et al. Barriers to timely diagnosis of interstitial lung disease in the real world: the INTENSITY survey. *BMC Pulm Med* 2018;18(1):9.
8. Spagnolo P, Ryerson CJ, Putman R, et al. Early diagnosis of fibrotic interstitial lung disease: challenges and opportunities. *Lancet Respir Med* 2021;9(9):1065–1076.
9. Mirza RD, Bolster MB, Johnson SR, et al. Assessing patient values and preferences to inform the 2023 American College of Rheumatology/American College of Chest Physicians interstitial lung disease guidelines. *Arthritis Care Res (Hoboken)* 2024;76(8):1083–1089.
10. Neumann I, Santesso N, Akl EA, et al. A guide for health professionals to interpret and use recommendations in guidelines developed with the GRADE approach. *J Clin Epidemiol* 2016;72: 45–55.

Correction to: Discovery of a Novel Missense Variant in NLRP3 Causing Atypical Cryopyrin-Associated Periodic Syndromes With Hearing Loss as the Primary Presentation, Responsive to Anti-Interleukin-1 Therapy

Birk-Bachar, M., Cohen, H., Sofrin-Drucker, E., Kropach-Gilad, N., Orenstein, N., Lidzbarsky, G., Kornreich, L., Tal, R., Amarilyo, G., Levinsky, Y. and Sokolov, M., 2024. Discovery of a Novel Missense Variant in NLRP3 Causing Atypical Cryopyrin-Associated Periodic Syndromes With Hearing Loss as the Primary Presentation, Responsive to Anti-Interleukin-1 Therapy. *Arthritis & Rheumatology* <https://acrjournals.onlinelibrary.wiley.com/doi/epdf/10.1002/art.42721>

As mentioned in our article, an important part of the patients' clinical evaluation included pure-tone audiometry at baseline and during follow-up of the affected family members. Unfortunately, we neglected to acknowledge two team members from the Speech and Language Center whose contributions were valuable to our work:

Professor Yael Henkin

Dr Ricky Kaplan-Neeman

Hearing, Speech and Language Center, Sheba Medical Center, Tel Hashomer,

Tel Aviv University, Israel

We regret the error.